NATIONAL CENTER FOR EARTHQUAKE ENGINEERING RESEARCH

ISSN 1088-3800

Post-Earthquake Reconstruction Strategies: NCEER-INCEDE Center-to-Center Project

Proceedings of the Workshop on Earthquake Engineering Frontiers in Transportation Facilities

Edited by G.C. Lee and I.M. Friedland

Technical Report NCEER-97-0005

INCEDE Report Number 1997-01

August 29, 1997

This Workshop was held in Buffalo, New York on March 10-11, 1997 and was supported by the Japan Society for the Promotion of Sciences and the U.S. National Science Foundation.

NOTICE

This report was prepared by the National Center for Earthquake Engineering Research (NCEER) and INCEDE (the Japan International Center for Disaster Mitigation Engineering). Neither NCEER, associates of NCEER, its sponsors, INCEDE nor any person acting on their behalf:

a. makes any warranty, express or implied, with respect to the use of any information, apparatus, method, or process disclosed in this report or that such use may not infringe upon privately owned rights; or

b. assumes any liabilities of whatsoever kind with respect to the use of, or the damage resulting from the use of, any information, apparatus, method, or process disclosed in this report.

Any opinions, findings, and conclusions or recommendations expressed in this publication are those of the author(s) and do not necessarily reflect the views of NCEER, the National Science Foundation, or other sponsors.

Proceedings of the Workshop on Earthquake Engineering Frontiers in Transportation Facilities

Held at
University Inn and Conference Center
Buffalo, New York
March 10-11, 1997

Edited by George C. Lee[1] and Ian M. Friedland[2]
Publication Date: August 29, 1997

Technical Report NCEER-97-0005

NSF Grant Number INT9512844

In cooperation with the
Japan International Center for Disaster Mitigation Engineering (INCEDE)

1 Director, National Center for Earthquake Engineering Research
2 Assistant Director for Bridges and Highways, National Center for Earthquake Engineering Research

NATIONAL CENTER FOR EARTHQUAKE ENGINEERING RESEARCH
State University of New York at Buffalo
Red Jacket Quadrangle, Buffalo, NY 14261

Preface

The 1994 Northridge and 1995 Kobe earthquakes have provided a significant amount of scientific data for researchers concerning earthquake hazard mitigation activities across a broad spectrum of disciplines. Because many of the issues in earthquake hazard mitigation research require multi-disciplinary efforts, collaboration between researchers and practitioners is seen to be more effective in addressing these issues than through individual investigator research approaches. This belief has led to the development of a project jointly funded by the U.S. National Science Foundation and the Japan Society for the Promotion of Sciences, which is being conducted by the U.S. National Center for Earthquake Engineering Research (NCEER) and the Japan International Center for Disaster Mitigation Engineering (INCEDE).

This project, which is known as the NCEER-INCEDE Center-to-Center project, is focused on the development of improved post-earthquake urban reconstruction strategies. It has been developed and is intended to fall under the umbrella of the U.S.-Japan common agenda on disaster mitigation, as agreed upon by the president of the United States and the prime minister of Japan in 1995. The subject matter addressed by the Center-to-Center project is relatively broad, but primarily concentrates on the Northridge and Kobe earthquakes. Cooperative investigations focus on key infrastructure systems addressing both short- and long-term issues. The emphasis in the Center-to-Center project is given to the technical and scientific aspects of post-earthquake reconstruction problems by focusing on cooperative research studies and analyses, although any and all areas of earthquake engineering related to infrastructure systems may be addressed.

During the first year of the project, key individuals from both NCEER and INCEDE met twice and a special workshop was held to identify key areas of study and the approaches for each center to pursue in a coordinated fashion. Three important components of post-earthquake activities were identified: (1) repair, restoration, and recovery of transportation systems; (2) repair, restoration, and recovery of water systems; and (3) emergency communications and management. The ability to assess the level of damage immediately following an earthquake is also considered to be an important issue under all three of these components.

To further this common Center-to-Center agenda, three specific tasks will be conducted during the first three years of the project. They are: (1) to document the experiences of organizations and agencies responsible for the restoration and reconstruction of transportation and water systems after the Northridge and Kobe earthquakes; (2) to assess ways of improving governmental and organizational capacity for managing post-disaster response, restoration, and early recovery; and (3) to develop a model reconstruction system that is both robust and resilient.

To further these goals, NCEER and INCEDE organized and conducted the Center-to-Center Workshop on Earthquake Engineering Frontiers in Transportation Facilities. The workshop was held in Buffalo, New York, on March 10 and 11, 1997, and consisted of presentations and discussions between Japanese and U.S. researchers and practitioners on earthquake engineering issues related to the design, construction, performance, and reconstruction of transportation

infrastructure in the U.S. and Japan. This first transportation-focused workshop concentrated on issues related to bridge engineering; future workshops under the Center-to-Center project are expected to address other modes of transportation as well, including transit and railway, and port and harbor facilities.

Discussions during the workshop resulted in a series of resolutions that are published in these proceedings for future reference. The conclusions of the workshop participants were that this first workshop provided an excellent vehicle for technology sharing and the identification of common problems and issues in earthquake engineering for transportation facilities; yet, there is still significant opportunity for improvement in bridge engineering practice in order to obtain more effective response and recovery following damaging earthquakes.

Appreciation is extended to Dr. Ken Sudo, Director, and Dr. Kimiro Meguro, both of INCEDE for their support and assistance in organizing the Japan-side participation in this workshop. Dr. Kazuhiko Kawashima of the Tokyo Institute of Technology is also recognized for his extensive efforts in coordinating the Japan-side presentations and participants. Appreciation is also extended to the U.S. National Science Foundation and the Japan Society for the Promotion of Sciences for their continued support of important activities like the Center-to-Center project.

Resolutions

The first Center-to-Center Project Workshop on Earthquake Engineering Frontiers in Transportation Facilities was held in Buffalo, New York on March 10 and 11, 1997. Jointly co-sponsored by the National Center for Earthquake Engineering Research (NCEER) in the United States and the International Center for Disaster-Mitigation Engineering (INCEDE) in Japan, the Center-to-Center Project attempts to learn from the experiences, and identify improved strategies for recovery, following damaging earthquakes. This collaborative effort focuses on promoting an increase in technology transfer, knowledge utilization mechanisms, and other areas as identified by NCEER and INCEDE. Financial support for the Center-to-Center Project is provided by the U.S. National Science Foundation (NSF) and the Japan Society for the Promotion of Science (JSPS).

Discussions at this first workshop on Transportation Facilities were structured around the technical areas of earthquake ground motions, soil behavior and response, underground structures, and the performance, analysis, and design and reconstruction of highway bridges during and following damaging earthquakes. Participants agreed that the workshop was successful and that it led to a greater understanding of the many issues involved in these areas both in the United States and Japan. However, participants also identified many problems yet to be resolved in these areas, and for other types of transportation facilities, and that additional research and studies are still needed.

The participants suggested that increased cooperation between the U.S. and Japan under the structure of the Center-to-Center Project would be beneficial to both countries for improving practice, policies, and procedures for preventing damage and for recovery following damaging earthquakes. As a result, the following resolutions were developed and approved during the workshop:

1. There are many topics of common interest to the U.S. and Japan in earthquake damage mitigation and reconstruction of transportation facilities. It is therefore resolved that continued cooperation between researchers and practitioners in these two countries be encouraged, and mechanisms for improved technology transfer and sharing be explored.

2. In view of the damage sustained to transportation facilities besides highways and bridges during the Northridge and Kobe earthquakes, and the resulting impacts on traffic flow in these regions, it is resolved that future workshops be held under Center-to-Center Project sponsorship to also examine the operation of traffic management and control systems (hardware and software), and address issues related to identifying damage and performance of port and harbor facilities, and transit and railway structures, in order to assist in the development of improved mitigation and post-earthquake recovery strategies.

3. Based on resolutions 1 and 2 above, it is further resolved that a second workshop on Earthquake Engineering Frontiers in Transportation Facilities be jointly organized by INCEDE and NCEER and held in Japan in approximately one year.

4. Based on the results of this first Transportation Facilities workshop, opportunities for collaborative research and information sharing should be further explored, and potential funding agencies for such collaborative research should be identified within the U.S. and Japan.

Participants of the NCEER-INCEDE Center-to-Center Workshop on Earthquake Engineering Frontiers in Transportation Facilities

Table of Contents

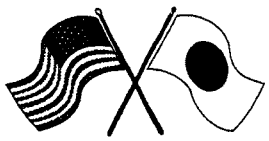

Opening Session

Session Co-chairs: Ian M. Friedland and Kazuhiko Kawashima

NCEER's Mission and Goals for the Center-to-Center Project: Cooperative Development of a Framework for Post-urban Earthquake Reconstruction Strategies

George C. Lee and Andrea S. Dargush

Center-to-Center (INCEDE-NCEER) Cooperative Research and US-Japan Common Agenda on Earthquake Related Issues and the Role of INCEDE Towards Goals of IDNDR

Ken Sudo, Tsuneo Katayama, Kimiro Meguro, Anura Srikantha Herath and Dushamante Dutta

NATIONAL CENTER FOR EARTHQUAKE ENGINEERING RESEARCH
Headquartered at the State University of New York at Buffalo

INSTITUTE OF INDUSTRIAL SCIENCE INCEDE UNIVERSITY OF TOKYO

NCEER's Mission and Goals for the Center-to-Center Project
Cooperative Development of a Framework for Post-Urban Earthquake Reconstruction Strategies

George C. Lee, Director, Andrea S. Dargush, Assistant Director for Research and Education
National Center for Earthquake Engineering Research
State University of New York at Buffalo

ABSTRACT

This paper summarizes the background and objectives of a Center-to-Center cooperative project on the development of post-urban earthquake reconstruction strategies between the International Center for Disaster Mitigation Engineering (INCEDE-Japan) and the National Center for Earthquake Engineering Research (NCEER-USA).

The subject matter is broad. This Center-to-Center project is limited to selected case studies of the Northridge and Kobe earthquakes. Investigation is focused on key infrastructural systems for which both short-term and long-term issues and concerns will be addressed. Emphasis is given to the technical and scientific aspects of post-earthquake reconstruction problems by focusing on cooperative research study and analysis.

This paper defines the background, the important issues and the selected aspects of studies we hope to conduct, to benefit those who plan to take part in the studies of this Center-to-Center project. Therefore, this paper is an open-ended description of the intent of the project with the hope that it can provide some direction for a more effective contribution by those who are interested in taking part in this Center-to-Center collaborative research effort.

INTRODUCTION

The 1994 Northridge and 1995 Kobe earthquakes have provided a significant amount of scientific data for researchers concerning earthquake hazard mitigation activities across a broad spectrum of disciplines. Because many issues of earthquake hazard mitigation studies require multi-disciplinary efforts, a Center-to-Center collaboration is seen to be more effective than individual investigator oriented approaches. This belief has led to the Center-to-Center project jointly funded by the Japan Society for the Promotion of Sciences and the US National Science Foundation. It is the first Center-to-Center collaborative effort between Japan and the US regarding earthquake engineering investigation and research. The project is being developed as a timely activity under the US-Japan common agenda on disaster mitigation agreed upon by the president of the United States and the prime minister of Japan in 1995.

The research plan discussed here will be the basis for US efforts during the second and third year of a three-year project on the development of post earthquake reconstruction strategies. It represents the US component in a US-Japan Collaborative Project between the National Center for Earthquake Engineering Research (NCEER), SUNY, Buffalo, and the International Center for Disaster Mitigation Engineering (INCEDE), Institute of Industrial Science, University of Tokyo, Japan. The project gives special emphasis to the experiences of recent events (Northridge and Kobe earthquakes).

Research objectives are carried out using the systems-integrated, multidisciplinary approach that has been successfully employed by NCEER over the past ten years. Research in primary focus areas of the project must yield not only fundamental knowledge on individual disciplinary-oriented issues but also provide insight to potential applications which may be used to address the problem. Interaction between disciplines is essential to reaching consensus on possible solutions, and the NCEER research matrix (Figure 1) provides a guiding framework to this approach. Participants include researchers from structural engineering, transportation

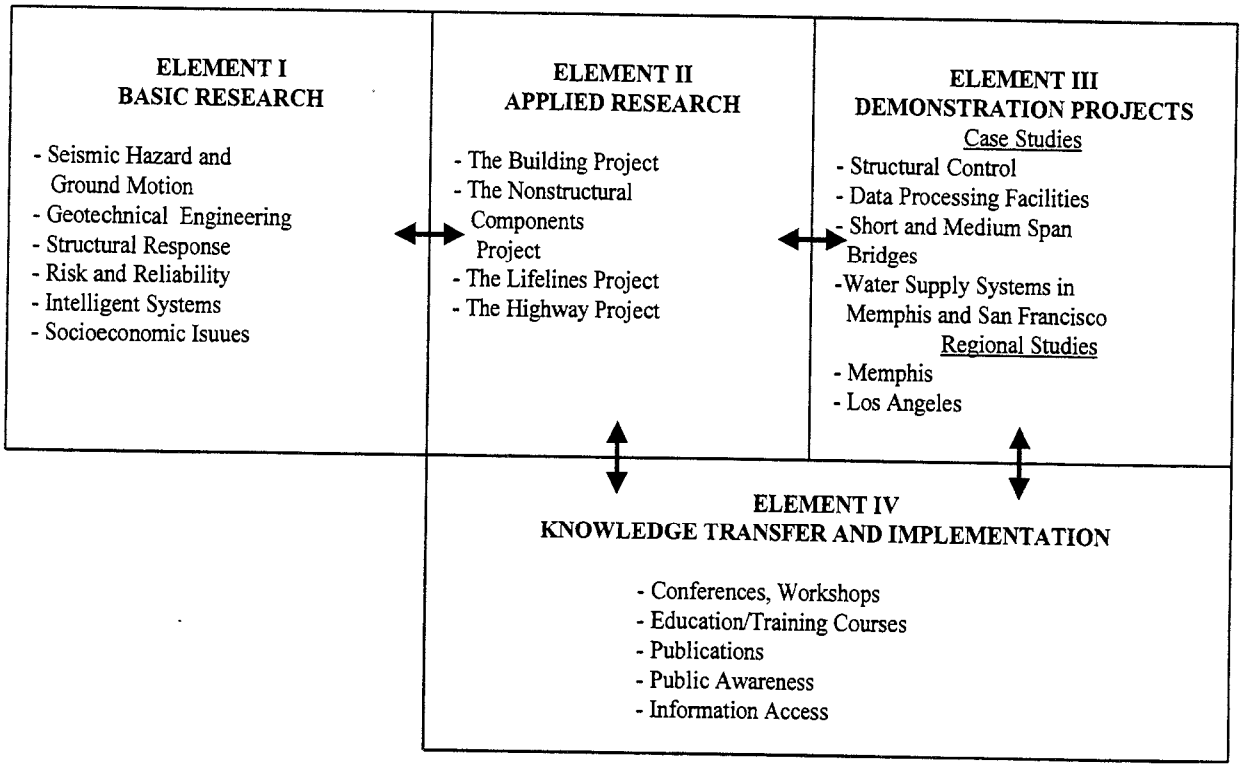

Figure 1. NCEER Research and Implementation Plan

engineering and other relevant engineering disciplines working with experts in utility management, socioeconomics, risk and reliability, urban planning and policy. Figure 2 relates the operational structure of the project.

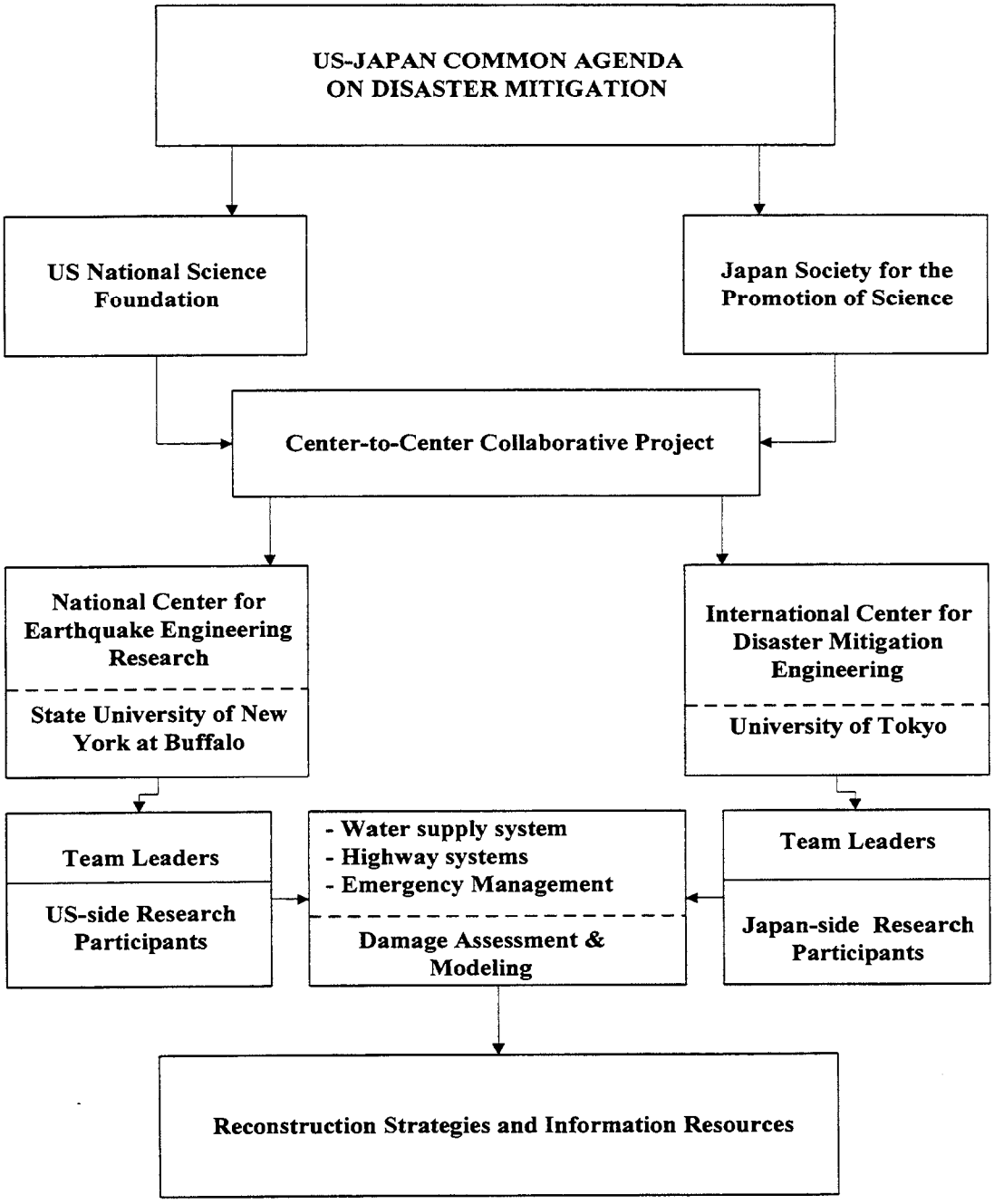

Figure 2. US-Japan Cooperative Research Process

The overall objectives of this project are to establish certain baseline data for post-disaster reconstruction, to define viable engineering, societal and financial strategies for recovery and reconstruction through shared information and experiences of the two recent major urban earthquakes. These strategies should serve to shorten the recovery period, improve the seismic resistance of the built environment and minimize cost. It is anticipated that results of this study

can reframe and improve the planning practices for global population centers to establish post-disaster reconstruction strategies.

BACKGROUND

Exactly one calendar year after the Northridge earthquake in California, the Kobe earthquake struck the city of Kobe in Japan, causing more than 5,000 deaths and a direct economic loss in excess of $120 billion. Both of these destructive earthquakes provide important learning opportunities to individuals concerned with earthquake hazard mitigation research and related implementation activities.

One striking feature of the recent earthquakes in California and Japan has been the impact of modern seismic codes on reducing the vulnerability in buildings constructed under these codes. These observations are evidence that sustained research efforts on earthquake hazard mitigation leading to the improvement of design codes and construction standards can certainly reduce the degree of loss and disruption from earthquakes to an urban center.

Since it is not possible to totally avoid loss and disruption due to the random nature of earthquakes, an important issue in earthquake hazard mitigation is post-event restoration and reconstruction. A major pressing need is to identify cost-effective strategies that both encourage recovery and mitigate against future damage. Studies of reconstruction suggest that during the rebuilding process, conflict exists between the need to "build back" and to "build better," between the need for rapid restoration and reconstruction and the need to further reduce future risks. One approach to address this conflict is to study reconstruction activities following recent major earthquakes in an effort to identify and document creative ways to establish a balance.

In general, knowledge of how such strategies were developed and used following the Kobe earthquake is particularly important for the US, given the significant potential that exists for catastrophic and near-catastrophic events in major urban areas. The US has not faced a comparable post-earthquake recovery challenge since the 1906 San Francisco event, and it is extremely important to identify repair, reconstruction, and recovery methods used after the Kobe event that have the potential for containing losses in future earthquakes. Similarly, following the Northridge earthquake, a number of innovative strategies were developed to facilitate recovery and mitigate future damage. Although different in magnitude and scope of impacts, the Kobe and Northridge earthquakes provide major opportunities for improving our mutual understanding about earthquake recovery processes.

For example, one of the effects that was prominent in both Northridge and Kobe is the severe damage sustained by utility and transportation systems, and the associated prolonged interruption of service. Lifeline systems have interactive interrelationships that can magnify damage and disruption of function. In Kobe, the inability of the transportation network to accommodate fire engines as a result of collapsed houses and buildings resulted in blocked access to burning buildings and cisterns. This difficulty continued in the early days following

the event, delaying not only repair and restoration but the ongoing search and rescue and other human-assistance efforts.

Individual utility lifelines suffered differing levels of damage and consequently different levels of service interruption. Water and gas systems developed considerable degrees of physical damage, with restoration further compounded by difficulties in location of damaged underground pipes.

Transportation systems are a special subset of lifeline systems and include highways, rail lines, airports and seaports. Recent earthquakes in California and Japan have again demonstrated that these systems can be extremely vulnerable to earthquake damage. Collapsed and partially-collapsed elevated structures have closed highway and rail lines for many months in both California and the Kobe region. As a consequence, access to affected regions has been seriously impeded with severe restrictions being placed on emergency response and the long-term business recovery of these regions. Expensive ground failures in the major sea ports of Oakland and Kobe have also lead to major disruptions in port traffic with uncertain long-term consequences for trade and commerce.

Trends in damage patterns to these systems confirm that older structures on soft sites are the most vulnerable. In general, newer systems sited on competent soils or engineered fills are considerable more resistant to earthquake ground motions. This is due to advances being made in the state-of-the-art and improvements being implemented in design codes and construction practices. The fact that the airports in both Japan and California sustained no serious damage during these recent events, is probably due to the fact that they were recently completed or extensively remodeled in recent years. By comparison the rail, highway and port facilities are much older (with some exceptions) in both countries and unless they have been seismically retrofitted, are at considerable risk.

In addition to socio-economic studies, improvements in structural performance are necessary for transportation systems. Like other lifelines, these systems are sensitive to soil conditions and variations in these conditions along their length. They may also be sensitive to spatial variation in the ground motion during an earthquake, particularly if supported on elevated sections that extend over many miles in length. These issues are not well understood and are examples of some of the engineering issues that must be addressed, in addition to the development of innovative repair and retrofit technologies.

Observations like these made in the aftermath of the Kobe earthquake are consistent with those for the Northridge event in a general sense, and therefore common lessons can be learned from both earthquakes. In the reconstruction of utility lifelines, judicious attention must be paid to the process of repair, restoration and retrofit as well as to the overall reconstruction of lifeline networks and systems from the viewpoint of city planning.

PARAMETERS AFFECTING POST-EARTHQUAKE ACTIONS

There are many interactive parameters which will influence post-earthquake actions. To simplify the matter, the project will focus on three sets of parameters: the engineering (physical infrastructure system) parameters, the cost and financial parameters, and the societal and policy parameters. For any normal reconstruction action of infrastructural systems, these three sets of parameters are simultaneously considered. However, their interactions will be different for post-earthquake actions. The examples of the engineering or physical infrastructure system to be reconstructed and some special issues may include:

Critical Facilities and Lifelines:

- Dams and reservoirs
- Fire stations and medical facilities
- Communication systems
- Transportation systems
- Water supply systems
- etc.

Reconstruction Issues

- Material choice
- Construction method
- Emerging technologies
- etc.

Examples of cost and financial issues include the cost of rebuilding versus repair, identification of sources of financing (e.g., public finance versus privatization versus international support), comparative cost analysis of pre-event strengthening versus post-event repair, economic models of restoration versus transformation, and analyses of amortization.

A range of societal and policy issues must also be considered. These can include: social attitudes toward restoration versus transformation; identification of desired urban patterns and levels of redevelopment; insurance modalities; access and egress routes; the role of open space; and actions which need to be taken to address abandoned areas. Local, state and federal policies play an influential role in the reconstruction process, as do public deliberations and effectiveness of communication between government and the public-at-large. Throughout the process, consideration must also be given to actions which should be taken to further reduce future disaster losses.

The actions to be taken to reconstruct the infrastructure system must follow a planned sequence based on the urgency and the priority established before the event. For convenience of discussion, we consider the following three groups of action items.

Emergency Response

- Medical care
- Search and rescue
- Evacuation
- Shelter
- Traffic control
- etc.

Urgent Restorations

- Essential facilities
- Critical lifelines (water, power, etc.)
- Housing and feeding
- Banking Systems
- etc.

Other Restorations and Recovery

- Production of public goods and services
- Institutional processes
- Application of new knowledge and technologies
- etc.

Each of the above actions has different characteristics. Strictly speaking, emergency responses are distinct from reconstruction activities. Urgent restorations, on the other hand, are reconstruction activities which give emphasis to rapid restoration of the essential functions of the community. Other restoration, however, may emphasize the accomplishment of certain long-term urban planning objectives. That is, "transformation issues."

It is understandable that each earthquake is unique and that the fragility of each community to earthquake ground motions is different. Thus, every earthquake will leave a distinct signature on the infrastructure system and the social environment of the community. Planning for the affected region must begin immediately after the earthquake (a fast track planning process) to monitor and guide the reconstruction activities. To have a set of reconstruction strategies developed prior to the event cannot eliminate post-event planning, but can greatly enhance the latter process, particularly impacting the long-term reconstruction projects.

THE CENTER-TO-CENTER PROJECT: A THREE-YEAR AGENDA (1995-1998)

Overall Objectives

The initial phase of the Center-to-Center project is three years. Expected activities during this three-year period are as follows. During year one, mutual understanding of the operations and emphases between the two centers is developed and targeted cooperative aspects of the collaborative project are established. Collection of data and technical information of the Northridge and Kobe earthquakes relevant to the focused aspects of study is initiated.

In year two, Japan- and US-side researchers continue to establish the database and share technical information. Where feasible, selected comparative studies will be carried out by small groups of investigators. US and Japanese information dissemination mechanisms will be cooperatively enhanced.

In year three, a multi-disciplinary team among US and Japanese experts will work to formulate "straw-man" post-disaster reconstruction strategies for optimal recovery. The straw-man will be made available to a wider group of scholars and practitioners for their comments and suggestions, which will be the basis for possible phase II actions of the Center-to-Center project.

Progress-to-Date

During the first year of the project (Fall 1995 - Fall 1996), key individuals from both centers met twice and a special workshop was held to identify key areas of study and the approaches for each center to pursue in a coordinated fashion.

Three important components of post earthquake activities were identified. They are: (1) repair, restoration and recovery of transportation systems; (2) repair, restoration and recovery of water systems; and (3) emergency communications and management. These focal areas and their critical elements are identified in Figure 3. Ability to assess damage conditions immediately after the earthquake is considered to be an important issue in all three systems under consideration.

The Japan-side has adopted the following approach for coordinating its activities. All researchers who are sponsored to conduct post-Kobe earthquake studies in these three areas are asked to (1) attend workshops co-sponsored by INCEDE, during the three year period; (2) present their research findings and discuss lessons learned with US researchers and (3) develop a two-page abstract summarizing key lessons learned. Researchers will also be encouraged to submit longer supporting documents detailing research findings. Near the end of the three year project period, INCEDE will compile the 2-page abstracts as a source book volume for post-Kobe earthquake reconstruction strategies.

NCEER-INCEDE Research Focuses	
Water Supply Systems • Social and economic impact of water supply distribution - service and business interruption - fire suppression capacity - public health effects • Application of advanced technologies for monitoring, control and damage detection • Development of measures and criteria for post-earthquake performance of lifeline and utility systems	
Highway Systems • Enhance existing databases (ground motion, structural performance, traffic impact, direct and indirect costs, etc.) for highway structures and systems • Develop experience-based systems analysis for loss estimation modeling and loss assessment, essential for developing reconstruction plans and strategies • Application of knowledge	**Emergency Management Issues** • Mutual learning about emergency management systems with emphasis given to intergovernmental emergency communication and coordination (Northridge and Kobe earthquakes) • Emergency responses of lifeline organizations and agencies in the Northridge and Kobe earthquakes
Damage Assessment and Modeling • Real-time assessment of large ground deformation after earthquakes (aerial photos, GPS, satellite reconnaissance) • Cost-effective methods for identifying non-exposed damage (i.e., underground pipeline systems) • Real-time damage/loss estimation modeling for emergency response/emergency management	

Figure 3. NCEER-INCEDE Research Focuses

NCEER has similarly asked prominent US researchers working on post-Northridge earthquake projects involving transportation, water and emergency management systems to attend US-Japan workshops to exchange views and information with their Japanese counterparts. NCEER will also request contributions from the US researchers summarizing findings and lessons learned from research in the three main areas of focus. The final form of these contributions has yet to be determined, but will defined and guided by the US-side project leaders (Figure 4).

George C. Lee University at Buffalo	Responsible for analyzing and synthesizing research and lessons learned on damage assessment, repair, and reconstruction of transportation facilities
M. Shinozuka University of Southern California	Responsible for analyzing and synthesizing research and lessons learned on damage assessment, repair, and reconstruction of water systems
Kathleen Tierney University of Delaware	Responsible for analyzing and synthesizing research and lessons learned on emergency management and reconstruction systems

Figure 4. US Research Team Leaders

RESEARCH PLAN - YEARS TWO AND THREE

During years two and three, NCEER project leaders have outlined the following specific tasks.

Task 1: Document the experiences of organizations and agencies responsible for the restoration and reconstruction of transportation and water systems after the Northridge and Kobe earthquakes.

The US coordinating team will review available documents and reports and visit state and local government organizations responsible for pre-earthquake planning and post-earthquake reconstruction for transportation systems and water delivery systems in the areas affected by the Northridge and Kobe events. The objective of this review will be to develop detailed information on how these organizations coordinated interagency repair, restoration, and recovery (including identification of mitigation goals for future preparedness efforts) and to document both positive and negative experiences. The plan is to involve one or more graduate students in field work in greater Los Angeles and the area affected by the Kobe earthquake.

In this phase of the project, we will obtain information on the following topics: (1) mitigation and reconstruction plans that existed prior to the two earthquake events, and the extent to which these plans were implemented following those events; (2) how decisions were made for restoration and reconstruction, including the procedures and processes that were used and the kinds of information that served as the basis for those decisions; (3) strategies for financing reconstruction; (4) the extent to which the mitigation of future earthquake damage was a consideration in the decisions that were made with respect to restoration and reconstruction; and (5) the factors that influenced post-disaster decisionmaking and the progress of reconstruction, including concern with economic, fiscal, and social impacts and infrastructure systems performance, future seismic safety concerns, and judgments about acceptable risk. Based on this information, we hope to draft a framework for optimal post-earthquake reconstruction strategies for transportation and water delivery systems.

This information will be obtained through interviews, site visits, and focus groups involving key decisionmakers as well as through analyzing pertinent documentary material such as after-action reports, progress reports, and documents prepared by other researchers. Specific results and recommendations will be requested.

Organization officials and researchers will be asked to provide feedback on the draft document, with special attention given to comparing the reconstruction strategies and actions with their research findings and experiences.

Pre-event planning is necessary for response, recovery and reconstruction. The planning process allows communities to have a fundamental understanding of potential earthquake risk and the level of resources available for post-event restoration of physical, social and economic systems. However, it is likely that results of research task 1 will reveal that reconstruction strategies cannot be formulated in general terms because they are very much dependent on local conditions and physical variables. Such conditions include the characteristics of the built environment, geological and soil conditions, the magnitude of the earthquake hazard, and social, economic and political factors. We will therefore undertake a second research task described below, which will constitute a major focus over the next two years.

Task 2: Assess ways of improving governmental and organizational capacity for managing post-disaster response, restoration, and early recovery.

When a major earthquake strikes, the ability to protect lives and property and to begin restoration efforts depends crucially on the performance of emergency communications and emergency management systems; critical systems and facilities must be able to survive and remain functional following a major earthquake or other disaster. Additionally, emergency procedures must be well-designed and well-understood by personnel who have emergency responsibilities, and plans must be implemented properly when the disaster occurs. Since not even the most well-formulated and detailed disaster plan addresses the range of situations emergency managers are likely to face, decisionmakers must also remain flexible and responsive to actual disaster conditions.

One major and perhaps overriding requirement in the post-impact period is the need for adequate information on the location and severity of damage and on what disaster-generated problems and which areas of the impact region require urgent attention and resources. An effective response is thus dependent on the ability to rapidly gather and process accurate information and to make decisions based on that information. Intergovernmental and interorganizational coordination (for example, among the different levels of government and between lifeline organizations and government emergency response agencies) is also critical during the emergency response and initial restoration/recovery periods. Again, this coordination cannot take place without adequate emergency communications capability, comprehensive pre-event planning, and effective implementation of response procedures.

New communications and data-management technologies offer great promise for improving emergency response capability following earthquakes and other disasters. Some of these technologies, such as GIS, were used in some response-related tasks following the Northridge earthquake, and an important element in our research plan will be to explore how technology can be used to enhance emergency operations.

Studies on emergency communications, response, and management issues have been undertaken on both the US and Japanese sides following the Northridge and Kobe events, and both countries stand to learn a great deal from such studies. For example, since the Kobe earthquake, researchers on the Japanese side have become more interested in gaining a detailed understanding of the structure and functioning of emergency operations systems in the US. On the US side, there is recognition that much can be gained from understanding the kinds of emergency response problems that are likely to develop following catastrophic and near-catastrophic earthquakes like the Kobe event, which was far more serious than any disaster experienced by the US in recent times. The current US emergency management system has not been tested by a major disaster like the Kobe earthquake (Northridge and even Hurricane Andrew were much less serious disasters), and it is important to document the lessons learned from the response to that disaster that are transferable to the US setting.

The information required in this task area will be collected in ways similar to those described for Task 1 – that is, through analyzing existing documentary material and research findings and through contacts with knowledgeable emergency management practitioners and researchers.

Task 3: Develop a model reconstruction system that is both robust and resilient.

In conventional planning for post-disaster reconstruction, planners typically collect information on the region's population and existing structures, trying to anticipate patterns of earthquake damage, suggest preemptive investments or regulations to mitigate damage, and suggest likely priorities for reconstruction. Extensive research has been done on sample cities' housing and infrastructure stock in order to try to predict earthquake damage, in the search for the ability to set reconstruction priorities before the event. The general assumption is that analytical and technical methods can be used to design an "optimal" solution in the face of uncertainties.

Though some aspects of the conventional approach have merit, such an approach is limited by the unpredictability and variability of earthquake disasters. Moreover, the social and political circumstances that develop after the emergency may pre-empt the effectiveness of pre-disaster plans for reconstruction. Studies on disaster response indicate that no amount of pre-planning can adequately prepare communities for all the issues they will face following a major disaster. Overall, rigid attempts to rationally optimize reconstruction prior to an event are likely to flounder, for the following reasons:

- Even in the rare cases where pre-event impact scenarios and post-event reconstruction plans do exist, earthquakes invariably produce unexpected and unanticipated consequences. Major seismic events can occur in places where they were not expected, as happened with the Great Kobe disaster, and in general it is difficult to pre-identify accurately which areas of a community's populations, elements of the infrastructure system, and sectors of the economy will be hardest hit. When a major earthquake strikes, those in charge of managing response, restoration, and recovery efforts must be flexible and able to respond to actual needs and demands, rather than following preconceived procedures that may prove irrelevant to the actual situation. Since the real situations decisionmakers face are typically quite different from the hypothetical ones on which their plans were based, a highly pliable approach is needed.

- Once the immediate emergency period has passed, decisions regarding recovery begin once again to be driven by political, economic, fiscal, and social considerations – considerations that again cannot be anticipated or quantified beforehand. Some proposed measures, such as projections for changes in land use planning goals typically engender political conflict. Strategies for decisionmaking, accommodating the legitimate concerns represented by diverse interest groups, and the resolution of conflicts will vary, depending on the community and societal setting. Once again, the emphasis must be placed on the capacity for taking these factors into account during the recovery process.

- Private-sector reconstruction decisions will be influenced by the availability of insurance, private credit, and government assistance. In light of the area's new disaster outlook after the earthquake, households, organizations, and firms will have to make decisions on where and how to reconstruct. Since economic conditions have the potential for shifting after an earthquake (industries that sustained the most damage may decide not to reconstruct locally or, as happened in Kobe because of damage to the port, communities may lose major revenue sources), decisions on reconstructing public infrastructure systems will have to be robust and responsive to changing economic conditions.

- Reconstruction decisions will evolve and change in the months and years after the disaster. As the new conditions are better understood, households and firms will reconsider their own decisions, and political forces and funding decisions will shift. Plans that assume static choices among priorities at one time period are likely to be misleading. Once again, the planning emphasis must be on building institutional capacity for robust response to evolving conditions.

- To be effective, reconstruction efforts must be prioritized and phased into a comprehensive planning effort. It is important to recognize that everything cannot be done all at once and that recovery, particularly from large events, will take time. The goal should be to shorten that time to the greatest extent possible, without compromising other important goals.

For the above reasons, we should examine an alternative approach in earthquake reconstruction planning: the development of institutional arrangements, information sources, decision making processes, and technological systems that support a systematic, intelligent approach to response and recovery. The proper design of such systems will require considerable research. The systems to be designed will likely be comprised of the following features:

- Pre-disaster preparation of geographic information systems and computer-aided visualization systems for spatial inventory of essential public facilities like hospitals, housing, roads and bridges, dams, underground infrastructure, potentially hazardous sites such as chemical storage facilities and gas tanks, etc. This base information must be maintained and continuously updated. (Since the data has many planning and public service uses even in the absence of a disaster, costs can be shared with other users.) Interactive access to the data following the disaster must be assured, which means systems must be resistant to damage and disruption. The purpose is to assure that post-earthquake conditions can be rapidly entered into the system to locate problem areas and speed up the rate at which reconstruction decisions can be made. Back up systems, including hard copy output of the most important information, should be available and regularly updated, in case of equipment malfunction during the disaster.

- A Formally-Designated Recovery Decision-Making body. Because reconstruction is a complex and multifaceted process, it is likely that coordinated reconstruction and recovery planning can be facilitated if a steering group is identified and given formal authority prior to the occurrence of a major earthquake. This approach to managing recovery has already been implemented in a limited basis in the US. Prior to the Northridge earthquake, the City of Los Angeles had formally adopted a recovery and reconstruction plan that outlined and assigned responsibility for a range of recovery-related tasks, and this plan was put into effect following the earthquake. NCEER research will (1) explore how the recovery plan was used following the Northridge event, including which areas of recovery were emphasized; (2) document lessons learned; (3) identify aspects of the recovery planning process that are transferable to other communities; and (4) suggest how recovery planning can be improved.

The robust reconstruction system described above depends heavily on computing and telecommunications technologies, and on the training and preparation of emergency service agents and task force members. Research is needed on the development of such robust systems. Research activities will include:

- Investigation and documentation of the reconstruction activities at Northridge, Kobe, and other places that have suffered earthquake damage. Should include investigation of the procedures and processes used in reconstruction decision making (Task 1).

- Investigation of the varying mechanisms, in both the US and Japan, which can be used to designate and train volunteers for post-disaster information collection.

- Comprehensive assessment of current options in computing and communications technologies, including issues of reliability, back-up, accuracy, protocols, formats, convenience and user-friendliness, cost, and usability for alternative purposes in non-emergencies.

While the outlined research agenda is recognized as an ambitious one for the remaining two year period of the project, the objectives proposed are important to the future development of improved post-disaster reconstruction strategies and it is our intention to move on as far as possible in the direction proposed. Progress will be monitored and feasibility of project objectives re-assessed after year two of the project.

REFERENCES

Benuska, L. (Ed.), "Loma Prieta Earthquake Reconnaissance Report," Earthquake Spectra, J. Earthquake Engineering Research Institute, Supplement to Volume 6, 1990, 448 pp.

Buckle, I.G. (Ed.), "The Northridge, California Earthquake of January 17, 1994: Performance of Highway Bridges," National Center for Earthquake Engineering Research Technical Report 94-0008, Buffalo, 1994.

Comartin, C.D., Greene, M. and Tubbesing, S.K. (Eds.), "The Hyogo-Ken Nanbu Earthquake, January 17, 1995: Preliminary Reconnaissance Report," Earthquake Engineering Research Institute Report 95-04, Oakland, 1995, 116 pp.

Goltz, J.D. (Ed.), "The Northridge, California Earthquake of January 17, 1994: General Reconnaissance Report," National Center for Earthquake Engineering Research Technical Report 94-0005, Buffalo, 1994.

Hall, J.F. (Ed.), "Northridge Earthquake, January 17, 1994 - Preliminary Reconnaissance Report," Earthquake Engineering Research Institute Report 94-01, Oakland, 1994, 114 pp.

---, "The Hanshin-Awaji, Japan Earthquake of January 17, 1995: Performance of Highway Bridges," National Center for Earthquake Engineering Research Technical Report, Buffalo, 1995, forthcoming.

---, "The Hanshin-Awaji, Japan Earthquake of January 17, 1995: Performance of Lifelines," National Center for Earthquake Engineering Research Technical Report 95-0015, Buffalo, 1995.

Todd, D., Carino, N. Chung, R.M., Lew, H.S., Taylor, A.W., Walton, W.D., Cooper, J.D. and Nimis, R., "1994 Northridge Earthquake - Performance of Structures, Lifelines, and Fire Protection Systems," National Institute of Standards and Technology Special Publication 862, Gaithersburg, 1994, 181 pp.

Center-to-Center (INCEDE-NCEER) Cooperative Research and US-Japan Common Agenda on Earthquake Related Issues and the Role of INCEDE towards Goals of IDNDR

Ken Sudo
International Center for Disaster-Mitigation Engineering
Institute of Industrial Science
The University of Tokyo

Tsuneo Katayama
National Research Institute for Earth Science and
Disaster Prevention
Science and Technology Agency

Kimiro Meguro
International Center for Disaster-Mitigation Engineering
Institute of Industrial Science
The University of Tokyo

Anura Srikantha Herath
International Center for Disaster-Mitigation Engineering
Institute of Industrial Science
The University of Tokyo

Dushamante Dutta
International Center for Disaster-Mitigation Engineering
Institute of Industrial Science
The University of Tokyo

ABSTRACT

This paper mentions the following topics: (1) the background and objectives of a Center-to Center cooperative project on post-urban earthquake reconstruction strategies which has been implementing jointly by the International Center for Disaster-Mitigation Engineering (INCEDE, Japan) and the National Center for Earthquake Engineering Research (NCEER, USA) ; (2) activities undertaken by INCEDE for accomplishing the objectives, organizing a research team consisting of 49 researchers from 17 research institutes of 7 universities in Japan who cover a diversity of research fields of earthquake disaster mitigation such as earthquake engineering, structural engineering, urban planning, disaster economics, medical relief, socio-economy and many others; and (3) a leading role of INCEDE in promoting IDNDR related activities in Japan.

Background and Objectives

The Northridge and Kobe earthquakes caused extreme damage to a variety of structures and system in Los Angeles and Kobe and surrounding areas. There is an urgent need for research to understand the major causes of damage and to develop methodologies to respond to problems

encountered in the recovery efforts as well as to prepare for a similar earthquake in a large urban area in the future. To learn from the experience and to identify strategies for recovery, a Center to Center Research Project under the name `Post-earthquake reconstruction strategies' was sponsored by National Science Foundation (NFS), USA and Japan society for the Promotion of Science (JSPS), Japan, was initiated.

There is an agreement between Both the Government of Japan and USA behind the project. Emphasis was given to Earthquake Disaster Mitigation Partnerships in the Joint communique issued after the Sixth US -Japan Joint High Level Committee Meeting on Science and Technology, May 2, 1996, Washington DC: "... Both sides expressed their support of a new Earthquake Disaster Mitigation Partnership through which cooperation in science and technology will enhance our ability to reduce the damage to communities caused by earthquakes. The priority themes for cooperation include quantifying the potential of future earthquakes: strengthening our ability to estimate losses; testing basic theories of the earthquake source; understanding near source motions; geological effects and structural response; reducing the seismic risks posed by steel buildings; strengthening evaluation and retrofit of existing buildings and infrastructure; developing performance-based design methods; improving real-time seismic information systems; and better controlling post-earthquake fires. Both sides also concurred that the enhancement of systems for natural disaster reduction such as the Pan Pacific Disaster Watch Network should be promoted. With regard to the International Arctic Research Center, both sides agreed to discuss the concrete concepts of cooperation. ..."

This study aims to develop post-earthquake reconstruction studies in a highly urbanized area from an engineering and social economic viewpoint based on the damage caused by the Northridge, California Earthquake of January 17, 1994, and the Hanshin-Awaji, Japan, Earthquake of January 17. 1995.

The objectives of the project are:

(1) To carry out a comprehensive comparative study of recent earthquake experiences in Northridge (USA) and Hanshin (Japan) in order to identify generic issues for post-disaster reconstruction;

(2) To conduct case studies and to identify exemplary technical, societal and financial strategies for the retrofitting and post-earthquake repair and restoration of the built environment in an optimal fashion;

(3) To carry out individual disciplinary-oriented research to fill knowledge gaps and simultaneously, to formulate one or more strategies for recovery using a system-integrated team approach involving multi-disciplinary experts;

(4) To exchange visiting researchers and students and to share experiences to enhance the spirit and substance of International Decade for Natural Disaster Reduction (IDNDR);

(5) To encourage and facilitate additional cooperative research efforts among earthquake engineers in Japan and US and to establish further joint efforts with other centers/research groups in both countries; and

(6) The results of this comprehensive effort will be documented in a series of technical reports for dissemination. Furthermore, it will provide an effective countermeasure for the recovery due to an earthquake which can strike not only Japan or USA but, any urbanized area in the world in the future.

Activities and Progress

The specific activities planned for the three years are:

(1) To obtain the latest and accurate information on the Northridge Earthquake in the US and the Hanshin Earthquake in Japan and exchange them. Then, carry out the first Center-to-Center coordination meeting in Japan, to decide on specific emphases and approaches, and to identify gaps

in the knowledge based in the chosen emphasis areas. Identify researchers and /or teams to carry out the studies;

(2) To perform case studies. Comparative studies, and disciplinary-based studies were needed. Multi-disciplinary team efforts will also begin in parallel to coordinate the disciplinary research efforts;

(3) To identify post-reconstruction strategies based on system-integrated consideration of above activities. Develop a draft document; and

(4) To seek comments and input on the draft document from a wider group of international experts, users and government officials, and revise the document for distribution.

In order to undertake these activities, both the INCEDE and NCEER held the first Coordination meeting in February 1996, titled as Japan-United States International Cooperation for Post-Earthquake Reconstruction Strategies. Issues identified in the workshop were compiled in resolution made in this meeting as follows:

(1) Group A: Water Systems, Power and Gas

1. Socio-economic impacts of water service disruption. Data collection and development of methods for identification/quantification of social and economic impacts of water service disruption. Apply to Northridge and Kobe. Disruption refers to loss of (1) portable water supply, and (2) fire water supply. Impacts are nuisance value, economic effects and public health effects.

2. Develop advanced technologies for monitoring, control, and damage detecting in water systems. Describe the new monitoring and control system proposed for the Kobe Water System. Identify and develop other approaches that may be applicable for water and gas systems. Identify and develop methods for rapid leak detecting of pipeline leaks following earthquake.

3. Develop performance measures and criteria for post-earthquake performance of lifeline, utility systems. Consider both engineering and socio-economic issues. Levels of performance should correspond to probability of earthquake occurrence. Performance measures may include systems functionality, or other system reliability guarantees.

4. Guidelines/Manual for alternative water supplies for post-earthquake use. Primary emphasis on alternative potable water supply sources, treatment and conveyance. Documentation of Kobe/Northridge experience. Compilation of practice /advanced technologies and development of decision process (flow .. etc.) guidelines, for use by local officials.

5. Develop standardized, publicly accessible database of water systems, and systems component performance. The initial focus should be on the Kobe and Northridge earthquakes, with a format allocating additional data sets in the future. Types of data may include field we may limited to:

* system performance
* geotechnical hazards
* ground motions
* component inventory
* component damage

Group B: Transportation

1. Enhance performance databases for highway structures and networks. The performance of structures and highway networks need to be carefully and completely documented in a scientifically consistent manner. Information to be collected and verified includes, ground motion, structural performance, traffic impacts, repair methods, direct and indirect costs. Both damaged and undamaged structures and networks in the affected region should be documented. The assembled database should be archived with a retrieval system and made available through the Internet and other electronic media to researchers and practitioners.

2. Develop improved loss models and reconstruction strategies for highway systems. Loss estimation and loss assessment models have been developed for Tokyo (by INCEDE) and Memphis (by NCEER). These models should be compared and improved as appropriate. Data collected in (1) above may also be used to improve these models. Cost benefit studies of various retrofit strategies

may be undertaken particularly if fragility functions for retrofitted structures and systems are developed. Traffic management experiences in Northridge and Kobe earthquakes should be compared and correlation with estimates from the above loss models attempted. Similarly, this economic impact of damage to the highways during Northridge and Kobe earthquakes should be compared and where possible used to calibrate the loss models. Other strategies to be explored include the development of resilient traffic monitoring sensors for real time assessment of earthquake impacts particularly in intelligent transportation systems currently under development in both countries.

Group C: Communications

1. Emergency management. a) U.S. emergency management system: Organization and operation. Japanese team visits U.S. for extended period to study and report on the intergovernmental emergency management system, including both plans and capabilities and actual performance in disaster situations. b) Emergency communication and coordination in the Kobe earthquake. U.S. researcher to collect data and write case study on intergovernmental communication and coordination in the emergency response period following the Kobe earthquake.

2. Emergency response of lifeline organizations in the Northridge and Kobe earthquakes. Using a common methodological strategy, U.S. researchers focusing on Northridge, and Japanese researchers, focusing on Kobe, will collect and compile data and write case studies on communication and coordination among major lifeline organizations (water, gas, electricity, transportation) during the emergency response and early recovery periods. Key issues include (1) extent to which lifeline organizations coordinated among themselves to reduce impacts and promote recovery; and (2) extent to which lifeline organizations were integrated into broader response and recovery activities undertaken by other organizations.

Group D: Damage Assessment

1. Real-time development of ground motion information.
2. Real-time assessment of large ground deformation after earthquake.
- Aerial photos
- GPS
- Satellite data
3. Real-time development of damage estimation model of facilities.
4. Real-time loss estimation for disaster management.
5. GIS-based decision support systems for effective disaster recovery.
6. Rapid screening and upgrading procedures for seismically vulnerable structures (e.g. underground pipelines, buildings) to ensure life safety performance , as a minimum.
7. Cost-effective methods for identifying non-exposed damage, e.g. buried foundations, steel connections, in ground structures like buried pipes.

Following up the identification of research issues, the INCEDE has organized a multi-disciplinary team consisting of 49 researchers from 17 research institutes. So that the following research fields are covered: epidemiology; infrastructure engineering; transportation; water supply; economics; humanitarian sociology; structural engineering; architectural engineering; earthquake ground motion; earthquake engineering; urban disaster engineering; GIS and MRS engineering; artificial intelligence; and urban planning.

The team met on 2 August, 1996 to discuss implementation strategy of this project with the following agenda:

- Brief explanation of activities up to the present
- Outline of the project implementation strategy
- General Discussion on the implementation
- Group discussion on individual research topics and the activity for the current year

- Report of the group plans and general discussion

It was decided that the team be divided into several groups in terms of research fields such as water and lifelines, transportation, communication, and realtime damage assessment.

The meeting recognized that compiling the digital information available on Northridge and Kobe earthquakes, being carried out at present as the first step in information gathering, would be an important contribution to the future generations. The use of WWW for the compilation, categorization and presentation of not only the materials being collected as part of the present research effort, but also the information available throughout WWW, would be continued with the support of all participating members.

Plans for the first year were decided as follows in this meeting:

(1) Water and lifelines

The water and lifelines group has decided to organize a domestic level group meeting on August 27 to finalize the outline of work and to discuss it in detail. However, the group gave emphasis to the importance of cooperative research between Japanese and US researchers. As a result, a workshop will be organized between Japanese and US researchers in USA in mid October, 1996.

(2) Transportation

The transportation group has planned to expand their research activities from the initially decided activities such as emergency traffic management/control system to hardware issues such as performance of bridges, traffic facilities, inspection and retrofitting of seismic resistivity of existing structures and demolishing etc. To cope up with the new dimension of work, the transportation group may be divided into two sub groups in near future. The group is planning to arrange a workshop in USA in March 1997 to discuss and exchange ideas and views between Japanese and US researchers involved in the group work.

(3) Communications

The communication group will be focusing on two areas. One is on the information gathering and dissemination related to earthquake experiences and the other is on the emergency communications. On the emergency communication, a trip will be made around middle of October 1996 to USA by a team of Japanese researchers. The main objective of the visit is to study emergency management practice in USA, especially the role of FEMA and related organizations. A second visit may be scheduled for late January 1997, coinciding with the US-JAPAN bi-lateral meeting on Urban Earthquake Disasters.

(4) Real Time Damage Assessment

The damage assessment group had joint discussions with the communication group during this meeting and has decided to continue their work jointly with the communication group. The group will be focusing mainly on the following issues; inspection of damaged structure and real time damage assessment system. The group will study the existing real time damage assessment systems in Japan such as SIGNALS of Tokyo Gas, UrEDAS and HERAS of Japan Railway, Kawasaki System of Kawasaki City, K-net of NIED, etc. and it will be compared with the existing systems in USA. The other group activities such as gathering of information, workshop with US counterparts and other related work will be carried out together with the communication group.

The meeting discussed about outcomes which the Project will have produced. The final product of the project is expected to consist of two parts. The first part would be individual in depth research on specific topics related to reconstruction strategies and would consist of journal paper type publications. The second product is envisaged as a book compiling best practice and lessons from the two earthquakes. Each item of the compilation would consist of not more than two pages. It would contain briefly the phenomena, figures and photographs describing the phenomena, and references for further reading. Each participant is urged to contribute around 15 such samples which would be

made available through WWW for discussion and refinement.

Dissemination of Outcomes to be Produced

The final product of the project will consist of two parts. The first part would be individual in depth research on specific topics related to reconstruction strategies and would consist of journal paper type publications. The second product is envisaged as a book compiling best practice and lessons from the two earthquakes. Each item of the compilation would consist of not more than two pages. It would contain briefly the phenomena, figures and photographs describing the phenomena, and references for further reading.

The source-book which this project will produce must be very much helpful to practitioners engaged in disaster management in local communities. There should be a mechanism which could make the source-book available to whoever needs. International communities for natural disaster reduction should take upon it. In this context, International Decade for Natural Disaster Reduction (IDNDR) could provide such machinery.

United Nations General Assembly proclaimed the International Decade for the Natural Disaster Reduction (IDNDR), beginning 1 January 1990, on its 44the session in December 1989. Goals of the Decade were identified as follows:

(1) To improve the capacity of each country to mitigate the effects of natural disasters expeditiously and effectively, paying special attention to assisting developing countries in the establishment, when needed, of early warning systems;

(2) To devise appropriate guidelines taking into account the cultural and economic diversity aiming nations;

(3) To foster scientific and engineering endeavors aimed at closing critical gaps in knowledge in order to reduce loss of life and property;

(4) To disseminate exiting and new information related to measures for the assessment, prediction, prevention and mitigation of natural disasters; and

(5) To develop measures for the assessment, prediction, prevention, and mitigation of natural disasters through programs of technical assistance and technology transfer, demonstration projects, and education and training, tailored to specific hazards and locations, and to evaluate the effectiveness of these programs.

All the five goals quote crucial role of science and technologies which deal with natural disasters and reduction of adverse effects from them. Indeed such scientific communities in the world as ICSU and IAEE took opportunities to enhance activities in the fields of natural disaster reduction, in developing new technologies, in disseminating technologies and knowledge through education and training, and in increasing policy maker's awareness about disaster, during the Decade.

In the Decade, the international community should have paid special attention to fostering international co-operation in the field of natural disaster reduction. However, actually it has undergone differently. Being closer to the end of the Decade, the United Nations has begun to discuss how the Decade should be closed. Scientific communities should urge the United Nations to bring together all outcomes from efforts by the communities, and people involved in disaster reduction from local level to policymaking level so that Decade outcomes could get visible to the world.

Both INCEDE and NCEER are requested to play leading roles in enhancing Decade related activities. Dissemination of the source-book and other products by the project to the world could be such activity.

Session 1
Ground Motion and Soils

Session Co-chairs: Andrea Dargush and Tsuneo Katayama

Seismological Aspects of the Hyougo-ken Nambu Earthquake, the Kobe Earthquake, of 17 January 1995
Ken Sudo and Kimiro Meguro

Future Directions in a National Portrayal of Seismic Hazard for Highway and Bridge Design
Maurice S. Power

Long Period Ground Motion due to the 1995 Hyogo-ken Nanbu, Japan Earthquake
Tatsuo Ohmachi, Shun'ichi Kataoka and Shojiro Kataoka

Site Liquefaction and Remediation
Mourad Zeghal, Korhan Adalier and Ahmed-W. Elgamal

Ground Displacement and Strain Caused by Soil Liquefaction During the 1995 Hyogoken-Nanbu Earthquake
Masanori Hamada and Kazue Wakamatsu

Reduction of Liquefaction Hazards by Deep Soil Mixing
Thomas D. O'Rourke and Siang H. Goh

SEISMOLOGICAL ASPECTS OF THE HYOUGO-KEN NAMBU EARTHQUAKE, THE KOBE EARTHQUAKE, OF 17 JANUARY 1995

Ken Sudo
International Center for Disaster-Mitigation Engineering
Institute of Industrial Science
The University of Tokyo

Kimiro Meguro
International Center for Disaster-Mitigation Engineering
Institute of Industrial Science
The University of Tokyo

ABSTRACT

The Kobe Earthquake of 17 January 1995 is mentioned in terms of seismological aspects: the focal process; geologic and tectonic settings; the background seismicity; and action by the Japanese Government.

FOCAL PROCESS

The Earthquake with the magintude 7.2 occurred at 5.46 hours (Japanese local time) right before dawn on 17 January 1995. The hypocenter was located at 135.05E, 34.60N, and 14km depths beneath the sea bottom of the Akashi-strait. The aftershocks were aligned in the NE-SW direction on the both sides of the epicenter, stretching almost 40 km lengths. The fault plane solution determined by analyses of seismic waves shows: (1) the earthquake was caused by the E-W compressional stress; and (2) the earthquake should have formed a right-lateral slip, although the rupture could not be seen clearly on the NE side of the hypocenter where the Kobe city is situated. It was very much consistent with the aftershock distribution.

Rupture processes which have been studied extensively by many researchers are almost consistent with each other: (1) the analyses of far field seismograms, seismograms at very distant seismic observatories, enables to estimate the size of the fault plane 40x20 km, the slip 2.1 m and the stress drop 10-20MPa. The duration time in which rock failure process lasted would be almost 11 sec; and (2) The near field seismogram analyses provided more detailed structure of the fault as well as its rupture process on the fault. However both the analyses do not seem to be able to generate such strong ground motion as having caused the devastating disaster.

There is a debate whether a precursory slip existed or was observed right before the outbreak of the earthquake. The precursory slip is observed in rock-failure experiment which is made to simulate earthquake occurrence. In order to find the slip, very much precise observation has focused on the first 10-100msec at the beginning of the seismic wave onset for earthquakes. So far any clear signal has neo been seen.

GEOLOGIC AND TECTONIC SETTINGS

Since the beginning of the 1980s' geological faults had been investigated in terms of their potential activities by trenching and excavating the respective fault sites. Dating of the soil surrounding the fault traces and offsets measurement provide us with their activities over a couple of thousands years past. This survey had identified the Nojima fault which caused this devastating earthquake as a fault potential to a large earthquake. There were a couple of faults which were similarly identified to be potential in the Kobe area. One of them was a fault running E-W direction close to the Kobe city, Arima-Takatsuki Fault. The Excavation of this fault has revealed, fortunately, that this fault was already activated only 400 years ago and its recurrence activity was estimated 1000-1500years.

It has been long-standing question why any fault trace could not been seen on the ground surface in the Kobe-area, although the earthquake made very much clearly the disaster belt. The aftershocks were distributed along a couple of active faults in the Kobe side.In order to elucidate this question, a committee to investigate active faults in and around Kobe area

BACKGROUND SEISMICITY

Almost a century since 1906, the focal area had been quiet seismically. However it is noted that three small earthquakes with magnitude between 1.5-3.3 preceded to the main shock 11hours before. In addition, anomaly was identified in the ground water upwelling, contamination of Rn Cl in the ground water and the strain change after the earthquake.

On the other hand, the observation did not enable us to predict the forthcoming earthquake. There was found a strong contrast in seismicities between seismicities before the Kobe earthquake and after the Kobe Earthquake in the region surrounding the Kobe. In particular in the region covering Osaka and Kyoto, clear increasing seismic activity has been found. The stress release along the faults which caused the devastating disaster has brought about some changes in the region, although we have not yet its mechanism.

ACTION BY JAPANESE GOVERNMENT

Realizing that measures against earthquake disasters are urged in many local and municipal governments, the Japanese Government enacted "The Special Act for Earthquake Disaster Management". As an important part of the measures, the Act set up "Earthquake Research and Investigation Headquarters" to promote intensively research activities to elucidate earthquake. The Minister of Science and Technology Agency has a mandate to put forward the Government to take relevant actions reflecting outcomes from research activities.

The Headquarters has decided to promote the following research: (1) intensive observation of seismicities on lands, under the sea bottom, precise measurements of crystal movements by GPS and some other sophisticated means, and investigation of geological faults by means of the fault trenching and boring, the seismic sounding, insitu--stress analyses of the crust and sea bottom topography; (2) intensive promotion of fundamental research on earthquake such as earthquake tectonics, earthquake mechanism and physical process, and probability analysis of earthquake occurrence.

In addition, strong ground motion research is intensively implemented, as well. The K-net, strong motion monitoring net work by the National Research Institute for Earth Science and Disaster prevention (NIED), covers the whole Japan islands to provide information about strongly shaking places quickly on earthquake occurrence.

FUTURE DIRECTIONS IN A NATIONAL PORTRAYAL OF SEISMIC HAZARD FOR HIGHWAY AND BRIDGE DESIGN

Maurice S. Power
Geomatrix Consultants
San Francisco, California

ABSTRACT

Issues involved in future directions for a national portrayal of the seismic ground shaking hazard for highway and bridge design in the United States include: choice of appropriate seismic ground motion parameters; risk representation in terms of basic approach (probabilistic, deterministic) and degree of conservatism; representation of site effects on ground motions; whether and how to include vertical ground motions, near-source ground motions, and spatial variations of ground motions in design; and other issues. In this paper, these issues are examined and possible future directions are indicated for representing the seismic ground motion hazard in nationally applicable codes and specifications. Areas are also identified where further research and development are needed to determine optimum ground motion characterizations.

INTRODUCTION

In studies being conducted for the Federal Highway Administration, the National Center for Earthquake Engineering Research (NCEER), through the NCEER Highway Project, has been evaluating issues and alternatives for the portrayal of seismic hazard for highway and bridge design in the United States. The focus is on possible changes in seismic ground motion representation in nationally-applicable guidelines and specifications, such as the AASHTO seismic design specifications for bridges (AASHTO, 1992, 1995). In May, 1997, NCEER will be conducting a workshop on the national representation of seismic ground motions for new and existing highway facilities. With attendance by bridge engineers, geotechnical engineers, and geoscientists, it is expected that this workshop will recommend future directions for national seismic hazard portrayal as well as identify areas where further research and development are needed to determine optimum characterizations of ground motions for guidelines and specifications.

In this paper, future directions for a national portrayal of seismic hazard for highway and bridge design are examined with respect to the following issues: ground shaking parameters; risk representation; site effects, vertical ground motions; near-source ground motions; spatial variations of ground motions; and other issues.

GROUND SHAKING PARAMETERS

Current specifications, codes, and model regulations (e.g., AASHTO, 1992, 1995 Specifications; 1994 Uniform Building Code, ICBO, 1994; 1994 NEHRP provisions, FEMA, (1994)) describe the national seismic hazard in terms of the effective or peak ground acceleration

(PGA). Elastic response spectral accelerations at different structural periods of vibration are then obtained by anchoring fixed response spectral shapes (for certain site conditions) to the PGA. The limitation of this approach is that response spectral shapes are strongly dependent on the regional seismic environment including the tectonic setting and the earthquakes magnitudes and source-to-site distances that contribute most to the seismic hazard. Figure 1 is an illustration of different spectral shapes for rock sites in the Western United States (WUS) (site in the San Francisco Bay region) and the Eastern United States (EUS) (site in New York City). These spectral shapes were obtained for a 500 year return period from a detailed probabilistic seismic hazard analysis in each region. The EUS spectrum contains high-frequency motion (periods less than 0.1 second) not present at the WUS site, which is a result of the harder rock conditions generally present in the EUS as compared to the WUS. The WUS spectrum contains more long-period motion, which is primarily a result of the dominance of larger magnitude earthquakes at the WUS site as compared to the EUS site.

Because of geographic differences in spectral content such as shown in Figure 1, there is increasing interest in the direct mapping of elastic response spectral values of ground motions at different periods of vibration, and attenuation relationships for spectral values now exist to permit mapping. In fact, a recent National Ground Motion Mapping Workshop, conducted by the Applied Technology Council (ATC) and cosponsored by the U.S. Geological Survey (USGS), NCEER, the Building Seismic Safety Council (BSSC), and the Structural Engineers Association of California (SEAOC) (ATC, 1995a), favored the mapping of elastic response spectral values as the parameters needed in codes for seismic structural analysis and design. At the same time, it was emphasized that peak ground motion parameters (peak ground acceleration, PGA, and peak ground velocity, PGV) are needed for evaluations of soil failure potential (e.g. liquefaction, deformations).

USGS has recently developed (1996) national ground motion maps for response spectral accelerations for periods of vibration of 0.2, 0.3, and 1.0 seconds as well as for PGA for three different probability levels (10%, 5%, and 2% probability of exceedance in 50 years). BSSC has proposed using spectral value maps based on the USGS mapping for the 1997 NEHRP Provisions for new buildings. Similarly, ATC/BSSC/FEMA (1996) have also proposed using these spectral value maps for the seismic rehabilitation of existing buildings. Thus, there appears to be a strong direction toward the use of maps of response spectral acceleration, rather than effective or peak ground acceleration, for the seismic design of facilities.

In mapping response spectral values, an issue is what should be the range of periods that the maps should address. There is a need in the highway and bridge engineering communities for spectral values over a wide period range, from very short-period values (less than 0.2 seconds) applicable to very stiff bridges that are common in the EUS, to long-period values (3 seconds or longer) applicable to long-span bridges or to bridges with tall slender piers or base-isolated structures (Buckle and Power, 1995). At present, our ability to confidently estimate long period motions (periods longer than 2 to 3 seconds) is less than for shorter period ground motions. The estimation of long-period ground motions is an area where further research is needed.

Duration and energy of ground shaking, while important to structural response, is not accounted for in the seismic loading formulations in current codes. However, there is increasing interest in utilizing these parameters in the seismic design process (e.g., Bertero, 1995; Chang and Mander, 1994; Krawinkler, 1995). Duration is also needed for soil failure and deformation evaluations. At the present time, nationally- applicable ground motion relationships that could permit the mapping of duration or energy are not available. However, estimates of duration may be approximately inferred by determining the dominant earthquake magnitude and source-to-site distance contributions to the seismic hazard at a site, because duration is strongly dependent on magnitude and distance and some correlations between duration, magnitude, and distance exist (e.g., Dobry et al. 1978). As illustrated in Figure 2 for a site in the Salt Lake City, Utah, area, it is possible to "deaggregate" the results of a probabilistic seismic hazard analysis to determine the magnitude and distance contributions for different ground motion levels or return periods, from which duration may be estimated using the available correlations. Thus deaggregation results at representative locations are considered to be an important output from national probabilistic seismic hazard mapping, and the USGS is providing such results from its recent mapping of response spectral values.

It is also recognized that inelastic response spectra are more directly indicative of structural performance at load levels beyond yield than elastic response spectra (e.g., Krawinkler, 1995). However, at present, there does not seem to be enthusiasm for mapping inelastic response spectral values primarily because they are engineering interpretations of ground motion effects and because of a preference for determining the inelastic response spectra directly from representative acceleration time histories (Krawinkler, 1995). Ultimately, practitioners would like to have suites or data bases of representative acceleration time histories for different regions of the country that could be used for dynamic analysis of structures. However, direct use of acceleration time histories are not applicable in the near-term for simplified code-type formulations of seismic loading.

RISK REPRESENTATION

The issue of risk representation refers to whether a probabilistic or deterministic approach should be used in national ground motion mapping and to the level of conservatism to be used for either approach. For past representations of the national hazard, probabilistically-based maps have been used. The California Department of Transportation (Caltrans) uses a deterministic map prepared for the state. A strong argument for the probabilistic approach is that the expression of the ground motions in terms of their probability of exceedance or return period for exceedance is directly related to risk. On the other hand, it has been pointed out that, in low or moderate seismicity areas, the "maximum" ground motions that might be experienced can far exceed those for probability levels that have been typically used in the past as a basis for the ground motions in seismic codes (e.g., 10% probability of exceedance in 50 years) and that, therefore, there may be insufficient protection for structures for rare but possible events in these areas. It has been argued that this situation could be alleviated by deterministically mapping ground motions for maximum earthquakes capable on defined seismic sources. Alternatively, use of a lower probability of exceedance (longer return period) in a probabilistic analysis could be considered. Deterministic approaches are difficult to implement in areas where discrete active

faults have not been defined principally because of the difficulty of defining source-to-site distances for purposes of estimating the ground motions.

At the National Ground Motion Mapping Workshop (ATC, 1995a), there was a strong preference for the probabilistic approach as a basic approach. However, deterministic maps were also desired for scenario earthquakes on major active faults. For the proposed 1997 NEHRP provisions for buildings, the USGS probabilistic ground motion maps are being used; however, deterministically-determined ground motion values are being used to place a ceiling on ground motions for locations close to highly active faults located in the Western U.S. This same approach is being proposed to define the upper-level ground motion for the seismic rehabilitation of existing buildings (ATC/BSSC/FEMA, 1996).

For either probabilistic or deterministic approaches, there is the issue of the level or degree of conservatism in the ground motion values. For the probabilistic approach, the issue is the appropriate probability level(s) or return period (s). In current national code-type ground motion representations (e.g., AASHTO Provisions, NEHRP Provisions, Uniform Building Code), a single probability level or return period (10% probability of exceedance in 50 years, or 475-year return period) has been used for all regions of the country. However, arguments can be made for using a lower probability level or longer return period in low seismicity regions. One argument is that ground motion estimates tend to be more uncertain for low-seismicity regions because seismic sources, seismicity rates, and ground motion attenuation functions tend to be less well defined than for high-seismicity regions. The greater uncertainty in the hazard in areas of lower seismicity is illustrated in Figure 3 for sites in New York City and Portland. As can be seen in Figure 3, the uncertainty band in the seismic hazard curve (measured from the 5th to the 95th percentile estimates of the hazard, i.e., 5th to 95th percentile confidence limits) is considerably wider for the lower-seismicity New York City site. To compensate for the additional uncertainty in low seismicity regions, longer return periods could be used. Another argument is that if a common probability level or return period is used in different regions, the probability of experiencing ground motions much higher than the design level motions is greater in low seismicity regions than in high seismicity regions because the ground motions in high seismicity regions are closer to those that may be associated with maximum earthquakes. Figure 4 illustrates the ratio of response spectral acceleration on rock for a 1 second period of vibration [Sa (1.0)] at a given annual probability (frequency) of exceedance to Sa (1.0) for an annual probability of exceedance of $2x10^{-3}$ (i.e., 500-year return period) for sites in San Francisco and New York City. Although such comparisons will depend on the specific ground motion parameter and site location, the general trend is as shown in Figure 4-- ground motions a certain factor higher than the design level have a higher probability of being exceeded in low seismicity regions than in high-seismicity regions. For example, in Figure 4, ground motions 1.5 times higher than the design level motions have an annual probability of exceedance of about $5x10^{-4}$ at the San Francisco site and $1.6x10^{-3}$ at the New York Site.

A probability level of 2% in 50 years (approximately 2,500-year return period) (with deterministic bounds near highly active faults as stated above) is used for the maps for the proposed 1997 NEHRP Provisions for new buildings. For design, it is proposed to use two-thirds of these map values, on the basis that most structures designed in accordance with the

provisions would be able to withstand the mapped ground motions (1.5 times the design values) without collapse. The guidelines for the seismic rehabilitation of new buildings (ATC/BSSC/FEMA, 1996) propose a "Basic Safety Objective" in which a building can withstand ground motions having a probability of exceedance of 10% in 50 years for a life-safety criterion and ground motions having a probability of exceedance of 2% in 50 years (with deterministic bounds discussed above) for a no-collapse criterion. The ATC-18 project (ATC, 1996a) suggests for the design of bridges functional evaluation ground motions having return periods in the range of 70 to 250 years (depending on the useful life of a bridge or other highway structure) and safety evaluation ground motions having a 950-to 2400-year return period.

In summary the current directions for national seismic risk representation in the U.S. appears to be toward: (1) continued use of probabilistic approaches for defining ground motion levels, possibly with deterministic ground motion bounds when ground motions become very large with the probabilistic approach close to highly active faults; (2) lower probability levels (longer return periods) and correspondingly higher ground motions, especially when associated with the performance objective of collapse prevention; and (3) possibly lower probability levels in low-seismicity areas compared to high seismicity areas, to reflect more uncertainty in probabilistic ground motion estimates in these areas, as well as greater rate of increase in ground motion levels with increasing return period in low seismicity areas compared to high-seismicity areas.

SITE EFFECTS ON SEISMIC HAZARD

It is expected that for code applications, national seismic hazard maps will continue to be prepared for a certain "reference "site condition" and "site factors" will then be used to estimate ground motions for other site soil types.

Site factors proposed to replace the simple site factors for site classes S1 through S4 that are in the current AASHTO provisions and the Uniform Building Code were developed at a Site Response Workshop held at the University of Southern California in 1992 (Rinne, 1994; Martin and Dobry, 1994). These site factors are in the form of multipliers to rock response spectra. There are separate site factors for the short-period range and the long-period range, whereas the S1-S4 factors apply only in the long-period range. Also, the proposed site factors are dependent on the level of shaking in rock, decreasing for higher levels of shaking reflecting nonlinear soil behavior and increased soil damping. These site factors are summarized in Table 1, and the corresponding site classifications are shown in Table 2. These site factors have been adopted into the 1994 NEHRP provisions for buildings, have been adopted for the 1997 Uniform Building Code, and have been proposed to Caltrans for their updated seismic specifications by the ATC-32 project (ATC, 1996b).

Recent studies by Crouse and McGuire (1996) and by Borcherdt (1996) and Borcherdt and Wentworth (1995) suggest that the nonlinear soil response aspects may be overemphasized in the short-period range with the new site factors and that the factor Fa should not decease as rapidly as shown in Table 1 with increase in shaking level. Data from the Northridge and Kobe earthquakes, which have not been fully analyzed to date, should provide additional insight into whether further changes to site factors should be considered.

VERTICAL GROUND MOTIONS

The present AASHTO Specifications do not contain specific requirements to design for vertical ground motions. The issue is whether, in certain cases, there should be explicit requirements to incorporate vertical ground motions in design and, if so, how to quantify them.

Recorded ground motion data from a number of recent earthquakes as well as ground motion modeling have shown that the ratio of vertical-to-horizontal response spectral values of ground motion are strongly dependent on the period of vibration and distance from the earthquake source. Results of statistical analyses of vertical-to-horizontal response spectral ratios by Egan et al. (1994) for earthquakes of magnitude equal to or greater than magnitude 6.5 recorded in California or similar tectonic environments (not including the Northridge earthquake data) are shown in Figure 5. The commonly-assumed two-thirds ratio is shown for reference. The results indicate that, for short periods of vibration and close distances from the causative faults, vertical-to-horizontal spectral ratios can substantially exceed the nominal two-thirds ratio and, in fact can substantially exceed unity at distances less than about 10 km. Figure 5 also indicates that the ratio of two-thirds is generally conservative for periods longer than about 0.2 to 0.3 seconds. The trends for high vertical-to-horizontal spectral ratios for short-period motions at near-source distances is well established from many analyses similar to that shown in Figure 7 including analyses of Northridge earthquake data (e.g., Niazi and Bozorgnia, 1992; Bozorgnia and Niazi, 1993; Niazi and Bozorgnia, 1994; Bozorgnia et al., 1994, 1995; Egan et al., 1994; Nisar and Golesorkhi, 1995).

EPRI (1993) carried out ground motion modeling studies to assess vertical-to-horizontal spectral ratios at EUS sites. Their results show dependence on differences in crustal models (Midcontinent and Gulf Coast) and site conditions (soil or rock). Figure 6 illustrates results of the EPRI modeling for rock sites for the Midcontinent crustal model. The general trend from the EPRI analyses are for higher short-period vertical-to-horizontal spectral ratios at closer distances, similar to the results for the WUS discussed above. However, numerically, the EPRI results for the EUS are somewhat different than those for the WUS, for example, higher vertical-to-horizontal ratios for longer periods.

NEAR-SOURCE GROUND MOTIONS

The special issue that arises with respect to near-source ground motions (other than their overall high amplitudes and the high vertical-to-horizontal spectral ratios discussed above) is the presence of an intermediate-to long-period pulse in the ground motion that is associated with the fault rupture process. Figure 7 provides two examples of pulsive motions from the Pacoima dam recording from the 1971 San Fernando earthquake and the Sylmar recording from the 1994 Northridge earthquake. The pulse can clearly be seen toward the beginning of the acceleration time histories and, for these records, has a period of about one second. However, other records may have pulsive motions occurring at periods somewhat shorter than one second to periods of several seconds. These pulsive motions contain a great deal of energy and can be very damaging to structures. The high velocities associated with the pulsive motion are shown in the figures.

It has also been found empirically, and is expected from seismological theory, that these longer-period, near-source ground motions are strongly directional in nature. The horizontal component of motion that is in a direction normal to the fault strike tends to have larger amplitudes than the component parallel to the fault strike. This is in contrast to short-period motions (say less than 0.5 seconds) in which there is no tendency for one horizontal component to be stronger than the other. Figure 8 is an example of directionality of near-source (within 10 km) longer-period ground motions for the 1979 Imperial Valley earthquake. The heavy line is the average ratio (from several individual recordings shown) of the response spectral values in the fault normal direction to the average of the response spectral values in the fault normal and fault parallel directions. It can be seen that for periods less than about 2 seconds for this earthquake, there is little or no tendency for the fault normal component to be higher than the average horizontal component, but at longer periods, the fault normal component averages about a factor of 1.4 times higher than the average horizontal component for this earthquake. For seismic design, ground motions are typically defined as the average horizontal component and taken to be equal in both horizontal directions. However, in the near-source region, there might be an expectation that the transverse and longitudinal longer-period components of ground motion exciting a bridge could be different, depending on the orientation of the bridge to the fault.

Although more research is needed about these near-source phenomena, there is enough data and knowledge to make an initial generalization of the phenomena for design purposes. The question is whether the phenomena can be quantified in specifications, codes, and guidelines in a way that is useful to and can be practically implemented by highway and bridge engineering practitioners.

SPATIAL VARIATIONS OF GROUND MOTIONS

For extended highway structures (bridges, tunnels, and other structures), ground motions may vary spatially along the structure. The variation includes the wave passage effect, which is the phenomena that seismic waves typically are not propagating perfectly vertically as they approach the ground surface, rather they propagate at some angle to the vertical and therefore arrive at different times at different points along the alignment of an extended structure. The wave passage effect can be characterized by an apparent velocity of seismic wave propagation along the axis of the structure. The spatial variation also includes attenuation and incoherency. Attenuation is a (generally) systematic decrease in ground motion amplitude with increasing distance from the earthquake source. Incoherence describes the differences in seismic wave form from point to point due to scattering and complex 3-D wave propagation. Incoherence can also be produced by differences in the wave mix from point to point for sites close to an extended seismic source.

For important bridges, procedures are available to quantify spatial variations of ground motions and develop multi-support foundation motions for use in the seismic analysis of the bridge. For code-type specifications and guidelines, an issue is whether certain classes of bridges and seismic environments could be defined for which spatial variations are not important enough

to quantify, and/or whether simpler methods could be defined to analyze for spatial variations or incorporate their effects in design (for example, by incorporating wave passage effects but not incoherence; or by increasing certain response quantities by certain factors to account for spatial variations of ground motion. This topic is being addressed in research for the NCEER Highway Project by Shinozuka and Deodatis (1995).

OTHER ISSUES

Some other issues involved in defining the national seismic hazard for highway structures include: (1) whether the mapped hazard should be portrayed as contours or zones; (2) whether upper and/or lower bounds should be placed on the hazard; (3) whether other modifications to the scientifically-defined hazard should be made before using it as a basis for design.

The AASHTO specifications as well as the NEHRP building provisions have portrayed the hazard as ground motion contours. On the other hand, the Uniform Building Code has opted for portraying the hazard as uniform (for design purposes) over broad zones. The contour portrayal leads to the most accurate spatial variation in the hazard. However, the zone approach offers the advantage of a simpler portrayal that could lead to more conservative design values if derived from the upper range or upper bound of ground motion values mapped over the zone. The degree of conservatism would be unequal over the zone, however.

Although the current AASHTO provisions do not place upper bounds on the mapped acceleration values, upper bounds have been placed in other current codes and regulations. Thus, at present, the largest peak (or effective) ground acceleration that appears on the maps of the 1994 Uniform Building Code and the 1994 NEHRP provisions for buildings is 0.4 g. The rationale has been that higher values (therefore higher seismic forces) would not necessarily lead to safer, better performing designs. However, the trend is in the direction of utilizing larger ("actual") ground motions, particularly in view of the high ground motions observed in recent earthquakes, such as Loma Prieta, Northridge, and Kobe. The 1997 Uniform Building Code will include "near-fault" factors, to recognize the higher-than-0.4g ground motions that occur in the near-source region of an earthquake. The proposed changes to the NEHRP provisions for 1997, discussed earlier, use actual calculated ground motions. The issue of placing lower bounds on the ground motions to be used in design relates to the desire to build in a certain degree of seismic resistance in low seismic areas and to have more resistance for rare, large events as discussed earlier. Lower bounds are proposed for the 1997 NEHRP provisions.

With respect to further modifying ground motion for use in a design procedure, another important issue is the long-period characterization of the ground motion. For both the equivalent lateral force method of analysis and the dynamic modal analysis method in the AASHTO Specifications, the long-period branch of the response spectrum decreases with increasing period as $1/T^{2/3}$, whereas for actual ground motions, the decrease is more typically as $1/T$. The $1/T^{2/3}$ characterization, which results in a slower decrease with increasing period and therefore higher long-period ground motions, dates back to the ATC-3 project for

buildings and the ATC-6 project for bridges (ATC, 1978 and 1981). As noted by Buckle and Power (1995), the two major reasons for introducing this conservatism in design of bridges as stated in ATC (1981) were: (1) The fundamental period of a bridge increases as the column height increases, the span length increases and the number of columns per bent decreases. Hence the longer the period the more likely that high ductility requirements will be concentrated in a few columns. (2) Instability of a bridge is more of a problem as the period increases. The question is whether these arguments are still compelling or whether the ground motion taken for design should be values more consistent with recorded ground motions. The trend, as reflected in proposed changes to both the UBC and the NEHRP provisions, is toward the actual ground motions and away from the decrease of long-period motions as $1/T^{2/3}$.

ACKNOWLEDGMENTS

The author wishes to acknowledge the continuing support of the Federal Highway Administration and the National Center for Earthquake Engineering Research for their work on the seismic vulnerability of new and existing highway construction through the NCEER Highway Project. In particular the author is involved in the characterization of the seismic hazard as it affects the design and retrofit of highway and bridge structures. This support is gratefully acknowledged.

REFERENCES

AASHTO, 1992, Standard specifications for highway bridges, division I-A: seismic design, American Association of State Highway and Transportation Officials, 15th Edition, Washington DC, 686 pp.

AASHTO, 1995, Standard specifications for highway bridges, division I-A: seismic design, American Association of State Highway and Transportation Officials, 15th Edition and Interims, Washington DC.

ATC/BSSC/FEMA, 1996, NEHRP Guidelines and commentary for the seismic rehabilitation of buildings, Ballot Version, prepared by Applied Technology Council (ATC-33 project) for Building Seismic Safety Council (BSSC), funded by Federal Emergency Management Agency (FEMA), publication nos. FEMA 273 and 274, September.

ATC, 1978, Tentative provisions for the development of seismic regulations for buildings, Report ATC-3-06, Applied Technology Council, 505 pp.

ATC, 1981, Seismic design guidelines for highway bridges, Report ATC-6, Applied Technology Council, 200 pp.

ATC, 1995a, National earthquake ground motion mapping workshop, preprints, Report ATC-35-2, Applied Technology Council.

ATC, 1996a, Seismic design criteria for bridges, current and future, Report ATC-18, Applied Technology Council.

ATC, 1996b, Review and revision of Caltrans seismic design procedures for bridges, Report ATC-32, Applied Technology Council.

Borcherdt, R.D., 1996, Preliminary amplification estimates inferred from strong ground motion recordings of the Northridge earthquake of January 17, 1995, Proceedings of the International Workshop on Site Response, v. 2, Yokosuka, Japan, organized by Port and Harbour Research Institute, Japan, January.

Borcherdt, R.D., and Wentworth, C.M., 1995, Strong ground motion generated by the Northridge earthquake of January 17, 1994: Implications for seismic design coefficients and building codes: Proceedings, Fifth International Conference on Seismic Zonation, Nice, France, October Vol., II, p. 964-971.

Bozorgnia, Y., and Niazi, M., 1993, Distance scaling of vertical and horizontal response spectra of the Loma Prieta earthquake, Journal of Earthquake Engineering and Structural Dynamics, Vol. 22, p. 695-707.

Bozorgnia, Y., Naizi, M., and Campbell, R.W., 1994, Vertical ground motion during the 1994 Northridge earthquake, Proceedings of 6th U.S.-Japan Workshop on the Improvement of Building Structural Design and Construction Practices, Vancouver British Columbia, Canada, Applied Technology Council publication ATC-15-5.

Bozorgnia, Y., Niazi, M., and Campbell, K.W., 1995, Characteristics of the free-field vertical ground motion, Earthquake Spectra, v. 11, no. 4, pp. 515-525.

Buckle, I., and Power, M., 1995, Ground motion issues and design values for bridges, Preprints: National Earthquake Ground Motion Mapping Workshop, Applied Technology Council, ATC-35-2, p. 11-1 - 11-8.

Chang, G.A., and Mander, J.B., 1994, Seismic energy based fatigue damage analysis of bridge columns, Part II: Evaluation of seismic demand, Technical Report NCEER-94-0013, National Center for Earthquake Engineering Research, State University of New York at Buffalo.

Crouse, C.B., and McGuire, J.W., 1996, Site response studies for purpose of revising NEHRP seismic provisions, Earthquake Spectra, v. 12, no. 3, pp. 407-439.

Dobry R., Idriss, I.M., and Ng, E., 1978, Duration characteristics of horizontal components of strong motion earthquake records: Bulletin of the Seismological Society of America, Vol. 68, no. 5, p. 1487-1520.

Egan, J.A., Makdisi, F.I., and Rosidi, D., 1994, Near-field vertical ground motions from the 17 January 1994 Northridge earthquake, were they unusual?: Poster presented at SSA-94, 89th Annual Meeting of the Seismological Society of America, April 5-7, Pasadena, California, Abstract No. 46 in Program for Northridge Abstracts.

Electric Power Research Institute (EPRI), 1993, Guidelines for determining design basis ground motions, Electric Power Research Institute Report TR-102293.

FEMA, 1994, NEHRP recommended provisions for seismic regulations for new buildings: Part 1 Provisions; Part II - Commentary, Report FEMA 222A and 223A, Federal Emergency Management Agency, Washington, DC, 220 pp. and 335 pp.

International Conference of Building Officials (ICBO), 1994, Uniform Building Code, vol. 2, Structural Engineering Design Provisions.

Krawinkler, H., 1995, The need for ground motion representation beyond elastic response spectral values, Preprints: National Earthquake Ground Motion Mapping Workshop, Applied Technology Council, ATC-35-2, p. 2-1 - 2-15.

Martin, G.R., and Dobry, R., 1994, Earthquake site response and seismic code provisions, NCEER Bull. 8, n. 4, p. 1-6; and Research Accomplishments, NCEER, 1986-1994, p. 121-129.

Niazi, M. and Bozorgnia, 1992, Behavior of near-source peak vertical and horizontal response spectra over SMART-1 array, Taiwan, Journal of Earthquake Engineering and Structural Dynamics, Vol. 21, p. 37-50.

Niazi, M., and Bozorgnia, Y., 1994, Vertical component of the ground motion in the near-source region of January 17, 1994 Northridge earthquake, Abstract, 89th Annual Meeting of Seismological Society of America, Pasadena, California, April 5-7.

Nisar, A., and Golesorkhi, R., 1995, Development of vertical design response spectrum for use in the near-field: Fifth International Conference on Seismic Zonation, Nice, France, October 17-19.

Rinne, E.E., 1994, Development of new site coefficients for building codes, Proceedings, Fifth U.S. National Conference on Earthquake Engineering, July 10-14, 1994, vol. III, p. 69-78.

Shinozuka, M., and Deodatis, G., 1995, Vulnerability assessment - seismic hazard and ground motion, summary of year 2 work, NCEER Highway Project Annual Report to Federal Highway Administration for Seismic Vulnerability of Existing Highway Construction.

Youngs, R.R., 1995, The need for detailed treatment in probabilistic seismic hazard mapping, Preprints: National Earthquake Ground Motion Mapping Workshop, Applied Technology Council, ATC-35-2, p. 6-1 - 6-13.

Youngs, R.R., Swan, F.H., Power, M.S., Schwartz, D.P., and Green, R.K., 1987, Probabilistic analysis of earthquake ground shaking hazard along the Wasatch Front, Utah: Assessment of Regional Earthquake Hazards and Risk Along the Wasatch Front, Utah, U.S. Geological Survey Open File Report 87-585, Vol. II, p. M-1-110.

TABLE 1

SITE COEFFICIENTS ADOPTED FOR 1994 NEHRP PROVISIONS AND 1997 UNIFORM BUILDING CODE

(a) Short-period Site coefficient, F_a

Soil Profile Type	Shaking Intensity				
	PGA = 0.1g	PGA = 0.2g	PGA = 0.3g	PGA = 0.4g	PGA = 0.5g
A	0.8	0.8	0.8	0.8	0.8
B	1.0	1.0	1.0	1.0	1.0
C	1.2	1.2	1.1	1.0	1.0
D	1.6	1.4	1.2	1.1	1.0
E	2.5	1.7	1.2	0.9	(--)[1]

(b) Long-period Site coefficient, F_v

Soil Profile Type	Shaking Intensity				
	PGA =0.1g	PGA =0.2g	PGA =0.3g	PGA = 0.4g	PGA =0.5g
A	0.8	0.8	0.8	0.8	0.8
B	1.0	1.0	1.0	1.0	1.0
C	1.7	1.6	1.5	1.4	1.3
D	2.4	2.0	1.8	1.6	1.5
E	3.5	3.2	2.8	2.4	(--)[1]

[1] site-specific geotechnical investigations and dynamic site response analyses should be performed.
Note: PGA refers to estimated peak ground acceleration on rock.

TABLE 2

DEFINITION OF SOIL PROFILE TYPES ADOPTED FOR 1994 NEHRP PROVISIONS AND 1997 UNIFORM BUILDING CODE

A Hard rock with measured shear wave velocity, $v_s >$ 5,000 ft/sec (1520 m/s).

B Rock with 2,500 ft/sec < v_s 5,000 (760 m/sec < v_s 1520 m/s).

C Very dense soil and soft rock with 1,200 ft/sec < v_s 2,500 ft/sec (360 m/s < v_s 760 m/s) or with either N > 50 or s_u 2,000 psf (100 kPa)

D Stiff soil with 600 ft/sec v_s 1,200 ft/sec (180 m/s v_s 360 m/s) or with either 15 N 50 or 1,000 psf s_u 2,000 psf (50 kPa s_u 100 kPa)

E Any profile with more than 10 ft (3 m) of soft clay defined as soil with PI > 20, w 40 percent, and s_u < 500 psf (25 kPa) or a soil profile with v_s< 600 ft/sec (180 m/s)

F Soil requiring site-specific evaluations:

1. Soils vulnerable to potential failure or collapse under seismic loading such as liquefiable soils, quick and highly sensitive clays, collapsible weakly cemented soils.

2. Peats and/or high organic clays (H > 10 ft [3 m] of peat and/or highly organic clay where H = thickness of soil).

3. Very high plasticity clays (H > 25 ft [8 m] with PI > 75).

4. Very thick soft/medium stiff clays (H > 120 ft [36 m]).

Note: v_s is shear wave velocity; N is Standard Penetration Test blow count; s_u is undrained shear strength. All values shown pertain to the average values in the top 100 feet of the soil profiles.

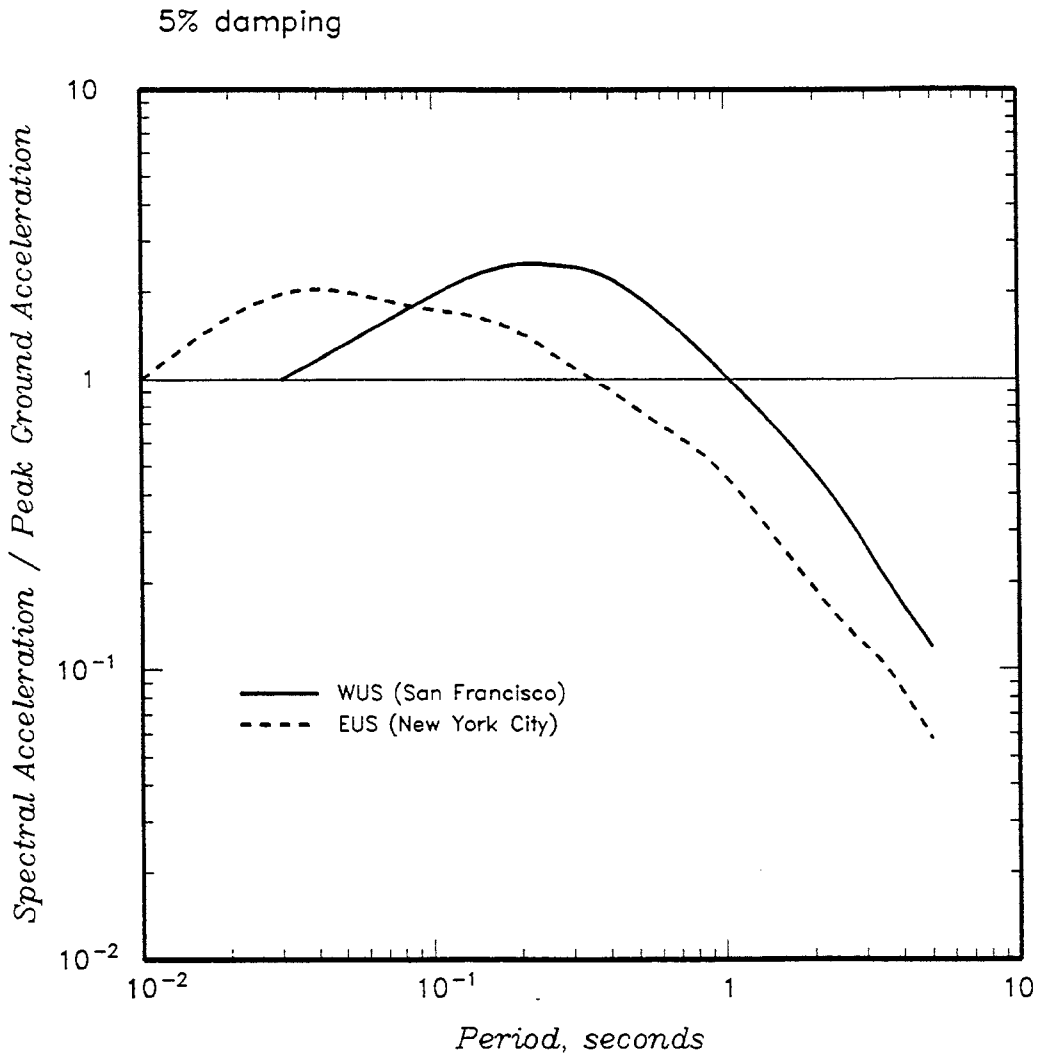

Figure 1. Comparison of equal-hazard response spectral shapes for rock ground motions for a 500-year return period—sites in western U.S. and eastern U.S.

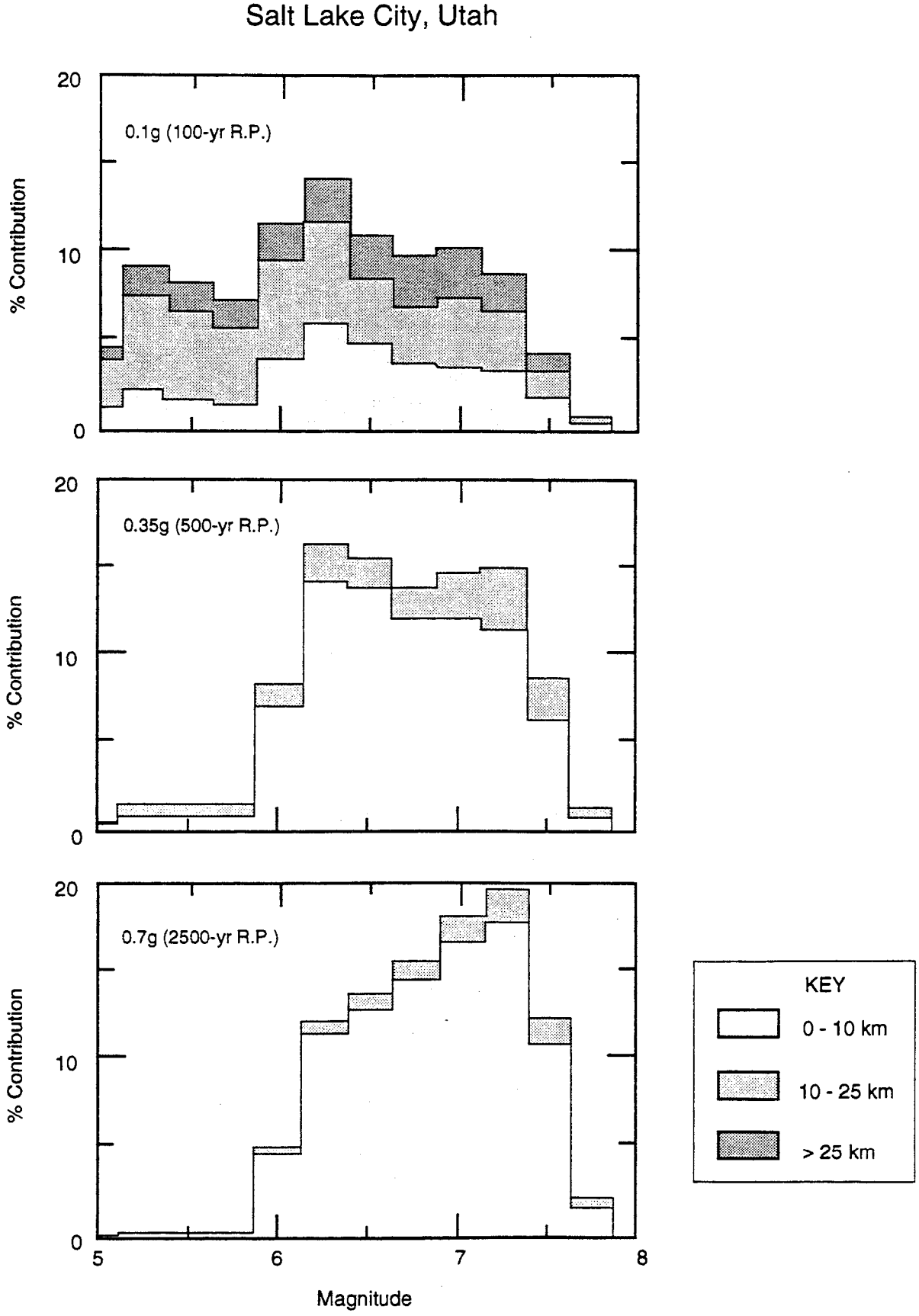

Figure 2. Example of de deaggregation of probabilistic seismic hazard to determine magnitude and distance contributions. (Youngs et al., 1987)

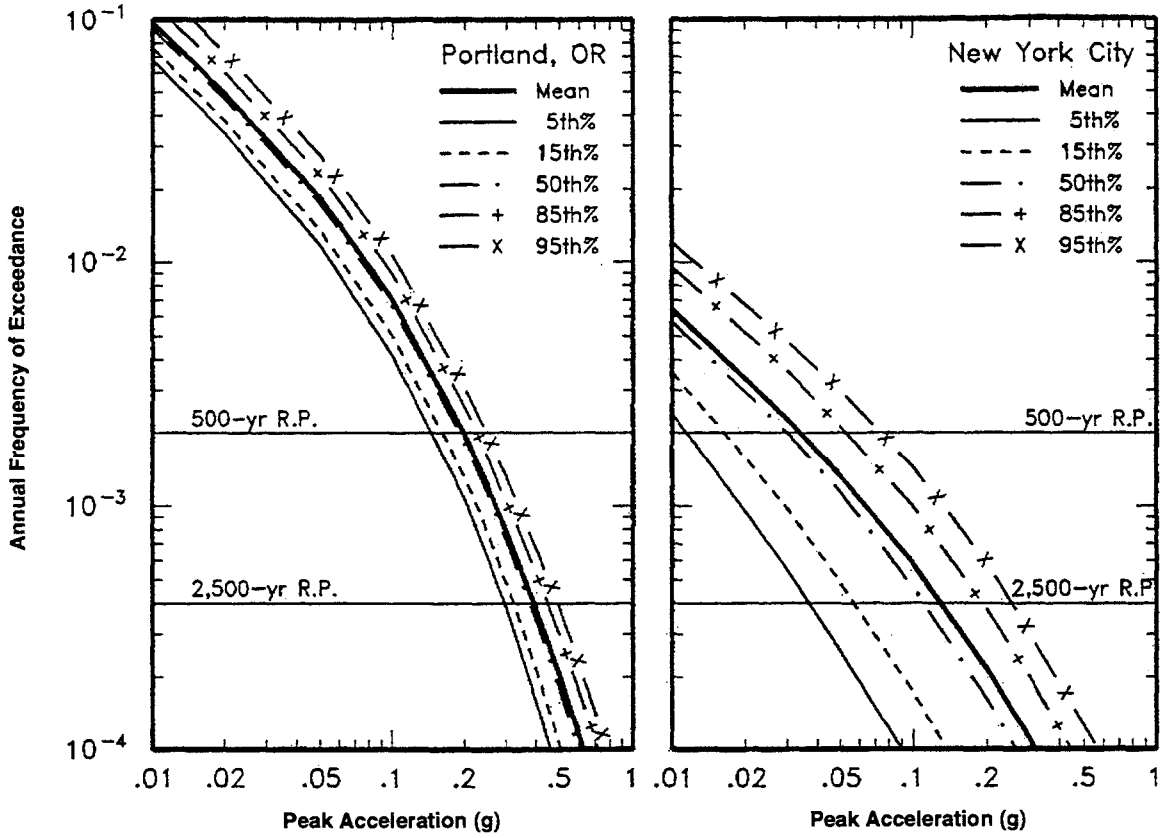

Figure 3. Seismic hazard curves for peak ground acceleration on rock illustrating uncertainty in hazard estimates (Youngs, 1995)

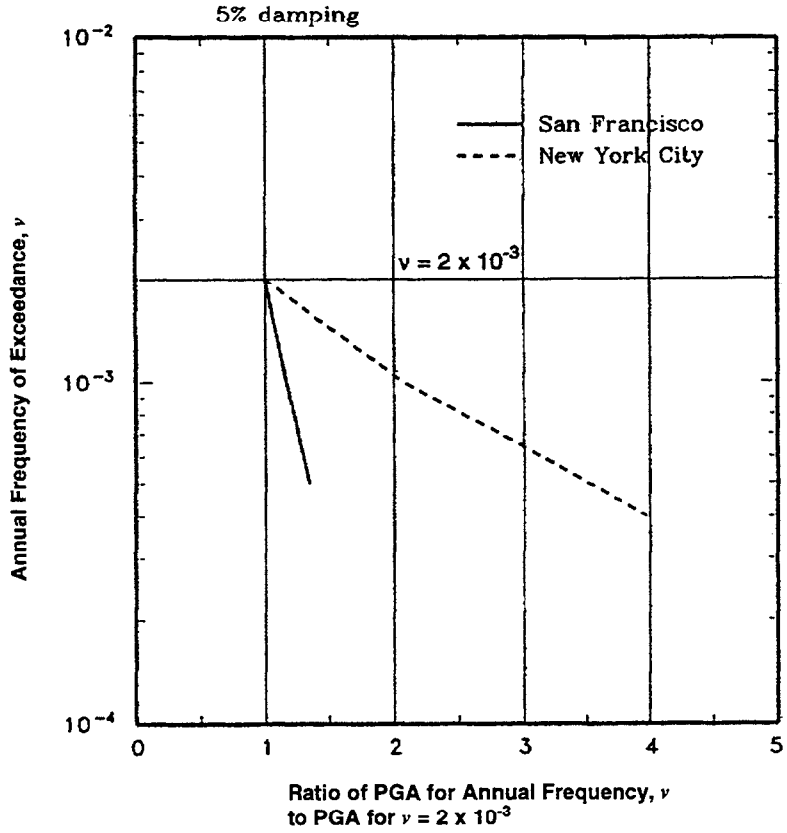

Figure 4. Effect of annual frequency of exceedance on relative amplitudes of peak ground acceleration (PGA) for sites in EUS and WUS

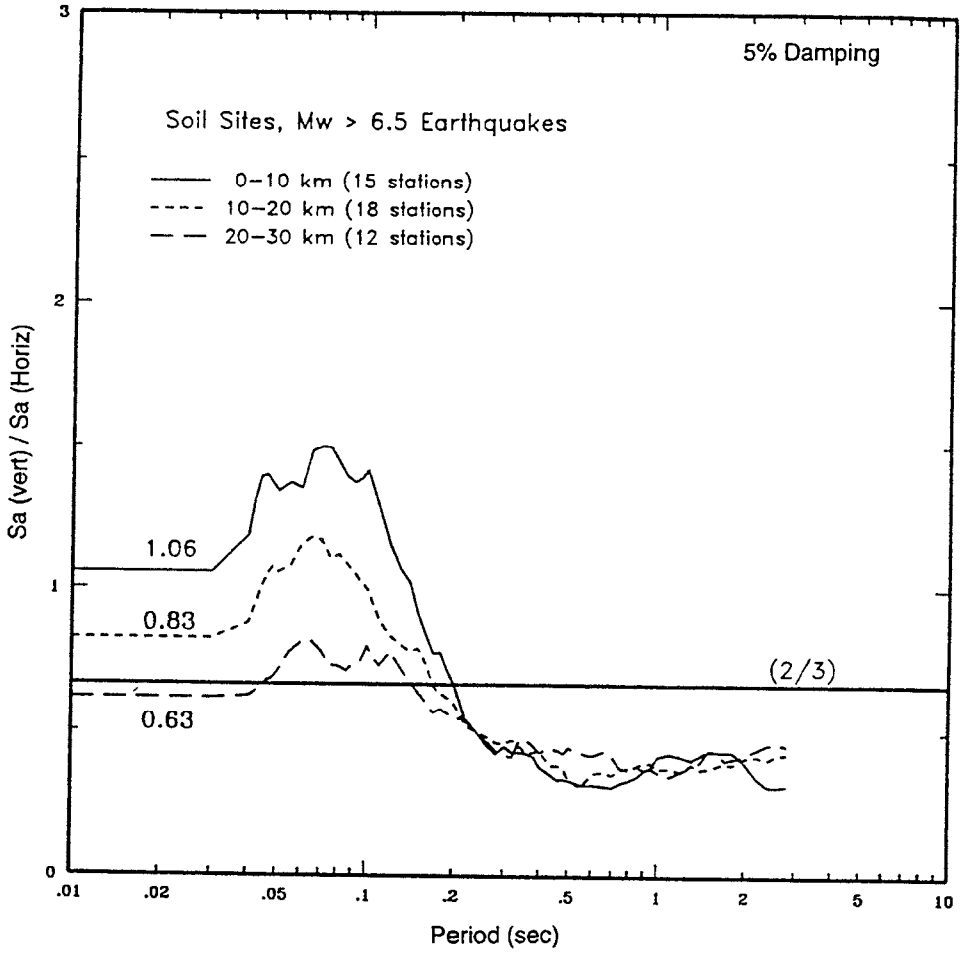

Figure 5. Ratios of vertical to horizontal response spectra for three distance ranges, magnitude ≥6.5 earthquakes, soil site recordings (Egan et al., 1994)

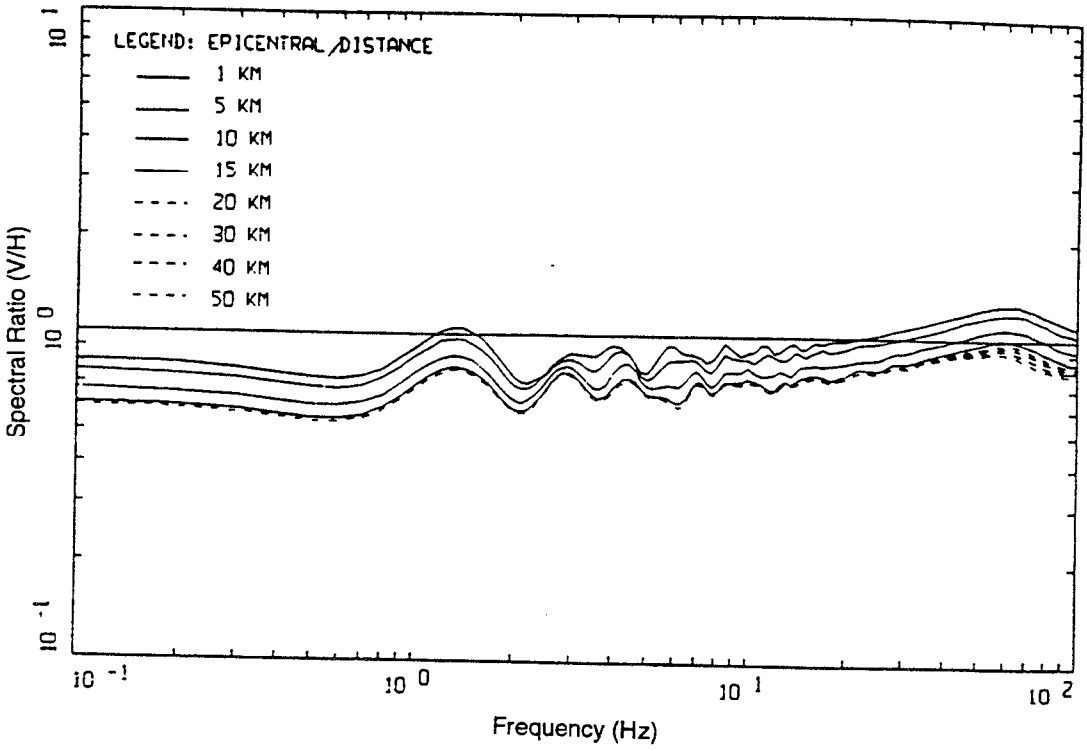

Figure 6. Ratios of vertical to horizontal 5% damped response spectra computed for the Midcontinent crustal model (EPRI, 1993)

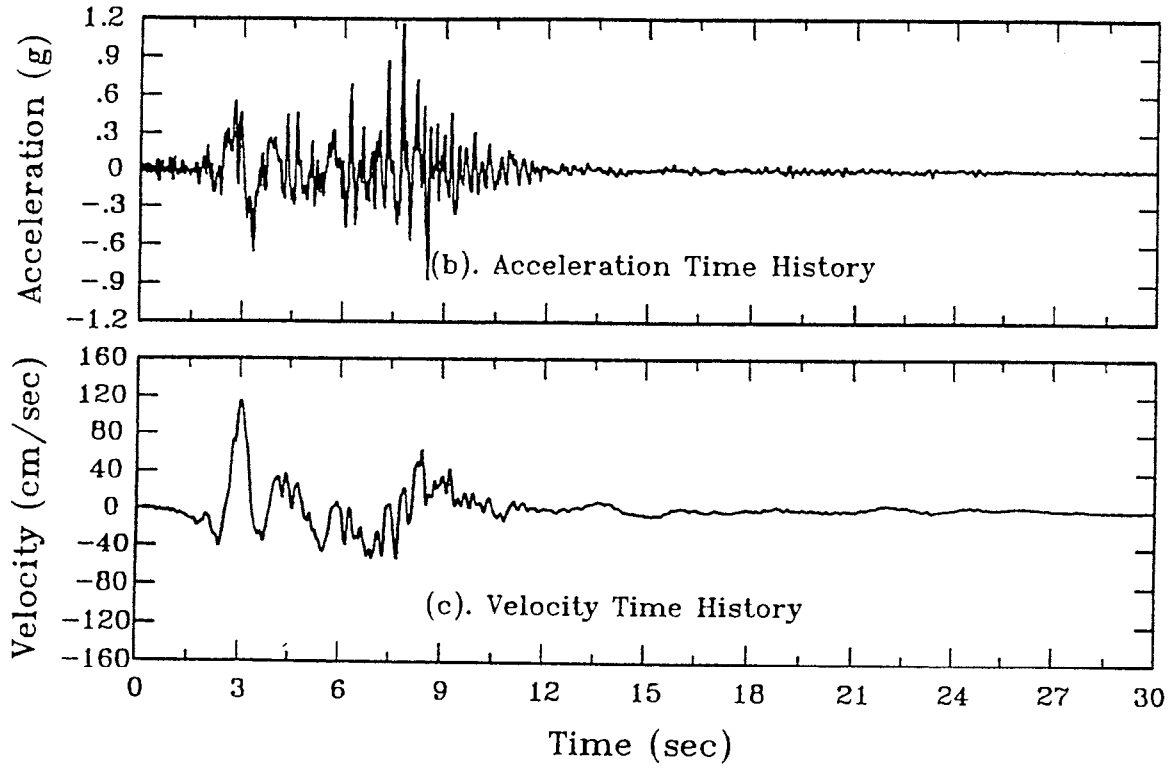

(a) Recording at Pacoima Dam Station, Component 164°, 1971 San Fernando Earthquake

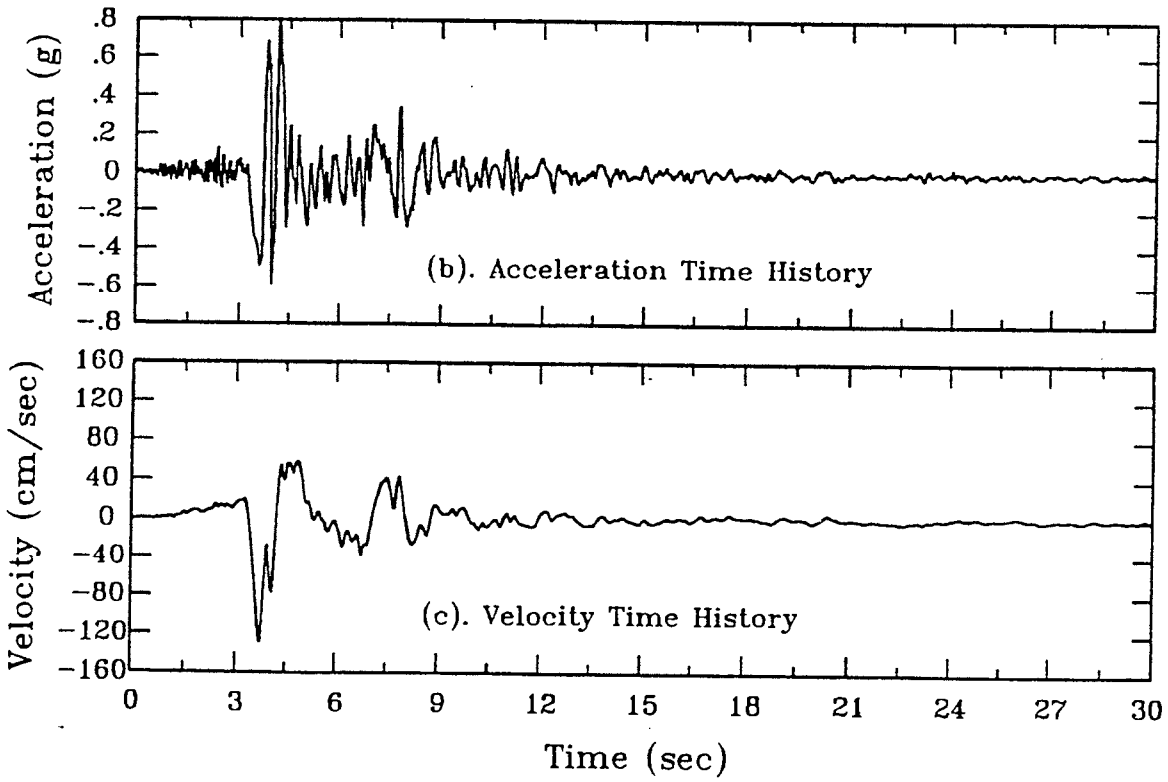

(b) Recording at Sylmar Station, Component 360°, 1994 Northridge Earthquake

Figure 7. Time histories of near-source ground motion recordings from 1971 San Fernando and 1994 Northridge earthquakes

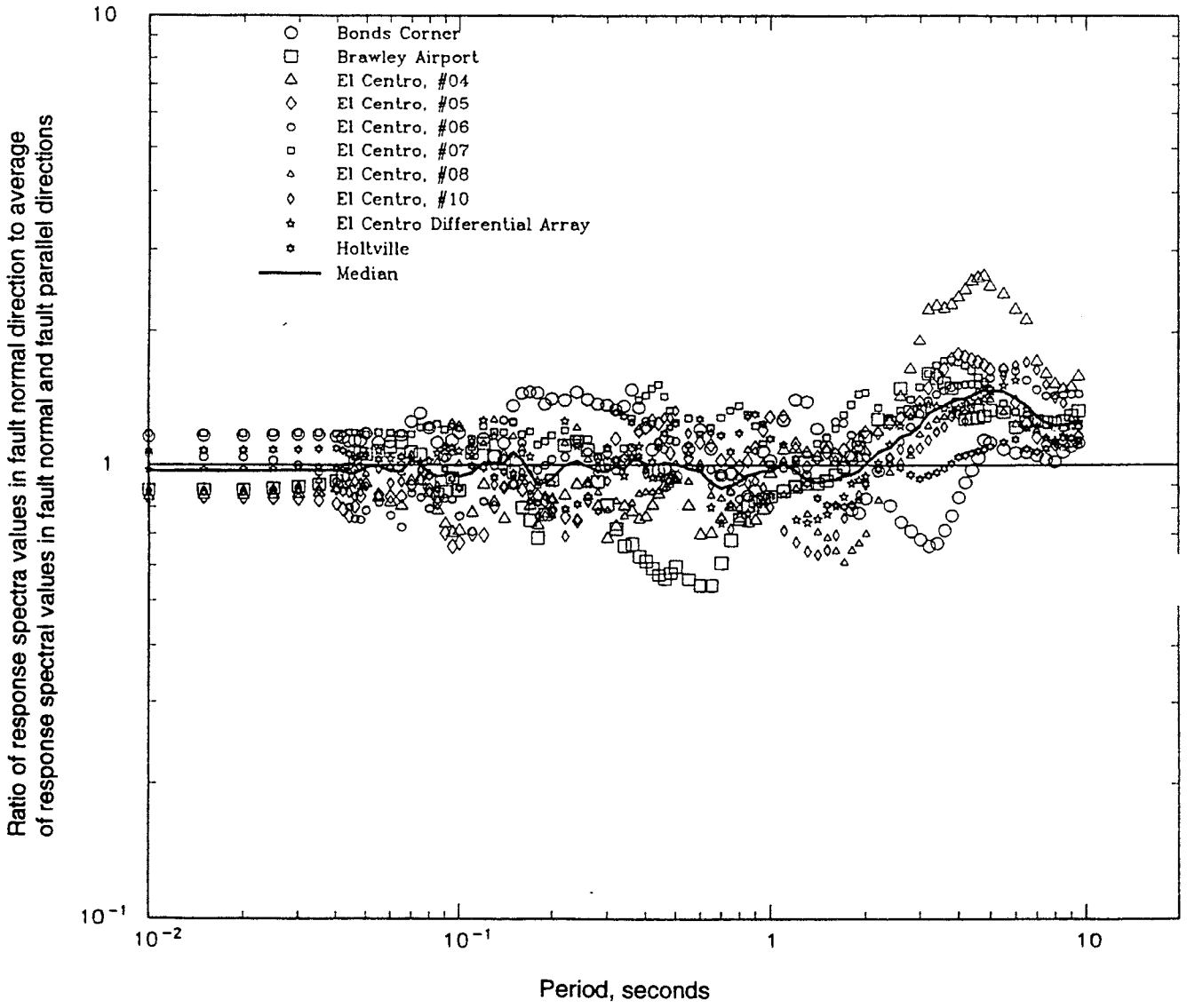

Figure 8. Directionality of near-source, long-period ground motions recorded during 1979 Imperial Valley Earthquake

LONG PERIOD GROUND MOTION DUE TO THE 1995 HYOGO-KEN NANBU, JAPAN EARTHQUAKE

Tatsuo Ohmachi
Professor, Department of Built Environment,
Tokyo Institute of Technology

Shun'ichi Kataoka
Graduate Student, Department of Built Environment,
Tokyo Institute of Technology

Shojiro Kataoka
Postdoctoral Scholar, Department of Civil Engineering,
California Institute of Technology

ABSTRACT

To develop a practical method to specify design ground motion, long period ground motion in and around the Osaka basin during the 1995 Hyogo-ken Nanbu earthquake is studied. First characteristics of observed ground motion at four sites are investigated. Then direction and velocity of wave propagation are estimated, using observed up-down component at very closely spaced stations. The velocities are close to the phase velocity of the fundamental mode Rayleigh wave. Direction of propagation is almost N30W. This means that the long period ground motion is due to the surface waves affected by 3-D topographical conditions. Using boundary element analysis, the 3-D effect on seismic ground motion is discussed. Direction of wave propagation is about N40W, and amplitude is almost identical to the observation.

INTRODUCTION

The 1995 Hyogo-ken Nanbu earthquake highlighted urgent necessity to take into account near-field ground motion in seismic design of urban facilities. Regarding the design ground motion, main effort seems to have been focused on the so-called short-period motion whose period is shorter than 1 or 2 second. As a result, several methods are now available for us to specify the short-period ground motion to a satisfactory level of accuracy as long as a design fault model is given. The methods include empirical or semi-empirical ones.

On the contrary, as for the longer period motion, there still remain some difficulties in specifying the design ground motion. Any reliable method has not been developed yet to date. A principal cause of the difficulties is the lack of good recordings of the motion with large intensity. However, the strong motion records of the Hyogo-ken Nanbu earthquake can give us a major breakthrough in this field, because there are some indicating almost 100 cm/s of response velocity for 5 % damping over the long period range. Among them, the present paper deals with those recorded in and around the Osaka basin.

In addition, 3-D simulation of the long period motion is applied as a supplement of the recordings. The model used in the simulation consists of the fault model of the main shock as well as 3-D configuration of a surface layer underlaid by the seismic bedrock. Although, due to the limitation of the computer,

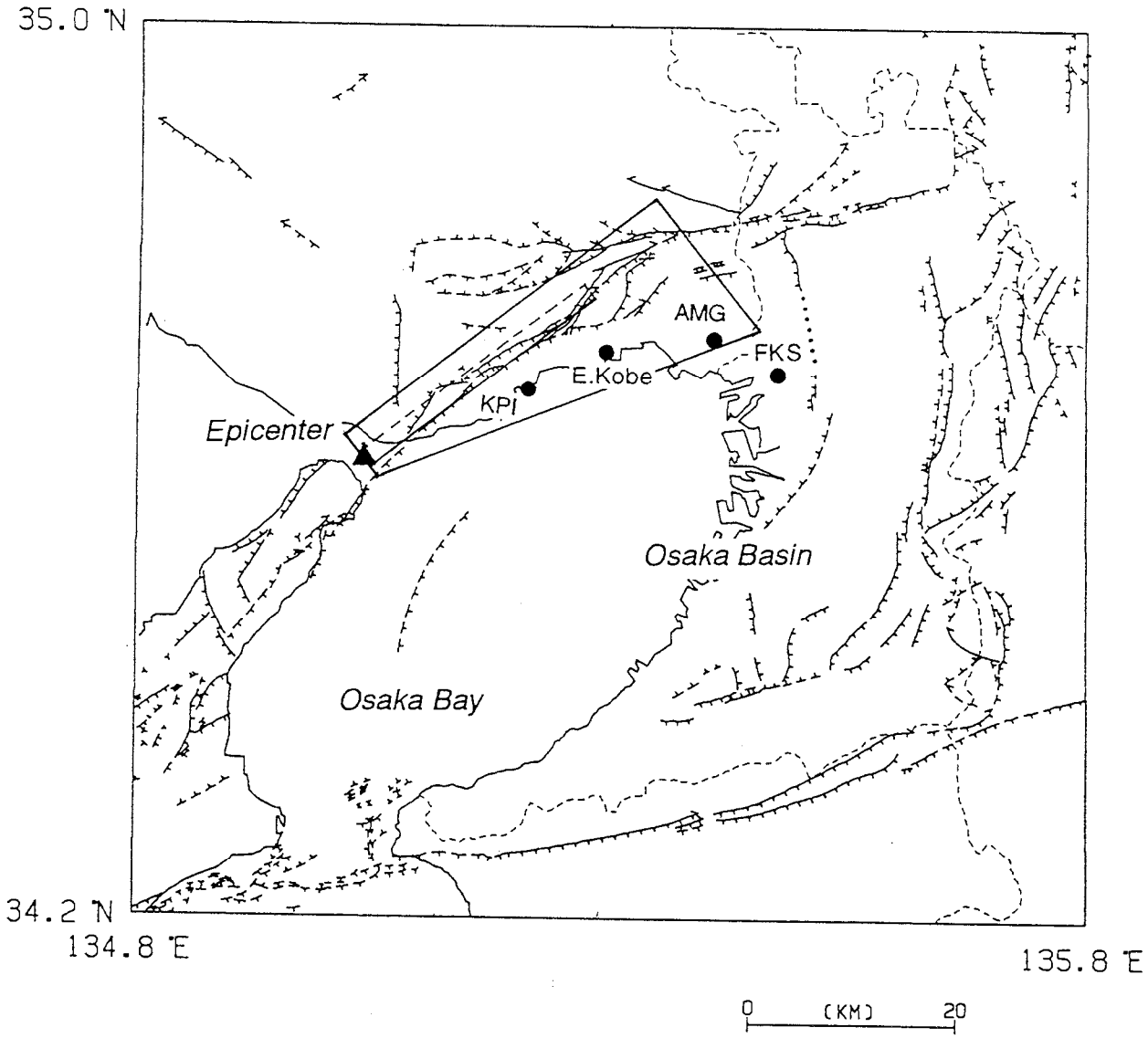

Figure 1. Map showing four strong motion stations (solid circle), epicenter (solid triangle) and active fault(——). The surface projection of fault model used in the numerical simulation is also plotted. The numerical modeling area is enclosed with trapezoid.

the model does not cover to the whole Osaka basin, common characteristics can be pointed out between the simulation and the observation.

OBSERVED GROUND MOTION

1. Characteristics of the recorded ground motion

The Osaka basin, as shown in Fig. 1, is bordered with active faults. The shape of the basin is elliptical with axis lengths of about 70 km by 30 km. The maximum thickness of the sediment layer is about 2.5 km at the middle of the basin. Because of its shape and impedance ratio, basin-induced surface waves are often observed in the basin[1].

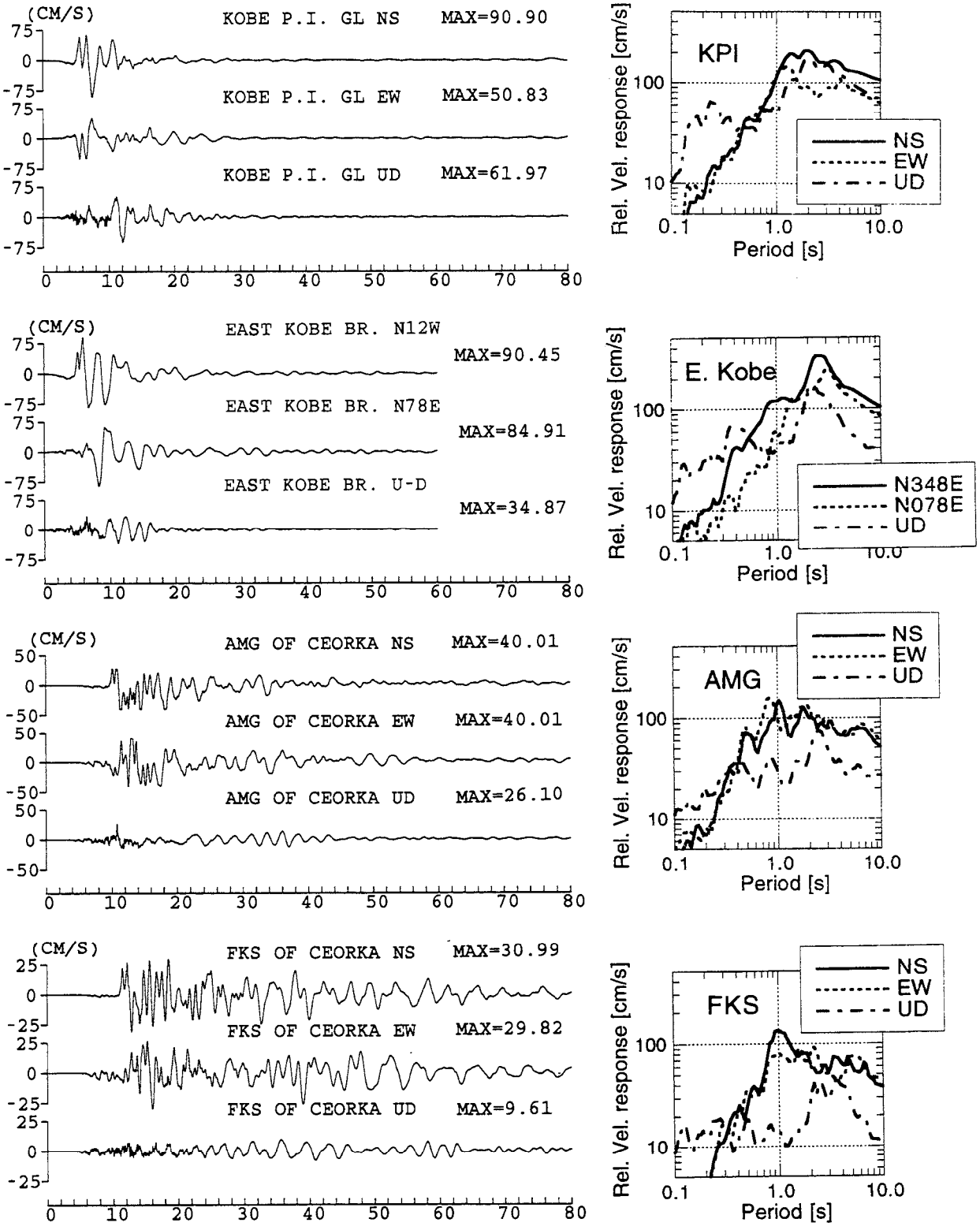

Figure 2. Velocity ground motions during 1995 Hyogo-ken Nanbu earthquake and relative velocity response spectra calculated from the ground motion at 4 sites, namely Kobe Port Island (KPI), East Kobe Bridge (E. Kobe), Amagasaki (AMG) and Fukushima (FKS). At AMG and FKS velocity type strong motion seismograms are installed. Horizontal component of Amagasaki are clipped. Start time of each time trace is aligned at 05:46:55.00, except E. Kobe. Response spectra are calculated with damping factor of 5%.

Fig. 2 shows ground motions observed at four sites and their velocity response spectra. Locations of the strong motion observation sites and the epicenter of the 1995 Hyogo-ken Nanbu earthquake are plotted in Fig. 1. Kobe port island (KPI) and East Kobe bridge (E. Kobe) are near-source sites while Amagasaki (AMG) and Fukushima (FKS) are located at 35 - 40 km distant sites from the epicenter. From Fig. 2, followings are pointed out.

1. In the near-source region, duration of intense ground motion was about 10 - 20 seconds, while at AMG and FKS, the duration was elongated to 40 to 50 seconds.
2. In the near-source region, waveforms are as simple as pulses, while at AMG and FKS, they are more complex.
3. The amplitude of vertical component at KPI is over 60 cm/s. The pulse of the vertical component appeared 6 sec. after S wave arrival.
4. Even in the near-source region, predominant period of the horizontal component differs from site to site. For example, at KPI, it is around 1.2 sec., while, at E. Kobe, 3 sec. The maximum response value is also different.
5. Velocity response of the horizontal component in the near-source region is over 100 cm/s in the range of 1 to 10 sec. While, at FKS, it is about 60 cm/s in the range of 1 to 7 sec.
6. There are peaks at around 5 sec. in both AMG and FKS spectra, but there is no peak in KPI and E. Kobe spectra at the period.
7. Each spectrum of the vertical component has a peak within 1 to 3 seconds. In this period range, response value of vertical component is almost the same as that of horizontal component.

2. Array analysis using observed ground motion

To identify the direction and velocity of wave propagation, an array analysis is essential. Several sets of strong motion records were obtained around FKS as shown in Fig.3. Up-down component records obtained at each station were used in this analysis because of its simplicity in comparison with horizontal one.

Semblance value[4] Sm was calculated to estimate the propagation direction and velocity, after adopting band-pass filtering. The semblance value Sm is defined as

$$Sm(\tau,\mathbf{S}) = \frac{\sum_{j=K_i-N/2}^{K_i+N/2} \left|\sum_{i=1}^{M} f_{i,j}\right|}{M \sum_{j=K_i-N/2}^{K_i+N/2} \sum_{i=1}^{M} |f_{i,j}|^2} \qquad (1)$$

where, M is the number of array stations, N is the length of a time window, $f_{i,j}$ is a band-pass filtered velocity seismograms of the j-th time sample at the i-th station. K_i is the number corresponding to the time $T=\tau+\mathbf{S}X_i$, where X_i is the horizontal position vector of the i-th station, $\mathbf{S}$ is a horizontal slowness vector, and $\mathbf{S}X_i$ is a inner product of the two vectors. τ is the center time of a time window at the origin. With the FKS station selected as the origin, Sm was repeatedly calculated for various values of $\mathbf{S}$ within a time window to find the maximum value of Sm, Sm_{max}. The direction and the velocity of wave propagation within the time window are then obtained from the value of $\mathbf{S}$ for Sm_{max}.

Fig. 4 shows results calculated for four periods; that is 2.50, 2.86, 3.57 and 4.55 sec. Fig. 4 indicates that the wave associated with the periods came from about N30W and that the longer period shows the larger velocity. It should be noted that, at FKS, the source fault is not located in the N30W direction.

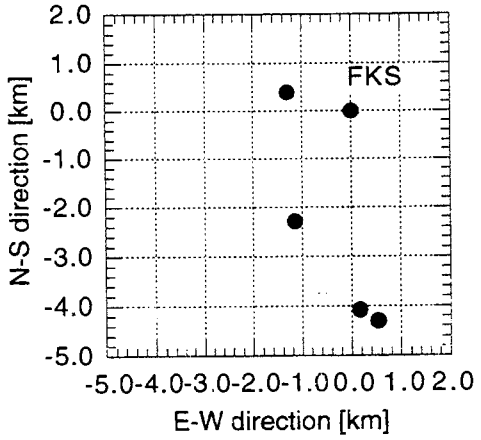

Figure 3. Relative location of the strong motion stations around FKS used in the array analysis.

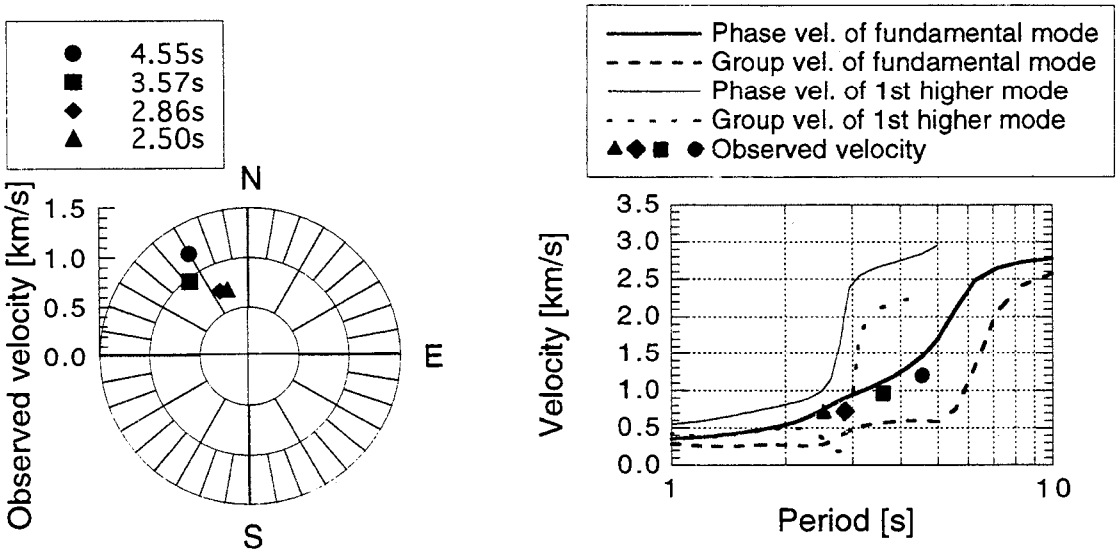

(a) Propagation direction and velocity

(b) Observed velocity and theoretical dispersion curve

Figure 4. Result of array analysis around FKS site using up-down component. The semblance value is used to determine the propagation direction and velocity. In the figure, numbers are center periods of adopted band pass filter.

Discussion by 3-D numerical simulation

1. Model

As observed records are limited in number, 3-D numerical simulation is desirable for the present purpose to investigate characteristics of wave propagation related to the long period ground motion. In this study, simulation using 3-D boundary element method (BEM)[5] is used for further discussion.

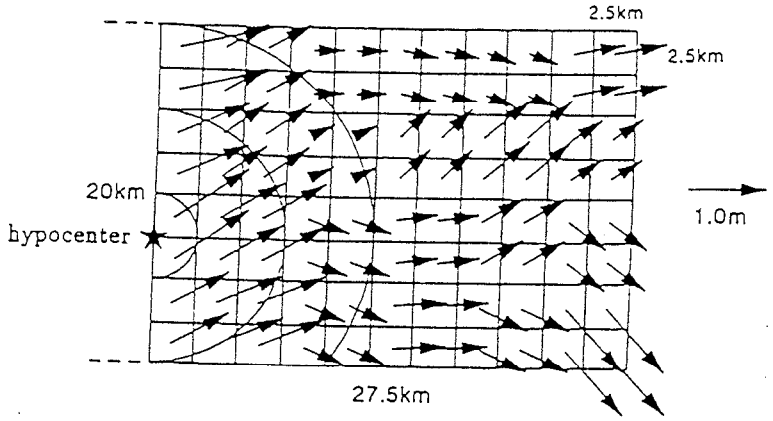

(a) Total slip vector distribution [Ide et al. (1996)].

Subsurface: v_P=2.5km/s, v_S=1.0km/s, ρ=2.1t/m^3, 1726nodes
Basement: v_P=5.4km/s, v_S=3.2km/s, ρ=2.7t/m^3, 513nodes

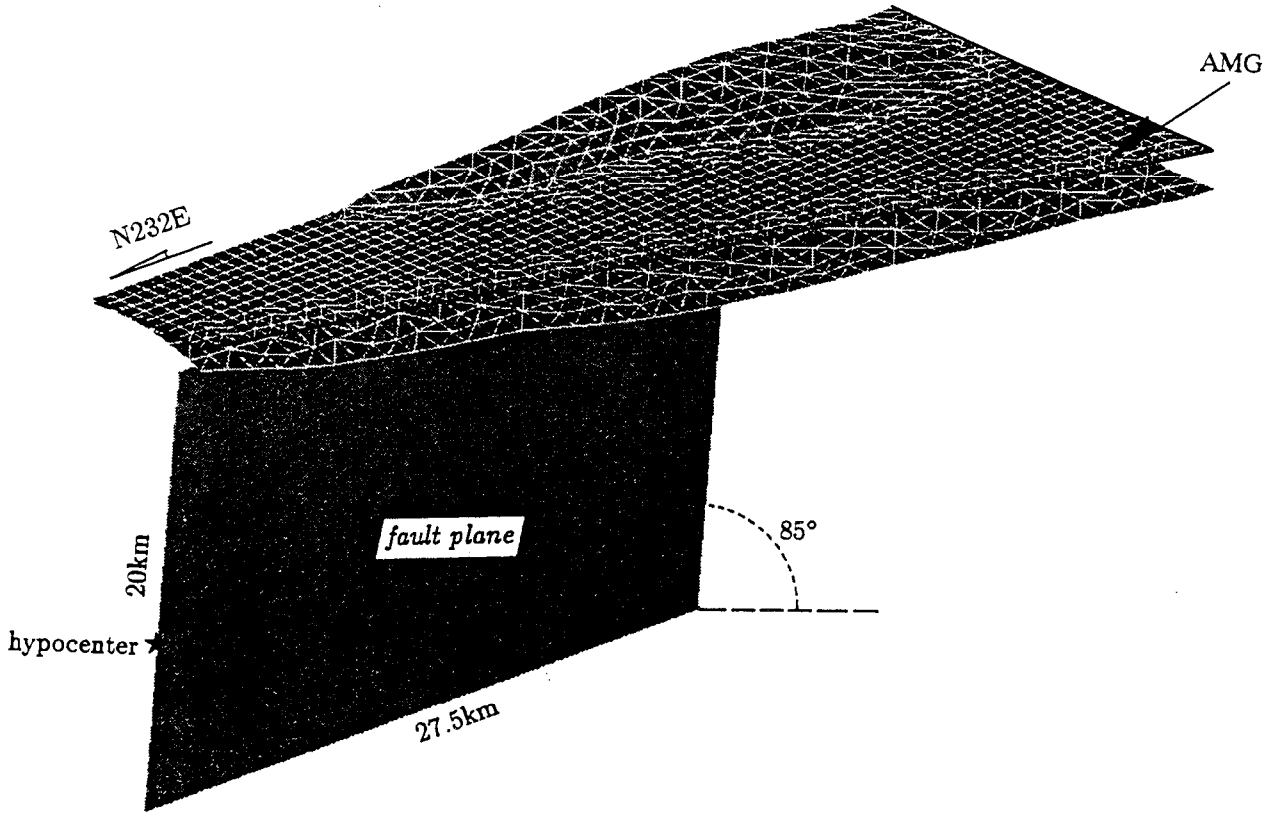

(b) 3D view of numerical model. Vp, Vs and ρ denote P and S wave velocities and mass density, respectively.

Figure 5. Numerical model used in the 3-D BEM simulation.

In Fig. 5, a numerical model used in the 3-D simulation is shown. In the simulation, a fault model presented by Ide et al.[6] was used. As their original source time function was complicated, is was simplified to a ramp function with rise time of 1 sec. in the simulation. The fault rupture was assumed to be propagated in all directions along the fault plane from the hypocenter at a constant velocity of 3 km/s. As the rise time was 1 sec., high frequency components are not produced by the faulting.

The ground is modeled by a single sedimentary layer overlying a semi-infinite basement rock. Properties[3,7] of both media shown in Fig. 5. No material damping was considered and grid spacing for the subsurface and the basement are about 0.6 km for sediment and 1 km for the rock, respectively. The simulation took us about 56 hrs. by using a CRAY C916/12256 super computer.

2. Check of simulation

The simulated motion was compared with the observed one at AMG, as shown in Fig. 6. In the time histories, initial S wave phase in the simulated motion looks similar to the observation. As for horizontal motion, the simulated motion agrees well with the observed motion in terms of the envelope shape. As for vertical component, dispersive motion which can be seen in the observation was well reproduced by the simulation. In spectra, both amplitudes and peak periods of simulated motions appear in a fairly good agreement with the observation for the period above 1 sec. Fig. 6 demonstrates the adaptability and limitation of the present simulation.

3. Array analysis using synthetic ground motion

In earlier section, the motion observed around FKS was found to come from N30W direction. In this section, instead of FKS, the AMG site was selected to investigate the propagation direction, because FKS is not covered by the numerical model. The AMG site is located at about 7 km north-west from the FKS. Ten sites around AMG spacing at about 1 km were selected for the array analysis, using up-down and fault parallel components with a result shown in Fig. 7. The semblance value was also calculated to estimate the propagation direction and velocity. Fig. 7 shows that both the up-down component and the fault parallel component motions were propagated in the same direction, that is, N40W. Phase velocities of the simulated waves are coincident with the theoretical phase velocities of Rayleigh and Love waves. Thus, the vertical and fault parallel components are estimated to be Rayleigh and Love waves, respectively, and these surface waves around AMG site are said to be much affected by 3-D topography of the Osaka basin. Hence the long period motion can called the basin-induced surface waves.

Although the basin-induced surface waves have often been observed in not only the Osaka basin but also Kanto plain, their amplitudes were much smaller that those observed during the 1995 Hyogo-ken Nanbu earthquake. The above mentioned characteristics such as the direction and the velocity of the waves are consistent with the findings in the previous studies. Accordingly, one of the most important findings of this study lies in the agreement of the simulation with the observation in the amplitude of the long period motion. Although the 3-D numerical simulation seems very promising, it should be improved to reduce time and job for practical application.

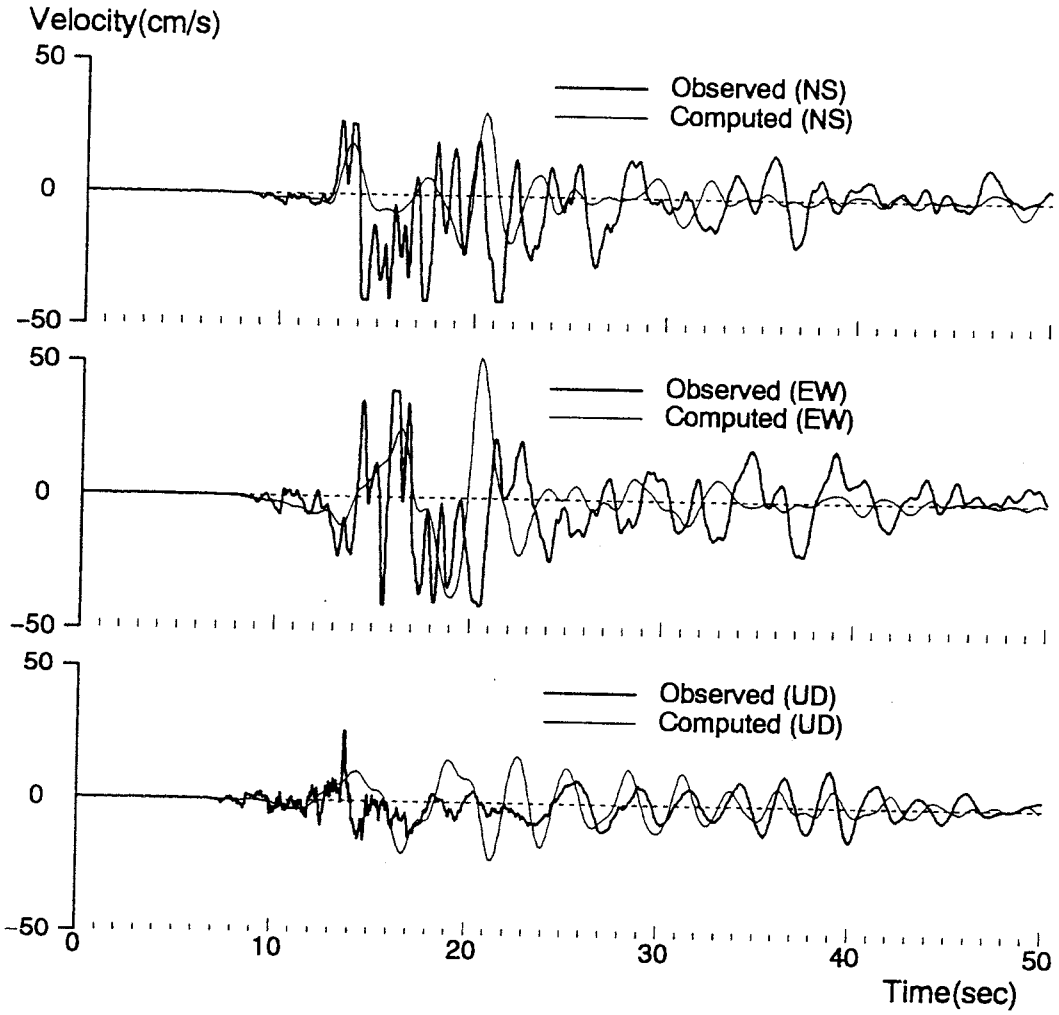

(a) Velocity traces

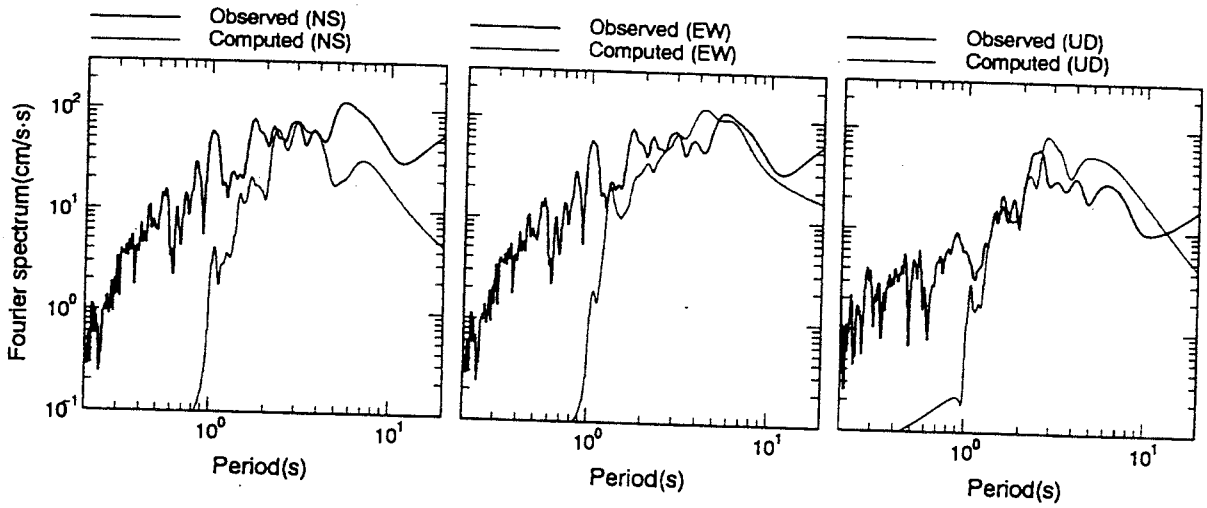

(b) Fourier spectra

Figure 6. Comparison of the synthetic ground motion with the observation at AMG

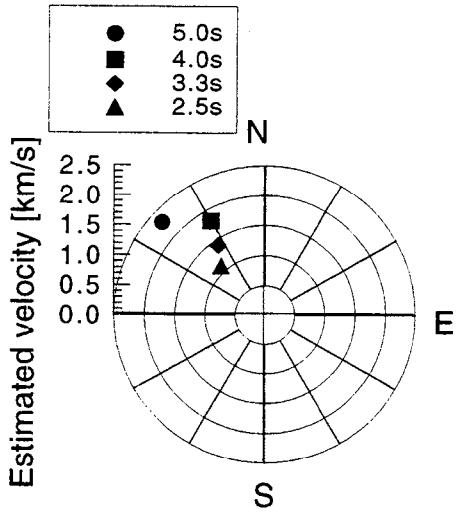

(a) Propagation direction and velocity of up-down component motion

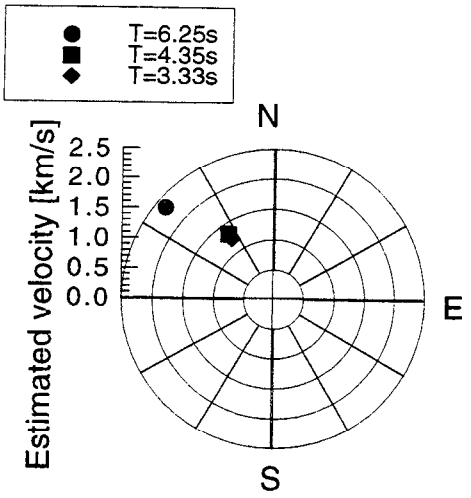

(b) Propagation direction and velocity of fault parallel component motion

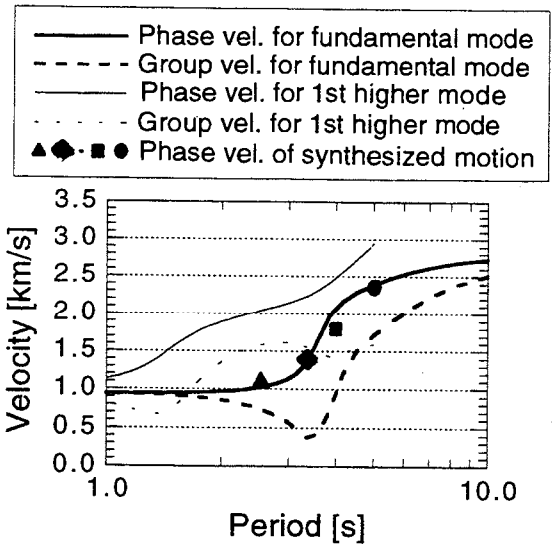

(c) Phase velocity of synthetic up-down component and theoretical dispersion curve of Rayleigh wave

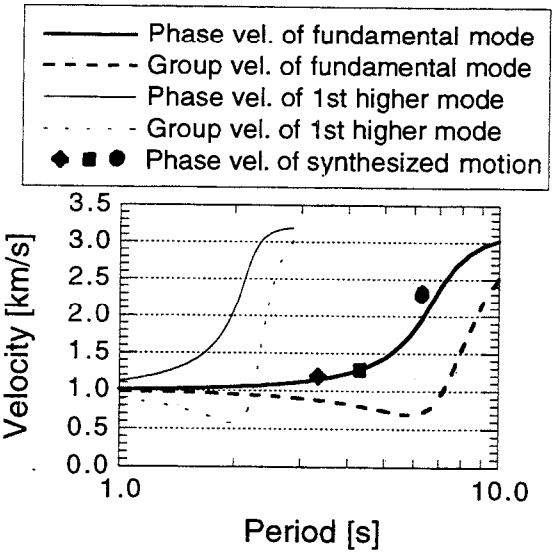

(d) Phase velocity of synthetic fault parallel component and theoretical dispersion curve of Love wave

Figure 7. Result of array analysis for synthetic ground motion around AMG site.

Conclusion

Conclusions drawn from the present study are the followings.

1. The long period motion observed at several stations can be regarded as surface waves propagated in the direction different from the radial one originating from the epicenter.

2. Thus, the long period motion is different from shorter period motion in some characteristics such as arrival time and wave propagation path, which are mainly dependent on 3-D configuration of the surface layer.

3. The 3-D numerical simulation has proved to show a good agreement with the observation, provided that two models are given to a satisfactory level of accuracy. One is a model of the seismic fault, and the other is the model of the ground structure to the depth of seismic bedrock.

4. At present, the 3-D simulation takes us much time and cost. For practical purpose, it seems necessary to develop a reasonable method for the simulation or some other substitutes.

Acknowledgment

Strong ground motion records in this study were provided by the CEORKA, the committee of earthquake observations and research in the Kansai Area. The authors would like to express their thanks to CEORKA and its member.

REFERENCES

1. Hatayama, K., K. Matsunami, T. Iwata and K. Irikura: Basin-induced Love waves in the eastern part of the Osaka basin, *J. Phys., Earth.*, **43**, 131-155, 1995.
2. Harkrider, D. G.: Surface waves in multilayered elastic media I. Rayleigh and Love waves from buried source in a multilayered elastic half-space, *Bull. Seism. Soc. Am.*, **54**, 627-679, 1964.
3. Kagawa, T., S. Sawada, Y. Iwasaki, A. Nanjo: On the modelization of deep sedimentary structure beneath the Osaka plain (in Japanese), *Proc. 22nd JSCE Earthq. Eng. Sympo.*, 199-202, 1993 .
4. Neidell, N. S. and M. T. Taner: Semblance and other coherency measures for multichannel data, *Geophysics*, **36**, 482-497, 1971.
5. Kataoka, Shojiro: Simulation of the 1995 Hyogo-ken Nanbu earthquake by a 3-D BEM (in Japanese), *Technical report, Department of civil engineering, Tokyo Institute of Technology*, **54**, 1996.
6. Ide, S., M. Takeo, Y. Yoshida: Source process of the 1995 Kobe earthquake: determination of spacio-temporal slip distribution by Bayesian modeling, *Bull. Seism. Soc. Am.*, **86**, 547-566, 1996.
7. Nakagawa, K., K. Shiono, N. Inoue, M. Sano: Geological characteristics and problems in and around Osaka basin as a basis for assessment of seismic hazards, *Special issue of Soils and Foundations*, 15-28, 1996.

SITE LIQUEFACTION AND REMEDIATION

Mourad Zeghal
Impact Forecasting, L.L.C., Chicago, IL 60606

Korhan Adalier
Civil Engineering Department, Rensselaer Polytechnic Institute, Troy, NY 12180

Ahmed-W. Elgamal
Civil Engng. and Engng. Mechanics Dept., Columbia University, New York, NY 10027

ABSTRACT

Two free-field downhole array seismic records are now available to document the underlying site liquefaction response mechanisms. Records of acceleration and pore pressure at the Wildlife Refuge (Imperial County, CA, USA) reflected liquefaction during the 1987 Superstition Hills earthquake. In 1995, liquefaction at Port Island (Kobe, Japan) was documented by a four accelerometer downhole array during the Hyogoken-Nanbu earthquake. Using these records, the associated shear stress-strain response is identified and employed as a guideline for development of liquefaction countermeasure techniques. A number of these techniques are discussed in view of the identified response mechanisms.

INTRODUCTION

Major seismic events such as the 1964 Niigata, the 1989 Loma Prieta, and the 1995 Kobe earthquakes, continue to demonstrate the damaging effects of liquefaction-induced loss of soil strength and associated lateral spreading (Seed 1966, Ishihara *et al.* 1987, Seed *et al.* 1990, Soils and Foundations 1996). Experimental laboratory research on soil liquefaction has provided valuable insight concerning excess pore-pressure buildup in saturated loose granular soils (National Research Council 1985). However, for engineering applications, there remains a need to further understand and identify the mechanisms of seismically induced soil deformation due to liquefaction, and associated stiffness and strength degradation.

In-situ seismic records of site liquefaction are scarce. Currently, downhole seismic records are only available for: (1) the Wildlife Refuge site (Imperial County, CA) during the 1987 Superstition Hills earthquake (accelerations and pore-pressures), and (2) the Port Island site (Kobe, Japan) during the 1995 Hyogoken-Nanbu earthquake. Such downhole acceleration and excess-pore-pressure records provide direct information on the mechanisms of site liquefaction; and associated stiffness degradation and lateral spreading. This valuable information is of paramount importance to the development of liquefaction countermeasure techniques.

A brief summary of the Wildlife Refuge and Port Island case histories is presented below. In view of the observed mechanisms, a number of liquefaction countermeasures are briefly discussed.

SHEAR STRESS-STRAIN RESPONSE

A simple identification procedure, proposed earlier in basic form for shake-table studies (Koga and Matsuo 1990), was developed and used to study the downhole earthquake response at Lotung (Zeghal and Elgamal 1993, Zeghal *et al.* 1995, Elgamal *et al.* 1996a). Using a shear beam model to

describe site seismic lateral response, shear stresses at levels z_i and $(z_{i-1}+z_i)/2$ may be evaluated as follows:

$$\tau_i(t) = \tau_{i-1}(t) + \rho_{i-1}\frac{\ddot{u}_{i-1}+\ddot{u}_i}{2}\Delta z_{i-1}, \quad i = 2,3,\cdots \tag{1}$$

$$\tau_{i-1/2}(t) = \tau_{i-1}(t) + \rho_{i-1}\frac{3\ddot{u}_{i-1}+\ddot{u}_i}{8}\Delta z_{i-1}, \quad i = 2,3,\cdots \tag{2}$$

in which subscripts i and $i-1/2$ refer to levels z_i (of the i^{th} accelerometer) and $(z_{i-1}+z_i)/2$ (halfway between accelerometers i and and $(i-1)$) respectively, $\tau_i(t) = \tau(z_i,t)$ is shear stress at level z_i, $\tau_1 = \tau(0,t) = 0$ at the stress-free ground surface, ρ_{i-1} = mass density of the z_{i-1} to z_i soil layer, $\ddot{u}_i = \ddot{u}(z_i,t)$ is absolute acceleration at level z_i, and Δz_i is spacing interval between accelerometers. These stress estimates (Eqs. 1 and 2) are second order accurate. The corresponding second-order accurate shear strains may be expressed as:

$$\gamma_i(t) = \frac{1}{\Delta z_{i-1}+\Delta z_i}\left((u_{i+1}-u_i)\frac{\Delta z_{i-1}}{\Delta z_i} + (u_i-u_{i-1})\frac{\Delta z_i}{\Delta z_{i-1}}\right), \quad i = 2,3,\cdots \tag{3}$$

$$\gamma_{i-1/2}(t) = \frac{u_i-u_{i-1}}{\Delta z_{i-1}}, \quad i = 2,3,\cdots \tag{4}$$

in which $u_i = u(z_i,t)$ is absolute displacement (evaluated through double integration of the recorded acceleration history $\ddot{u}(z_i,t)$).

WILDLIFE REFUGE, CALIFORNIA USA

The Wildlife Refuge site is located on the west side of the Alamo river, Imperial County in Southern California. Evidence of liquefaction was observed at or near the site following the 1930, 1950, 1957, 1979, and 1981 Imperial Valley (Youd and Wieczorek 1984) earthquakes. These observations triggered an interest in Wildlife which in an insightful effort, was instrumented in 1982 (Fig. 1, Youd and Wieczorek 1984) by the United States Geological Survey (USGS). On November 24, 1987, the Wildlife site was shaken by the Superstition Hills earthquake ($M_W = 6.6$), causing a sharp increase in recorded pore-water pressure (Holzer *et al.* 1989). In addition, subsequent field investigations showed evidence of site liquefaction and ground fissures. Fig. 2 depicts the NS and EW components of the recorded accelerations at ground surface and 7.5 m depth; and the associated excess pore-water pressure measured at 2.9 m depth (piezometer P5, Fig. 1). As shown in Fig. 2, the surface records displayed peculiar acceleration spikes (Holzer *et al.* 1989) associated with simultaneous instants of pore-pressure drop.

Fig. 3 displays the shear stress-strain history during the Superstition Hills earthquake evaluated using Eqs. 1-4 (Zeghal and Elgamal 1994, Zeghal *et al.* 1996). A dramatic loss of soil stiffness due to liquefaction is depicted by this stress-strain history. This was further manifested by the effective stress histories at 2.9 m depth (location of piezometer P5, Fig. 1), evaluated from the acceleration and excess pore pressure records of Fig. 2. Shear stress versus effective vertical stress ($\sigma'_v = \sigma_v - p$, where p is excess pore pressure measured by P5, and σ_v is total vertical stress at P5) may be interpreted as an effective stress path.

During the initial phase (stage 1 [0 s to 13.7 s], Fig. 2), the site showed no evidence of significant stiffness degradation (Fig. 3); and no appreciable rise in pore pressure was recorded by piezometer P5 (Fig. 2). During the strong shaking phase (stage 2 [13.7 s to 20.6 s], Figs. 2 and 3), the site experienced a clear and gradual stiffness degradation associated with a sharp increase in pore water

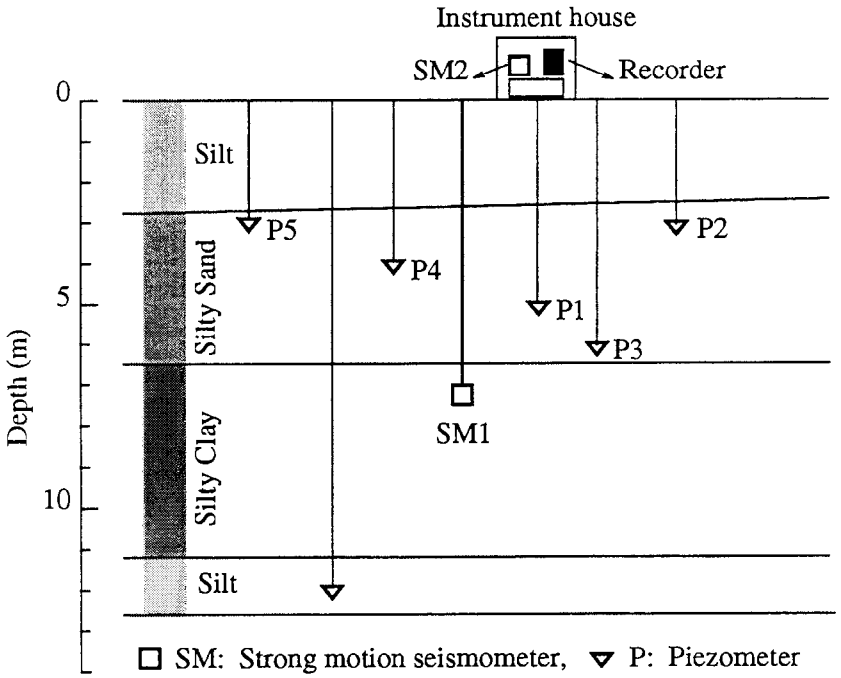

Figure 1: Cross-section and instrumentation at the Wildlife Refuge site (after Bennett *et al.* 1984).

pressure. Soil stiffness and yield strength continued to decrease during stages 3 and 4 ([20.6 s to 96.0 s], Figs. 2 and 3). Cycles of large shear strain were developed during these stages, with a peak strain of 1.5 % at 36 s (Fig. 3). During stages 2-4, site response was marked by shear stress-strain hardening at large strains (Fig. 3). This hardening was more pronounced in the negative direction where acceleration spikes occurred along with instantaneous pore pressure drops (Fig. 2). Such asymmetric hardening was most probably associated with the presence of a nearby free slope towards which permanent ground deformations were observed (Holzer *et al.* 1989). At low effective confining pressures (high excess pore pressures, stage 4), the effective stress-path (Fig. 3) clearly exhibited a reversal of behavior from contractive to dilative as the line of phase transformation was approached (National Research Council 1985).

Thus, this case history clearly showed (for the first time), an in-situ mechanism of shear stress-strain hardening at large strain excursions during liquefaction. Such a mechanism has been observed in a number of experimental studies (e.g., Koga and Matsuo 1990, Arulmoli *et al.* 1992, Taboada and Dobry 1993), and is a consequence of soil dilation at large strain excursions, which results in associated instantaneous pore-pressure drops (Vucetic and Dobry 1988).

PORT ISLAND, KOBE JAPAN

Port Island is a reclaimed island located on the west-south side of Kobe, Japan. In the phase completed by 1981, 436 ha were reclaimed by bottom-dumping from barges (Nakakita and Watanabe 1981). Soil in the artificial reclaimed layer (O'Rourke 1995, Sitar 1995) consisted of decomposed weathered granite fill (Masa soil mined from the nearby Rokko mountains). A downhole accelerometer array was installed at the North-West corner of Port Island (Fig. 4) in August 1991 (Iwasaki 1995a). The array consisted of triaxial accelerometers located at the surface, 16 m, 32 m, and 83 m depths. All instruments were linked to a common triggering mechanism, and hence the recorded

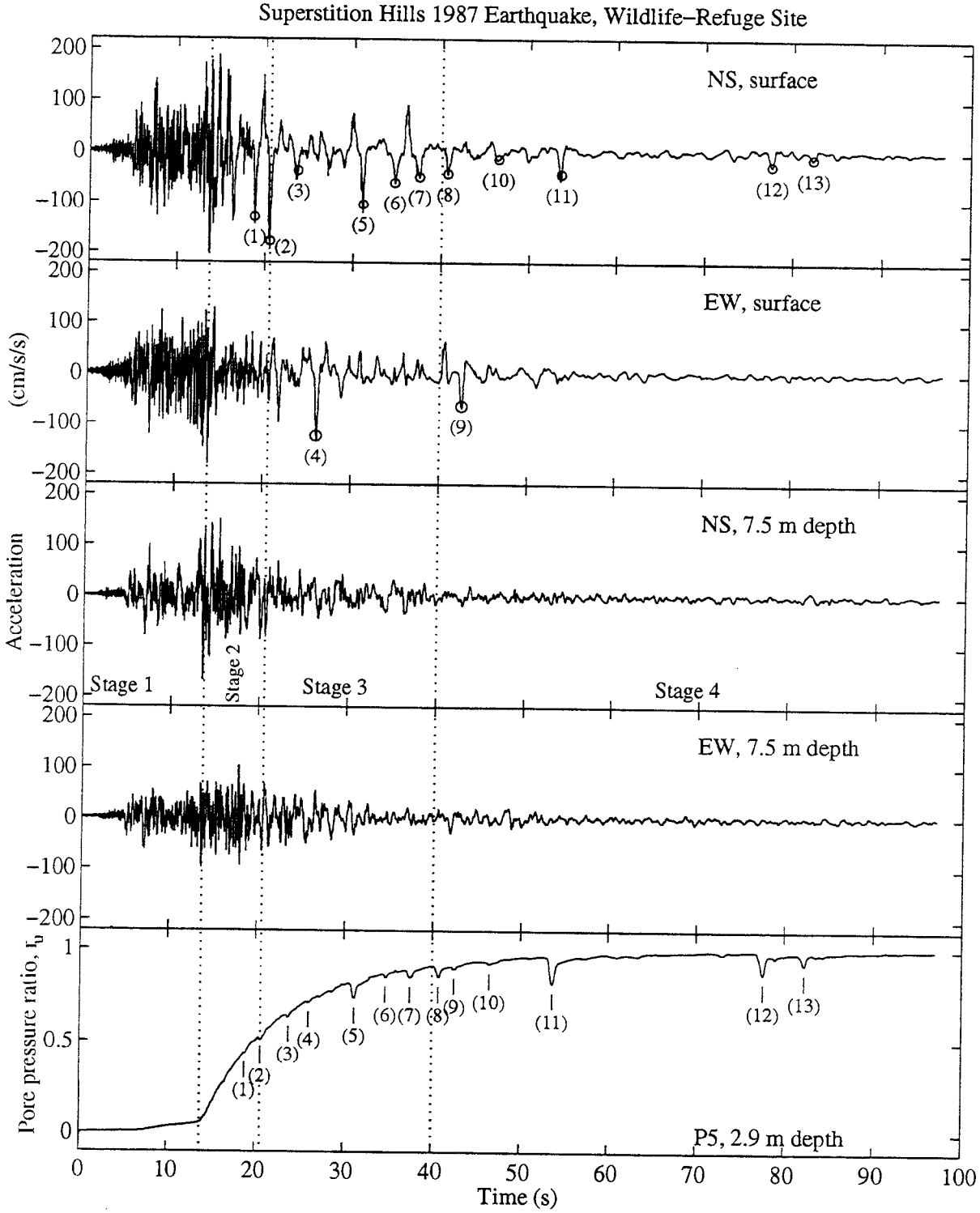

Figure 2: Wildlife Refuge site NS and EW surface and downhole (at 7.5 m depth) accelerations, and associated pore water pressure (at 2.9 m depth) during the Superstition Hills 1987 earthquake.

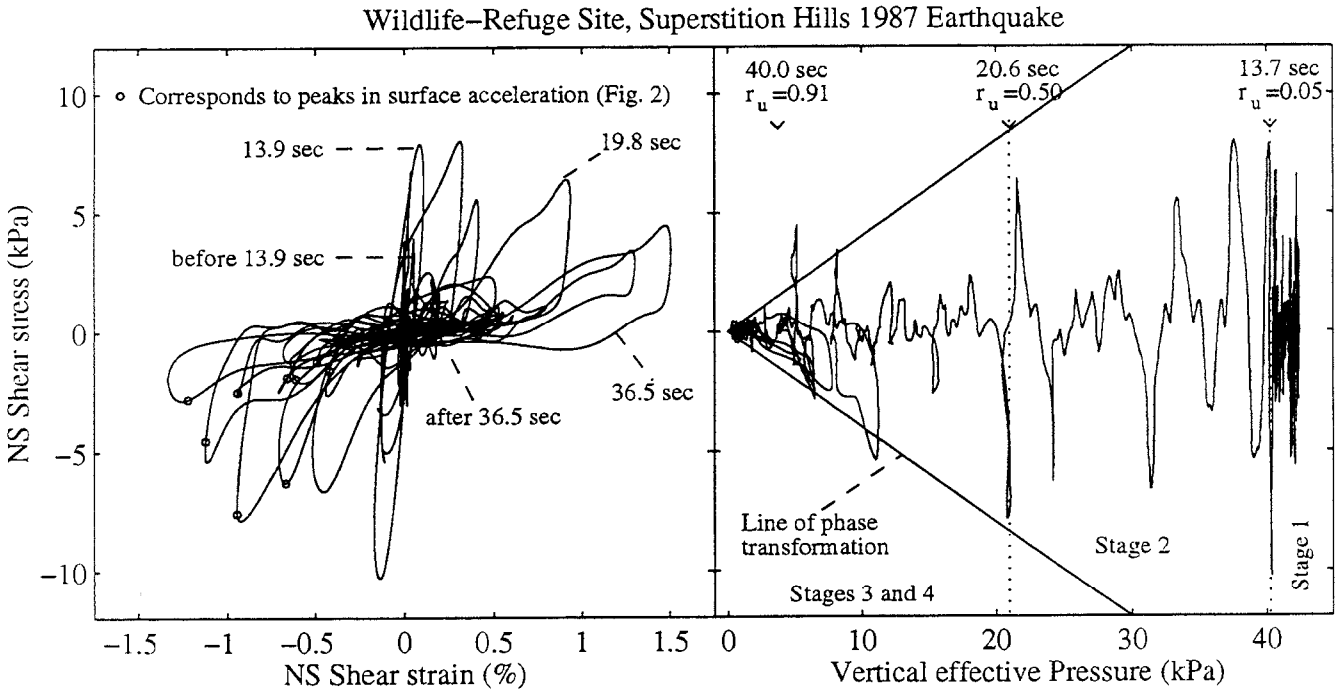

Figure 3: Wildlife Refuge site NS shear stress-strain and effective stress-path histories during the Superstition Hills 1987 earthquake (Zeghal and Elgamal 1994).

earthquake data were synchronized.

As shown in Fig. 4, the downhole array site consists of: (1) an artificial, reclaimed, loose surface layer down to about 19 m depth, (2) an alluvial clay layer between 19 m and 27 m depth, (3) sand and sand with gravel strata interlayered with clay between 27 and 61 m depth, (4) a diluvial clay layer between 61 m and 82 m depth, and (5) sand with gravel layers interlayered with clay starting at about 82 m depth. The water table was located at 4 m depth approximately. A Standard Penetration Test (SPT) and a geophysical shear wave velocity profile of the soil strata around the downhole array are also shown in Fig. 4 (Iwasaki 1995a, b). In the upper 20 m layer (Fig. 4), low Standard Penetration Test (SPT) blow counts prevailed (average uncorrected N-values of about 6 blows/ft). Such low values in a granular fill are indicative of high liquefaction susceptibility (Seed *et al.* 1983).

Using the recorded downhole accelerations (Fig. 5) and Eqs. 1-4, the shear stress-strain response was evaluated (Elgamal *et al.* 1996b). Selected representative cycles of this response are shown in Fig. 6. Two remarkably different response patterns were exhibited at the site. Below 32m depth, the shear stress-strain histories showed an essentially linear soil response, with no appreciable reduction in soil stiffness. On the other hand, at shallow depths, the stress-strain histories indicated: (1) a noticeable reduction in stiffness with a slight shear strain hardening at elevation 24m (Fig. 6), and (2) an abrupt sharp loss of stiffness and reduction of yield strength near the surface at 8m depth.

MECHANISMS OF SITE LIQUEFACTION

The Wildlife Refuge and Port Island sites exhibited two remarkably different response mechanisms. In first approximation, the responses may be contrasted along the lines presented in Table 1.

Following liquefaction, the Port Island site response was marked by large strains and small stresses,

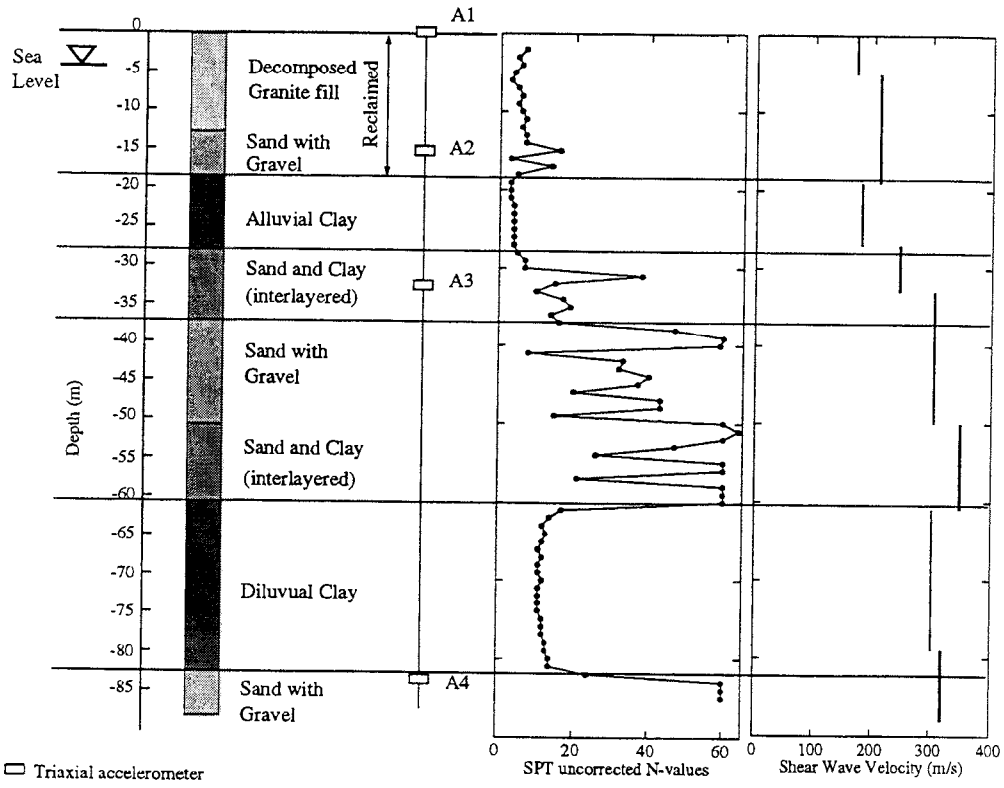

Figure 4: Soil profile and instrumentation at the Port Island site (after Iwasaki 1995a).

while at the Wildlife site the response was associated with a regain in shear stiffness and strength at large strain excursions. This regain is due to a tendency for dilation at large strains during liquefaction (cyclic mobility), and is of importance in restricting the extent of accumulated lateral cyclic deformation. This phonemenon is an essential ingredient in liquefaction remediation techniques involving densification, as mentioned below.

LIQUEFACTION COUNTERMEASURES

The soil improvement techniques discussed below are divided into four main categories: (1) densification, (2) drainage, (3) solidification, and (4) inclusions (Adalier 1996). A brief description of each with a number of relevant references follows. In view of the liquefaction mechanisms contrasted above, the potential beneficial outcomes of these techniques for the Wildlife Refuge and Port Island sites are described in Table 2.

Densification Methods

Densification increases liquefaction resistance due to the associated decrease in void ratio or increase in relative density, and mean effective stress (increase in lateral stresses). Densification can be achieved using several methods such as vibro-compaction, vibro-replacement, deep dynamic compaction, deep blasting, compaction grouting, and displacement piles. A comprehensive description of these methods can be found in ASCE (1977), in a state-of-the-art paper by Mitchell (1981), and in Broms (1991). Densification of loose soils has been the most popular method of reducing earthquake related liquefaction potential. However, most densification techniques (e.g., vibro-densification) have limited application to existing structures because of settlement and damage concerns.

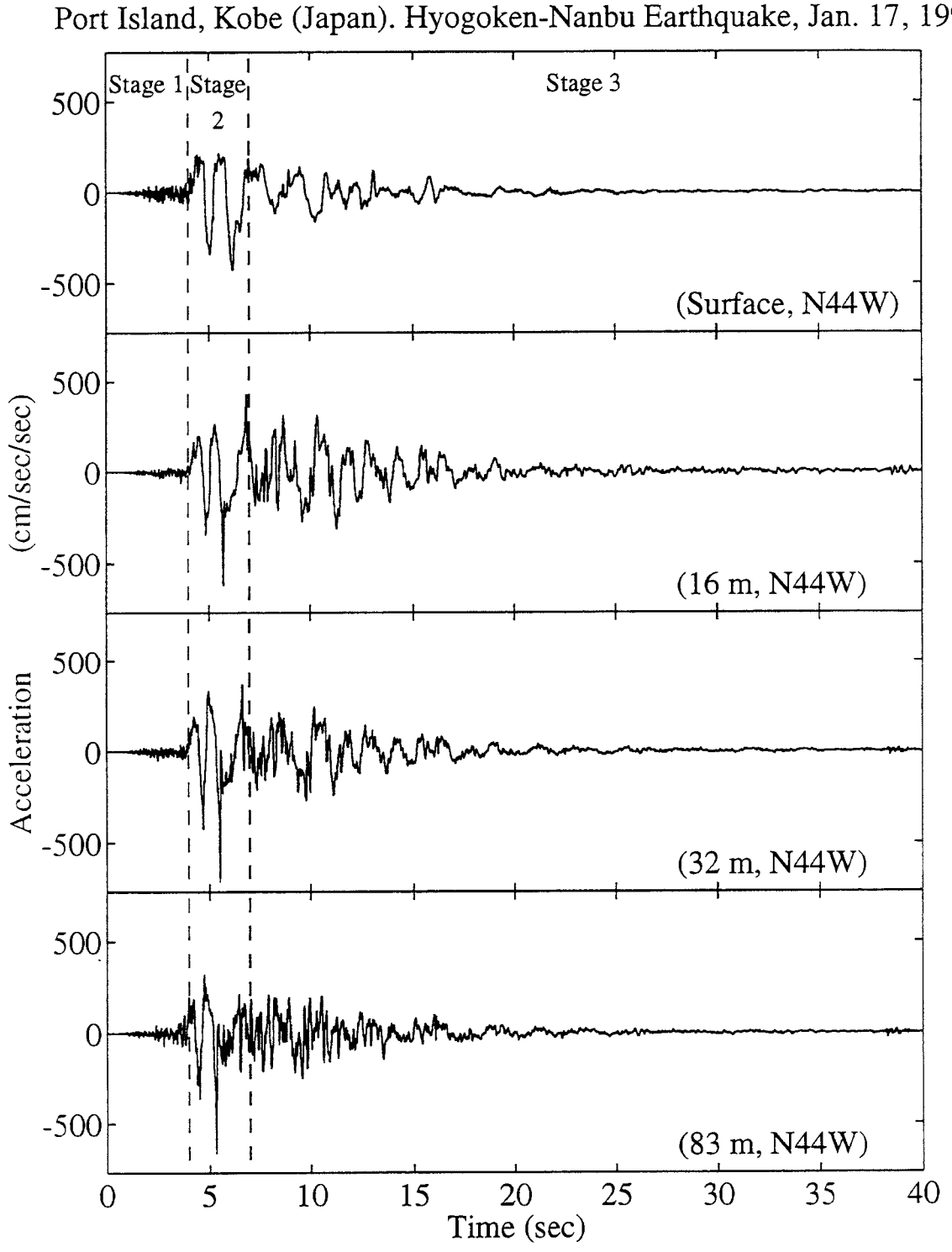

Figure 5: N44W accelerations at ground surface and downhole stations (at 16 m, 32 m and 83 m depths, after Iwasaki 1995a).

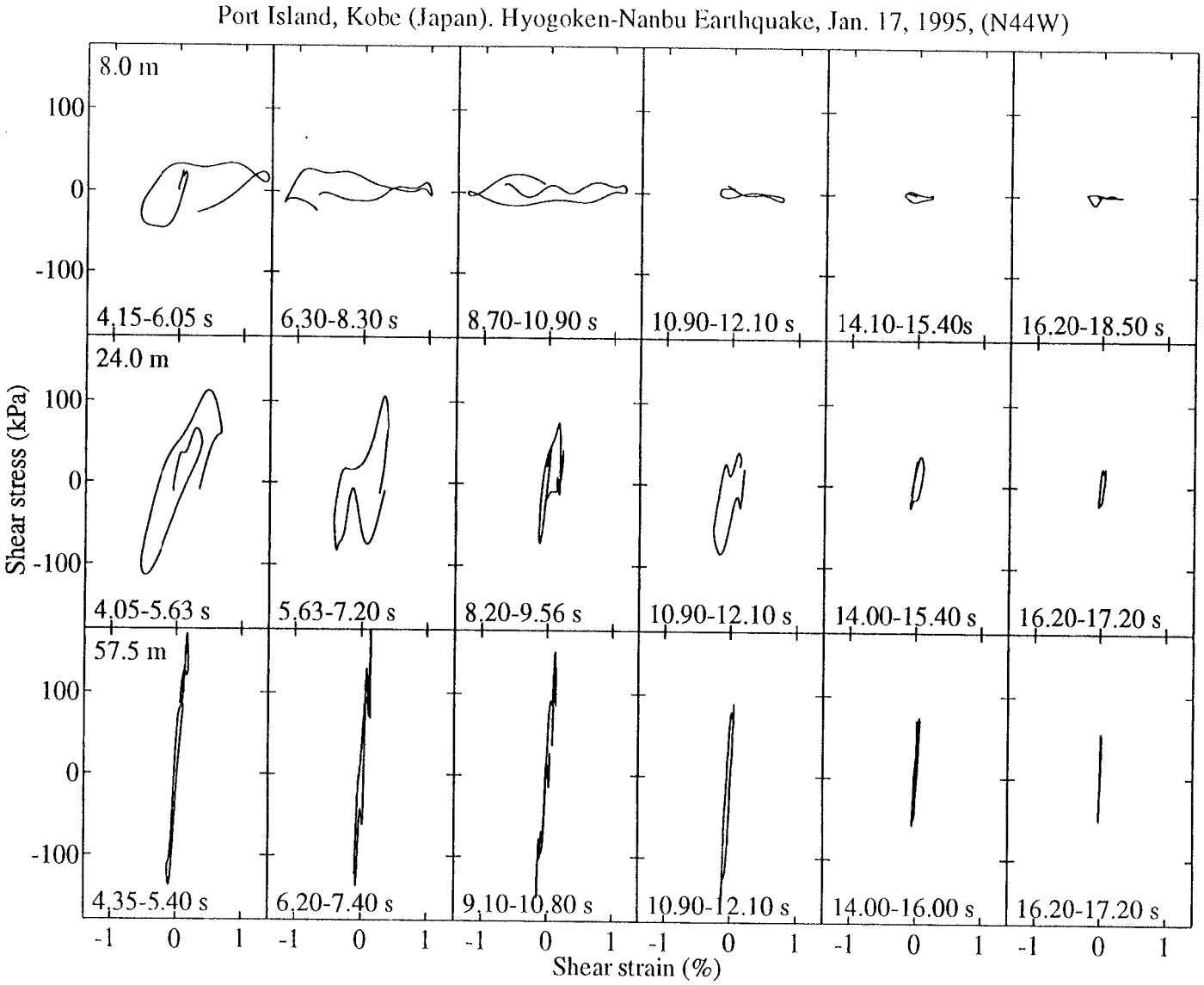

Figure 6: Selected N44W shear stress-strain cycles midway between accelerometers, at 8.0 m, 24.0 m and 57.5 m depths (Elgamal *et al.* 1996b).

Table 1: Contrast in Wildlife Refuge and Port Island response mechanisms.

Parameter	Wildlife Refuge site	Port Island site
Level of base accel. towards loss of stiffness	0.15 g	0.07 g
Duration of shaking leading to loss of stiffness	7 sec (13 sec to 20 sec)	2 sec (5 sec to 7 sec)
Peak input acc. and duration after liquefaction	0.06 g / 15 sec	0.2 g / 7 sec
Liquefied zone	within upper 7 m	within upper 16 m
Cyclic strains	1.5 %	1.5 %
Site condition	nearby slope	level
Downslope strains	> 1.5 %	—
Post-liquefaction shear mechanism	cyclic mobility	—
Duration of liquefied state	> 15 min. (Holzer *et al.* 1989)	> 4 min. (Elgamal *et al.* 1996b)
Vertical settlement	few cms (Holzer *et al.* 1989)	> 0.5m nearby (Soils and Foundations 1996)

Vibro-techniques: These methods involve driving a vibratory probe into the soil, and densifying the soil surrounding the probe during driving and withdrawal. Gravel or crushed stones are introduced into the hole created by a vibro-probe, and compacted (stone column technique or vibro-replacement). Mitchell (1970, 1981), Welsh (1987), Moseley (1993), Xanthakos *et al.* (1994), and Adalier (1996) provide useful information about vibro densification techniques.

Deep Dynamic Compaction: This technique involves repeated dropping of heavy weights from heights of up to 40 m onto the ground surface. Shock waves created by the impact densify the soil. Deep dynamic compaction can improve all soils except for cohesive ones below the groundwater table. The main limitation of this method is its potential to damage surrounding structures due to large vibrations, noise, and flying debris. Leonards *et al.* (1980), Lukas (1986), and Slocombe (1993) comprehensively discuss the general uses of this method. Important theoretical aspects are reported by Menard and Broise (1975), Scott and Pierce (1975), and Hansbo (1978).

Deep Blasting: This method involves detonation of charges at some specified depth. The shock waves created by blasting densify the saturated soil layer. Blasting is effective only in saturated soils, and is especially effective in saturated cohesionless soils with low fines content (about 20 % or less). This method is the least expensive and quickest among all densification techniques. However due to environmental dangers, it is mostly used at isolated sites. Comprehensive discussions about this method are reported by Prugh (1963), Mitchell (1970), Ivanov (1980), and Jeffries (1991).

Compaction Grouting: This procedure involves pumping a low slump thick grout under high pressures (usually ranging between 700 to 2800 kPa) to displace and compact the surrounding soil (producing an increased confinement effect). Applications include granular soils with high fines

Table 2: Applicability of different remedial techniques to Wildlife and Port Island sites

Technique	Case	Outcome
Drainage	**Wildlife**: applicable **Port Island**: not applicable since the shaking was very strong with a rapid excess pore pressure buildup (2 sec duration, see Table 1).	Control of pore pressures leading to reduction of vertical settlements and lateral deformations.
Drainage with densification (e.g., stone columns).	Applicable in both cases.	Densification of surrounding soil (increase in relative density), and introduction of stiff elements to increase shear resistance.
Densification	**Wildlife**: most densification techniques may not be suitable since the soil contains a large portion of fines. **Port Island**: All densification methods could be used for this site (note that deep dynamic compaction has an economical treatment depth of about 12 m). Port Island areas treated with vibrocompaction experienced deformations substantially lower than those of the surrounding untreated zones (Soils and Foundations 1996). Compaction grouting may not be economical for the large areas involved in both cases.	Reduction of liquefaction potential and settlement, and increase in cyclic mobility (to reduce lateral deformation).
Solidification	Solidification methods are relatively expensive and uneconomical for both cases. Furthermore, limited area application (e.g., sparce stabilized zones or cells within a large soil mass) may not be be sufficient for eliminating liquefaction induced deformation at Port Island (since the shaking was too violent).	Elimination of liquefaction in treated soil volume. Reduction in available pore water, decrease in liquefaction potential, and increase in overall stiffness in the areas confined by treated zones.
Inclusions	**Wildlife**: applicable. **Port Island**: applicable, but should be designed for a 0.7 g level of ground motion	Introduction of stiff elements to increase shear resistance, reduce liquefaction potential, and provide resistance against lateral deformation of the ground.

content, giving it an edge over other densification methods. A major advantage of grouting lies in that it can be used in small, difficult-to-access areas and as a remedial measure beneath or adjacent to an existing structure. Warner (1982) reports an overall history of this technique. Graf (1992) discusses current practice, and Rubright and Welsh (1993) describe the method comprehensively.

Displacement Piles: Piles of timber, steel or prestressed concrete are driven compacting the surrounding soil by displacement as well as by vibration. Detailed information about this method is given by Iyengar (1981), and Solymar and Reed (1986).

Drainage Techniques

Use of relief wells such as gravel drains (stone columns) or prefabricated drains are typical examples for increasing drainage in soil systems. It is believed that installation of stone columns (gravel drains) by vibro-replacement mitigates liquefaction potential by: (1) increasing the surrounding soil density, (2) providing drainage to control pore pressures, and (3) introducing stiff elements (stone columns) that can potentially carry higher stress levels and provide a deformation restricting effect (Priebe 1991, Baez and Martin 1993, Adalier 1996). Among the comprehensive studies on drainage are Seed and Booker (1977), Tokimatsu and Yoshimi (1980), Iai (1988), and Onoue *et al.* (1991).

Solidification Methods

These methods involve the introduction of stabilizing chemicals (e.g., cement, bentonite, and sodium silicates) by either injection (e.g., injection grouting) or mixing (e.g., jet grouting and deep-soil-mixing). These methods are relatively expensive, and are generally only considered for limited areas to construct stabilized zones or cells within a larger soil mass (improved grid shape); or for situations where other soil improvement techniques cannot be used (e.g., small, difficult-to-access areas, or under existing structures). Comprehensive information regarding different solidification methods is reported in Mitchell (1981), Winterkorn and Pamukcu (1991), and Adalier (1996).

In general, injection grouting can be effective in sands with less than 20 % fine material (silt and clay). On the other hand, jet grouting which involves mixing with grout by fracturing the soil with high pressure water or air jets can be effective in any type of inorganic soil. More detailed information about grouting techniques is reported by Mitchell (1981), Welsh (1987), Moseley (1993), Xanthakos *et al.* (1994), and Adalier (1996).

The deep-soil-mixing technique whereby soil is physically mixed with cementing material via mixing augers, can be used for any type of soil (Taki and Yang 1991, Jasperse and Ryan 1992). A complete discussion about the deep-soil-mixing technique is reported by Toth (1993).

Inclusions

This method involves formation of inclusions in the soil using concrete, timber, or steel piles, and sheet piles. Such techniques usually rely on the ability of inclusions to reduce shear stress and restrict shear strains in the soil. In addition, depending on the installation method (driving or placing), it can densify the surrounding soil and enhance liquefaction resistance. Generally, these techniques have enjoyed little popularity as liquefaction countermeasure methods. Thorough discussions may be found in Kramer and Holtz (1991), and Adalier (1996).

SUMMARY AND CONCLUSIONS

The conducted study showed the role of downhole acceleration records in assessing the mechanisms of site amplification, stiffness degradation and liquefaction. At the Wildlife Refuge and Port Island sites, the estimated stress-strain histories showed that: (1) site stiffness and strength decreased

steadily with excess pore pressure buildup, (2) at high excess pore pressure levels, site response was characterized by large strains and small stresses, and (3) during liquefaction, significant shear strength may evolve at large shear strains, due to the cyclic mobility effect. A number of guidelines were drawn for liquefaction countermeasure strategies. A brief review of liquefaction countermeasures was presented showing the effect of each technique in mitigating the observed detrimental liquefaction effects.

ACKNOWLEDGMENTS

This research was supported by the United States Geological Survey (grant No. 1434-94-G-2397), the National Science Foundation (grant No. MSS-9057388), and the National Center for Earthquake Engineering Research (grant No. 90-1503); with matching funds from Earth Mechanics Inc. Port Island downhole acceleration data were provided by the Committee of Earthquake Observation and Research in the Kansai Area (CEORKA), Japan, with the help of Dr. Y. Iwasaki.

REFERENCES

Adalier, K. (1996). "Mitigation of Earthquake Induced Liquefaction Hazards," Ph.D. Thesis, Rensselaer Polytechnic Institute, Troy, NY.

Arulmoli, K., Muraleetharan, K. K., Hossain, M. M. and Fruth, L. S. (1992). "Verification of Liquefaction Analyses by Centrifuge Studies Laboratory Testing Program Soil Data Report," Report, The Earth Technology Corporation.

ASCE (1977). *Soil Improvement, History, Capabilities, and Outlook.* ASCE Committee on Placement and Improvement of Soils, Geotechnical Engineering Division, New York.

Baez, J. I., and Martin, G. R. (1993). "Advances in the design of vibro systems for the improvement of liquefaction resistance," Symposium of Ground Improvement, Vancouver Geotechnical Society, Vancouver, B.C.

Bennett, M. J., McLaughlin, P. V., Sarmiento, J. S., and Youd, T. L. (1984). "Geotechnical Investigation of Liquefaction Sites, Imperial Valley, California," *U.S.G.S. Open-File Report* 84-252.

Broms, B. B. (1991). "Deep Compaction of granular soils," *Foundation Engineering Handbook*, 2nd Edition, Von Nostrand Reinhold, New York, NY, 814-832.

Elgamal, A.-W., Zeghal, M., Parra, E., Gunturi, R., Tang, H. T., and Stepp, C. J. (1996a). "Identification and Modeling of Earthquake Ground Response I: Site Amplification," *Soil Dynamics and Earthquake Engineering*, Vol. 15, No. 8, 499-522.

Elgamal, A.-W., Zeghal, M. and Parra, E. (1996b). "Liquefaction of an Artificial Island in Kobe, Japan," *Journal of Geotechnical Engineering*, ASCE Vol. 122, No. 1.

Graf, E. D. (1992). "Compaction Grout; 1992," Proc., Grouting, Soil Improvement, and Geosynthetics, New Orleans, R. H. Borden, R. D. Holtz and I. Juran (eds.), Geotech. Spec. Pub. No. 30, ASCE, Vol. 1, 257-287.

Hansbo, S. (1978). "Dynamic Consolidation of Soil by Falling Weight," *Ground Engineering*, 11 (5), 27-31.

Holzer, T. L., Youd T. L. and Hanks T. C. (1989). "Dynamics of Liquefaction During the 1987 Superstition Hills, California, Earthquake," *Science*, Vol. 244, 56-59.

Iai, S. (1988). "Large scale model tests and analysis of gravel drains," Report of the Port and Harbor Research Institute, Vol. 27, No.3.

Ishihara, K., Anazawa, Y., and Kuwano, J. (1987). "Pore Water Pressures and Ground Motions Monitored During the 1985 Chiba-Ibaragi Earthquake," *Soils and Foundations*, Vol 27, No. 3, 13-30.

Ivanov, P. L. (1980). "Consolidation of saturated soils by explosions"" Proc. Int. Conf. on Compaction, ENPC, Paris, 1, 331-337.

Iwasaki, Y. (1995a). Georesearch Institute, Osaka, Japan, Personal communication.

Iwasaki, Y. (1995b). "Geological and Geotechnical Characteristics of Kobe Area and Strong Ground Motion Records by 1995 Kobe Earthquake, Tsuchi-to-Kiso," *Japanese Society of Soil Mechanics and Foundation Engineering*, Vol. 43, No. 6, 15-20 (in Japanese).

Iyengar, M. (1981). "Improvement of characteristics of a liquefiable soil deposit by pile driving operations," *Inter. Conf. on Recent Advances in Geotech. Earthq. Eng. and Soil Dyn., St. Louis, Mo.*

Jasperse, B. H., and Ryan, C. R. (1992). "Stabilization and fixation using soil mixing,"*Grouting, Soil Improvement and Geosynthetics*, ASCE Geotech. Spec. Pub. No. 30, 1273-1284.

Jeffries, M. G. (1991). "Explosive Compaction," *Geotechnical News*, 29-31.

Koga, Y. and Matsuo, O. (1990). "Shaking Table Tests of Embankments Resting on Liquefiable Sandy Ground," *Soils and Foundations*, Vol. 30, No. 4, 162-174.

Kramer, S. L., and Holtz, R. D. (1991). *Soil Improvement and Foundation Remediation with Emphasis on Seismic Hazards.* A Report of a workshop sponsored by the National Science Foundation and held at the University of Washington, Dept. of Civil Eng., Seattle, Washington, Aug. 19-21.

Leonards, G. A., Cutter, W. A., and Holtz, R. D. (1980). "Dynamic compaction of granular soils," J. Geotech. Eng., ASCE, Vol. 106, 35-44.

Lukas, R. G. (1986) "Dynamic compaction for highway construction," Vol. 1, Design and Construction Guidelines, Federal Highway Administration, Office of Research and Development, U.S. D.O.T., Washington, D.C., Report No. FHWA/RD-86/133, July.

Menard, L., and Broise, Y. (1975). "Theoretical and practical aspects of Dynamic Consolidation," *Geotechnique*, Vol. 15, No. 1, 3-18.

Mitchell, J. K. (1970). "In place treatment of foundation soils," J. of Soil Mech. and Found. Div., ASCE, Vol. 96, No.SM1, 73-110.

Mitchell, J. K. (1981). "Soil Improvement State-of the-Art Report," Session 12, Proc. of the 10th Int. Conf. on soil Mech. and Found. Eng., Stockholm, Vol. 4, 506-565.

Moseley, M. P. (1993). *Ground Improvement.* Chapman and Hall, Pub. by CRC Press Inc., Florida.

Nakakita, Y., and Watanabe, Y. (1981). "Soil stabilization by Preloading in Kobe Port Island," *Proceedings of the 9th International Conference on Soil Mechanics and Foundation Engineering*, Tokyo, Japan, 611-622.

National Research Council (1985). *Liquefaction of Soils During Earthquakes*, Committee on Earthquake Engineering, National Academy press, Washington D. C.

Onoue, A., Ting, N., Germaine, J. T., Whitman, R. V., and Mori N. (1991). "Smear zone around a drain pile and well resistance of drains," Geo-Coast' 91, Yokohoma, Japan.

O'Rourke, T. D. (1995). "Geotechnical Effects," *Preliminary Report from the Hyogoken-Nanbu Earthquake of January 17, 1995*, National Center for Earthquake Engineering Research Bulletin, SUNY, Buffalo, Vol. 9, No. 1.

Priebe, H. J. (1991). "Vibro Replacement - design criteria and quality control," Deep Foundation Improvements: Design, Construction, and Testing, ASTM STP 1089, M. I. Esrig and R. C. Bachus (eds.), ATSM, Philadelphia, 62-72.

Prugh, B. J. (1963) "Densification of soils by explosive vibrations," Proc. ASCE, J. of Construction Division, ASCE, Vol. 89, No. CO1, 79-100.

Rubright, R., and Welsh, J. (1993). "Compaction Grouting," Ch. 6, in *Ground Improvement*, Moseley M. P. (ed.), Chapman and Hall (Pub.).

Scott, R. A., and Pierce R. W. (1975). "Soil compaction by impacts," *Geotechnique*, Vol. 25, No. 1, 19-30.

Seed, H. B. (1966). "Landslides During Earthquakes Due to Soil Liquefaction," *Journal of Soil Mechanics and Foundations Division*, ASCE, Vol. 94, No. SM5, Sept., 1053-1122.

Seed, H. B., Idriss, I. M., and Arango, I. (1983). "Evaluation of Liquefaction Potential Using Field Performance Data," *Journal of Geotechnical Engineering*, ASCE, Vol. 109, No. 3, 458-482.

Seed, R. B., Dickenson, S. E., Riemer, M. F., Bray, J. D., Sitar, N., Mitchell, J. K., Idriss, I. M., Kayen, R. E., Kropp, A., Hander, L.F. Jr., and Power, M. S. (1990). "Preliminary Report on the Principal Geotechnical Aspects of the October 17, 1989, Loma Prieta Earthquake," Report No. EERC-90-05, Earthquake Engineering Research Center, University of California, Berkeley.

Slocombe, B. C. (1993). "Dynamic Compaction," Ch. 2, In Ground Improvement, Moseley M. P. (ed.), Chapman and Hall (Pub.).

Soils and Foundations (1996). "Special Issue on Geotechnical Aspects of the January 17, 1995 Hyogoken Nambu Earthquake," *Soils and Foundations*, Japan Geotechnical Society, January 1996.

Solymar, Z. V., and Reed, D. J. (1986). "A comparison of foundation compaction techniques," *Canadian Geotechnical Journal*, Vol. 23, No. 3, 271-280.

Sitar, N., Ed. (1995). "Geotechnical Reconnaissance of the Effects of the January 17, 1995, Hyogoken-Nanbu Earthquake Japan," *Report No. UCB/EERC-95/01*, Earthquake Engineering Research Center, Berkeley, California.

Taboada, V. M. and Dobry, R. (1993). "Experimental Results of Model 1 at RPI," *Proceedings of the International Conference on the Verification of Numerical Procedures for the Analysis of Soil Liquefaction Problems*, Arulanandan, K. and Scott, R. F., eds., Vol. 1, Davis, CA, 3-17, Balkema.

Taki, D, and Yang, D. S. (1991). "Soil-Cement mixed wall techniques," *Geot. Eng. Congress 1991*, Boulder, F. G. McLean, D. A. Campbell and D. W. Harris (eds.), Geot. Spec. Pub. No. 27, ASCE, Vol. 1, 289-309.

Tokimatsu, K., and Yoshimi, Y. (1980). "Effects of vertical drains on the bearing capacity of saturated sand during earthquakes," Proc. of Int. Conf. on Eng. for Protection from Natural Disasters, Asian Institute of Technology, Jan., 643-655.

Toth, P. S. (1993). "In Situ soil mixing," Chap. 9 in *Ground Improvement*, Moseley M. P. (ed.), Pub. by Chapman and Hall, London, 218 p.

Vucetic, M. and Dobry, R. (1988). "Cyclic Triaxial Strain-Controlled testing of Liquefiable Sands," *Amer. Soc. Testing Mat.*, Spec. Tech. Publ. 977, 475-485.

Warner, J. (1982). "Compaction Grouting - the first thirty years," ASCE Specialty Conf. On Grouting in Geotechnical Engineering, New Orleans.

Welsh, J. P. (ed.) (1987). Soil Improvement - A Ten Year Update. Geotechnical Special Publication No. 12, ASCE, NY, NY.

Winterkorn, H. F., and Pamukcu, S. (1991). "Soil Stabilization and Grouting," Chap. 9 in *Foundation Engineering Handbook*, H-Y. Fang (ed.), 2nd Ed., Pub. by Van Nostrand Reinhold, NY, NY.

Xanthakos, P. P., Abramson, L. W., and Bruce, D A. (1994). *Ground Control and Improvement.* A Wiley-Interscience Publication, John Wiley and Sons Inc., New York, NY, 910p.

Youd, T. L., and Wieczorek, G. F. (1984). "Liquefaction During 1981 and Previous Earthquakes Near Westmorland California," U.S. Geological Survey Open-File Report 84-680.

Zeghal, M. and Elgamal, A.-W. (1993). "Lotung Site: Downhole Seismic Data Analysis," Rep., Department of Civil Engineering, Rensselaer Polytechnic Institute, Troy, NY.

Zeghal, M., Elgamal, A.-W., Tang, H. T., and Stepp, J. C., "Lotung downhole array: evaluation of soil nonlinear properties," *Journal of Geotechnical Engineering*, ASCE, Vol. 121.

Zeghal, M. and Elgamal, A.-W. (1994). "Analysis of Site Liquefaction Using Earthquake Records," *Journal of Geotechnical Engineering*, ASCE, Vol. 120, No. 6, 996-1017.

Zeghal, M., Elgamal, A.-W., and Parra, E. (1996). "Identification and Modeling of Earthquake Ground Response II: Site Liquefaction," *Soil Dynamics and Earthquake Engineering*, Vol. 15, No. 8, 499-522.

GROUND DISPLACEMENT AND STRAIN CAUSED BY SOIL LIQUEFACTION DURING THE 1995 HYOGOKEN-NANBU EARTHQUAKE

Masanori Hamada
Department of Civil Engineering
Waseda University, Tokyo, Japan

Kazue Wakamatsu
Institute of Industrial Science
University of Tokyo, Japan

ABSTRACT

This paper introduces an outline of liquefaction-induced ground displacements during the 1995 Hyogoken-Nanbu earthquake, which were measured by an aerial survey, and describes the characteristics of the ground displacements. It also outlines the ground strain caused by the liquefaction, which were analyzed from the measured ground displacement, and discusses a relationship between the magnitude of the ground strain and the damage rate of buried pipes.

INTRODUCTION

The 1995 Hyogoken-nanbu earthquake caused a significant soil liquefaction in an extensive area of reclaimed land in Kobe and its neighboring cities. The soil liquefaction also induced large ground displacements in the horizontal direction, which resulted in serious damage to buried lifeline facilities and foundations of bridges and buildings. The authors have investigated the liquefaction during the earthquake and its caused damage to various kind of civil engineering structures. They also measured the liquefaction-induced ground displacements in reclaimed lands along the waterfront of Hanshin area by an arial survey using both pre- and post-earthquake photographs and by referring to the results from field surveys. They investigated the characteristics of the ground displacements and the strains, and discussed the relationship between the damage rates of buried pipes and the ground strains.

METHODS OF MEASUREMENT AND ACCURACY OF GROUND DISPLACEMENT

Liquefaction-induced ground displacements were measured on the two manmade islands (Port and Rokko Islands), and other reclaimed land areas in Kobe and the neighboring cities.
Two sets of aerial photographs, which were taken in the same area before and after the earthquake, are necessary for measurement of ground displacements. The following sets of aerial photographs were used for the measurement:

Pre-earthquake	Scale:	1/12,500
	Date:	May 1990, May 1993 and May 1994
Post-earthquake	Scale:	1/8,500,
	Date:	Jan. (18th-21st .) 1995

Three dimensional coordinates before as well as after the earthquake were measured on objects fixed on the ground surface such as manholes and corners of drainage channels, and/or of corners on roofs of reportedly un-damaged structures. The liquefaction-induced ground displacements were obtained by subtracting coordinates before the earthquake from ones after the earthquake.

The accuracy of each aerial survey before and after the earthquake depends on the reduction scale of the aerial photographs, human errors in reading the coordinates etc. The accuracy of the present aerial survey before the earthquake was estimated to be ±24 cm horizontally and ±27 cm vertically, while the one after the earthquake was estimated as ±23 cm horizontally and ±46 cm vertically. An attention should be paid to the fact that these accuracies were estimated as a standard variation of the residual errors. The maximum error in this measurement is ±56 cm horizontally and ±54 cm vertically before the earthquake, while ±84 cm horizontally and ±98 cm vertically after the earthquake. It should be noted, therefore, that errors of such magnitude may occur at some observation points. The accuracy of the surveys after the earthquake can be improved, however, if the coordinates of the standard control points will be measured with a higher accuracy in the future.

The accuracy of liquefaction-induced ground displacements is given as a root-mean square of the accuracies before and after the earthquake, and is estimated as ±33 cm horizontally and ±53 cm vertically.

Relative displacements between two observation points, namely ground strains are important to discuss earthquake resistance of inground structures. The accuracy of relative displacements depends on the scale reduction of the aerial photographs. The accuracy of the relative displacement (in the horizontal direction) is 7.6×10^{-6} m before the earthquake and 12.8×10^{-6} m after the earthquake in the scale of the aerial photos. The accuracy of the relative displacement before and after the earthquake was estimated to be 9 cm and 11 cm, respectively. Therefore, the accuracy of the relative displacement was estimated to be 14 cm as a root mean square of the above two standard variations. The complete results of the measurements was reported in a report by in Hamada et al. (1995).

Several typical example of the ground displacements and their caused damage will be presented in the following section .

CHARACTERISTICS OF LIQUEFACTION-INDUCED GROUND DISPLACEMENT

Distribution of Ground Displacement As mentioned later, quaywalls moved towards the sea and canals, and consequently the liquefied ground in a wide area behind quaywalls largely displaced in the same direction. An investigation into the range where the ground displacements were caused and into the displacement distribution pattern from the quaywall line is one of important aspects for earthquake resistant design of structures.

Figure 1 shows examples of horizontal ground displacement distributions along lines in the north-south direction perpendicular to west-east shorelines in six reclaimed lands. In the figure, plus of vertical axis indicates southward displacements and minus represents northward displacements. It can be seen that the horizontal displacements decrease with increasing distance from the sea and become mostly constant not depending on the distance from the quaywalls. In man-made lands, i.e., Port and Rokko Islands, the displacements decrease rapidly, and become less than 1 meter in the area several ten meters away from the shorelines. In contrast, they decrease gradually in the mainland-side reclaimed ground such as Mikage-hama, Uozaki-hama, Fukae-hama and Nishinomiya-hama. The displacements in Port and Rokko Islands change their directions from south to north wards around the center of the islands. Whereas, in the mainland-side reclaimed ground, they turn their directions at immediately in front of northern quaywalls. This means that mostly whole area of the reclaimed ground moved toward south i.e., towards the sea.

The relation between horizontal ground displacement and distance from the quaywall lines can be schematically illustrated as shown in Fig. 2. As above-mentioned, the horizontal displacements decrease within some distance from the sea, and then become mostly constant The zone where the

displacement decreases rapidly were considered to be affected directly by the movement and/or collapse of quaywalls, therefore, we called simply as "affected zone" in the following, as shown in Fig. 2. The distribution of the ground displacements can be separated into two parts: the first part is that directly affected by the movement of quaywalls and the second one independent of the quaywall movement.

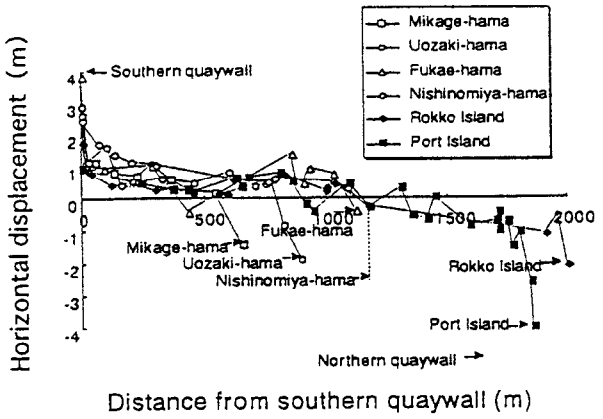

Fig. 1 Horizontal ground displacement against distance from quaywall for the north-south sections through six reclaimed lands

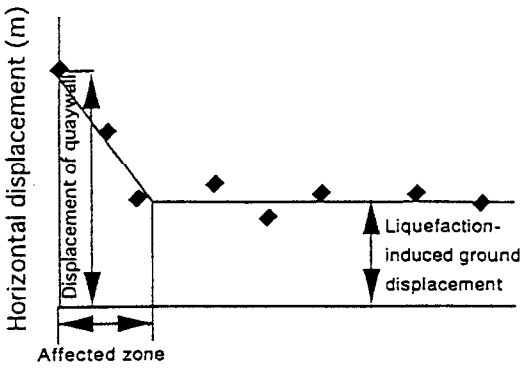

Fig. 2 Schematic diagram showing relationship between horizontal ground displacement for distance from quaywall

Correlation with Thickness of Liquefied Soil and Effect of Soil Improvement Hamada et al. (1986) have pointed out that liquefaction-induced horizontal ground displacements during the 1987 Nihonkai-chubu and the 1964 Niigata earthquakes correlated to thickness of liquefied soil layer. Fig. 3 shows a relationship between the ground displacements in the areas where they become mostly constant away from the quaywalls and the thickness of the liquefied soil. Some correlation can be seen in mainland-side islands, however, in Port and Rokko Islands, the displacements are much smaller not depending on the thickness of liquefied soil layer.

Figures 4 and 5 show horizontal ground displacements for lines across soil improved zones in Port and Rokko Islands, respectively. The ground displacements in the improved zones are approximately within ±33 cm, within the accuracy of the measurement mentioned in **6.1**, which indicates that the ground displacements were negligibly small in the improved zones. It can be concluded that the soil improvement in the central districts of the two islands restrained the ground displacement. In addition, the higher ground level i.e., deeper ground water table in the areas might contribute to reduce the displacements.

Zone Affected by the Displacement of Quaywall In "affected zone", the magnitude of the horizontal ground displacements change almost linearly, which resulted in increase of relative displacement, namely ground strain. The most of the serious damage to structures associated with liquefaction-induced ground displacements occurred within the "affected zone". Figure 6 shows relationship between horizontal displacements of quaywalls and length of affected zones from the quaywalls. Clear correlation can not be found, however upper limits of the distance of the affected zones increases with the quaywall displacements. For example, when quaywalls moved by 3meters, the effects extends to the inland about 200 meters away from quaywalls. The length of affected zones are sometimes very small although wall displacements exceed 3 meters. The probable reasons for this are as follows; 1) effect of improved soils and/or existence of foundations of structures near quaywalls; 2) effect of a large thickness of unliquefiable soil layer due to the deeper water table.

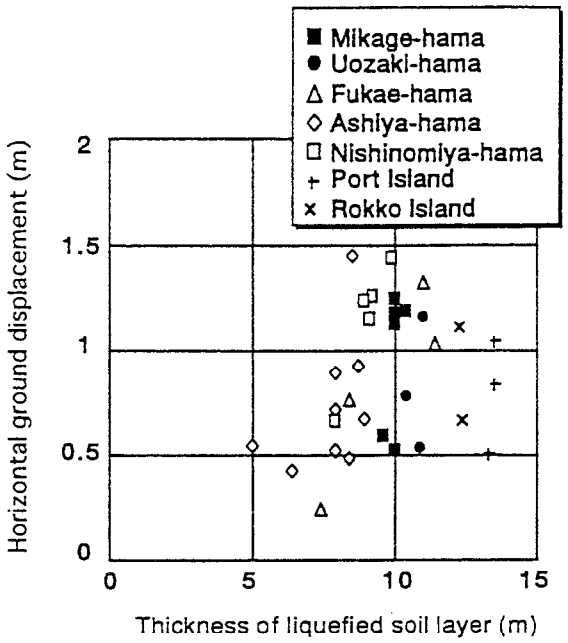

Fig. 3 Horizontal ground displacement against thickness of liquefied soil layer

Horizontal Displacement of Quaywall Figures 7(a) and (b) shows horizontal displacements of quaywalls in several reclaimed lands, and Fig. 8 shows the mean displacement in each lands. The displacements are larger on south side of Rokko Island, north side of Port Island and east side of Fukae-hama. Whereas, displacements on the north side are smaller than that on other sides except in both Port and Rokko Islands. According earthquake motion records during the earthquake, north-south components of ground motions were generally predominant. The result in Fig. 8 shows that the displacements of the north and south sides quaywalls, which can be considered to be affected more strongly by the earthquake ground motion, are not necessarily dominant. The mean displacements in Fig. 8 are arranged in order of nearer islands from the source faults. The result in Fig. 8 also shows that the quaywall displacements are not necessarily larger in the areas nearer from the earthquake source. The fact above-mentioned suggests that the quaywalls did not moved only due to the inertia force acting on them.

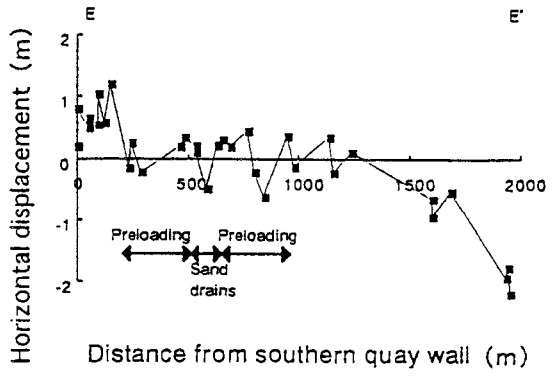

Fig. 4 Horizontal ground displacement for a line across improved zones in Port Island

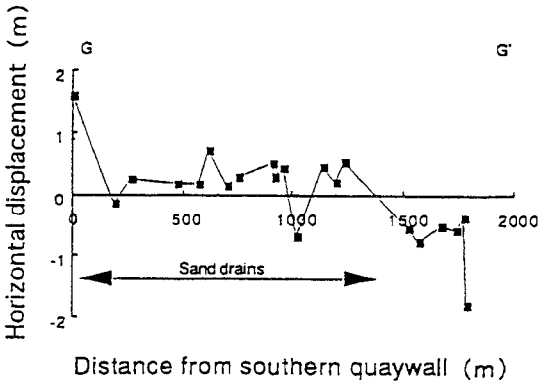

Fig. 5 Horizontal ground displacement for a line across improved zones in Rokko Island

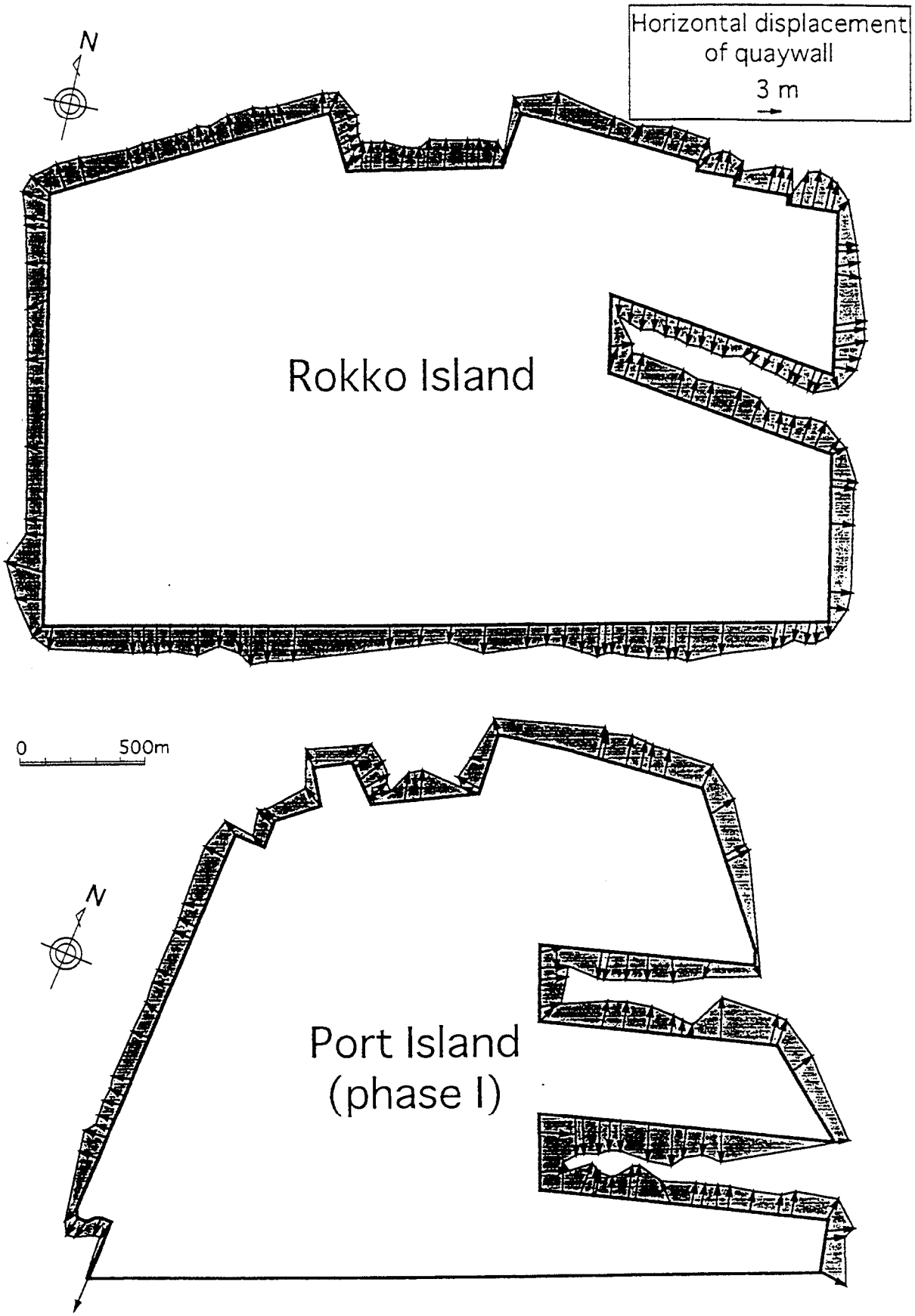

Fig 7(a) Horizontal displacement of quaywalls

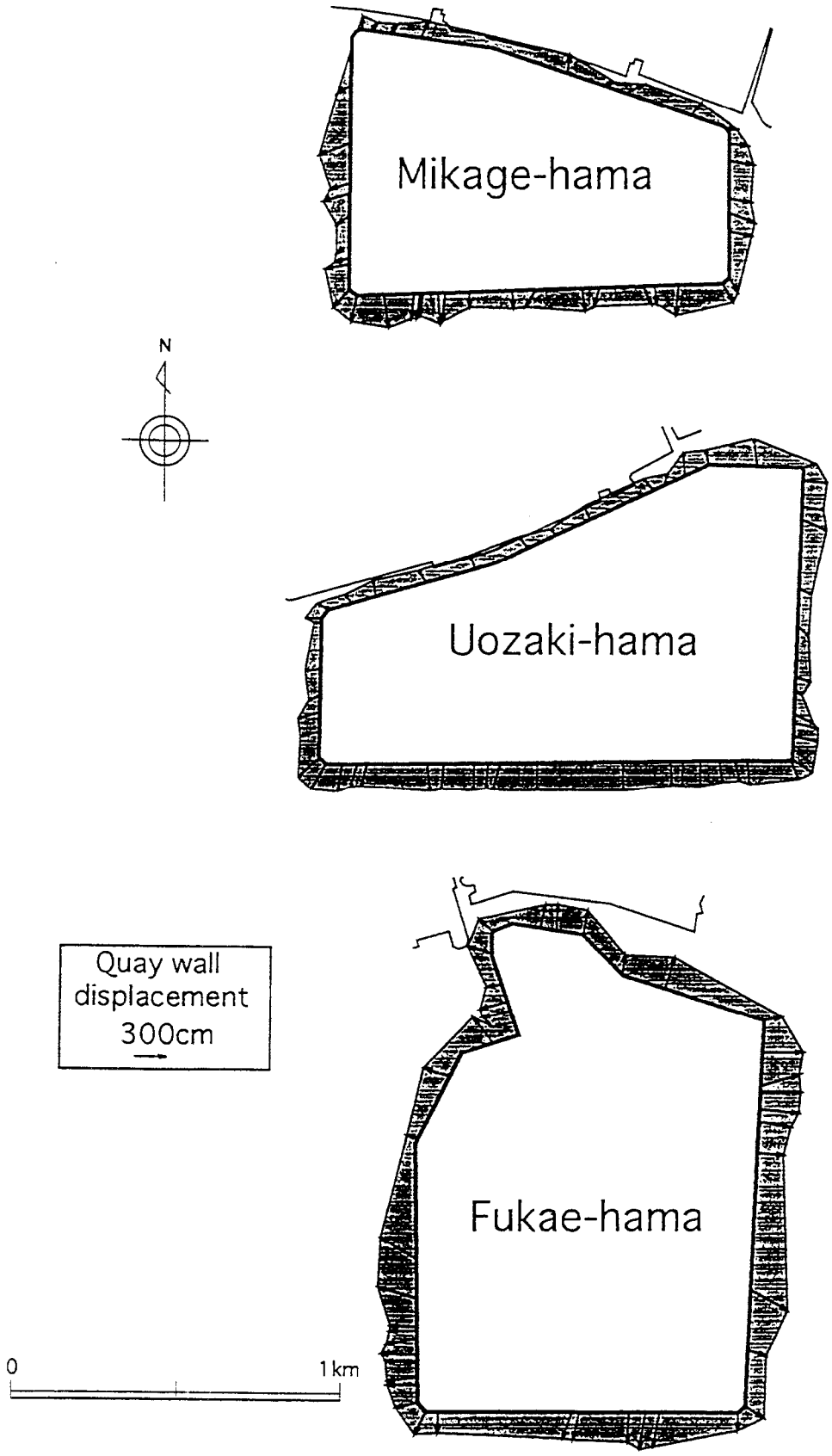

Fig 7(b) Horizontal displacement of quaywalls

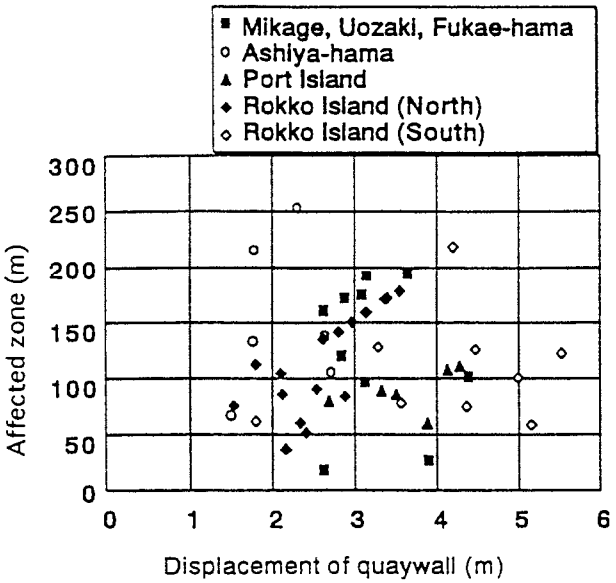

Fig. 6 Relationship between horizontal displacements of quaywalls and length of affected zones

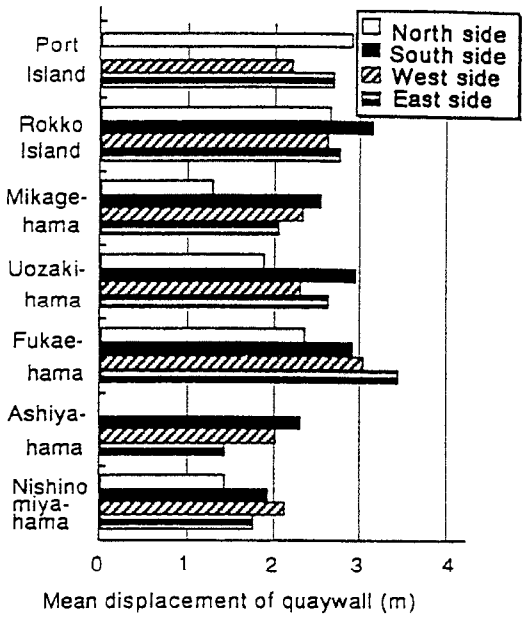

Fig. 8 Mean horizontal displacement of quaywalls

LIQUEFACTION-INDUCED GROUND STRAIN

Ground strains have a more deterministic influence to performances of buried pipes of lifelines such as gas, water, sewage and electricity during an earthquake than ground displacements. Therefore, ground strains caused by the Hyogoken-nanbu earthquake were calculated according to the following procedure, and a correlation between the ground strain and damage to buried pipes was investigated.

1) The displacement function in each quadrangle with a side of about 100 m, shown in Fig. 9 is assumed to be linear, as shown by the following formula (1). Namely, the strains in a cell are assumed to be constant.

$$u = \alpha_1 x + \beta_1 y + \gamma_1$$
$$v = \alpha_2 x + \beta_2 y + \gamma_2 \qquad (1)$$

where,
x, y : Coordinates in the east-west and south-north directions,
u, v : Components of ground displacements in the respective directions.

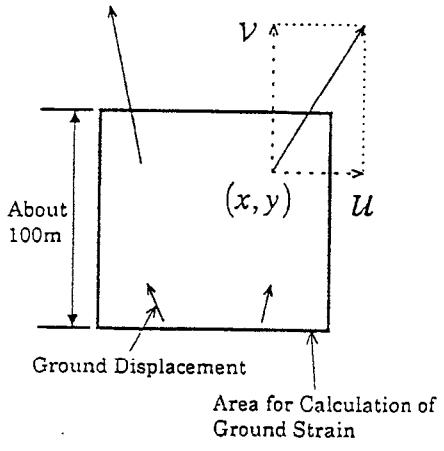

Fig. 9 Schematic diagram showing procedure of calculation of ground strain

2) Six coefficients α_1 , α_2 , β_1 , β_2, γ_1 and γ_2 are determined from the ground displacements measured in a quadrangle using the Least Square Approximation. For the determination of ground strains, at least three displacement vectors are necessary in each quadrangle. The

permanent ground strains on horizontal plane are obtained as the differentials of the displacement function.

As for the above-mentioned procedure, it should be noted that the magnitude of the calculated ground strains depends on the size of the quadrangles. The performance of a buried structure with a large dimension such as conduits and tunnels is governed by ground strain in a wider area, but that of buried pipes is governed by ground strains in comparatively smaller area. Therefore, the influence of the size of quadrangles should be carefully examined when a correlation between the damage to buried structures and ground strains is discussed.

Figure 10 shows one example of the calculated ground strains in the north-eastern area of Rokko Island. The large movement of the quaywalls triggered the ground displacement behind them. And so, the displacement of the ground close to the quaywalls is much larger than that away from the quaywalls. Therefore, the ground strain was calculated in two kinds of areas. The first area is within 100 meters from quaywalls and the second area more than 100 meters away from quaywalls. Figure 10 (a) shows the ground strain in the area within about 100 m from quaywalls, while Fig. 10 (b) is for the result in the area away from quaywalls. A large tensile strain was caused along quaywalls and its maximum reaches 7%. On the contrary, the ground strain in the area more than 100 meters away from quaywalls is comparatively smaller. It should be noted that compressive strains are also caused in both areas.

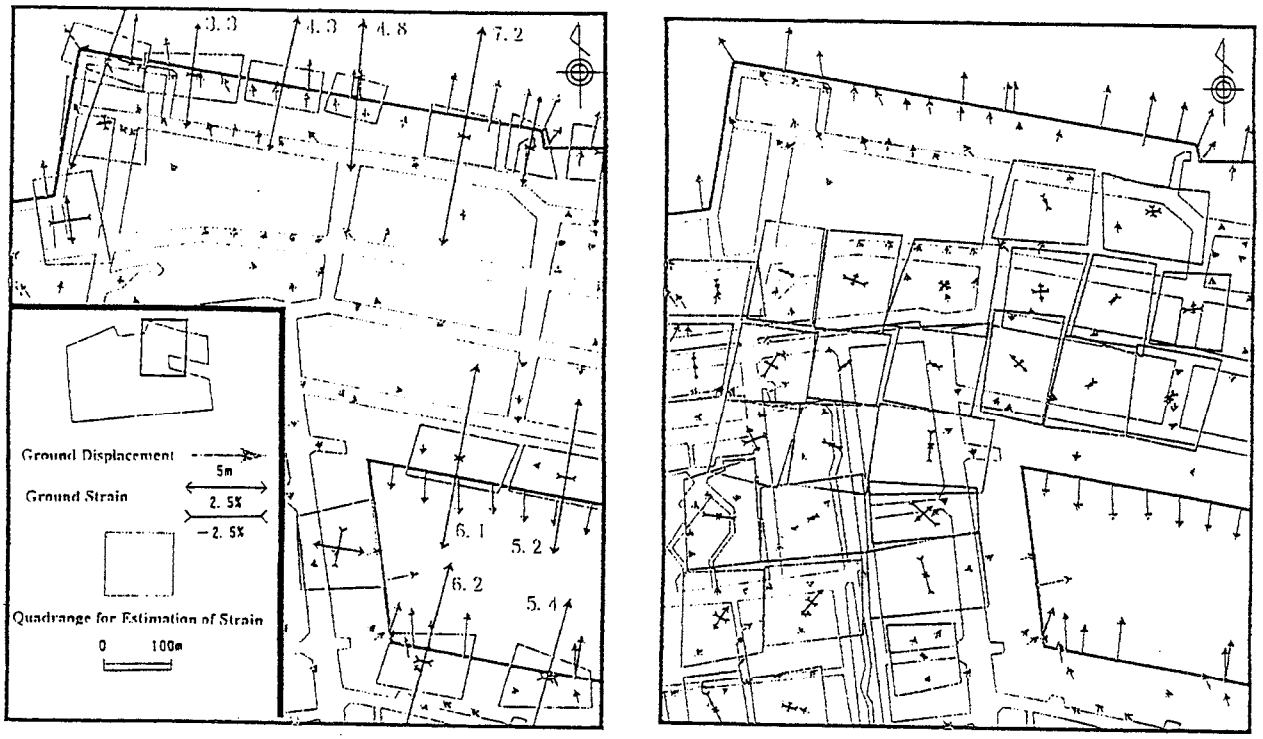

a) area within about 100 m from quaywalls b) area more than 100 m away from quaywalls

Fig. 10 Calculated ground strains in the north-eastern area of Rokko Island

Figures 11 and 12 show probability of occurrence of the ground strains in Rokko and Port Islands and the reclaimed ground in the mainland-side such as Fukae, Uozaki, Nishinomiya etc. As mentioned previously, tensile strains are much larger than compressive strains, and particularly are predominant in the area along quaywalls. For example, in Port Island the mean value of tensile strains along quaywalls is 2.4% (see Fig. 11), but the one away from quaywalls is about 0.6% (Fig. 12). The mean value of compressive strains is comparatively smaller, below 1.0% in all areas. The result shown in Figs. 11 and 12, can be referred for an evaluation of a standard value of an input ground strain for the earthquake resistant design of buried structures. However, relationships between the magnitude of ground strains and damage rate of buried structures should be also taken into consideration for the evaluation of the standard design value of ground strains.

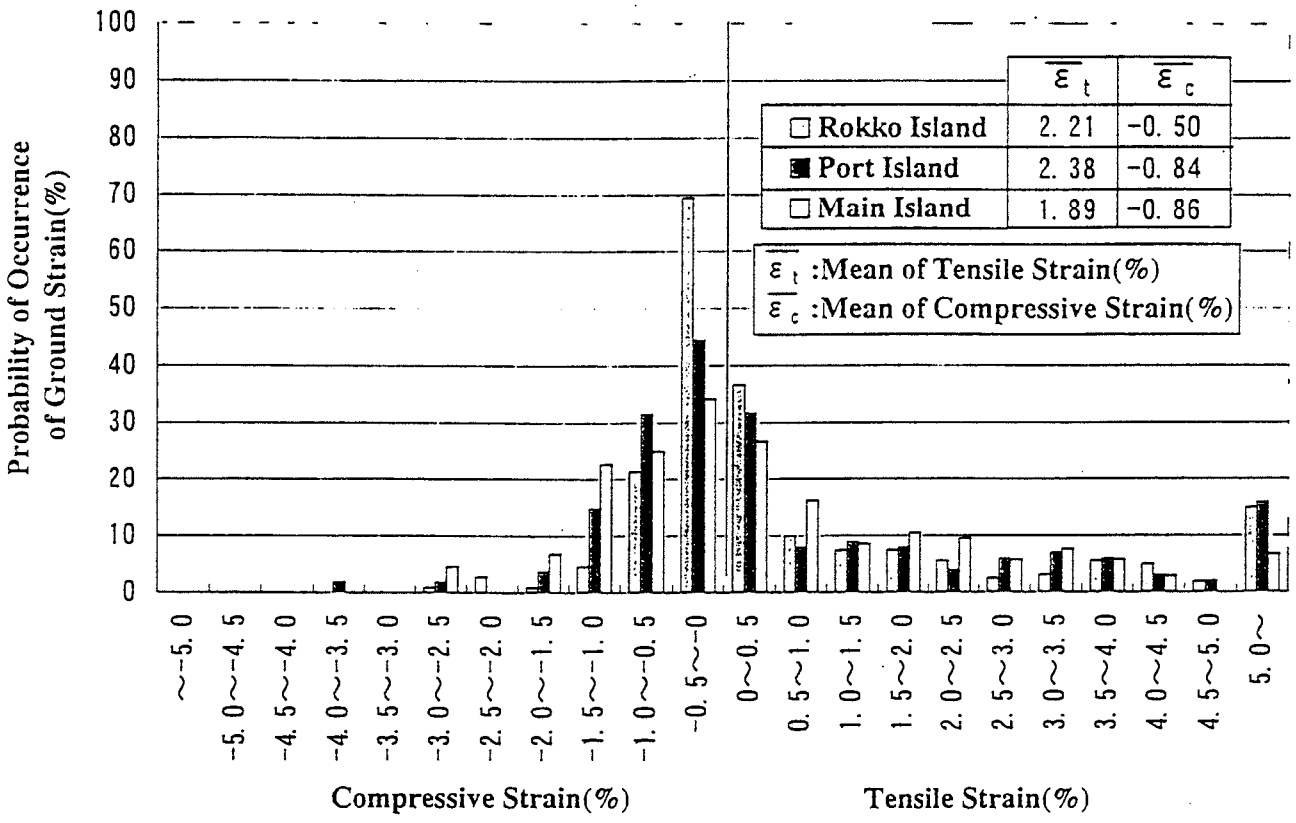

Fig. 11 Probability of occurrence of the ground strains in Rokko and Port Islands and the reclaimed ground in the mainland (within 100 m from quaywalls)

Figure 13 shows an example of relationships between the damage rate (ductile iron pipes in Kobe) and ground strain in the axial direction[23]. It can be seen from the figure that the cast iron pipe was hardly damage when the ground strain was below 0.2%, but the damage rate reached mostly 100% above 0.6% ground strain. Figure 14 shows another example of a relationship between damage rate of concrete buried pipes for sewage and ground strains. The damage rate means, a ratio of the number of damaged spans between neighboring two manholes to the total number of inspected spans. A trend can be recognized from the result that the damage rate gradually increases as ground strains.

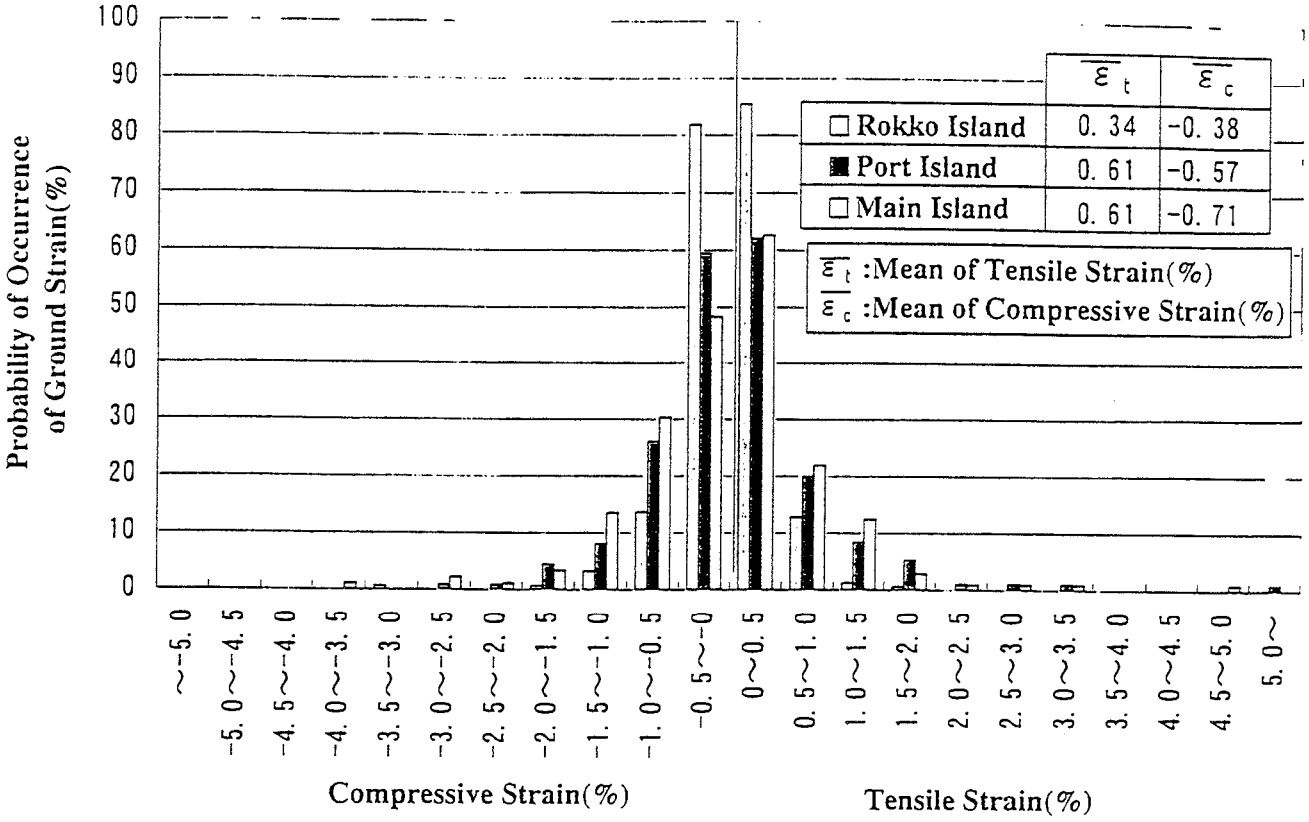

Fig. 12 Probability of occurrence of the ground strains in Rokko and Port Islands and the reclaimed ground in the mainland (more than 100 m away from quaywalls)

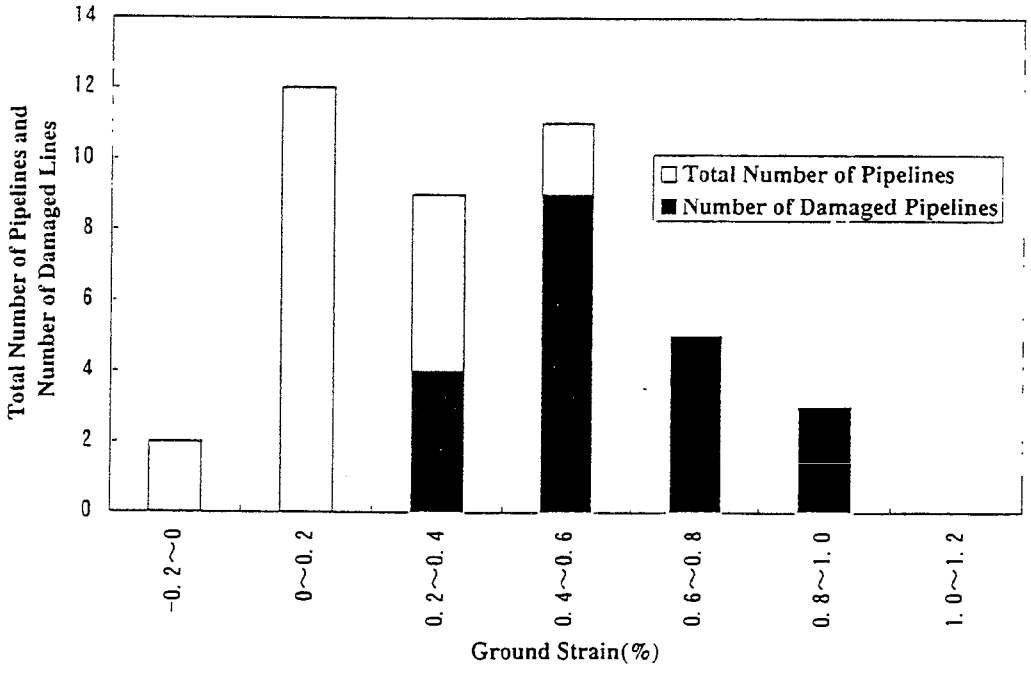

Fig. 13 Relationship between the damage rate of ductile iron pipes and ground strains in the axial direction[3)]

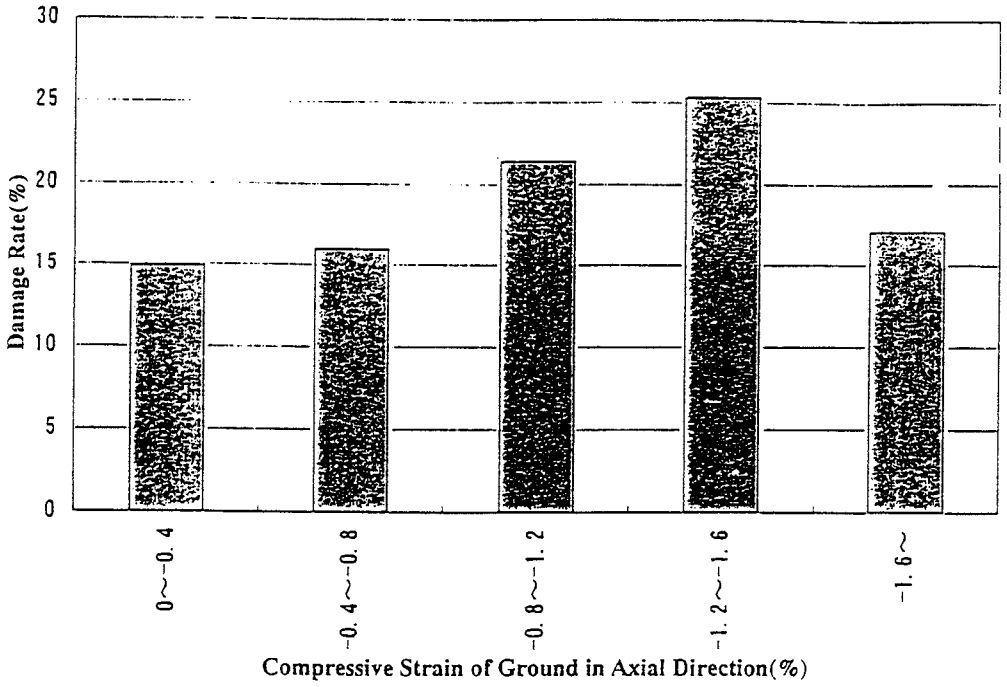

Fig. 14 Damage rate of concrete buried pipes for sewage and ground strains

CONCLUSIONS

Based on the investigation into the liquefaction-induced ground displacements and strains, and damage to buried pipes and foundations of structures in the 1995 Hyogoken-Nanbu earthquake, the following conclusions are obtained:

1) The soil liquefaction induced large ground displacements in the horizontal direction along the shoreline in the reclaimed lands in Kobe and neighboring cities. The ground displacements were also observed in the inland several hundred meters away from the shoreline.

2) Many structures such as buried pipes and foundation piles of buildings and civil engineering structures were damaged due to the liquefaction-induced ground displacement.

3) Horizontal ground displacement along lines perpendicular to shorelines decrease within some distance from the sea, and then become mostly constant not depending on the distance from the quaywalls. In two man-made lands, the displacements decrease rapidly, and become less than 1 meter in the area several ten meters away from the shorelines. In contrast, they decrease gradually in the mainland-side reclaimed ground.

4) Ground strains were calculated from the measured ground displacements. The results show that large tensile ground strains were caused in the area along quaywalls and its maximum reaches several %, but the one away from the quaywall is comparatively smaller, below 1%. Compressive strains of the ground were also caused but much smaller than tensile strain.

REFERENCES

1) Hamada, H., Isoyama, R. and Wakamatsu, K.: *The Hyogoken-Nanbu (Kobe) Earthquake, Liquefaction, Ground Displacement and Soil Condition in Hanshin Area*, Association for Development of Earthquake Prediction, 1995.

2) Hamada, M., Yasuda, S., Isoyama, R. and Emoto, K.: *Study on Liquefaction Induced Permanent Ground Displacements*, Association for Development of Earthquake Prediction, Tokyo, 1986.

3) Engineering Work Division of Japan Water Association: *Damage to Water Pipes and its Analysis on the Great Hanshin and Awaji Earthquake*, 1995

REDUCTION OF LIQUEFACTION HAZARDS BY DEEP SOIL MIXING

T.D. O'Rourke
S.H. Goh
School of Civil and Environmental Engineering
Cornell University
Ithaca, NY

ABSTRACT

One of the most promising technologies for site improvement involves deep soil mixing (DSM), whereby cements and hardening agents are mixed in situ with native soil to increase strength and stiffness properties. This method proved to be effective in stabilizing potentially liquefiable soil at several sites during the Kobe earthquake, including the Oriental Hotel, where partial coverage by DSM columns was successful not only in controlling lateral spread but in preventing liquefaction.

This paper describes a simplified analytical approach for modeling the dynamic response of DSM at liquefiable sites. The approach combines two-dimensional models of DSM panels oriented both parallel and perpendicular to the direction of strongest ground motion to account for three-dimensional distortion of the DSM grid. Maximum and average soil shear strains from the analysis are used to estimate the ratio of excess pore pressure to effective overburden stress on the basis of published laboratory data.

Analytical results compare very favorably with two separate sets of centrifuge test data. The analytical model correctly predicts the observed behavior of DSM-reinforced soil at the Oriental Hotel during the Kobe earthquake. DSM is effective in reducing liquefaction potential because it provides reinforcement to restrict shear strain in the soil mass. The proposed analytical approach correctly accounts for observed performance and provides a means of assessing the appropriate DSM grid dimensions for effective site improvement.

INTRODUCTION

One of the most promising technologies for site improvement involves deep soil mixing (DSM), whereby cements and hardening agents are mixed in situ with native soil to increase strength and stiffness properties. This method proved to be effective in stabilizing potentially liquefiable soil at several sites during the Kobe earthquake, including the Oriental Hotel (e.g., Hamada and Wakamatsu, 1997), where partial coverage by DSM columns was successful not only in controlling lateral spread but in preventing liquefaction. An important aspect of this application was the use of DSM columns to create rectangular cells to enclose liquefiable sands, thereby reducing substantially the amount of soil needing treatment. Currently, there are no reliable analytical or design procedures for deciding on the appropriate geometry and coverage by DSM columns. Because the issue of optimal coverage is critical for the rational and cost-effective use of

all ground improvement methods, the development of appropriate modeling and design procedures for DSM has fundamental ramifications for the entire suite of site remediation technologies.

This paper describes a simplified analytical approach to modeling the earthquake performance of DSM grids at liquefiable sites. The approach is based on estimating cyclic shear strains in the DSM-reinforced ground and relating these strains to excess pore pressures by means of published laboratory data (e.g., Dobry, et al., 1982). The paper describes the analytical approach, which combines two-dimensional models of DSM panels oriented both parallel and perpendicular to the direction of strongest ground motion to account for three-dimensional grid distortion. Analytical results are compared with centrifuge test measurements. The model also is used in conjunction with strong motion records at Port Island (e.g., Elgamal, et. al., 1996) to evaluate the response of DSM-reinforced fill beneath the Oriental Hotel. The analytical results are then compared with field observations of performance.

CYCLIC SHEAR STRAIN EFFECTS ON LIQUEFACTION

In this paper, the cyclic strain approach is adopted for predicting pore pressure buildup and liquefaction of saturated cohesionless soils. The foundation of this approach was laid by Silver and Seed (1971) and Youd (1972), who produced experimental evidence to show that densification of dry sands is controlled by cyclic strains rather than cyclic stresses, and that there exists a threshold shear strain below which densification does not occur. Since the tendency for a sand to densify when dry is related directly to its tendency to develop excess pore pressure when saturated, it follows that cyclic strains are an appropriate and fundamentally sound basis for predicting pore pressure generation in potentially liquefiable soils.

Dobry and Ladd (1980) and Dobry et al. (1982) proposed an approach that uses cyclic strains rather than cyclic stresses to characterize earthquake-induced loading and liquefaction resistance. Figure 1 shows the pore pressure ratio r_u (defined as the ratio of excess pore pressure to the effective confining stresses) produced by 10 strain-controlled cycles of loading on two different sands prepared by three different methods at three different initial effective confining pressures (Dobry and Ladd, 1980). The fact that pore pressures are relatively insensitive to factors other than cyclic shear strain amplitude for a given number of loading cycles is demonstrated in the figure and is an important feature of the cyclic strain approach. Figure 1 also shows the modulus reduction factor, defined as the ratio of secant modulus under strain to maximum soil modulus, as a function of cyclic shear strain. The experimental range in modulus reduction factor for sands (Seed and Idriss, 1970) also is plotted in the figure. Modulus degradation is accompanied by increased pore pressure as cyclic strains exceed values of approximately 10^{-2} percent.

Figure 2 shows the variation of pore pressure ratio with cyclic shear strain for Monterey No. 0 sand prepared at a relative density of 60% and a confining pressure of 95.6 kPa (Dobry, et al., 1982) for various numbers of strain cycles. Such relationships can be used as a basis for the prediction of pore pressure generation under field conditions, in

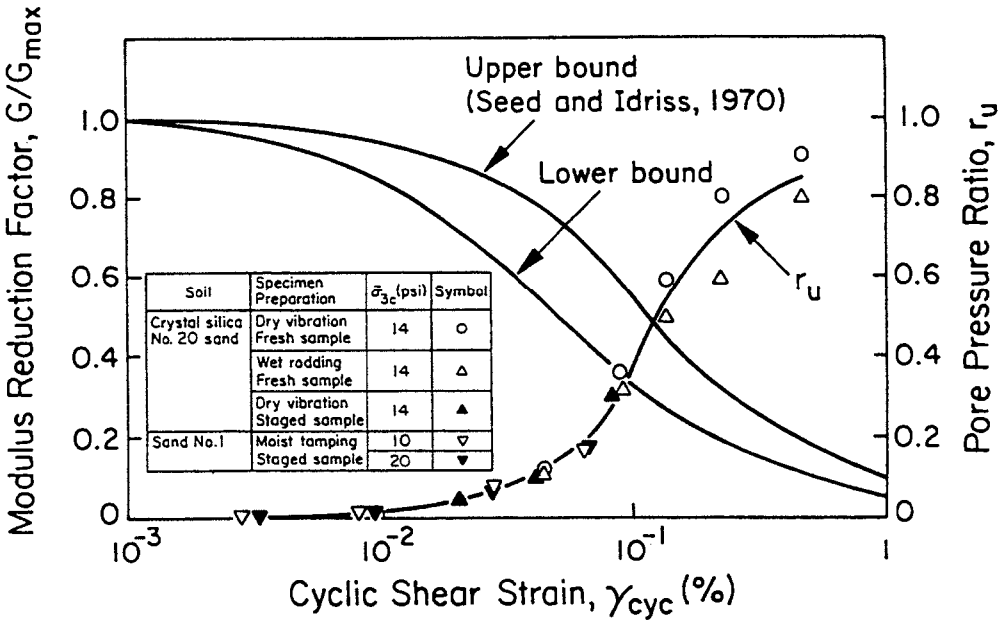

Figure 1 Measured pore pressure ratio after 10 cycles of loading in strain controlled cyclic triaxial tests (Dobry and Ladd, 1980) and the range of modulus reduction factor with cyclic shear strain for sands (Seed and Idriss, 1970).

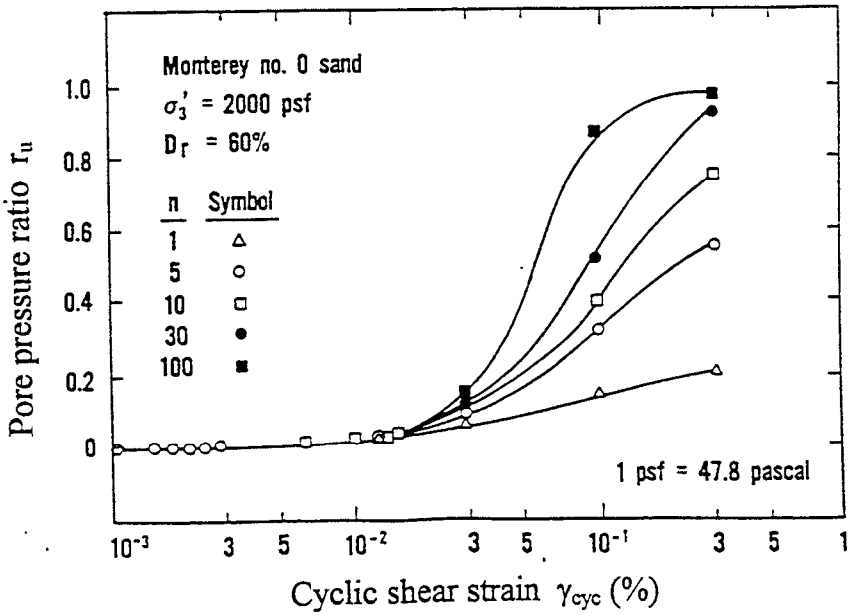

Figure 2 Pore pressure buildup as a function of cyclic shear strain for Monterey No. 0 sand at D_r = 60% , confining pressure = 95.6 kPa (2000 psf) and various number of cycles (Dobry, et al., 1982).

which soil strain profiles are first determined using analytical or numerical procedures that account for dynamic loading and then correlated by means of laboratory data to probable increases in pore pressures.

The cyclic strain approach requires that soil strain profiles be determined to a reasonable level of accuracy before strain amplitudes are correlated to the pore pressure increases using plots like those shown in Figures 1 and 2. The finite element method (FEM) provides an appropriate analytical procedure for simulating soil deformation under earthquake excitation and is employed in this work to obtain soil strain distributions resulting from seismic acceleration-time records.

ANALYTICAL MODEL

General Procedure

In this section, the procedure for implementing a simplified strain-based liquefaction model is described. The key steps are listed in the flow chart in Figure 3, of which the three most important elements are: 1) idealization of the 3-D problem into a 2-D equivalent model so that plane strain analysis can be performed, 2) 2-D FEM analysis to obtain shear deformation of the wall parallel to the direction of strong motion, and 3) plate analysis to obtain the flexural component of wall deformation perpendicular to the direction of strong motion.

Plane strain idealization of 3-D soil structure interaction

To keep the method simple and computationally efficient, some simplifications and idealizations are necessary. The most important of these is to model the DSM walls and soil contained within the DSM wall system as an equivalent homogeneous material with transformed elastic moduli appropriate for plane strain finite element analyses, as explained in Appendix A. This is shown graphically in Figure 4(a). However, this transformation results in a soil-structure system that causes the wall to deform in a shape that is dominated by shear (Figure 4(b)). A more realistic deformed profile of the wall is shown in Figure 4(c), which also reflects flexural deformation. This additional component is modeled using plate analysis, as explained below.

2-D FEM analysis for shear deformation

Figure 5 shows the finite element mesh used for the plane strain analysis of the idealized soil-structure system subjected to earthquake motions. It is discretized using eight-noded isoparametric quadrilaterals, with the nodes along the bottom edge restrained in both the horizontal and vertical directions. The vertical edges are modeled as viscous transmitting boundaries (Lysmer, et al., 1969) which minimize the reflection of energy back into the finite domain.

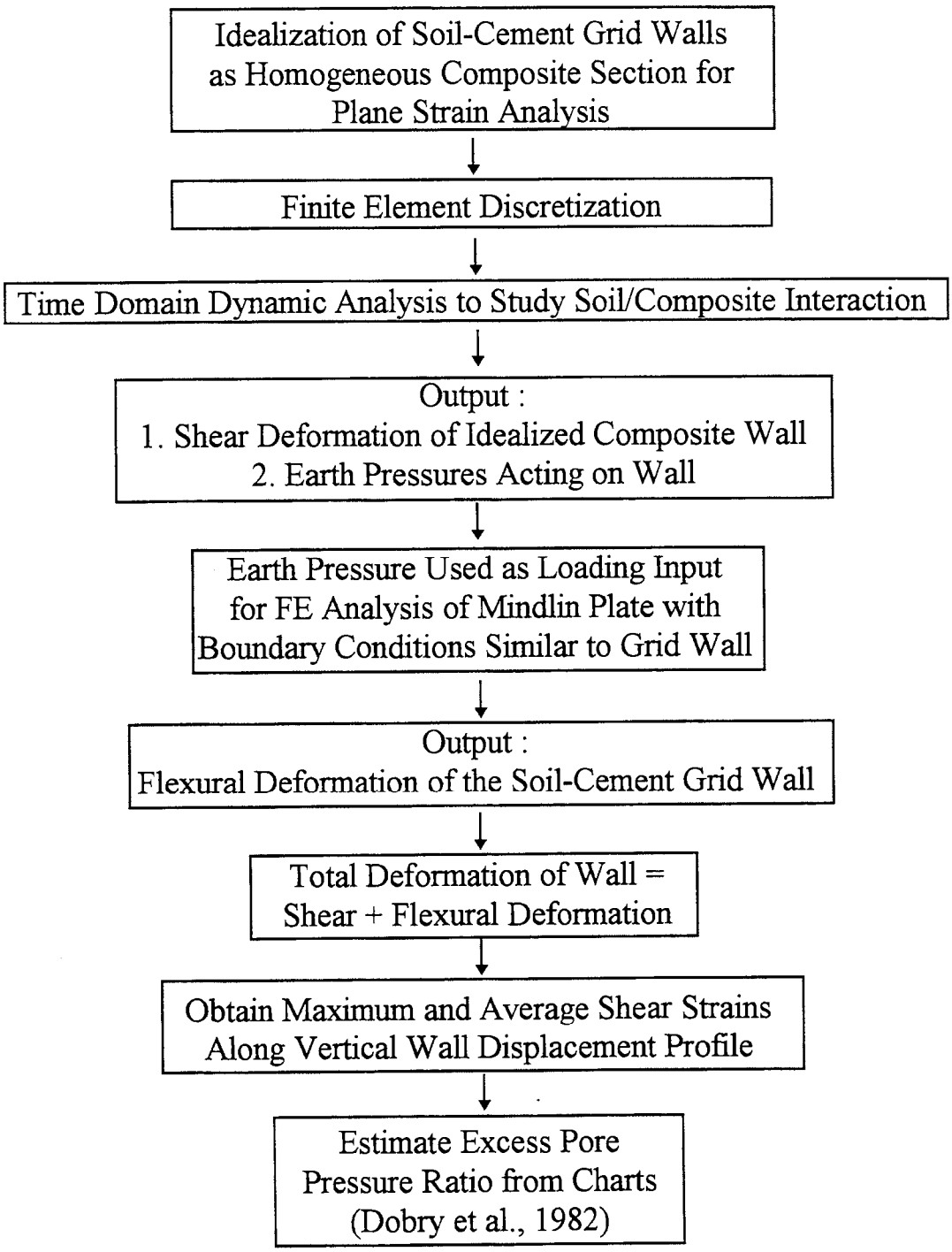

Figure 3 Flow chart showing the general analytical procedures

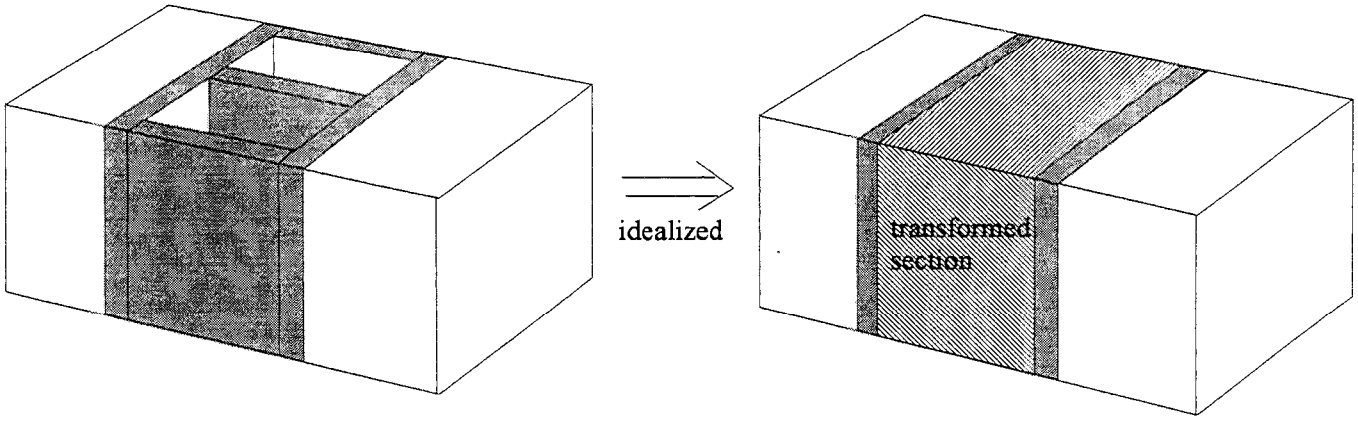

(a) Transformed section

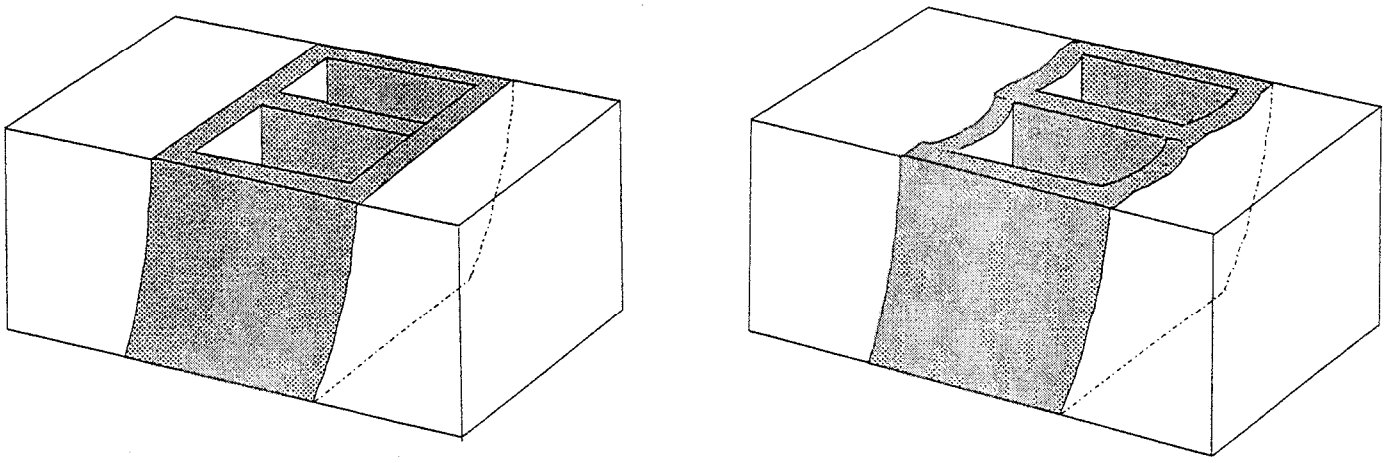

(b) Shear deformation

(c) Shear + Flexure

Figure 4 2-D Idealization and Modes of Deformation

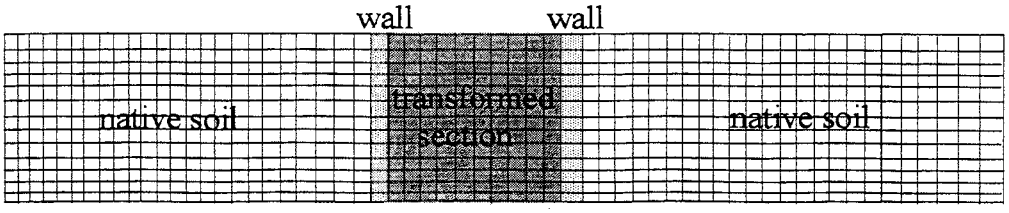

Figure 5 Typical finite element mesh used for DSM analysis

The earthquake accelerations $\ddot{u}_b(t)$ at the base of the liquefiable layer are used as the input excitations. These are applied in the form of inertial forces by writing the global equation of motion as

$$[\mathbf{M}]\{\ddot{\mathbf{u}}\} + [\mathbf{C}]\{\dot{\mathbf{u}}\} + [\mathbf{K}]\{\mathbf{u}\} = -[\mathbf{M}][\mathbf{1}]\ddot{u}_b(t) \quad (1)$$

Equation (1) is solved in the time domain using the standard Newmark time integration scheme (Newmark, 1957).

Since the surrounding soil, wall, and transformed section are modeled as linear, elastic materials, no permanent deformations are incurred. In the absence of permanent strains, the critical deformed profile of the wall is obtained when the wall achieves its maximum displacement from an initial vertical position. Due to the homogeneity of the transformed section, the resultant wall displacement profile is caused mainly by shear, as shown in Figure 4(b). The plane strain analysis does not yield the flexural deformation brought about by inertial forces conveyed to wall elements oriented perpendicular to the direction of strong motion.

Plate analysis for flexural deformation

To model the component of flexural deformation, the computed horizontal soil stresses adjacent to the wall at the instant of maximum wall deflection are used in a plate-bending analysis. The analysis is performed with a finite element code based on the Mindlin plate formulation (Hinton and Owen, 1984). The wall is modeled as a plate with both vertical edges and the bottom edge fixed; the top edge is unrestrained. Since the applied pressure is obtained from the preceding plane strain analysis, this analytical approach does not account for the horizontal variation in soil stresses (perpendicular to the wall subjected to flexure) which may arise due to arching effects associated with wall deformation.

By neglecting arching effects, the simplified model is conservative. Such conservatism is reasonable, and even desirable, because there are considerable uncertainties in our current state of knowledge about DSM properties, soil response under large strain, and the three-dimensional transfer of dynamic stresses.

The displacements along the centerline of the wall are obtained from plate analysis and combined with the displacements obtained from the plane strain, transformed-section analysis. The resultant profile is then used to determine the maximum and average shear strains along the depth of the wall. Using plots, like those in Figures 1 and 2, these strain values can be correlated to the buildup of pore pressure.

To account for soil modulus degradation with increasing shear strains, it is necessary to check that the computed average strains along the depth of the wall are consistent with the values of soil modulus assumed in the elastic analysis. This requires that several trial analyses be performed so that the assumed and predicted modulus converge to a value compatible with the soil strain levels.

Some of the preliminary results obtained using the method described above are presented and discussed in the following sections.

CENTRIFUGE TEST RESULTS

In this section, the strain-based analytical approach is used to study the pore pressure response of a liquefiable soil contained within a DSM structure tested in a centrifuge. The experiments were carried out by Suzuki, et al. (1989) and Babasaki, et al. (1991). Figure 6 shows the plan and section views of one of the centrifuge models (Suzuki, et al., 1989), referred to as Model B. The soil was prepared in two layers : a base layer consisting of compacted fine aggregates and a upper layer comprising a saturated liquefiable sand. The groundwater table was maintained at the top of the liquefiable soil. The DSM structure was composed of three cells, the lengths of which were varied to study the effect of different cell lengths on liquefaction response. Another model (Babasaki, et al., 1991), referred to as Model C, used a DSM structure with more interconnected cells, but a smaller cell width (7 cm) perpendicular to the earthquake motion. Two series of tests were performed with this model in which the water level in the liquefiable sands was varied from the ground surface (test series 1) to an equivalent 1-m depth below ground surface (test series 2). This model is not shown in Figure 6, but the model test results are plotted in Figure 7. There was also a control experiment with no DSM structure that was used to obtain the free-field response of the saturated sand.

The experiments were performed at centrifugal acceleration levels of 100g. All model dimensions shown in Figure 6, therefore, must be multiplied by 100 to obtain the prototype dimensions under field conditions, corresponding to :

thickness of the saturated sand layer	: 10 m
width of DSM cell	: 10 m (Model B)
(normal to direction of earthquake shaking)	: 7 m (Model C)
length of DSM cell	: 5 m, 10 m and 20 m
(in the direction of earthquake shaking)	(Model B)
	: 5 m, 7.5 m, 10 m, 12.5 m and 18.5 m (Model C)

In the simplified procedure proposed here, it is necessary to use a value of the degraded soil modulus that is compatible with the level of strain sustained. The experimental range in the modulus reduction factor has already been presented in Figure 1. Using the degradation model proposed by Drnevich (1972), it is possible, for a particular number of shearing cycles (N) and a reference strain level (γ_r), to obtain a specific G/G_{max} vs. γ_{cyc} relationship that falls within the two experimental bounds plotted in Figure 1. The value of G_{max} was estimated as 51,000 kPa, using the Hardin and Drnevich (1972) equation for sands isotropically consolidated under a pressure σ'_c. With

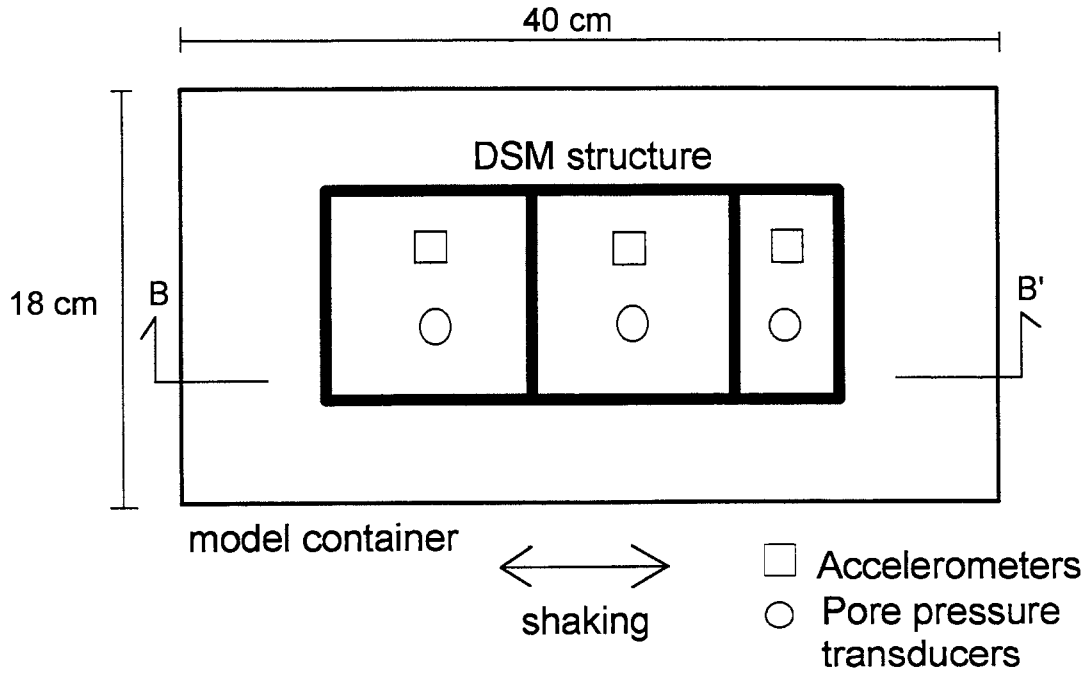

a) Plan View

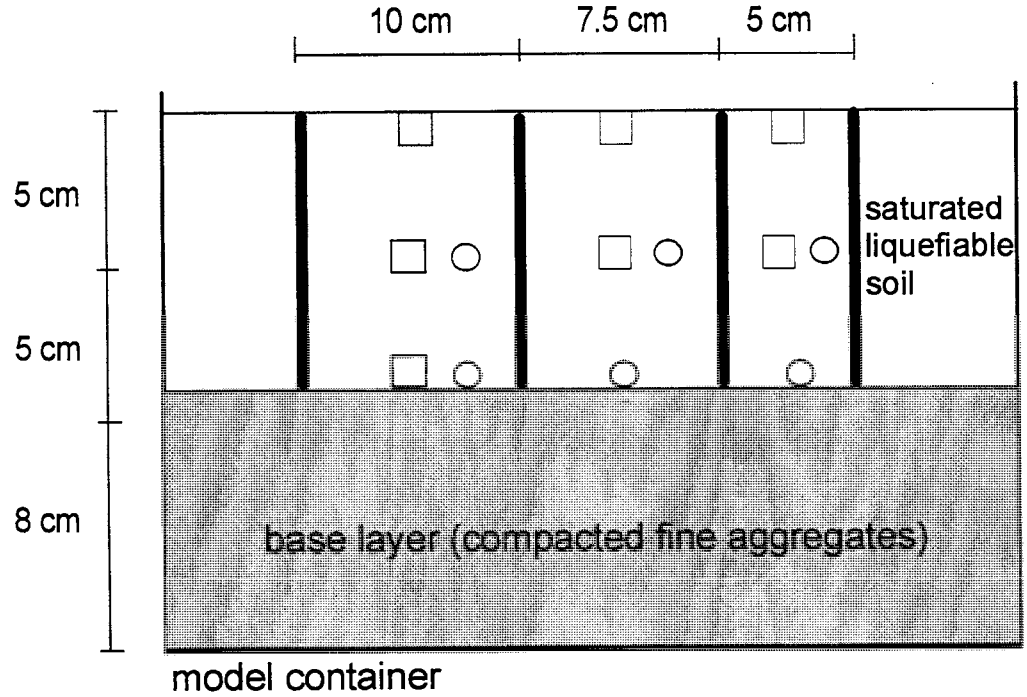

b) Cross-section B-B'

Figure 6 Centrifuge experiment setup

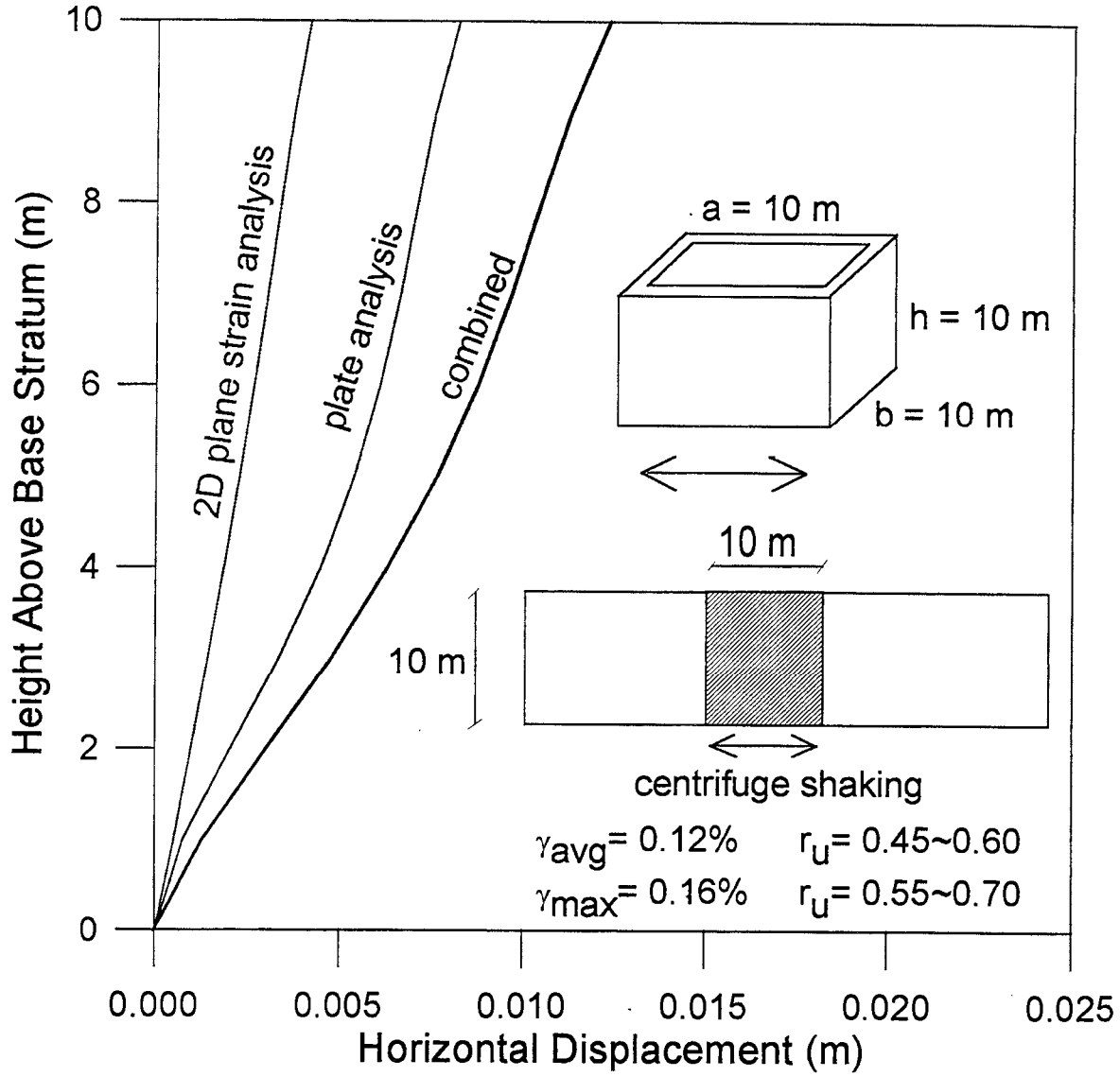

Figure 7 Computed displacement profiles for the centrifuge experiments

this value of G_{max} and the appropriate modulus reduction relationship, trial analyses were performed until the degraded shear modulus and r_u converged on the same level of cyclic shear strain.

The numerical model used a finite element mesh similar to that shown in Figure 5. For the input loadings, the acceleration time records used in the centrifuge experiments were digitized and applied to the finite element model using Equation (1).

The shear modulus of the DSM model walls was estimated from seismic wave velocity and low-strain cyclic triaxial tests on sandy soil treated with slurry cements (Shibuya, et al., 1992). The experimental results show a shear modulus range of approximately 500 to 750 MPa at strain levels compatible with wall deformation. A modulus of 650 MPa was used in the analyses.

Figure 7 shows the computed displacement profiles for the Model B cell with width, length, and depth of 10 m. The shear and maximum flexural deformations from the plane strain and plate analyses, respectively, are plotted and combined to show the maximum deflection. Average and maximum shear strains were calculated from the maximum deflection and used in conjunction with Figure 2 to estimate a range of r_u for 10 to 30 equivalent strain cycles.

The results of the Model B and C centrifuge experiments, together with those from the numerical analyses, are plotted in Figure 8. In this figure, r_u is plotted as a function of the length/depth ratio (a/h) of the cell wall. The experimental results show that r_u increases with higher values of a/h. These results are consistent with the trend predicted by the numerical analyses that are represented by high-low bars delineating the range of analytical results associated with 10 and 30 cycles of equivalent strain.

Figure 8 shows that the analytical and experimental results compare favorably for centrifuge test data. In the next section, the simplified approach is used to predict the field performance of an actual DSM structure used for foundation improvement. The case study involves the performance of the Oriental Hotel during the 1995 Kobe earthquake.

PERFORMANCE OF ORIENTAL HOTEL DURING THE KOBE EARTHQUAKE

The foundation system of the Oriental Hotel consisted of drilled shafts within a DSM grid wall (Hamada and Wakamatsu, 1996). The site of the earthquake, together with the location of the hotel plan and profile views of its foundation system, are shown in Figure 9. Although the surrounding area experienced substantial liquefaction and lateral spread (see Figure 9b for lateral displacement and settlements), the soil and drilled shafts within the DSM structure were relatively unaffected.

As shown in Figure 9, the DSM walls of the Oriental Hotel consist of cells, which vary in shapes and sizes, and would require a 3-D model for a rigorous analysis. However, the method of transformed sections described earlier was used for an approximate analysis. In the case of the Oriental Hotel, the soil masses contained in the cells along the

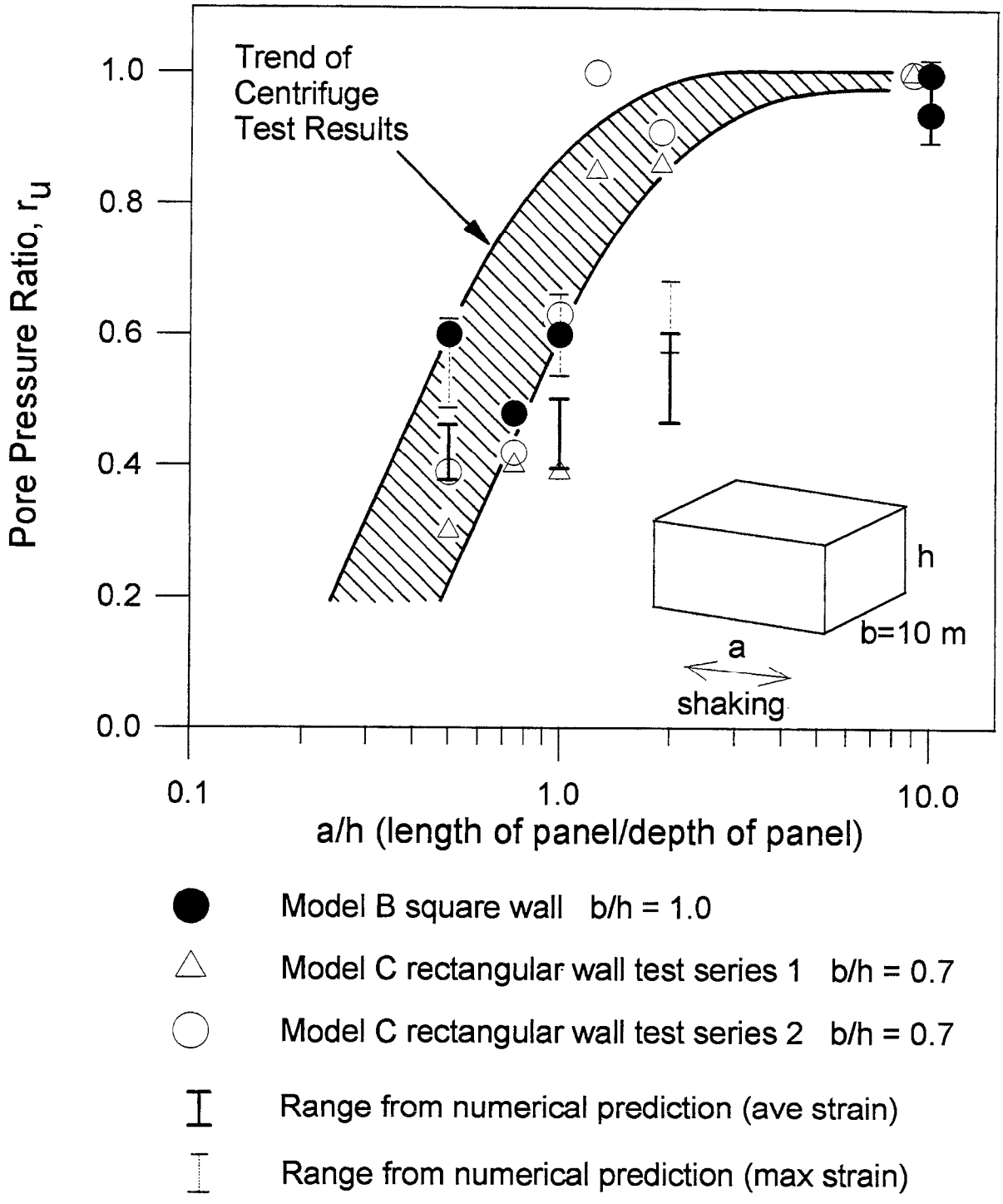

Figure 8 Pore pressure ratios vs a/h from centrifuge tests and numerical analyses

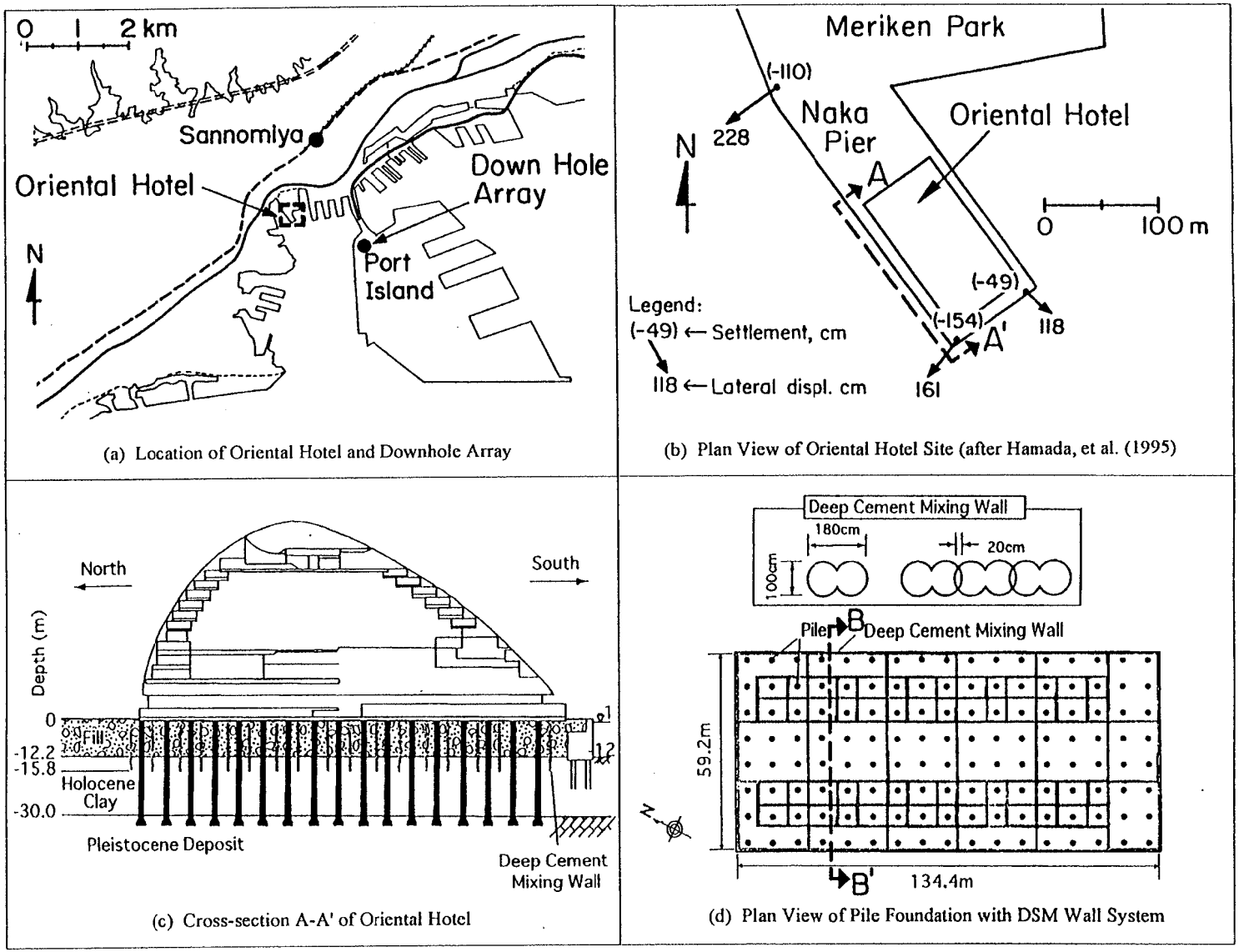

Figure 9 Composite Figure Showing Hotel and Foundation System

cross-section B-B' (Figure 9d) were deemed to be the most susceptible to liquefaction because they have the largest length/depth ratio. Hence, the DSM walls along this section, together with the enclosed soil masses, were transformed into an equivalent homogeneous block appropriate for 2-D plane strain analysis (see Appendix A). A finite element mesh similar to that shown in Figure 5 then was used for analyzing the deformation response of the critical section.

The accelerations at the base of the liquefiable layer were reported by Elgamal, et al. (1996), and are shown in Figure 10. This acceleration record has been resolved in the direction corresponding to the longitudinal axis of the hotel. It was used as the input base accelerations for the finite element analyses.

Figure 11 shows the computed displacement profiles for the critical DSM section of the Oriental Hotel. It can be seen that the shear deformation computed from the 2-D plane strain analysis is quite small compared to the flexural deformation computed from the plate analysis. This observation highlights the important role that three-dimensional flexural effects play in the overall deformation of the system, and also shows how the neglect of these effects may lead to unconservative results.

From Figure 11, the resultant total displacement profile yields an average strain of 0.84% and a maximum strain of 0.93%. By using the r_u relationship plotted in Figure 2, an r_u of approximately 0.9 is predicted. The high values of pore pressure suggest that the soil was close to initial liquefaction. Such a condition probably was not severe enough to cause significant damage or produce surface evidence of liquefaction.

CONCLUSIONS

This paper describes a simplified analytical approach for modeling the dynamic response of DSM at liquefiable sites. The approach combines two-dimensional models of DSM panels oriented both parallel and perpendicular to the direction of strongest ground motion to account for three-dimensional distortion of the DSM grid. Maximum and average soil shear strains from the analysis are used to estimate the ratio of excess pore pressure to effective overburden stress on the basis of published laboratory data.

Analytical results compare very favorably with two separate sets of centrifuge test data. The analytical model correctly predicts the observed behavior of DSM-reinforced soil at the Oriental Hotel during the Kobe earthquake. DSM is effective in reducing liquefaction potential because it provides reinforcement to restrict shear strain in the soil mass. The proposed analytical approach correctly accounts for observed performance and provides a means of assessing the appropriate DSM grid dimensions for effective site improvement.

ACKNOWLEDGMENTS

Part of the research reported in this work was supported by the National Center for Earthquake Engineering Research, Buffalo, NY, under Contract Nos. R91591-A and

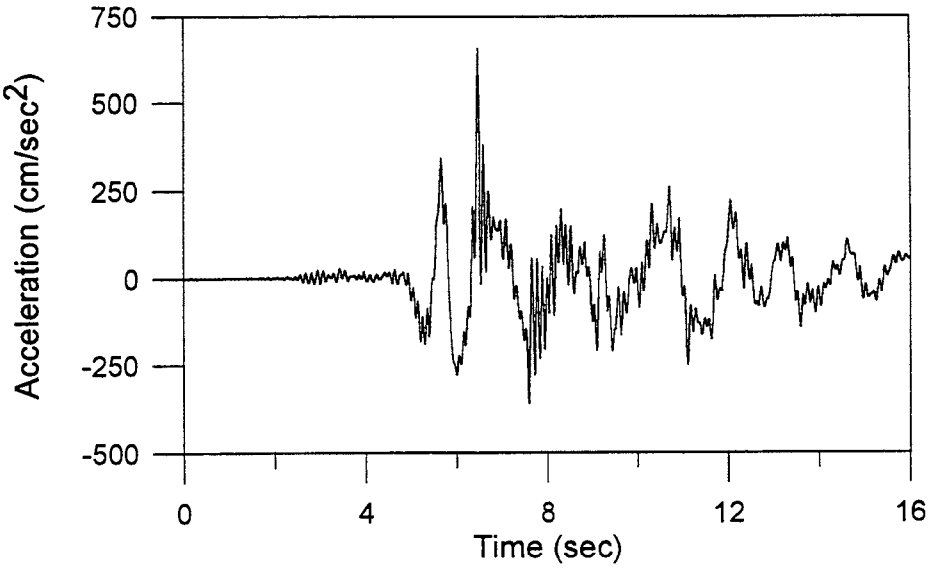

Figure 10 Input acceleration time history for the Kobe earthquake (along the major axis of the Oriental hotel)

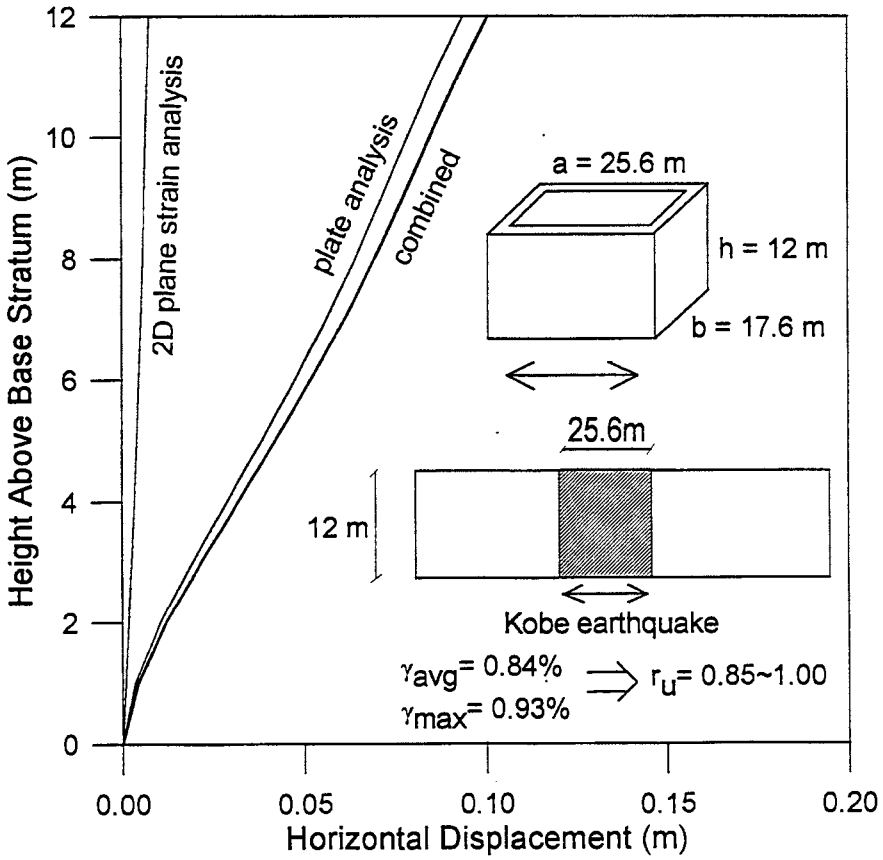

Figure 11 Computed displacement profiles for the Kobe earthquake

R91612. The authors gratefully acknowledge the assistance of S.M.W. Seiko, Inc., Hayward, CA, and particularly Dr. D.S. Yang of Seiko, in obtaining information pertaining to centrifuge test results and the Oriental Hotel. Part of the work was supported by S.M.W. Seiko, Inc. Assistance in preparing the manuscript and figures was provided by L. McCall and A. Avcisoy.

REFERENCES

Babasaki, R., Suzuki, K., Suzuki, Y., and Fujii, S. (1991). "Cell type foundation improved by deep cement mixing method against soil liquefaction (part 2) centrifugal vibration tests on cell type foundation," *Proceedings*, 26th Geotechnical Engineering Research Conference, Nagano, Japan.

Castro, G. (1975). "Liquefaction and cyclic mobility of sands," *Journal of the Geotechnical Engineering Division*, ASCE, Vol. 101, No. GT6, pp.551-569.

Dobry, R., and Ladd, R.S. (1980). Discussion to "Soil liquefaction and cyclic mobility evaluation for level ground during earthquakes," by H.B.Seed and "Liquefaction potential: science versus practice," by R.B.Peck, *Journal of the Geotechnical Engineering Division, ASCE*, Vol. 106, No. GT6, pp. 720-724.

Dobry, R., Ladd, R.S., Yokel, F.Y., Chung, R.M., and Powell, D. (1982). "Prediction of pore water pressure and liquefaction of sands during earthquakes by the cyclic strain method," *NBS Building Science Series 138*, National Bureau of Standards, Gaithersburg, MD.

Drnevich, V.P. (1972). "Undrained cyclic shear of saturated sand," *Journal of the Soil Mechanics and Foundations Division*, ASCE, Vol. 98, No. SM8, pp. 807-825.

Elgamal, A.W., Zeghal, M., and Parra, E. (1996). "Liquefaction of reclaimed land in Kobe, Japan," *Journal of Geotechnical Engineering*, ASCE, Vol. 122, No. 6, pp. 39-49.

Hamada, M., Isoyama, R., and Wakamatsu, K. (1995). "The 1995 Hyogoken-Nanbu (Kobe) earthquake - liquefaction, ground displacement and soil condition in Hanshin area," School of Science and Engineering, Waseda University, Tokyo, Japan, Aug.

Hamada, M. and Wakamatsu, K. (1996). "Liquefaction, ground deformation and their caused damage to structures," *The 1995 Hyogoken-Nanbu Earthquake*, Japan Society of Civil Engineers, Tokyo, Japan, June, pp. 45-92.

Hardin, B.O. and Drnevich, V.P. (1972). "Shear modulus and damping in soils: measurements and parameter effects," *Journal of the Soil Mechanics and Foundations Division*, ASCE, Vol. 98, No. SM6, pp. 603-624.

Hinton, E. and Owen, D.R.J. (1984) *Finite Element Software for Plates and Shells*, Pineridge Press, Swansea, U.K.

Lysmer, J. and Kuhlemeyer, R.L. (1969). "Finite Dynamic Model for Infinite Media", *Journal of Engineering Mechanics Division*, ASCE, 95(4), pp 859-877.

Newmark, N.M. (1959). "A Method of Computation for Structural Dynamics", *Journal of the Engineering Mechanics Division*, ASCE, Vol. 85, pp 67-94.

Seed, H.B. and Idriss, I.M. (1970). "Soil moduli and damping factors for dynamic response analyses," *Report EERC 70-10*, Earthquake Engineering Research Center, University of California, Berkeley.

Shibuya, S., Tatsuoka, F., Teachavorasinskun, S., Kong, X.J., Abe, F., Kim, Y.-S., and Park, C.-S. (1992). "Elastic deformation properties of geomaterials," *Soils and Foundations*, Vol. 32, No. 3, pp. 26-46.

Silver, N.L. and Seed, H.B. (1971). "Volume changes in sands during cyclic loading," *Journal of the Soil Mechanics and Foundations Division*, ASCE, Vol. 97, No. SM9, pp. 1171-1190.

Suzuki, Y., Suzuki, K., and Babasaki, R. (1989). "Cell type foundation improved by deep cement mixing method against soil liquefaction (part 4) centrifugal vibratory tests on anti-liquefaction effects," *Proceedings*, Research Conference of Japan Society of Architecture, Kyushu, Japan.

Youd, T.L. (1972). "Compaction of sands by repeated shear straining," *Journal of the Soil Mechanics and Foundations Division,* ASCE, Vol.98, No.SM7, pp.709-725.

APPENDIX A
EQUIVALENT TRANSFORMED SECTION FOR PLANE STRAIN ANALYSIS

To perform a plane strain analysis, it is necessary to transform the compartmentalized soil-wall section shown in Figure A1 into an approximately equivalent homogeneous section shown in Figure A2.

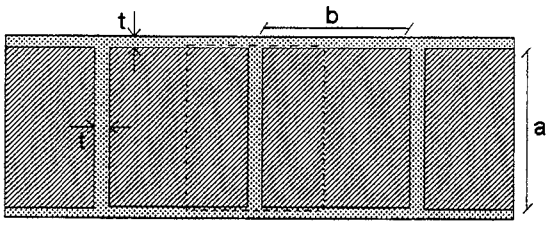

Figure A1 Original soil-wall system

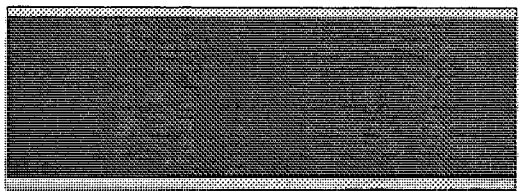

Figure A2 Transformed section

The procedures are illustrated in Figures A3(i) - (iii).

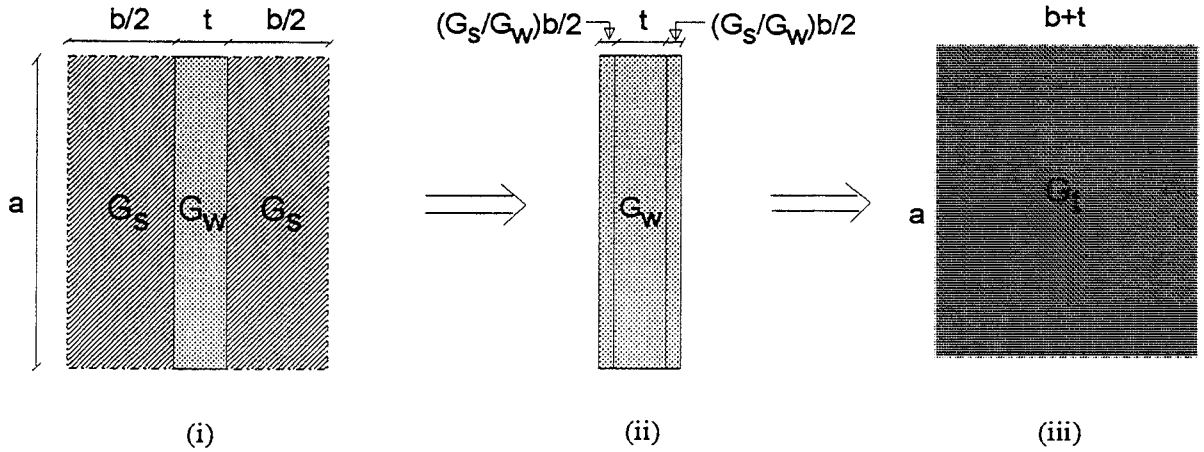

Figure A3 Steps in obtaining the transformed section

Figure A3(i) shows the plan view of a representative unit of the soil-wall mass. Using the method of transformed sections, the soil mass can be converted into an equivalent wall of thickness $(G_s/G_w)b$. Although this results in a homogeneous section, the dimensions have been modified and a further transformation is needed to convert this homogeneous section (of shear modulus G_w) into one which retains the original dimensions but having a transformed modulus G_t.

The transformation from the section shown in Figure A3(ii) to that shown in Figure A3(iii) is accomplished by the relationship given below :

$$G_w A'_w = G_t A_{unit} \quad \text{(a1)}$$

where A'_w = area of the homogeneous transformed section with $G = G_w$

$$= [t + (G_s / G_w)b]\, a \quad \text{(a2)}$$

A_{unit} = area of one representative unit of the original soil-wall compartment

$$= [t + b]\, a \quad \text{(a3)}$$

Hence an estimate of G_t can be obtained as

$$G_t = \frac{G_w\left[t + (G_s / G_w)b\right]}{[t + b]} \quad \text{(a4)}$$

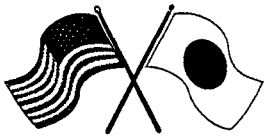

Session 2
Underground Structures

Session Co-chairs: Maurice Power and Tatsuo Ohmachi

NATIONAL CENTER FOR EARTHQUAKE ENGINEERING RESEARCH
Headquartered at the State University of New York at Buffalo

INSTITUTE OF INDUSTRIAL SCIENCE INCEDE UNIVERSITY OF TOKYO

GIS ASSESSMENT OF WATER SUPPLY DAMAGE FROM THE NORTHRIDGE EARTHQUAKE

T.D. O'Rourke
S. Toprak
School of Civil and Environmental Engineering
Cornell University
Ithaca, NY

ABSTRACT

The 1994 Northridge earthquake resulted in the most extensive damage to a US water supply system since the 1906 San Francisco earthquake. Three major transmission systems, which provide over three-quarters of the water for the City of Los Angeles, were disrupted. Los Angeles Department of Water and Power (LADWP) and Metropolitan Water District (MWD) trunk lines (nominal pipe diameter $\geq$ 600 mm) were damaged at 74 locations, and the LADWP distribution system required repairs at 1013 locations. The widespread disruption provides a unique opportunity to evaluate the geographic variability of the damage, the most vulnerable pipelines, and the relationship among damage, transient motion, and permanent ground deformation.

This paper describes how a geographical information system (GIS) was developed for the earthquake response of the LADWP system. Damage patterns are evaluated for each type of pipeline and related to seismic intensity, measured transient motion, locations of high water table, and locations of permanent ground deformation. Key factors affecting earthquake damage are discussed.

INTRODUCTION

The 1994 Northridge earthquake led to significant disruption of the water supply system of Los Angeles, causing damage at 15 locations in the three transmission systems providing water from Northern California, 74 locations in water trunk lines (nominal pipe diameter $\geq$ 600 mm), and 1013 locations in the Los Angeles Department of Water and Power (LADWP) distribution pipeline network. The damage was distributed over approximately 1200 km^2. Damage of such a widespread nature invites questions about its spatial variability and its relationship with parameters such as earthquake intensity, peak acceleration, peak velocity, groundwater levels, and areas of permanent ground deformation (PGD). Large water supply systems are composed of pipelines constructed with different materials, diameters, and joint characteristics. Hence, there also are questions about how the damage patterns are influenced by different material and mechanical characteristics.

Questions related to spatial variability are well suited for evaluation with geographical information systems (GIS). This paper provides a description of how a GIS database was assembled for water supply damage caused by the Northridge earthquake. The characteristics of the Los Angeles water supply are discussed, and graphical information is provided regarding the

overall statistics and spatial patterns of pipeline damage. Various spatial relationships between earthquake damage and seismic intensity are explored. Local patterns of damage and repair also are examined relative to groundwater levels and zones of liquefaction-induced PGD.

EARTHQUAKE DAMAGE DATABASES

The earthquake-induced damage to water pipelines and the database developed to characterize this damage have been described by O'Rourke, et al. (1996), and only the salient features of this work are summarized here. Geographic information system databases for lengths of trunk lines according to pipe composition and size were assembled with ARC/INFO software (ESRI, Inc., 1994). All LADWP and Metropolitan Water District (MWD) trunk lines within the area covered by the LADWP system were digitized from 1:12,000 scale pipeline maps provided by LADWP.

The trunk line repair database was assembled from repair statistics provided by LADWP and MWD, as well as extensive discussions with engineers of both organizations. The distribution line repair database was organized from repair statistics developed for the State of California Office of Emergency Services (OES). After a careful evaluation of the 1405 original OES repair records, it was determined that 1013 were valid for damage at distribution mains and hydrants. Reliable information about pipe composition could be found for 964 repairs, and this portion of the database is used in this paper for evaluating percentages of pipeline damage according to composition.

The distribution pipeline database was supplemented by databases developed for the trunk line and aqueduct systems. Repairs to all LADWP and MWD trunk lines within the City of Los Angeles were characterized and located in the GIS. The repairs to all transmission pipelines upstream of the Jensen and City of Los Angeles water treatment facilities were similarly assembled in the GIS database.

LOS ANGELES WATER SUPPLY SYSTEM

Figure 1 shows that the portion of the Los Angeles water supply system most seriously affected by the Northridge earthquake superimposed on the topography of Los Angeles. The water supply system includes transmission lines, trunk lines and distribution lines. All large diameter pipelines upstream of the treatment plants are considered to be transmission facilities.

Figure 2 presents charts showing the relative lengths of LADWP and MWD trunk and distribution lines, according to pipe composition. It should be noted that the vertical axis in Figure 2c is logarithmic scale. The figures were developed from LADWP statistics, valid as of June, 1994. Because statistics on ductile iron (DI) pipe are not provided in LADWP summaries of total pipeline length, the percentage of DI pipe was estimated on the basis of evaluations of the digitized portion of the system. The MWD trunk lines include pipelines within the area of the LADWP system designated by MWD as feeder lines. Total lengths of approximately 700 km and 300 km for LADWP and MWD trunk lines, respectively, are included in the database, and the pie charts in each figure show the relative percentages of the combined LADWP and MWD trunk lines associated with different types of pipe material. The concrete category includes precast

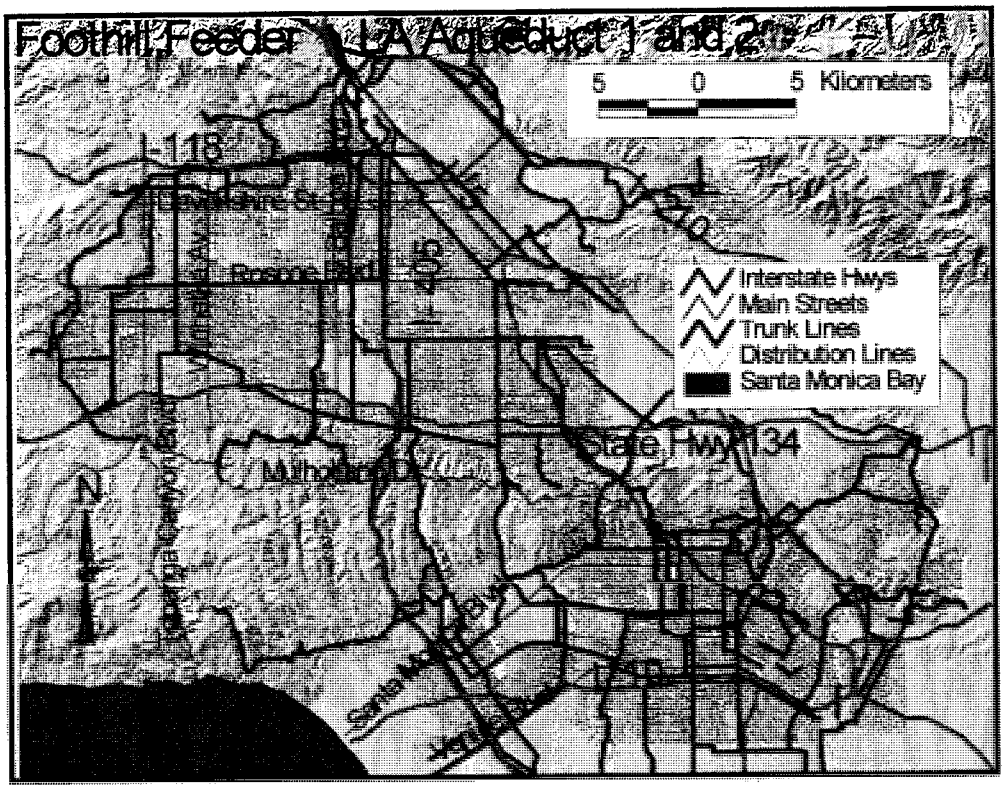

Figure 1. Map of Los Angeles Water Supply System Affected by Northridge Earthquake

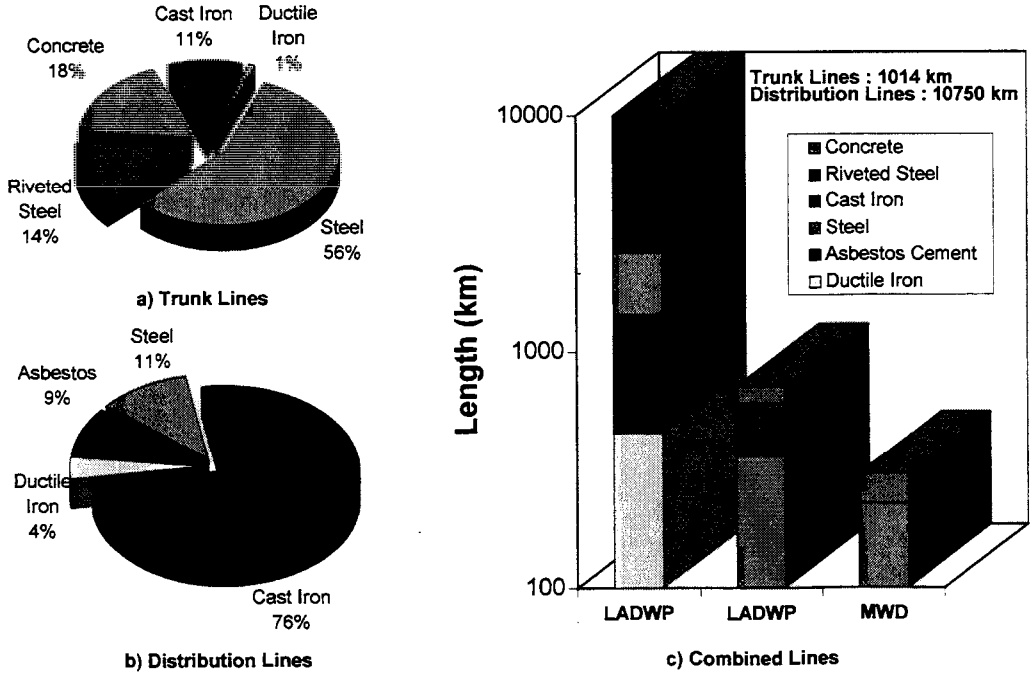

Figure 2. Composition Statistics of Water Trunk and Distribution Lines

concrete, prestressed concrete, reinforced concrete, and concrete cylinder pipelines. About 70% of the trunk lines are composed of steel, with 14% associated with riveted steel and 56% associated primarily with steel pipe connected by welded slip joints. The total length of the distribution lines is 10,750 km. About 76% and 11% of the distribution lines composed of cast iron and steel, respectively.

Figure 3 shows cast iron (CI) pipeline density in the study area. Pipeline density is presented in terms of pipe length contours, obtained by overlaying a 2 km x 2 km mesh onto distribution lines and determining the CI pipeline length in each mesh area. The length of pipelines in each area is divided by the same area to provide a normalized parameter independent of grid size. Contours then were drawn from the spatial distribution of normalized lengths, each of which were centered on its tributary area.

The figure illustrates that CI pipelines are distributed at a relatively high density throughout the City of Los Angeles. Since 76% of the water distribution system consists of CI pipelines with widespread distribution throughout the city, this type of pipeline can be used most effectively to evaluate the distribution and characteristics of damage over the entire area.

Figure 4 shows pipe length contours for steel distribution pipelines, developed in a manner similar to that for Figure 3. Comparison of Figures 3 and 4 shows a significant difference between the density patterns for CI and steel pipe. Steel pipelines are concentrated mostly in hillsides and mountains.

NORTHRIDGE EARTHQUAKE DAMAGE

Figure 5 shows the locations of transmission lines and associated repairs superimposed on a topographic map. The map illustrates an area to the north of City of Los Angeles. Elevation contours at 50 m intervals were obtained from Digital Elevation Model (DEM) files. Locations of repairs are marked by solid circles, with the numbers of repairs indicated at locations of concentrated damage. Locations of welded slip joint repairs are identified separately. As shown in the figure, the aqueduct systems that supply water from northern California are the Foothill Feeder, operated by MWD, and Los Angeles Aqueducts No. 1 and 2, operated by LADWP. A description of damage sustained by LADWP and MWD transmission lines has been provided by Lund (1995). In total, there were 11 repair locations in LADWP Aqueducts No. 1 and 2, of which 4 involved either circumferential cracks or compressive buckling at welded slip joints. Excessive axial pullout occurred at 2 Dresser couplings.

Damage to the MWD transmission system occurred near the Jensen Filtration Plant at a welded slip joint of a 2160-mm steel pipeline and as cracks and leakage in a reinforced concrete conduit. Damage was sustained by another steel pipeline at a sleeve-type coupling and in an area of differential settlement and horizontal movement adjacent to the Jensen Plant.

Figure 6 presents a map of trunk line repair locations in the northwestern portion of San Fernando Valley. Sixty-seven of the 74 trunk line repairs were located in this region, with the highest concentrations of damage in the Van Norman Complex, near the intersection of Balboa

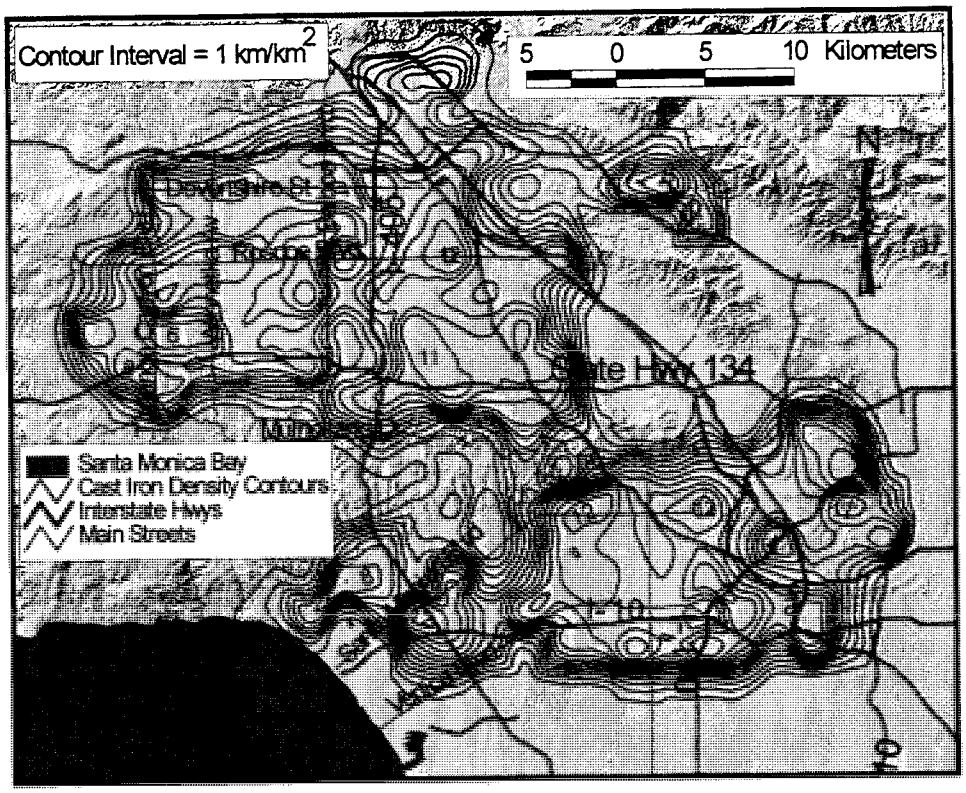

Figure 3. Cast Iron Pipeline Density Map

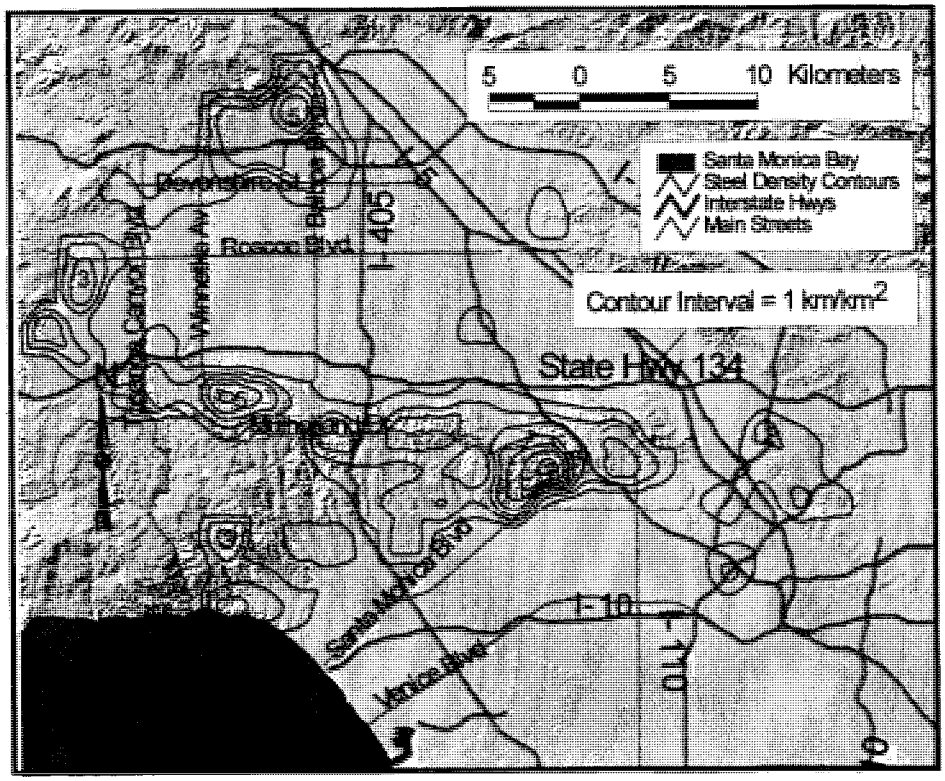

Figure 4. Steel Pipeline Density Map

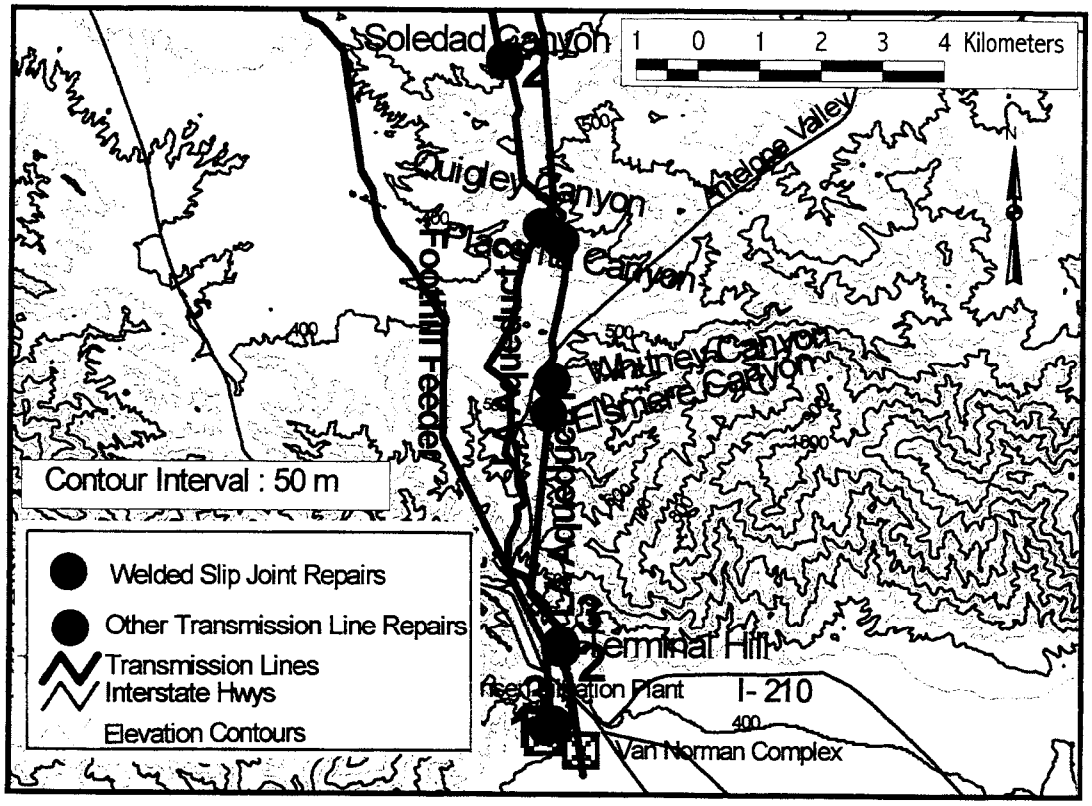

Figure 5. Water Transmission Line Damage

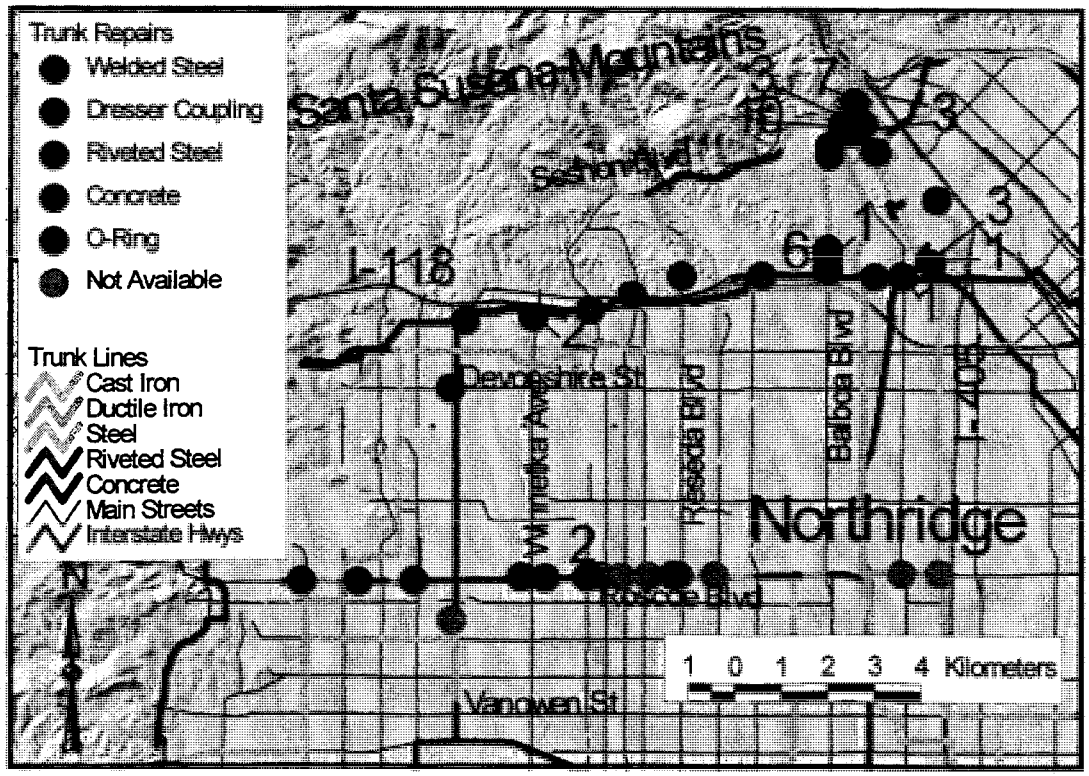

Figure 6. Water Trunk Line Damage

Blvd. and Rinaldi St., and along Roscoe Blvd. At locations of multiple repairs, a number is shown that represents the sum of repairs made at that location.

Figure 7 presents a map of distribution pipeline repair locations and repair rate contours for CI pipeline damage. The repair rate contours were developed by dividing the map into 2 km x 2 km areas, determining the number of CI pipeline repairs in each area, and dividing the repairs by the distance of CI main in that area. Contours then were drawn from the spatial distribution of repair rates, each of which was centered on its tributary area. The 2 km x 2 km grid was found to provide a good representation of damage patterns for the map scale of the figure. These contours are especially well suited for comparing damage with the spatial distribution of strong motion parameters, as discussed in a forthcoming section.

Figure 8 presents a map of pipeline repair locations and repair rate contours for steel pipelines. The map and contours were developed in a manner similar to that for the CI pipeline repair rate contours. Both Figures 7 and 8 need to be evaluated relative to the spatial patterns of density for CI and steel pipelines presented in Figures 3 and 4, respectively. For example, Figure 4 shows that steel pipelines are located mostly at higher elevations surrounding the San Fernando Valley. Steel pipeline repairs, therefore, are located in these areas.

The overall statistics of pipeline damage are summarized in Figure 9 in the form of pie and bar charts. As with Figure 2, please note that the bar chart scale is logarithmic. Most repairs to trunk lines occurred in steel pipelines, with 80% of all repairs in riveted and continuous wall steel piping. Sixty-six percent of repairs were in continuous wall steel pipe, whereas only 56% of all trunk lines were composed of this type of pipe. The steel trunk lines were damaged heavily by compressive wrinkling of welded slip joints, with this type of damage recorded at 20 locations. There also were 10 reported locations of pullout at compression couplings.

Seventy-one percent of the distribution line repairs were in CI pipelines, which constitute 76% of the system (see Figure 2). Twenty-two percent of the repairs were in steel pipelines, which constitute only 11% of the system (see Figure 2). The relatively high concentration of steel pipeline repairs is associated with various types of steel, such as Mannesman and Matheson steel, which are prone to corrosion, as well as damage at certain types of elastomeric joints that are vulnerable to creep and leakage.

EARTHQUAKE DAMAGE VS. SEISMIC INTENSITY

Figure 10 shows the repair rate contours for CI pipelines superimposed on zones of Modified Mercalli Intensity (MMI) mapped by USGS (Dewey, et al., 1995). The locations of highest repair rate coincide with areas of MMIX and MMVIII.

Figures 11 and 12 show the repair rate contours for CI pipelines superimposed on zones of peak acceleration and velocity measured by free-field strong motion instruments. The free-field records used to plot peak acceleration and velocity zones are identical to those described by Chang, et al. (1996) in their evaluation of the engineering implications of the earthquake motion. The records from approximately 240 rock and soil stations were used. The maximum horizontal acceleration of 1.78 g measured at the Tarzana-Cedar Hill Nursery was removed from the

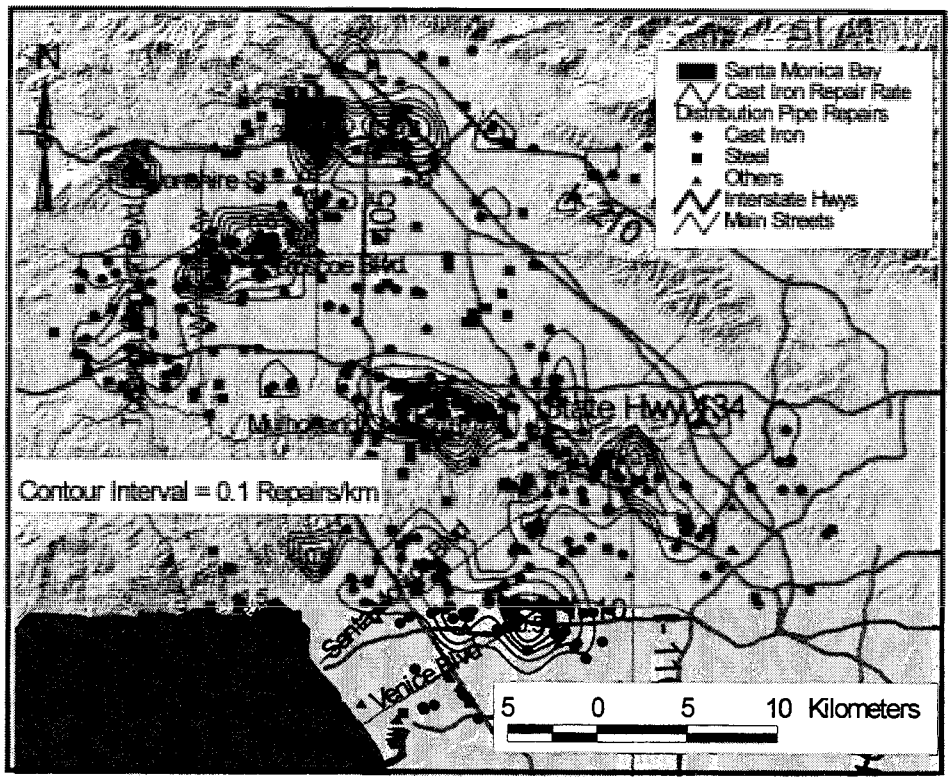

Figure 7. Cast Iron Pipeline Repair Rate Contours

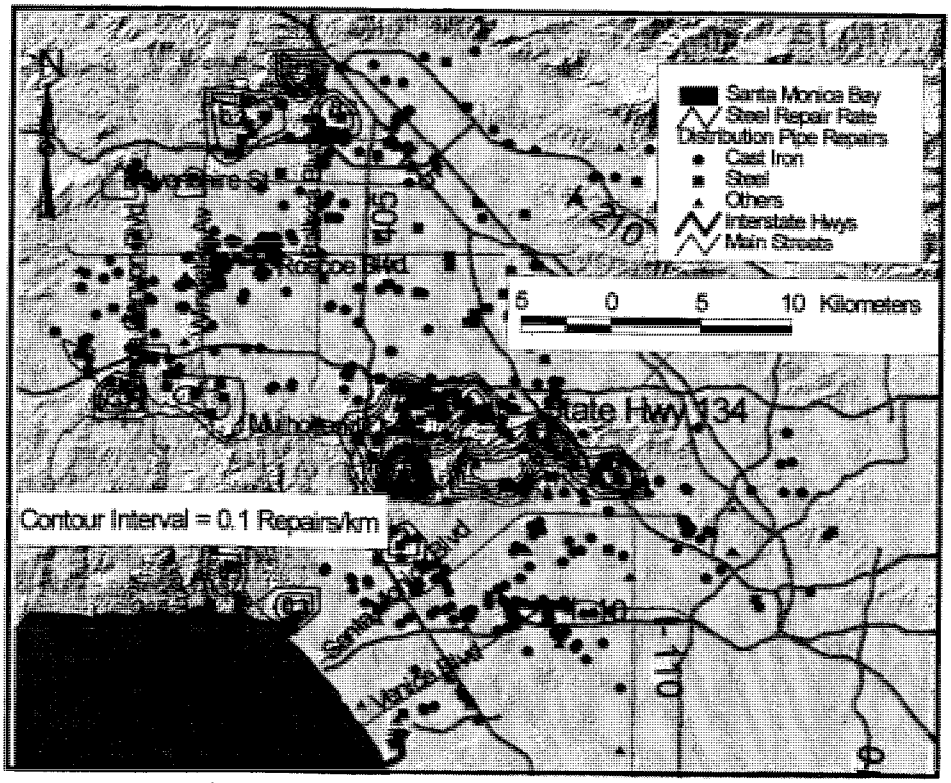

Figure 8. Steel Pipeline Repair Rate Contours

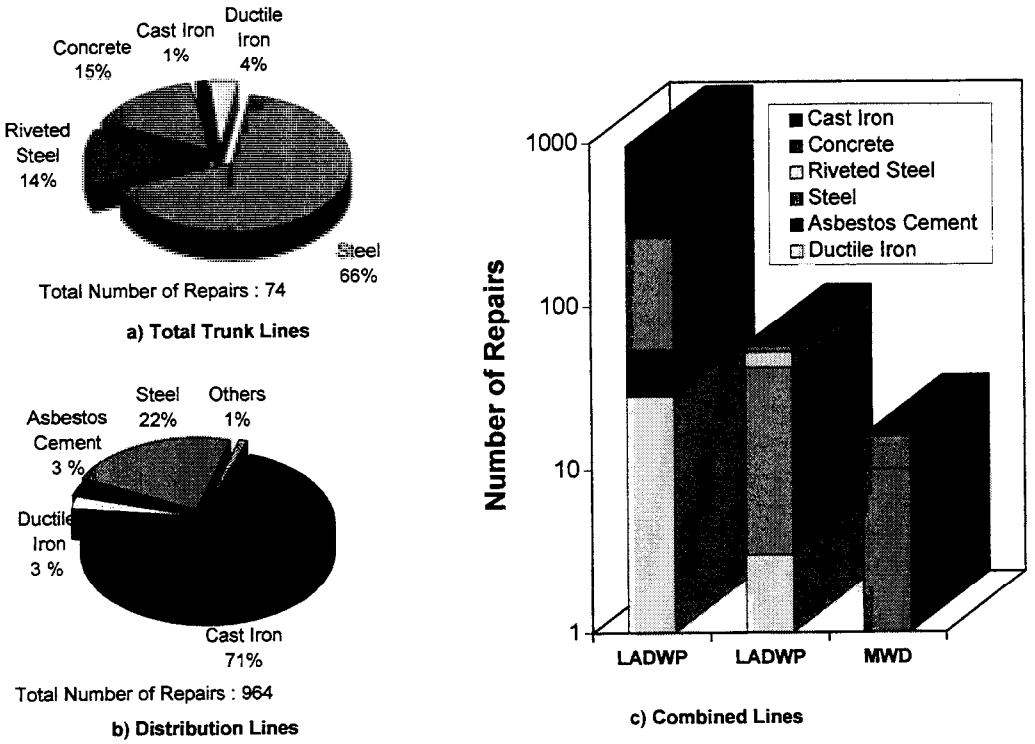

Figure 9. Repair Statistics of Water Trunk and Distribution Lines

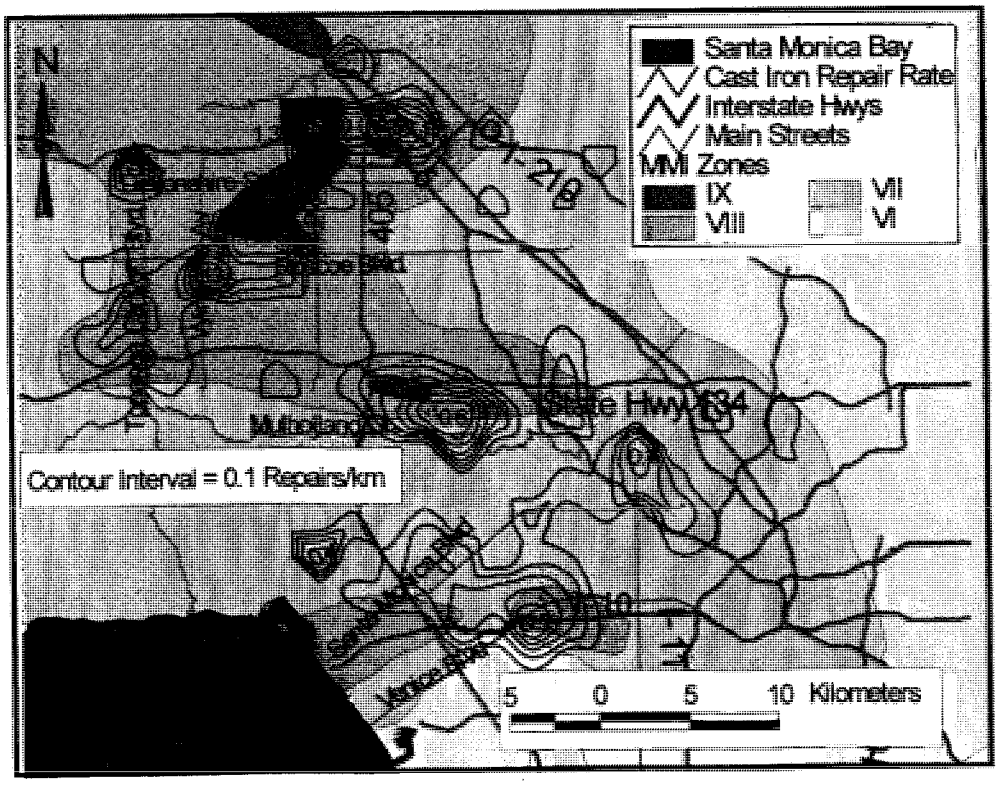

Figure 10. Pipeline Repair Rate Contours vs. MMI

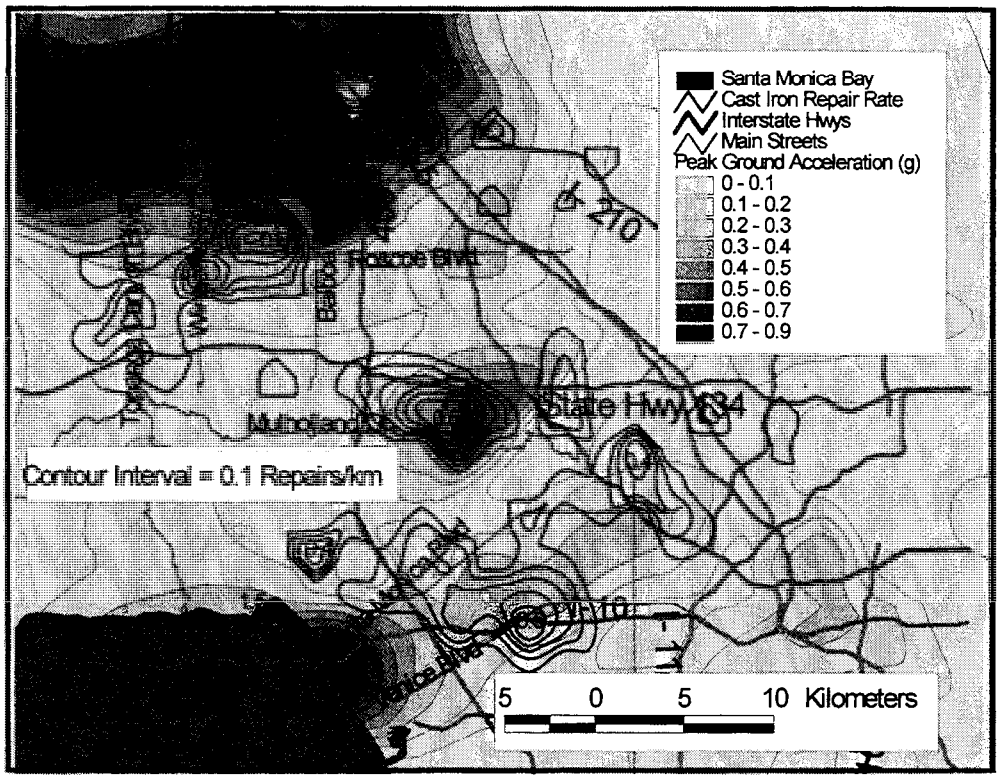

Figure 11. Pipeline Repair Rate Contours vs. Peak Ground Acceleration

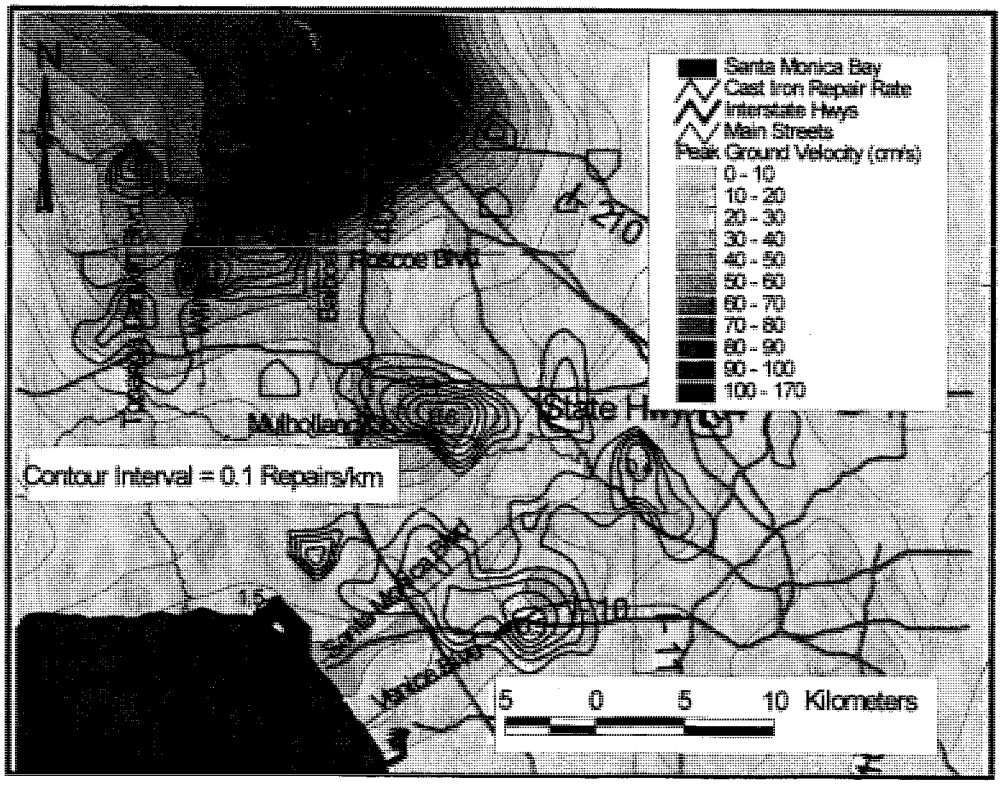

Figure 12. Pipeline Repair Rate Contours vs. Peak Ground Velocity

database prior to GIS evaluation to avoid distortions from possible topographic influences. In addition, records from stations at dam abutments were screened when a station downstream of the dam was available, again to minimize distortion from topographic effects.

The zones of highest peak acceleration coincide reasonably well with the locations of highest repair rate, especially near the northern edge of the San Fernando Valley, the Santa Monica Mountains, and the Los Angeles Basin. The zones of highest peak velocity show similar spatial correlation with repair rate concentrations. The velocities do not coincide as well with repair concentrations in the Los Angeles Basin, but correlate better with CI pipeline repairs in the western and central portions of San Fernando Valley.

It is notable that high concentrations of repair rate occur in the northern portion of the Santa Monica Mountains in the Sherman Oaks area. This location coincides with a zone of extensive slope movements, ground fissures, and cracking of artificial fill described by Barrows, et al. (1995). Ground failure of this type is likely affected by acceleration levels, which were very high in the Sherman Oaks area, as illustrated in Figure 11. Zones of high acceleration, therefore, would be expected to correlate with locations of ground failure and thus PGD effects on pipelines. In contrast, zones of high velocity would be expected to correlate well with locations of high transient ground strain and be correlated less directly with PGD.

LOCAL PATTERNS OF DAMAGE

Figure 13 shows CI pipeline repair rate contours in the western and central portions of San Fernando Valley superimposed on the outline of high groundwater level zones that are taken from Tinsley, et al. (1985) and Los Angeles County (1990). The highest repair rate concentrations occur in pre- and post-1944 zones with groundwater approximately 3 m deep. Holzer, et al. (1996) report that locations within this area experienced PGD from both liquefaction and failure of soft clay sediments. It appears that the high groundwater table helps to delineate locations of liquefiable sands and soft clay, both of which are susceptible to large transient strains associated with site amplification. They are also susceptible to ground failure.

Figure 14 shows locations of pipeline repair and repair rate contours near the intersection of Balboa Blvd. and Rinaldi St. This area was influenced by liquefaction-induced lateral spread (Holzer, et al., 1996) that contributed to catastrophic failure of a gas transmission and two water trunk lines (O'Rourke and Toprak, 1995). A 0.5 km x 0.5 km was used to determine repair rates in this area. The local repair rates are exceptionally high, with a maximum value of 4.5 repairs/km.

CONCLUSIONS

Geographical information systems (GIS) are well suited for evaluating the spatial relationships between water supply system damage and factors such as seismic intensity, peak acceleration, peak velocity, groundwater levels, and locations of ground failure. Spatial correlations between water pipeline damage and each of these parameters were examined for the 1994 Northridge earthquake. Good correlations between pipeline repair rates and both peak acceleration and peak velocity were found, although neither parameter was observed to provide consistently strong correlations at all locations of concentrated repair. It appears that zones of

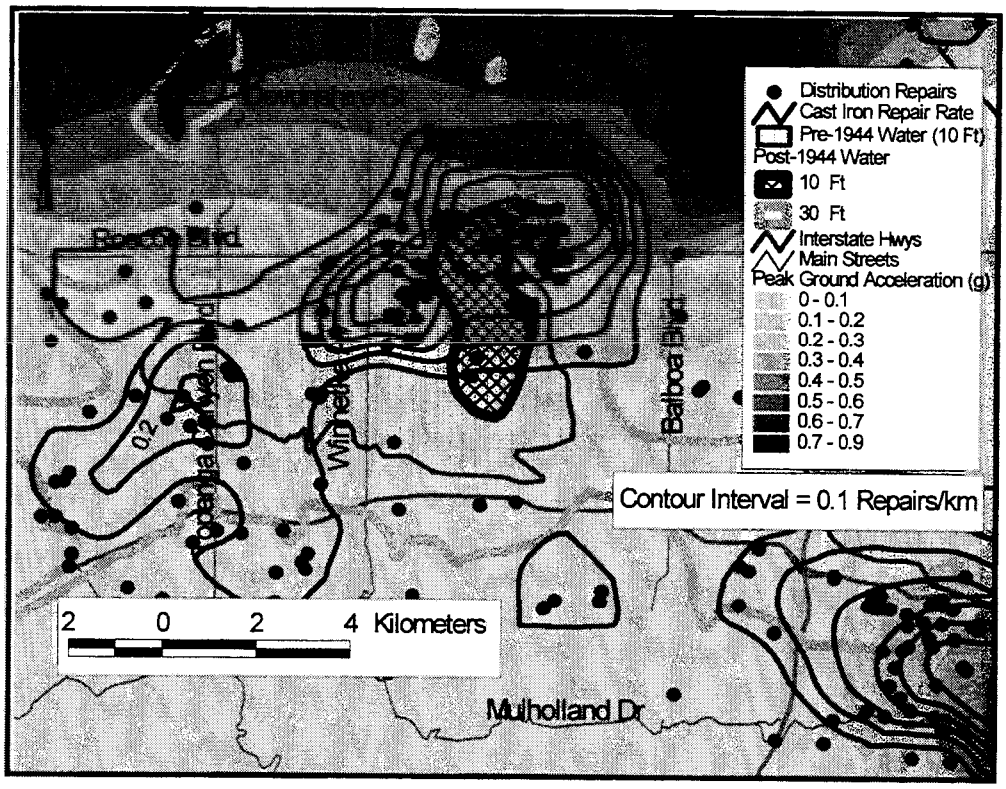

Figure 13. San Fernando Valley Pipeline Repair Rate Contours, Peak Ground Acceleration, and Ground Water Table

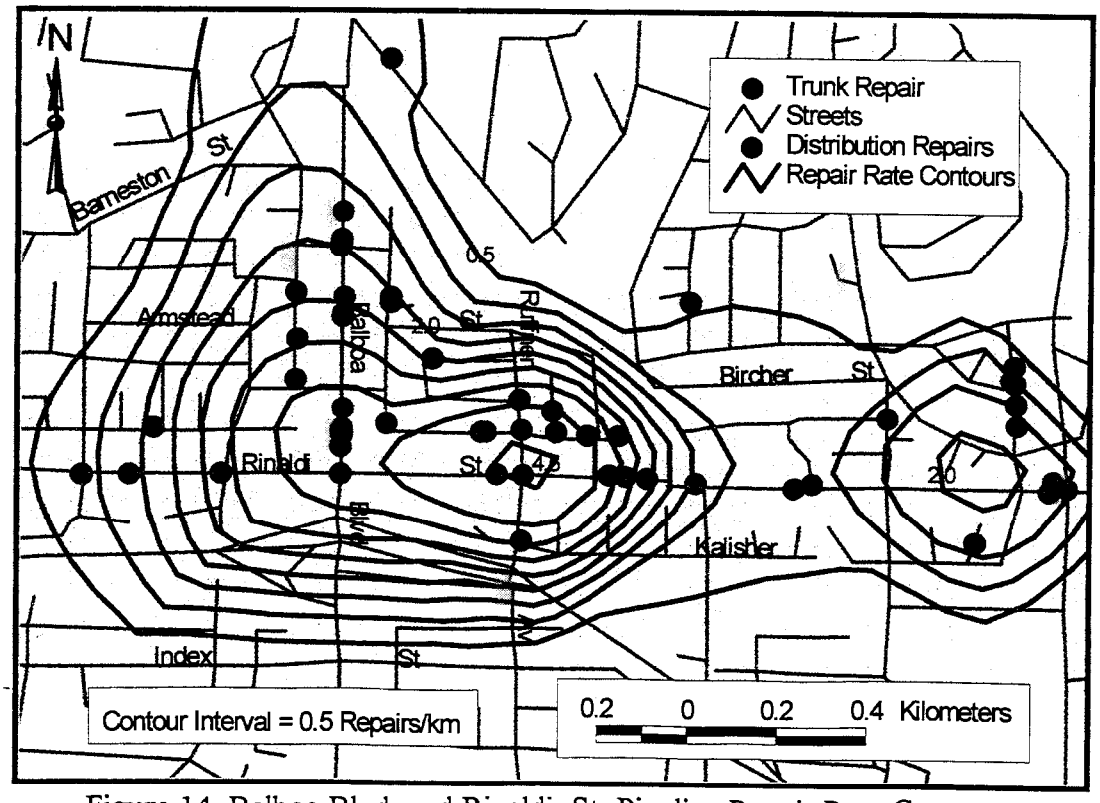

Figure 14. Balboa Blvd. and Rinaldi St. Pipeline Repair Rate Contours

high peak acceleration coincide with locations of ground failure and thus PGD effects on pipelines. In contrast, zones of high velocity would be expected to correlate well with locations of high transient ground strains. Zones of high groundwater level in the western and central portions of San Fernando Valley help to delineate locations of liquefiable sands and soft clay, both of which are susceptible to large transient strains associated with site amplification. They also are susceptible to ground failure. There is a strong spatial correlation between pipeline repair rates resulting from the Northridge earthquake and high groundwater levels in the San Fernando Valley.

ACKNOWLEDGMENTS

The research reported in this paper was supported by the National Center for Earthquake Engineering Research, Buffalo, NY under Contract Nos. R91598 and R91605. The authors wish to express their deep gratitude to Mr. H. Dekermenjian of LADWP for his interest and assistance in obtaining pipeline and pipeline repair data. Thanks are also extended to Mr. N. Blaze of EQE, Inc., Mr. C. Davis of LADWP, and Mr. D. Wright of MWD for their assistance in obtaining valuable information. The manuscript was prepared by L. McCall, and A. Avcisoy helped prepare the figures.

REFERENCES

Barrows, A.G., Irvine, P.J., and Tan, S.S. (1995). "Geologic surface effects triggered by the Northridge earthquake," The Northridge, California, Earthquake of 17 January 1994, *Special Publication 116*, M.C. Woods and W.R. Seiple, Eds., California Division of Mines and Geology, Sacramento, CA, pp. 65-88.

Chang, S.W., Bray, J.D., and Seed, R.B. (1996). "Engineering implications of ground motions from the Northridge earthquake," *Bulletin of the Seismological Society of America*, Vol. 86, No. 1B, Feb., pp. 5270-5288.

Dewey, J.W., Reagor, B.G., Dengler, L., and Moley, K. (1995). "Intensity distribution and isoseismal maps for the Northridge, California, earthquake of January 17, 1994," *U.S. Geological Survey Open-File Report 95-92*, U.S. Department of the Interior, Washington, DC.

ESRI (1994). *The ARC/INFO User's Guide*, Environmental Systems Research Institute, Inc., Redlands, CA.

Holzer, T.L., Bennett, M.J., Tinsley, J.C. III, Ponti, D.J., and Sharp, R.V. (1996). "Causes of ground failure in alluvium during the Northridge, California earthquake of January 17, 1994," *Technical Report NCEER-96-0012*, National Center for Earthquake Engineering Research, Buffalo, NY, pp. 345-360.

Los Angeles County (1990). *Technical Appendix to the Safety Element of the Los Angeles County General Plan, Hazard Reduction in Los Angeles County*, Department of Regional Planning, Dec.

Lund, L. (1995). "Water systems," in Northridge Earthquake Lifeline Performance and Post-Earthquake Response, A.J. Schiff, Ed., *TCLEE Monograph No. 8*, ASCE, August, pp. 96-131.

O'Rourke, T.D. and Toprak, S. (1995). "Case history of pipeline response to ground deformation at Balboa Blvd., 1994 Northridge earthquake," *Proceedings*, Sixth U.S.-Japan Workshop on Earthquake Disaster Prevention for Lifeline Systems, Osaka, Japan, July, pp. 3-20.

O'Rourke, T.D., Toprak, S., and Sano, Y. (1996). "Los Angeles water pipeline system response to the 1994 Northridge earthquake," *Technical Report NCEER-96-0012*, National Center for Earthquake Engineering Research, Buffalo, NY, pp. 1-16.

Tinsley, J.C., Youd, T.L., Perkins, D.M., and Chen, T.F. (1985). "Evaluation of liquefaction potential," Evaluating Earthquake Hazards in the Los Angeles Region - An Earth-Science Perspective, *U.S. Geological Survey Professional Paper* 1360, J.I. Ziony, Ed., U.S. Department of the Interior, Washington, DC, pp. 263-316.

EFFECTS OF LIQUEFACTION-INDUCED LARGE GROUND DISPLACEMENT ON EARTHQUAKE RESISTANCE OF FOUNDATIONS DURING THE HYOGOKEN-NANBU EARTHQUAKE

Masanori Hamada
Department of Civil Engineering
Waseda University, Tokyo, Japan

Kazue Wakamatsu
Institute of Industrial Science
University of Tokyo, Japan

ABSTRACT

This paper introduces performances of foundations under a condition of liquefaction-induced ground displacement and investigates the effects of the ground displacements on the earthquake resistance of the foundations. It also introduces some examples of undamaged foundations even when the surrounding ground largely moved horizontally.

INTRODUCTION

The 1995 Hyogoken-nanbu earthquake caused a significant soil liquefaction in an extensive area of reclaimed land in Kobe and its neighboring cities. The soil liquefaction also induced large ground displacements in the horizontal direction, which resulted in serious damage to buried lifeline facilities and foundations of bridges and buildings. The authors have investigated the liquefaction during the earthquake and its caused damage to various kind of civil engineering structures. They also measured the liquefaction-induced ground displacements in reclaimed lands along the waterfront of Hanshin area by an arial survey using both pre- and post-earthquake photographs and by referring to the results from field surveys.[1] Typical examples of damage related liquefaction-induced ground displacements are presented. In addition, the authors discuss the performances of foundations in the area of the liquefaction and large ground displacements, by referring to the types of the foundation, and sought effective countermeasures in the liquefied ground.

DAMAGE TO BRIDGE FOUNDATIONS

Foundations of Rokko Liner The "Rokko Liner" is a railway, which is connecting J.R. Sumiyoshi St. in mainland and the Rokko Island. It was reported that many foundations of bridges of the railway moved towards the sea with a magnitude of several ten centimeters due to liquefaction-induced large ground displacements. Photo. 1 shows that a steel girder of the railway dropped due to movement and inclination of its concrete caisson foundation of a diameter of 6.0 meters and a depth of about 40 meters. The ground in the neighborhood consists of filled soil with a thickness of about 20 meters overlying soft Holocene clay of the original seabed sediment as shown in Fig. 1, and the foundation was penetrated into the Pleistocene gravel layer at a depth of about 40 meters below the ground surface.

According to an on-ground survey conducted by Kobe city government the top of the caisson foundation moved about 60 cm towards the sea. As shown in Fig. 2, the quaywalls in front of the railway foundation displaced towards the sea, at a maximum about 3.5 meters, and consequently the ground behind the quaywalls widely moved towards the sea. Many ground fissures, about 30-

50 cm wide were caused due to the large tensile strain of the ground as shown in Photo. 2. The ground in Photo. 2 moved towards the sea, from the right to the left, and the ground surface had been originally flat before the earthquake, but largely inclined.

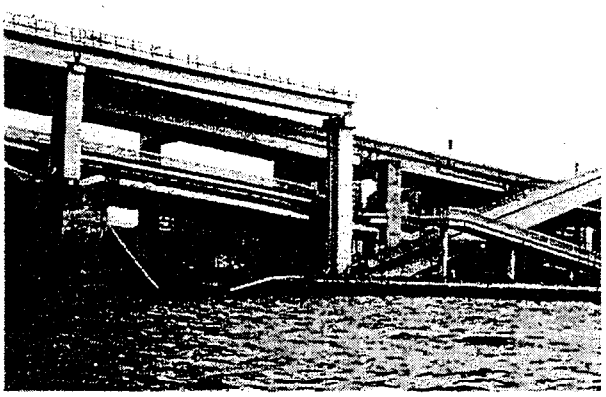

Photo.1 Bridge girder dropped due to ground displacement (A in Fig. 2)

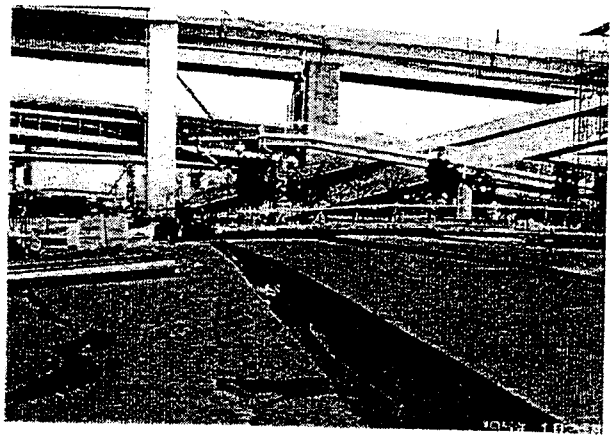

Photo. 2 Ground fissure due to ground strain in northern part of Rokko Island

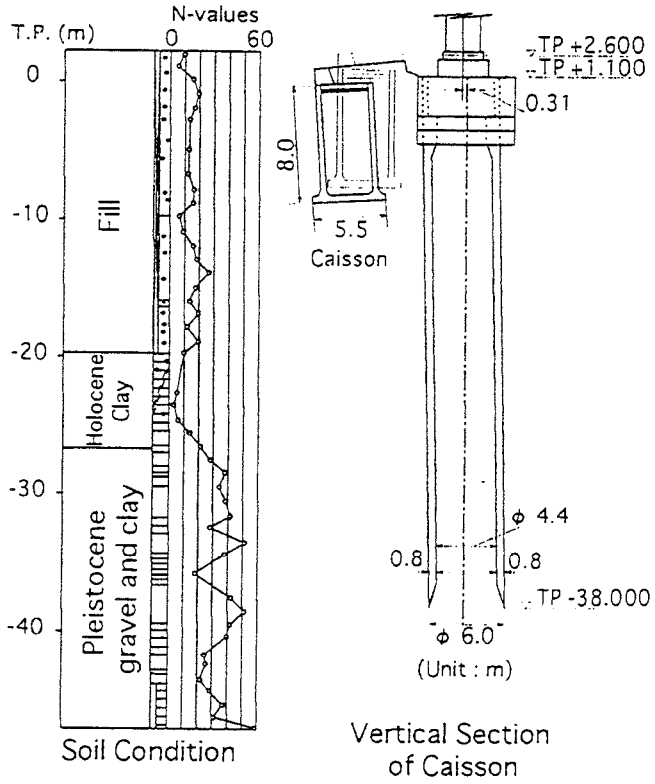

Fig. 1 Profile of caisson foundation and soil in neighborhood (Rokko Liner)[2)]

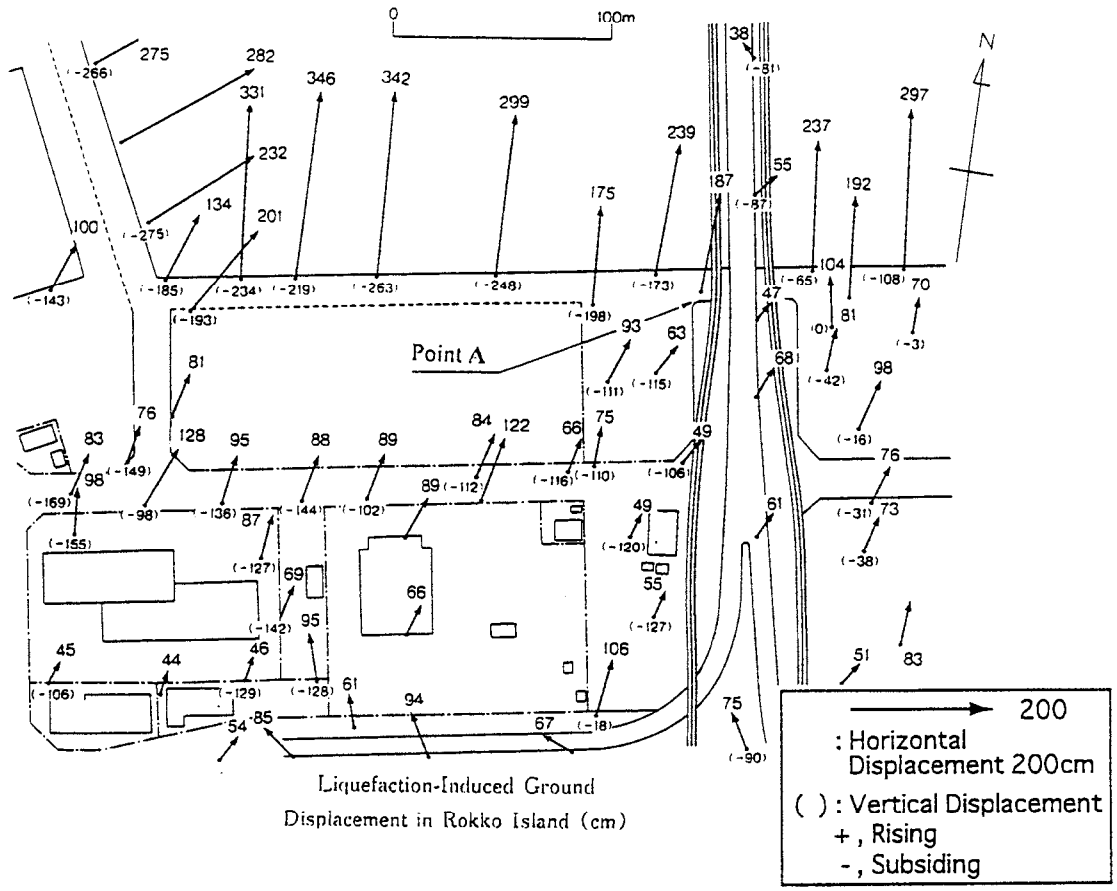

Fig. 2 Liquefaction-induced ground displacement on northern part of Rokko Island[1)]
(At point A a steel girder of the railway dropped)

Bridge Piers of No. 5 Bay Highway The No. 5 Bay Highway is connecting Osaka city and Rokko Island in Kobe city, and was constructed in 1993. The bridges of this highway did not suffer any critical damage because it was designed by latest design code. However, many bridge foundations moved and/or inclined due to liquefaction-induced large ground displacements.

Figure 3 shows displacements of the ground measured by the authors and the movement of top of bridge piers measured by a committee of Japan Road Association[3)]. The light colored sand in Photo. 3 boiled out of the ground surface, and it can be recognized that the ground in the neighborhood of the highway bridge, caused a significant liquefaction. The bridge piers displaced in the same direction with the displacement of the surrounding ground, but the magnitude of the displacement of the piers is smaller than that of the ground. The maximum displacement of the top of the piers was about 90 cm, while the surrounding ground moved about 1-2 meters. These piers have cast-in-place concrete pile foundations, but it was reported that many of them had been significantly cracked, and were reinforced after the earthquake.

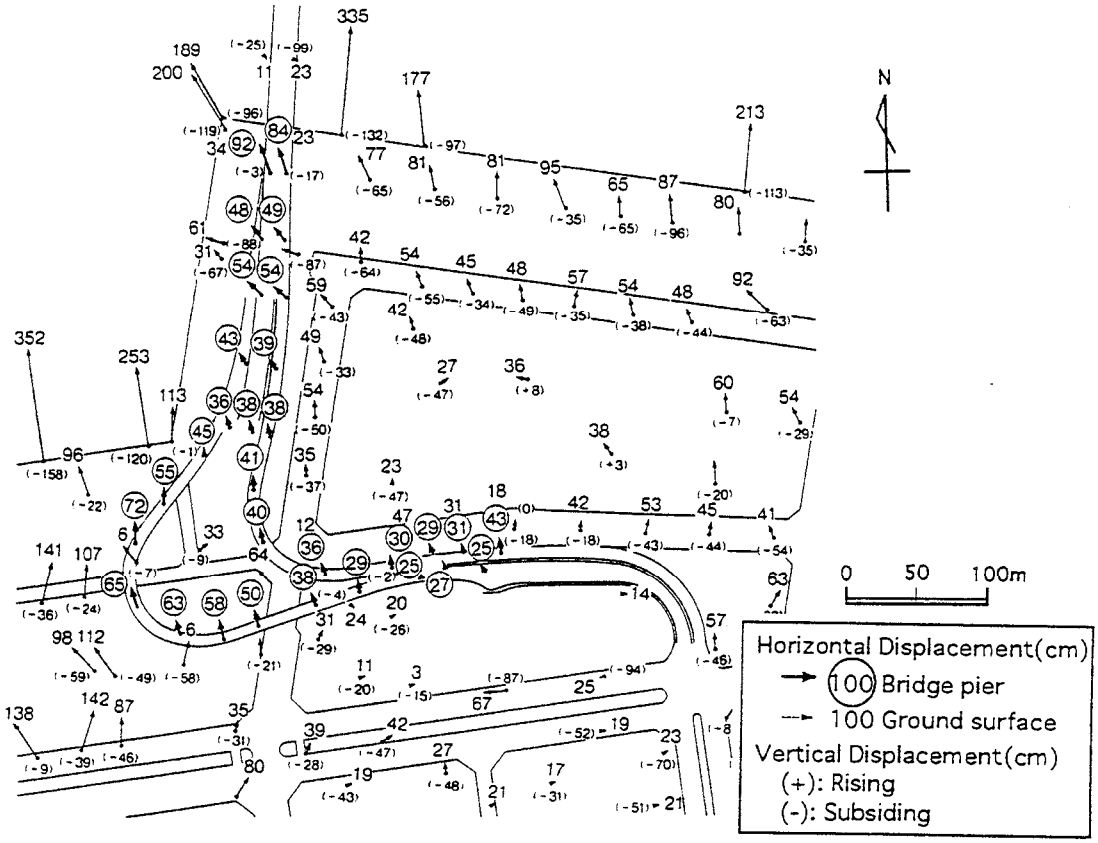

Fig. 3 Displacements at ground surface[1] and at top of bridge piers[3] at northern part of Rokko Island

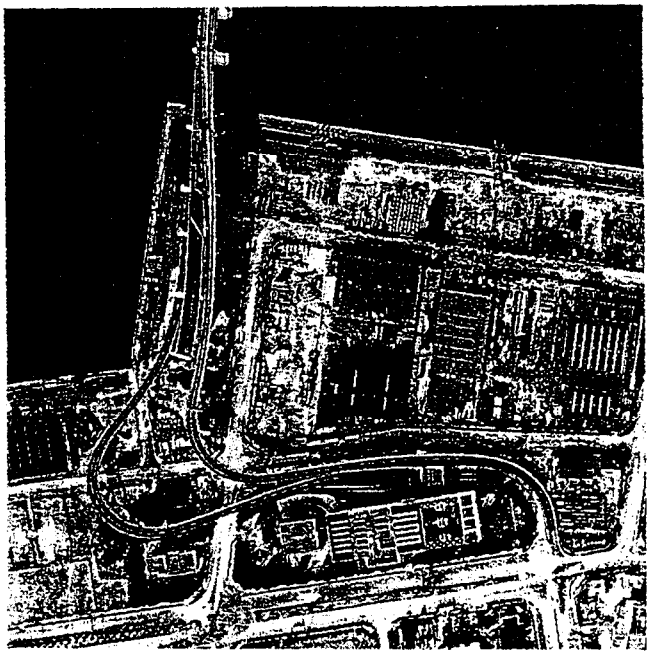

Photo. 3 The No. 5 Bay Highway in Rokko Island

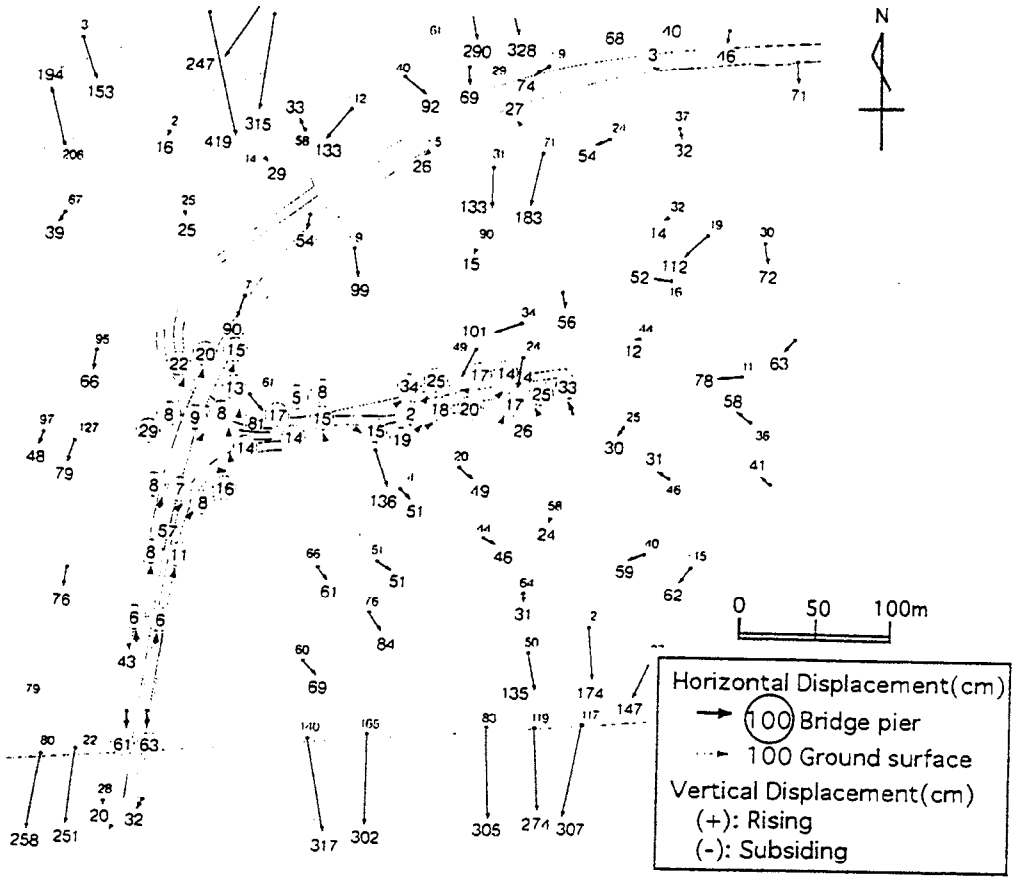

Fig. 4 Displacements at ground surface[1] and at top of bridge piers[3] at southern part of Uozaki-hama

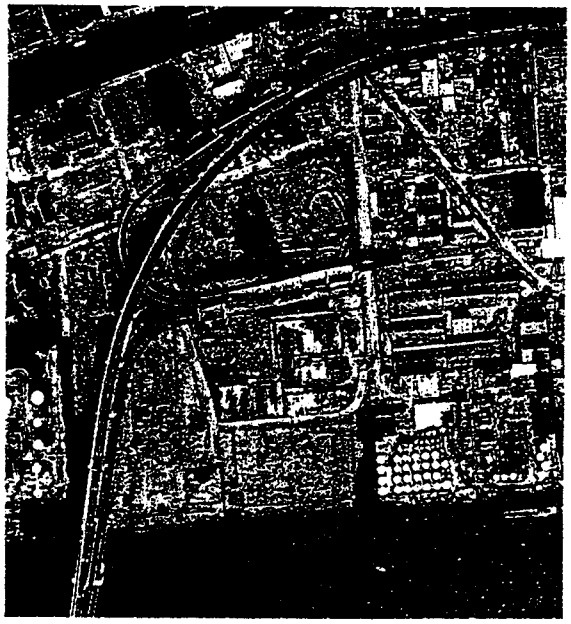

Photo. 4 The No. 5 Bay Highway in Uozaki-hama

Photo. 4 shows the same highway and its surrounding area in Uozaki-hama after the earthquake. Some amount of sand boil deposit was also observed on the ground surface. The highway bridges reportedly had inground wall foundations. Figure 4 shows the displacements at tops of the bridge piers as well as at the ground surface, which were measured by previously mentioned investigation groups. Compared with the displacement of the bridge piers in Port Island, which had cast-in-place concrete pile foundations, the displacements of the piers with inground wall foundations in Uozaki-hama are much smaller. This suggests that inground wall foundations are more effective to counter the ground displacements.

Figure 5 is a relationship between the displacements of the bridge piers and those at the ground surface[3]. It can be said that displacements of the piers with inground walls and caisson foundations are smaller than those of the piers with pile foundations. The result in Fig. 5 also suggests that inground walls and caissons are more effective for the foundations in the ground with a high potential of liquefaction and its induced ground displacement.

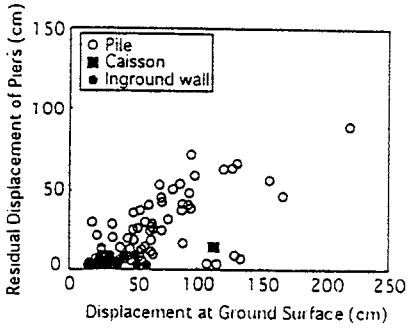

Fig. 5 Relationship between the displacements of the bridge piers and those at the ground surface[3]

DAMAGE TO LIFELINE FACILITIES

Higashi-nada Sewage Treatment Plant The Higashi-nada Sewage Treatment Plant locates in Uozaki-hama which was reclaimed from the sea, and suffered a severe liquefaction. Figure 6 shows the plan of the plant and ground displacements measured by aerial survey. The ground along a canal moved towards the water at a maximum about 3 meters. Photo. 5 shows a concrete pier of a bridge crossing the canal inclined due to displacement of its foundation, where the top of the pier was restrained to move because of the rigidity of the bridge girder. Photo. 6 also shows a similar example of evidences of the ground movement toward the canal. A concrete foundation of stairs up to a bridge crossing the canal was separated from the stairs due to ground displacement toward the canal.

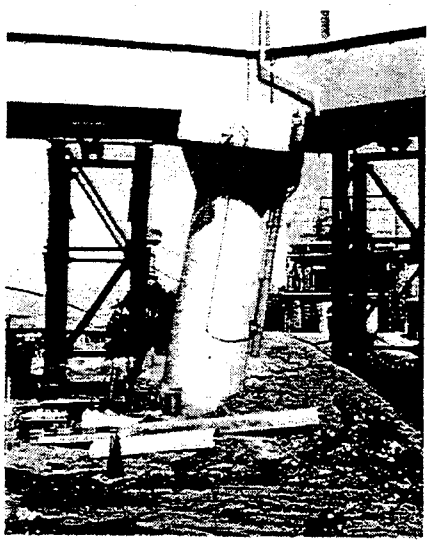

Photo. 5 Inclined concrete pier due to ground displacement (A in Fig. 6)

Photo. 6 Separation between stairs of over-canal bridge and its concrete foundation due to ground displacement toward the canal (left) (B in Fig.6)

The sewage facilities in the plant suffered severe damage and the function of the plant was perfectly lost after the earthquake. Photo. 7 is floating and separation of inground concrete conduit due to buoyancy of the liquefied soil as well as due to ground displacement in the horizontal direction, while Photo. 8 shows breakage of a concrete foundation pile of the control building. Furthermore, it was reported that joints of concrete casting of precipitation basins were largely separated due to horizontal displacement of the surrounding ground.

As mentioned above, many facilities and buildings were significantly damaged due to liquefaction and it's related ground displacement. However, it should be noted that some facilities and buildings with specific foundations hardly suffered any damage in this plant, even when the surrounding ground moved significantly, as mentioned later.

Photo. 7 Floating and separation of concrete conduit due to ground displacement (Courtesy of Mr. K. Takenaka, C in Fig. 6)

Photo.8 Breakage of foundation pile of the control building (Courtesy of Mr. K. Takenaka)

Movement of petroleum storage tanks A large number of petrochemical storage tanks located in reclaimed area, most of which suffered significant liquefaction and its caused large ground displacement during the earthquake in Kobe, Ashiya and Nishinomiya cities. Many tanks moved toward the sea and inclined when quaywalls of the tank yard collapsed or largely moved. However, any tank did not fall down, and any large leakage of oil and its product which could have induced a serious fire was not reported at the time of the earthquake, except the following instance of the leakage of liquid propane gas.

Photo. 9 shows a yard of petrochemical storage tank, which locates in Mikage-hama where also suffered severe liquefaction during the earthquake. It was reported that a large amount of liliquefied ptopane gas le propane gas leaked from a valve of pipeline at Point A in Fig. 7, and a large number of residents in the neighborhood was requested to evacuate at the time of the leakage. The report which was compiled by a committee of Ministry of International Trade and Industry of Japan[4] said that a direct cause of the leakage was a large deformation of the valve due to the ground deformation in horizontal as well as in vertical directions.

Figure 7 shows the ground displacements of the tank yard measured by aerial survey. The quaywall in front of the tank yard moved towards the sea at maximum about 4 meters. It should be noted that the northern boundary of the yard, more than 200 meters away from the southern shore line still moved toward the south with a magnitude of about 2 meters. This means that the whole area of the tank yard moved to the south, namely toward the sea. A large tensile strain was caused

by the relative displacement of the ground between the south and the north areas of the tank yard, and it can be assumed that this large ground strain deformed the valve of the pipeline.

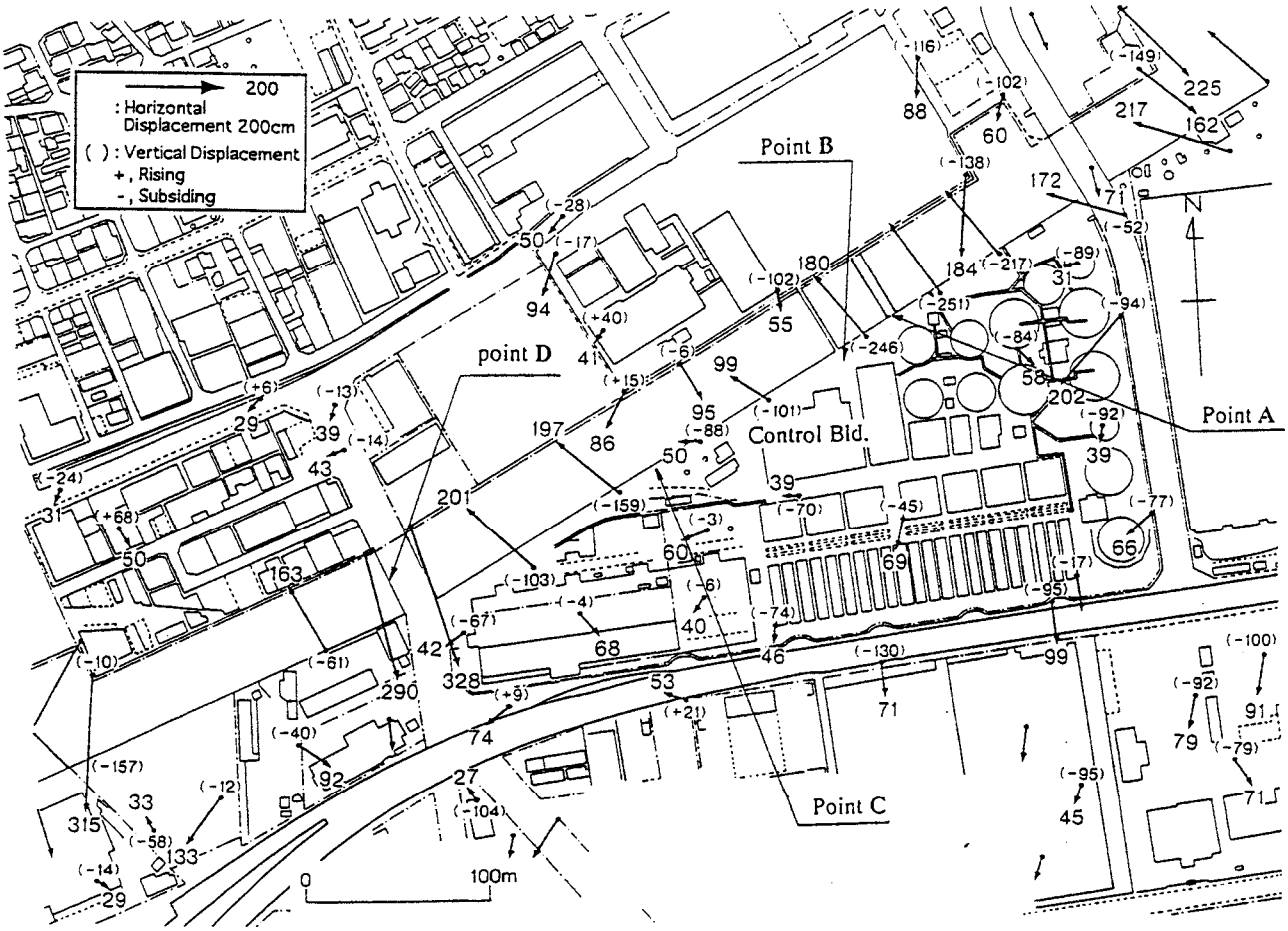

Fig. 6 Plan of Higashinada Sewage Treatment Plant and ground displacements[1)]

Photo. 9 Petrochemical storage tank yard in Mikage-hama

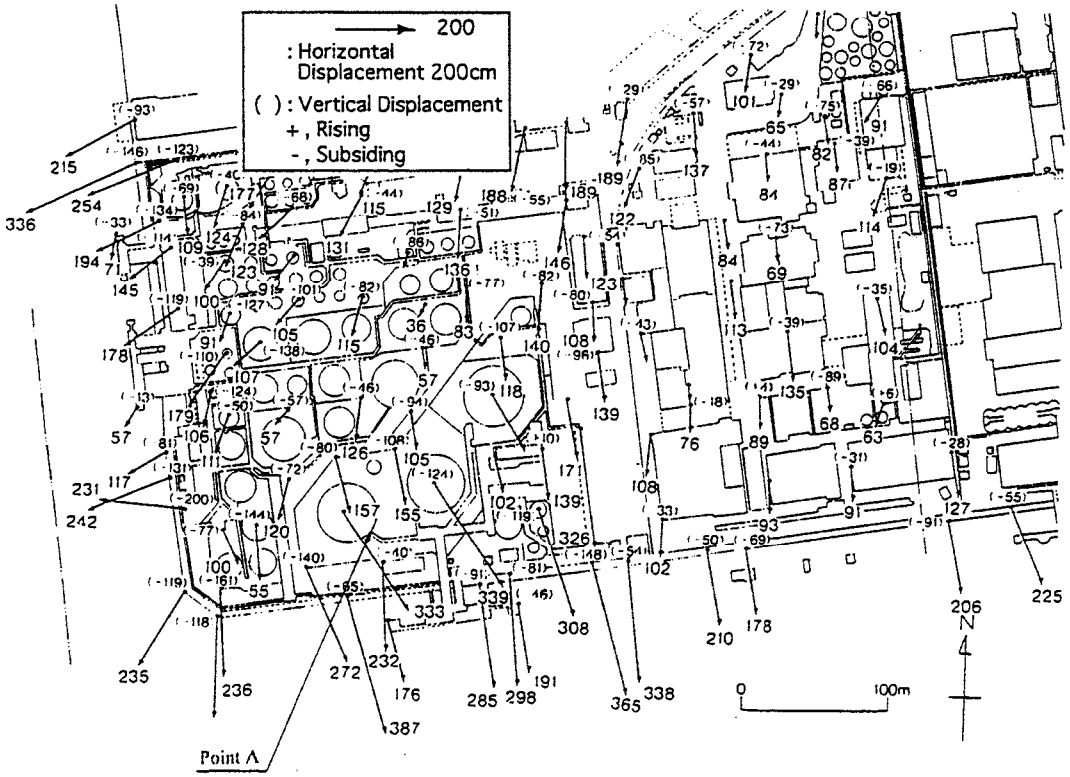

Fig. 7 Liquefaction-induced ground displacement at petrochemical storage tank yard in Mikage-hama[1)]

CASE STUDIES ON EFFECTIVE COUNTERMEASURES OF FOUNDATIONS AGAINST LIQUEFACTION AND LARGE GROUND DISPLACEMENT

The liquefaction and its induced large ground displacement caused significant damage to foundations of buildings, bridges and various kinds of industrial facilities. However, some foundations proved to have resisted against the liquefaction and large ground displacements during the earthquake. The authors investigated the structural characteristic such foundations in order to pursue effective countermeasures of foundations in liquefiable ground.

Higashi-nada Sewage Treatment Plant. As mentioned previously, a large number of the foundations of the facilities of the Higashi-nada sewage treatment plant was severely damaged due to liquefaction and its induced ground displacements. However, some facilities and buildings survived without any damage or with very slight damage even in the area where the ground moved 2-3 meters in the horizontal direction.

Figure 8 shows a plan of the sewage plant, and three ranks of differential settlements of the buildings and the facilities of the plant. It can be found that not only the structures close to the canal but also those away from the canal suffered large differential settlements. Furthermore, it should be noted that deferential settlements of some structures along the canal is very small, although the surrounding ground largely moved towards the canal. It seems that the distance of a building from the canal did not have a direct influence to the degree of differential settle-ments. For an example, differential settlements of the storage tanks which located in northern-east corner of the plant varies into three ranks. It is also noteworthy that a half part of the control building caused a large differential settlement, but another half part hardly suffered any settlements. The result shown in Fig. 8 seems to give us an instructive information to consider an effective countermeasures of foundations against liquefaction and its caused large ground displacements.

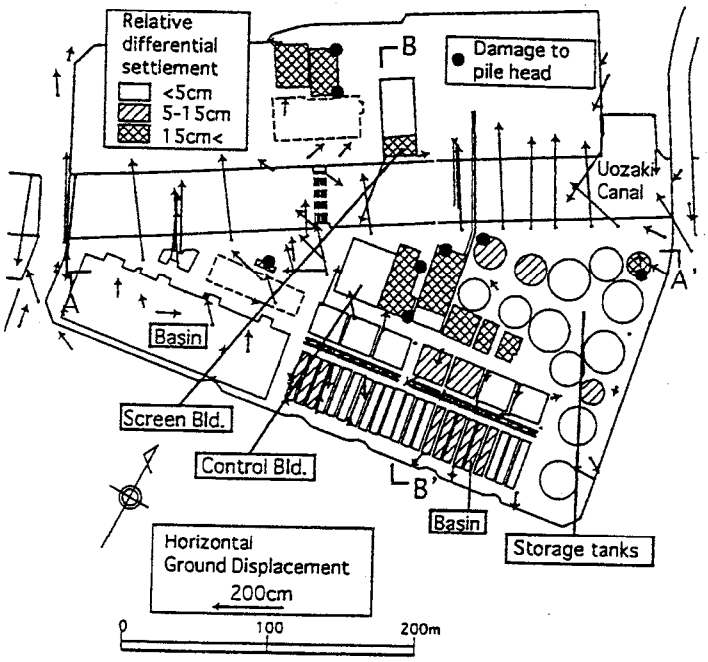

Fig. 8 Plan of Higashinada Sewage Treatment Plant showing ranks of differential settlement and horizontal ground displacement

Figure 9 shows a cross section along the A-A' line in Fig. 8. It is clear that differential settlements of structures with an inground portion is smaller than those of structures without any inground portion. The half part of the control building, which has no basement suffered large differential settlement, but another half part of the building with a basement did not induce any settlement. It is also interesting to note that the magnitude of differential settlements of the tanks depends on the depth of their inground portions.

Figure 10 is a cross-section along B-B' line in Fig. 8. This figure also shows that the magnitude of differential settlements depend on the depth of inground portion of structures. A building (

Screen Building in Fig. 8) along the canal consists of two parts. A large differential settlement above 15 cm was observed in a part without any basement, while no differential settlement was found in another part with a basement.

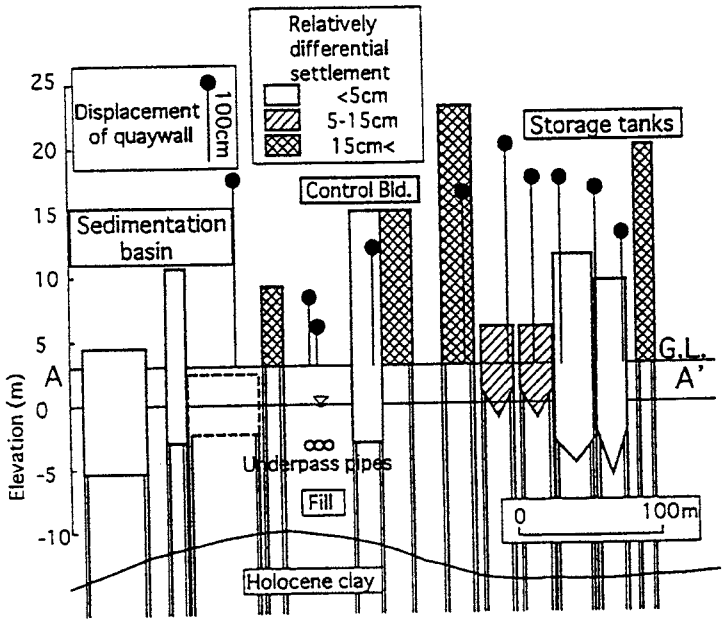

Fig. 9 Depth of foundations and ranks of differential settlement of structures along A-A' line

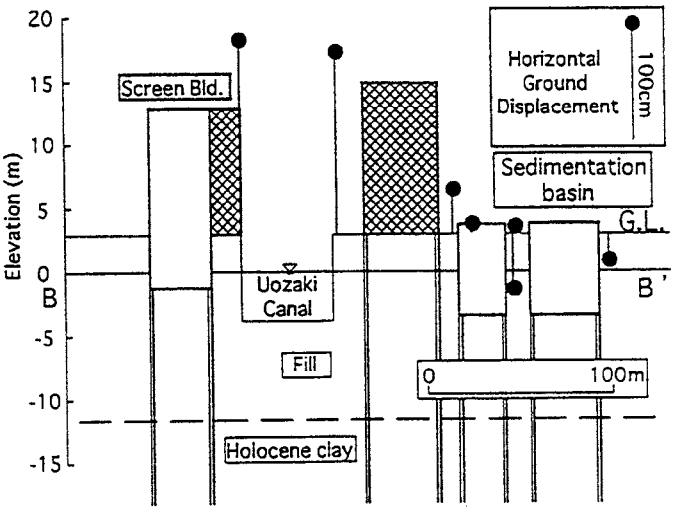

Fig. 10 Depth of foundations and ranks of differential settlement of structures along B-B' line

Shimagami Pumping Station The Shimagami pumping station located along a shore line at Nagata ward in Kobe city. The distance of the building from the quaywall is only 8 meters. As shown in Fig. 11 the quaywall moved towards the sea at a maximum about 3 meters, and consequently the ground behind the quaywall displaced toward the sea. However, the building of the pumping station with a height of about 16 meters hardly suffered any damage, besides the surrounding ground subsided more than 1.0 meter. This building has a basement with a depth of about 8 meters for northern half of the building and about 11 meters for southern half, and is supported by cast-in-place concrete piles of a diameters of 1.0-1.5 meters as shown in Fig. 12. An inground wall, named as SMW (Soil Mixing Wall), with a width of 45 cm, was built for the excavation of the basement. This inground wall remained after the construction of the building and surrounded the concrete piles. It can be guessed that the existence of the inground wall had a great influence to prevent damage to the foundation piles, in addition to the existence of the basement.

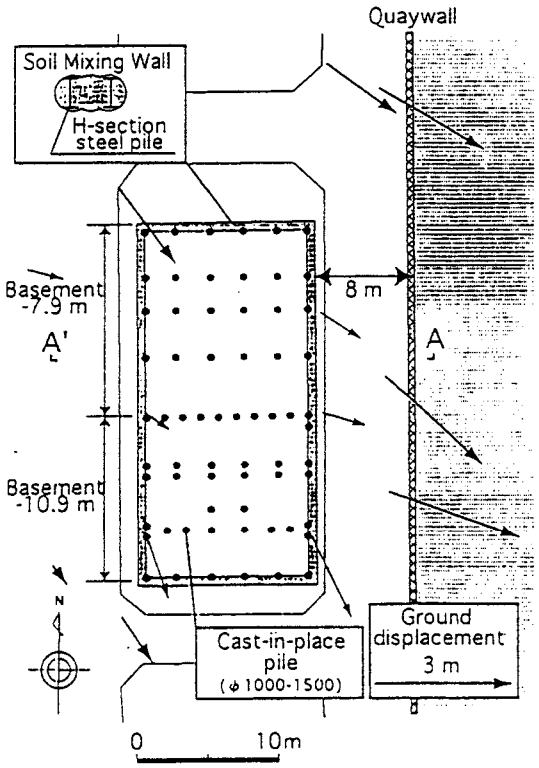

Fig. 11 Plan of Shimagami Pumping Station and liquefaction-induced ground displacement

The liquefaction around the building caused a large settlement of the ground surface. Photo. 10 shows ground subsidence and top of the inground wall, which appeared after the earthquake.

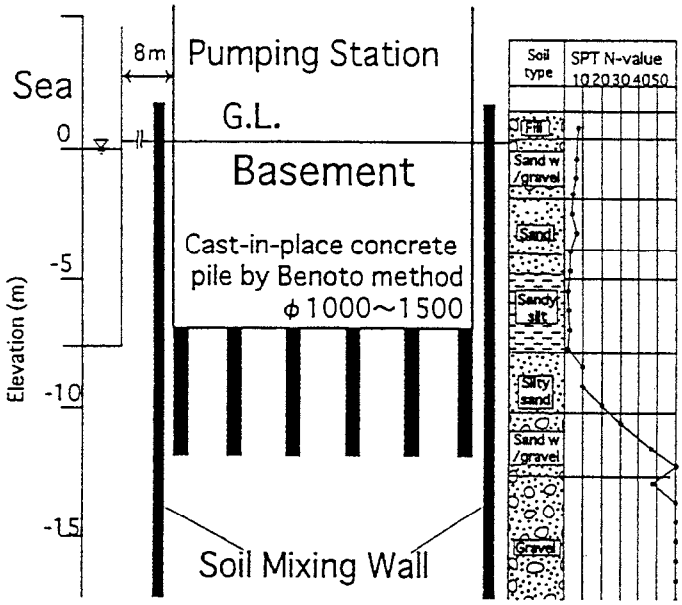

Fig. 12 Cross section of Shimagami Pumping Station

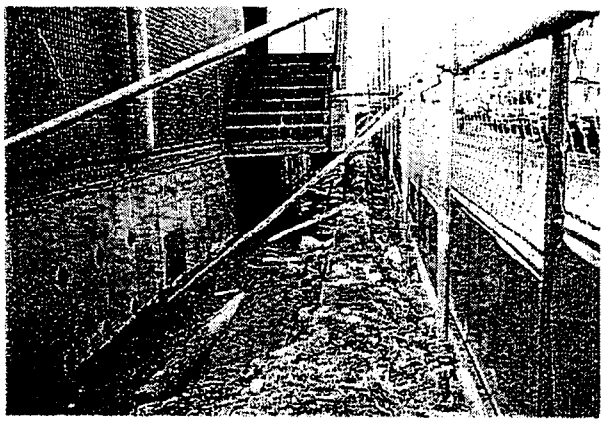

Photo. 10 Inground wall of Shimagami Pumping Station, which appeared after the earthquake due to ground subsidence

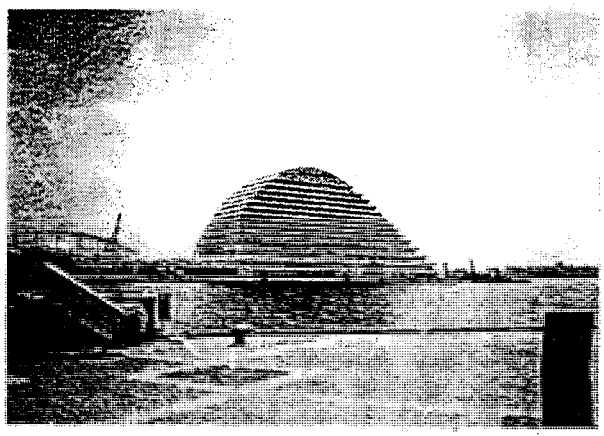

Photo. 11 Oriental Hotel on Central Pier of Kobe Port

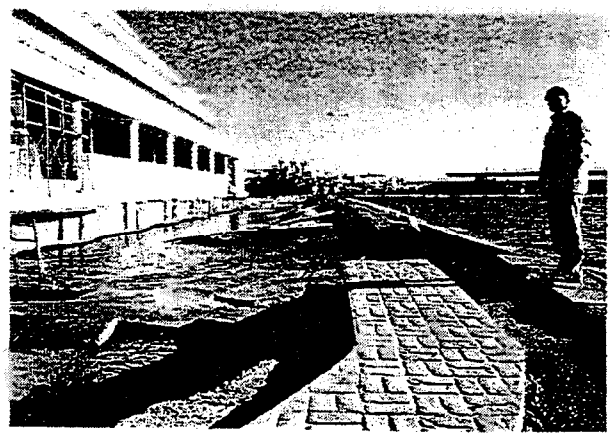

Photo. 12 The ground in front of the hotel moved towards the sea and subsided

Foundation of The Oriental Hotel The Oriental Hotel shown in Photo. 11 located on the Central Pier of Kobe Port, and has 60m height above ground surface. The quaywalls in front of the building moved towards the sea and subsided shown Photo. 12. The hotel building was constructed on cast-in-place concrete piles of a diameter of about 1.0 meter and length of about 30 meters. The thickness of the reclamation is about 12 meters and the foundation piles reached into a firm Pleistocene gravel layer.

It was reported that at the stage of the structural design of this building, lateral flow of the liquefiable soil beneath the building towards the sea was considered to seriously affect the stability of the building[5]. Therefore, inground walls was designed and constructed to avoid the lateral flow of foundation ground. As shown in Fig. 13, The inground walls, which consist of continuous cast-in-place piles with a diameter of 1.0 meter and length of 12-19 meters, were constructed by mixing cement slurry into the ground, and the wall reached into non-liquefiable soil layer through the reclaimed liquefiable layer.

It was reported that this hotel building did not suffer any structural damage and any settlement, and that no trace of the liquefaction was found on ground surface under the building, when the foundation was excavated after the earthquake[5].

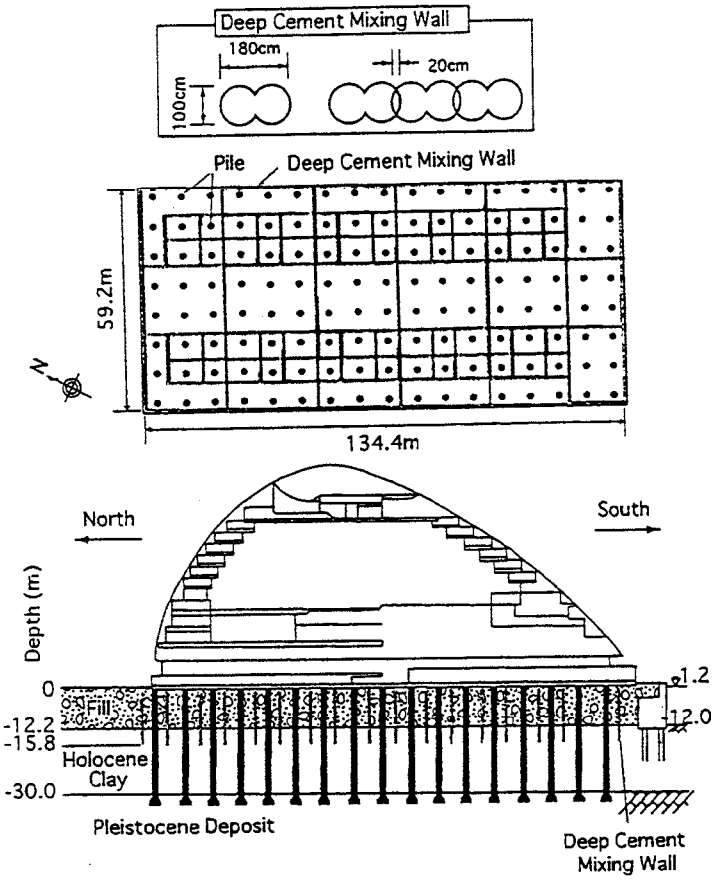

Fig. 13 Section and plan of foundation of Oriental Hotel[5]

CONCLUSIONS

Based on the investigation into the liquefaction, its induced ground displacement and performances of various kinds of structures in the 1995 Hyogoken-nanbu earthquake, the following conclusions are obtained:

1) Many structures settled and/or tilted with severe damage to their foundation piles due to liquefaction and/or large ground displacement. In contrast, structures supported on improved soils sustained little damage although the surrounding subsoil's liquefied.

2) The structures with a basement, inground portion, inground wall such as soil mixing wall, continuous concrete wall, and/or deep cement mixing wall survived with no or little damage. The building supported on nodular friction pile foundation also performed well.

REFERENCES

1) Hamada, H., Isoyama, R. and Wakamatsu, K.: *The Hyogoken-Nanbu (Kobe) Earthquake, Liquefaction, Ground Displacement and Soil Condition in Hanshin Area*, Association for Development of Earthquake Prediction, 1995.

2) Investigation Committee of Great Hanshin and Awaji Earthquake Disaster: *Report on the Great Hanshin and Awaji Earthquake*, Japanese Geotechnical Society, 1996 (in Japanese).

3) Committee of Japan Road Association: *Report on Damage to Highway Bridge in the Hyogoken-nanbu Earthquake*, 1995 (in Japanese).

4) Japan Association of Safety of High Pressure Gas: Interim Report on Leakage of Propane Gas in the Hyogoken -nanbu earthquake, 1995 (in Japanese).

5) Suzuki, Y., Saito, S., Onimaru, S., Kimura, T., Uchida, A. and Okumura, R.: Grid-shape stabilized ground improved by deep cement mixing method against liquefaction for a building foundation, *Tuchi-to-Kiso*, Japanese Geotechni-cal Society, Vol. 44, No. 2, pp. 46-48, 1996 (in Japanese with English abstract)

PERFORMANCE OF CORRUGATED METAL PIPE (CMP) CULVERTS DURING PAST EARTHQUAKES

T. Leslie Youd and Chris J. Beckman
Department of Civil and Environmental Engineering
Brigham Young University
Provo, Utah 84602

ABSTRACT

To evaluate culvert performance during earthquakes, we reviewed reconnaissance reports from six earthquakes and conducted field investigations in areas shaken by three of those earthquakes. Hundreds of CMP culverts were in place in areas strongly shaken by these earthquakes. Lack of reported or observed damage to all but ten of these structures indicate that CMP culverts generally perform performed very well during earthquake shaking. Of the ten damaged culverts, all but one were in areas of ground failure caused by liquefaction or slope instability. The one culvert not in an area of ground failure suffered minor damage due to increased lateral pressures cracking a head wall and slightly deforming the pipe inlet. Damaging ground failures included embankment penetration into liquefied foundation soils, lateral spread, ground oscillation and slope instability. Diameters of culverts ranged from 0.45 m to 3.6 m.

INTRODUCTION

The performance of culverts is important to the safety and reliability of highways during and after large earthquakes. Culverts, however, have received little attention in the earthquake engineering literature. To provide information on performance of these structures, we reviewed reconnaissance reports from several earthquakes and conducted field investigations to inspect both damaged and undamaged culverts shaken by recent earthquakes. Where damage occurred, we studied both the culvert and the surrounding ground to determine the cause of the poor performance. For this paper, corrugated metal pipe (CMP) culverts are considered; a more in-depth treatment of these and other types of culverts is given in a research report (Youd and Beckman, in press).

Following a literature review, we contacted highway officials in Idaho and California to obtain reports and locations of culverts damaged by recent earthquakes. In some instances, the highway officials had inspected both damaged and undamaged culverts and could confirm either good or poor performance. In many instances, however, we assumed that lack of reported damage was indicative of good performance. During the field reconnaissance, we inspected a number of these culverts to verify the assumed good performance.

The types of culverts commonly used in highway construction include corrugated metal pipe, synthetic pipe, concrete pipe, and concrete boxes. The most common use of culverts is for drainage beneath roadway embankments. In these instances, culverts are placed beneath the

roadway to allow excess runoff to harmlessly flow beneath the roadway. Larger culverts may also be placed to allow pedestrians or vehicles to pass beneath busy roadways. Most drainage culverts are constructed of corrugated metal pipe (CMP). The corrugations, parallel ridges and furrows around the circumference of the pipe, give the culvert added strength. CMP is usually galvanized for corrosion resistance. CMP is widely used because of its strength, versatility, ease of placement, and low cost.

TABLE 1 Corrugated Metal Pipe (CMP) Culverts Investigated in This Study

No.	Location	Ground Effects	Diam.	Damage
1	Portage Highway, 1.6 km south of Portage, Alaska (1964 earthquake)	Penetration of fill into foundation	0.91 m	Ends deflected upward 2 m
2	Mile Marker 40.4, Seward Highway, Alaska (1964 earthquake)	Penetration of fill into foundation	?	Ends deflected upward 0.5 m
3	Mile Marker 46.6, Seward Highway, Alaska (1964 earthquake)	Penetration of fill into foundation	?	Ends deflected upward
4	Route 5/210 intersection, Sylmar, Calif. (1971 earthquake)	Lateral spread	1.07 m	Severe joint separation
5	Route 5, south of Roxford St., Sylmar, Calif. (1971 earthquake)	Increased lateral earth pressure	3.6 m	Fractured headwall
6-25	20 culverts, Summit Road, Santa Cruz County (1989 earthquake)	Area of diffuse tectonic deformation	various	No damage
26	Jetty Road north of Moss Landing, Calif. (1989 earthquake)	Penetration and lateral spread of fill	0.76 m	Split and ends deflected
27	Elkhorn Road east of Moss Landing, Calif. (1989 earthquake)	Penetration of fill into foundation	0.76-0.91 m	Ends deflected upward 0.5 m
28	Spanish Ranch Road, Santa Cruz County (1989 earthquake)	Slump of hillside and roadway	0.91 m	Pipes rotated and separated
29	Port of Mori, Hokkaido, Japan (1993 earthquake)	Lateral Spread	0.46 m	Separated from headwall
30-31	Route 405, San Fernando, Calif. (1994 earthquake)	No visible ground disturbance	0.38-0.46 m	No damage
32	Lower San Fernando Dam, Calif. (1994 earthquake)	Increased lateral pressure	2.4 m	Lateral collapse

CORRUGATED METAL PIPE (CMP) CULVERT PERFORMANCE

Table 1 lists 32 CMP culverts that we specifically studied either through field inspection or from critical review of descriptions in published earthquake reconnaissance reports. Of these 32 culverts, one collapsed laterally due to increased horizontal pressures, six buckled or bent, two were pulled apart at joints, two were slightly damaged (easily repairable), and 21 were undamaged. Many more CMP culverts were located in the affected areas, the total of which we did not determine. None of these additional culverts were reported as damaged, either by local highway officials whom we interviewed, or in published reports. We drove over or by many of these culverts during our field investigation without seeing evidence of deformed or patched roadway surfaces indicative of damage to the roadway or underlying culverts. Thus, we infer that these culverts performed well and were not significantly damaged by earthquake shaking.

As noted in Table 1, the seven most severely damaged culverts were at sites disturbed by ground failure. Several different modes of ground failure were involved in the culvert damage.

Penetration of Embankments into Foundation Materials

The most common mode of ground failure causing damage to CMP culverts has been penetration of highway embankments into softened foundation materials. This softening was usually caused by liquefaction. At some localities, lateral spread as well as embankment penetration occurred. A schematic representation of embankment penetration and resulting damage is illustrated in Figure 1. The following case histories illustrate this type of ground failure and culvert damage.

Alaskan Culverts. Prior to the 1964 Alaska earthquake, a 0.9-m-diameter CMP culvert was placed beneath a 1-m to 2-m high highway embankment that crosses a marshy area about 1.6 km south of Portage, Alaska. The highway provided access to the Portage Glacier area. Liquefaction was widespread in the marsh sediments as evidenced by sand boils, fissures, ground settlement, lateral spread, and ground oscillation. These phenomena led to severe damage or collapse of several highway and railway bridges, differential settlement of highway and railway grades, and general subsidence of the ground surface. As diagramed in Figure 1 and photographed in Figure 2, penetration of the highway fill pressed the center section of the culvert downward into an underlying marsh deposit. As a result, the pipe buckled, most likely at a joint, and the ends of the culvert were deflected upward out of the ground. This action raised the left end of the culvert about 2 m above the ground surface (McCulloch and Bonilla, 1970). Liquefaction of foundation sediment most likely caused this damage.

Similar damage occurred to two additional culverts beneath the Seward Highway, one at highway mile marker 40.4 and the other near 46.6. These localities lie 50 to 55 km southwest of Portage. Both culverts were placed in marshy areas to allow local seepage and runoff to pass beneath the embankment. Kachadoorian (1968) reported that the culvert at marker 40.4 deflected upward with outer ends rising as much as 0.5 m. He also noted that the ends of culvert at mile marker 46.6 were deflected upward, but did not give an amount. Embankment penetration into foundation soils appears to have caused this culvert damage.

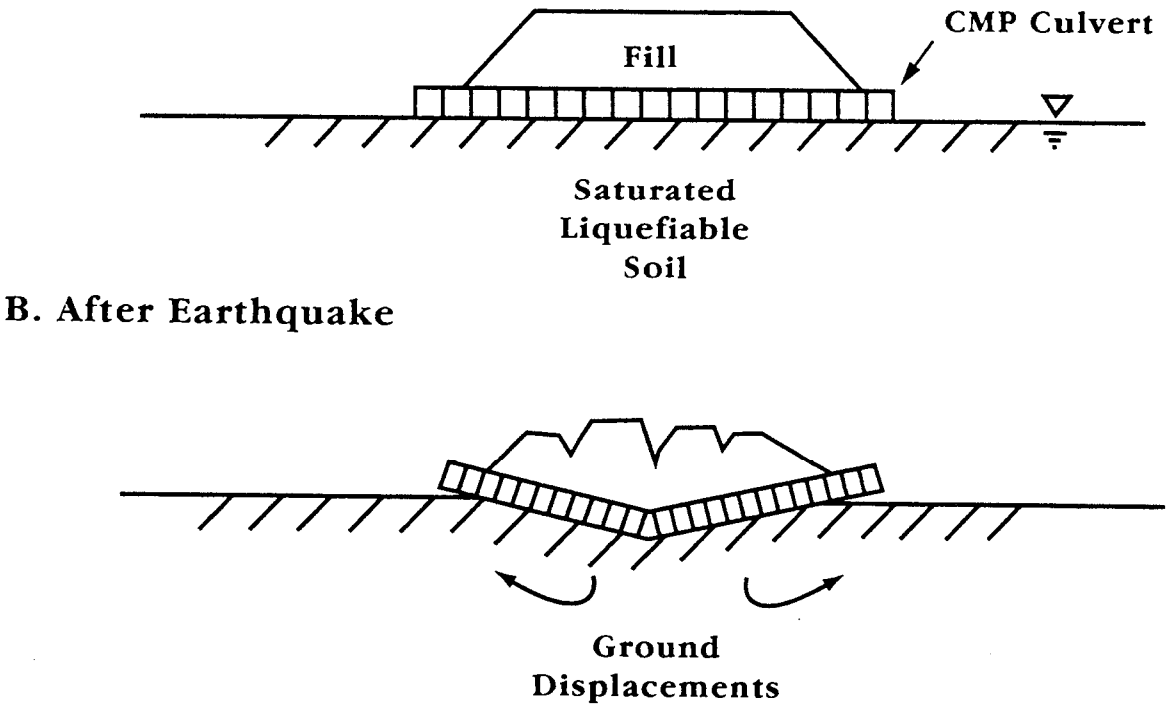

FIGURE 1. Schematic Diagram of Embankment Penetration into Foundation and Consequent Culvert Damage

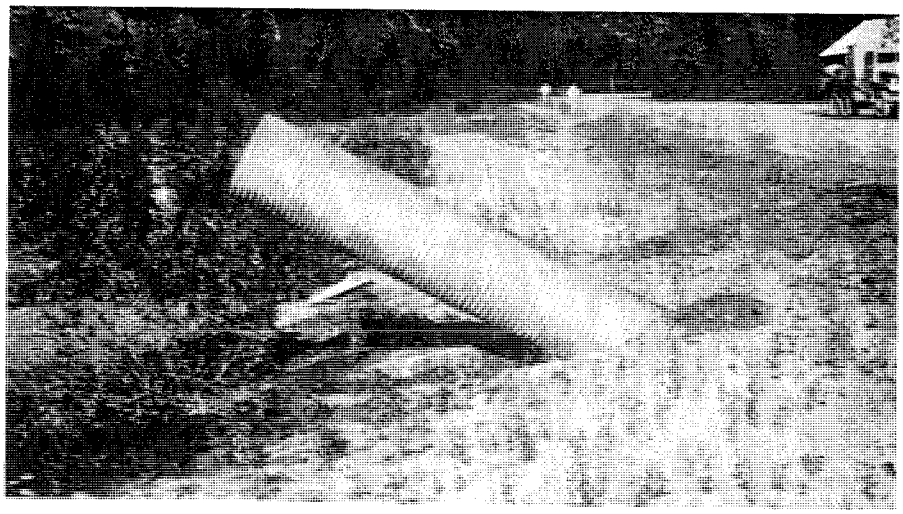

FIGURE 2. End of 0.9-m-diameter CMP Culvert Elevated About 2 m Above Ground Surface by Embankment Penetration South of Portage, Alaska (After McCulloch and Bonilla, 1970)

Jetty Road Culvert. During the 1989 Loma Prieta, California earthquake, a 100-m-long segment of Jetty Road subsided as much as 1 m and spread laterally as much as 6 m. This locality is a few kilometers north of the community of Moss Landing. The subsidence and spreading left open fissures as wide and as deep as a few meters. This ground disturbance blocked the exit of several vehicles and their occupants, leaving them stranded at the beach. A single 0.76-m-diameter CMP culvert had been placed beneath the embankment to accommodate flow of drainage and tidal waters. Prior to the earthquake, that culvert was partially plugged with sediment, greatly restricting the tidal flow. As a consequence, a freshwater marsh had formed inland from the culvert (Kenneth Gray, California State Parks, Monterey, California, oral communication, June, 1994)

During the earthquake, the roadway embankment penetrated about 1 m into the foundation soil and spread laterally about 6 m, as noted above. This action fractured and pulled apart the culvert, and deflected the ends upward out of the marsh (Figure 3). Eye witnesses reported that the ends of the culvert were about 6 m farther apart after the earthquake than before.

By the time of our visit, nearly 5 years after the earthquake, the roadway had been rebuilt, with six new 0.76-m-diameter CMP culverts placed to carry the flow of Elkhorn Slough. Because of the increased capacity of these culverts, a considerable volume of tidal water was flowing through the culverts; this flow was rapidly converting the former freshwater marsh inland from the culvert into a nearly barren tidal marsh.

Figure 1 shows the general mechanism of failure for the Jetty Road culvert. In this instance, however, lateral spread of the embankment fill also fractured the CMP and pulled it apart. Liquefaction of foundation material apparently allowed penetration and spreading of the fill.

Elkhorn Road Culverts

The second site of damaged culverts is at the Elkhorn road crossing over Elkhorn Slough, about 5 km east of Moss Landing, California. The road was constructed on a 1- to 2-m-high (pre-earthquake) embankment placed over the broad marsh. Seven 0.9-m -diameter CMP culverts were placed beneath the roadway to carry both natural drainage and tidal flows. During the earthquake, the roadway subsided as much as 0.5 m to 1 m over a distance of few hundred meters. This subsidence was caused by penetration of the fill into the foundation sediment, apparently as a consequence of liquefaction. The penetration of the fill bent or buckled the CMP culverts, causing the ends to deflect upward with the ends rising as much as 0.6 m as shown in Figure 4.

The culverts continued to function, however, with near capacity quantities of water freely flowing through most pipes. Although the road surface had been smoothed and patched prior to the time of our visit, no new filling or grading had occurred. The damaged pipes and the highway fill were in much the same condition as they were immediately after the earthquake. Considerable tidal flow was passing through the damaged culverts which were mostly submerged, even at low tides.

FIGURE 3 Damage to Jetty Road North of Moss Landing, California. View southeastward of Disturbed Embankment and Deflected End of CMP Culvert (Photograph by Ken Gray, Dept. of Parks and Recreation, Monterey County, Calif.)

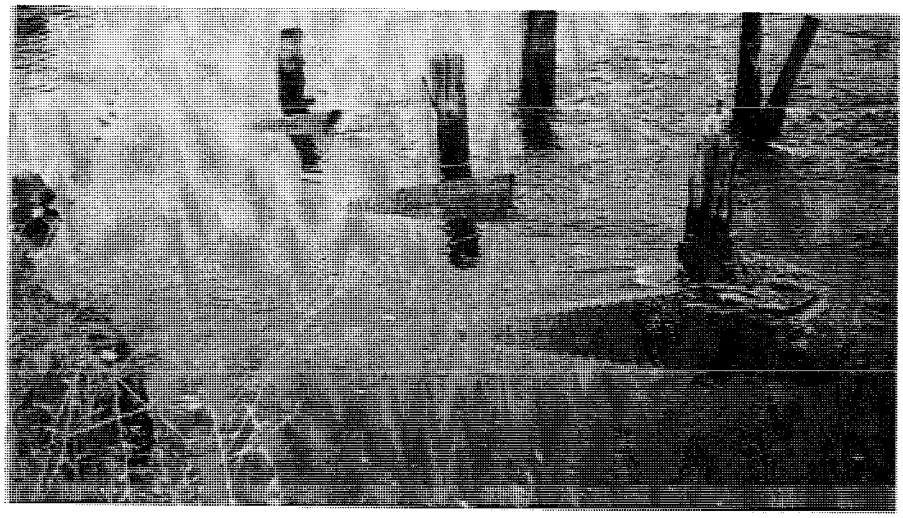

FIGURE 4 CMP Culverts Deflected Upward Due to Penetration of Elkhorn Road into Softened Marsh Sediment (Photograph by C. Beckman)

Slumping of Fill and Foundation Materials

The slumping of fill and foundation materials is capable of damaging roadways and culverts placed on such unstable ground. This type of failure usually occurs along steep slopes, where weaker materials tend to slide during earthquake shaking. Our survey identified only one CMP culvert damaged by slumping.

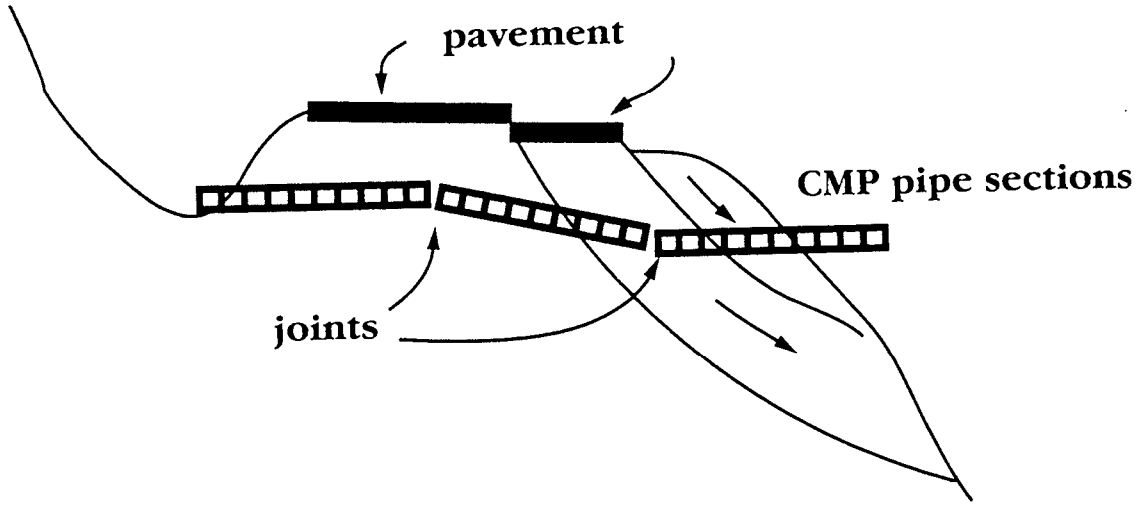

FIGURE 5 Diagram of Slump and Culvert Damage Beneath Spanish Ranch Road

Spanish Ranch Road Culvert. A 0.9-m-diameter CMP was placed beneath Spanish Ranch Road in the Santa Cruz Mountains prior to the 1989 Loma Prieta earthquake. Spanish Ranch road winds precipitously along a steep mountain side east of Santa Cruz, California. The culvert consisted of three 6-m long segments of CMP with a 100-mm to 200-mm long over-wraps of corrugated metal over each joint. The culvert was covered by about 1 m of compacted fill.

Strong ground shaking during the 1989 Loma Prieta earthquake generated a slump that intersected the outer third of the roadway and underlying culvert. The slumped ground rotated and slid downward about 1 m. The ground movement did not crush nor tear the CMP culvert, but rather rotated the pipes while stretching the joints (Figure 5). Joints connecting the pipe sections were pulled apart as much as 150 mm on the top and the bottom of the first and second joints from the inlet, respectively. The CMP pipes were undamaged, but were rotated as much as five degrees. The wrap of corrugated metal over the joints remained in place, covering the openings and preventing highway fill from entering the culvert. The culvert continued to function without interruption for at least five years after the earthquake by allowing drainage to flow freely beneath the roadway. The highway was temporarily repaired by crowding the embankment against the mountain side.

Summit Road CMP Culverts. As noted in Table 1, many culverts are in service beneath Summit Road which traverses the crest of the Santa Cruz Mountains east of Santa Cruz, California. Being in the epicentral region of the 1989 Loma Prieta earthquake, this area was strongly shaken (peak accelerations in excess of 0.4 g), and disturbed by a diffuse zone of tectonic deformation. The zone of deformation was characterized by a broad band of disperse and discontinuous surface ruptures (U.S.G.S. staff, 1990; Aydin et al., 1992). We inspected three culverts at random and slowly drove over the remaining culverts searching for pavement damage or repairs indicative of damage or deformation to the underlying pipe. We also matched locations of culverts with fissures mapped by the U.S.G.S. staff (1990), and found that no single

fracture intersected any of the culverts. No pavement damage or repairs were observed, which indicates that these culverts performed well. From this good behavior, we conclude that strong ground shaking in the absense of ground failure or groud deformation is not detrimental to well-constructed CMP culverts.

Increased Lateral Earth Pressures

Earthquake shaking may transiently or permanently increase lateral earth pressures acting against buried structures such as culverts. Visual inspection of the interior of the three CMP culverts located on Summit Road and the damaged culvert beneath Spanish Ranch Road (noted above) revealed no signs of deformation due to increased lateral pressures from the 1989 Loma Prieta earthquake. We also did not discover any reports of deformation of CMP culverts beneath highways due to lateral pressures generated by earthquake shaking. During the 1994 Northridge earthquake, however, a 2.4-m-diameter CMP culvert that had been placed beneath the reshaped Lower San Fernando dam collapsed horizontally as a consequence of increased lateral soil pressure.

Lower San Fernando Dam CMP Culvert. During the 1971 San Fernando earthquake, hydraulically a placed fill within the Lower San Fernando Dam liquefied, leading to a massive flow failure. This failure carried a large segment of embankment, including the crest of the dam, into the reservoir (Seed et al., 1975). After the earthquake, a replacement dam was constructed about one mile upstream from the failed dam. The old dam was then reshaped and is now used as a flood control structure.

While reshaping the old dam, a 2.4-m-diameter CMP storm drain was placed beneath the reconstructed fill. The inlet to the new CMP drain was in a shallow pond that formed in front of the reshaped dam. Water from the pond percolated through the dam, saturating the foundation and lower layers of the fill. After placing the storm drain, a gently sloping compacted berm was placed across the upstream face of the dam.

The Lower San Fernando dam was strongly shaken by the 1994 Northridge earthquake with estimated peak ground accelerations ranging from 0.4 g to 0.8 g (Bardet and Davis, 1995). This shaking liquefied saturated materials beneath the upstream berm, generating numerous fissures and sand boils on or near the lower part of that structure (Figure 6). The zone affected by fissures and sand boils was about 130 m wide (north to south up the face of the berm), and 420 m long (east to west across the berm). Most of the fissures paralleled the crest of the dam and were pulled apart in extension with openings as wide as 300 mm. This geometry indicates a lateral spread origin for the fissures, with ground displacement toward the lowland in front of the dam. Other sets of fissures, mostly near the abutments and over the buried storm drain, were oriented perpendicular to the crest of the dam. These fissures were likely generated by transient ground oscillations across the face of the berm.

Approximately 100 m of the new CMP storm drain passed through the zone of liquefied effects. In May 1994, the storm drain was excavated, revealing a 75-m-long section of CMP pipe that had collapsed laterally inward (Figure 7). The northern terminus of the collapsed

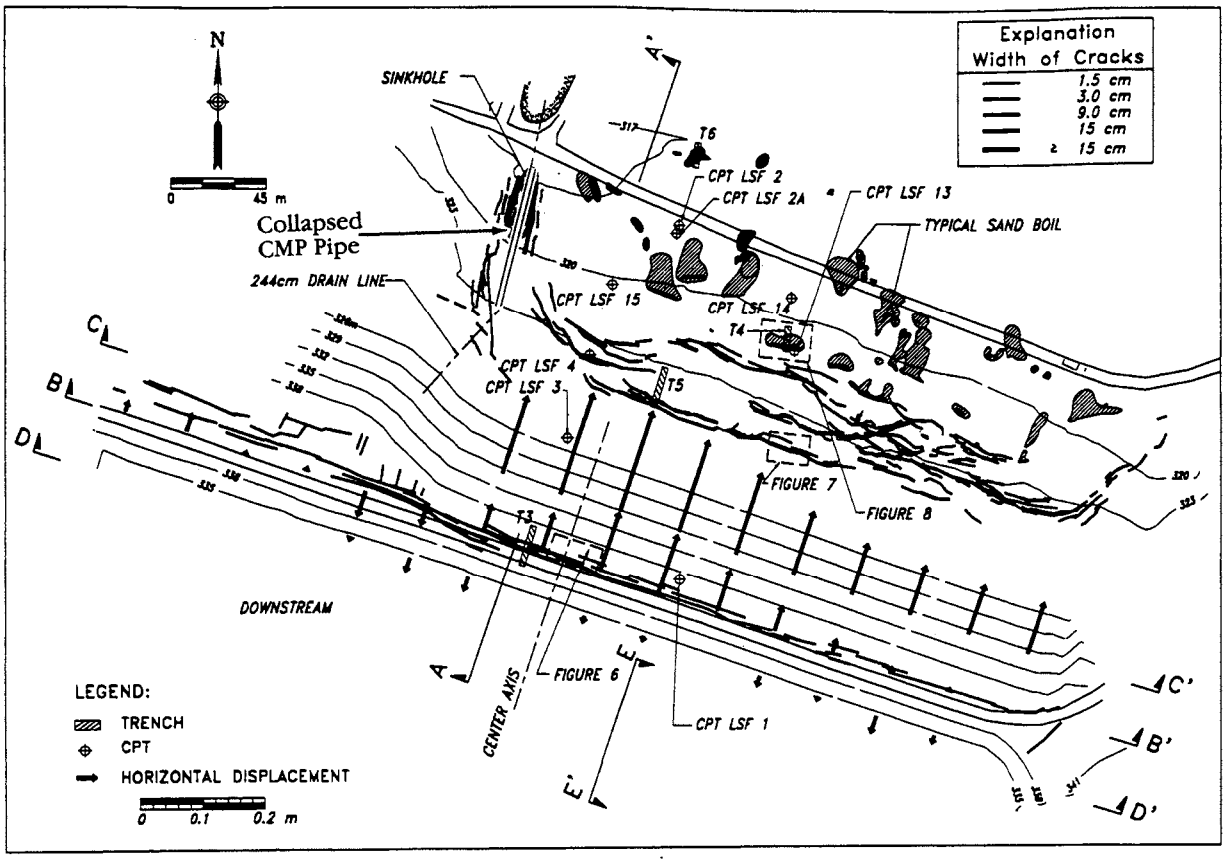

FIGURE 6 Upstream Berm at Lower San Fernando Dam Showing Alignment of Buried drain That Collapsed, and Localities of Ground Fissures and Sand Boils(After Bardet and Davis, 1995)

section of CMP pipe was approximately 18 m inland from the toe of the fill; the southern terminus of collapsed CMP was near a connection of the CMP to an old reinforced-concrete pipe (Bardet and Davis, 1995). The thickness of compacted fill over the collapsed pipe ranged from about 4 m at the northern end of the collapsed section to more than 12 m over the southern terminus of collapse. The ground water level at the time of failure was roughly 1 m below the invert of the pipe, but may have varied in depth within the embankment (Bardet and Davis, 1995).

The laterally inward collapse indicates that failure was induced by transient or permanent increases of lateral earth pressure acting against the pipe, and that the lateral earth pressure was greater than vertical earth pressures at the time of failure. Prior to the earthquake, vertical earth pressures were likely somewhat greater than lateral pressures, given that the pipe was buried beneath a thick section of compacted fill. Thus, a large increase of lateral earth pressure must have occurred during the earthquake. Also, because collapse occurred only within the zone of liquefaction effects, liquefaction-related phenomena most likely contributed to the failure. The depth of burial also may have been a factor influencing failure.

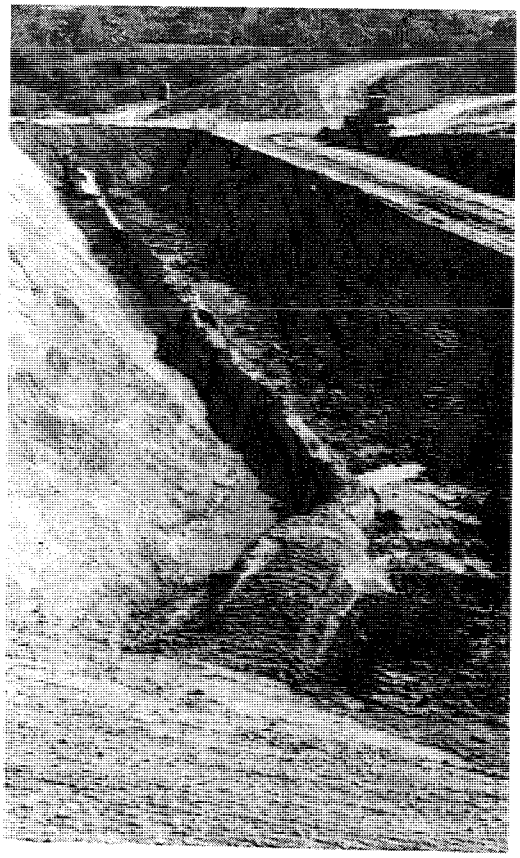

FIGURE 7 View Southward of Laterally Collapsed 2.4-m-Diameter CMP Pipe Beneath Lower San Fernando Dam. (Courtesy of J.P. Bardet, University of Southern California)

We suggest two plausible mechanisms for generating the large increases of lateral earth pressure that collapsed the pipe.

(1) Lateral earth pressure generally increases during vibratory compaction of soils (Youd and Craven, 1975). Thus, earthquake shaking could have compacted soils around the culvert and increased lateral earth pressures. Laboratory test results indicate however, that vibratory compaction alone is unlikely to generate lateral earth pressures great enough to exceed vertical pressures, particularly during an earthquake of relatively short duration (Youd and Craven, 1975). Thus, increased lateral earth pressure due to seismic compaction alone was probably not capable of laterally collapsing the CMP pipe.

(2) Liquefaction of soils below the water table may have decoupled overlying soil layers, allowing them to oscillate back and forth in a form of ground failure called ground oscillation. This phenomenon typically fractures the decoupled soil layers into large blocks that oscillate in different modes and phases. Impacts between oscillating blocks can generate large transient lateral earth pressures capable of crushing a buried CMP culvert. The magnitudes of these transient earth pressures are a function of the thickness of the oscillating block.

The many ground fissures within the lower part of the berm provide evidence of ground oscillation. Fissures trending laterally across the face of the berm indicate oscillation in a north-south direction with some permanent downslope displacement or lateral spread. Fissures trending longitudinally up the face of the berm, including those at the margins of the berm and over the buried storm drain, indicate that oscillation also occurred across the berm in an east-west direction. The fissures over the drain indicate that a plain of separation developed at that locality. Impacts between the mobilized blocks on either side of the culvert likely generated large pulses of lateral earth pressure capable of collapsing the culvert.

Based on this evidence and reasoning, we conclude that lateral pressures generated by ground oscillation caused the collapse of the 2.4-m-diameter CMP. We also conclude that in areas where the depth of the fill above the top of the pipe was less than about 3.5 m, the CMP pipe was sufficiently strong to resist induced lateral pressures without collapse. Given that collapse of CMP occurred adjacent to the connection with the old reinforced-concrete pipe, we conclude that the greater wall thickness and consequent strength of an older section of concrete pipe was sufficient to withstand transient increases of lateral stresses without fracturing the pipe.

Lateral Spread

Route 5/210 Intersection CMP Culvert. During the 1971 San Fernando earthquake, the Foundation Section (1973) of the California Department of Transportation (CALTRANS) gave the following brief report of damage to a CMP culvert near the Route 5/210 Interchange:

> A 42-inch (1-m) corrugated steel pipe also suffered severe joint separation in this area. It was believed that this pipe could be repaired without replacement.

Although the location of this culvert is not clearly specified and our interviews with CALTRANS personnel provided no more information, the culvert likely was located in a lowland south of the interchange which was displaced by the Juvenile Hall lateral spread during the 1971 earthquake (Youd, 1971; 1973). During the field investigation, we searched unsuccessfully for this culvert, but could not find it. This culvert may have been removed or replaced. Lateral displacements, as large as 1.8 m in the Juvenile Hall spread, likely generated the separations at pipe joints noted above. Again, the damage was concentrated at joints with little noted damage to the pipe sections.

Other CMP Culvert Damage

Several culverts experienced cracking of concrete headwalls placed around the ends of CMP culverts to restrain lateral movements of soil placed over and around inlets and outlets. The culverts noted here are in the northern part of the San Fernando valley, and the head walls were fractured during the 1971 San Fernando earthquake. This damage did not require major repairs or culvert replacement. The headwall cracking was partly due to increased lateral earth pressures against the headwalls and partly due to transient or permanent deformations of CMP culverts which formed deformable inclusions within the brittle concrete walls.

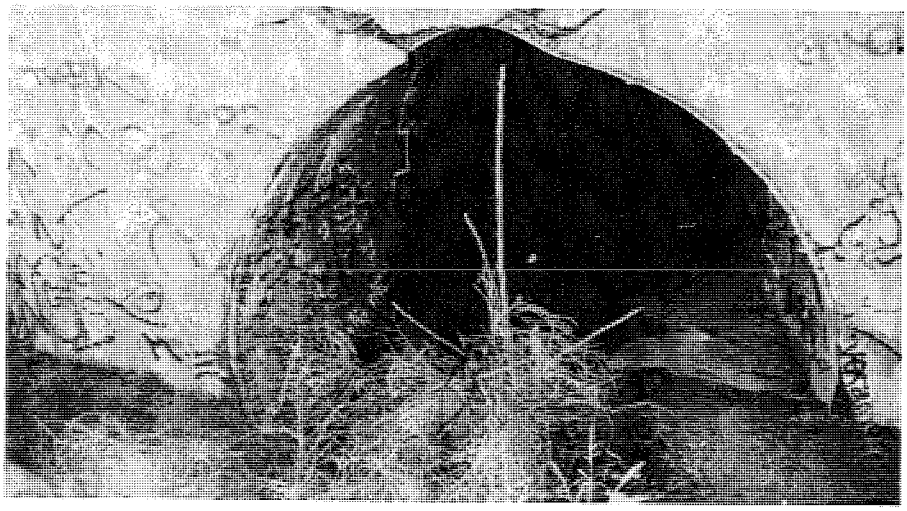

FIGURE 8 Fractured Headwall and Deformed Inlet of CMP Culvert Beneath Route 5 About 600 m south of Roxford Street, Sylmar California. Photographed After the January 1995 Northridge earthquake.

Figure 8 shows a fractured head wall and distorted inlet to a 3.6-m-diameter CMP culvert beneath Route 5 about 600 m south of the Roxford Street underpass. The culvert was constructed from bolted curved plates of corrugated steel. More than 6 m of fill cover the central part of this culvert. During the 1971 San Fernando earthquake, a 200-mm-thick segment of head wall above the culvert crown at the inlet fractured and broke away from the wall. As shown in the photograph, the culvert was also locally deformed at the inlet. In this instance, the pipe deformation did not extend beyond 1 m from the pipe inlet. A retaining wall that extended northward from the inlet was also fractured and bulged outward due to increased lateral earth pressures generated during the 1971 earthquake.

This culvert is within the area strongly shaken by the 1994 Northridge earthquake. A re-inspection of the culvert about a year after the 1994 earthquake revealed that no repairs had been made and no additional detectable damage occurred to the pipe and headwall during the 1994 earthquake. Ground shaking during both the 1971 and 1994 earthquakes was intense at this locality with peak accelerations exceeding 0.5 g. The reasons for the lack of significant additional damage during the 1994 earthquake are not clear. One possible explanation is that the general water table in the area likely dropped significantly after the 1971 event. In 1971, the culvert outlet was near the shoreline of lower Van Norman Lake. That lake was drained after the 1971 earthquake likely lowering the water table beneath the freeway embankment. Although there were no visible signs of liquefaction or ground failure at the locality in 1971, foundation soils may have been saturated and softer than in 1994, allowing greater transient ground displacements and increases in lateral pressure.

CONCLUSIONS

To evaluate culvert performance during earthquakes, we reviewed reconnaissance reports from six earthquakes and conducted field investigations in areas shaken by three of those earthquakes. Hundreds of CMP culverts were in place in areas strongly shaken by these earthquakes. Lack of reported or observed damage to all but ten of these structures indicate that CMP culverts generally perform performed very well during earthquake shaking. Thirty-two CMP culverts, including the ten damaged structures, were specifically examined through field inspection or critical literature review. Diameters of these culverts ranged from 0.45 m to 3.6 m. Of the ten damaged culverts, eight required repairs or replacement. Only two of those culverts were nonfunctional after earthquake shaking. Based on this performance, we draw the following conclusions:

1. CMP culverts have performed very well during earthquakes, except in areas of ground failure or ground disturbance. Of the ten damaged culverts identified, all but one were in areas of ground failure caused by liquefaction or slope instability. The one culvert not in an area of ground failure suffered minor damage due to increased lateral pressures cracking a head wall and slightly deforming the pipe inlet.

2. Penetration of roadway embankments into softened or weakened foundation soils has been the most common cause of damage to CMP culverts. This damage was usually a consequence of soil liquefaction. Embankment penetration pushes mid-sections of culverts downward, bending or buckling the pipe and deflecting end-sections upward. In most instances the pavement and overlying roadway were also severely disrupted.

3. Liquefaction-induced lateral spread pulled apart three CMP culverts primarily through failure at the joints. Differential axial and lateral ground displacements generated extensional or flexural forces within the culverts causing separations at the joints or tearing of the pipe.

4. Increased lateral earth pressures laterally collapsed one 2.4-m-diameter CMP culvert over a length of about 75 m. This culvert was buried beneath 4.2 m to 12 m of compacted fill overlying liquefiable deposits. Transient pulses of lateral stresses generated by liquefaction-induced ground oscillation apparently caused the collapse of this CMP structure. The same pipe was undamaged where liquefaction occurred, but the depth of cover was less than 3.5 m.

5. Several smaller-diameter CMP culverts (<1.2 m) were inspected and found to be undeformed even though they were located in areas of intense seismic shaking or in areas where liquefaction occurred. These seismic effects should have transiently or permanently increased lateral earth pressures, but did not perceptibly deform the culvert sections. Depth of cover over these culverts ranged up to 6 m. This performance indicates that well constructed and uncorroded small-diameter (<1.2 m) CMP culverts are sufficiently strong to resist lateral deformation due to seismic effects.

6. Slumping of fill and foundation soils down one steep slope deformed and pulled apart one CMP culvert. In this instance, about 1 m of differential vertical displacement across a 18-m-long culvert did not rupture or deform individual pipe sections, but rotated individual pipes by as much as 5 degrees. This disturbance caused as much as 200 mm of pull-apart at the joints. An over-wrap of corrugated metal over the joints remained in place, however, and prevented fill or other debris from entering the culvert. This culvert remained in service for several years after the earthquake.

ACKNOWLEDGMENTS

This project is part of the Highway Project being conducted in behalf of the Federal Highway Administration (FHWA) by the National Center for Earthquake Engineering Research (NCEER) under FHWA Contract DTFH61-92-C-00106 Task 106-B(I). Support, including funding, from FHWA and NCEER is gratefully acknowledged. Information on damaged and undamaged culverts in their jurisdictions was provided by highway officials from the California Department of Transportation, Los Angeles, Monterey, and Santa Cruz Counties, California, the Idaho Department of Transportation, and Custer County, Idaho.

REFERENCES

Aydin, Atilla, Johnson, Arvid M., and Fleming, Robert W., 1992, "Right-lateral-reverse surface rupture along the San Andreas and Sargent faults associated with the October 17, 1989, Loma Prieta, California, earthquake," *Geology*, vol. 20, p. 1063-1047, December 1992.

Bardet, J.P., and Davis, C.A., 1995, "Failure of Underground Pipe in the Van Norman Complex During the 1994 Northridge Earthquake," *Proceedings*, 4th U.S. Conference on Lifeline Earthquake Engineering, in press.

Foundation Section (California Division of Highways, Materials and Research Department), 1973, "Earthquake Damage to California Highways," in, *The San Fernando, California, earthquake of February 9, 1971*, Vol. 2, p. 235-246.

Kachadoorian, Reuben, 1968, "Effects of the Great Earthquake of March 27, 1964, on the Alaska Highway System," U..Geological Survey Professional Paper 545-C, 66 p.

McCulloch, D.S. and Bonilla, M.G., 1970, "Effects of the Earthquake Of March 27, 1964, on The Alaska Railroad," U.S. Geological Survey *Professional Paper* 545-D, 161 p.

Seed, H.B., Lee, K.L., Idriss, I.M., and Makdisi, F.I., 1975, "The Slides in the San Fernando Dams During the Earthquake of February 9, 1971," *Journal of the Geotechnical Engineering Division*, ASCE, Vol. 101, No. GT7, p. 651-688.

U.S.G.S. Staff, 1990, Fracture Map of the Santa Cruz Mountains, Loma Prieta Earthquake, U.S. Geological Survey, Menlo Park, California.

Youd, T.L., 1971, Landsliding in the vicinity of the Van Norman Lakes, in The San Fernando, California, Earthquake of February 9, 1971, U.S. Geological Survey *Professional Paper* 733, p. 105-109.

Youd, T.L., 1973, "Ground Movements in Van Norman Lake Vicinity During San Fernando Earthquake," in, *The San Fernando, California, earthquake of February 9, 1971*, Vol III, p. 197-206.

Youd, T.L., and Craven, T.N., 1975, "Lateral Stress in Sands During Cyclic Loading," *Journal of the Geotechnical Engineering Division*, ASCE, Vol. 101, No. GT2, p. 217-221.

Youd, T.L., and Beckman, C.J., in press, "Highway Culvert Performance During Earthquakes," National Center for Earthquake Engineering Research Technical Report.

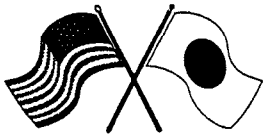

Session 3
Analysis & Structure Performance
Part I

Session Co-chairs: Thomas O'Rourke and Masanori Hamada

SIMULATION OF COLLAPSE PROCESS OF ELEVATED EXPRESSWAY BRIDGES DUE TO THE 1995 KOBE EARTHQUAKE

Kimiro Meguro
International Center for Disaster-Mitigation Engineering,
Institute of Industrial Science, The University of Tokyo, Tokyo, Japan
E-mail: meguro@incede.iis.u-tokyo.ac.jp

Tsuneo Katayama
National Research Institute for Earth Science and Disaster Prevention,
Science and Technology Agency, Tsukuba, Japan

ABSTRACT

At 5:46 a.m. (local time) on January 17, 1995, the Great Hanshin (Hyogo-Ken Nanbu or Kobe) earthquake hit the Hanshin-Awaji area, Japan. The damage due to this earthquake was the worst earthquake disaster in Japan since the 1923 Great Kanto earthquake. Over 100,000 houses and buildings collapsed and many modern civil infrastructures such as elevated bridges of highways and railways, and port facilities, etc. were also heavily damaged. In addition, fires broke out razing many houses after the quake. The death toll was more than 6,300 including deaths due to various problems following the earthquake. Unfortunately, most deaths were caused due to collapse of structures. To mitigate casualties due to earthquakes, it is important to study the mechanism of collapse of structures during earthquakes. In this study, using the Extended Distinct Element Method (EDEM), which is applicable to both a composite and continuous medium, and a perfect discrete one, the collapse mechanism of structures during the 1995 Great Hanshin earthquake is studied. Although the phenomena treated in this study were difficult to be simulated by the conventional methods such as the finite element method, the numerical results obtained agree well with the actual earthquake damage.

INTRODUCTION

To mitigate casualties due to earthquakes, it is important to study the mechanism of collapse of structures during earthquakes. The Great Hanshin earthquake of 17 January, 1995 caused over 100,000 collapsed houses and buildings, many heavily damaged civil infrastructures, and more than 6,300 deaths. Most of the deaths were due to collapse of structures.

To assure the safety of the general public in the event of future earthquakes, it is vital to analyze the collapse of structures. The process which is used in analyzing the behavior of structures in a collapse, addressing the problems such as, "Where and how do they undergo collapse?", "Is the time of collapse short or long?", "How far would the fragments of structural members fly and/or move in the process of collapse?", and "Would the collapse of structures be partial or overall?", is expected to greatly reduce the domains of structure collapse behavioral uncertainties. It is hoped that the knowledge of engineering concerned with collapse of structures will pave way in bringing forth approachs which could clarify these uncertainties. For example, we may undertake such architectural designs which allow partial structural collapse but prevent complete collapse. The means of such an analysis at present is the Extended (or Modified) Distinct Element Method (EDEM, MDEM) (Iwashita and Hakuno, 1990, Meguro *et al.*, 1988, Meguro *et al.*, 1991) which were developed from the distinct element method (Cundall, 1971).

In this study, using the EDEM, the mechanism of collapse of structures during the 1995 Great Hanshin earthquake is studied by simulating various modes of collapse process of structures, especially, elevated exepressway bridges, reported after the quake.

EXTENDED DISTINCT ELEMENT METHOD

Although the conventional distinct element method (DEM) used in geotechnical engineering has proved very useful, only a few applications are heard in other media (Meguro and Hakuno, 1989a, Meguro and Hakuno, 1992, Meguro and Hakuno, 1994). The use of DEM was extended to the fracture analysis of structures, usually analyzed only by the methods based on continuum equations such as the FEM. The EDEM was originally developed by the research group including the first author of the paper. A computer algorithm has been written which can be used both for geotechnical engineering and for various other media as well. This method maintains continuity of the elements because it includes the additional spring called pore-spring or joint-spring which represents the effects of the material surrounding the elements. **Figure 1** shows the EDE modelling.

The equations of motion of an element, i, having the mass, mi, and the moment of inertia, Ii, are

$$mi \cdot d^2u/dt^2 + Ci \cdot du/dt + Fi = 0 \quad (1)$$

$$Ii \cdot d^2\phi/dt^2 + Di \cdot d\phi/dt + Mi = 0 \quad (2)$$

in which Fi is the sum of all the forces acting on the element; Mi the sum of all the moments acting on it; Ci and Di the damping coefficients; u the displacement vector; and ϕ the rotational displacement.

The time histories of u and ϕ are obtained step-by-step in the time domain by the explicit numerical integration of equations (1) and (2).

As forces acting on an element are of two kinds, Fi and Mi are expressed as

$$Fi = Fie + Fip + mi\,(g+\alpha) \quad (3)$$

$$Mi = Mie + Mip \quad (4)$$

where Fie is the sum of forces from all the elements in contact; and Fip, from all the material surrounding it. Mie and Mip are the sums of all the moments from all the elements in contact and from all the material surrounding it respectively. These forces are obtained from the deformations of the element and pore-springs (joint-springs) set in the normal and tangential directions. In equation (3), g is the acceleration due to gravity and α is the external acceleration acting on it. As the fracture criterion of the pore-spring, a critical tensile strain (β) is specified in the normal direction, and Coulomb's equation is used in the tangential direction.

A new concept regarding the application of the EDEM is also proposed in this study: the EDEM can be taken as an extended lumped mass system, the field of application of which is extended to the discontinuous media, unlike the standard lumped mass system which is applicable only to the continuous media.

The EDEM is a conceptual model realized with a unique idea incorporated, wherein elements

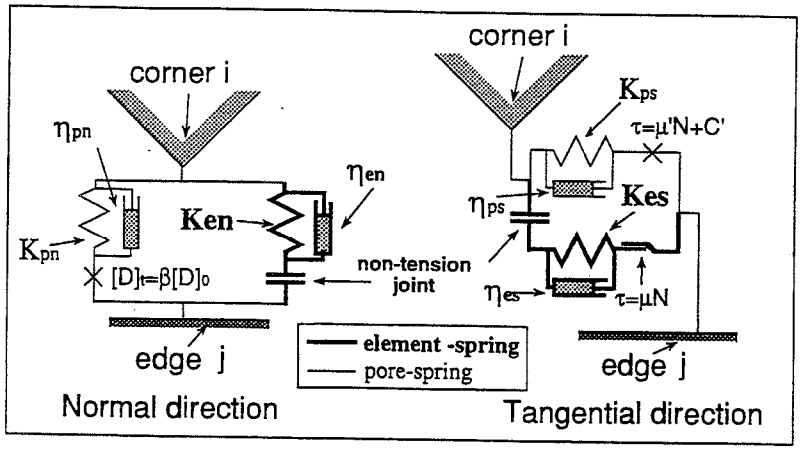

Fig. 1. EDE modelling

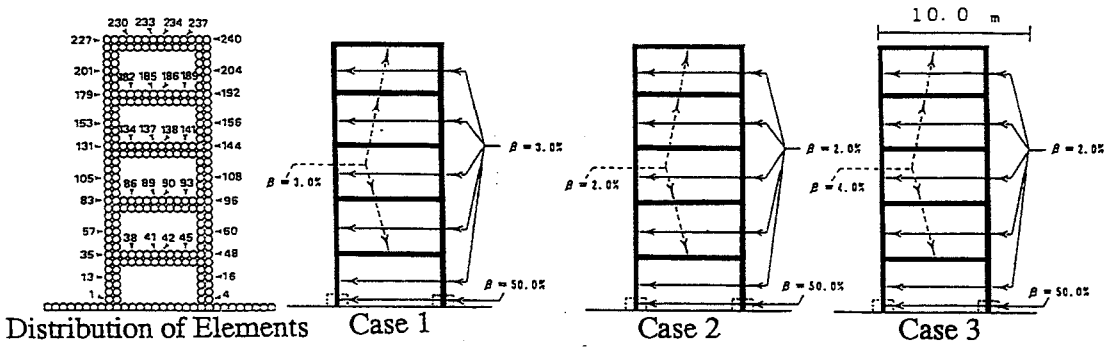

Fig. 2. Building models

are each recognized as a unitary element of motion, a key to solve the equation of motion, and an interaction among elements is regarded as a spring action. In another aspect, the EDEM is taken as a lumped mass system, a subsystem of the composite, multi-degree-of-freedom (MDOF) system. Reference will now be made to "What is the most outstanding difference between the lumped mass system branched off from the MDOF system which is generally applied as a means for the dynamic response analysis, and the EDEM system?" The difference lies between the respective system configurations, the former being characterized in that only continuous bodies can be analyzed while the latter, featuring its configuration, enables behavioral tracking over such a scope from a continuous body to a discontinuous body. Taking note of this system configuration, the EDEM system may be grasped as a means for the response analysis (extended MDOF) following the MDOF system characterized by an extended scope of application.

Depending upon the material characteristics of the medium concerned and the scales of the structures to be modeled by the EDEM, it is impractical and beyond the operational capability of present computers to have models in which the elements have one-to-one correspondence with those in the real medium. For example, in the case where basic vibration and subsequent collapse modes, both of which

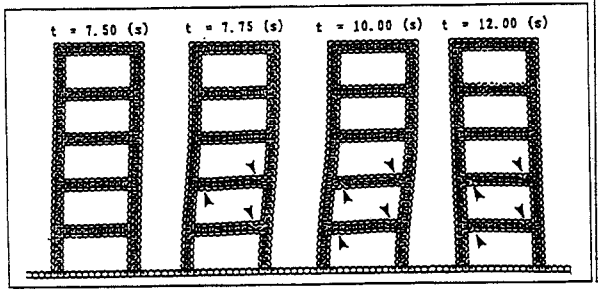

Fig. 3(a). Seismic response analysis of a slender building (Case1: Example of earthquake damage to weak-beam-type buildings)

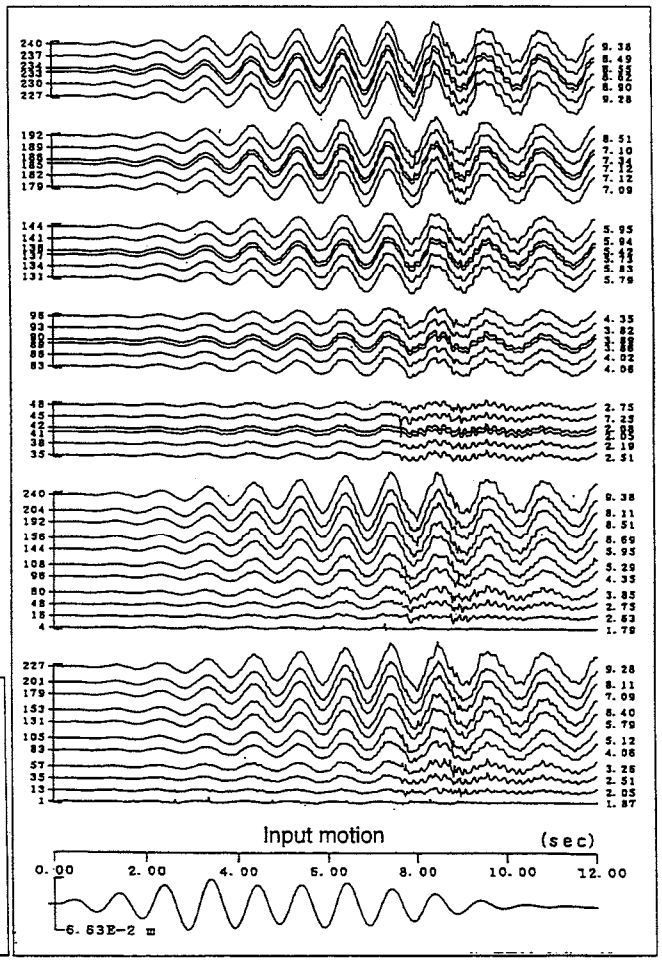

Fig. 3(b). Time-history of response velocity (Horizontal comp. with Case 1)

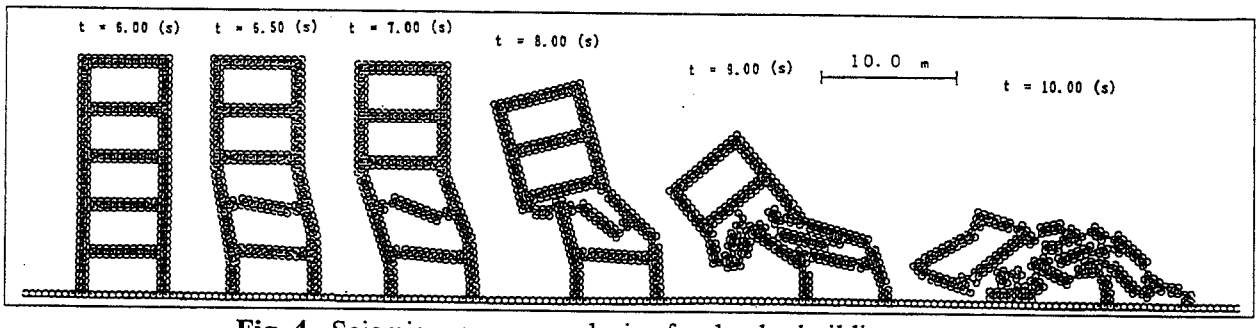

Fig. 4. Seismic response analysis of a slender building
(Case 2: Example of earthquake damage to weak-colomn-type buildings)

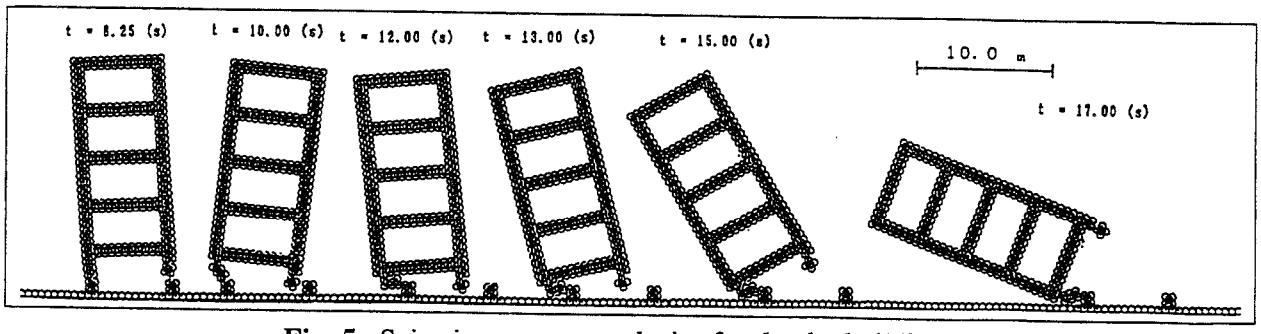

Fig. 5. Seismic response analysis of a slender building
(Case 3: Collapse of a slender building due to resonance)

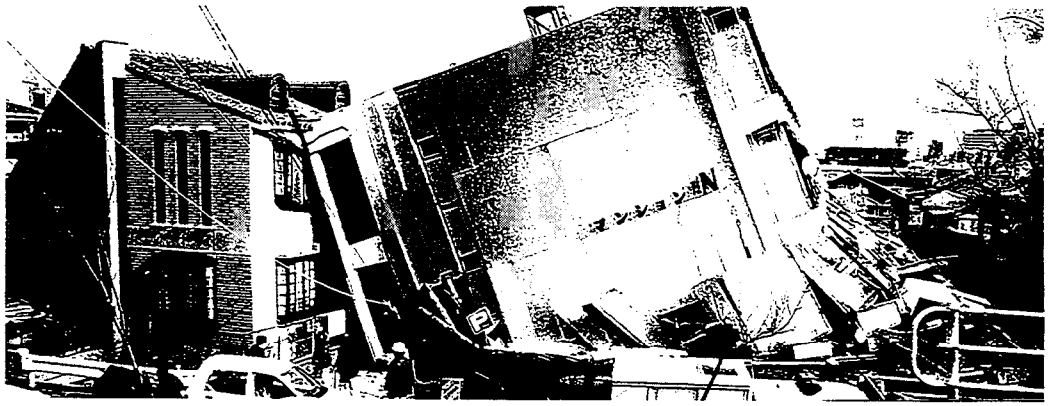

Photo 1 Tumbling-type collapse of buildings

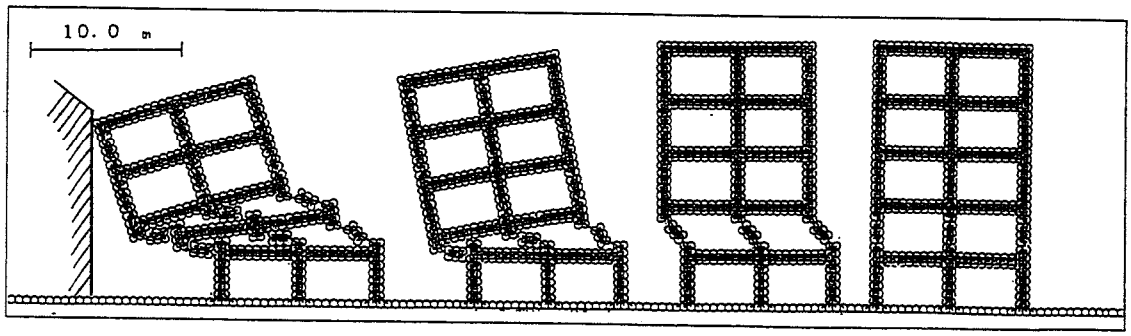

Fig. 6. EDE simulation of the tumbling-type collapse

hold significance in engineering, are required to be clarified, there is no need to model at the material level involving a large number of elements. In such a case, it is useful to consider the EDEM as an extended MDOF system, which can be applied to the collapse behavior of structure.

The dynamic response analysis by the conventional MDOF system is very difficult when analyzing the dynamic behavior in the stage of structural collapse initiation or in the process wherein structural collapse is progressing. However, the dynamic response analysis following the EDEM system allows us to simulate the collapse behavior of structures from a sound state to a complete collapse. Therefore, with the EDEM system dynamic response analysis, the structural vibration characteristics can vary with the outbreak of collapse, and keeping pace with the progress of collapse can phenomenally be illustrated in a state of spontaneity.

Examples of the EDE simulation are shown in **Figs. 2** to **5** (Meguro and Hakuno, 1989b). These are the analyses of dynamic behavior of the slender structures due to excitation. In case of the simulation using the model of case 1, cracks appear at the left and/or right beam-column connections of the 2nd and 3rd floors at 7.75 sec (**Fig. 3 (a)**). The effects of appearance and slips between the cracks can be seen in the velocity response at the joint corners. Because of the damage due to cracks, dynamic properties of the structure system is changed. Its natural period become longer as shown in **Fig. 3 (b)**.

NUMERICAL RESULTS

To study the mechanism of collapse of structures due to past earthquakes, Meguro and Hakuno simulated various modes of collapsed structures, some of which are shown in **Figs. 6** to **8** (Hakuno and Meguro, 1993). After the 1995 Great Hanshin earthquake, these types of structural collapse were observed in the affected areas (**Photos 1-3**).

In addition to the collapse of houses and building structures, elevated bridges of highways

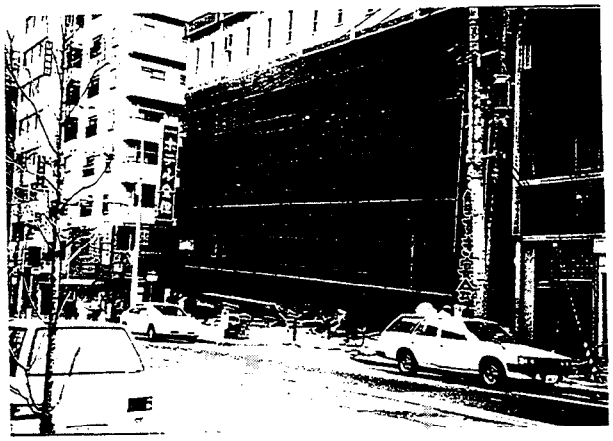

Photo 2 Damage to the first floor collapse-type

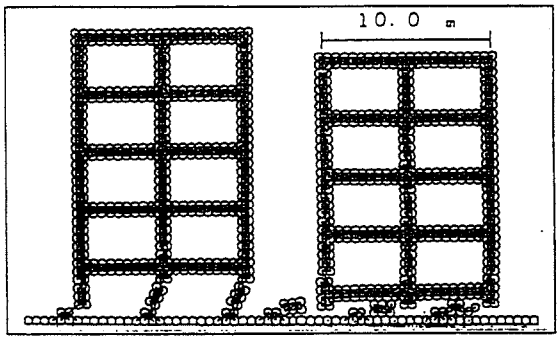

Fig. 7. EDE simulation of the damage to the first floor collapse-type

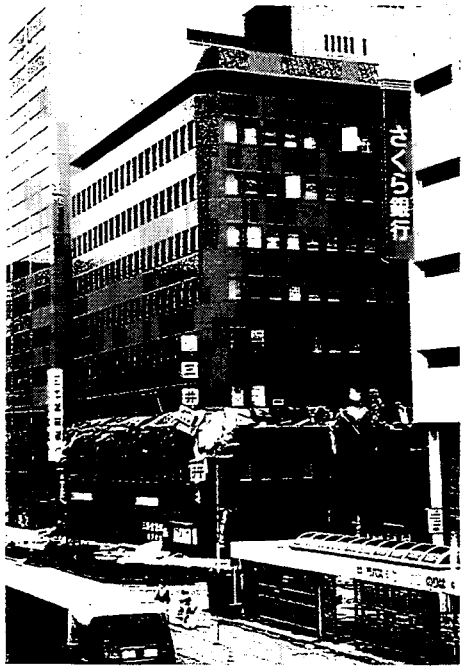

Photo 3 Damage to an intermediate floor collapse-type

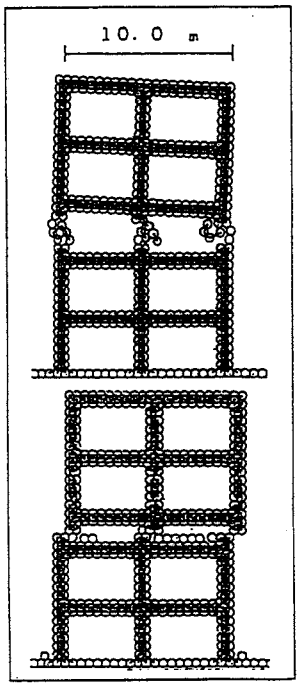

Fig. 8. EDE simulation of the damage to an intermediate floor collapse-type

and railways were also severely damaged due to the 1995 Great Hanshin earthquake. Since the earthquake occurred early in the morning, fortunately, casualties due to the damage of civil infrastructures such as highways and railways were not so many. If the earthquake had hit during daytime when the people were outside and using infrastructures, many people may have been killed or severely injured due to the collapse of these structures. **Photos 4** and **5** show the collapse of elevated bridges of Hanshin Expressway. Considering the damage in **Photo 4**, although the piers didn't collapse but suffered some damage at the bottom, two adjacent simple-beam decks fell down due to dislocation of the bearing supports (**Fig. 9**). Seventeen piers spanning over 630 m of pilz-type bridges were destroyed and the bridges collapsed (**Photo 5**). To

Photo 4 Damage to elevated expressway bridges (Fallen two adjacent simple-beam decks)

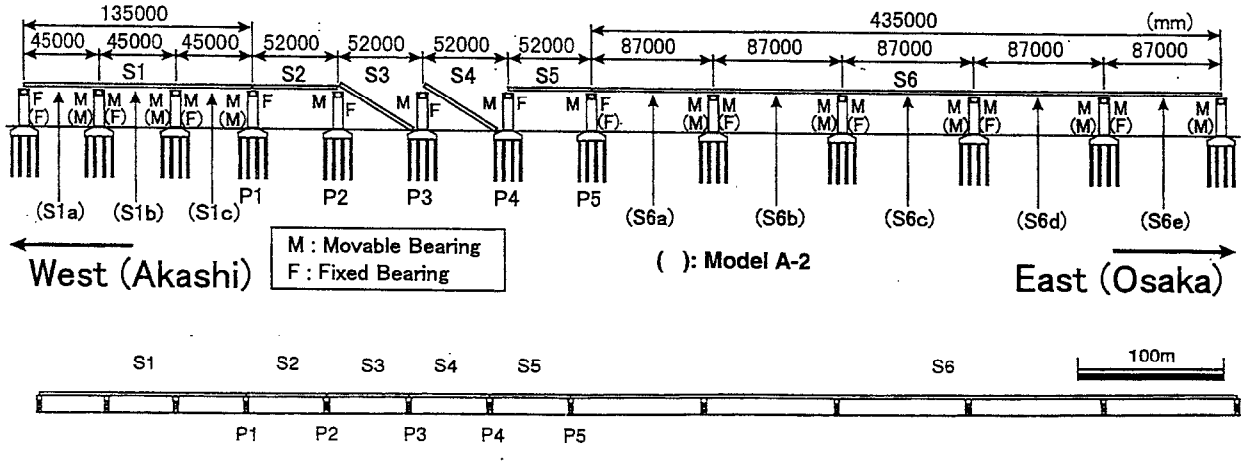

Fig. 9. Overview of the objective damaged bridges and simulation model (Model A)

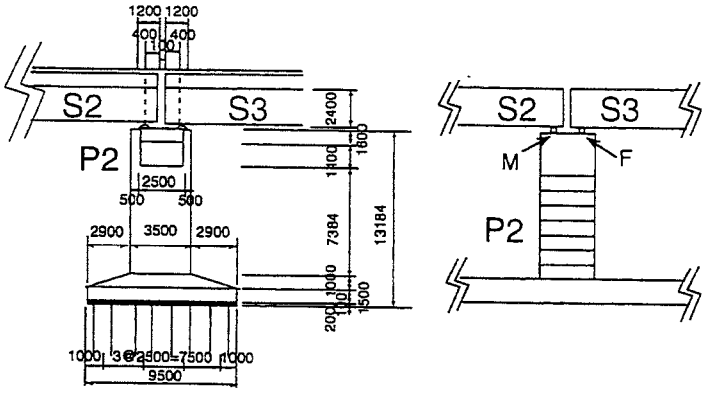

Fig. 10. Size of the bridges and close up of the simulation model (Model A)

Photo 5 Collapse of pilz-type bridges

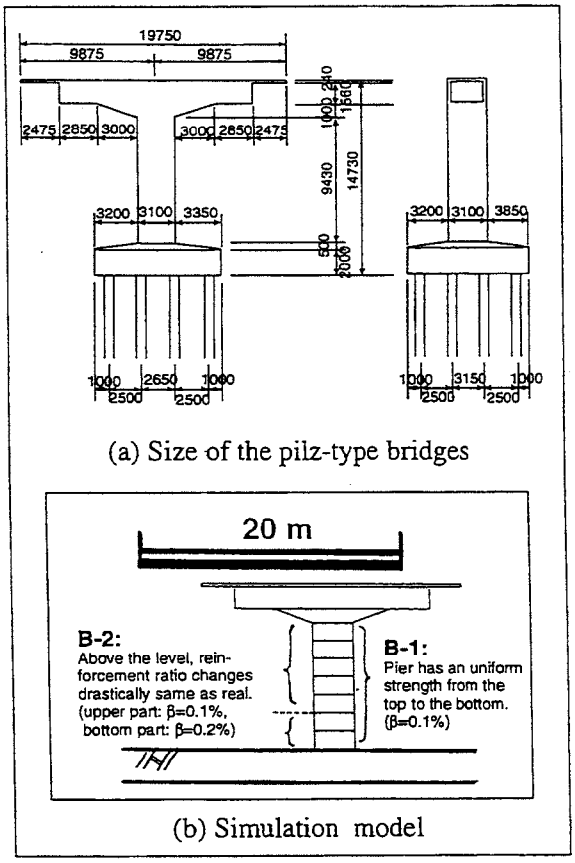

(a) Size of the pilz-type bridges

(b) Simulation model

Fig. 11. Size of the pilz-type bridges and simulation model (Model B)

study the collapse mechanism of these elevated bridges, the fracture process of the damage was simulated using the EDEM.

Figures 9 to **11** show the damaged elevated bridge models (Models A and B) for EDE simulation. Considering the fracture mode of the damage and computational time, we reduced the number of elements used and made the model simple. Since the ground motion at these sites were not recorded, numerical integrated displacement motion from the North-South (N-S) and East-West (E-W) components of the ground acceleration records at Kobe Marine Meteorological Observatory were used in the simulation (**Fig. 12**). Based on the locations of seismic faults and bridges, and their collapse modes, E-W component was used for the Model A, and N-S component was used for the Model B.

Simulation Results using Model A

Effects of the time lag of seismic load at the bases: Using the Model A in **Fig. 9**, a series of simulations with and without consideration of time lag due to wave propagation were carried out. Namely, one case without input time lag, and four cases with the lag based on the assumption that the seismic wave in **Fig. 12** (b) propagated from the left (east) to the right (west) with different apparent wave velocity (Va=500, 1000, 3000, 5000, ∞ m/s).

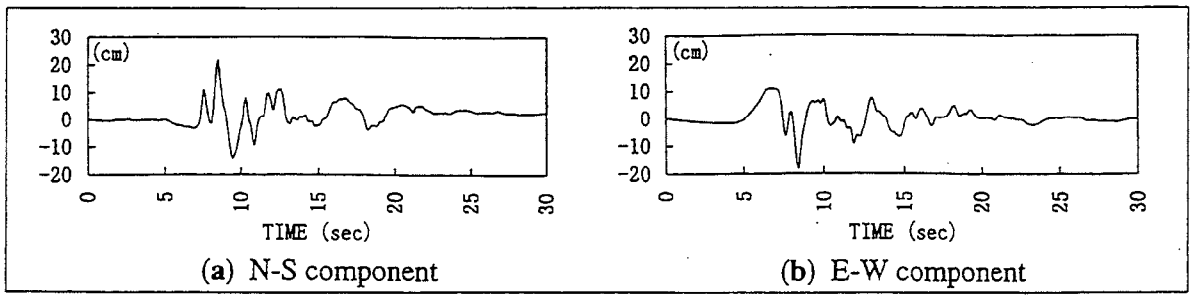

Fig. 12. Input groung motions

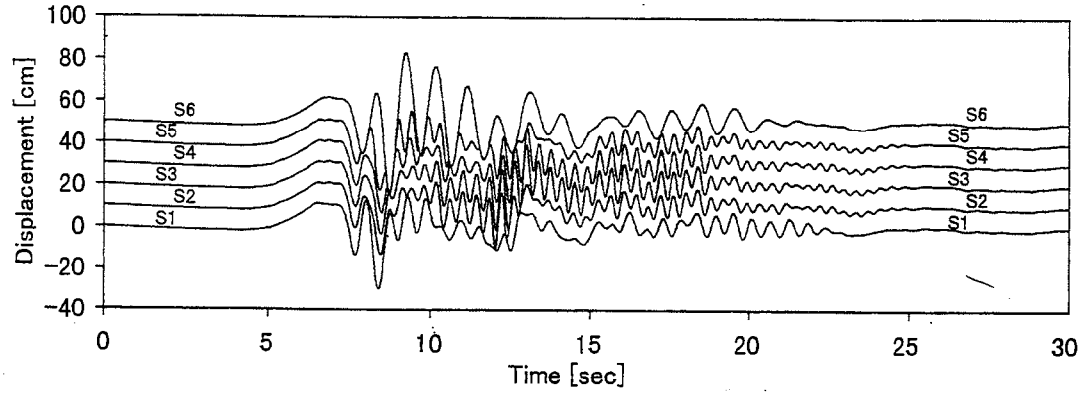

Fig. 13. Dynamic diplacement response of each deck (Model A-1, Va=3,000 m/s)

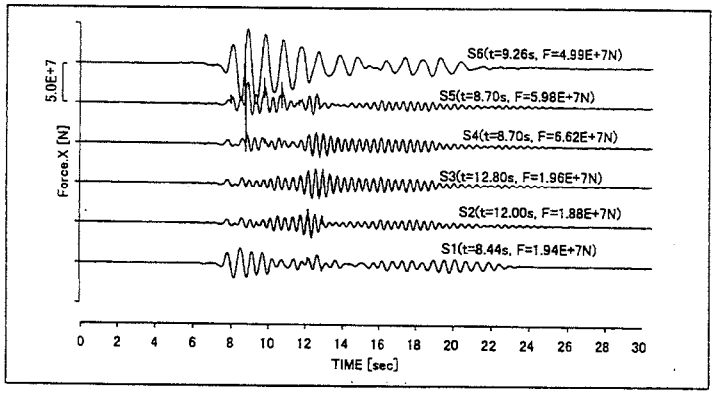

Fig. 14. Time-history of forces acting on fixed bearings (Model A-1, Va=3,000 m/s)

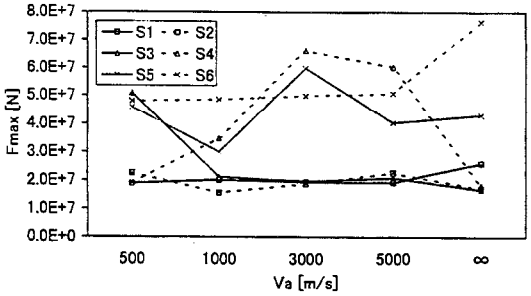

Fig. 15. Comparison of maximun force acting on fixed bearing (Model A-1)

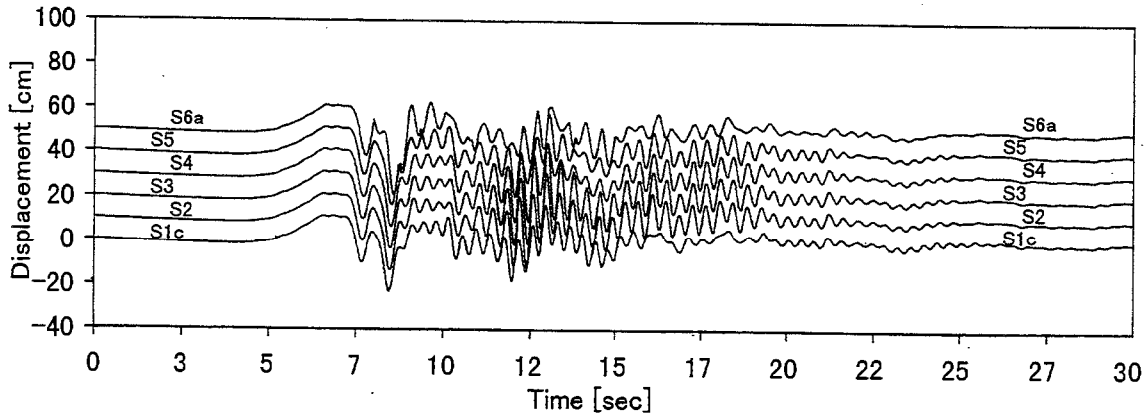

Fig. 16. Dynamic diplacement response of each deck (Model A-2, Va=3,000 m/s)

Some of the simulation results are shown in **Figs. 13** and **14**. Displacement response of each deck is drawn considering the gap of 10 cm between each two decks in **Fig. 13**. **Figure 14** shows the time history of the forces acting on each fixed bearing. From these two figures, we can see that there are poundings between decks and impulsive forces are acting due to their effects. In this simulation, the conditions that although pounding between decks can be occurred, joint-spring between elements are not destroyed. When the maximum forces acting on each fixed bearing are compared of five cases (**Fig. 15**), the case of Va=3,000 m/s is the severest case among acceptable apparent wave velocities.

Effects of the difference of dynamic properties between decks: As a big difference of dynamic properties among S1, S2 to S5, and S6 can be considered one of the main reasons of the collapse, next, we tried to study the effects. A virtual model (Model A-2) was made by dividing the continuous long-span S1 deck into three simply supported (S1a-S1c) decks and also S6 deck into five simply supported decks (S6a-S6e) as shown in the **Fig. 9**. Using the same conditions of the previous simulation, dynamic response analysis was performed under the condition that Va is 3,000 m/s. Numerical simulation results are shown in **Figs. 16** and **17**. This case, severe poundings like in the previous case are not appeared because the dynamic properties of decks S1 and S6 became similar to S2 to S5 decks by dividing them. With the comparison of these two results, it can be noted that the effects of the difference of dynamic properties due to the different structural type had an important role in the mechanism of collapse.

Effects of pounding between decks on collapse of bridges: Dynamic fracture analyses of the bridges were carried out by using apparent wave velocity, Va=3,000 (m/s). **Figs. 18** and **19** show the simulation results. **Figure 19** is a close up of the dynamic displacement response during 7 to 10 (sec) in which severe poundings are observed. From these figures, we can say that due to a series of poundings between decks propagating from east to west, all the fixed bearings broke around 8 (sec) resulting two simply supported decks of the elevated bridge fell down as shown in **Fig. 20**. The collapse mode obtained here is very similar to that of actual damage as shown in **Photo 4**. The difference between actual case and simulation is that S3 and S4 decks fell down in real damage, while S2 and S3 did in the simulation. Considering the uncertainties of input ground motions and some boundary conditions, this simulation results explains the mechanism of the damage as shown in **Photo 4**. As a next case, simulation using the Model A-2, in which S1 and S6 are divided, was carried out. Figure 15 shows the dynamic displacement response of each deck. Comparing the result with normal case, it should be noted that the displacements are relatively very small and the effects of different dynamic properties of bridges played a important role in collapse mechanism.

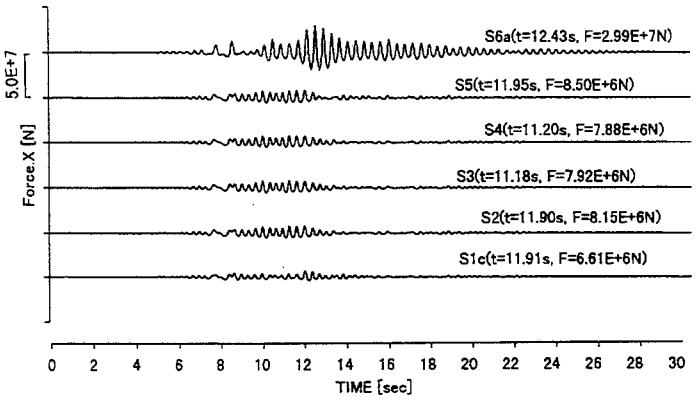

Fig. 17. Time-history of forces acting on fixed bearings (Model A-2, Va=3,000 m/s)

Simulation Results using Model B

With the model in **Fig. 11**, collapse process of the damage to elevated expressway bridges due to overturning was simulated. This was the symbolic damage during the Kobe earthquake shown in **Photo 5**. Simulations of collapse process of two different cases (B-1 and B-2) are

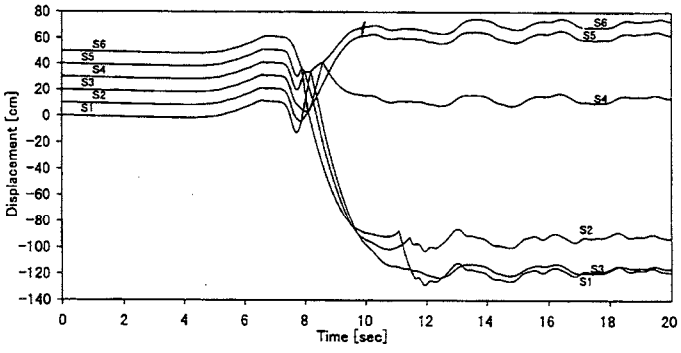

Fig. 18. Dynamic displacement response of each deck during collpapse process (Model A-1,Va=3,000m/s)

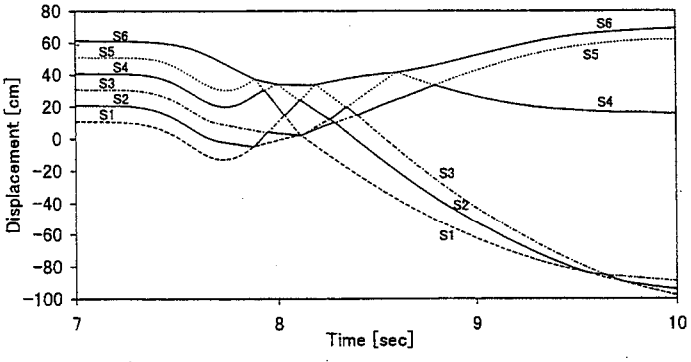

Fig. 19. Close up of the displacement response during 7 to 10 sec (Model A-1,Va=3,000m/s)

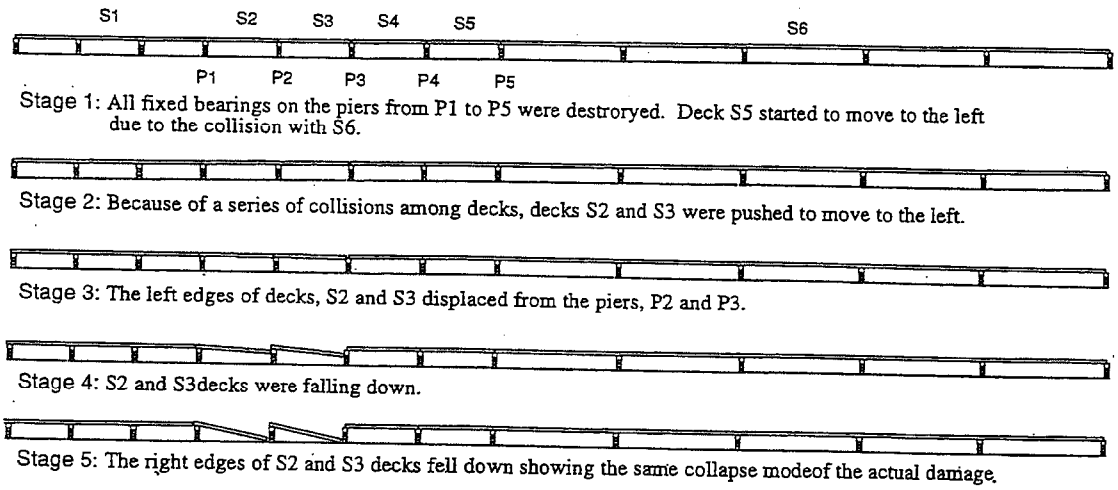

Fig. 20 (a). EDE Simulation of collapse process of elevated expressway bridges (Model A-1, Va=3,000m/s)

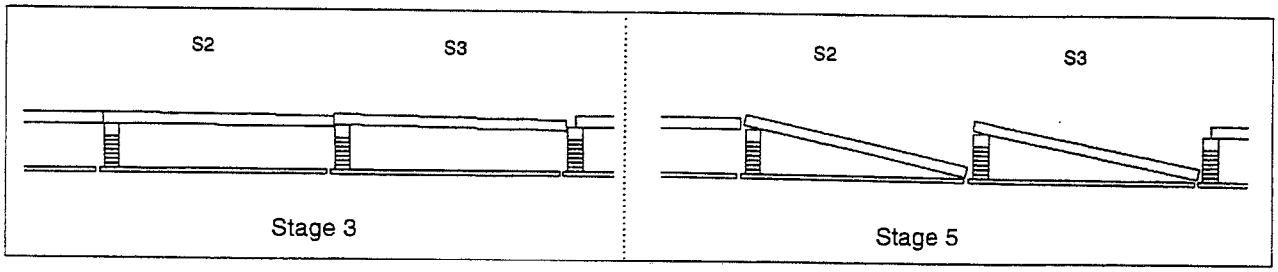

Fig. 20(b). Close up of collapsed parts

shown in **Fig. 22**. **Figure 22** (a) is a result under condition that the pier has an uniform strength from the top to the bottom (B-1), while the pier in **Fig. 22** (b) has a discontinuous plane where the reinforcement ratio changes drastically same as real (B-2). **Figure 23** shows the displacement-acceleration relation of the deck. With time, the bridge inclined and finally, overturned. Although the exact collapse process is not reported, the final collapse modes obtained in this study agree with those of the real damage.

CONCLUSION

Using the EDEM, we tried to simulate the collapse process of structures due to the 1995 Great Hanshin earthquake in order to study the mechanism of the damage. These simulations are based on the new concept of the EDEM application in which the EDEM is taken as an enhanced lumped mass system. Although the phenomena treated in this study were difficult to be simulated by the conventional methods such as the finite element method, the numerical results obtained by the EDEM agree well with the real earthquake damage.

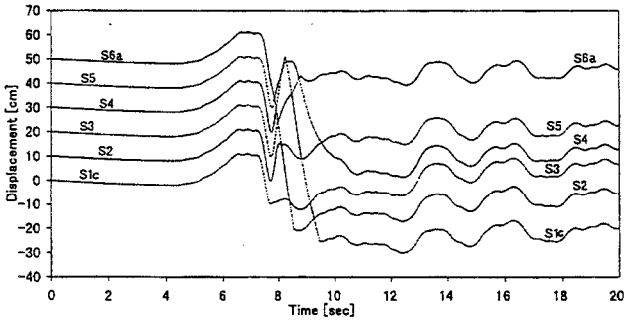

Fig. 21. Dynamic displacement response of each deck during collpapse process (Model A-2,Va=3,000m/s)

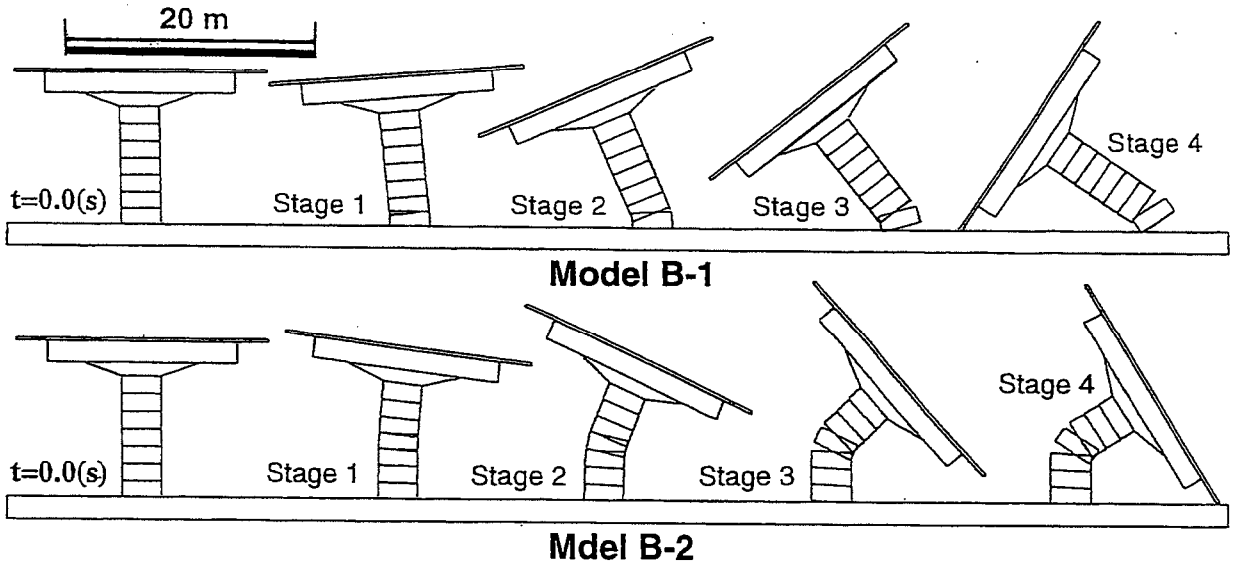

Fig. 22. EDE simulation of collapse process of pilz-type elevated expressway bridges (Model B)

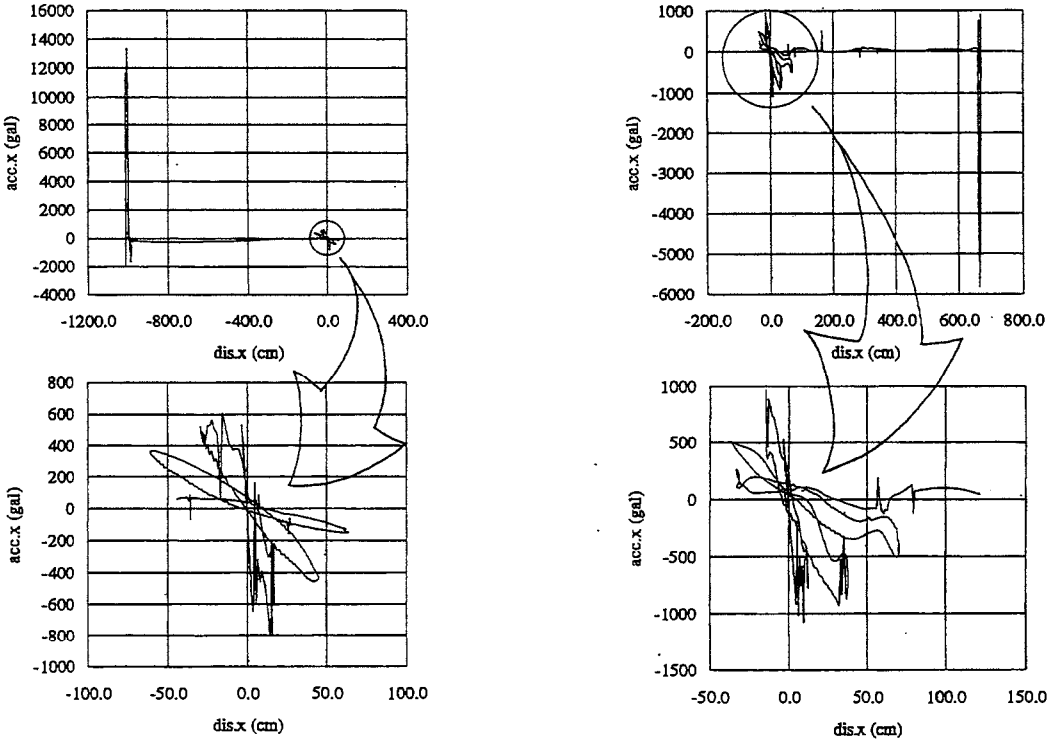

(a) Model B-1 (b) Model B-2

Fig. 23. Displacement-acceleration relation of the deck (Model B)

Examining the simulation results, a conclusion can be drawn that the macro models of these structures would be capable of demonstrating to some extent as to how structures would undergo local collapse, whereby the models be allowed to account for the process or the mechanism of actual earthquake-caused structural collapse with certain accuracy. Although the EDEM is required to go through improvements over various points, the results for fracture as a whole, generally replicate observed earthquake damage.

REFERENCES

Cundall, P. A. (1971). A computer model for simulating progressive, large scale movement in blocky rock Systems, *Proc. of Symp. ISRM, Nancy, France,* **Vol. 2**, 129-136.

Hakuno, M. and K. Meguro (1993). Simulation of concrete-frame collapse due to dynamic loading, *ASCE Journal of Engineering Mechanics,* **Vol. 119, No. 9**, 1709-1723.

Iwashita, K. and M. Hakuno (1990). Modified distinct element method simulation of dynamic cliff collapse, *Structural Eng./Earthquake Eng., Japan Society of Civil Engineers (JSCE),* **Vol. 7, No. 1**, 133-142.

Meguro, K., K. Iwashita and M. Hakuno (1988). Fracture tests of masonry concrete elements by granular assembly simulation, *Proc. of 9WCEE,* **Vol. 6**, 181-186.

Meguro, K. and M. Hakuno (1989a). Fracture analyses of concrete structures by the modified distinct element method, *Structural Eng./Earthquake Eng., JSCE,* **Vol. 6, No. 2**, 283-294.

Meguro, K. and M. Hakuno (1989b). Extended distinct element analysis of collapse process of structures, *Proc. of 10th Annual Conf. on Natural Disasters, Japan society on natural disaster science,* 26-27 (in Japanese)

Meguro, K., K. Iwashita and M. Hakuno (1991). Fracture analyses of media composed of irregularly shaped regions by the extended distinct element method, *Structural Eng./Earthquake Eng. , JSCE,* **Vol. 8, No.3**, 131s-142s.

Meguro, K. and M. Hakuno (1992). Simulation of collapse of structures due to earthquakes using the extended distinct element method, *Proc. of 10WCEE,* **Vol. 7**, 3793-3796.

Meguro, K. and M. Hakuno (1994). Application of the extended distinct element method for collapse simulation of a double-deck bridge, *Structural Eng./Earthquake Eng., JSCE,* **Vol. 10, No. 4**, 175s-185s.

EVALUATION OF BRIDGE DAMAGE DATA FROM THE 1994 NORTHRIDGE, CA EARTHQUAKE

Nesrin I. Basöz and Anne S. Kiremidjian
The John A. Blume Earthquake Engineering Center
Stanford University
Stanford, CA 94305

ABSTRACT

Data on bridge damage from earthquakes is becoming increasingly more available. Such data, however, have not been systematically studied with the objective to evaluate damage characteristics and to correlate these to observed or estimated local ground motions. This paper presents the results from a project in which bridge damage data from the 1994 Northridge earthquake are studied. Structural characteristics that are highly correlated with the observed damage are identified. Bridges are grouped by these structural characteristics and empirical fragility curves are developed for these groups. Only about two percent of the bridges that were exposed to ground shaking experienced damage and only 6 of these bridges collapsed. The analyses of data on bridge damage showed that concrete structures designed/built with older design standards were more prone to damage under seismic loading.

INTRODUCTION

The January 17, 1994 Northridge, California earthquake caused serious damage to bridges in the region, resulting in disruptions to the transportation system. The earthquake was of moderate size (a moment magnitude of 6.7) and occurred at 4:31 am local time. These two factors contributed to the low number of casualties. The impact of bridge closures on emergency response activities immediately after the earthquake was negligible. Closure of the damaged bridges, however, caused major rerouting of traffic during the months following the earthquake.

In this paper, results are presented from a project primarily sponsored by NCEER and the NCEER Highway Project on "Seismic Vulnerability of Highway Construction", with funding provided by the Federal Highway Administration (FHWA). In that project, data on bridge damage from the Loma Prieta and Northridge earthquakes are studied to correlate observed bridge damage to: (*i*) structural characteristics of a bridge, (*ii*) local ground motions, and (*iii*) repair cost. In order to achieve these objectives, first statistics on structural characteristics of bridges, ground shaking levels at bridge sites, damage characteristics and repair cost are performed. Next, empirical damage probability matrices and fragility curves are developed from data on bridge damage. In addition, correlation between structural characteristics and observed damage are determined. Detailed discussion of the procedures and complete results from the analysis can be found in Basöz and Kiremidjian [1997]. In this paper, only the results from the Northridge earthquake are presented.

Despite the high ground motion levels observed in the 1994 Northridge, CA earthquake, only about two percent of all the bridges in the area experienced major damage. The analyses of data on bridge damage showed that concrete structures designed/built with older design standards were more prone to damage under seismic loading. The ground shaking level, skew angle, abutment type, pier type and span continuity are found to be the structural characteristics that show the highest correlation with the observed damage. A total of about $150,000,000 repair cost is reported for the damaged bridges. Repair and/or reconstruction of the collapsed structures formed a large portion of the total repair cost.

ANALYSIS METHOD FOR BRIDGE DAMAGE DATA

Characteristics of the Database

The database compiled for the Northridge earthquake consists of four main type of data: (*i*) structural characteristics, (*ii*) bridge damage, (*iii*) repair cost, and (*iv*) ground motion levels and soil characteristics at bridge sites. A relational database management system (RDBMS), dBase™, is used to compile and perform queries for data on bridge damage and structural characteristics of bridges. In addition, a geographic information system (GIS), Arc/Info™, is used to obtain the ground motion levels at each bridge site.

Structural Characteristics: Several structural characteristics of bridges are compiled in a database for the groups of bridges that were exposed to ground shaking in the Northridge earthquake. These structural characteristics include abutment type, number of spans, type of superstructure and substructure, length and width of the bridge, skew, number of hinges at joints and bents, abutment and column foundation types, and design year to represent design standards, such as column reinforcement and seat width. These structural attributes are obtained from the Structural Maintenance System (SMS) database compiled and managed by Caltrans. The detailed descriptions for each of these attributes can be found in the OSM&I Guide [Caltrans, 1993]. In addition, more detailed information on structural characteristics is obtained from Caltrans for some of the damaged bridges. Caltrans is currently in the process of compiling a database that includes information on abutment, bent/pier/column and bent/pier/footing details, such as seat width and type of bearings, footing type and column/footing connection. However, only about 15 percent of all the California bridges are currently in this database hence, the detailed information in this database could not be used in the statistical analyses due to scarcity of data.

Bridge Damage: Detailed damage descriptions and the corresponding damage states are compiled for bridges damaged in the Northridge earthquake. The damage descriptions are obtained mainly from bridge damage reports compiled by Caltrans [1994]. These descriptions are cross-referenced with those provided by Buckle [1994], EERI [1995], and Yashinsky [1995]. Judgment is used to treat inconsistencies in the interpretation of the observed damage data where inconsistencies exist.

The database on bridge damage specifies four damage states for bridges damaged in the Northridge earthquake (*minor*, *moderate*, *major* and *collapse*). The bridge damage data are used in correlation studies to obtain ground motion-damage relationships.

Damage State Definitions: Currently, no guidelines for evaluating physical bridge damage exists. The terms *minor*, *moderate* and *major* damage are subjective. Definitions of damage states for columns, abutments, and joints and connections for concrete bridges are proposed which are developed based on the observed bridge damage in the Northridge earthquake [Basöz, 1996]. A questionnaire is prepared to acquire expert opinion on the proposed damage state definitions. The questionnaire is given to bridge engineers at Caltrans. The feedback provided by the bridge engineers is used to modify some of the damage state definitions.

Repair Cost: The estimated repair cost values for bridges damaged in the Northridge earthquake are compiled in a database. These estimated repair costs are obtained from supplementary bridge reports compiled by Caltrans following the Northridge earthquake. The database includes total estimated repair cost and a more detailed information on repair work and cost for each bridge that has been repaired. The repair cost ratio, defined as the ratio of repair cost to replacement cost of a bridge, is calculated for all the damaged bridges. The replacement cost of a bridge is estimated to be $\$90/ft^2$ based on the 1995 cost books.

Ground Motion Levels: In addition to structural characteristics, soil type at each bridge site and peak ground acceleration (PGA) levels observed in the Northridge earthquake are compiled. In order to obtain empirical ground motion-damage relationships for the set of bridges damaged in the Northridge earthquake, two sets of peak ground acceleration (PGA) values are used as the ground motion levels: (*i*) PGA values reported by USGS [1994], which are obtained from the contours of observed PGA recordings in horizontal direction and are reported in USGS Open-File Report 94-197 [1994], and (*ii*) PGA values reported by WCFS [1995] that are obtained from the contours of average of the PGA values measured in the E-W and N-S directions. Recorded ground motion levels were used to scale the parameters of empirical Green's functions which were used in simulating the ground shaking levels [Somerville et al., 1996]. The PGA value at a given bridge site is obtained within GIS by overlaying the ground shaking map and the bridge location map. Subsequently, the highest PGA values obtained at a bridge site were 1.55g and 0.66g for the USGS and WCFS maps, respectively. Since the PGA levels from the two data sets varied considerably the correlation studies are performed for both data sets. Results based on USGS [1994] PGA levels are presented in this paper.

Classification of Bridges

The compiled inventory of bridges is reviewed to: (*i*) select bridges to be used in correlation studies, (*ii*) select structural characteristics (attributes) that best describe the seismic response of bridges, and (*iii*) verify the correctness of the attribute values included in the bridge inventory database.

Data Sets: Several data sets are used for statistical analyses. All the analyses are performed for the state bridges since most of the reported damage pertain to state bridges. First, all highway state bridges are selected and gathered in the *highway bridge data set*. Statistics on design year and ground shaking levels are obtained for this data set. Most of the bridge damage pertained to concrete structures. The number of damaged steel bridges was not large enough for statistical analysis. Therefore, concrete bridges are selected from the *highway bridge data set*.

One of objectives of this research is to identify the effect of various structural characteristics on bridge damage. In order to study the effect of structural component types on bridge damage, such as effect of abutment type (monolithic or non-monolithic), and effect of number of columns per bent, bridges with single abutment type and one column bent type are compiled in a database called the *homogeneous data set*. That is, in order to determine the effect of each characteristics, only bridges with homogeneous structural characteristics are selected from the *concrete highway bridge data set*. For example, a bridge with a seat type abutment (non-monolithic), and a diaphragm type (monolithic), is defined as a *heterogeneous* bridge and excluded from the *homogeneous data set*. Similarly, a bridge with both multiple and single column bents is defined as a heterogeneous bridge, and is excluded from the *homogeneous data set*. Bridges with incomplete information are also excluded from this data set.

Another criterion in the data selection relates to the correlation analyses. A complete data set for correlation analyses requires that all the bridges exposed to a given ground shaking level be included. In order to satisfy this requirement, a minimum PGA level is selected as a threshold value. This PGA level is determined based on the available ground motion maps. That is, only bridges that were exposed to peak ground acceleration (PGA) level of 0.15g or larger are compiled. The data set that satisfies this condition is extracted from the *homogeneous data* set and is referred as the *correlation data set*.

The bridges in the *correlation data set* are grouped first by the superstructure type and substructure material. Then, these bridges are further classified into sub-categories based on other structural characteristics, such as number of spans, abutment type, column bent type and span continuity. The classification scheme used in this task is adapted from the bridge classification developed by Basöz and Kiremidjian [1996] under another project submitted to the National Center of Earthquake Engineering Research. The damaged bridges are classified into these classes in order to group bridges that are expected to experience similar damage levels under a given seismic loading. The correlation studies are also carried out using the bridge classification defined by the National Institute of Building Sciences (NIBS) Manual [RMS, 1995].

Reliability of the Database: Caltrans currently has two database systems: the first one (SMS) follows the FHWA National Bridge Inventory System but is more detailed, and the second one (BIRIS) is a database that stores bridge books and drawings for all the bridges. The bridge books include detailed reports from each bridge inspection. For some of the 25,000 bridges in the state of California, discrepancies exist between the two databases.

The two databases are compared to verify the correctness of the attribute values for bridges that were damaged in the Northridge earthquake. The abutment type and column bent type are found to be more likely to have errors than the other attributes that are of interest for this research. For example, only in few cases (for 2 to 3 percent of the damaged bridge data set) the values of the design year and skew attributes were found to be erroneous.

Where there are discrepancies between the two databases, the structural plans are investigated with the assistance of bridge engineers from Caltrans to determine the correct

attribute values. In order to evaluate the effect of error inherent in the database on the results of the correlation studies, several analyses performed using sample data sets with corrected and uncorrected data. The correction of attribute values in the database is very time consuming and is beyond the scope of this project task to correct all the erroneous attribute values in Caltrans SMS database. However, the correction of the available bridge inventories is crucial for vulnerability assessment of bridges based on these inventories.

Correlation Studies

Correlation analyses are performed using the data on bridge damage and repair cost compiled for the Northridge earthquake. The correlation studies are performed to accomplish the following objectives:

(*i*) To determine the structural characteristics that best represent damage such that bridges can be grouped using these characteristics,

(*ii*) To obtain ground motion-damage relationships for bridges with similar structural characteristics,

(*iii*) To obtain ground motion-repair cost ratio relationships to estimate direct economic losses due to damage to bridges,

(*iv*) To correlate damage and repair cost ratio.

The data on bridge damage are compiled in the form of damage matrices, i.e., the number of bridges with each level of observed damaged at different PGA levels. Then, the damage probability matrices (DPMs), i.e., the probability of being in a damage state given the ground motion level are obtained for each group of bridges. The damage matrices are used as input data to logistic regression analysis to obtain empirical fragility curves both unconditional and conditional on damage. Similar procedures are used to obtain empirical fragility curves for the repair cost ratio. Table 1 shows the types of empirical fragility curves developed based on bridge damage observed in the Northridge earthquake. Comparison of observed damage data to currently available ground motion-damage relationships [ATC, 1985; RMS, 1995] are presented in Basöz et al. [1997].

EXAMPLE STATISTICS AND RESULTS

The bridges in the Greater Los Angeles area, including Los Angeles, Ventura, Riverside, and Orange Counties, were exposed to ground shaking during the 1994 Northridge earthquake.

Table 2 lists the number of state and local bridges and the number of damaged state bridges in each of the four counties. A database that includes state and local bridges for the four counties is extracted from the Bridge Maintenance Database compiled by Caltrans [1993]. The

TABLE 1. Characteristics of Data Groups Used in Correlation Analyses

Dependent Variable	Independent Variable	Data Set Grouped by	Conditional on damage
damage state	PGA values reported by USGS [1994]	- detailed classification based on Basöz and Kiremidjian [1996], - NIBS classes, - number of spans, - design year	no
			yes
	PGA values reported by WCFS [1995]	- detailed classification based on Basöz and Kiremidjian [1996], - number of spans, - design year	no
			yes
	design year		no
repair cost ratio	PGA values reported by USGS [1994]	- detailed classification based on Basöz and Kiremidjian [1996], - number of spans, - design year	no
	PGA values reported by WCFS [1995]	- detailed classification based on Basöz and Kiremidjian [1996], - number of spans, - design year	no
	damage states		yes

structural characteristics, structural type and material, number of spans, abutment type, span continuity, design year indicating the seat width and column longitudinal reinforcement, substructure type, skew, and foundation type, are included in this database.

The bridge damage from the Northridge earthquake pertained mostly to state bridges in Los Angeles and Ventura Counties. Bridges in these two counties also experienced much higher accelerations in the Northridge earthquake than bridges in Riverside and Orange Counties. A total of 63 bridges were exposed to peak ground acceleration (PGA) levels of 0.15g or higher in Riverside and Orange Counties. As shown in Table 2, 3533 state and 2571 local bridges are located in the four counties. Of the 3533 state bridges, 3318 (1902 bridges in Los Angeles County, 312 in Ventura County, 462 in Orange County and 642 in Riverside County) carry highway traffic and gathered in the *highway bridge data set*. The number of bridges in the *highway bridge data set* by superstructure type and substructure material are shown in Table 3.

TABLE 2. Distribution of State and Local Bridges and the Number of Damaged State Bridges in the Greater Los Angeles Area

County	Number of State Bridges	Number of Local Bridges	Total Number of Bridges	Number of Damaged Bridges
Los Angeles	2097	1553	3650	228
Riverside	644	338	982	-
Orange	463	505	968	-
Ventura	329	175	504	5

TABLE 3. Distribution of Highway Bridges in Los Angeles, Ventura, Orange and Riverside Counties by Structural and Material Type

	concrete girder	steel girder	truss	tunnel	timber	arch	suspension	unknown
concrete	2396	119	4	0	0	12	1	4
steel	9[1]	3	0	0	1	0	0	0
N/A	708	32	0	4	0	15	0	6
timber	0	0	0	0	4	0	0	0

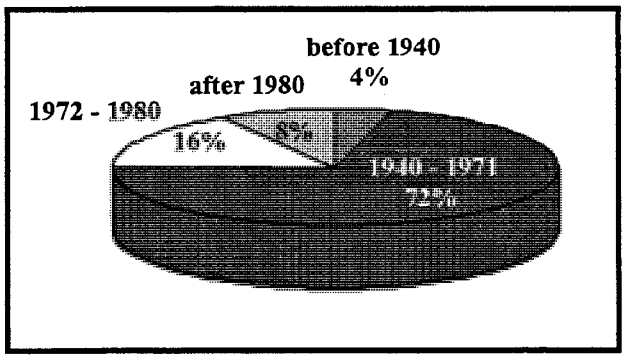

FIGURE 1. Distribution of State Highway Bridges in Los Angeles, Ventura, Orange and Riverside Counties by Design Year

Figure 1 shows the distribution of these bridges by design year. Seventy six percent of the bridges in the *highway bridge data set* were designed by pre-1971 design standards. As shown in Table 3, majority of the bridges in the four counties are concrete structures. Furthermore, more than 85 percent of the bridges damaged in the Northridge earthquake were concrete structures. Therefore, the statistical analyses are conducted mainly for the concrete bridges. Figure 2 shows the recorded PGA values [USGS, 1994] and the state bridges of the four counties. The PGA value at a given bridge site is obtained within GIS.

[1] These 9 bridges have concrete slab type superstructure and have both concrete and steel column bents.

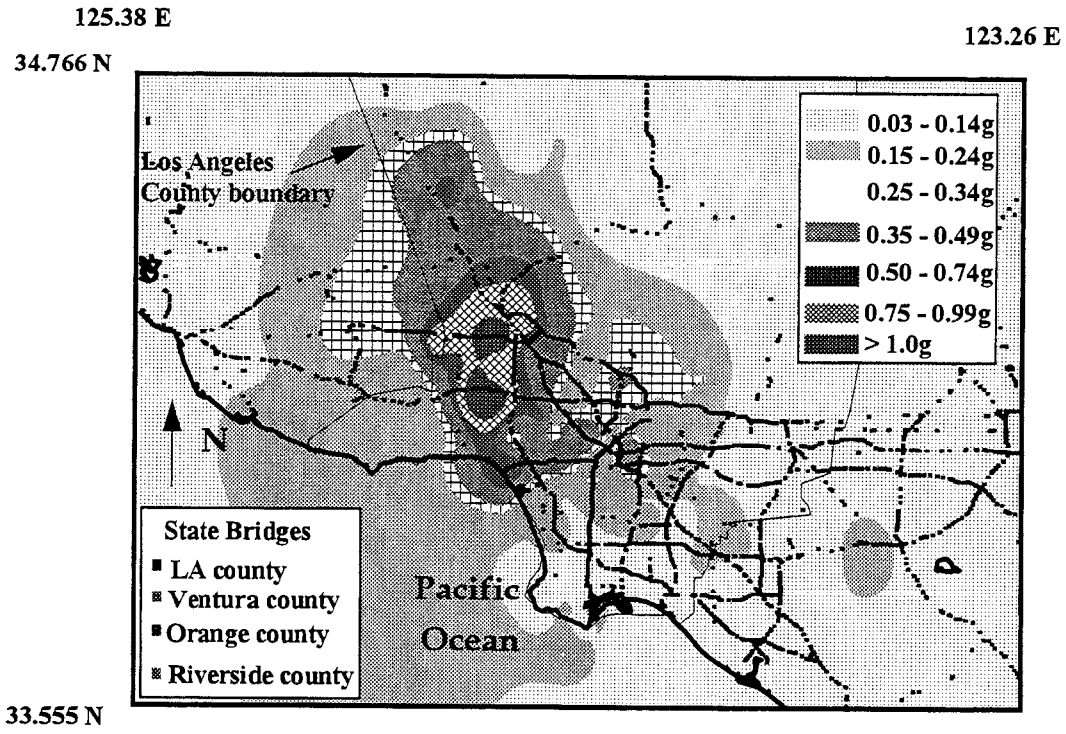

Figure 2. PGA levels observed in the Greater Los Angeles area from the Northridge earthquake [USGS, 1994].

Figure 3 shows the distribution of damaged bridges by design year and damage state. Seventy seven percent of the damaged bridges were designed with pre-1971 design standards. Eighty percent of the damaged bridges were multiple span bridges. As examples of empirical fragility curves developed in this research, Figures 4 and 5 show fragility curves for multiple span bridges. Note that the empirical fragility curves shown in Figure 5 are conditional on damage, i.e., they show the probability of being in (or exceeding) a particular damage state given a bridge is damaged. The PGA values shown on the horizontal axis are the observed values reported by USGS [1994].

For the repair cost data, a database is compiled from the supplementary bridge damage reports provided by Caltrans. A total of about $150,000,000 was reported as repair cost in these reports. The total repair cost for the six collapsed bridges constitute the seventy five percent of the repair cost of all damaged bridges. The database includes total estimated repair cost and a more detailed information on repair work and cost for 130 bridges in Los Angeles and Ventura Counties. Tables 4 and 5 show estimated repair cost of damaged bridges by damage state, and structural type and number of spans. Figures 6 and 7 show fragility curves for repair cost ratio for multiple and single span bridges.

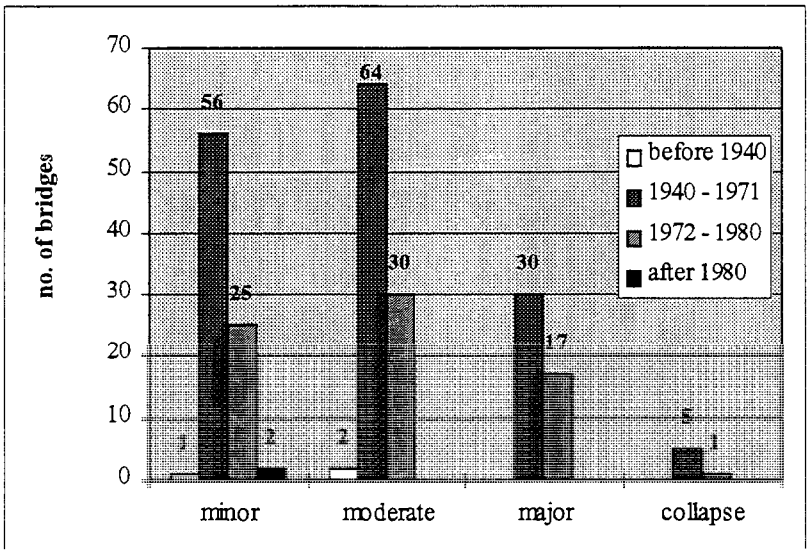

FIGURE 3. Distribution of All Damaged Bridges by Design Year and Damage State

TABLE 4. Distribution of Estimated Repair Cost by Damage State

Damage state	Number of Bridges	Estimated repair cost
collapse	6	$121,765,750
major	47	$18,398,057
moderate	93	$6,895,731
minor	85	$446,950

TABLE 5. Distribution of Estimated Repair Cost by Structural Type and Number of Spans

Superstructure Type	Number of Spans	Number of Bridge	Estimated Repair Cost
concrete girder	> 1	610	$133,347,138
concrete girder	= 1	223	$1,273,000
steel girder	> 1	36	$2,288,750

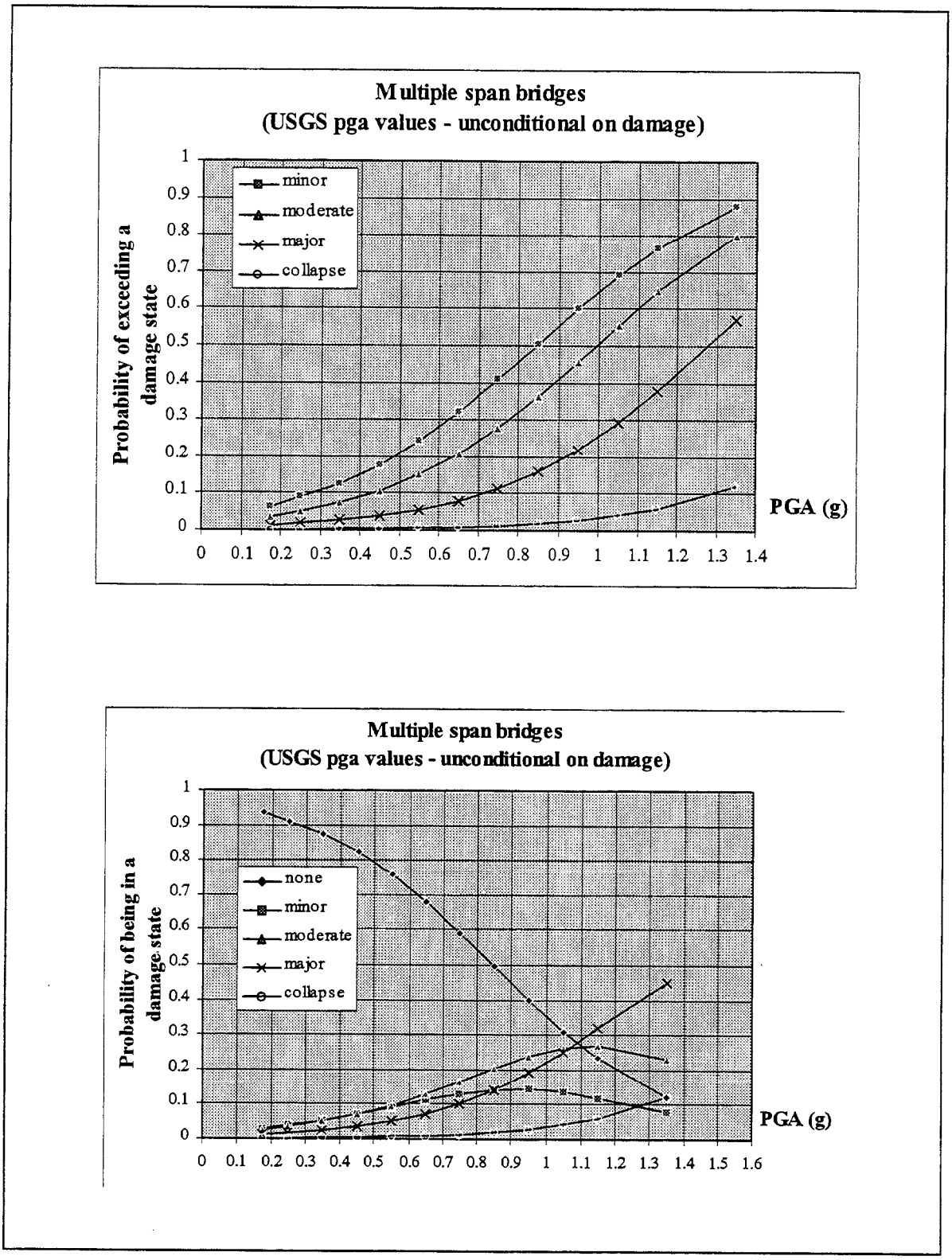

FIGURE 4. Empirical Fragility Curve for Multiple Span Bridges, Unconditional on Damage

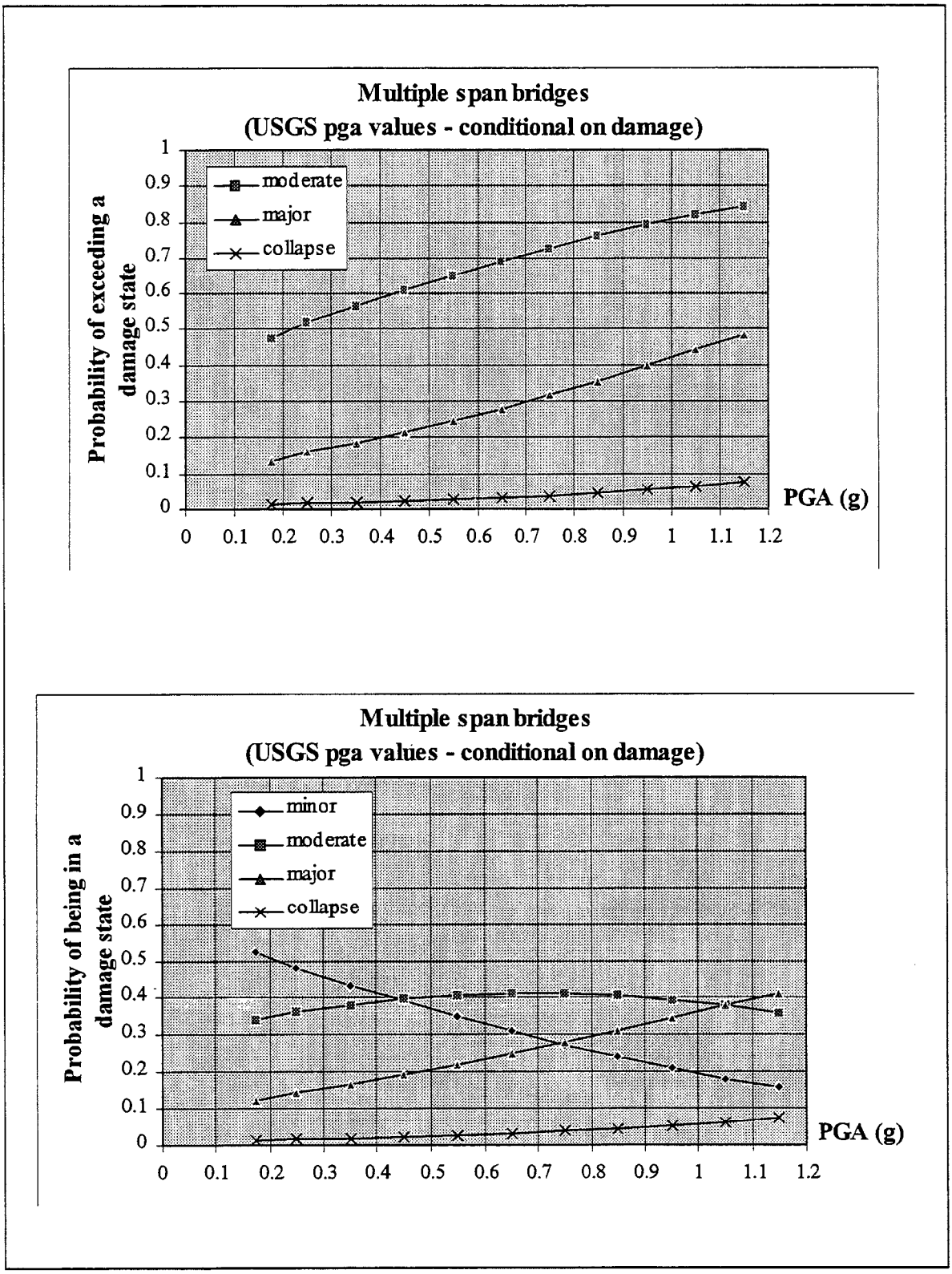

FIGURE 5. Empirical Fragility Curve for Multiple Span Bridges, Conditional on Damage

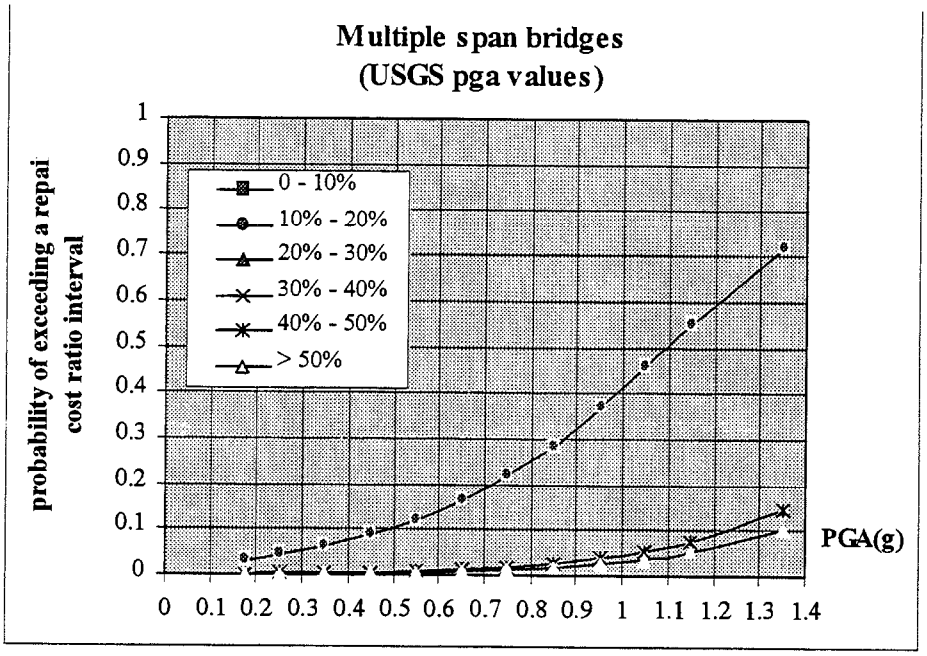

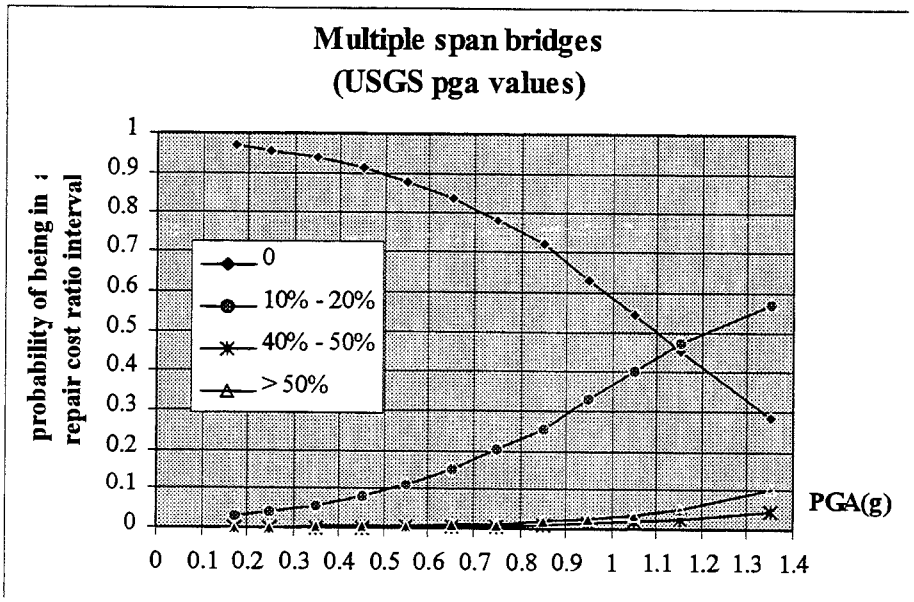

FIGURE 6. Empirical Fragility Curve for Multiple Span Bridges, Unconditional on Repair Cost Ratio

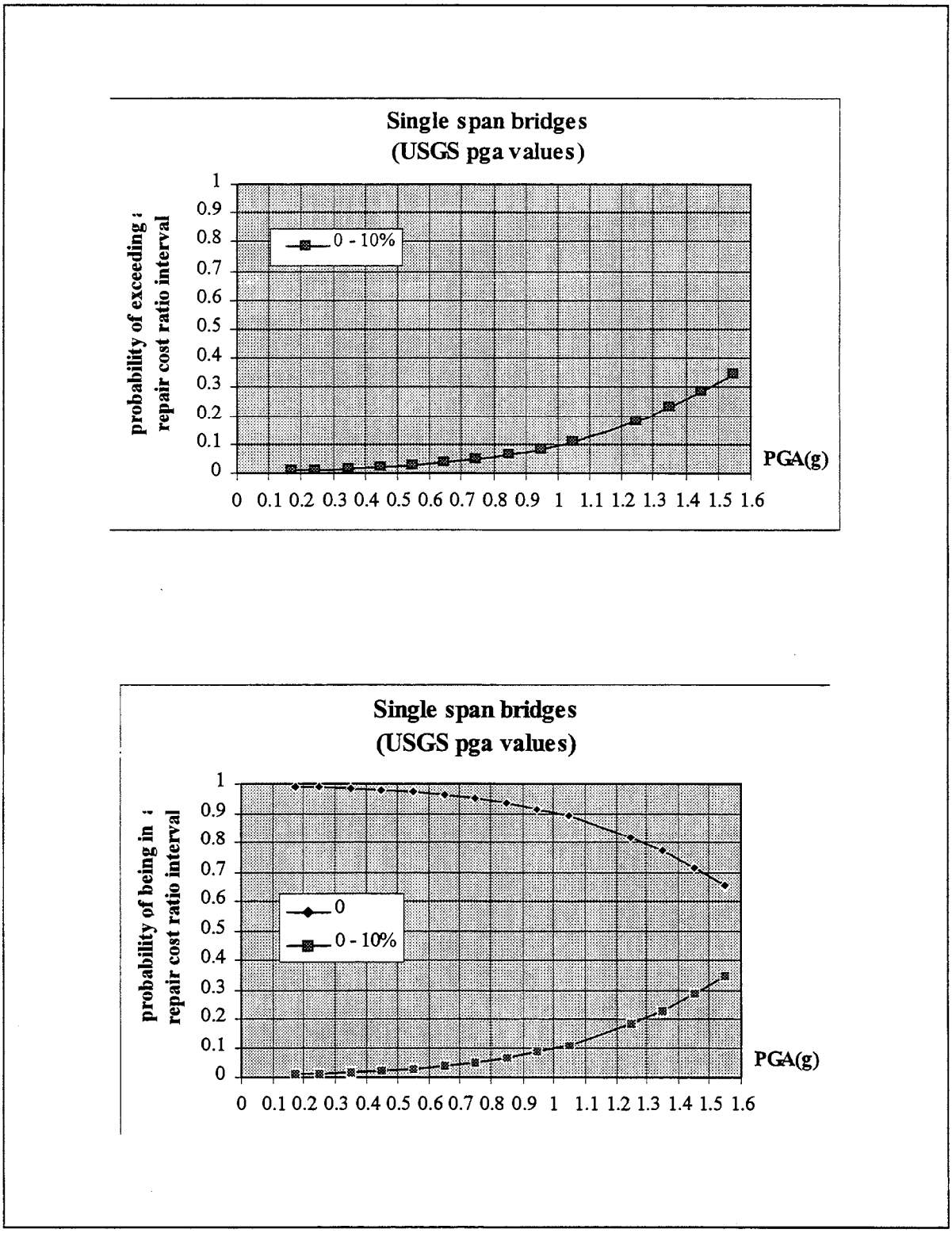

FIGURE 7. Empirical Fragility Curve for Single Span Bridges, Unconditional on Repair Cost Ratio

DISCUSSION OF THE RESULTS AND CONCLUSIONS

The Northridge earthquake provided valuable information to evaluate bridge damage and its impact on the performance of the highway system. Only about two percent of the bridges that were exposed to ground shaking experienced damage and only 6 of these bridges collapsed. Most of the damaged bridges were designed with pre-1971 design standards. Bridges with non-monolithic abutment types, in-span hinges and single column bents performed poorly as observed in previous earthquakes.

Currently available bridge classes and the corresponding ground motion-damage relationships are rudimentary and do not properly estimate the observed damage from the Northridge earthquake. The method used in this research utilizes the observed damage data to develop empirical fragility curves which can and should be improved as more data become available. PGA levels, skew, span continuity, abutment type, and number of spans were found to correlate well with the observed damage. These are the characteristics used in the classification by Basöz and Kiremidjian [1996] and suggests that data shows good agreement with the structural characteristics used in that bridge classification.

Empirical fragility curves are only developed for concrete bridges since the available data for steel bridges were not sufficient. These fragility curves are obtained for concrete bridges grouped by various structural characteristics. Due to scarcity of data for some groups of bridges, the empirical fragility curves could not be obtained. The fragility curves developed in this research should be modified as more data become available.

Damage states for components of concrete bridges are defined. The damage state definitions proposed in this research can be used to: (*i*) develop analytical fragility curves, (*ii*) to assess the vulnerability of bridges, and (*iii*) to develop a post-earthquake investigation form that will assist to compile bridge damage more consistently than the current practice.

Repair cost ratio-ground motion relationships are developed for bridges grouped by various structural characteristics. The observed repair cost ratio for single span bridges was not more than 10 percent while for multiple span bridges repair cost ratios as high as 50 percent were observed. The empirical repair cost-damage relationships and the repair cost ratio-ground motion relationships can be used to estimate the direct loss due to damage to bridges in earthquakes.

A comprehensive database is compiled for the 1994 Northridge, California earthquake. This database includes information on bridge damage and the structural characteristics that are important for vulnerability assessment of bridges. This type of a database provides an essential base to improve our understanding of bridge damage from past earthquakes. The results from this research can be used to assist in decisions for mitigation, such as prioritization of bridges for seismic retrofitting, and during post-earthquake response and recovery activities.

REFERENCES

ATC-13, [1985]. *Earthquake Damage Evaluation Data for California*, Report ATC-13, Applied Technology Council, Redwood City, California.

Basöz, N. [1996]. *Risk Assessment for Highway Transportation Systems*. Ph.D. Dissertation, Department of Civil Engineering, Stanford University. (July).

Basöz, N., and A. S. Kiremidjian. [1997]. *Evaluation of Bridge Damage Data from Recent California Earthquakes*, to be submitted to NCEER.

Basöz, N., A. S. Kiremidjian, S. A. King, and K. H. Law. [1997]. "Characteristics of Bridge Damage in the 1994 Northridge, CA Earthquake.", submitted to Earthquake Spectra.

Basöz, N., and A. S. Kiremidjian. [1996]. *Prioritization of Bridges for Seismic Retrofitting. Technical Report No. 118.* John A. Blume Earthquake Engineering Center, Civil Engineering Department, Stanford University, Stanford, California.

Buckle, I. G. [1994]. *The Northridge, California Earthquake of January 17, 1994: Performance of Highway Bridges*, Technical Report NCEER-94-0008.

California Department of Transportation, (Caltrans). [1993]. *OSM&I Coding Guide for SMS.* Division of Structures, Office of Structures Maintenance and Investigations, Sacramento, California.

California Department of Transportation, (Caltrans). [1994]. *The Northridge Earthquake*, Caltrans PEQIT Report, Division of Structures, Sacramento, CA.

EERI. [1995]. *Northridge Earthquake of January 17, 1994 Reconnaissance Report*, Earthquake Spectra, Earthquake Engineering Research Institute, Oakland, California.

Risk Management Solutions (RMS). [1995]. *Development of a Standardized Earthquake Loss Estimation Methodology.* Prepared for the National Institute of Building Sciences by Risk Management Solutions, Inc., Menlo Park, California.

Somerville, P., C. Saikia, D. Wald, and R. Graves. [1996]. "Implications of the Northridge Earthquake for Strong Ground Motions from Thrust Faults." *Bulletin of Seismological Society of America.* Vol. 86, No. 1B, (February). S115-S125.

USGS. [1994]. US Geological Survey, *Open-File Report 94-197.* Menlo Park, California.

Woodward-Clyde Federal Services (WCFS). [1995]. *Contoured Ground Motion Parameters for the 1994 Northridge Event.* ASCII files.

Yashinsky, M., P. Hipley, and Q. Nguyen. [1995]. *The Performance of Bridge Seismic Retrofits During the Northridge Earthquake.* Caltrans Office of Earthquake Engineering, Sacramento, California.

EXAMINATION OF PERFORMANCE OF MENSHIN ELEVATED HIGHWAY BRIDGES DURING THE KOBE EARTHQUAKE

Masato Abé, Yozo Fujino, and Junji Yoshida

Department of Civil Engineering, The University of Tokyo,

Hongo 7-3-1, Bunkyo-ku, Tokyo 113, Japan.

ABSTRACT

Performance of a Menshin (base-isolated) bridges during 1995 Kobe earthquake and aftershocks is studied using measured data. Two four span continuous bridges are studied: bridge A which is supported by laminated rubber bearings and bridge B which is supported by lead rubber bearings. The first half of the paper shows that the motion of superstructures can be approximated by a single-degree-of-freedom (SDOF) equivalently linearized system. In the second half of the paper, the identified damping and stiffness values of the bearing is compared with those calculated from original force-displacement relationship by applying equivalent linearization, and are found to be in agreement.
SDOF motion

1. INTRODUCTION

Application of Menshin (base-isolation) design has become very popular after 1995 Kobe earthquake. However, there are very few records to verify the actual performance of base-isolation in bridges in large earthquakes. Matsunohama district in the Bay shore route of the Hanshin Expressway, which locates about 35 km east of epicenter of Kobe earthquake (Figure 1 and 2), had extensive instrumentation of accelerometers, and seismic responses of various positions at the main shock and after shocks are recorded (Naganuma et. al. 1995).

The Matsunohama district has two base-isolated bridges: one is supported by laminated rubber bearings, and the other is supported by lead rubber bearings (LRB). The first bridge is called bridge A, and the second is called bridge B, in the current paper for simplicity. Both bridges A and B are continuous four span girder bridges as shown in the elevations of Figure 3. Bridge A consists of 13 steel I-girders, and Bridge B is made of two steel box girders. The girder of Bridge A is supported by laminated rubber bearings at P-21, P-22, and P-23, and by Teflon sliding bearings at P-20 and P24. In Bridge B, LRB is used at P-29, P-31, and P-32, and pivot roller bearings are used at P-28 and P-33.

Piers P-23 in Bridge A and P-32 in Bridge B are instrumented. Figure 4 shows the locations of accelerometers in each pier. The accelerometers at underground, footing and pier top have three measurement components (horizontal two directions and vertical), and the accelerometer at the girder has one component in longitudinal direction.

The maximum acceleration observed in the main shock and after shocks in January 17th are shown in Tables 1 and 2 for both bridges. All the listed records are in the longitudinal direction of the girder. The peak ground acceleration at the main shock was over 100 gal [cm/s].

The purpose of the paper is to evaluate the performance of base-isolated bridges using these observed records. Stress is placed on the evaluation of the performance of bearing, and the analysis of the relationship between the accelerograms of the pier top and girder. Because only the longitudinal acceleration of girder is available, the longitudinal response is studied. Single-degree-of-freedom structures are employed to approximate the response of the girder. After establishing the structural model, the stiffness and damping of the bearings are evaluated using equivalent linearization technique.

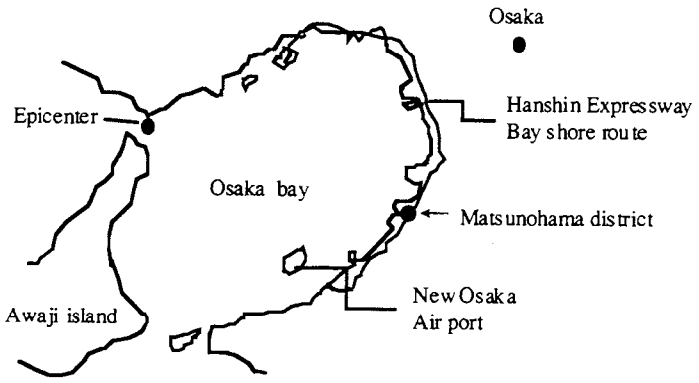

Figure 1. Location of Matsunohama district.

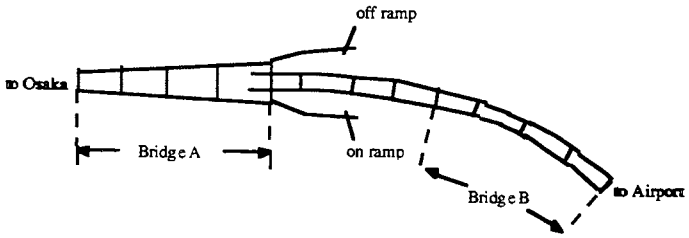

Figure 2. Plan of Matsunohama district.

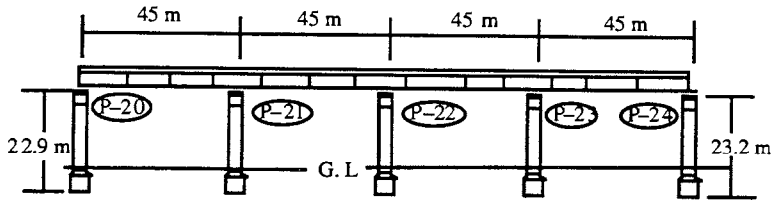

(a) Bridge A

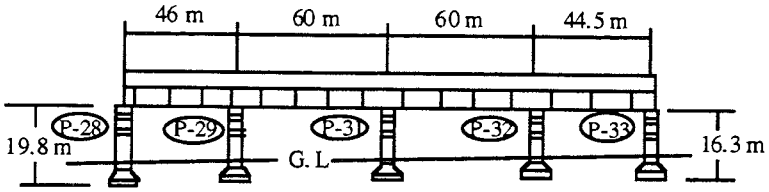

(b) Bridge B

Figure 3. Elevation of the instrumented bridges.

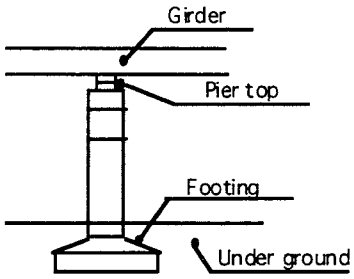

Figure 4. Location of accelerometers.

Table 1. Observed acceleration at Bridge A

	Time	Max. acc. at underground [gal]	Max. acc. at footing [gal]	Max. acc. at pier top [gal]	Max. acc. at girder [gal]
Main shock	5:46:59	149	113	228	217
After shock	5:50:23	17.7	12.3	22.3	19.4
After shock	5:53:21	13.5	9.10	38.9	14.8
After shock	6:42:59	4.96	2.70	8.14	8.86
After shock	7:38:43	19.3	15.0	26.5	28.2

Table 2. Observed acceleration at Bridge B

	Time	Max. acc. at underground [gal]	Max. acc. at footing [gal]	Max. acc. at pier top [gal]	Max. acc. at girder [gal]
Main shock	5:46:59	124	87.8	209	134
After shock	5:50:23	19.0	12.4	15.9	7.49
After shock	5:53:21	15.9	10.8	28.1	5.89
After shock	6:42:59	3.30	2.38	2.95	3.75
After shock	7:38:43	12.6	13.5	16.1	16.9

2. SUPERSTRUCTURE MOTION

The longitudinal motion of the girder is modeled by an SDOF model as shown in Figure 5. Using this model, the motion of superstructure during the main shock is simulated in this section.

The damping ratio and the natural frequency of the model is identified by minimizing the error of root mean square of Fourier spectrum of measured and calculated responses between 1 to 5Hz. In calculating Fourier spectrum, duration of earthquake is defined by the first and the last exceedance of 20% of the magnitude of the maximum acceleration.

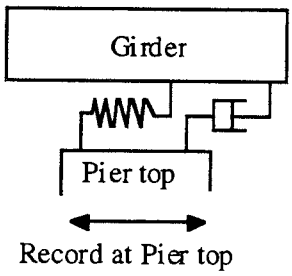

Figure 5. SDOF model for analysis

2.1. BRIDGE A

Figure 6 shows the measured and identified accelerogram of the response of the girder of Bridge A. The measured and computed results show good agreement. The identified natural frequency and damping ratio are 1.26Hz and 14%. Figure 7 shows the corresponding Fourier spectrum. Again, excellent agreement is observed.

The superstructure can be approximated by the SDOF model, which implies that the girder of Bridge A behaved like a rigid body in the longitudinal direction. Hence, the oscillatory dynamics of the girder can be neglected to analyze the seismic performance of base-isolated bridges.

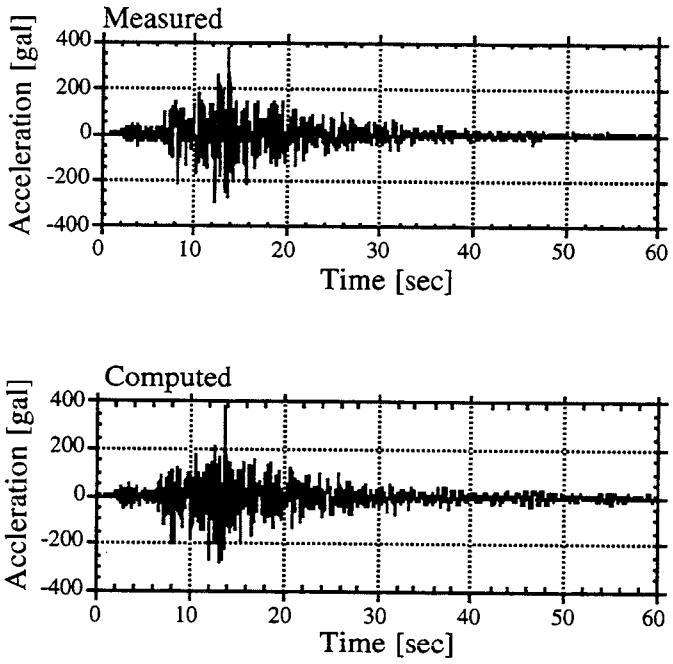

Figure 6. Measured and computed accelerograms for Bridge A

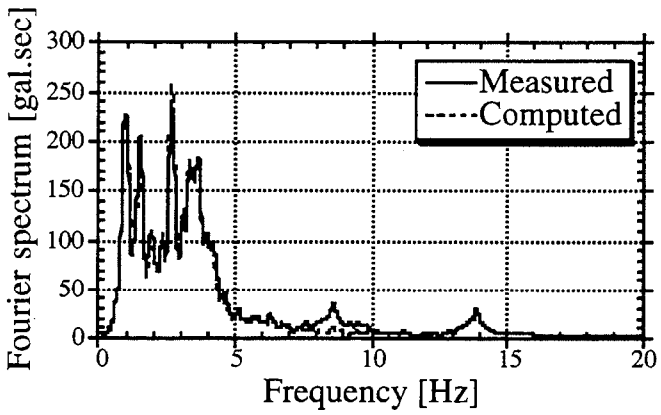

Figure 7. Fourier spectrum of accelerogram of Bridge A

2.2. BRIDGE B

Figure 8 shows the measured and calculated response of the girder. The identified values for natural frequency and the damping ratio are 1.23Hz and 16% respectively. The responses do not agree as well as the case of Bridge B. By looking at the Fourier spectrum in Figure 9, this discrepancy is caused by higher frequency components especially around 15Hz.

One of the possible causes of this high frequency component is that it was induced by pounding of the side block of the bearing and the upper bearing. The side block and the upper bearing has the spacing of 5mm. This possibility can easily rejected, because this frequency component appears even for small after shocks where the displacement of the girder is well below 5mm. The other possibility is the effect of eccentricity of center of gravity and center of rigidity. Because Bridge B is curved with radius of 560m, the rigid body rotational mode of the girder is weakly coupled with the longitudinal mode. The frequency of this coupled mode is calculated and is found to be around 1Hz. Besides, the participation factor of rotational mode subject to transversal excitation is small. Hence, this possibility is also rejected.

The accelerometer is attached at the lateral beam as shown in Figure 10. This lateral beam is much more flexible than the main girder, so the high frequency component may be caused by the local vibration of this lateral beam. To clarify the cause of high frequency component, field testing is conducted by installing a portable accelerometer at the girder. Figure 11 shows the ambient vibration observed at the main girder and the lateral beam where the original accelerometer is attached. It can clearly be seen that the high frequency component is only observed at the lateral beam. Therefore, it is appropriate to filter out this high frequency component when the global response of the superstructure is of interest.

Figure 12 shows the measured acceleration filtered except for the band of 0.5Hz and 10Hz. It agrees well with the previous computed result in Figure 8.

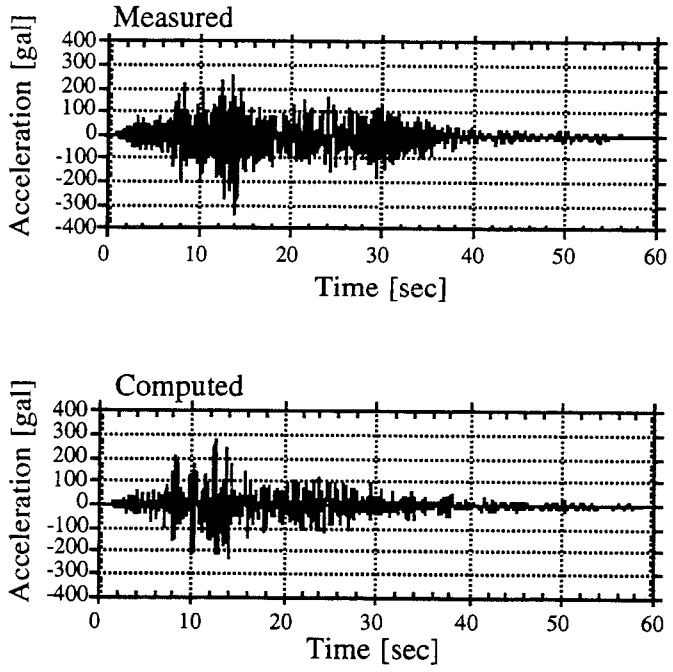

Figure 8. Measured and computed accelerograms for Bridge B

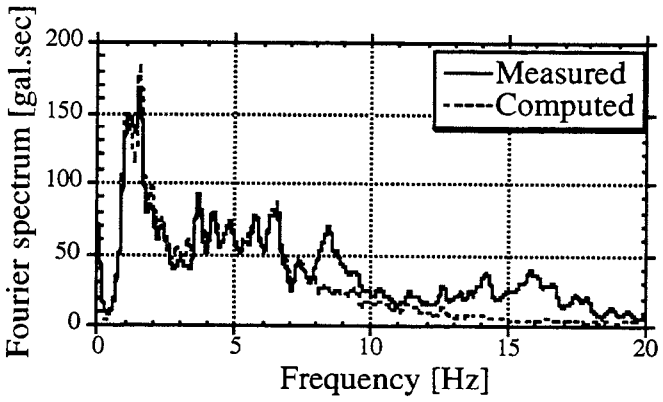

Figure 9. Fourier spectrum of accelerogram of Bridge B

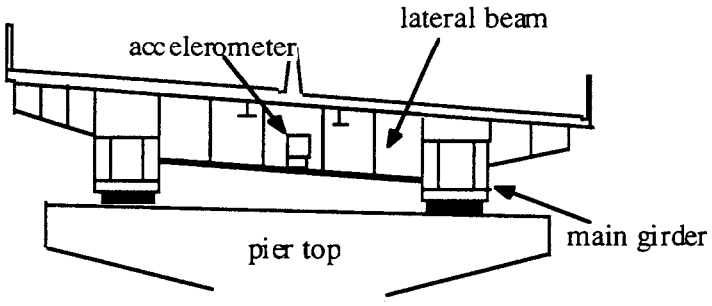

Figure 10. Attachment of accelerometer of Bridge B

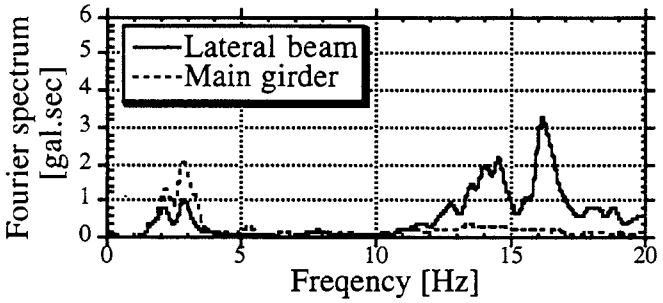

Figure 11. Fourier spectrum of accelerogram at the lateral beam and main girder of Bridge B

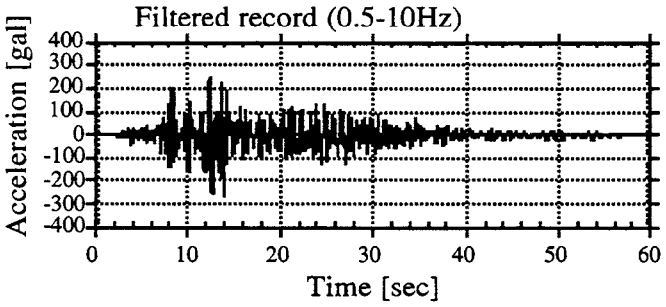

Figure 12. Accelerogram measured accelerogram with band-pass filter (0.5Hz-10Hz)

3. EVALUATION OF DAMPING AND STIFFNESS OF BEARINGS DURING EARTHQUAKES

In the previous section, seismic response of superstructures of Bridge A and B are well described by the SDOF model which assumes rigid body motion of the girder. The stiffness and damping of the SDOF model were identified by the observed accelerograms. In this section, these identified stiffness and damping are compared with the characteristics of bearings whose force-displacement relationship was tested before installation (Hiromatsu, et. al., 1994). To estimate the stiffness and damping from the experimentally obtained force-displacement relationship, equivalent linearization (Skinner, et. al., 1993) using the measured maximum displacement is employed. The displacements are obtained by integrating the accelerograms in frequency domain with band-pass filter from 0.5Hz to 10Hz.

3.1. BRIDGE A

The force-displacement relationship of the laminated rubber bearings in Bridge A is shown in Figure 13. For this bearing, only the monotonic loading test results were available. The estimated stiffness and damping of the rubber bearing obtained by equivalent linearization are shown by solid column in Figure 14. The identified stiffness and damping values are shown by the column with diagonal lines. The horizontal axis of Figure 14 shows the maximum displacement for each event. The most left column corresponds to the response of the main shock, and after shocks are sorted in the order of maximum displacement.

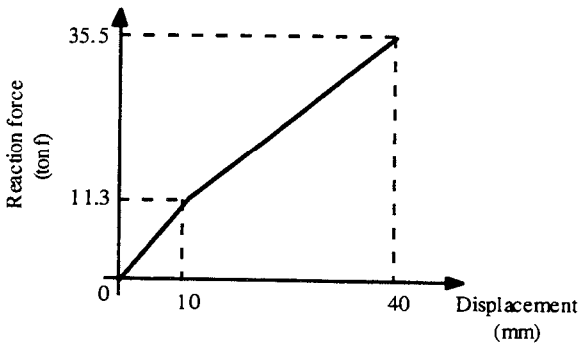

Figure 13. An example force-displacement relationship for laminated rubber bearing.

It can clearly be seen that the identified values are generally larger than that of the values obtained by equivalent linearization, because of the contribution of friction of Teflon sliding bearings at P-20 and P-24. The effect of the friction is shown by the columns with dots. The left column shows the maximum possible effect by friction and the right column show the smallest possible contribution. These variation comes from the velocity dependency of Teflon sliding bearing. The maximum value for friction coefficient is taken between 0.19 and 0.034 according to the response velocity and the minimum value is set to 0.025 following experimental observations and code specifications (Shimoda, 1990, Japan Highway Association, 1991).

The estimated equivalent stiffness and damping with friction generally show good agreement with the identified values, with slight discrepancy for the largest and the smallest events. For the largest main event, the equivalent stiffness and damping give underestimation of identified values, which may be caused by the effect of rubber stuffed at the connection to the adjacent girders. The overestimation at the smallest event may be due to the fact that the Teflon sliding bearing can have extremely low friction coefficient at low velocity and the minimum value of 0.025 used here may have overestimated the real friction.

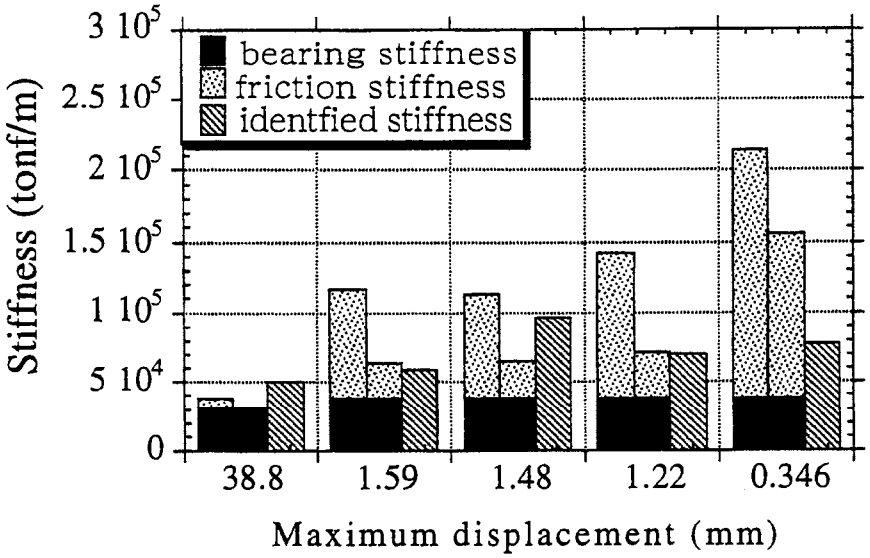

(a) Equivalent stiffness

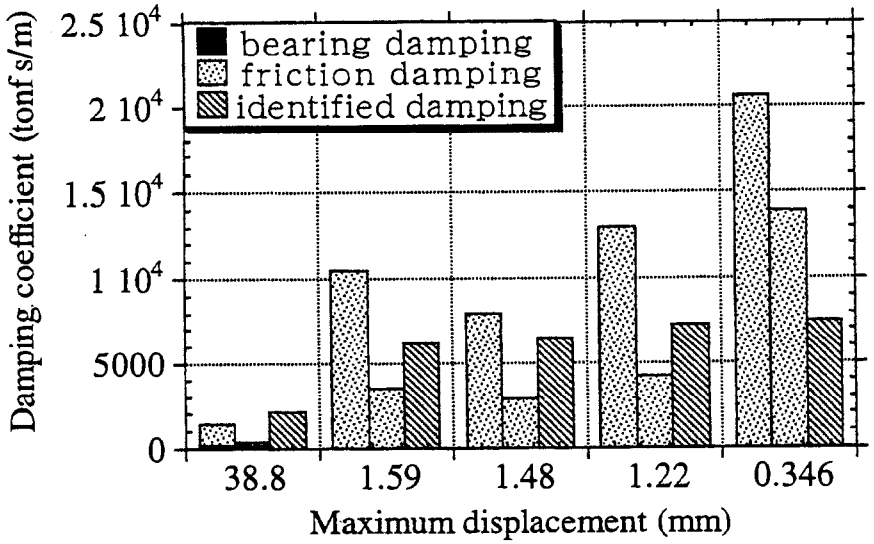

(b) Equivalent damping coefficient

Figure 14. Comparison between estimated and identified stiffness and damping coefficeint of Bridge A

3.2. BRIDGE B

Cyclic loading test results for one of the LRB's are shown in Figure 15. Figure 15a shows the hysteresis loop for relatively large displacement, and it can clearly be seen that the force-displacement relationship is well approximated by bilinear characteristics. However, for smaller displacement, the bearing has much lower stiffness as shown in Figure 15b, because the lead is mostly rigid and the deformation is concentrated to the rubber part for small displacement. The equivalent stiffness and damping are directly calculated from the secant and the area of the loop.

Figure 16 shows the comparison between estimated values by equivalent linearization and identified values. Because both sides of the continuous girder is supported by pivot roller bearings, friction effect is included in addition to the effect of LRB. The maximum friction is estimated to 0.05 and the minimum to 0.001. The estimated and identified values are shown to agree well.

Although the effect of friction is the main cause of the uncertainty for both Bridges A and B, this effect becomes smaller for larger earthquake responses. Hence, the performance of base-isolation is not reduced by the effect of these friction of other types of bearings for medium or larger earthquakes.

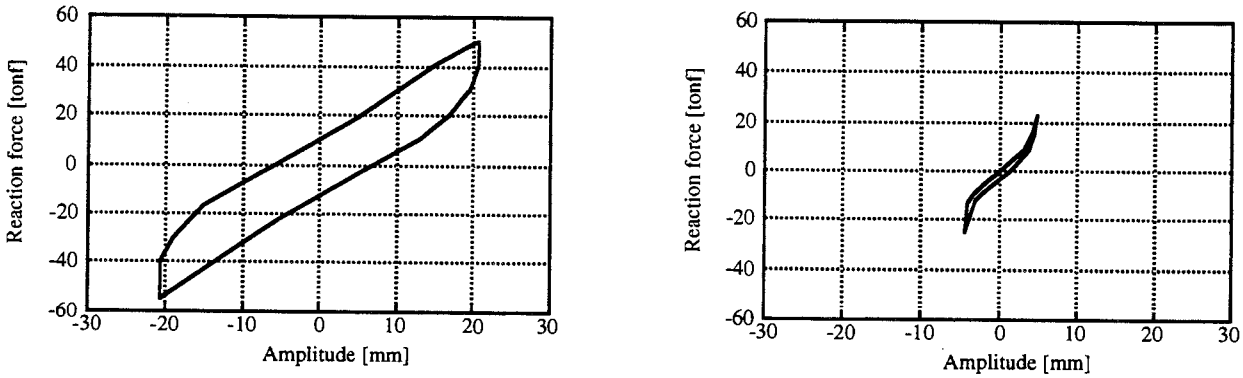

(a) Strain amplitude 16%

(b) Strain amplitude 4%

Figure 15. An example force-displacement relationship for LRB.

4. SUMMARY

Performance of base-isolated bridges with laminated rubber bearings and LRB's in 1995 Kobe earthquake is studied using observed data. The major findings are as follows:

1. Longitudinal motion of superstructure can be approximated by a simple single degree of freedom system for both bridges, which implies that the girder behaves like a rigid body during earthquake.
2. The stiffness and damping of the bearings calculated form experimentally obtained force-displacement relationship by equivalent linearization is compared with the values identified directly from observed data. The stiffness and damping of the bearings are found to be consistent to the original hysteresis. The major discrepancy between the estimated and identified data are caused by the effect of friction at the ends of girder.

In this study, the relationship between the observed data at the pier top and the girder is used to clarify the performance of bearings. Construction of more sophisticated model to recreate the relation between the far-field, footing, and pier top data is currently underway to verify the effect of base isolation to the total structural system, and to study the effect of base-isolation for larger earthquakes where yielding of the piers are possible.

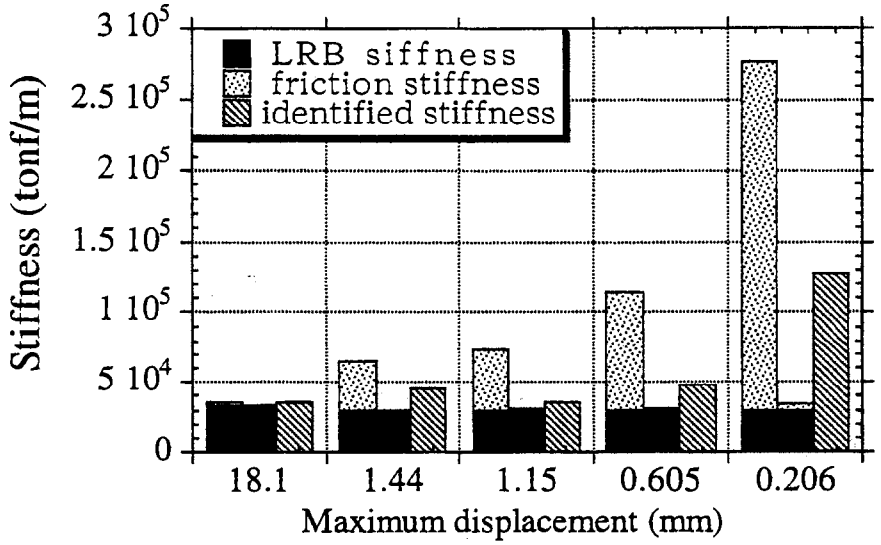

(a) Equivalent stiffness

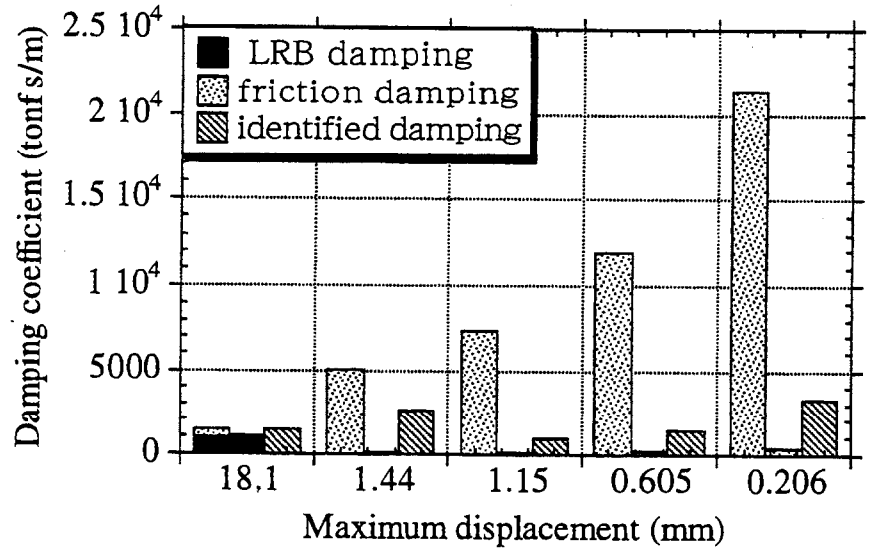

(b) Equivalent damping coefficient

Figure 16. Comparison between estimated and identified stiffness and damping coefficeint of Bridge B

ACKNOWLEDGMENT

The authors wish to express their gratitude to the Hanshin Expressway Authority for providing the measured data and the technical support in the field measurement.

REFERENCES

Horimatsu, M., Sasaki, N., Komatsu, I., and Nakaya, S., 1994, "Vibration experiments and dynamic response analysis using the actual highway bridge with base isolators," *Journal of Bridge and Foundation*, April issue, pp.24-32 (in Japanese).

Japan Highway Association, 1991, *Reference Manual of Bearings for Highway Bridges* (in Japanese).

Naganuma, T., Horie, Y., Kobayashi, H., and Sasaki, N., 1996, "The analysis of seismic response of the bridge with Menshin bearings during the Hyogo-ken Nanbu earthquake," *Fourth U.S.-Japan Workshop on Earthquake Protective Systems for Bridges*, Osaka, Japan.

Shimoda, I., 1990, "Component test of bearing material for use in friction pendulum seismic isolators," *Engineering Mechanics Conference, Japan Society of Mechanical Engineers* (in Japanese).

Skinner, R. I., Robinson, W. H., and McVerry, G. H., 1993, *An Introduction to Seismic Isolation*, John Wiley & Sons.

LIQUEFACTION-INDUCED DAMAGE TO BRIDGES

T. Leslie Youd
Department of Civil Engineering
Brigham Young University
Provo, Utah

ABSTRACT

Liquefaction-induced lateral spread is a major cause of earthquake damage to bridges built across streams and rivers. Lateral spreads are characterized by horizontally displaced ground with extensional deformations at the head of the feature, shear deformations along the margins, and compressed ground at the toe. Displacements generally range from a few centimeters to several meters and are directed down mild slopes or toward a free-face, such as an incised river channel. Such displacements thrust bridge abutments and piers riverward, generating large shear forces in connections and compressional forces in the superstructure. These forces have sheared connections, allowing decks to be thrust into, through, or over abutment walls, or causing decks to buckle. In other instances, connections have remained intact with the deck acting as a strut, holding tops of piers and abutments in place while the bases of these elements are displaced toward the river. These actions have inflicted severe damage and even bridge collapse. This paper reviews the performance of bridges during past earthquakes to illustrate types of damage as a consequence of liquefaction-induced ground displacement.

INTRODUCTION

The following text is reproduced from a paper entitled Liquefaction-Induced Damage to Bridges published by the author in Transportation Research Record 1411 (10). Liquefaction-induced ground failure is a major causes of earthquake damage to bridges. Bridges spanning rivers are particularly vulnerable to liquefaction because such structures commonly are founded on floodplain alluvium in areas with high a ground water levels. These conditions--recent deposition and high ground water--are characteristics of sediments with high liquefaction susceptibility. Floodplain topography--including gentle slopes and incised river channels--are characteristic of areas susceptible to liquefaction-induced lateral spread.

Lateral spreads (Figure 1) are characterized ground displacement down mild slopes or toward a free face, such as an incised channel. Lateral displacements may range from a few centimeters to several meters and are generated by a combination of gravitational and seismic forces. Bridge piers and abutments founded on a lateral spread are usually transported riverward with the spreading ground. Consequent differential displacements between foundation elements create severe stresses and/or deformations within the bridge structure. To illustrate and categorize the types of damage inflicted by lateral spreads, several case histories of bridge damage are reviewed herein.

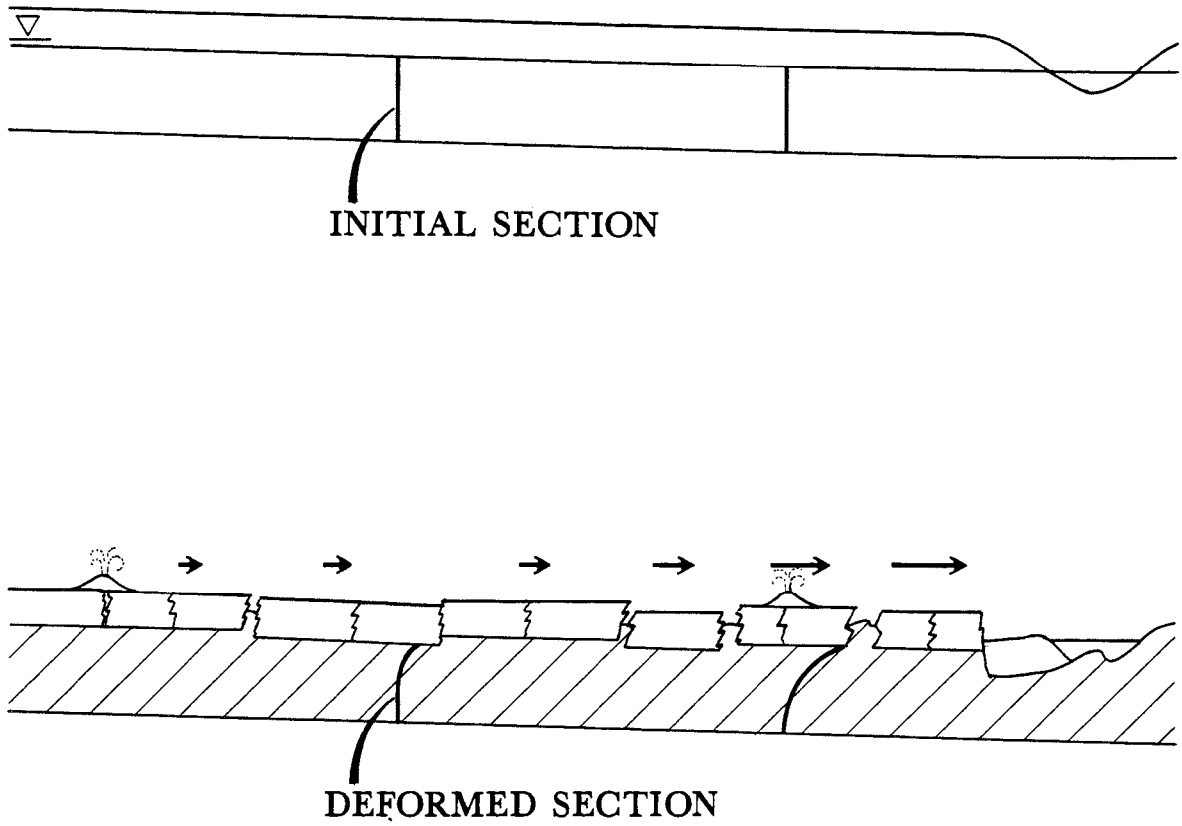

Figure 1. Diagram of a lateral spread showing liquefied layer, ground displacement, and disrupted ground surface. (After National Research Council (7)).

BRIDGE DAMAGE DURING PAST EARTHQUAKES

1868 Hayward, California Earthquake

One of the first instances of bridge damage caused by liquefaction-induced lateral spread in the U.S. apparently occurred during the 1868 Hayward, California earthquake. Halley (3) noted the following: "The drawbridge on the line of the S.F. and O.R.R. was thrown out of place about eight inches [0.2 m], and as the locomotive and nearly all the cars were at San Antonio, no train left Oakland at 8 o'clock." This description is not very clear, but the type of damage, compression of the bridge structure, is typical of damage inflicted by lateral spread.

1886 Charleston, South Carolina Earthquake

The evidence is more explicit that liquefaction-induced lateral displacement damaged several bridges during the 1886 Charleston, South Carolina earthquake. For example, Earle Sloan (as quoted by Peters and Hermann (8)) penned the following cryptic notes concerning the Bacous bridge over the Ashley River: "[The damage] affords evidence of tendency of banks to approach center of channel. Here expressed by compression of bridge causing one plank to

overlap another seven inches [0.18 m] and jamming joints." The same investigator gave the following description of the railroad bridge over Rantowles Creek:

> Close inspection revealed fact that there had been a vibratory movement of sufficient energy to have caused entire [word missing] plastic earth with included piling on each side of "draw" to bodily approach channel of stream; the piling which affords no indication of relative movement from enclosing earth has dragged attached bents from vertical position and jerked superstructure from opposite sides to center line with a violence wrecking rails, bulging up stringers, forcing up caps of bents, mortised and spiled with 4 inch tenons, to top of latter, and in general affording liberal indications of shortening of distance separating the banks. Superstructure on both sides of "draw" was violent flexured both transversely and vertically with accumulated length of rail. Latter accumulation accounted for by near summit of involved grade where joints are liberally parted.

These descriptions document lateral movements and the damage they caused. Ground displacements as great as several tenths of a meter shifted abutments and piers toward the centers of the channels, compressing bridge decks with attendant bulging up of stringers and overlapping of planks. Documented ground disturbances--including ground fissures and sand boils--confirm that liquefaction was widespread near these bridges.

1906 San Francisco, California Earthquake

Lateral spreads generated by the 1906 San Francisco earthquake damaged several bridges, including the highway bridge over the Salinas River south of Salinas, California (Figure 2). Lateral displacement of the floodplain physically displaced both ground and pile foundation about 1.8 m northward toward the river channel. The bridge trusses and deck were strong enough to remain intact and were essentially undamaged. The deck, which remained attached to the tops of the piers, acted as a strut, holding the tops of the piers in place while their bases shifted riverward. This motion left the southern pier inclined, with the top of the pier tilted outward, away from the river.

1964 Prince William Sound, Alaska Earthquake

The most devastating earthquake damage to bridges in U.S. history occurred during the great Alaskan earthquake of 1964. Liquefaction and lateral spread damaged 266 railway and highway bridges, collapsing about 20 and damaging many others beyond repair. This destruction severely impaired the surface transportation system in southern Alaska for many months after the earthquake.

In nearly all instances, the Alaskan bridges were compressed as a consequence of lateral ground displacement. Those displacements inflicted different types of damage, depending on the amount of ground displacement, the strengths of various structural elements, and the orientation of the bridge relative to the river. The general types of damage are shown by the following illustrations.

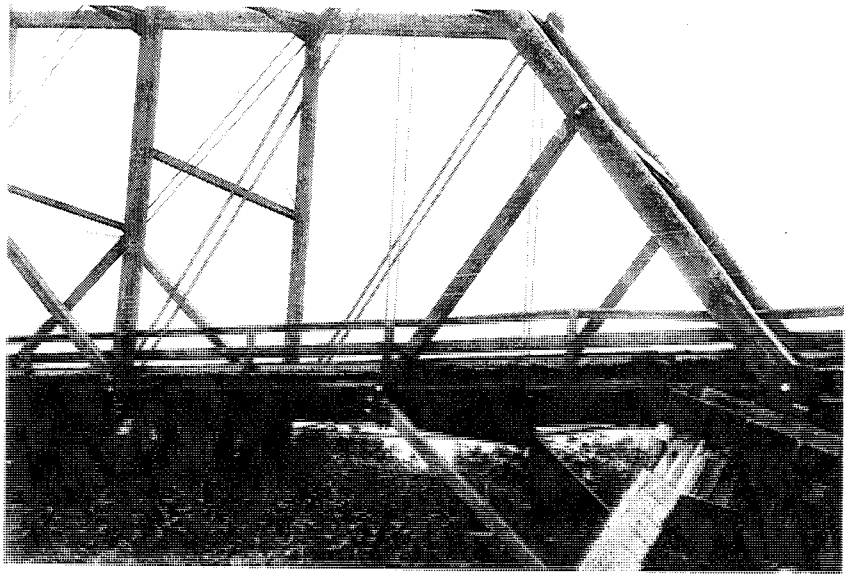

Figure 2. Highway bridge over Salinas River south of Salinas California that was damaged by lateral ground displacement during the 1906 San Francisco earthquake. The ground displacement physically moved the base of the southern pier 2.8 m toward the river (photograph by J.C. Branner, courtesy of Stanford University Archives).

Railway Bridges. According to McCulloch and Bonilla (6), 125 railway bridges and 110 culverts were damaged or destroyed during the 1964 Alaska earthquake. None of those bridges collapsed, although many were irreparable and had to be replaced. The estimated cost to repair and replace these structures was about $2.5 million (1964 value). For comparison, the cost to regrade, repair, and realign railway embankments, which were also severely impacted by ground failure and ground subsidence, was nearly $9 million. McCulloch and Bonilla recorded the following general description of ground displacements and consequent damage to railway bridges, most of which were timber structures:

> In all but six bridges, the net compression shown by interbent measurements exceeded the net extension. Net compression was generally 20 inches [0.50 m] or less, regardless of bridge length, but in two bridges compression was as large as 64 and 81.5 inches [1.62 and 2.07 m].
>
> In addition to having their supporting bents torn free, most stringers were put into compression by converging streambanks. Distances between streambanks were decreased by as much as 6.5 feet [2.0 m]. As a result, the stringers acted as struts, and either jammed into the fillers on the bulkheads or, where compression was greater, drove through the bulkhead planks. In some bridges most of the compression was released at one end, and the stringers were thrust up over the top of the bulkhead onto one of the approach fills.

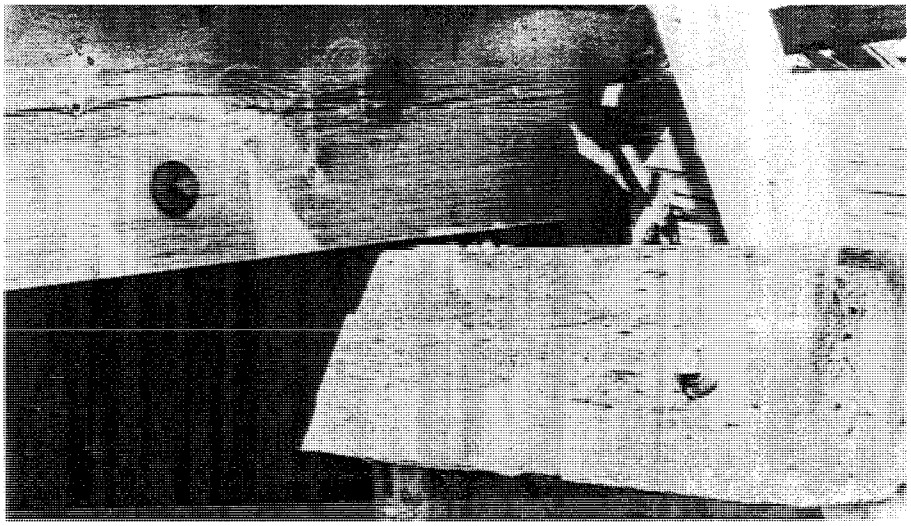

Figure 3. Stringers of bridge 61.9 that were driven though the bulkhead wall by convergence of the stream banks during the 1964 Alaska earthquake (after McCulloch and Bonilla (6)).

Figure 4. Highway bridge over Resurrection River that was compressed by lateral spreading during the 1964 Alaska earthquake. The compression thrust the deck into and fractured the abutment wall while ground displacement carried the adjacent pier streamward, fracturing that element at the ground line (after McCulloch and Bonilla (6)).

Compressive forces not released by failures at the bulkheads produced lateral deflections in the decks of several bridges. Stringers were either thrown into long horizonal bends, or were broken at sharp kinks, with as much as 8 feet [2.4 m] of lateral deflection at the apex of the bends.

Figure 5. Stream bank convergence of about 0.18 m buckled the deck of the Alaska railway bridge at milepost 63.0 (after McCulloch and Bonilla (6)).

The following examples of damaged railway bridges illustrate these effects. The damage to the bridge at milepost 61.9 is representative of stringers thrust through bulkhead walls (Figure3). This bridge consisted of seven 4.5-m long spans supported on interior timber pile bents with timber bulkheads at either end. About 0.5 m of streambank convergence compressed the bridge structure, tearing stringers from their seatings and thrusting the loosened stringers through the bulkhead walls.

A similar type of failure occurred to a highway bridge over one of the channels of the Resurrection River near Seward. The banks of the river spread into the channel, causing more than 0.3 m of convergence between bridge abutments (Figure 4). The narrowing of the channel thrust the bridge girders and deck into the abutment wall, which fractured and rotated under the impact, allowing the deck to penetrate about 0.3 m into the adjacent fill. The ground displacement carried the adjacent bridge pier about 0.3 m toward the channel, with the top of the pier remaining attached to the deck. As shown in the figure, this displacement fractured the pier at the ground line and tilted the upper part of the pier outward, away from the river.

The bridge at milepost 37.3 is representative of a structure that fractured and buckled due to compressional forces applied by the converging stream banks (Figure 5). This bridge was composed of five 4.5-m long spans. The stream banks converged about 0.18 m, causing the deck to buckle horizontally by about 1.2 m (6). A few similarly stressed bridge decks buckled upward rather than laterally.

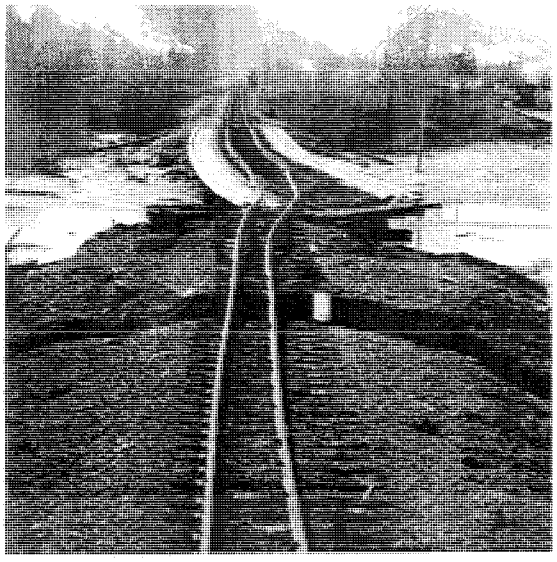

Figure 6. The Alaska railroad bridge at milepost 63.0 was compressed by lateral ground displacement, causing near end of the bridge to shear connections with the bulkhead and skew to the right (After McCulloch and Bonilla, (6)).

Bridges that crossed streams at oblique angles commonly skewed, rather than buckled, under ground-induced compressional forces. For example, the railway bridge at milepost 63.0 (Figure 6) skewed horizontally as a consequence of about 2.8 m of stream bank convergence. The bridge was a 58.4-m long structure supported by 14 pile bents. The convergence of the stream banks shifted the pile bents streamward on both sides of the channel. Because the direction of ground displacement was at an angle to the longitudinal axis of the bridge, the compressional generated horizontal forces between the deck and the southern bulkhead. These forces fractured the stringer connections at the bulkhead, and deflected deck 2.4 m eastward (to the right in Figure 6). The deck rotated and bowed horizontally as a unit, breaking connections between some pile caps and stringers and dragging others laterally with the displaced deck.

In their field investigations, McCulloch and Bonilla (6) found no instances where piles had sunk to greater depths than their pre-earthquake positions. Conversely, in several instances, the piles had risen. McCulloch and Bonilla attribute that rise to lateral spread of the ground toward river channels, which compressed sediments within the channels, causing channel beds to heave upward and lift the piles with the rising soil. Buoyancy of the piles and upward pull by arching superstructures also may have contributed to the upward movement.

Highway Bridges. Highway bridges were affected even more severely than railway bridges during the 1964 earthquake. Kachadoorian (5) classified more than twenty highway bridges as destroyed, by which he generally meant that foundations had failed and decks had collapsed. Nearly all of this destruction was caused by lateral displacement of piers and abutments. These displacements broke connections with the superstructure, leaving decks unsupported. One collapsed bridge--the structure over Twentymile River--is shown in Figure 7.

Figure 7. Collapsed highway bridge across Twentymile River (bridge nearest camera); damaged but intact railway bridge behind highway structure (after McCulloch and Bonilla (6)).

This and other severely damaged bridges were at localities of intense liquefaction effects--including ground oscillation and lateral spread--as described by Kachadoorian (5):

> The seismic shaking and lateral displacement of the sediments pulled the wood ties off the caps, and the superstructure became independent of the substructure. The deck or superstructure had a vertical as well as a horizontal component of movement during the earthquake. Eventually the wood bents failed beneath the superstructure and the bridge collapsed. In many bridges the wood piles were driven through the reinforced concrete deck [Figure 7]. Eye witness reports show that the decks had an up-and-down motion period of about 1 second. That is, a wave apparently passed through the deck, and, as it passed through, the superstructure moved up and down in about a 1-second cycle.

Kachadoorian then indicates that the up and down motions caused impacts between the piles and bridge decks (after the pile caps had failed) that drove the piles through the deck.

This description of bridge failure indicates that seismic shaking liquefied the underlying soils, which in turn spread laterally toward the river channel. That ground movement pushed the pile bents riverward, shearing connections with the superstructure. The ground apparently did not move in a single uniform motion, but oscillated back and forth and up-and down in waves as it migrated toward the river. This oscillatory movement caused the bridge deck to vibrate vertically--and apparently out of phase with the underlying ground--generating intense impacts between the deck and the detached piles, with the piles eventually punching through the paved surface as the deck fell to the ground.

In addition to bridges classified as "destroyed," Kachadoorian classified more than seventy bridges as severely damaged. Such a rating generally meant that abutments and pile bents shifted horizontally, breaking connections with superstructure. This action was accompanied by ramming of decks into abutment walls, severely damaging either stringers or trusses, or the abutment, as illustrated in Figure 3. However, none of the severely damaged bridges collapsed.

With respect to post-earthquake pile elevations, Kachadoorian (5) noted that after the earthquake, most of the piles beneath destroyed or severely damaged highway bridges were lower, but by no more than about 0.1 m. The reason for this penetration of piles is not given, but it may have been caused from pounding by the deck. This small amount of settlement indicates that major loss of pile-bearing resistance did not occur.

In total, Kachadoorian (5) classed 92 highway bridges (45 percent of those in the heavily shaken area) as destroyed or severely damaged. An additional 49 bridges (24 percent of the total) were classed as slightly to moderately damaged. The estimated cost to repair or replace these structures was more than $25 million (1964 value). The tenfold greater monetary damage to highway bridges compared to railway bridges indicates the greater destruction to the highway structures.

1964 Niigata, Japan Earthquake

Three months after the 1964 Alaskan earthquake, a large earthquake struck the west coast of Japan near the city of Niigata. That earthquake generated some of the most widespread and spectacular effects of liquefaction of any modern earthquake. The combined effects of the 1964 Alaska and 1964 Niigata earthquakes forcefully drew the world's attention to the destructive capability of liquefaction; rigorous studies of the liquefaction phenomenon were initiated immediately thereafter.

Liquefaction-induced lateral spread during the Niigata earthquake caused bank convergence of as much as 23 m across the 250-m wide Shinano River (4). Those displacements severely damaged one railway and three highway bridges. For example, several deck segments of the Showa highway bridge collapsed into the river, as a consequence of ground displacement (Figure 8). Hamada and others (4) give the following description of that collapse:

> There were obvious signs that a violent collision had occurred between the girders themselves and the abutment on the left bank. From the above, it can be conjectured that a large horizontal force had been exerted on the girder from the abutment on the left bank, and this is considered to have been one of the causes of the collapse. There were also signs that the bridge pier foundations on the left bank had moved toward the center of the river. In particular, pier P_6 had tilted considerably toward the right bank. It may be considered that such movement of the bridge pier foundations also contributed to the collapse.

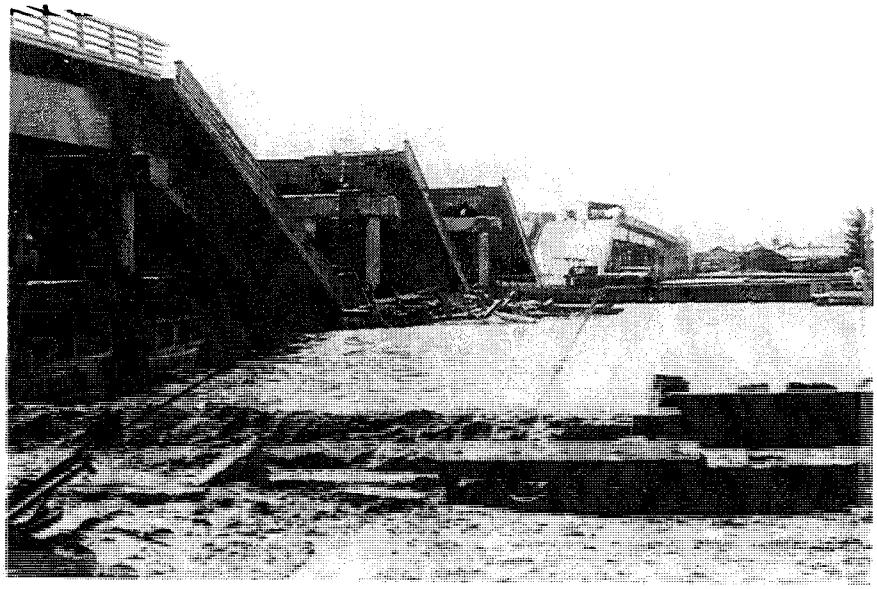

Figure 8. Showa highway bridge that collapsed into the Shinano River during the 1964 Niigata, Japan earthquake (from T.L. Youd photo collection).

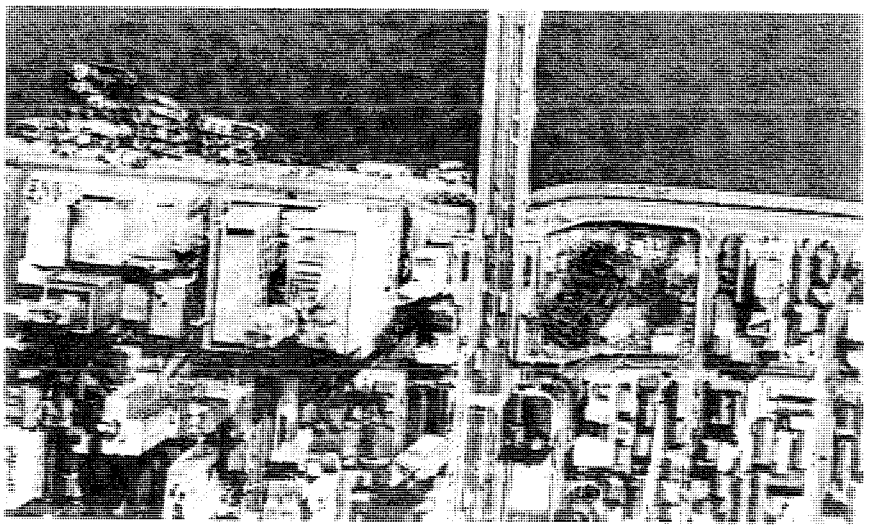

Figure 9. Aerial view of Bandai Bridge showing curved revetments along water-bank interface. The curvature was caused by lateral ground displacements during the 1964 Niigata earthquake (After Hamada et al. (4))

The steel-pipe piles supporting another pier, P_4 (located within the river), were extracted and examined after the earthquake. The deformed shapes of those piles indicate that about 0.5 m of lateral displacement had occurred at the level of the river bed, and that ground displacement reached depths as great as 7 to 8 m below the bed.

As noted by Hamada and others, horizontal displacement of the piers supporting the Showa bridge was much less than displacement of the ground a short distance either upstream or downstream from the bridge. This reduced displacement indicates that the bridge restrained ground deformation. Other bridges across the Shinano River impeded lateral ground movements as well. In the latter instances, the decks remained attached to the piers and acted as struts or braces, increasing resistance to ground displacement. For example, the post-earthquake aerial photograph reproduced as Figure 9 shows reconstructed river revetments above and below the Bandai Bridge. Those revetments formed a straight line before the earthquake. The revetments were pushed toward the river during the earthquake and then reconstructed in their post earthquake position. The reduced ground displacement near the bridge is graphically illustrated by the landward curvature of the reconstructed revetments. Further evidence that the bridges restricted bank displacements is given by Hamada and others (4) who calculated vectors of ground displacement from photogrammetric analyses of pre- and post-earthquake aerial photographs. Those vectors indicate that river bank displacements were about 8 to 9 m upstream from the Bandai Bridge, but only about 4 to 5 m near the bridge. Thus the bridge apparently restrained lateral ground movements by about 4 m.

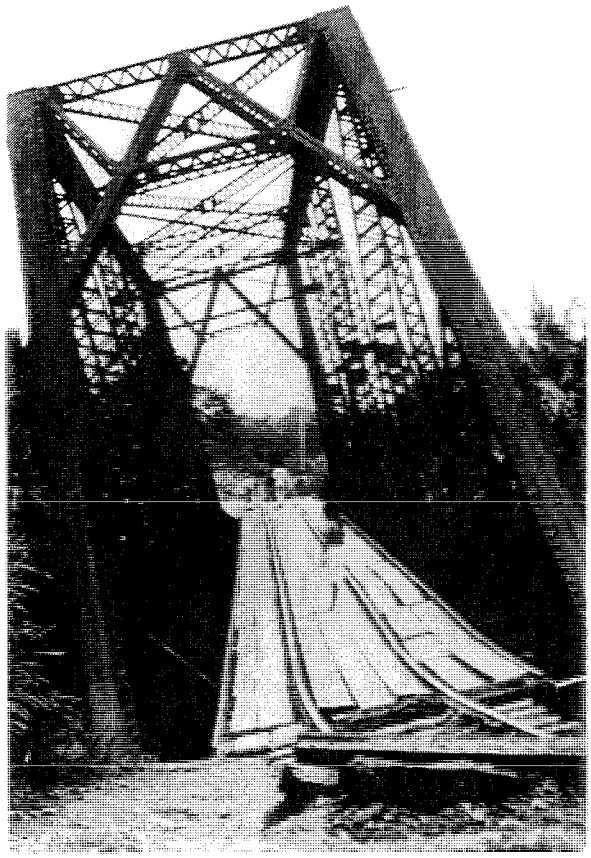

Figure 10. Railway bridge over the Rio Bananito that tipped during the 1991 Costa Rican earthquake; lateral ground displacement pushed the supporting caissons from the bridge seatings leaving the truss unsupported (photograph courtesy of Laboratorio de Ingeniria Seismica de la Universidad de Costa Rica).

1991 Limon Province, Costa Rica Earthquake

Du ring the 22 April 1991 Limon Province, Costa Rica earthquake, eight major highway and railway bridges collapsed, and several other bridges were severely damaged. All of these bridges were at river crossings and in nearly all instances, liquefaction-induced ground displacement was the cause of damage.

The modes of bridge damage in Costa Rica were generally similar to those described above; that is, lateral displacement of floodplain deposits pushed abutments and piers riverward, shearing connections and causing other damage. In several instances, connections between the foundation and the deck readily sheared, preventing the deck from acting as a strut or brace. The connection failures allowed the abutments and piers to readily shift or tilt toward the river channel, removing support from the superstructure. An example of this type of failure is illustrated by the tipped railroad bridge over the Rio Bananito near Bananito Sur (Figure 10). The steel-truss single span bridge was supported by four 1.5 m by 2.1 m oval-shaped concrete caissons, one placed under each corner of the truss. Liquefaction and lateral spread on both sides of the river pushed the tops of the caissons inward removing support from the truss which dropped and tilted. Displacements of the tops of the caissons ranged from 1.9 to 5.7 m (9).

Youd and others (9) surveyed the bridge site after the earthquake and compared measured distances with those noted on the bridge plans (Table 1). Differences between the pre- and post-earthquake distances were small and fall within the range of survey and construction error. These comparisons indicate that the abutments and piers withstood earthquake shaking and the development of liquefaction, without significant permanent displacement. In particular, the

Figure 11. Caissons beneath the Rio Bananito railway bridge that were pushed riverward by lateral ground displacement during the 1991 Costa Rica earthquake (photograph by T.L. Youd).

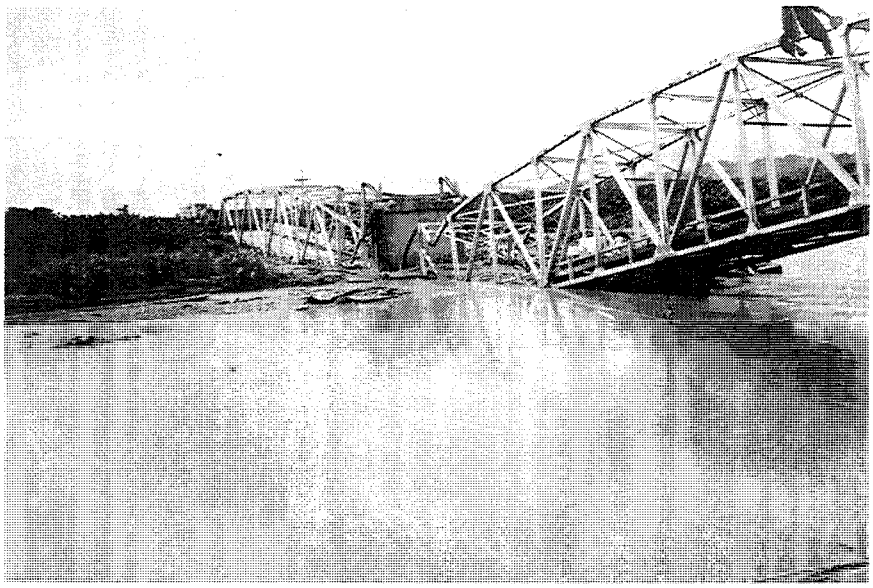

Figure 12. Highway bridge that collapsed into the Rio Estrella during the 1991 Costa Rica earthquake (photograph by T.L. Youd).

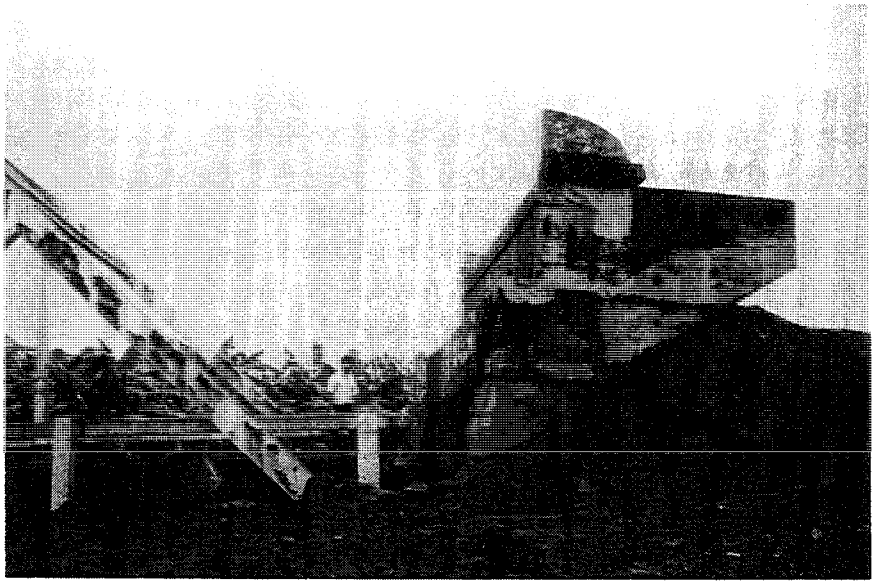

Figure 13. Liquefaction-induced settlement and deformation of approach fill adjacent to southern abutment of Rio Estrella highway bridge (photograph by T.L. Youd).

TABLE 1.--COMPARISON OF PLAN AND MEASURED POST-EARTHQUAKE DISTANCES BETWEEN BRIDGE ELEMENTS FOR THE HIGHWAY BRIDGE OVER RIO ESTRELLA (2)

Distance Between Centers Of Bridge Seats From:	Plan (m)	Post-Earthquake (m)
North Abutment to Pier 1	25.00	24.96
Pier 1 to Pier 2	75.00	75.02
Pier 2 toSouth Abutment	75.00	75.24
North to South Abutments	176.32	176.14

foundation beneath the southern abutment remained in place, even though liquefaction and substantial ground disruption occurred in the immediate vicinity (Figure 13). This abutment consisted of a concrete wall supported on two substantial groups of piles, which extend to depths of about 14 m below river level (2).

PREDICTION OF GROUND DISPLACEMENT AND BRIDGE DAMAGE

Two pieces of information required to assess bridge safety against ground failure: an estimate of ground displacement and an assessment of bridge capability to withstand that displacement. Some progress has been made over the past few years in developing techniques for evaluating ground displacement. Case histories have been compiled from which the primary factors controlling displacement have been identified and regression analyses have produced predictive models (1). Several investigators have also applied analytical techniques to estimate ground movements, but more development and verification of those techniques are required. The second component, assessment of the capability of bridges to resist ground displacement, is practically unstudied. Likewise, the effectiveness of remedial measures that might be used to strengthen bridges or to stabilize the ground to resist displacement has not been widely researched. It is beyond the scope of this paper to further discuss these topics, except to note that much more research attention is required to develop engineering guidelines for design or retrofit of bridges to withstand liquefaction-induced ground displacements.

CONCLUSIONS

1. Lateral spread has been the primary cause of liquefaction-induced damage to bridges. Lateral ground displacements have pushed abutments and piers riverward, creating large shear forces at connections and compressio+nal forces within the superstructure.

2. Compressional forces generated by lateral ground displacement generally cause one of the following reactions:

a. The superstructure may act as a strut, bracing tops of abutments and piers and holding them relatively in place, while the bases of these elements shift streamward with the spreading ground. this action leaves piers and abutments tilted outward away from the river.

b. The connections between the foundation and the superstructure may fail, allowing piers and abutments to shift or tilt toward the river with little restraint. In this instance, the deck may impact the backwall of the abutment, which may either fracture the wall allowing the deck to penetrate into the embankment, or deflect the deck upward and over the abutment and embankment.

c. The deck may buckle laterally or vertically, causing severe damage to the superstructure.

3. Only limited study has been made of bridge damage caused by ground displacement or of mitigative measures to prevent such damage. More research is needed on this topic.

REFERENCES CITED

1. S.F. Bartlett and T.L. Youd (1992). Empirical Prediction of Lateral Spread Displacement. National Center for Earthquake Engineering Research, Technical Report NCEER-92-0021, 1992.
2. Earthquake Engineering Research Institute (1991). Costa Rica Earthquake Reconnaissance Report. *Earthquake Spectra*, Vol. 7, Supplement B.
3. W. Halley (1876). The Centennial Year Book of Alameda County, California. Oakland, 1876.
4. M. Hamada, S. Yasuda, R. Isoyama, and K. Emoto (1986). Study on Liquefaction Induced Permanent Ground Displacements. Association for the Development of Earthquake Prediction, Tokyo, Japan.
5. R. Kachadoorian (1968). Effects of the Earthquake of March 27, 1964, on the Alaska Highway System. U.S. Geological Survey *Professional Paper* 545-C.
6. D.S. McCulloch and M.G. Bonilla (1970). Effects of the Earthquake of March 27, 1964, on the Alaska Railroad. U.S. Geological Survey *Professional Paper* 545-D.
7. National Research Council (1985). Liquefaction of Soils During earthquakes. Washington, D.C., National Academy Press.
8. K.E. Peters and R.B. Hermann (1986). First-Hand Observations of the Charleston Earthquake of August 31, 1886, and Other Earthquake Materials. *Bulletin* 41, South Carolina Geological Survey.
9. T.L. Youd, K.M. Rollins, A.F. Salazar and R.E. Wallace (1992). Bridge Damage Caused by Liquefaction During the 22 April 1991 Costa Rica Earthquake. *Proceedings*, 10th World Conference on Earthquake Engineering, Madrid, Spain, vol. 1, p. 153-158.
10. Youd, T.L. (1993). Liquefaction Induced Damage to Bridges, *Transportation Research Record* No. 1411, p.35-41.

An Analysis of Damage to Hanshin Elevated Expressway during 1995 Hyogoken Nambu Earthquake

Yozo FUJINO, Masato ABE and Satoko ABE
Department of Civil Engineering, University of Tokyo
Bunko-ku, Tokyo 113, Japan

Abstract Damage to Hanshin Expressway 'Kobe Route' (P1 to P718) is decribed with structural characteristics. It is shown that many single piers suffered large residual inclination due to seismic-induced plastic deformation. Damage to the section from P200 to P300 is investigated in detail and it is found that almost all the single RC piers in this section received either severe damage above the ground level or large residual inclination. The observed damage mode of the circular RC piers, i.e. flexure and/or shear, is in good agreement with the mode predicted from the strength analysis. However, the agreement is not so good in the case of rectangular RC piers and the reason is discussed. Finally, nonlinear dynamic FE-based response analysis of a single RC pier(P223) with fixed base is conducted, but large residual inclination observed is not simulated even when there is a mass eccentricity at the pier top.

Introduction

Elevated expressway in the epicentral area were severely damaged or even completely collapsed during the Kobe Earthquake. The Hanshin Expressway 'Kobe route' is not exceptional. It took 20 months to restore the elevated structures and to reopen the route. The Kobe Route of a total length 25 km from Nishinomiya to Kobe West (Tsukimiyama) (Fig.1) was subjected to near-field strong ground motion and as a result large portion of the Kobe Line suffered serious damage. In Uozaki-Fukae, elevated RC bridges were collapsed and overturned over 600m length. Many RC single piers had brittle shear-type failure. Almost all the single steel piers had local buckling to some degree and some were completely fractured(Ref. 1).

Although damage level of many piers was very high in the Kobe Route, it is also true that damage to many RC piers judges by visual inspection is moderate or mild. Fig.2 shows the damage level of the RC single piers along. the Kobe Route. The damage level is basically estimated visually based on the appearance of the above-ground damage. In Fig.2, B_s and C_s means that the damage level in the underground was found to be very severe during the restoration although the damage seen above the ground level was judge to be B (severe) or C (mild). It is rather suprizing that almost half of the piers were classified into the damage level 'D' (very mild damage or practically no damage).

The damage level in Fig.2 clearly shows that the spatial variation of the damage level is rather random along the route; no consistent trend can be found. Of course, the ground motion level and the ground condition would have been different from place to place along the Kobe Route. The type of the bridge structures also varies along the Route. Hence it would be very difficult to completely elucidate the reason(s) of the damage level of each pier and each bridge component. However, it

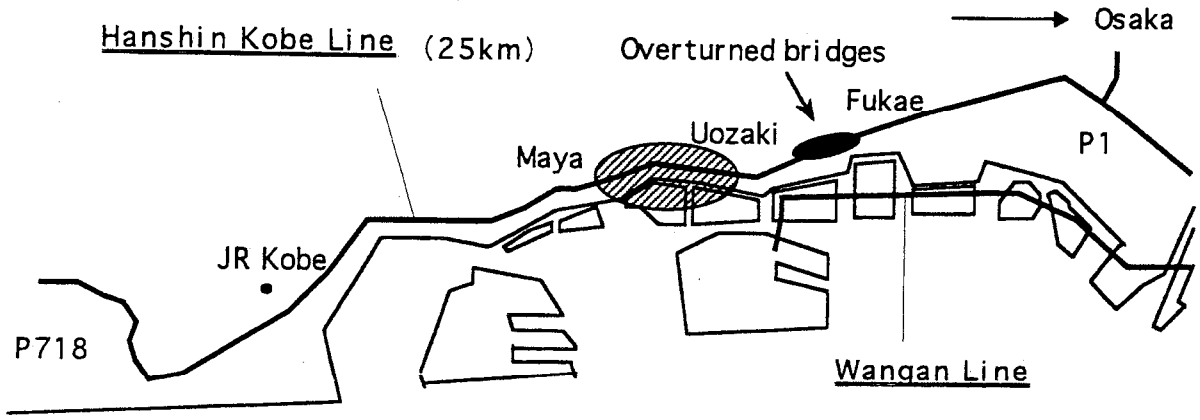

Fig. 1 Kobe Route of Hanshin Expressway

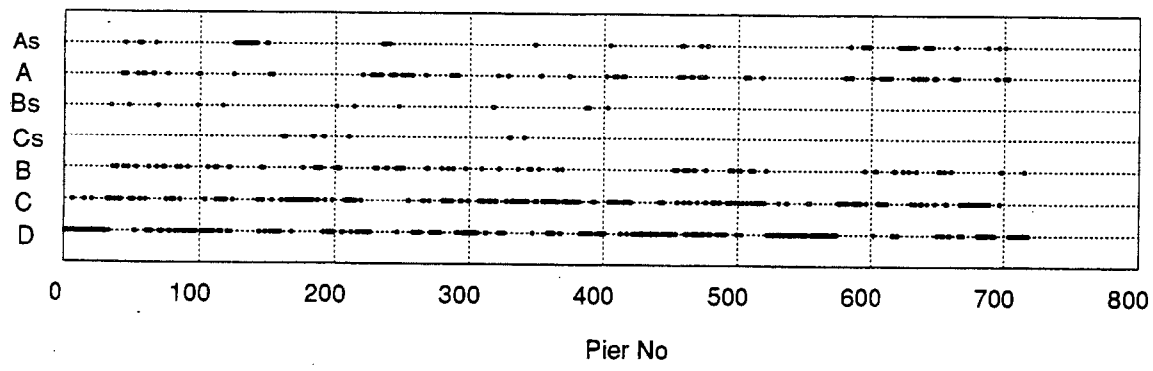

Fig. 2 Damage level of piers in Kobe Route(P1 - P718)
(As:collapse, A: very severe, B; severe, C: mild, D: very mild
or no damage, Bs & Cs; very severe(initially evaluated by B & C, respectively)

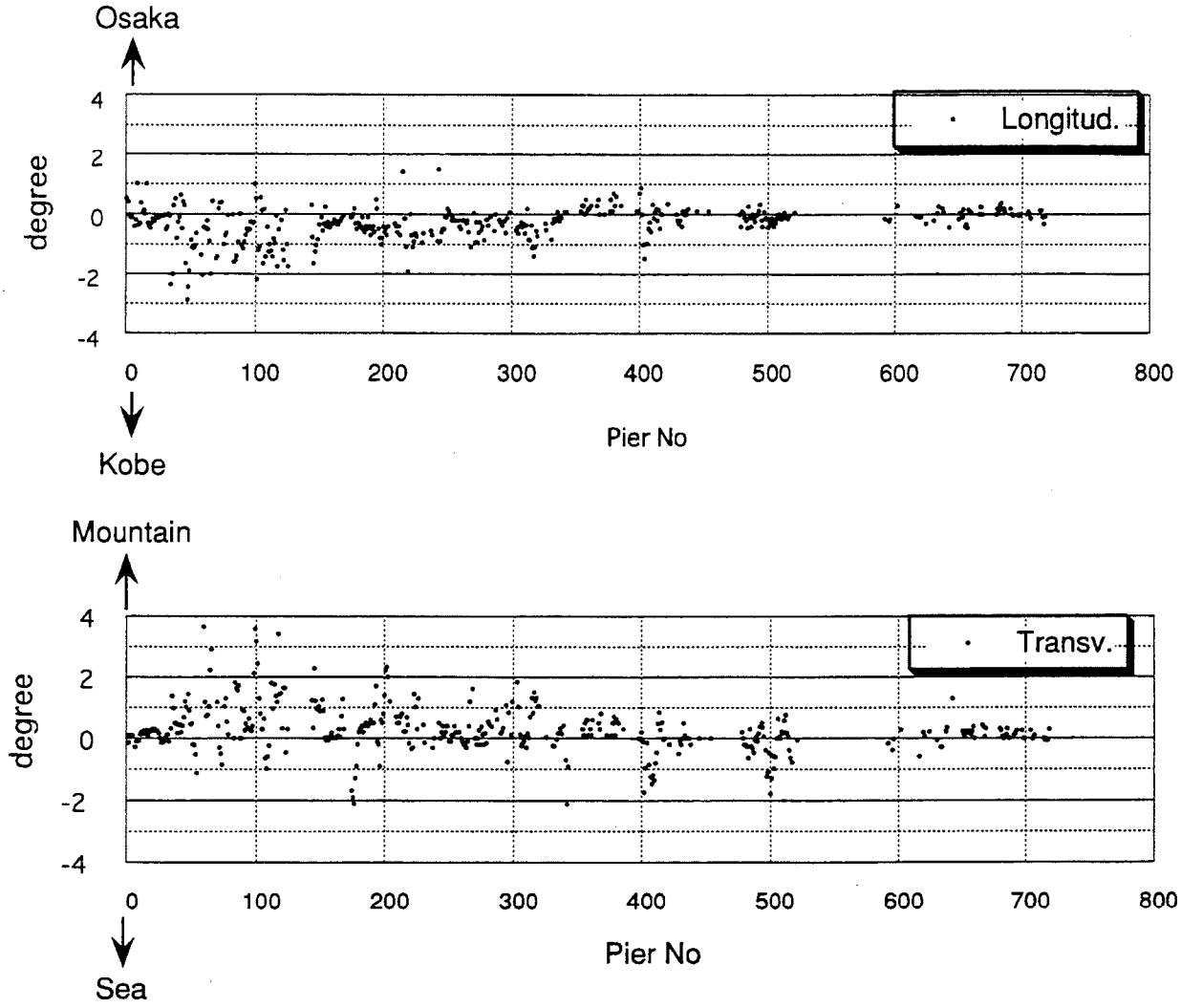

Fig. 3 Residual inclination of piers(P1 - P718)

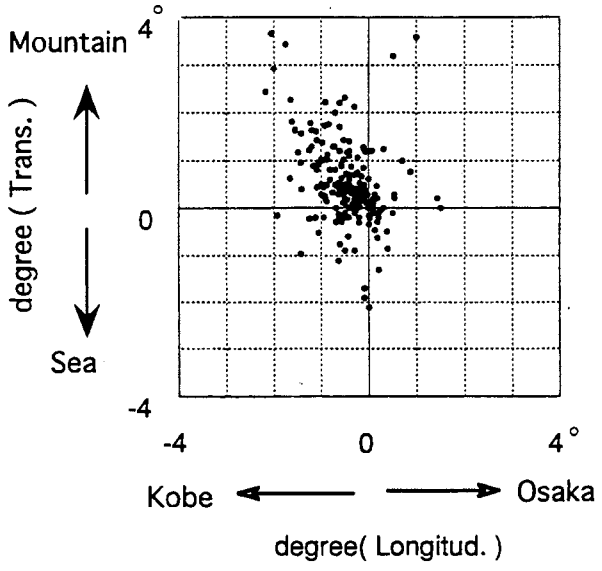

Fig. 4 Direction of residual inclination of piers (P1 - P718)

should be noted from a view point of earthquake engineering, extensive damage/undamage data were obtained in this earthquake and this information is extremely valuableto to understand the performance of the bridge structure under seismic excitation.

This study attempts to clarify the damage to elebvated bridges in the Kobe Route from mechanics and dynamics points of view. Since the Kobe Route is very long and dealing with the whole route involves many difficult issues, attention in this study is paid primarily to the section from P200 to P300.

Structure characteristic and damage to Kobe Route

The Kobe Route was constructed in 1960's to 1970s as a part of the Hanshin Expressway and completely adopted the elevated type. The height of the piers is about 10m in average and the span length along the route varies 20m to 80m. Most of the superstructur in the route are simply-supported spans and continuous spans are employed only in long span in order to cross the major street. Almost 90% of the girders is either steel I-girders or box girders. Many single piers(approx. 80%) were used to provide the space for traffic beneath the elevated expressway. Piled foundation is extensively employed because of the ground condition.

Right after the earthquake, reconstruction and repair of the bridge structures for restoration of the Kobe Route started. One of the measurements was the level of the inclinations of the pier (Fig.3). Piers with the damage level A_s B_s and C_s and A were basically demolished and no measurements were made.

Large residual inlination of piers causes the difficulty of placing the girders and visual uneasiness. Piers with more than 1° inclination were decided to demolish. Among 280 piers demolished, 88 piers were removed simply because of the large inclination.

It is interesting to note that the large inclination occurred in P50 to P300. Although the piers in the west is closer to the epicenter, the inclination in the west part is smaller. Correlation between the damage level (Fig.2) and the residual inclination of the piers(Fig.3) is seemingly not identified.

Fig. 4 shows the direction of the residual inclination of the piers, indicating the principal direction of the inclination is north-west which is alomost perpendicular to the fault ruputured during the 1995 Hyougoken Nambu earthquake.

Some correlation between the inclination and the ground condition is found, but clean explanation of the spatial distribution of the large pier inclination remains unanswered.

Damage level analysis of the section from P200 to P300

The ground motion would be significantly different over the Kobe Route of a 25 km length and the ground condition indeed varies along the route. This make the damage analysis be difficult on the same basis. The section from P200 to P300 (4.5 km length) is therefore selected for a detailed study.

In this section, almost all the piers are of RC single type as shown in Fig. 5a. Most of the girders are simply-supported ones with less than 50 m (Fig.5 b, c) and the spans of which length is 75m are part of the continuous girders. The girder in this portion are of steel. Most of the piers are of circular section (Fig.5d). Some of T-shape single piers are eccentric in mass.

Fig. 6a shows the damage to the piers from P200 to P300. The damage level is very much scattered; almost 50% of the piers suffered minor damage whereas 30% of the piers over severely or

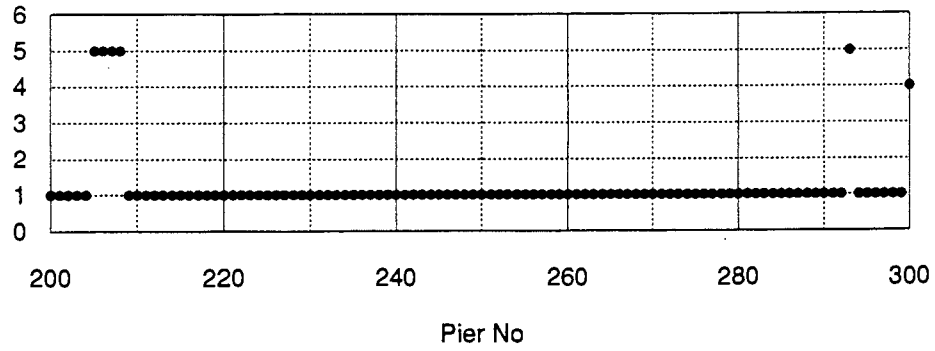

a) Type of RC piers(P200 - P300)
(1: single, 2: Special-type single, 3: Rigid single 4: Framed, 5: Special-type framed)

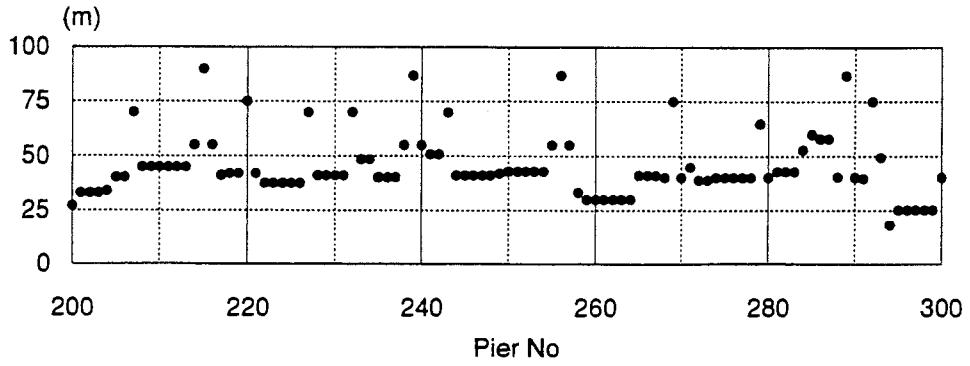

b) Span length

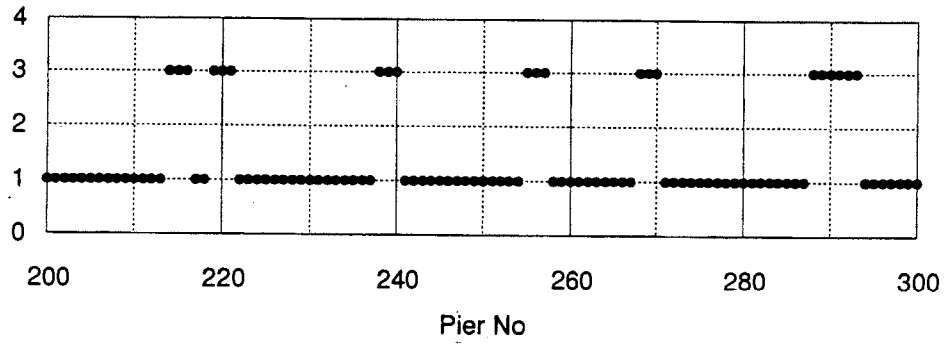

c) Number of spans

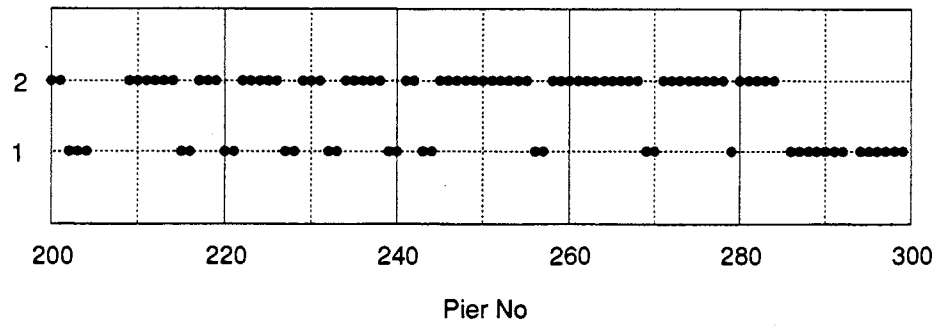

d) Type of pier section(1: rectangular, 2: circular)

Fig. 5 Structural characteristics of the section from P200 to P300

completely damaged. This fact is rather difficult to accept because the type of the bridge structures in this section is similar to each other and the ground motion in this 4.5 km length would not be so different.

As shown in FIg. 3, the residual inclination of the piers in the section is relatively large. According to Ref.1, the inclination angles 0.2° ,0.5° ,1.0° and 2.0° corresponds roughly to the ductility factors 1.2, 3.0, 6.0 and 12.0. This implies that piers with the residual inclination > 0.5° (suffered the damage A_s or at least A. If the overall damage is defined to be either (A_s ,A,B_s,,C_s) or the residual inclination >0.5° , almost all the piers are heavily damaged with some exceptions (Fig.6c). Comparing Fig. 6a and Fig. 6b, interestingly one can find that many piers with the damage level D have large residual inclination. Careful investigation of the whole damage of the bridge structure shows the exceptions in Fig. 6c are explainable; for example P205-208, and P293 are not single RC but framed piers. P216, P221 and P290 carries continuous girders and the steel shoes (fixed) were broken; the lateral force reduction in these piers can be expected. P239, P246, P248, P269 and P279 are the damage level B, which means the damage is not so mild. Considering these, the overall damage level from P200 to P300 is not scattered, but is consistently high.

Damage mode analysis of single RC piers from P200 to P300

As well known, the damage mode of RC piers under horizontal seismic force can be classified roughly into either flexure, shear or their combination. Among these, the shear mode failure is non-ductile and to be avoided. However, the seismic code at 1960s and 1970s did not pay enough attention to the brittle shear fracture and consequently did not require adequate transverse reinforcement for shear in the aseismic design of piers. Indeed, some of the piers had shear or flexural-shear failures in the Kobe route, resulting in catastrophic collapses.

The shear capacity and flexural moment capacity of RC piers can be computed easily using available prediction formulars(Refs 2 and 3). The ratio of shear to flexural capacity of a single piers under the horizontal load is defined as

r = shear capacity x pier height / (flexural capacity - moment due to eccentricity)

This ratio r indicates

r > 1 : flexural failure mode

r < 1 : shear failure mode

The reinforcements of the RC single piers were collected from Hanshin Public Expressway Corporation(HPEC) and the ratio, r was computed from the design dimensions (Fig.7). In the piers from P200 to P300, there was no termination of the longitudinal reinforcements in the middle of the piers. Fig. 8 shows the failure modes observed in the piers of the circular section (Fig. 8a) and the ratios, r computed (Fig.8 b). Almost all the values of r is > 1 and the failure mode is actually flexural except two (P219, P267). The two piers suffered the damage level A and the shear capacity might be decreased due to the flexural damage.

Fig. 9 shows the results for the rectangular section. In Hanshin Expressway, generally the rectangular piers carry long span girders. According to the aseismic bridge design code employed at 1960s, longitudinal reinforcements in the piers is increased to meet large bending moment due to large weight of the long span whereas the transverse reinforcement is not proportionally increased. The values of the ratio in many piers are therefore less than 1.0 and the shear failure was indeed

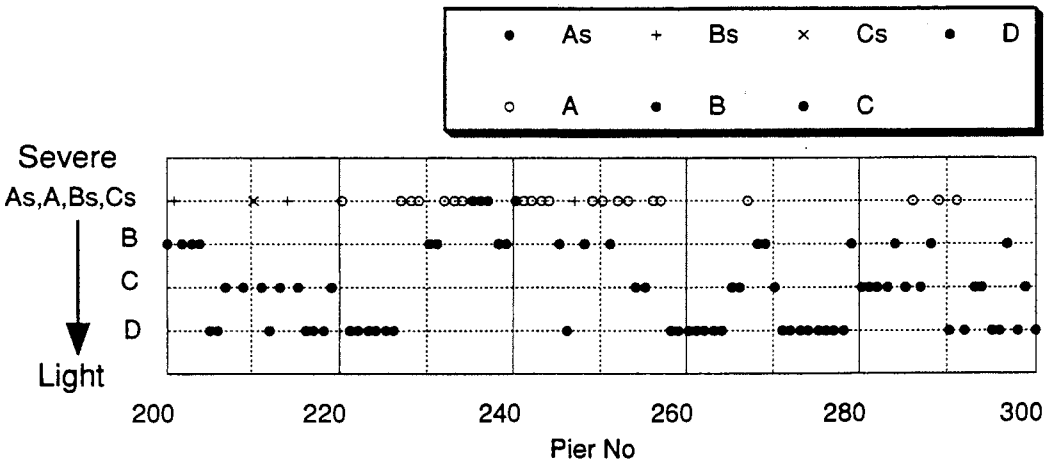

a) Damage level judged by Hanshin Public Expressway Corporation

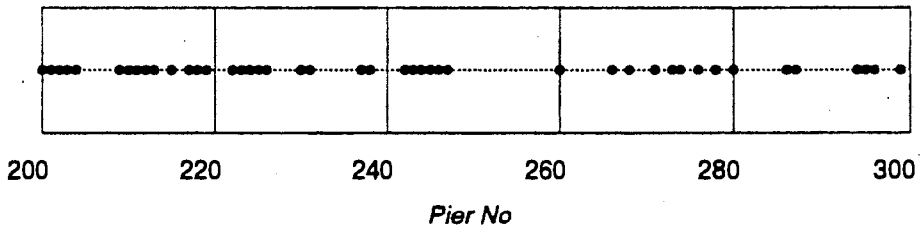

b) Piers with residual inclination > 0.5°

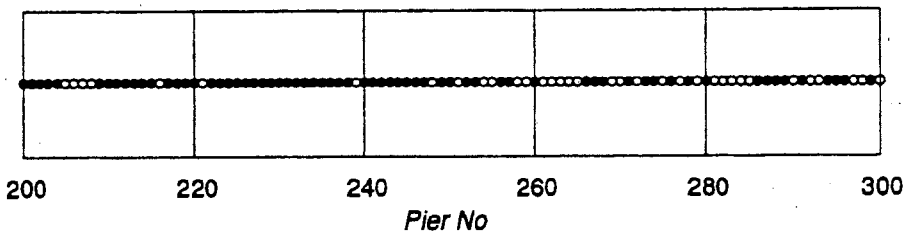

c) Severe damage(either (As+A+Bs+Cs) or inclination > 0.5°)

Fig. 6 Damage level from P200 to P300

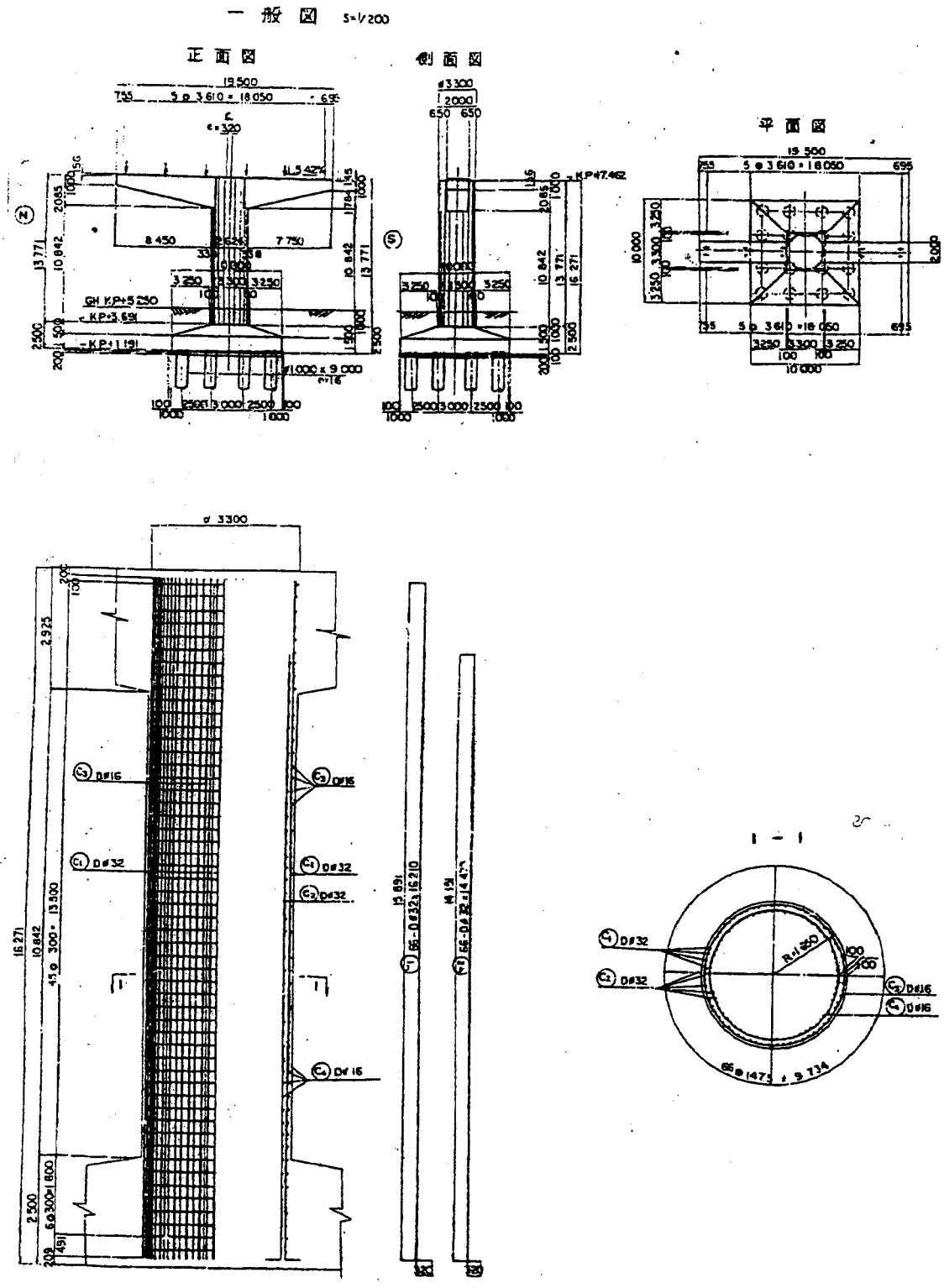

Fig. 7 Reinforcement of P223 in Kobe Route

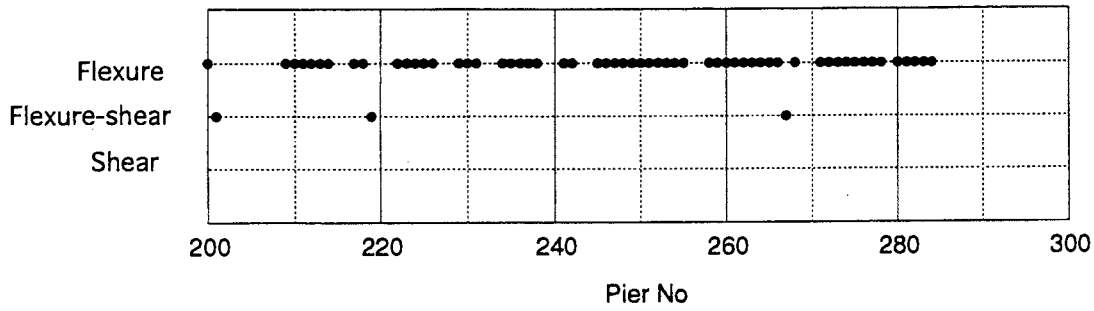

a) Damage mode observed

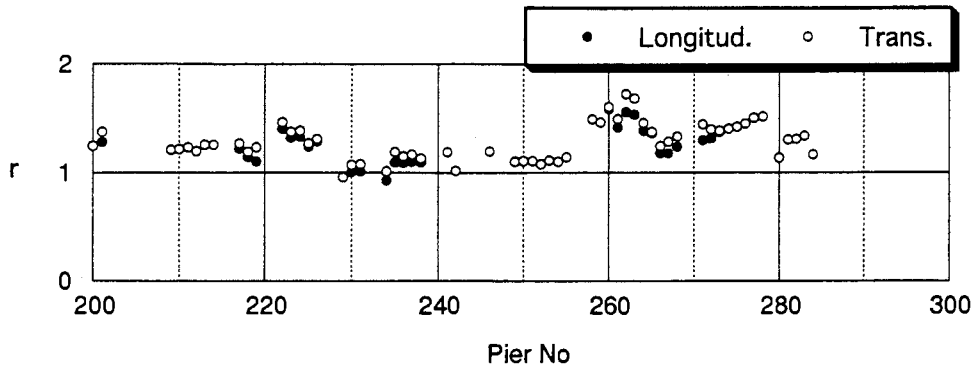

b) Ratio of shear to flexural capacity

Fig. 8 Damage mode and the ratio, r (circular section)

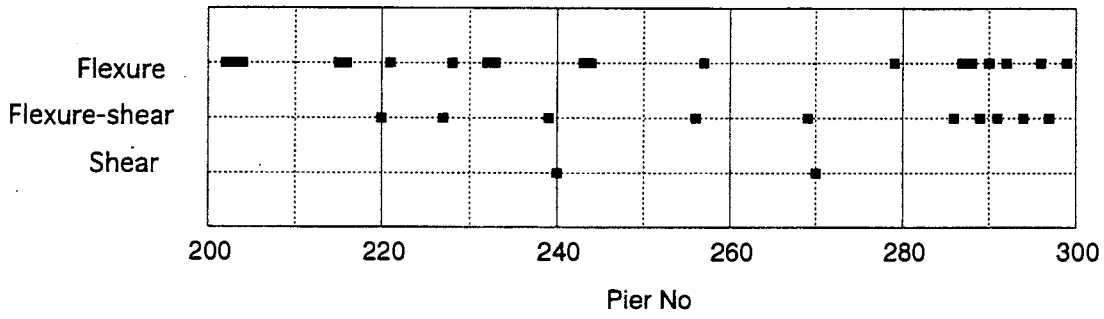

a) Damage mode observed

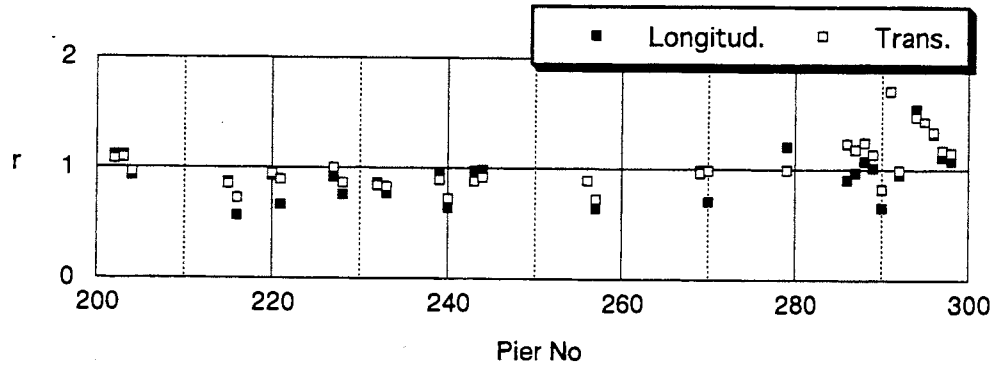

b) Ratio of shear to flexural capacity

Fig. 9 Damage mode and the ratio, r (rectangular section)

observed in these piers. Agreement between the observed failure mode and prediction is not so good; there are several exceptions. The damage to P257 occurred at the middle of the pier and the failure mode of P233 seems to be flexure-shear form photo although the mode is flexure according to HPEC. P215 suffered large residual inclination(1.43° in the transverse direction).P216, P221 and P290 carry continuous girders with fixed shoes; broken shoes might have acted as a fuse to these piers. Disagreement between the prediction and the actual mode can be reasonably explained in some of the exceptions, but some remains unexplainable.

Nonlinear dynamic response using FE formulation

The residual inclination of many piers in Kobe Route is found to be very large (Fig.3). These large inclinations are either due to the damage to the piers or due to other causes. To clarify this, nonlinear response analysis is conducted herein. The FEM computer code for simulating the 3-D nonlinear behavior of RC members under dynamic loading has been developed by Maekawa and Okamura(Ref. 4) and was used in the numerical analysis. The nonlinear modeling of the concrete utilizes the Maekawa model, while the nonlinear model of steel (re-bars) developed by Kato was included in the code.

Pier, P223 with circular section is selected for the numerical simulation(Fig. 10). In this pier, the damage level above the ground level was D, but the large residual inclination 1.43° was found in the transverse direction. The pier itself is not symmetric and the center of the mass is 0.35m apart from the pier axis toward the north. The horizontal ground motion measured at JR Takatori Station is used as an input(NS component, maximum gal;606). The average yield strengths for both concrete and reinforcing steel bar were employed.

The transverse response under the one-directional motion was computed. The foundation of the pier is not modeled and fixed base is assumed. Dynamic effect of girders is not taken into account and treated as distributed mass. Fig.10a shows the time history response of the angle of the pier (top displacement / pier height); the maximum angle is almost 1.5° , but the residual angle is much less than 0.5° . The response under a larger eccentricity (mass center is apart from the pier axis by 1.5m) is also computed for comparison (Fig.10b). It was confirmed that in these two cases, the maximum shear force in the pier did not exceed the ultimate shear capacity. The residual inclination is increased due to the mass eccentricity. However, the computed residual inclination is still much less than 1.43-° . The large residual inclination is not explained yet. The foundation flexibility has to be included in the model. Effect of material strength, ground motion, and so on has to be studied carefully. The study is undergoing and conclusive remarks on the residual inclination of the piers cannot be made at present.

Concluding remarks

An analysis on the damage of Hanshin Expressway suffered during the Hyogoken Nambu Earthquake was made. Special attention was paid to the piers from P200 to P300. The study can be summarized as follows;

(1) The large residual inclination of the piers was observed in Hanshin Expressway.

(2) The damage level in piers can be explained in a consistent manner, considering both the above-ground damage and the residual inclination of piers together.

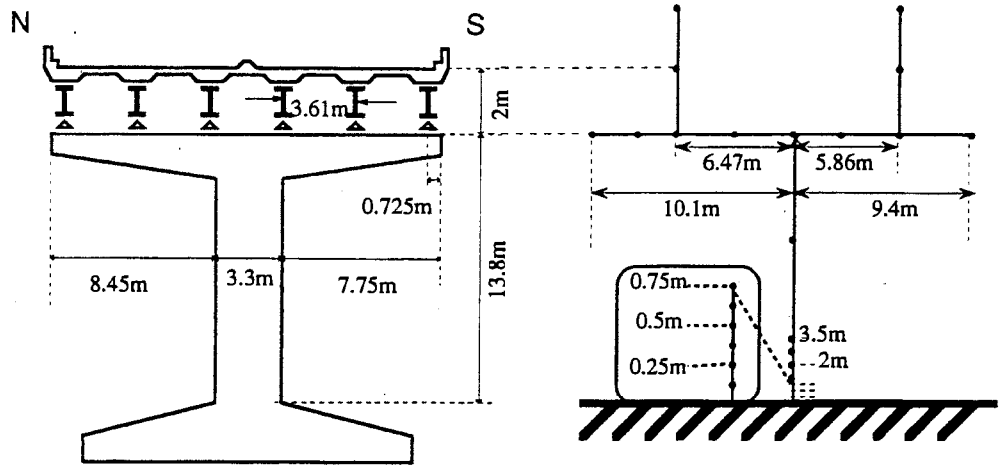

Fig. 10 FE Model of pier, P223

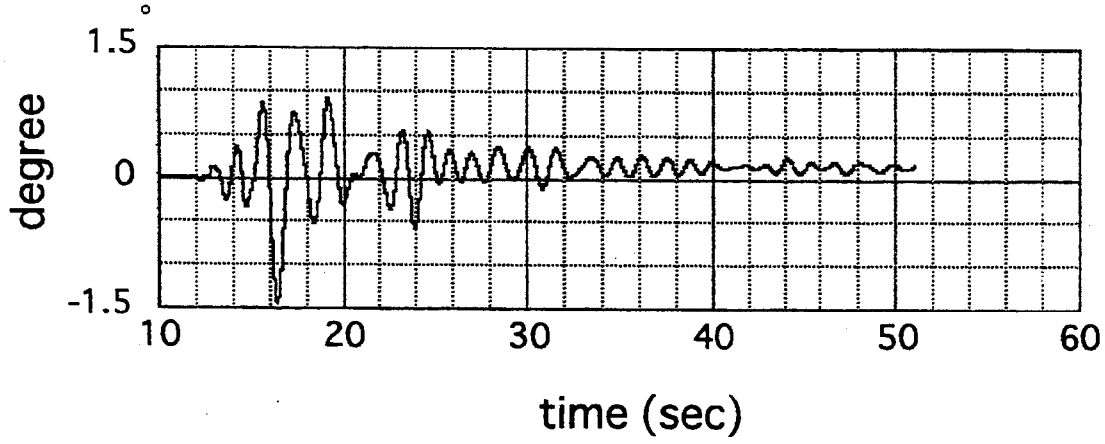

Fig. 11 Time history response at top inclination angle(P223)

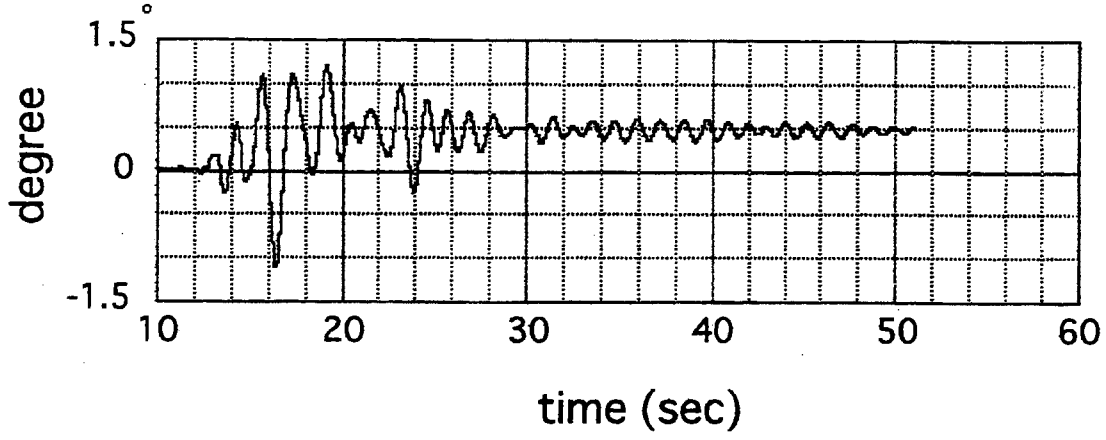

Fig. 12 Time history analysis at top inclination angle
(P223 with large eccentric mass, 1.5m(assumed))

(3) The ratio of shear to flexural capacity, r can predict the actual failure modes of RC single piers.
(4) Large residual inclination (displacement)observed in the piers is not explained yet from the nonlinear FE dynamic analysis. Further study including refinement of the model is needed to elucidate the residual inclination.

Acknowledgment

The authors express their sincere thanks to Hanshin Public Expressway Corporation for providing us with data and information. Special thanks are to Kitazawa,M., Hayasi, H., Ishizaki, H., Kousa, K. and Yasuda, F. of HPEC. Prof. H. Okamura, Univ. of Tokoyo made valuable comments during the study and Prof. K. Maekawa, Univ. of Tokyo allowed the authors to use the computer code DCOM2. This study is partially supported by grant-in-aid from the Ministry of Education ,Japan.

References

1) Ministry of Construction, Japan: Investigation report on damage to road bridges in 1995 Hyogoken Nanbu Earthquake, 1995 Dec.
2) JSCE; Design Standard for Concrete Structures, 1996-version, 1996.
3) Niwa, J et al: Re-evaluation of RC members without shear reinforcement, Journ. of JSCE, No.372/V-5, 1986.8
4) Okamura, H. and Maekawa, K.: *Nonlinear analysis and constitutive laws for reiforced concrete*, Giho-do, 1991.5
5) Abe, S.: A sysnthetic analysis of the damage of the elevated highway bridges during the Great Hanshin Earthquake, Master Thesis, Graduate School of Engineering, University of Tokyo,pp.1-64.

SEISMIC RESPONSE OF BRIDGES TO DIFFERENTIAL SUPPORT GROUND MOTION

George Deodatis and Sanjay Arwade
Department of Civil Engineering and Operations Research
Princeton University
Princeton, New Jersey

Masanobu Shinozuka
Department of Civil Engineering
University of Southern California
Los Angeles, California

ABSTRACT

A methodology is presented to generate spatially varying seismic ground motion time histories at a number of prescribed locations on the ground surface, compatible with prescribed response spectra and duration of strong ground motion, and reflecting the wave propagation and loss of coherence effects. The prescribed locations can correspond to different local soil conditions and therefore different response spectra can be assigned to each location. This methodology is then used in a case study of the SR14/I-5 Interchange that has partially collapsed during the 1994 Northridge earthquake. This case study includes a set of different scenario earthquakes with different velocities of wave propagation, different angles of incidence of seismic waves with respect to the axis of the bridge, and combinations of vertical and horizontal components of ground motion. It was concluded that the maximum stress at critical locations of the bridge can show increases up to 18%, compared to the case of identical support ground motion.

METHODOLOGY TO GENERATE RESPONSE SPECTRUM COMPATIBLE AND CORRELATED SEISMIC GROUND MOTION TIME HISTORIES

The methodology is capable of generating acceleration time histories at several specified locations on the ground surface, according to user-supplied response spectra. It should be mentioned that different locations can correspond to different local soil conditions, and consequently different response spectra can be assigned to each location. In addition, a duration of strong ground motion can be specified through a modulating (envelope) function, and the simulated time histories will reflect a prescribed velocity of wave propagation and a specified loss of coherence law through a complex coherence function.

The methodology is now described following Deodatis (1996a), by considering three points on the ground surface (in general any number of points can be considered). The acceleration time histories at these three points are modeled as a uniformly modulated, trivariate, non-stationary stochastic vector process. In general, the three points correspond to different local soil conditions. Consequently, a different target acceleration response

spectrum $RSA_j(\omega)$; $j = 1,2,3$ is assigned to each one of the three points. In addition, complex coherence functions $\Gamma_{jk}(\omega)$; $j,k = 1,2,3$; $j \neq k$ are prescribed between pairs of points, and modulating functions $A_j(t)$; $j = 1,2,3$ are assigned at each point. The simulation of the acceleration time histories is then performed according to the iterative scheme shown in Table 1. This scheme is not expected to perfectly converge at all frequencies as the number of iterations increases (perfect convergence at frequency $\omega = \omega^*$ is expressed as: $\frac{RSA_j(\omega^*)}{RSA^{(j_j)}(\omega^*)} = 1$; $j = 1,2,3$, where $RSA^{(j_j)}(\omega)$ is defined in Table 1). This is why no convergence criterion is included in the flowchart of Table 1. As will be shown in the numerical example that follows, only a small number of iterations is usually needed (in most cases less than ten) for a sufficiently accurate convergence at every frequency. For more details about the iterative process described in Table 1, the reader is referred to Deodatis (1996a).

At this point it should be mentioned that the idea for upgrading the individual power spectral density functions depicted in Table 1 has been suggested by Gasparini and Vanmarcke (1976) for one-dimensional and uni-variate stochastic processes. Two alternative methodologies to generate ground motion time histories compatible with prescribed response spectra, coherence function, velocity of wave propagation, and duration of strong ground motion, have been suggested by Hao et al. (1989) and by Abrahamson (1993).

An example taken from Deodatis (1996a) is presented now to demonstrate the capabilities of the methodology. Three locations are considered on the ground surface as indicated in Fig. 1. Point 1 corresponds to rock or stiff soils (Uniform Building Code (UBC) Type 1), point 2 corresponds to deep cohesionless or stiff clay soils (UBC Type 2), and point 3 corresponds to soft to medium clays and sands (UBC Type 3). The corresponding acceleration response spectra specified by the Uniform Building Code (International Conference of Building Officials 1994) for a peak ground acceleration of 200 cm/sec^2 are plotted in Fig. 2. Acceleration time histories will be generated at the three points defined in Fig. 1 to be compatible with the corresponding three response spectra shown in Fig. 2. A velocity of wave propagation of 2 km/sec is prescribed with the direction indicated in Fig. 1. Abrahamson's coherence function (Abrahamson 1993) is selected since it has the advantage that it can be used for a broad range of soil conditions. The resulting coherence functions between points 1 and 2 and points 1 and 3 are plotted in Fig. 3. Finally, the duration of strong ground motion is controlled using the Jennings et al. model (Jennings et al. 1968) with parameters defined in Fig. 4.

The acceleration time histories are generated at 6,144 time instants, with a time step $\Delta t = 3.07 \cdot 10^{-3}$ sec, over a length equal to $6,144 \cdot 3.07 \cdot 10^{-3} = 18.85$ sec. They are plotted after ten iterations in Fig. 5. Their corresponding response spectra are computed and plotted versus the prescribed UBC response spectra in Fig. 6. The agreement between prescribed and computed response spectra is very good for all three locations. In addition, the three generated time histories shown in Fig. 5 reflect the prescribed velocity of wave propagation of 2 km/sec, Abrahamson's specified coherence law, and the modulating (envelope) function defined in Fig. 4.

CASE STUDY ON THE SR14/I-5 INTERCHANGE

The southbound SR14/I-5 separation and overhead structure is located at mile post 24.5 on Route 5 in Los Angeles County approximately 24 miles northwest of downtown Los Angeles and is generally aligned in the north-south direction. The bridge is a ten-span structure divided into five frames by four expansion joints. It has seat-type abutments and single column bents. The total length is 1582 ft with an overall width of 55 ft. The structure is curved to a radius of 2235 ft. Figure 7 taken from Buckle (1994) shows elevation, plan and section views of the viaduct.

The viaduct failed spectacularly on January 17, 1994. The entire frame 1 from abutment 1 to the hinge in span 3-4 collapsed, with total disintegration of the column at pier 2, and an apparent punching through the superstructure of pier 3. The bridge unseated off abutment 1, moving about 5 ft north, and also unseated off the hinge adjacent to pier 4, again ending up in a final position some distance north of its original plan position. The right exterior shear key at abutment 1 was damaged. However, the left shear key had little visual damage. The pier 3 bent cap was inclined towards pier 4 and the measured ground separation from the column at pier 4 was approximately six inches north-south and four inches east-west. The predominant motion of the structure appeared to be in the north-south direction.

In this study, a three-dimensional finite element model of the viaduct was constructed based on the "as built plans" of the structure, and then this model was subjected to response spectrum compatible, spatially varying ground motions generated using the methodology described in the previous section. The purpose of this study is to show that spatially varying ground motion can lead to increased bridge response when compared to spatially constant ground motion.

Ground Motion

A total of 18 scenario earthquakes were considered by varying the velocity of seismic wave propagation v, the angle of incidence of seismic waves with respect to the axis of the bridge θ ($\theta = 0$ when seismic waves propagate parallel to the axis of the bridge, and $\theta = 90^o$ when seismic waves propagate at an angle of 90^o with respect to the axis of the bridge), and by considering combinations of horizontal and vertical components of ground motion. These 18 cases are described in Table 2.

The Caltrans acceleration design response spectrum for 80-150 ft alluvium, 5% damping, and 0.5g peak ground acceleration was selected for all supports of the bridge (see Fig. 7). Abrahamson's coherence law (Abrahamson 1993) was chosen to describe the coherence loss between pairs of supports. Finally, the Jennings et al. envelope (Jennings et al. 1968) was used to define the duration of strong ground motion (see Fig. 4).

A set of generated displacement time histories at the 11 supports of the bridge is plotted in Fig. 8 for Case #6 in Table 2.

Bridge Model

The motion of interest in this study is the motion of the center axis of the bridge. For this reason, the structure is modeled with 1-D frame elements running along the neutral axis of the superstructure box girder. The section properties of these elements are chosen to represent the full width and depth of the box girder. The ANSYS computer code was selected for the dynamic analysis.

Dynamic Analysis and Conclusions

For each of the 18 scenario earthquakes considered (refer to Table 2), the structure was analyzed using identical and differential support ground motion (dynamic time history analysis). The following ratio is computed for each section of the bridge (deck sections, pier sections) in order to quantify the effect of the spatial variation of ground motion on the dynamic response of the structure:

$$\rho = \frac{\text{maximum value of stress computed using spatially varying ground motion}}{\text{maximum value of stress computed using spatially constant ground motion}}$$

It is obvious that the ratio ρ indicates the increase ($\rho > 1$) or decrease ($\rho < 1$) in the maximum value of the stress for a specific section of the bridge caused by differential support ground motion, compared to the corresponding case of identical support ground motion.

Values of ρ for the five segments of the deck are provided in Table 3. Similar values are available for the columns.

From Table 3, it can be seen that certain sections of the deck can experience maximum stress increases of the order of 16%-18% when analyzed using spatially varying ground motion (compared to a corresponding dynamic analysis using identical support ground motion). Since the "Standard Specifications for Highway Bridges" of AASHTO (1996) require either a response spectrum dynamic analysis or a time history dynamic analysis for bridges with more than 6 spans like the SR14/I-5 Interchange, it is recommended to use the time history dynamic analysis option involving response spectrum compatible ground motion time histories that will reflect the wave propagation and loss of coherence effects. Such a dynamic analysis has to be performed by considering a few scenario earthquakes by varying the angle of incidence of seismic waves with respect to the axis of the bridge and by considering different (realistic) velocities of wave propagation. It is expected that one or more of these scenario earthquakes (that are design response spectrum compatible) will produce maximum stresses that will be higher than the corresponding maximum stresses obtained from a dynamic analysis using identical support ground motion. The set of dynamic analyses recommended here can be used to design new bridges or to analyze existing bridges for retrofitting and strengthening purposes.

ACKNOWLEDGMENTS

This work was supported by the National Science Foundation under Grant # BCS-9257900 with Dr. Clifford J. Astill as Program Director, and by the NCEER Highway Project (FHWA Contract DTFH61-92-C-00106).

REFERENCES

Abrahamson, N.A. (1993). "Spatial Variation of Multiple Support Inputs," *Proceedings of 1st U.S. Seminar on Seismic Evaluation and Retrofit of Steel Bridges*, a Caltrans & University of California at Berkeley Seminar, San Francisco, October 18.

Buckle, I.G. (1994). "The Northridge, California Earthquake of January 17, 1994: Performance of Highway Bridges," *Technical Report NCEER-94-0008*, National Center for Earthquake Engineering Research, State University of New York at Buffalo.

Deodatis, G. (1996a). "Non-Stationary Stochastic Vector Processes: Seismic Ground Motion Applications," *Probabilistic Engineering Mechanics*, Vol. 11, No. 3, pp. 149-167.

Deodatis, G. (1996b). "Simulation of Ergodic Multi-Variate Stochastic Processes," *Journal of Engineering Mechanics*, ASCE, Vol. 122, No. 8, pp. 778-787.

Gasparini, D. and Vanmarcke, E.H. (1976). "Simulated Earthquake Motions Compatible With Prescribed Response Spectra," Technical Report, Department of Civil Engineering, Massachusetts Institute of Technology, Publication No. R76-4.

Hao, H., Oliveira, C.S. and Penzien, J. (1989). "Multiple-Station Ground Motion Processing and Simulation Based on SMART-1 Array Data," *Nuclear Engineering and Design*, Vol. 111, No. 3, pp. 293-310.

International Conference of Building Officials. (1994). "Uniform Building Code," Vol. 2.

Jennings, P.C., Housner, G.W. and Tsai, N.C. (1968). "Simulated Earthquake Motions," Technical Report, Earthquake Engineering Research Laboratory, California Institute of Technology.

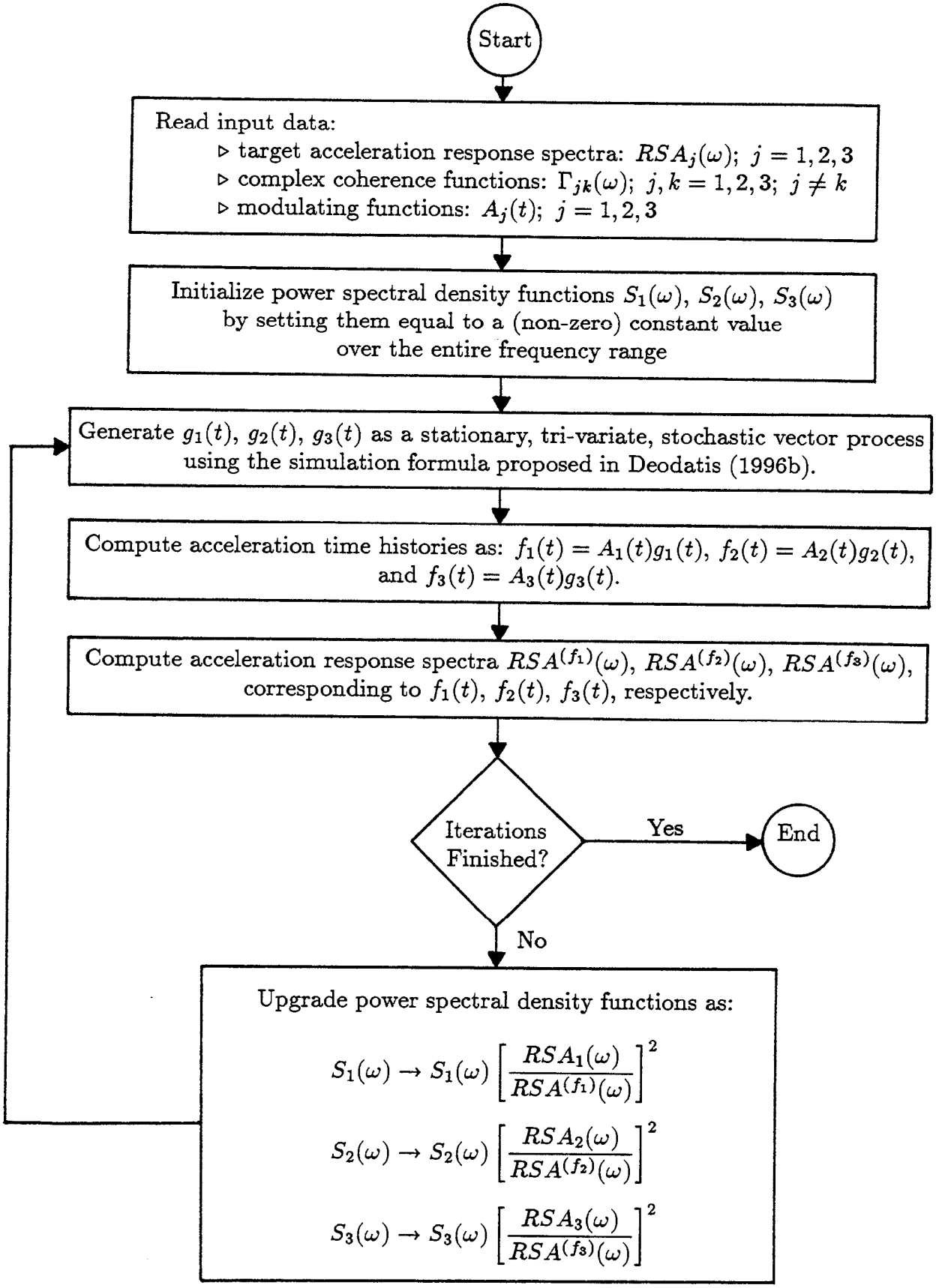

Table 1. Iterative Scheme to Simulate Response Spectrum Compatible Acceleration Time Histories at Three Points On the Ground Surface.

Table 2. The 18 Scenario Earthquakes

Case #	**Velocity v** (m/sec)	**Angle θ** (degrees)	**Ground Motion Components**
1	1,000	0	Horizontal only
2	1,200	0	Horizontal only
3	1,400	0	Horizontal only
4	1,600	0	Horizontal only
5	1,800	0	Horizontal only
6	2,000	0	Horizontal only
7	2,200	0	Horizontal only
8	2,400	0	Horizontal only
9	2,600	0	Horizontal only
10	2,800	0	Horizontal only
11	2,000	10	Horizontal only
12	2,000	20	Horizontal only
13	2,000	30	Horizontal only
14	2,000	40	Horizontal only
15	2,000	60	Horizontal only
16	2,000	90	Horizontal only
17	2,000	0	Horizontal + Vertical
18	2,000	30	Horizontal + Vertical

Table 3. Values of ρ in the Five Segments of the Deck for the 18 Scenario Earthquakes

Scenario #	ρ for segment 1	ρ for segment 2	ρ for segment 3	ρ for segment 4	ρ for segment 5
1	1.18	0.98	0.96	1.05	1.06
2	1.14	0.98	0.97	1.06	1.05
3	1.13	1.00	0.98	1.07	1.03
4	1.13	1.00	0.99	1.07	1.04
5	1.13	1.00	0.99	1.06	1.04
6	1.12	1.01	0.99	1.05	1.04
7	1.12	1.02	1.00	1.05	1.04
8	1.11	1.02	1.00	1.05	1.03
9	1.11	1.02	1.00	1.05	1.03
10	1.12	1.01	0.99	1.05	1.04
11	1.12	1.02	0.99	1.06	1.05
12	1.12	1.02	1.00	1.06	1.05
13	1.10	1.03	1.00	1.06	1.04
14	1.09	1.05	1.00	1.05	1.05
15	1.05	1.06	0.99	0.99	1.03
16	1.00	0.96	0.99	0.99	0.99
17	0.70	1.10	1.04	1.16	0.65
18	1.07	1.07	1.03	1.01	1.09

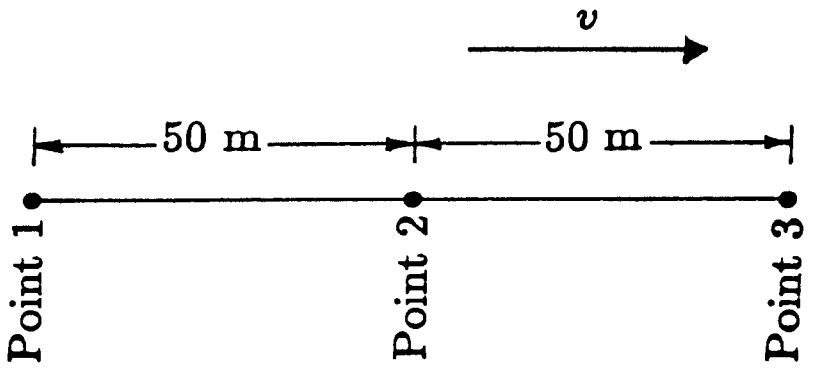

Fig. 1 Configuration of points 1, 2, and 3 on the ground surface along the line of main wave propagation.

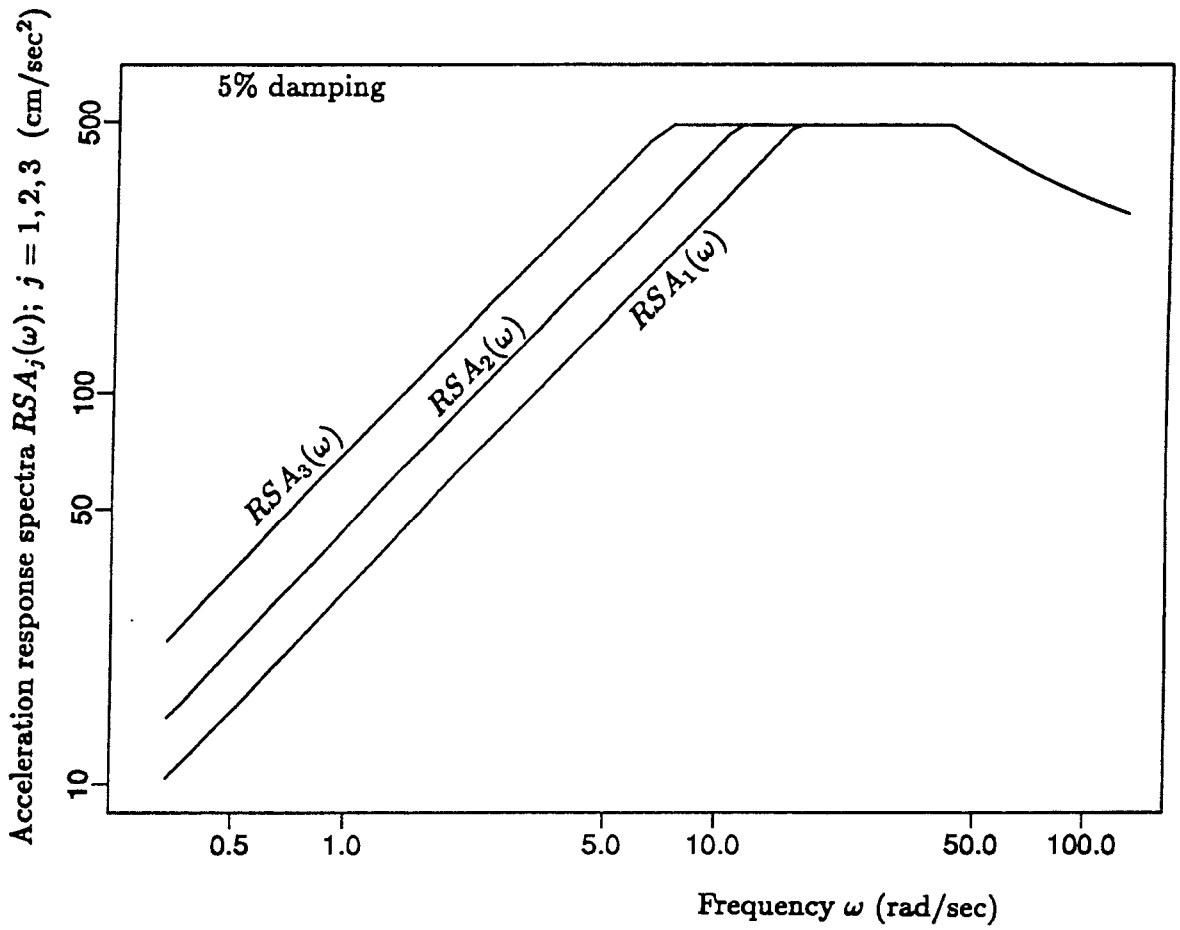

Fig. 2 Uniform Building Code acceleration response spectra assigned to points 1, 2, and 3, respectively (refer to Fig. 1 for location of three points).

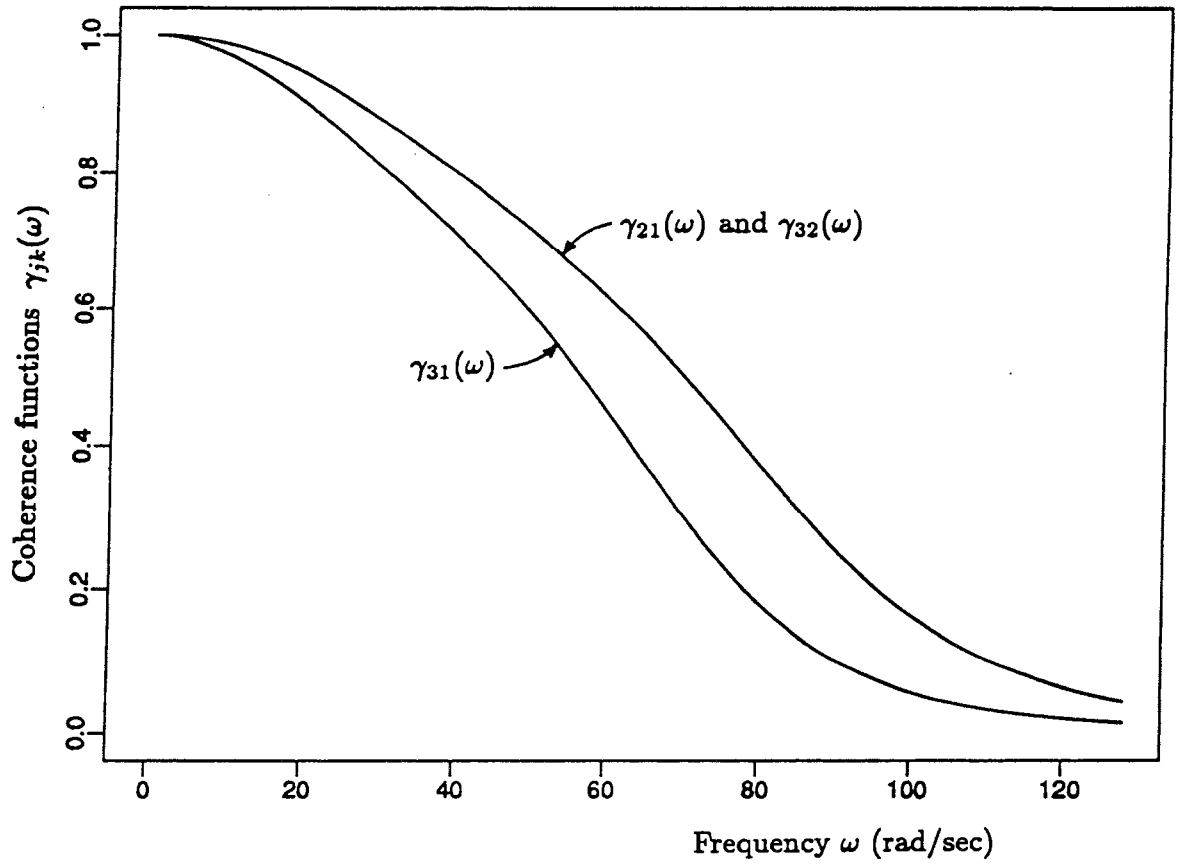

Fig. 3 Coherence functions using Abrahamson's model between points 1 and 2 (or 2 and 3) and points 1 and 3.

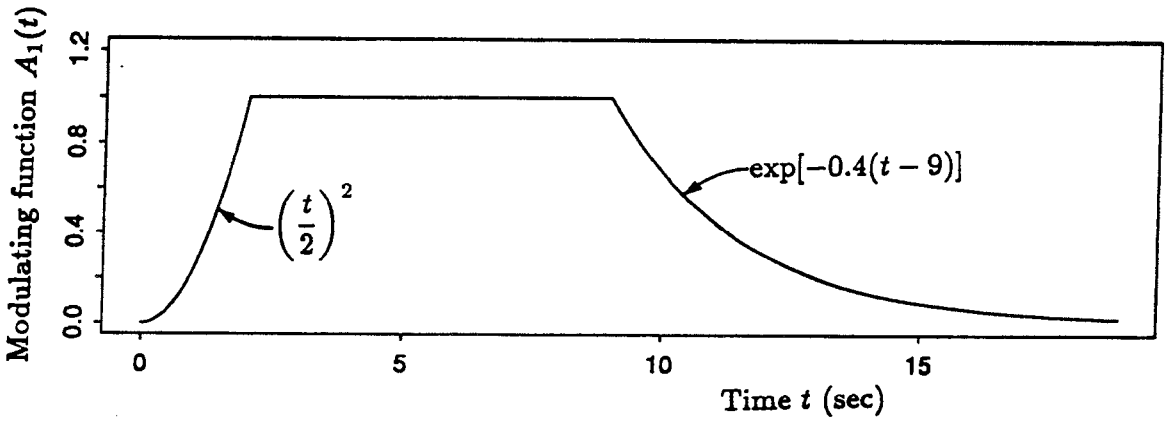

Fig. 4 Jennings et al. model used for envelope function.

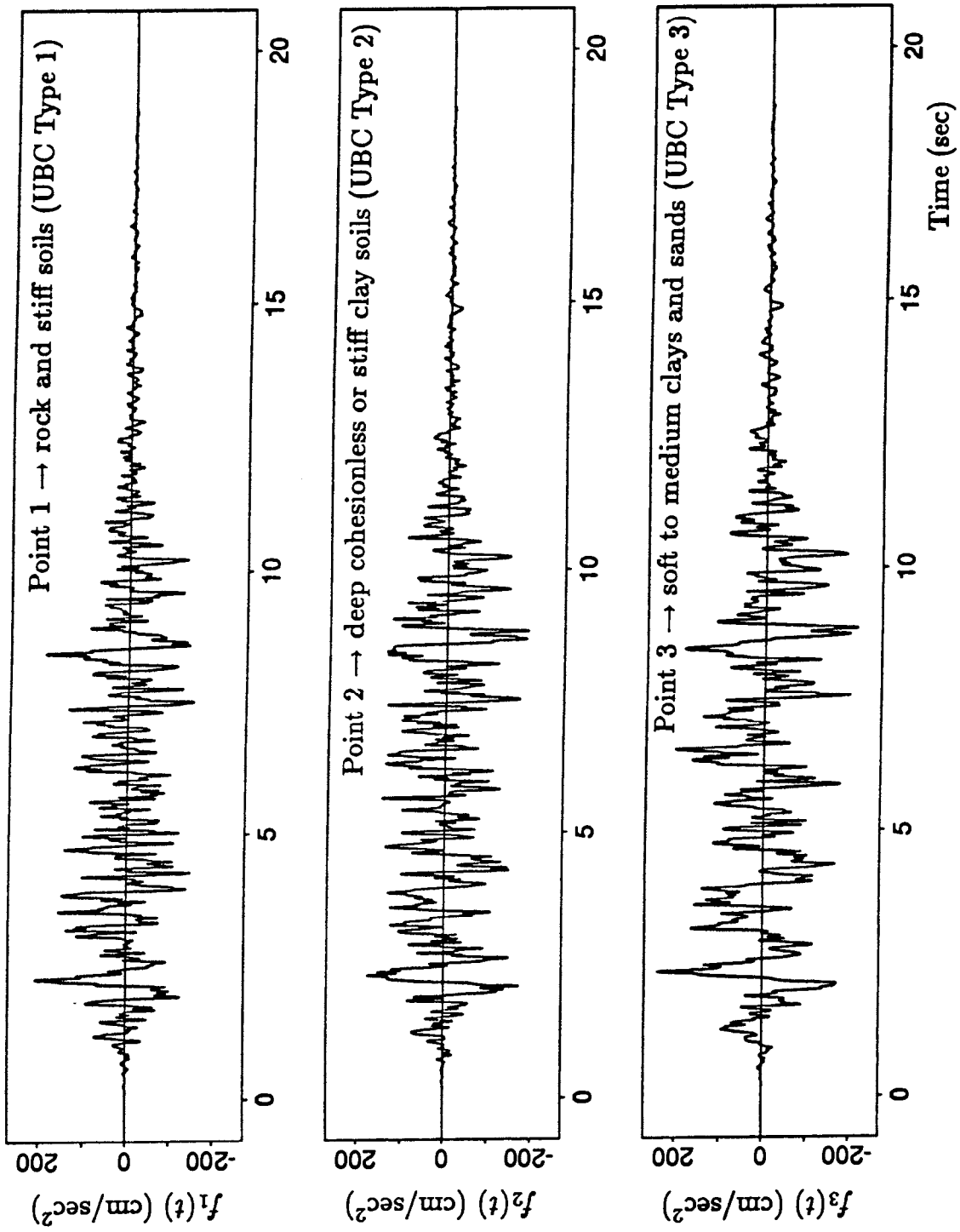

Fig. 5 Generated acceleration time histories at points 1, 2, and 3 defined in Fig. 1.

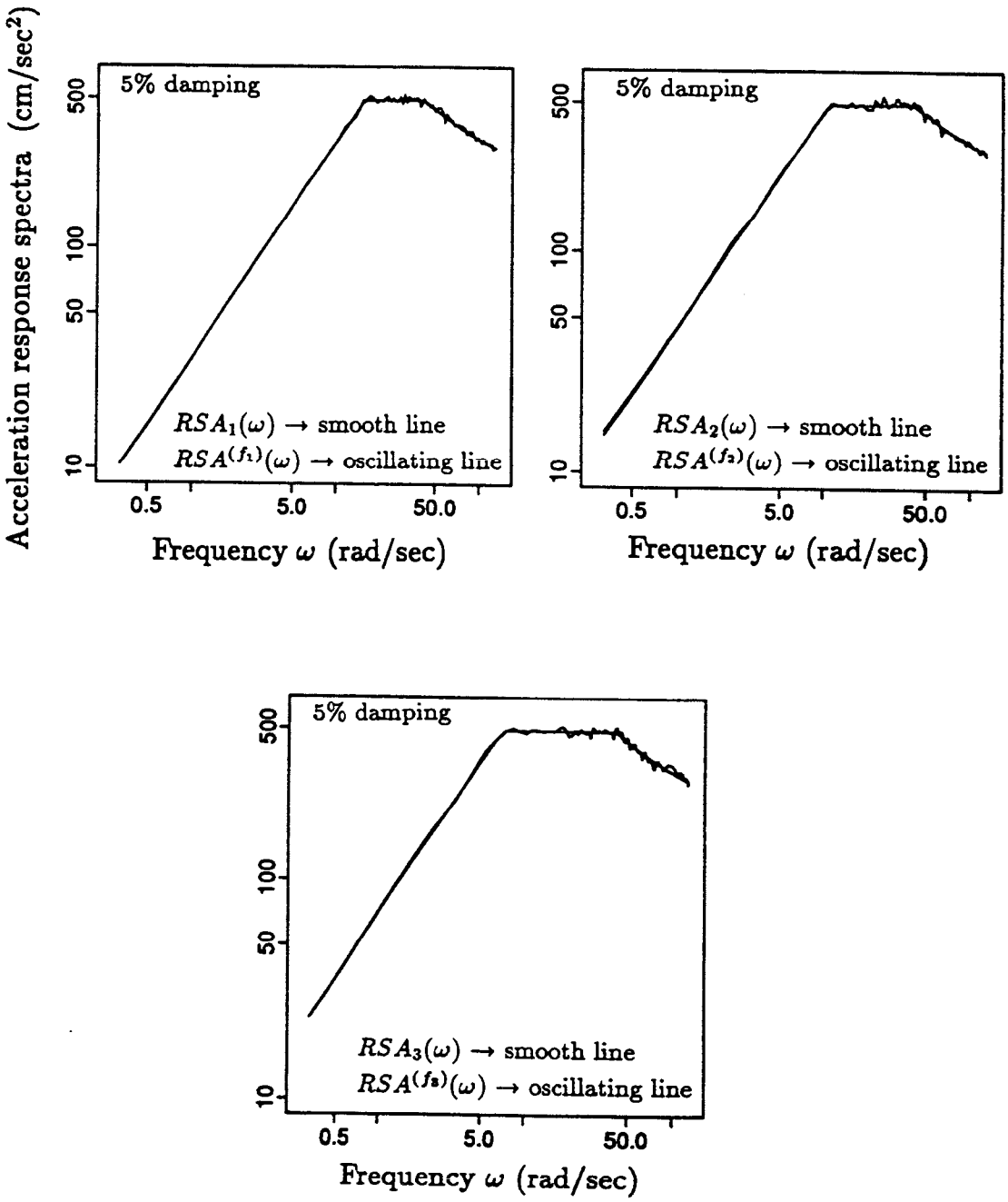

Fig. 6 Acceleration response spectra $RSA^{(f_j)}(\omega)$; $j = 1, 2, 3$ computed using the generated acceleration time histories shown in Fig. 5 versus the UBC acceleration response spectra $RSA_j(\omega)$; $j = 1, 2, 3$.

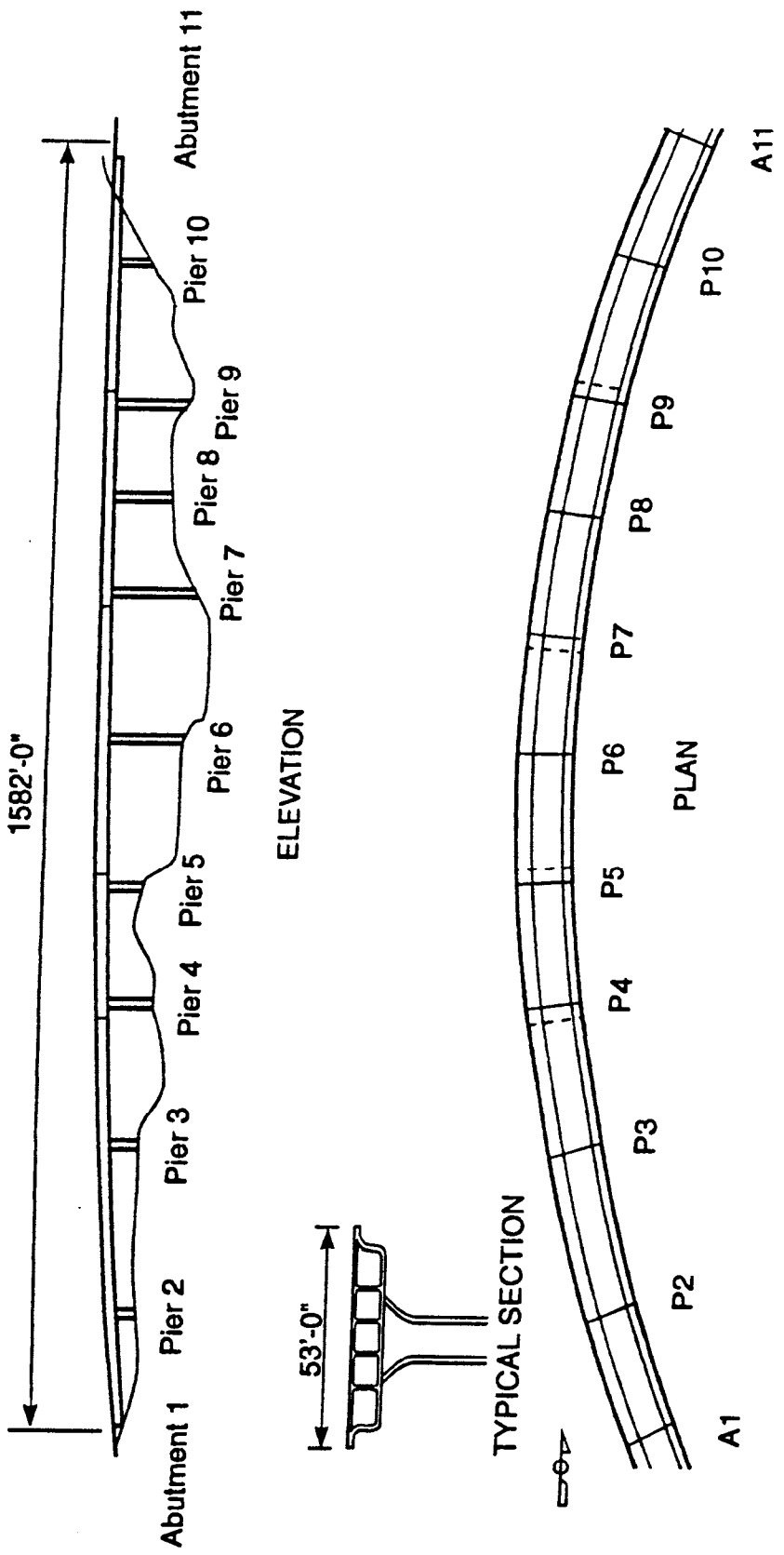

Fig. 7 Elevation, plan and section views of the southbound SR14/I-5 separation and overhead taken from Buckle (1994).

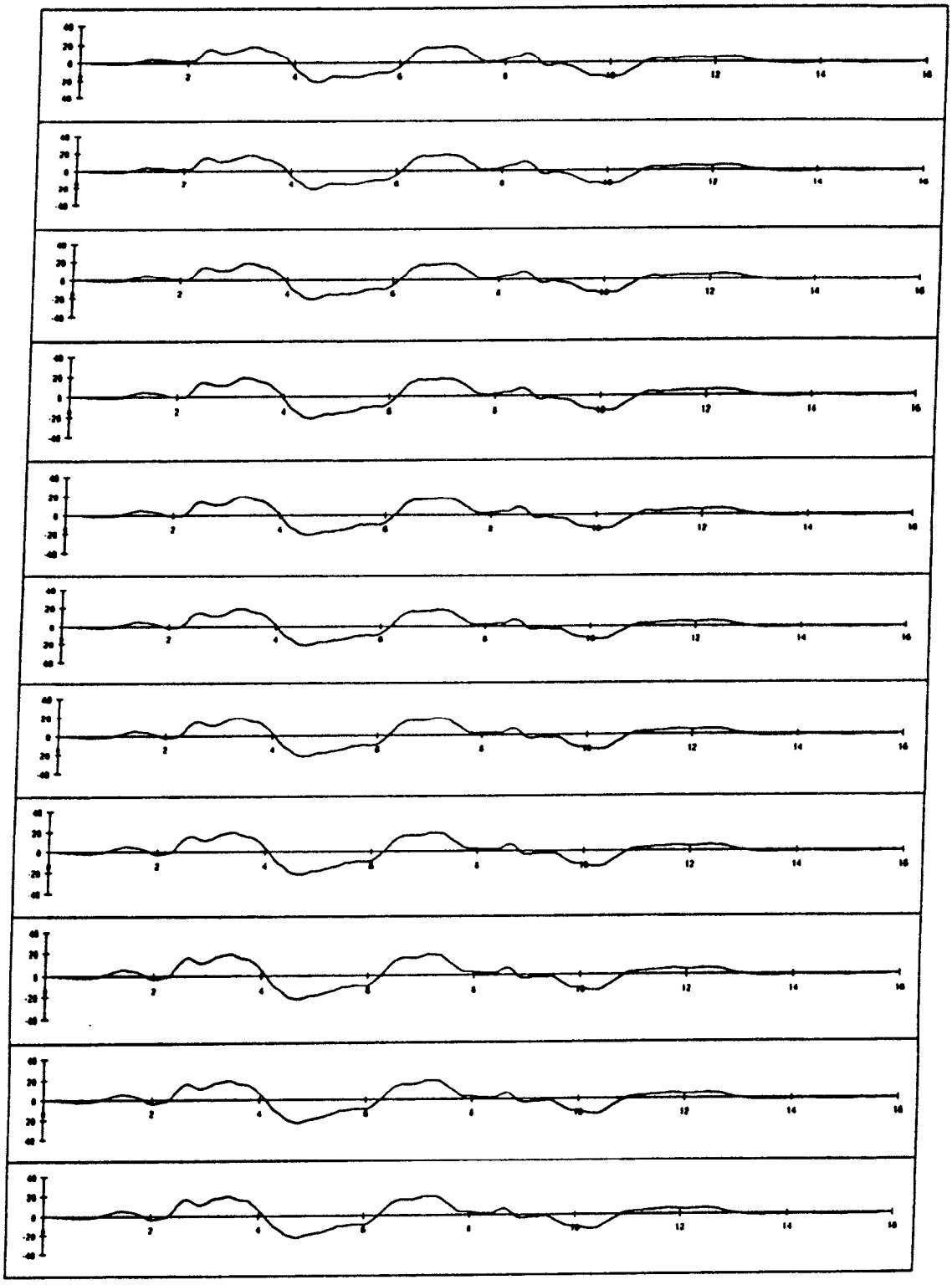

Fig. 8 A set of generated displacement time histories in cm, at the 11 supports of the bridge for Case #6 in Table 2.

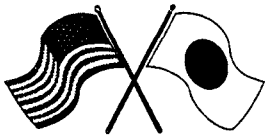

Session 4
Analysis & Structure Performance
Part II

Session Co-chairs: T. Leslie Youd and Yozo Fujino

DYNAMIC RESPONSE BEHAVIOR OF PRESTRESSED CONCRETE VIADUCT UNDER SEVERE EARTHQUAKE

Wael Zatar
Graduate School of Engineering
Saitama University, Japan

Hiroshi Mutsuyoshi
Department of Civil Engineering
Saitama University, Japan

ABSTRACT

In order to clarify inelastic behavior of prestressed concrete (hereafter PC) girders of a viaduct under severe earthquakes, four small scale PC specimens were designed to represent experimental parts of models for viaduct structures. Three specimens were tested under statically reversed loading. The last viaduct model was tested using a substructured pseudo-dynamic test and then a cyclic loading was applied to the same specimen till failure. The inelastic response analysis based on one component model for the analytical modeling of members was conducted during the substructure pseudo-dynamic test. Response analyses for the same viaduct model were performed.
KEYWORDS: earthquake resistant structures; viaduct structures; partially prestressed concrete; substructured pseudo-dynamic test; dynamic analysis; elasto-plastic behavior.

1. INTRODUCTION

Because of the importance of viaduct structures and elevated bridges in the construction of highways and railways, especially in Japan, various loading tests have been carried out for the elevated bridges to study the inelastic behavior of reinforced concrete bridge piers subjected to severe ground motions. Since the girders of these bridges are generally hinged to the piers, only the piers are subjected to earthquake forces. On the other hand, because of the fixation between girders and piers in viaduct structures, not only the piers but also the girders may have some damage. Yet not enough tests have been performed to study the inelastic behavior of PC girders of viaduct structures. The objectives of this study are to obtain the inelastic response behavior of such PC viaduct structures due to severe earthquake excitation.

In the present study, four structural models were selected so that they can represent actual viaduct structures. Four cantilever PC members from these models were tested experimentally among which the significant difference was the amount and arrangement of prestressing tendons and reinforcing bars. Three specimens of PC girders for the viaduct models were tested experimentally through being subjected to static cyclic loading imposed by an actuator. A substructured pseudo-dynamic test using an amplified excitation of Hyogo-Ken Nanbu 1995 earthquake was carried out for the last PC viaduct model. All the members of the model except for the experimental member were treated analytically during the pseudo-dynamic test using one component model. Takeda's model [4] was used for the restoring force-displacement model of RC piers. After the completion of the substructured pseudo-dynamic test, a cyclic loading test was performed till failure of the specimen. Response analyses were carried out for the same viaduct model and a comparison between the experimental and analytical results was conducted in terms of hysteretic load-deformation characteristics and time histories.

2. OUTLINE OF TESTS

2.1. Dimensions of test specimens

Four partially PC specimens representing the experimental girder members of the viaduct models were tested. They had the same dimensions but they differed in the amount of prestressing tendons and reinforcing bars for the purpose of studying the influence of restoring force characteristics on the resulting response behavior. Details of specimens are shown in Fig. 1 and Table 1. The upper part of the specimens that represent the PC girders has depth of 25 cm, width of 20 cm and length of 200 cm. The PC girder parts were placed monolithically with lower parts that represent the RC piers of the viaduct models. The lower part has depth of 50 cm, width of 40 cm and length of 120 cm. The lower part of specimen was rigid enough to represent the actual case of piers for a viaduct structure as well as to enable the observation of the damage that can occur in the girder during a real earthquake excitation. The compressive strength of concrete is about 400 kgf/cm^2, yielding points of reinforcing bars D13 and D16 are 3600 kgf/cm^2 and 3400 kgf/cm^2 respectively while those of prestressing tendons are 10500 kgf/cm^2 for D17 and 12200 kgf/cm^2 for D11. All specimens were designed so that the shear capacity is higher than flexural one.

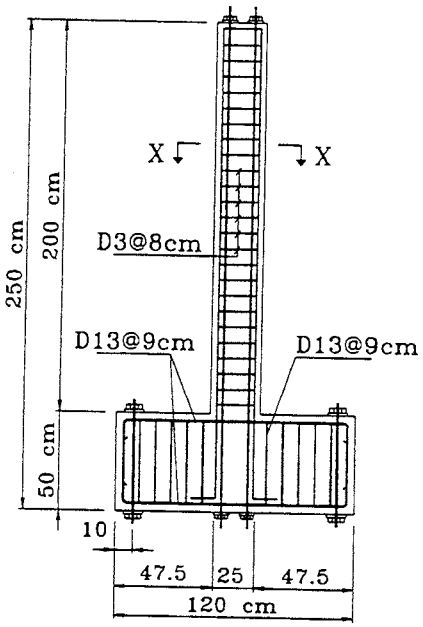

Fig.1 Test specimens

Table 1 Reinforcement provided to specimens

Specimen No.	Prestressing tendons		Reinforcement		Remarks
	R.S. *	L.S. **	R.S. *	L.S. **	
A-1	D17	--	2D6	2D6	Cyclic test
A-2	D17	D11	2D6	2D13	Cyclic test
A-3	D17	D17	2D6	2D6	Cyclic test
B	D11	D11	2D13	2D13	PSD test***

* R.S. : Right side of specimen at the test setup
** L.S. : left side of specimen at the test setup
*** PSD : Substructured pseudo-dynamic test

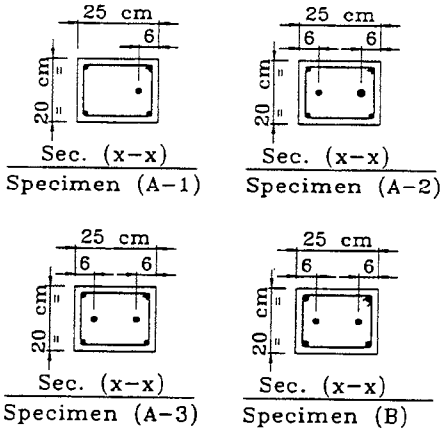

2.2. Reversed cyclic loading tests

Reversed cyclic loading tests were carried out for specimens A-1, A-2 and A-3. The purpose of conducting these tests was to clarify the load-displacement characteristics of PC girders when changing the amount and arrangement of prestressing tendons and reinforcing bars in the cross section. Specimens were tested using the same setup shown in Fig. 2 which consisted of the specimen, actuator, reaction wall, testing floor, data logger and measuring devices. All specimens were fixed to the testing floor using side supports, steel bars and high strength bolts. The loading point was fixed at a height of 150 cm from the face of the PC member for all specimens. The yielding displacement considered in this study for the prestressing tendons and the reinforcing bars are the displacement corresponding to their

yielding loads. The repetition of each cycle was 10 times. The applied displacements imposed to the specimens through the actuator were multiples of the reinforcing bars yielding displacement.

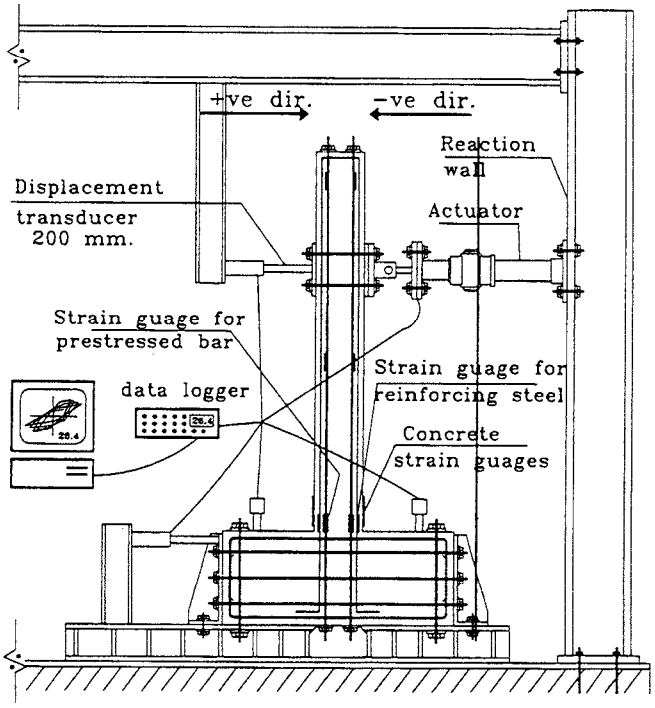

Fig. 2 Loading setup

2.3. Substructured Pseudo-dynamic test

2.3.1. Structural model

The considered viaduct which has a scale of 1/10 of the actual ones is shown in Fig. 3. The PC girder of a viaduct structure is taken in this study as the experimental substructure where it might undergo extensive plastic deformations when a severe earthquake occurs. For simplicity and due to the difficulty of implementing members with varying inflection points, it was assumed that the viaduct girder is symmetric with respect to the center of each bay and thus only half of one girder bay was taken in this study as the experimental member (Fig. 3). The members numbering scheme is shown in Fig. 4.

2.3.2. Experimental procedures

In order to obtain inelastic response behavior for the PC viaduct structure shown in Fig. 3, substructured pseudo-dynamic testing technique [2] was used in which load was applied quasi-statically during the test and the dynamic effects are simulated numerically. Specimen B was taken as the experimental part of the viaduct model. Analytical inelastic mechanical model and its restoring force-displacement model were used for all members in the structure except the PC girder [2] where its restoring force was measured directly from the loading test system. One component model proposed by Giberson [1] was used for the inelastic member model in which the spring stiffness was determined using Otani's method [3]. Takeda's tri-linear model [4] was used for the RC piers. This model includes concrete cracking and yielding. Such a realistic conceptual model recognizes the continually degrading stiffness due to bond slip, shear cracks and energy absorption characteristics of the structure during load application. The earthquake excitation used was the modified Hyogo-Ken Nanbu (NS 1995) earthquake where the time scale was reduced to half the original one while the maximum ground acceleration was 818 gal (Fig. 5) to allow the observation of the resulting

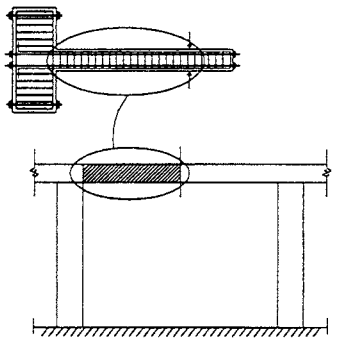
Fig. 3 Test specimens

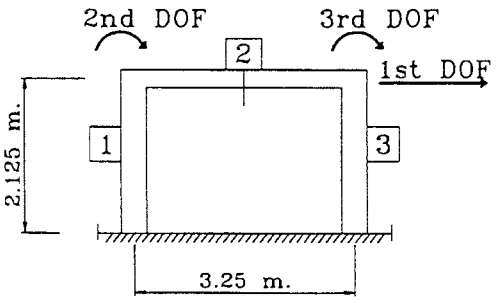

Fig. 4 Model used for pseudo-dynamic test.

response. The time interval was taken 0.005 sec during the test. After the completion of the substructured pseudo-dynamic test, a reversed cyclic test was performed on the same specimen till failure occurred in order to obtain the ultimate limit state. The used system in the substructured pseudo-dynamic test consisted of the specimen, loading actuator, personal computer that analyzed the inelastic earthquake response of the viaduct model and controlled the input/output data, measuring devices and another personal computer used for output data acquisition. The test procedures are as follows:

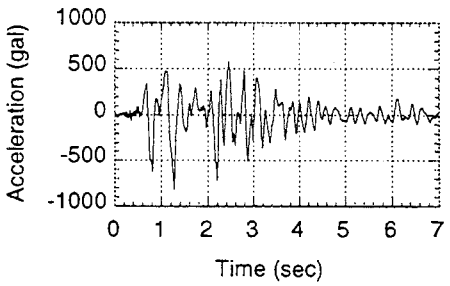

Fig. 5 Input ground acceleration for the 4th viaduct model

1- The displacement of the girder is calculated analytically by the program.
2- By means of a D/A converter, the calculated displacement is converted from digital value to analog one that can be applied to the specimen through the actuator.
3- Immediately after the actuator gives the required displacement to the specimen, the restoring force is measured using the displacement transducer fixed to the specimen at the same level of the actuator, The computer records this restoring force after converting the data from analog to digital through an A/D converter.
4- The previous restoring force is used in the next step.
5- The previous steps (step 1-4) are repeated for the entire duration of the input earthquake.

3. TEST RESULTS

The hysteresis loops for all the tested specimens of the viaduct models indicated stiffness degradation, bauschinger effect for both the unloading and reloading and pinching of hysteretic load-deformation curves. The inelastic response behavior of the PC girder changed during conducting the tests because of shear cracks occurred at critical sections. As a consequence, the load carrying capacity deteriorated. Therefore, adequate ductility without decrease of the load carrying capacity should always be maintained.

3.1. Reversed cyclic loading tests

Fig. 6 shows the load-displacement curve of specimen A-1. The test was continued, after reaching the ultimate load, till the load decreased to about 80% of the ultimate load. In the left side of the load-displacement curve, the maximum displacement was about 11 times the yielding displacement of the reinforcing bars and about 3 times the yielding displacement of the prestressing tendon. In the right side of load-displacement curve, the maximum displacement was about 13 times the yielding displacement of the reinforcing bars. The hysteresis loop shows that the deformational capacity is different between the two directions of load application because of the unsymmetric arrangement of prestressed tendons. The skeleton curve for the left side of the load-displacement curve can be approximated by a skeleton curve for prestressed concrete because the relative contribution of prestressing tendon is dominant in the resulting response behavior. On the other hand

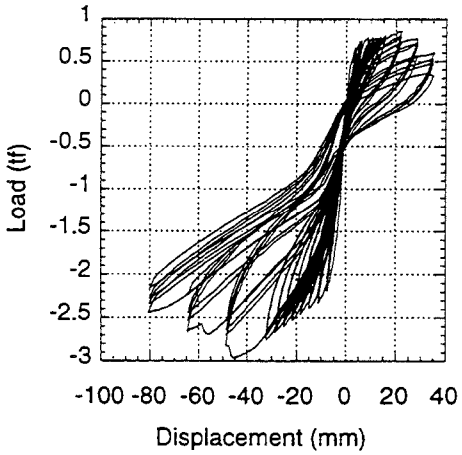

Fig. 6 Load-displacement curve for specimen (A-1)

the skeleton curve for the right side of the load-displacement curve can be approximated by a tri-linear model for reinforced concrete member.

Fig. 7 shows the load-displacement curve for specimen A-2. After the ultimate load was reached, the test was continued on the left side of the load-displacement curve till the load decreased to about 80% of the ultimate load. The test was then stopped in this direction. The corresponding displacement reached about 4 times the yielding displacement of the prestressing tendon D17. At this stage of the test, the prestressing tendon D11 that resisted the positive direction of load application did not reach yielding. Consequently, the test continued in this positive direction till the displacement reached about 8.5 times the yielding displacement of the reinforcing bars. It can be observed from the hysteresis loop that the skeleton curve for the right side of the load-displacement curve can be approximated by a skeleton curve for prestressed concrete. The last observation can be attributed to the relative ratio of prestressing tendons to reinforcing bars in the specimen. The ultimate load is different in the two directions of load application because of the unsymmetrical arrangement of prestressing tendons and reinforcing bars in the cross section.

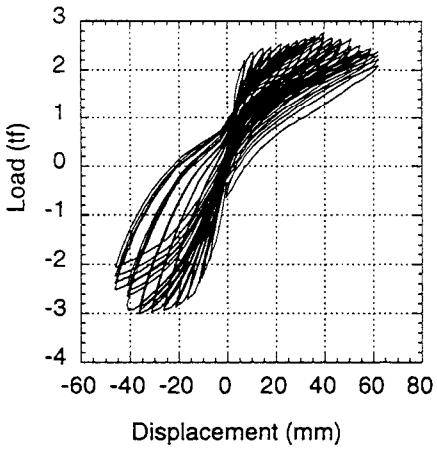

Fig. 7 Load-displacement curve for specimen (A-2)

Fig. 8 shows the load-displacement curve for specimen A-3. The test was performed after yielding of the prestressing tendons till the displacement reached about 2.5 times the yielding displacement of the prestressing tendons. The skeleton curve for both the right and left sides of the load-displacement curve can be approximated by a skeleton curve for prestressed concrete because the resistance of the cross section is dependent mainly on the prestressing tendons rather than the reinforcing bars.

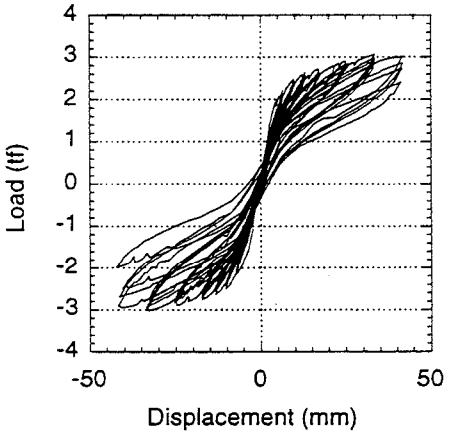

Fig. 8 Load-displacement curve for specimen (A-3)

3.2. Substructured pseudo-dynamic test

Fig. 9 shows the time history of the actuator load for the substructured pseudo-dynamic test of specimen B of the 4th viaduct model shown in Fig. 3. The resulting hysteresis loops is shown in Fig. 10-C & 10-D in which the bauschinger effect and pinching of the hysteresis loops can be observed. The hysteresis loops for the other members are shown in Fig. 10-A, 10-B, 10-E and 10-F. It can be seen that not only the RC piers but also the PC girders undergo extensive damage during the earthquake excitation. The time history of the response acceleration in Fig. 11 shows that the time

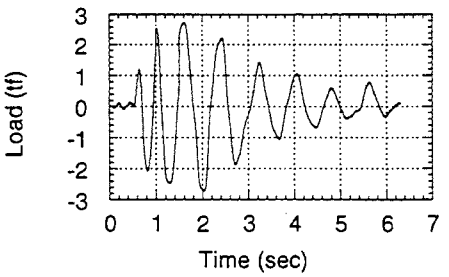

Fig. 9 Time history of actuator load for the 4th viaduct model

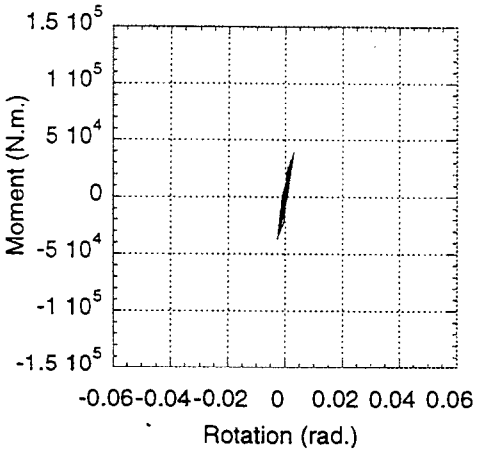

Fig. 10-A Moment rotation curve for top joint of member No. 1

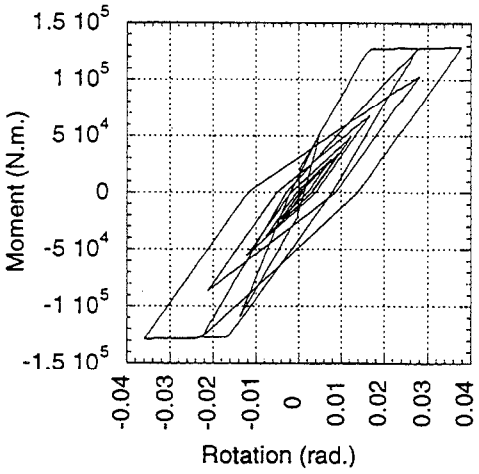

Fig. 10-B Moment rotation curve for end point of member No 1

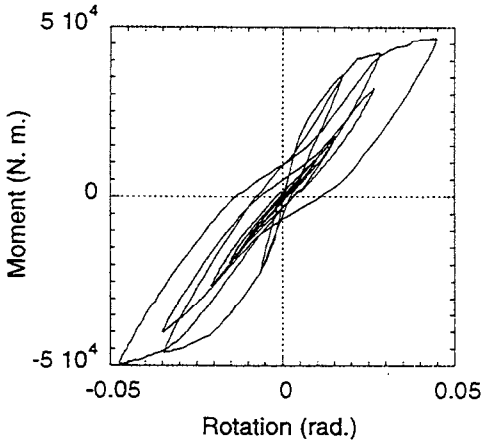

Fig. 10-C Moment rotation curve for left point of member No 2

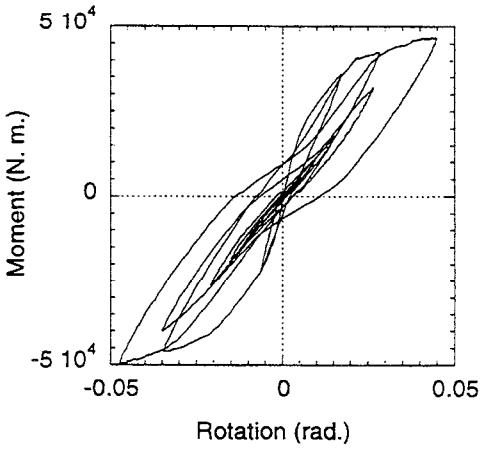

Fig. 10-D Moment rotation curve for right point of member No 2

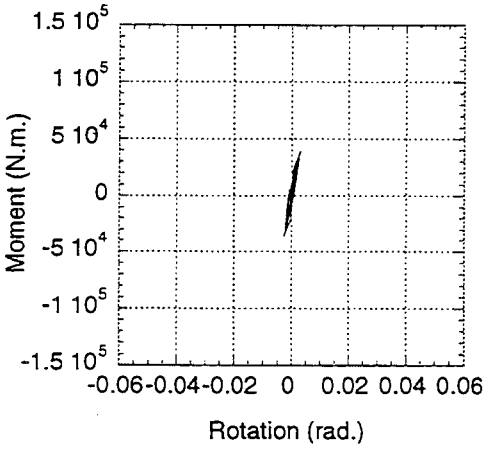

Fig. 10-E Moment rotation curve for top joint of member No. 3

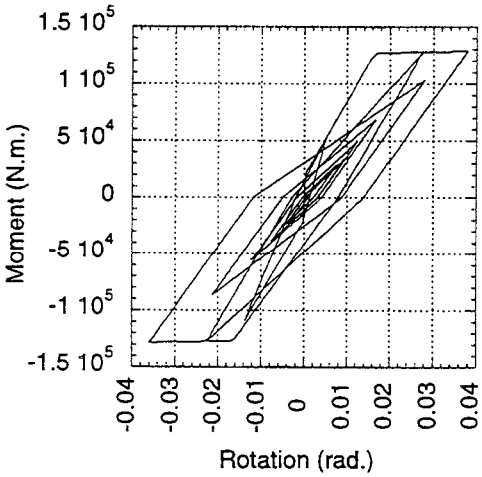

Fig. 10-F Moment rotation curve for end point of member No 3

Fig. 10 Experimental moment rotation curves for substructured pseudo-dynamic test of the 4th viaduct model

and direction of the max. acceleration are consistent with the time and direction of the max. input ground acceleration. The max. acceleration was about 12 m/sec^2. The time history of the displacement shown in Fig. 12 verified the previous observation.

The previous viaduct model was treated analytically using the same program used for analyzing the RC piers during the substructured pseudo-dynamic test. The time histories for acceleration and displacement are shown in Fig. 13 and Fig. 14. The corresponding hysteresis loops are shown in Fig. 15-A to Fig. 15-F for both the PC girder and the RC piers. A comparison between the analytical and experimental results showed good agreement .

After the completion of the pseudo-dynamic test, a cyclic loading test for the same specimen was conducted. Fig. 16 shows the resulting load-displacement curve. The test continued till the displacement reached about 5 times the yielding displacement of the prestressing tendons.

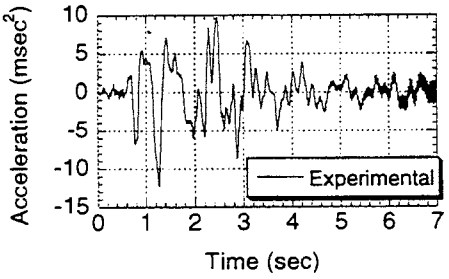

Fig. 11 Acceleration time history of the 4th viaduct model

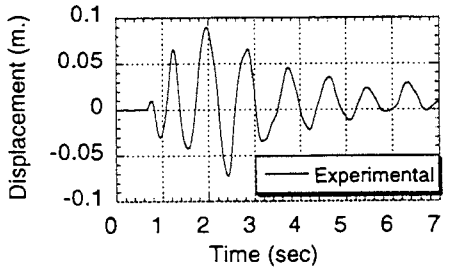

Fig. 12 Displacement time history of the 4th viaduct model

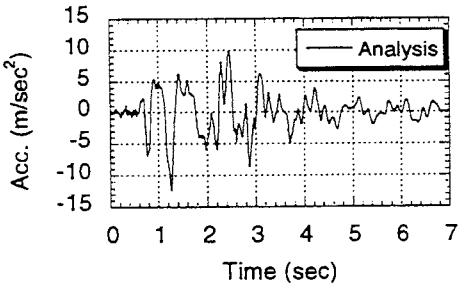

Fig. 13 Acceleration time history of the 4th viaduct structure

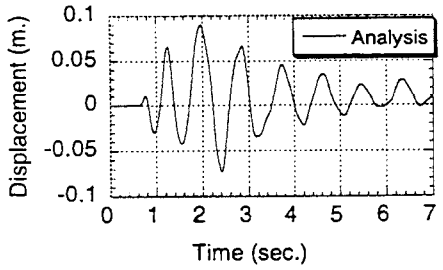

Fig. 14 Displacement time history of the 4th viaduct structure

4. CONCLUSIONS

In order to clarify the inelastic response behavior of partially PC girders of a viaduct under severe earthquake, four small scale PC specimens were made which can represent half of a PC girder of a viaduct model structure. The main difference among the specimens was in the relative ratio of prestressing tendons to reinforcing bars. While cyclic loading tests were carried out for three specimens, substructured pseudo-dynamic test was carried out for the 4th viaduct model. One component model was used for analyzing the RC piers. After the completion of the substructure pseudo-dynamic test, cyclic loading test was conducted till failure of the specimen. Response analyses were also conducted using the same

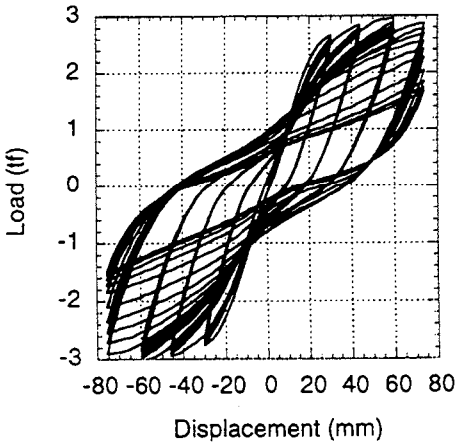

Fig. 16 Load displacement curve for cyclic loading of specimen (B)

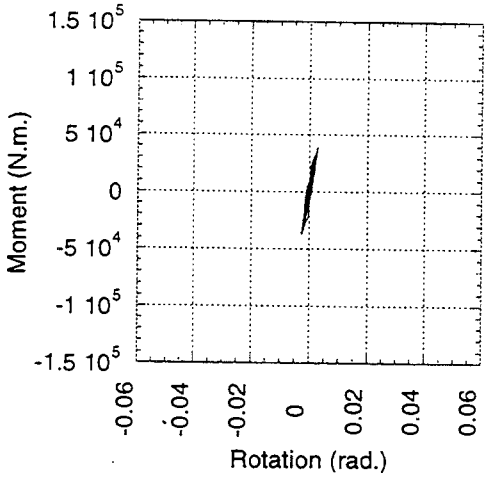

Fig. 15-A Moment rotation curve for top of member No.1

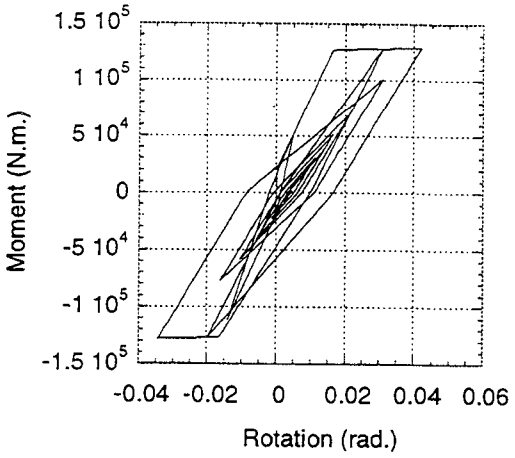

Fig. (15-B) Moment rotation curve for bottom end of member No. 1

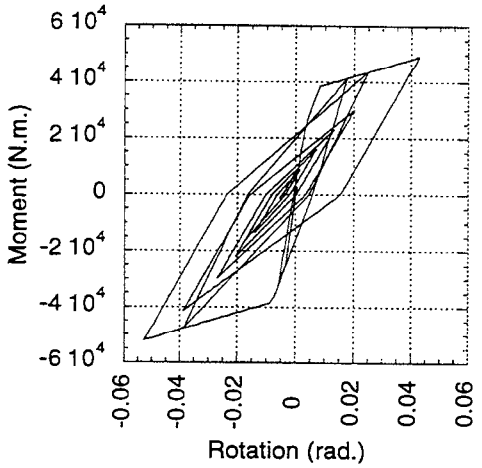

Fig. 15-C Moment rotation curve for left end of member No. 2

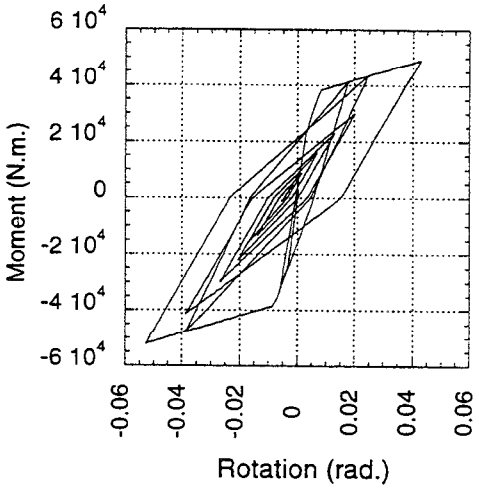

Fig. 15-D Moment rotation curve for right end of member No. 2

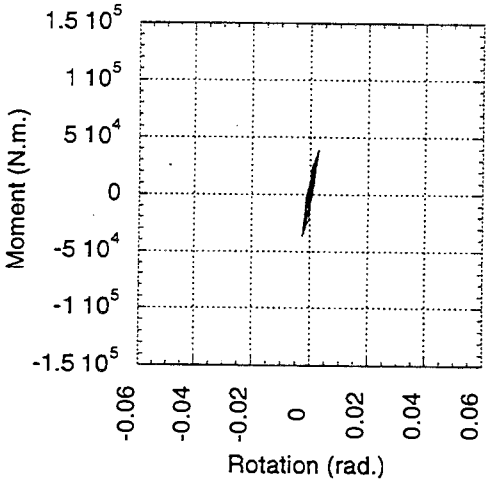

Fig. 15-E Moment rotation curve for top of member No.3

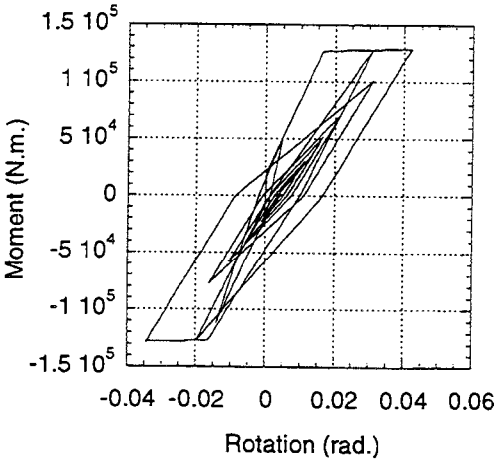

Fig. (15-F) Moment rotation curve for bottom end of member No. 3

Fig. 15 Analytical moment rotation curves for the 4th viaduct model

viaduct model and then a comparison between both the analytical and experimental results was performed. From experimental and analytical results, it can be concluded that:

1) Not only the RC piers but also the PC girders are subjected to inelastic deformation that may cause a considerable damage. As a consequence, adequate care should be given to the PC girder design to satisfy the requirements of a seismic resistant structure.
2) In general, since PC girder is designed mainly to resist dead and live loads, Prestressing tendons and steel bars are arranged unsymmetrically in the cross section. Therefore, they can not resist the reversed loading resulted from earthquake excitation whereas one direction will suffer severe damage.
3) A good agreement between the analytical and experimental results for the 4th viaduct model was obtained.
4) The inelastic response behavior of PC girder of a viaduct can be remarkably changed due to shear cracks. Consequently, the load carrying capacity decreases for all specimens. Therefore, adequate ductility without decrease of the load carrying capacity should always be maintained in order to ensure a seismic resistant structure of the viaduct girders.

ACKNOWLEDGMENT

The author would like to acknowledge the cooperation provided by members of R/C lab. of Saitama university during the experimental program. The financial support of Grant-in-aid of the Ministry of Education, Science and Culture is greatly appreciated.

REFERENCES

1. Giberson, M.F., "Two Nonlinear Beams With Definitions of Ductility, Proc. of ASCE, Vol. 95, No. ST2, 1969.
2. Mutsuyoshi, H., Machida, A., Sadasue, K., and Oba, S. "Earthquake Response Behavior of First-Level Girder in R/C Frame Structure Based on Pseudo-dynamic Test Method," Transactions of JCI, Vol. 14, pp.289-296, 1992.
3. Otani, S., "Inelastic Analysis of R/C Frame structures," Proc. of ASCE, Vol. 100, No. ST2, 1974.
4. Takeda, T., Sozen, M. A., and Nielsen, N. N., "Reinforced Concrete Response to Simulated earthquake," Journal of the Structural Division, ASCE, Vol. 96, No. ST2, paper 7759, Dec., 1970, pp.2557-2573.

EFFECT OF VERTICAL GROUND MOTION ON BRIDGE DECK RESPONSE

Chih-Peng Yu, Daniel S. Broekhuizen, Jose M. Roesset,
John E. Breen, and Michael E. Kreger
The University of Texas at Austin
Austin, Texas

ABSTRACT

The effect of vertical ground motion on vertical response accelerations of bridge decks is evaluated. A series of parametric studies of the seismic response of highway bridges subjected to various accelerograms recorded during the 1994 Northridge earthquake is conducted in the frequency range using three-dimensional linear member formulation with distributed masses. Analyses are carried out both with two-dimensional planar models and, to a limited extent, three-dimensional models. The parameters considered in the study include not only the bridge dimensions but also the stiffness characteristics of the foundations.

INTRODUCTION

Vertical components of ground motion are rarely taken into account in the seismic design of regular buildings or highway bridges. Seismic design of these structures is normally performed considering either one horizontal component of motion at a time, or occasionally, two horizontal components of motion, but neglecting always the vertical motion. It is commonly believed and widely accepted that vertical vibrations are much less important than horizontal vibrations and that they can be neglected without impairing the safety of structures. This is because vertical accelerations decay rapidly with distance and are normally smaller than the horizontal accelerations, unless one is close to the causative fault.

One of the potential effects of vertical accelerations on seismic response of highway bridges is possible cracking on the side of the girder without post-tensioned reinforcement or with minimum reinforcement designed using a load balancing technique. This could occur if girders were subjected to significant upward accelerations (larger than gravity). The effect would be more important if the vertical component had a significant amount of energy in the high frequency range (close to the natural vertical frequency of the structures).

BACKGROUND

On Monday, January 17, 1994, a magnitude 6.8 earthquake occurred in Northridge, California. Vertical accelerations in excess of 0.6 g were recorded at various locations. Among them, a vertical acceleration of 1.18 g was recorded at Tarzana-Cedar Hill [1]. Thus, vertical accelerations were unusually large in the Northridge area due to the proximity to the fault. Yu et al. [2] computed ratios of maximum vertical to maximum horizontal ground accelerations recorded by the U.S. Geological Survey (USGS) and the California Strong Motion Instrumentation Program (CSMIP) [3,4] and determined that, except for the Arleta records of CSMIP (which had a ratio of approximately 1.7) and a limited number of other

points, maxima for vertical components of motion were approximately half of maxima for corresponding horizontal components of motion. In current UBC and AASHTO specifications, the vertical component of motion can be neglected or has an amplitude of one-third that of the horizontal motion if it is considered. Therefore, it is obvious that vertical accelerations can be higher in the epicentral region than those implemented in the codes.

For prestressed concrete girders designed using the load balancing method, the bending moment due to eccentric post-tensioning is normally used to balance approximately two-thirds the bending moment due to dead load. Absence of the dead load or vertical forces acting upward could then cause tension cracks. Broekhuizen [5] calculated the tensile stresses in the box girders of three California bridges due to a 1 g upward acceleration and compared them with allowable tensile stresses specified by the AASHTO specification. He concluded that any tensile cracks that may possibly occur due to the effect of vertical accelerations should not be a major problem since present design practice is to provide continuous reinforcement in the top of girders over piers and at the bottom of girders at mid span.

OBJECTIVE AND SCOPE

The objective of the study was to investigate the potential effect of vertical accelerations on the dynamic response of bridges with prestressed concrete girders or decks. Realistic data from three bridges (Ramps L, M, and C of the SR14/15 interchange) and the accelerograms recorded by CSMIP at Sylmar Hospital were used. The Sylmar Hospital station has an epicentral distance of approximately 16 kilometers, and the bridge site is approximately 3 kilometers west of the station.

A series of parametric studies using symmetric simple frames and bridges was carried out first to provide an initial impression of the importance of vertical response accelerations and vertical ground motions. For the simple models, cross section properties associated with pier-3 and the box girder of Ramp-L of the SR14/15 interchange were used [5,6]. Because real bridges normally consist of unsymmetric configurations with many spans and different foundation types, the relation between structural dimensions and maximum vertical accelerations due to a given ground motion is more difficult to predict than for simple models. Three interior frames of Ramp-L were used to study whether the responses obtained with simple models can be generalized to predict the overall response of more-complicated bridges. Ramp-L was finally studied using both straight and curved models to investigate the effect of the assumed configurations (idealized straight versus actual curved shape) on the computed response.

EARTHQUAKE CHARACTERISTICS

Figure 1 illustrates the accelerograms and absolute acceleration spectra for the Sylmar records. Figures 1(a) and 1(b) show the characteristics of the ground motion in the E-W direction with a maximum ground acceleration of 0.6 g. Two significant peaks, signifying predominant frequencies, can be observed in Fig. 1(b); one in the range from 1.5 to 3 Hz and the other at approximately 9 Hz. Figures 1(c) and 1(d) show the corresponding curves for the N-S component with a maximum ground acceleration of 0.84 g. The predominant frequency

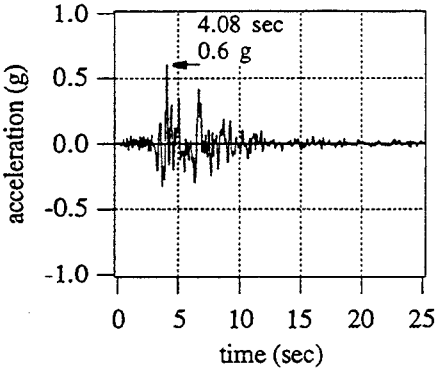

(a) accelerogram in E-W direction.

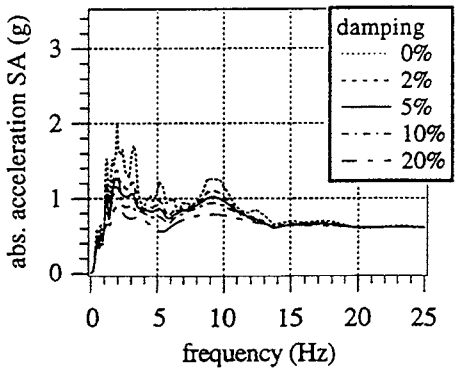

(b) SA spectrum for E-W component.

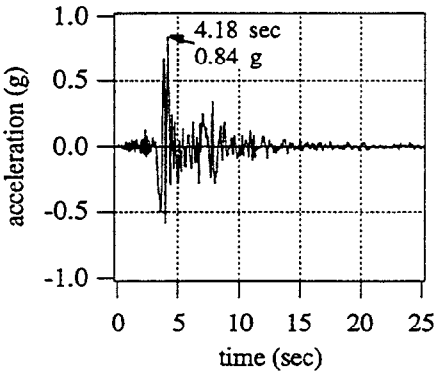

(c) accelerogram in N-S direction.

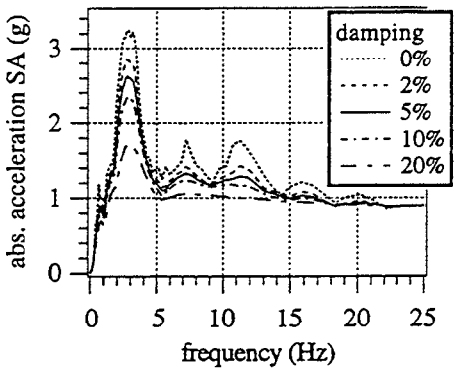

(d) SA spectrum for N-S component.

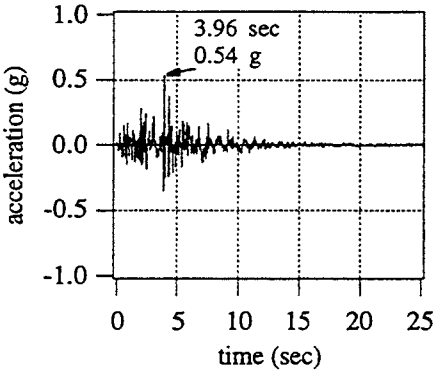

(e) accelerogram in vertical direction.

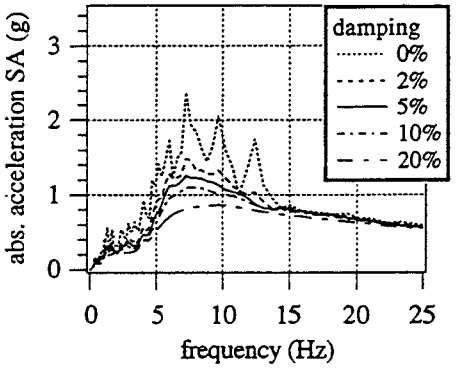

(f) SA spectrum for vertical component.

Fig. 1 Time histories and absolute acceleration spectra for Sylmar Hospital records

is approximately 3 Hz with two minor peaks at 7 and 11 Hz. Finally, Figs. 1(e) and 1(f) show waveforms and spectra for the vertical direction, which had a maximum acceleration of 0.54 g. The response spectra exhibit a broad range of frequencies from 6 to 12 Hz with significant amplitudes. Ground motions obtained at four other CSMIP stations during the Northridge earthquake were also used by Broekhuizen [5] with the 3-D bridge model to investigate the relative importance of vertical ground motions to vertical girder accelerations. The additional ground motions were obtained at the Downtown station at Pacoima Dam, LACC North station at Century City, LA County Fire Station at Newhall, and City Hall Grounds station at Santa Monica. The records obtained at these locations had maximum vertical accelerations ranging from 0.2 to 1 times the maximum horizontal ground accelerations.

NUMERICAL MODEL

A 3-D linear member formulation in the frequency domain was implemented allowing consideration of distributed transverse and axial masses and rotational mass moments of inertia as well as shear deformations. This model is able to reproduce all wave propagation effects. To account for soil-structure interaction effects, dynamic foundation stiffnesses were derived using elastic soil springs and dashpots added at the sides and bottom of the soil foundation interfaces. These dynamic stiffnesses were then added to the structural model at the base of the piers. Once the total dynamic stiffness matrix was assembled, the equilibrium equations were solved for each specific frequency using as input for the support motion the amplitude obtained from the Fourier transform of the earthquake record.

Ramp-L of the SR14/15 interchange is a curved bridge with single-bent columns and multi-cell box girders. The bridge was modeled as a space frame using the 3-D linear member formulation with equivalent cross section properties. Although the box girder is usually skewed with respect to the longitudinal axis, the cross section properties were calculated neglecting the skew and inclination of the bridge.

For soil-structure interaction, the soil springs and dashpots were calculated based on soil data obtained by Stokoe [7] near Olive View Hospital. The formulation and data for the structural members as well as the soil properties are summarized by Yu [6].

PARAMETRIC STUDY

Vertical acceleration of the deck can be due directly to vertical ground motion (exciting the vertical modes of vibration) or result from the coupled modes associated with flexural vibrations of the columns and girders due to horizontal ground motion. The relative importance of these modes and of the vertical vibration depend on the frame configuration (including span length, column height, and connection type) and on the frequency content of the ground motion. Effects of changing span length and column height on natural frequencies of simple frames were studied first using symmetric single-span frames and three-span bridges with columns fixed at the base. Figure 2 illustrates the configurations of the simple frames and three-span bridge.

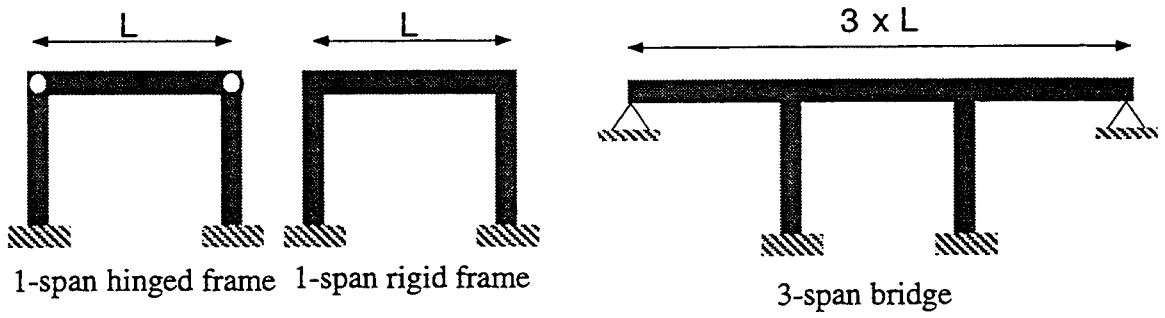

Fig. 2 Simple models for parametric studies

Vertically-Induced Acceleration

Figure 3 illustrates the influence of various span lengths and column heights on the vertical response of bridge decks for simple frames and three-span bridges. Figures 3(a) and 3(b) indicate that the highest maximum accelerations (at mid span) occur for span lengths near 20 to 30 m. This is supported by Fig. 4 which shows transfer functions for vertical accelerations at mid span due to a unit vertical acceleration at the supports. As mentioned earlier, the vertical component of the Sylmar records has predominant frequencies ranging from 6 to 12 Hz, and thus a trend of increasing vertical response accelerations is expected when natural frequencies of the models approach this range. The three-span model has slightly higher responses than the single-span frames since the former has larger transfer function amplitudes at its frequency peaks.

Figures 3(c) through 3(f) indicate for span lengths of approximately 30 m that large vertical accelerations occur for column heights of 10 to 15 m, then the responses decrease up to a column height of approximately 40 m, and then the trend reverses and vertical response increases for longer columns. As column heights initially increase beyond 10 to 15 m, the frequency of the fundamental vertical mode drops below the predominant frequency range for the vertical component of ground motion. As the columns get longer, the response frequencies for the higher modes of vertical response decrease and fall into the predominant frequency range for the vertical component of ground motion. For longer span lengths (for instance, the 61 m length used to assemble the data in Figs. 3(e) and 3(f)), vertical response appears to increase with increase in column height. Once again, this is due to higher response modes approaching the predominant frequency range for the vertical component of ground motion. These observations are supported by transfer functions computed by Broekhuizen [5].

Horizontally-Induced Vertical Acceleration

For the three-span bridge, lower horizontally-induced vertical accelerations are expected because the abutments at the two ends restrict movement. It is shown in Fig. 5 that only single-span rigid frames with long span lengths and short column heights experience significant vertical accelerations due to the horizontal base excitation. Figures 5(a) and 5(b) show an increasing trend for maximum acceleration as span length increases. This occurs

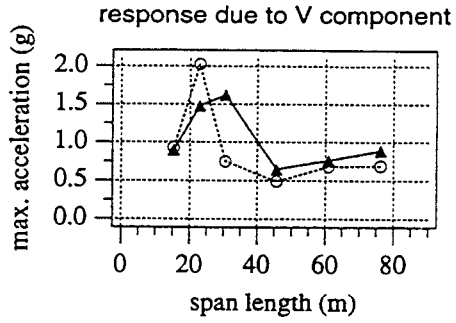

(a) column height = 6m

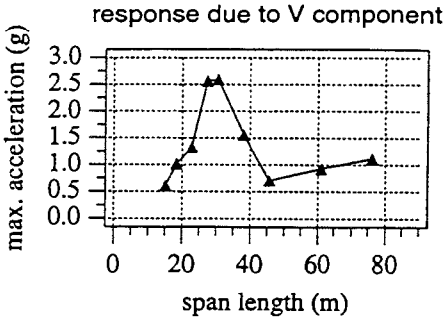

(b) column height = 6m

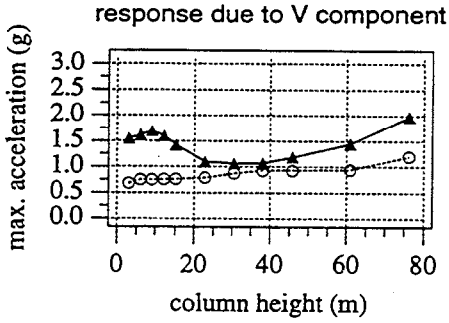

(c) span length = 30.5m

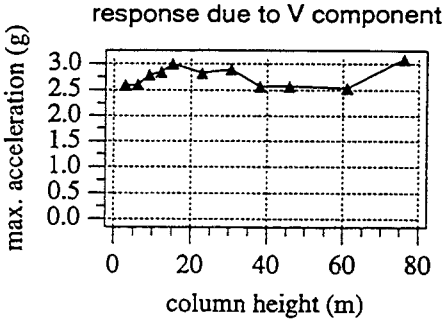

(d) span length = 30.5m

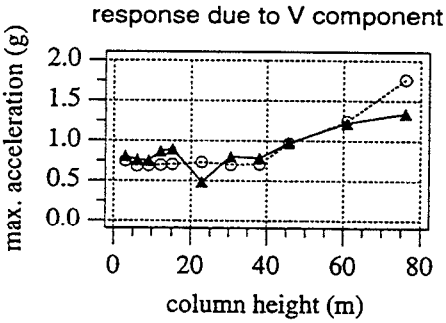

(e) span length = 61m

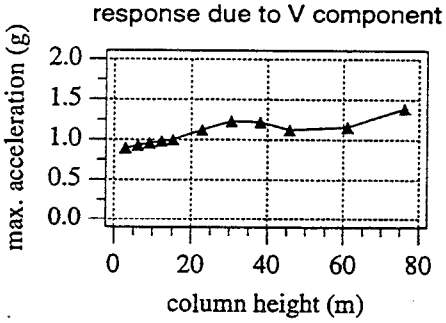

(f) span length = 61m

(a) (c) (e) : responses of 1-span frame

(b) (d) (f) : responses of 3-span bridge

Fig. 3 Variation of response accelerations at mid-span with span length and column height due to Sylmar Hospital Vertical record

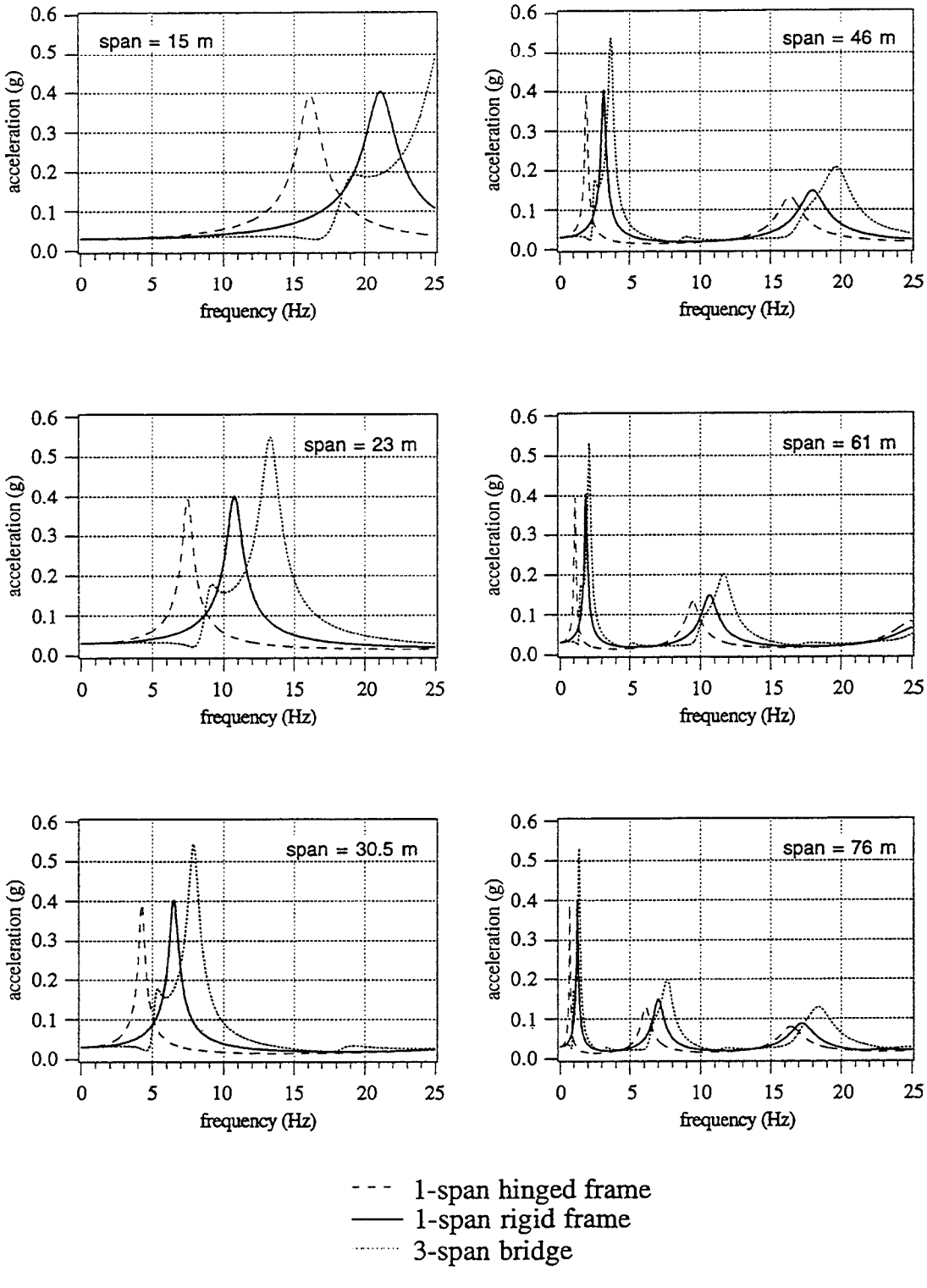

Fig. 4 Transfer functions for vertical accelerations due to a unit vertical acceleration at the supports

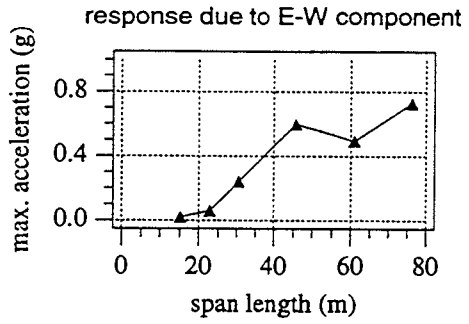

(a) column height = 6m

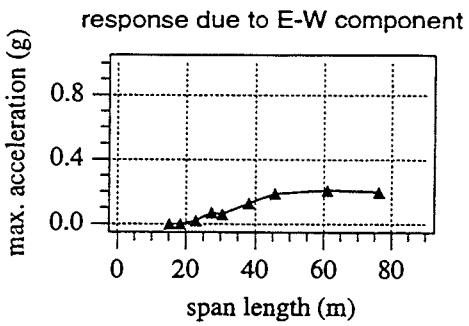

(b) column height = 6m

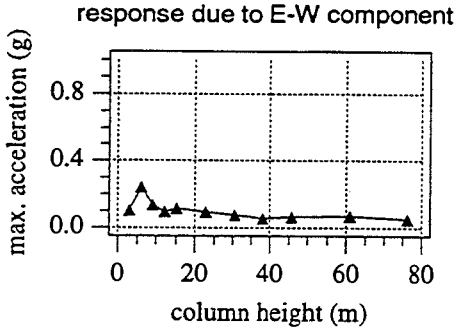

(c) span length = 30.5m

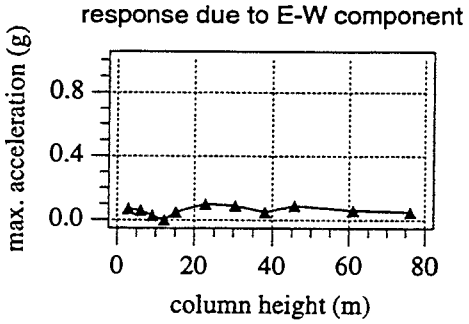

(d) span length = 30.5m

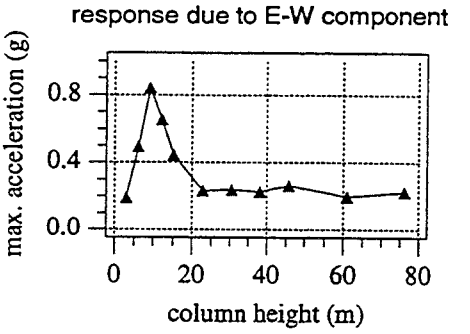

(e) span length = 61m

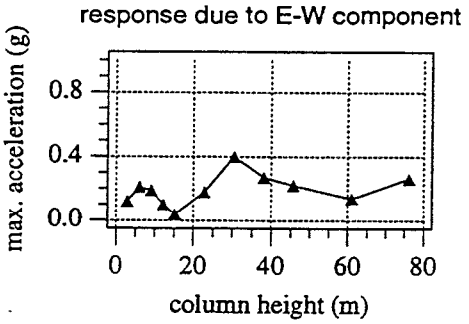

(f) span length = 61m

(a) (c) (e) : responses of 1-span frame

(b) (d) (f) : responses of 3-span bridge

Fig. 5 Variation of response accelerations with span length and column height at quarter-spans due to Sylmar Hospital E-W record

because the natural frequencies of the structures move towards the dominant frequency range of the E-W component of motion (1.5 to 3 Hz) as span length increases. Figures 5(c) through 5(f) illustrate that the largest amplification for the single-span frames occurs for a column height from 6 to 9 m. On the other hand, for the three-span bridges, the largest amplification occurs for longer columns. For the three-span bridges with 61 m spans, a column height of approximately 30 m leads to a higher maximum acceleration than do shorter columns.

From this portion of the study, it appears that horizontal ground motion could be important for bridges consisting of long spans with columns of certain heights. The critical height of the columns depends on the horizontal stiffness of the bridge and the horizontal constraints applied to the system. Based on the realistic data used for the above study, it seems that short columns tend to result in high amplification for single-span frames while the constraints provided by the abutments can lead to higher values of the critical column height.

Soil-Structure Interaction

Accounting for soil-structure interaction effects implies a more flexible system, and thus, an effective natural period longer than that of the structure on a rigid base. In addition, the effective damping of the system will also be different and often larger than that of the structure alone due to the energy dissipated into the soil. The effect of soil-structure interaction on vertical deck acceleration was investigated for different foundation types. Two foundation types were considered: shallow footings and deep (pile) foundations. Both footings resting directly on the soil and supported by piles were considered for the first type. Friction and end-bearing piles were considered for the second. Figure 6 illustrates the resulting types of foundations; (a) spread footings, (b) footings supported by a pile group, (c) friction piles, and (d) end-bearing piles socketed in rock.

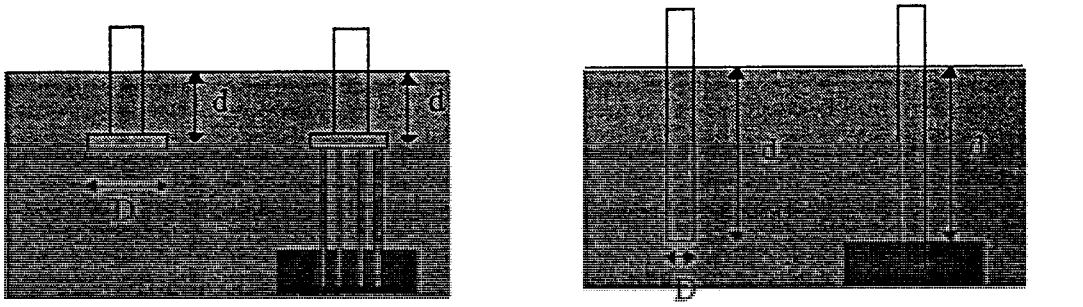

a. spread footings b. pile supported footings c. friction piles d. end bearing piles

Fig. 6 Foundation types

In these foundation models, embedded portions of the piers were assumed to have the same cross section properties as the columns. The dimension of the footings was three times the diameter of the piers. The bottom springs and dashpots for pile-supported footings were calculated from a pile group with 32 concrete piles (8 rows in the longitudinal direction by 4

in the transverse direction with 1.07 m spacing) having 0.4 m diameter and 7.6 m length. These properties were selected from the data presented in reference [6] for the pile group supporting pier-5 of Ramp-M. The shear wave velocity of the soil was 183 m/sec.

Figures 7 and 8 show the maximum vertical accelerations at mid span due to the vertical components of motion for simple models supported by different foundations (including rigid bases). The figures demonstrate that floating foundations tend to result in lower maximum accelerations than stiffer foundations. Including the foundations leads to similar overall trends as obtained for rigid bases. The differences between the two stiffer foundations and the rigid bases are not significant, and the two floating foundations yield approximately the same maximum accelerations for all cases.

The E-W component of motion resulted in vertical accelerations that were typically smaller than those obtained for the vertical component of motion [5]. The various foundation types resulted in very similar results for different span lengths. Increases or decreases in the resulting maximum vertical accelerations depended on how the natural frequency was affected by the foundation and on the frequency content of the horizontal component of motion. The four foundation types resulted in increases in the effective column heights of approximately 3 to 6 m.

Simplified Models versus Complete Model

Figure 9 illustrates simplified models of three interior frames of Ramp-L. Figures 9(a), 9(b), and 9(c) correspond with Frames 3, 2, and 4, respectively. There are two models for each frame; the first (frame model) is the isolated frame separated from adjacent spans, and the second (bridge model) is the frame with its adjacent spans connected to abutments (by means of pin supports). Results obtained with these simplified models were compared to those obtained using the complete model of Ramp-L. Figures 9(d) and 9(e) show the elevation and plan of Ramp-L.

Vertical accelerations were computed for the Sylmar E-W component of ground motion, the vertical component of motion, and the combination of the E-W and vertical components of motion. Figures 10 and 11 illustrate the maximum vertical accelerations computed for the motions listed above for the simplified models and complete model of Frame-3 and Frame-4. In both figures, the predictions for the simplified models are poor for horizontally-induced vertical accelerations and good to very good for vertical excitation. In general, the bridge model appears to yield better predictions of response than the frame model.

Figure 12 shows the comparison between vertical accelerations obtained with the straight and curved models of Ramp-L. Vertically-induced vertical accelerations obtained with these two nine-span models are nearly identical. As expected, the horizontally-induced vertical accelerations predicted using these two models are different. However, as long as the vertical component of motion dominates the vertical acceleration responses, differences between vertical accelerations for the two models subjected to combined E-W and vertical components of motion are relatively small as shown in Fig. 12(c).

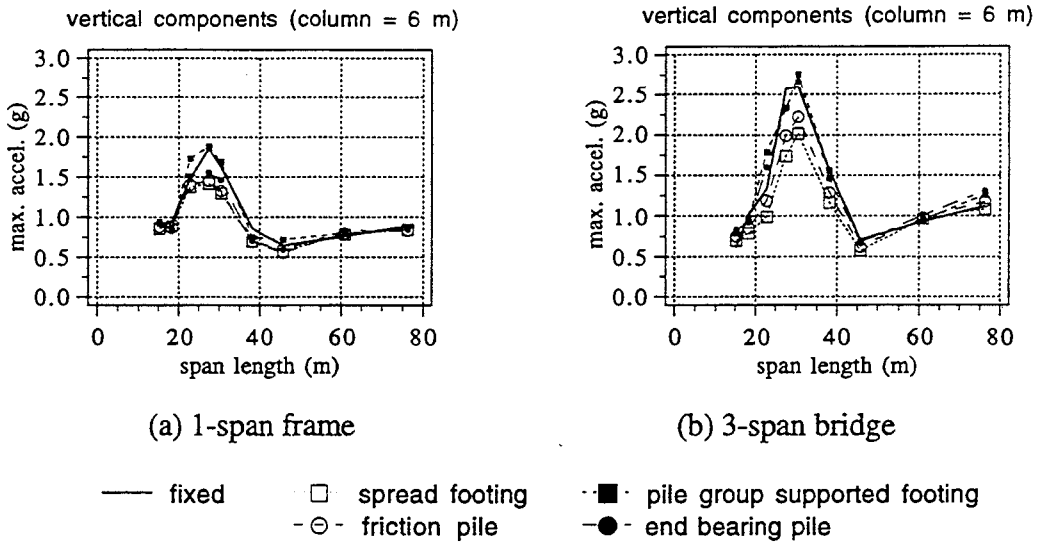

Fig. 7 Effect of foundation types on maximum accelerations for simple models with different span lengths (due to Sylmar vertical component)

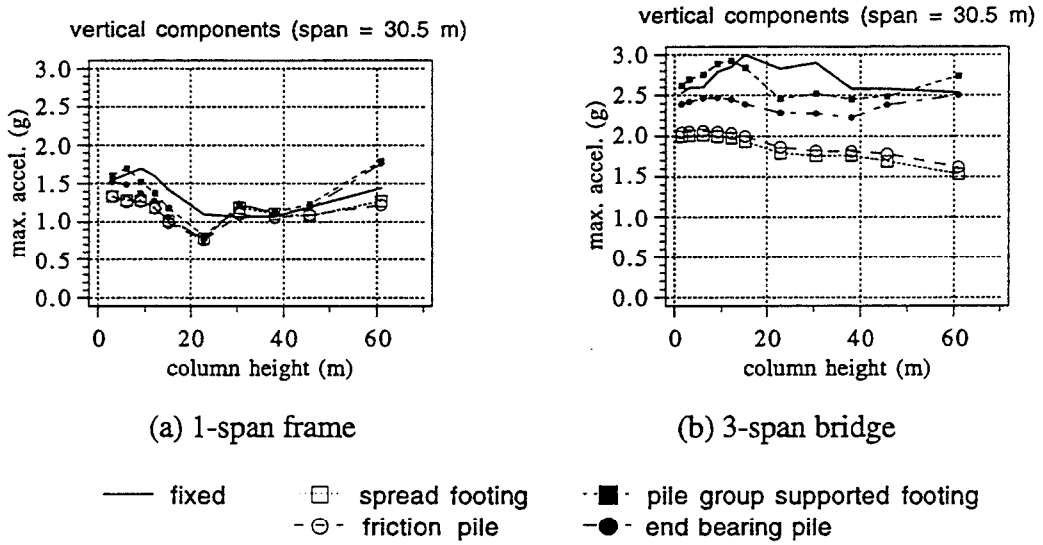

Fig. 8 Effect of foundation types on maximum accelerations for simple models with different column heights (due to Sylmar vertical component)

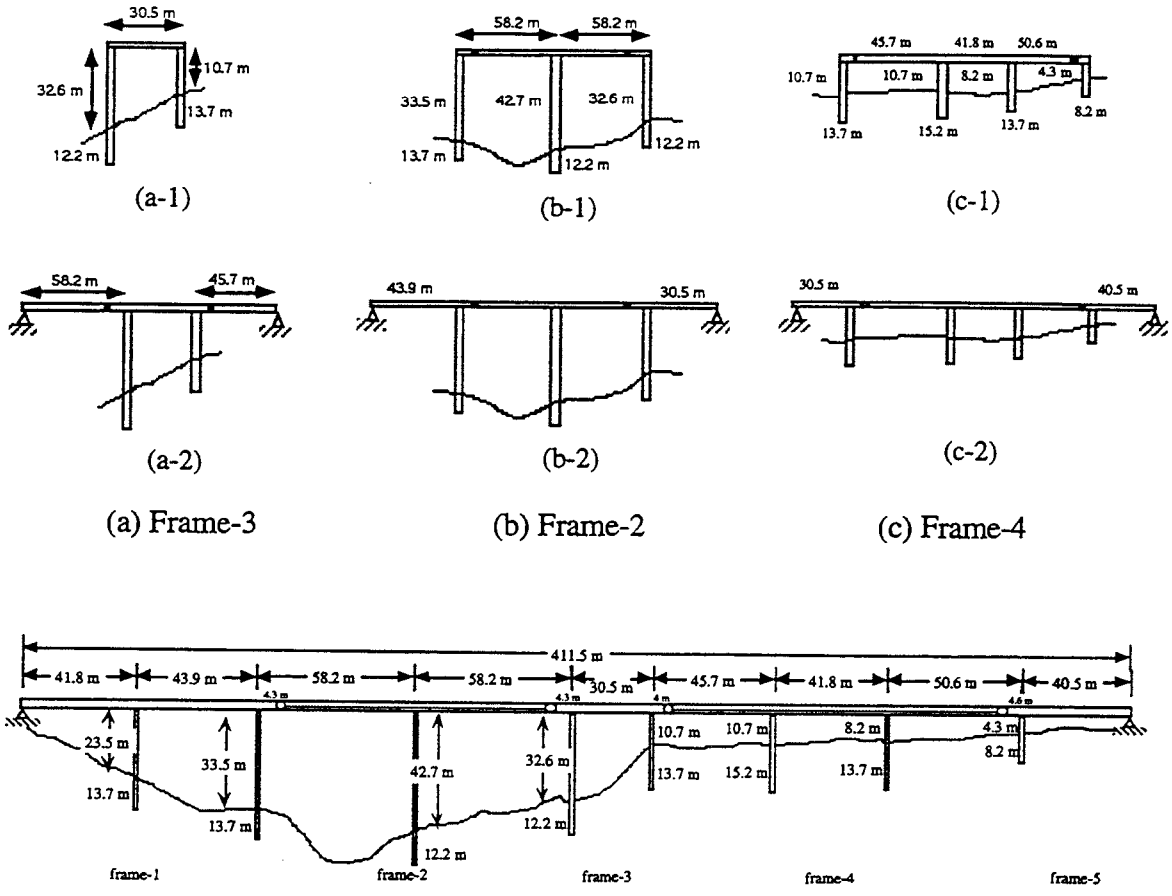

Fig. 9 Simplified models and configuration of Ramp-L

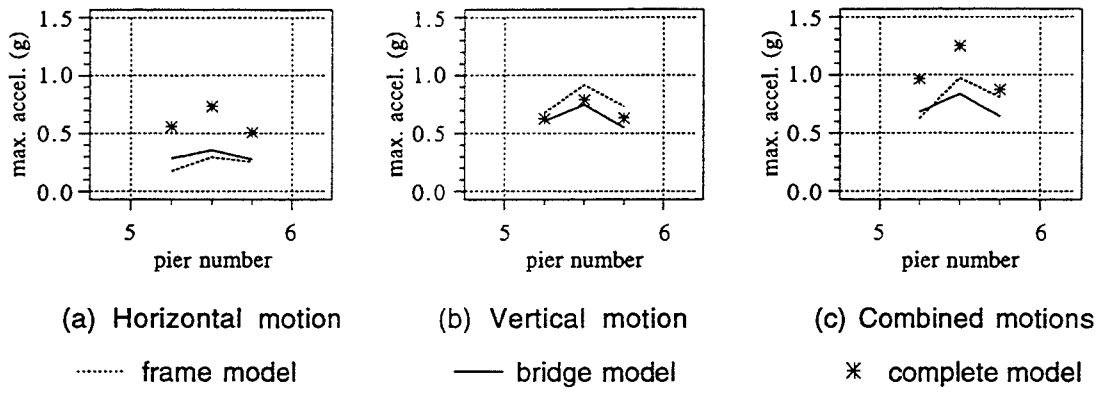

Fig. 10 Comparison between models for Frame-3 (single-span case)

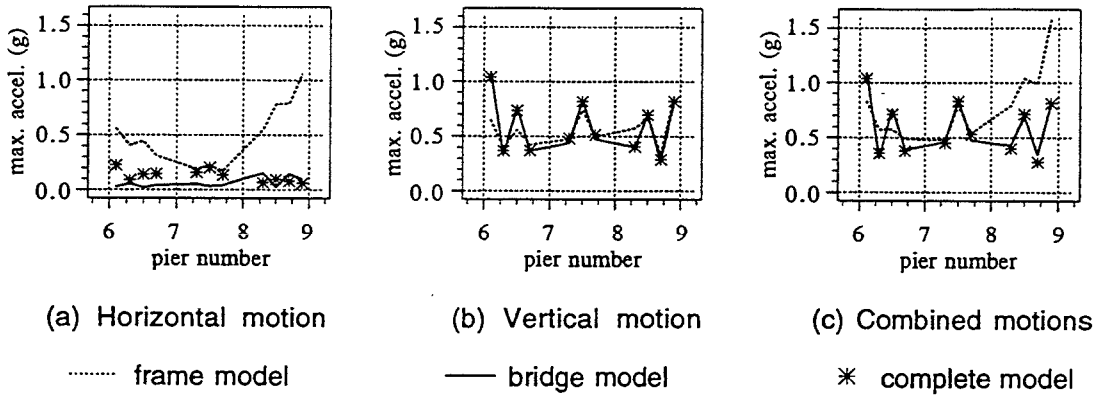

Fig. 11 Comparison between models for Frame-4 (three-span case)

CONCLUSIONS

Several conclusions were derived from the numerical results obtained in this study. They include the following:

- Vertical components of motion provide the most significant input for vertical deck accelerations. The effect of horizontal components can be important when bridges consist of long spans with columns of certain heights (typically short columns). Constraints provided by abutments can result in higher critical column heights.

- Vertical deck accelerations obtained for realistic models were large enough in some cases to crack prestressed concrete super-structures. However, current detailing practice should ensure that reinforcement will be present to preclude unrestricted growth of cracks.

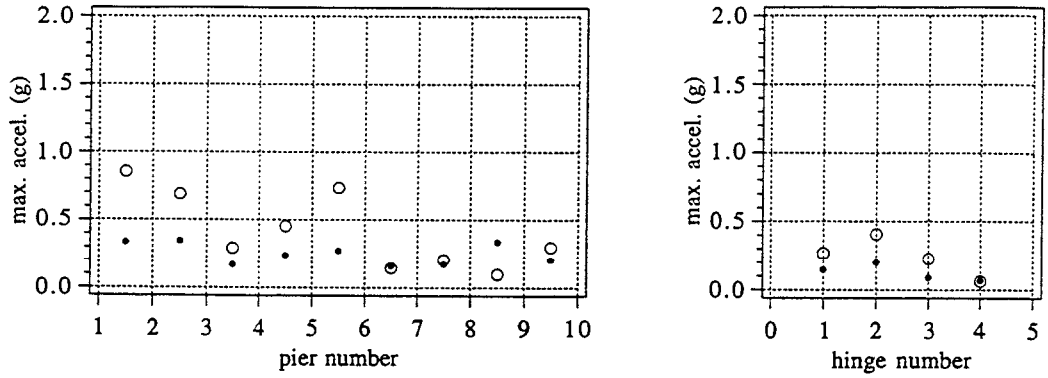

(a) maximum vertical accelerations due to E-W component.

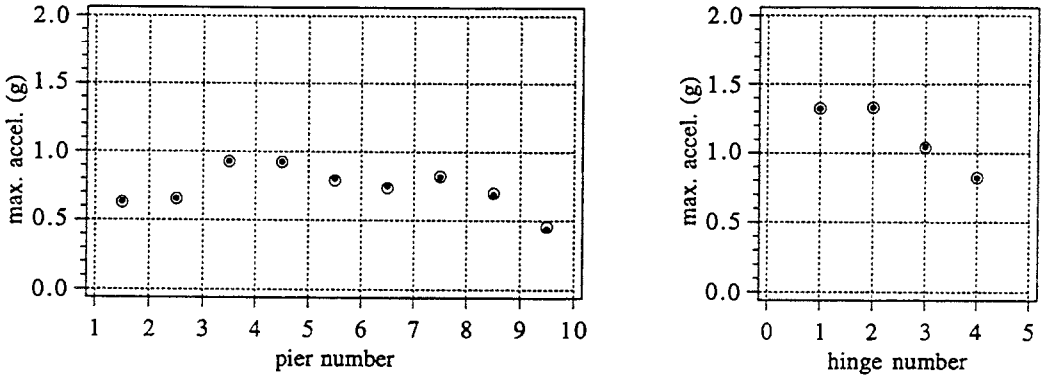

(b) maximum vertical accelerations due to vertical component.

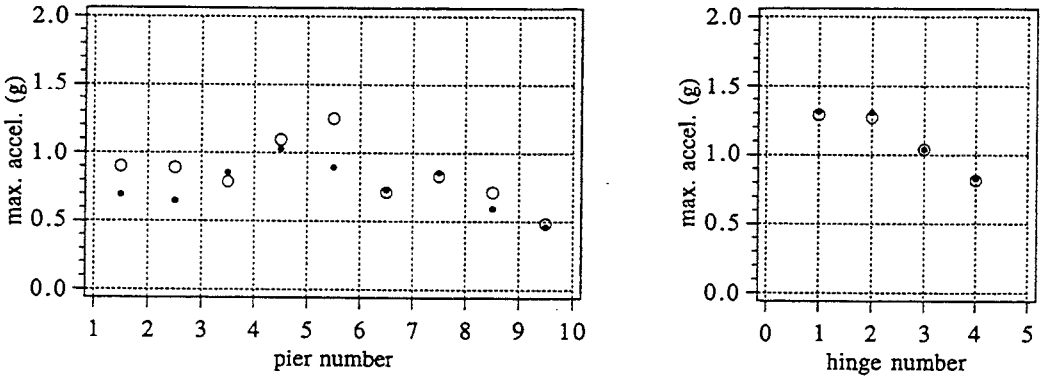

(c) maximum vertical accelerations due to combined E-W and vertical components.

○ straight model ● curved model

Fig. 12 Comparison between straight and curved models for Ramp-L

- Foundation effects can be accounted for by considering a more flexible system. Floating foundations tend to result in lower maximum accelerations than stiffer foundations. The general trends observed for models with fixed bases were not seriously affected by the foundation types.

- The primary conclusions in relation to vertical response due to vertical ground motion obtained from the parametric studies on simple frames remained valid when considering more realistic bridge models. Predictions from simplified models are poor for horizontally-induced vertical accelerations.

- Vertically-induced vertical accelerations obtained with straight and curved models of Ramp-L were nearly identical. Horizontally-induced vertical accelerations predicted using these two models were different. Differences in vertical response of the two models to combined E-W and vertical components of motion were not significant because the vertical component of motion dominated vertical response.

ACKNOWLEDGEMENTS

The authors wish to acknowledge the National Science Foundation for supporting this work. The work was performed at The University of Texas at Austin under NSF Grand No. CMS-9412525.

REFERENCES

1. Darragh, R., et al., "Preliminary Processed Data for Tarzana-Cedar Hill Nursery A from the Northridge Earthquake," California Strong Motion Instrumentation Program, Division of Mines and Geology, Department of Conservation, The Resources Agency, State of California, Report OSMS 94-12B, 1994.
2. Yu, Chih-Peng, Broekhuizen, Daniel S., Roesset, Jose M., and Breen, John E., "Effect of Vertical Ground Motions on Bridge Deck Accelerations," American Society of Civil Engineers, Structural Journal, under review.
3. Darragh, R., Cao, T., et al., "Processed CSMIP Strong-Motion Records from the Northridge Earthquake," Release No. 1 and No. 3, California Strong Motion Instrumentation Program, Division of Mines and Geology, Department of Conservation, The Resources Agency, State of California, Report OSMS 94-06B and Report OSMS 94-09, 1994.
4. Todd, D., Carino, N., et al., "1994 Northridge Earthquake: Performance of Structures, Lifelines, and Fire Protection Systems," National Institute of Standards and Technology, Special Publication 862, ICSSC TR14, 1994.
5. Broekhuizen, Daniel S., "Effect of Vertical Accelerations on Prestressed Concrete Bridges," Master of Science Thesis, The University of Texas at Austin, May, 1996, 245 pp.
6. Yu, Chih-Peng, "Effect of Vertical Earthquake Components on Bridge Responses," Ph.D. Dissertation, The University of Texas at Austin, December 1996, 302 pp.
7. Stokoe, K.H., and Joh, S., Report for NSF project, No. CMS-9416433, in progress.

DEVELOPMENT AND APPLICATION OF A NEW MODEL FOR FRACTURE BEHAVIOR ANALYSIS OF STRUCTURES

Kimiro Meguro
Associate Professor, International Center for Disaster-Mitigation Engineering,
Institute of Industrial Science, The University of Tokyo

Hatem Tagel-Din
Graduate Student, Department of Civil Engineering, The University of Tokyo

ABSTRACT

A new method for fracture analysis of reinforced concrete structures is proposed. The concrete is modeled as an assembly of distinct elements made by dividing the concrete virtually. These elements are connected by distributed springs in both normal and tangential directions. The reinforcement bars are modeled as continuos springs connecting elements together. Local failure of concrete is modeled by failure of springs connecting elements when the stress calculated from forces acting on springs exceed the critical stress. The element formulation and the computer code were developed and the accuracy of the method were verified by comparing many experimental results. In these experiments, the results showed good agreement in determining the failure load, the load-deflection relations, the prediction of crack initiation, crack location and crack propagation. The formulations used to develop this method are simple and efficient in modeling the mechanical behavior of RC structures.

INTRODUCTION

Failure analysis of reinforced concrete structures has been mainly carried out using the Finite Element Method (FEM). However, the FEM assumes that elements are connected by nodes and in most of FEM codes, these nodes are not permitted to separate during the analysis. Moreover, separation of elements at node location results in stress singularity at the crack location. The FE analysis is appropriate especially before the generation of extensive cracking. On the other hand, many techniques were developed to deal with cracks. These techniques, such as Smeared Crack approach[1)], assume that no separation occurs between elements. The effects of cracking are only considered on the element stiffness matrix. Therefore, it is difficult to follow the crack propagation using smeared crack approach. This makes the prediction of the crack initiation, crack location, and crack width or length difficult. Moreover, the use of relatively large-sized elements makes this prediction of cracking properties difficult. While, Discrete Crack Methods[1)] assume that the location of cracks and direction of crack propagation are predefined .

Many other methods were developed to deal with these problems. The Rigid Block and Spring Method, RBSM[2)], is one of them. The main advantage of this method is that it simulates the cracking process with relatively simple technique compared with the FEM, while the main disadvantages is that crack propagation depends mainly on the element shape, size and arrangement. Spring stiffness is not calculated accurately so that the calculated displacements were not of reliable accuracy. Each element cannot behave as one body independent from surrounding elements. Thus the RBSM can be applied only to predict failure load.

One of the recent methods to deal with fracture analysis of concrete is the Modified or Extended Distinct Element Method (MDEM or EDEM)[3)]. This method can follow the highly non-linear geometric changes of the structure during failure, however, the main disadvantages of this method are that in some cases accuracy is not enough for quantitative discussion and it needs relatively long CPU time compared with the FEM.

The proposed method assumes that the region studied is an assembly of virtually divided small blocks. These blocks are connected by distributed springs in normal and tangential directions. The formulations for spring stiffness and spring failure conditions were developed so that the springs surrounding the element totally represent the block deformations and failure. Although simple material models and failure criteria were incorporated, the highly non-linear behavior, i.e. crack initiation and crack propagation of the studied problems could be followed with high accuracy till reaching global failure of the structure.

NUMERICAL MODEL

Element Formulation

The two elements shown in Figure (1) are assumed to be connected by pairs of normal and shear springs located at contact points which are distributed around the element edges. Referring to Figure (1), each pair of springs totally represent stresses and deformations of a certain area of the studied elements. The total stiffness matrix is determined by summing the stiffness matrices of individual spring around each element. Failure of springs is modeled by assuming zero stiffness for the spring being considered. Consequently, the developed stiffness matrix is an average stiffness matrix for the element according to the stress situation around the element. In the 2-dimensional model, three degrees of freedom are considered for each element and deformations are assumed to be small. This leads to a relatively small stiffness matrix which is only of size (6X6). Stiffness matrix is developed for an arbitrary contact point with one pair of normal and shear springs as shown in Figure (2). Equation (1) shows the upper-left quarter of stiffness matrix. In this formulation, the element stiffness matrix depends on the contact point location (distance L and the angles θ and α) and the stiffness of normal and shear springs which are determined according to the stress and strain situations at the contact point location.

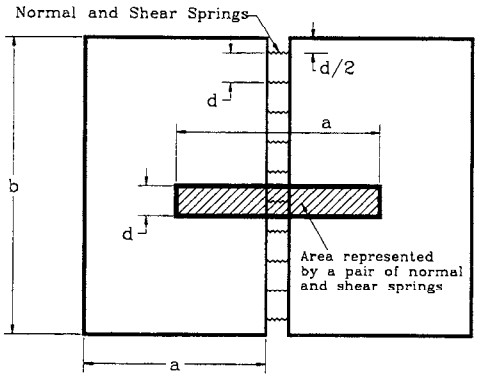

Fig. (1) Spring distributions and area of influence of each spring

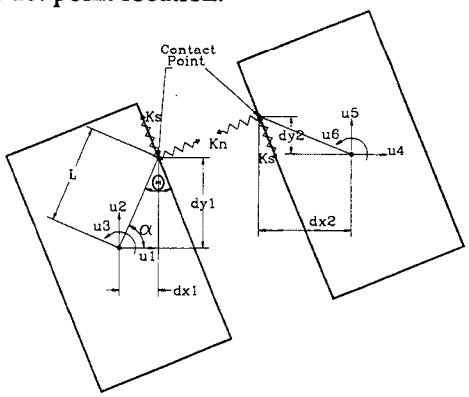

Fig. (2) Element shape, contact point and degrees of freedom for two elements

$$\begin{bmatrix} \begin{matrix}\mathrm{Sin}^2(\theta+\alpha)K_n \\ +\mathrm{Cos}^2(\theta+\alpha)K_s\end{matrix} & \begin{matrix}-K_n\mathrm{Sin}(\theta+\alpha)\mathrm{Cos}(\theta+\alpha) \\ +K_s\mathrm{Sin}(\theta+\alpha)\mathrm{Cos}(\theta+\alpha)\end{matrix} & \begin{matrix}\mathrm{Cos}(\theta+\alpha)K_sL\mathrm{Sin}(\alpha) \\ -\mathrm{Sin}(\theta+\alpha)K_nL\mathrm{Cos}(\alpha)\end{matrix} \\ \begin{matrix}-K_n\mathrm{Sin}(\theta+\alpha)\mathrm{Cos}(\theta+\alpha) \\ +K_s\mathrm{Sin}(\theta+\alpha)\mathrm{Cos}(\theta+\alpha)\end{matrix} & \begin{matrix}\mathrm{Sin}^2(\theta+\alpha)K_s \\ +\mathrm{Cos}^2(\theta+\alpha)K_n\end{matrix} & \begin{matrix}\mathrm{Cos}(\theta+\alpha)K_nL\mathrm{Cos}(\alpha) \\ +\mathrm{Sin}(\theta+\alpha)K_sL\mathrm{Sin}(\alpha)\end{matrix} \\ \begin{matrix}\mathrm{Cos}(\theta+\alpha)K_sL\mathrm{Sin}(\alpha) \\ -\mathrm{Sin}(\theta+\alpha)K_nL\mathrm{Cos}(\alpha)\end{matrix} & \begin{matrix}\mathrm{Cos}(\theta+\alpha)K_nL\mathrm{Cos}(\alpha) \\ +\mathrm{Sin}(\theta+\alpha)K_sL\mathrm{Sin}(\alpha)\end{matrix} & \begin{matrix}L^2\mathrm{Cos}^2(\alpha)K_n \\ +L^2\mathrm{Sin}^2(\alpha)K_s\end{matrix} \end{bmatrix} \quad (1)$$

Determination of Spring Stiffness

In this analysis, it is assumed that each normal and shear spring stiffness represents a certain area of the connected blocks. Figure (2) shows the location of springs around one edge of the element. The spring stiffness is calculated simply by Equation (2)

$$K_n = \frac{E*d*T}{a} \text{ and } K_s = \frac{G*d*T}{a} \quad (2)$$

where, d is the distance between springs, T is the thickness of the element and "a" is the length of the representative area, E and G are the Young's and shear modulus of concrete, respectively. For steel springs, the term (d*T) is replaced by the area of the steel bar while E and G are the Young's and shear modulus of steel, respectively.

Numerical Analysis Procedure

Figure (3) shows the flow chart of the model proposed. The program automatically generates elements and contact springs. Moreover, the reinforcement spring location is defined by its coordinate according to the steel bar position. The global failure is achieved by having singularity in the global stiffness matrix. This singularity means that the structure has no further resistance for carrying loads. It should be noted also that using tangent modulus for the compression springs requires the use of relatively small load increments to get stable solutions. In addition, small load increments are required to follow cracking in the studied problem.

MATERIAL MODELING

Material models used for concrete are shown in Figure (4). For the tension model, Young's modulus is assumed constant till failure of springs occurs (Figure (4-a)). For the compression model, a parabolic stress-strain relation is adopted (Figure (4-b)). After reaching the peak stress, the Young's modulus is assumed to be zero to avoid negative stiffness. For the shear model, shear modulus is assumed constant till reaching the cracking point. After cracking, the shear stiffness is assumed to be zero at the location of failed springs in tension (Figure (4-c)). As for steel, the tension and compression models are assumed to be bilinear. When steel stress reaches yield stress, Young's modulus is assumed to be 1% of its original value.

After the assemblage of the global stiffness matrix, the displacements of the elements are determined using the following well-known formula

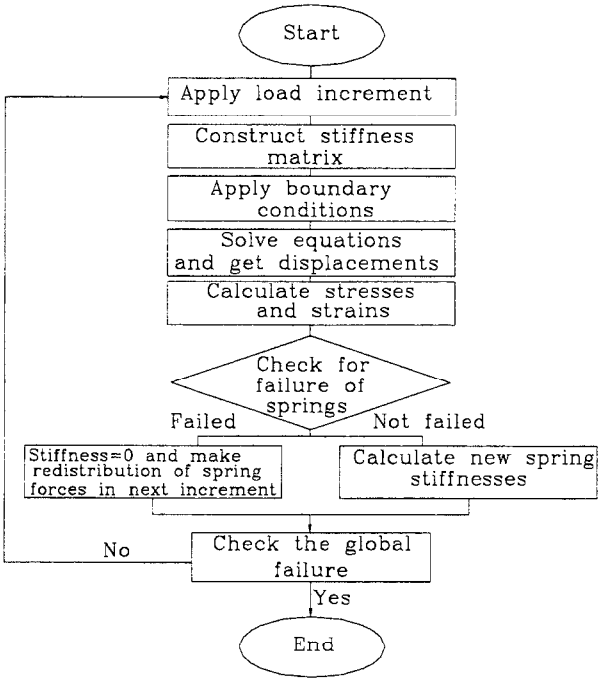

Fig. (3) Flow of analysis

$$[K_G][U] = [F] \quad (3)$$

Where $[K_G]$ is the global stiffness matrix, [U] is the unknown displacement vector and [F] is the global load vector. After the determination of displacements, the strains are calculated by determining the new relative displacement between the ends of the springs.

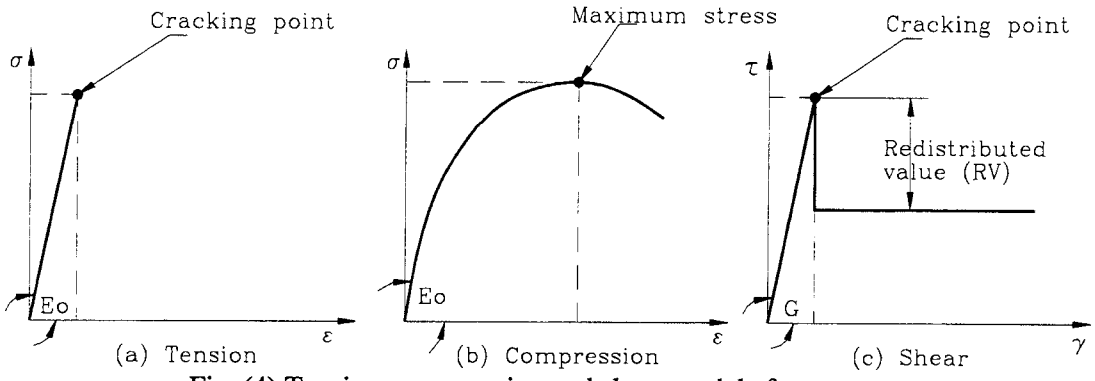

Fig. (4) Tension, compression and shear models for concrete

FAILURE CRITERIA

One of the main problems accompanying the use of blocks for representation of reinforced concrete is the modeling of diagonal cracking. The assumption that the cracks are allowed to propagate along the element edges only increases the stiffness of the structure in nonlinear conditions. To overcome this problem, the following technique is used. It mainly depends on way of determination of the principal stresses at the contact point. Referring to Figure (5), the shear and normal stress components (τ and σ_1) at point (A) are determined from the normal and shear springs attached at the contact point location. The secondary stress (σ_2) was calculated from normal stresses in points (B) and (C), as shown in Figure (5). Therefore,

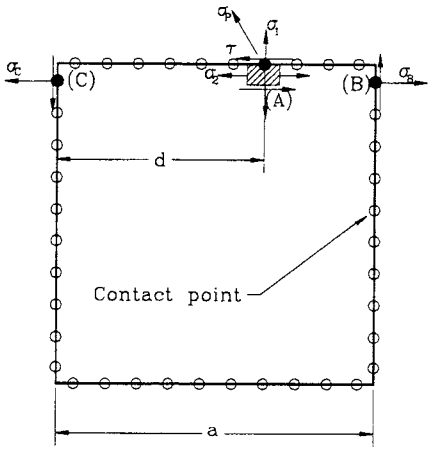

Fig. (5) Principal stress determination at contact points

$$\sigma_2 = \frac{d}{a}\sigma_B + \frac{(a-d)}{a}\sigma_C \tag{4}$$

Hereafter, the principal tension is calculated:

$$\sigma_p = \left(\frac{\sigma_1 + \sigma_2}{2}\right) + \sqrt{\left(\frac{\sigma_1 - \sigma_2}{2}\right)^2 + (\tau)^2} \tag{5}$$

This value of principal stress, σ_p, is compared with the tension resistance of concrete. When σ_p exceeds the critical value of tension resistance, the normal and shear spring forces are redistributed in the next load increment by applying the shear and normal spring forces in the reverse direction. These redistributed forces are transferred to the element centroid as a force and moment, and then these redistributed forces are applied to the structure in the next load increment. The redistribution of spring forces at the crack location is very important for following the proper crack propagation. For the normal spring, the whole force value is redistributed to have zero tension stress at the crack faces. Although shear springs at the location of tension cracking might have some resistance after cracking due to the effect of friction and interlocking of aggregates at the crack faces, the shear stiffness is assumed zero after crack occurrence. Having any shear resistance at the crack face reduces the tendency of the crack to open in further load increments because of the rigid body motion of the attached elements. To consider the effect of friction and aggregate interlocking, a redistributed value (RV), shown in Figure (4-c), is adopted.

NUMERICAL RESULTS IN MONOTONIC LOADING

Simulation of the Effects of Element Size and The Number of Springs

Adjustment of element size in the analysis is very important. Simulation of structures using elements of large size leads to increasing the structure stiffness and failure resistance of the structure. This means that the calculated displacements become smaller and the failure load gets to be larger than the actual one. To make this effect clear, we carried out a series of simulations using the laterally loaded cantilever shown in Figure (6). All material properties were taken constant and elastic analysis was performed using the proposed method. The results were compared with the theoretical results of elastic structure. The percentage of error in maximum displacement and the CPU time (CPU: DEC ALPHA 300 MHz) are also shown in Figure (6). To discuss the effect of the number of connecting springs, the analyses were performed using two models with 20 and 10 springs connecting each pair of adjacent element faces for each case of different element size. From the figure, it is evident that increasing the number of base elements leads to decreasing the error but increasing the CPU time. Use of only one element at the base leads to about 30% error in the theoretically calculated displacement. This error reduces to less than 1% when the number of elements at the base increase to 5. However, the CPU time increases rapidly. When we compare the results using 20 and 10 springs, although the accuracy of the results of 10 springs model is same as that in case of 10 springs, the CPU time in case of 10 springs is almost half of that in case of 20 springs. It should be emphasized that using rigid elements, calculated displacements become smaller than the actual displacements when the size of element is not small enough. From this figure, it can be concluded that usage of large number of elements together with relatively few number of connecting springs leads to very high accuracy in reasonable analysis time. To improve the accuracy in case of elastic analysis, it is advisable to increase the number of elements rather than increasing the number of connecting springs.

It should be also noted that in the previous analysis using rigid elements, like RBSM[2], the results obtained were of poor accuracy. This may be due to:

- The spring stiffness not being determined in a proper way to simulate the element deformation,
- The use of relatively large sized elements, and
- The use of relatively small number of springs between edges which leads to an inaccurate failure mechanism.

The number of springs per face is also an important parameter. Although the effect of number of springs in the elastic analysis is not large, its effect in non-linear analysis, especially after the generation of cracks, becomes larger. This effect will be discussed in next section.

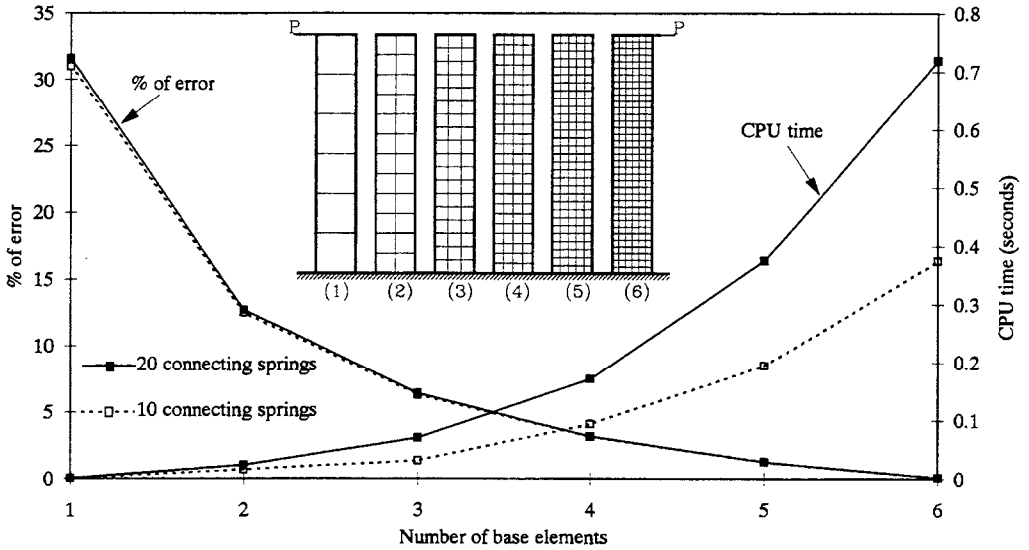

Fig. (6) Relation between the number of base elements, % of error and CPU time

Two-Storied RC Wall Subjected to Monotonic Loading

To verify the accuracy of the model, the simulation results are compared with the experimental results of a two-storied RC wall. The shape of the wall, reinforcement and loading location are shown in Figure (7). Reference (4) gives more details on the columns, beams and wall reinforcement, or the material properties. The wall is modeled using 1,845 square elements. The number of springs between each two adjacent faces is 10. Reinforcement locations are defined by their nearest spring coordinates. For vertical reinforcement, x-coordinate is defined at the steel bar location while for horizontal reinforcement, y-coordinate is defined.

Figure (7) shows a comparison between measured and calculated load-rotation relations. First, to discuss the effects of load increment in failure analysis, three models of different load increments, calculated by dividing the estimated failure load by 50, 250 and 500, with the constant number (10) of springs were used. Next, to study the effects of the number of connecting springs between faces, additional simulations were carried out using the case of 250 load increments with 5 and 2 springs between faces and the results were compared with that with 10 springs. The failure load calculated in all cases were within the range from 64 to 70 tf while the measured one was 67 tf. The calculated failure load using the FEM was 64 tf[1]. In general, the calculated failure loads are very close to the measured ones. The results of 50, 250 and 500 increments are almost congruent till at least 90% of failure load. It should be emphasized that the CPU time of analysis of 500 increments is 10 times that of 50 increments. To avoid long CPU time, load increments can be reduced after about 90% of expected failure load. Moreover, it can be noticed easily from Figure (7) that the agreement between experimental and numerical results is fairly good for 250 increments with 10 or 5 connecting springs. Surprisingly, for the case of 250 increments with only 2 springs connecting each two adjacent faces, the results are also reliable till reaching failure of the structure. It is noted also that using few number of load increments leads to the results in slightly higher failure load (70 tf) while using a few number of connecting springs gives slightly lower one (64 tf). This means that our model gives reliable results even when using a few number of connecting springs or few number of load increments.

Although increasing the number of springs leads to increasing the CPU time required for assembling the global stiffness matrix, the time required for the solution of equations, which is dominant when the number of elements is large, does not change because the number of degrees of freedom is independent of the number of springs used. This means that we can use larger number of springs between edges without significant change of the CPU time of analysis. On the other hand, as the total number of connecting springs used is generally large, it is necessary to use automatic mesh and spring generation. Moreover, increasing the number of springs leads to increasing the computer memory capacity required.

Figure (8) shows the relation between load and the number of failed springs for each increment. Cumulative curves also show the total number of failed springs till that increment. It can be noted that although the number of increments in both cases are different, both cumulative curves close each other. This gives good indication that the solution is generally stable. Excessive cracking begins to appear when the applied load is about 28 tf. At the same load, behavior of the structure begins to be highly nonlinear.

Figure (9) shows the deformed shape during the application of load in case of 500 load increments with 10 springs. The location of cracks and crack propagation can be easily observed. The location of cracks and crack propagation are very similar to those obtained from the experiment. This means that the proposed model can be applied for fracture behavior of RC structures, such as, failure load, deformations, crack generation, crack location and crack propagation, etc.

It should be emphasized that although the shape of elements used in the analysis are squares, it does not affect the crack generation or crack propagation in the material. Diagonal cracks, as shown in Figure (9), coincide well with those obtained from the experiment. In analysis using rigid elements, like RBSM[2], shapes and distributions of elements were decided based on the assumption that cracks were generated and propagated in previously expected locations and directions.

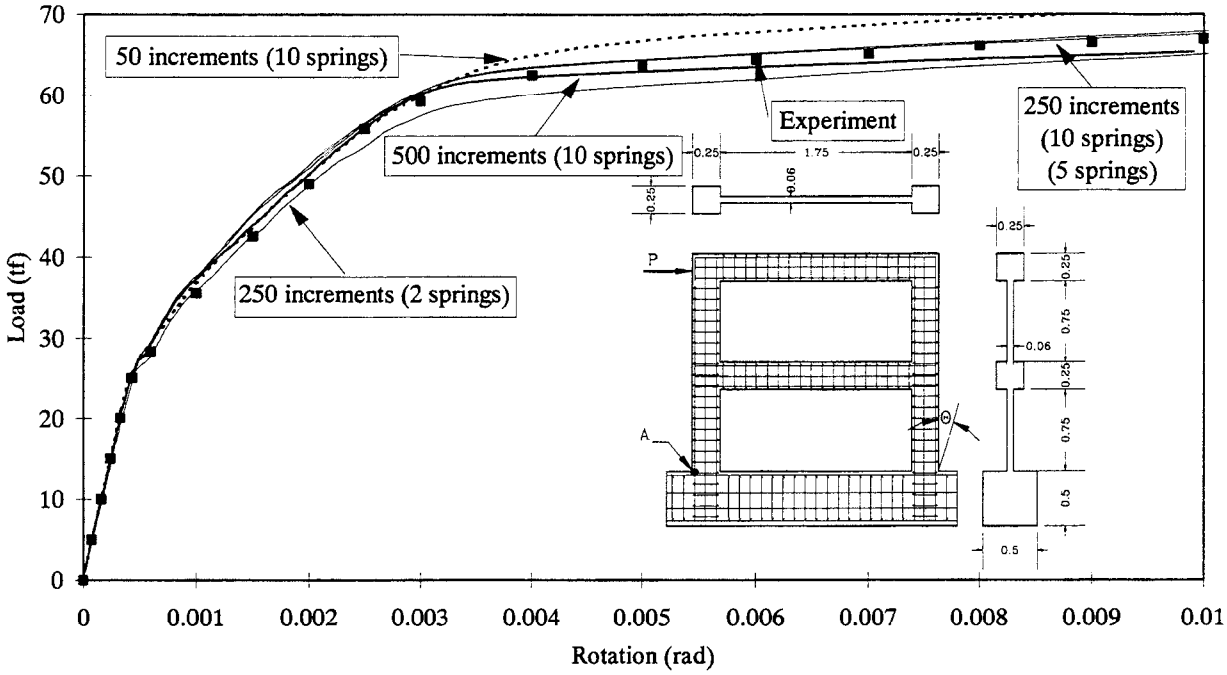

Fig. (7) Relation between load and wall rotation for 2-storied RC wall

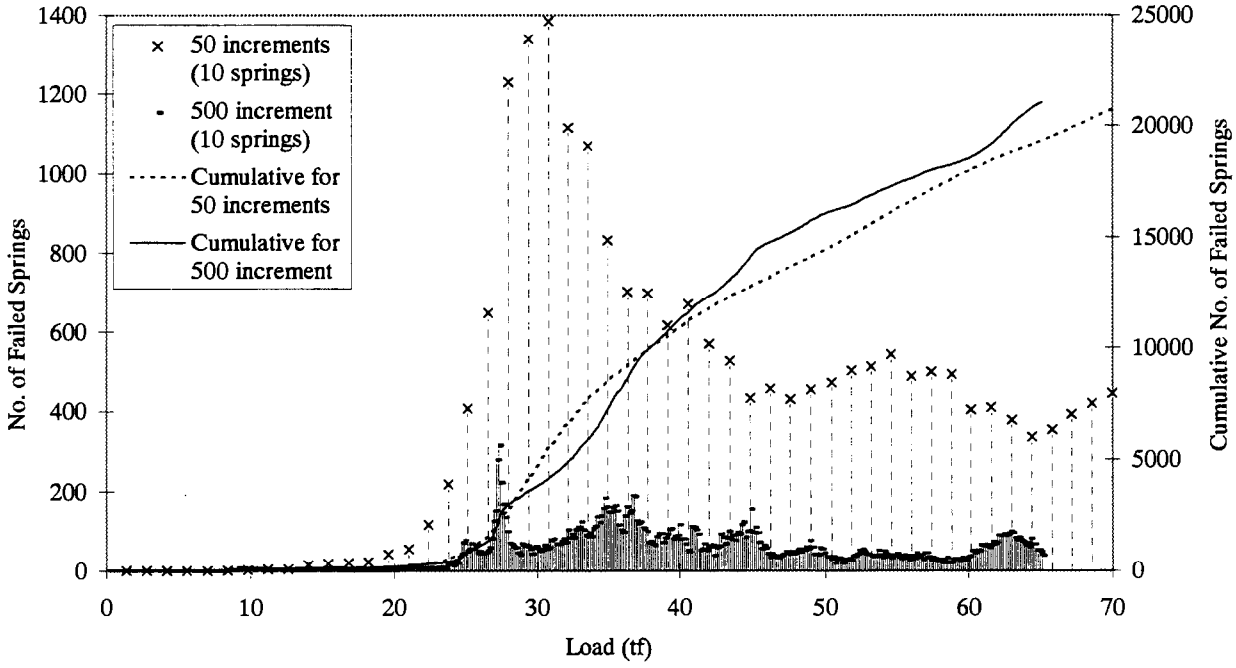

Fig. (8) Relation between load and the number of failed springs for 2-storied RC wall

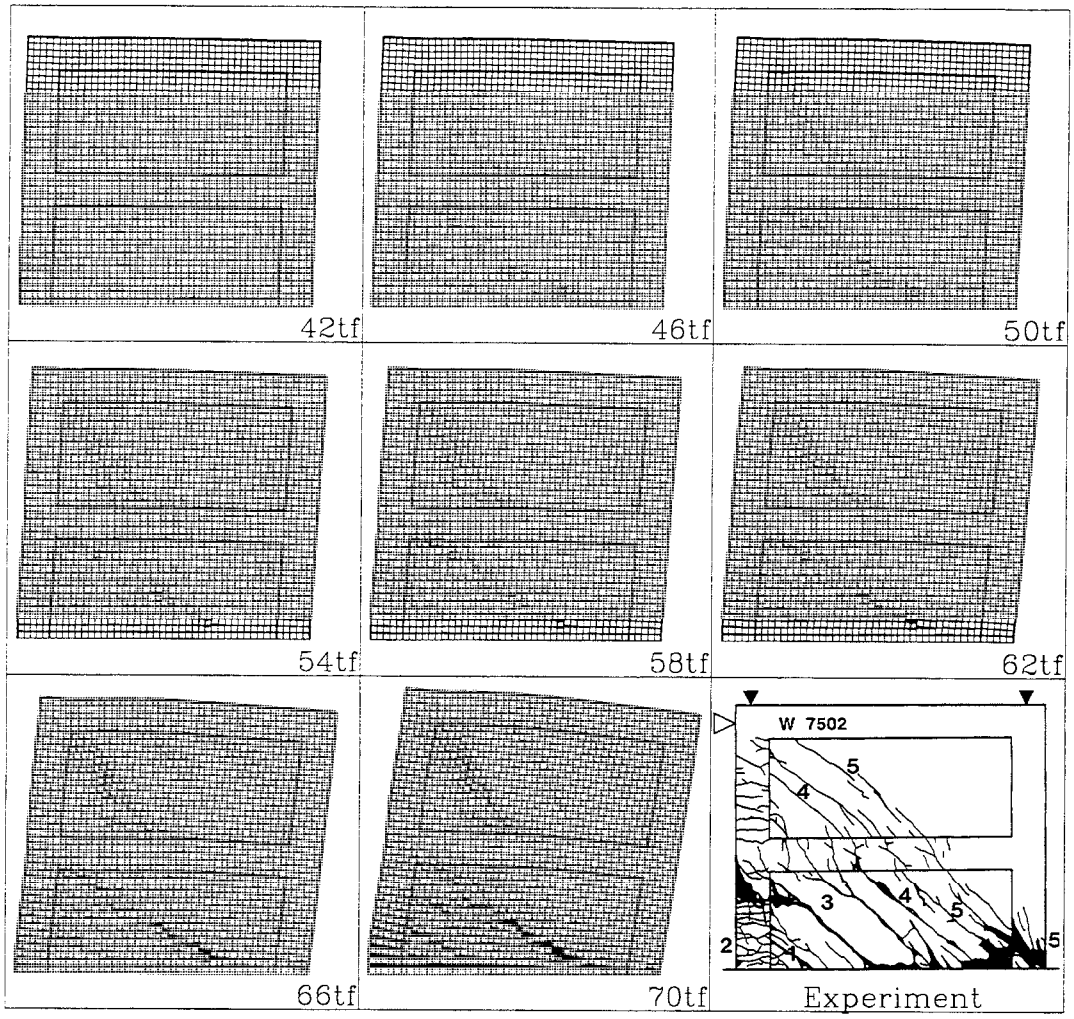

Fig. (9) Deformed shape and crack locations of the 2-storied RC wall structure
(in case of 500 increments with 10 springs between each two adjacent faces, Simulation Scale Factor=30)

RC Deep Beam

The second verification example is an RC deep beam. Dimensions, loading conditions and reinforcement details[5] are shown in Figure (10). Analysis of such type of problems is relatively difficult because reinforcement exists only in tension area near the support. This means that concrete behavior in most of the beam is almost like plain concrete. Numerical analysis is performed for only half of the beam because of symmetry. The model is divided into 2,700 square elements. The number of springs between each two adjacent element faces is 10.

Figure (10) shows the relation between load and deformation under the applied load given from the experiment and simulated by the proposed technique and the FEM[6]. It can be noticed easily that the proposed technique gives good agreement with the experimental results in both deformations and failure load. The results obtained by the proposed technique are better than those by the FEM. The measured failure load was found to be about 88 tf. The calculated failure load is about 91 tf using the proposed technique and about 98 tf using the FEM. Moreover, the deformations before failure using the proposed technique is much better than those calculated by the FEM.

Figure (11) shows the deformed shape during loading. The right-down corner of Figure (11) shows the location of cracks after the exeriment[6]. It can be easily noticed that the deformed shape agrees well with the experimental one.

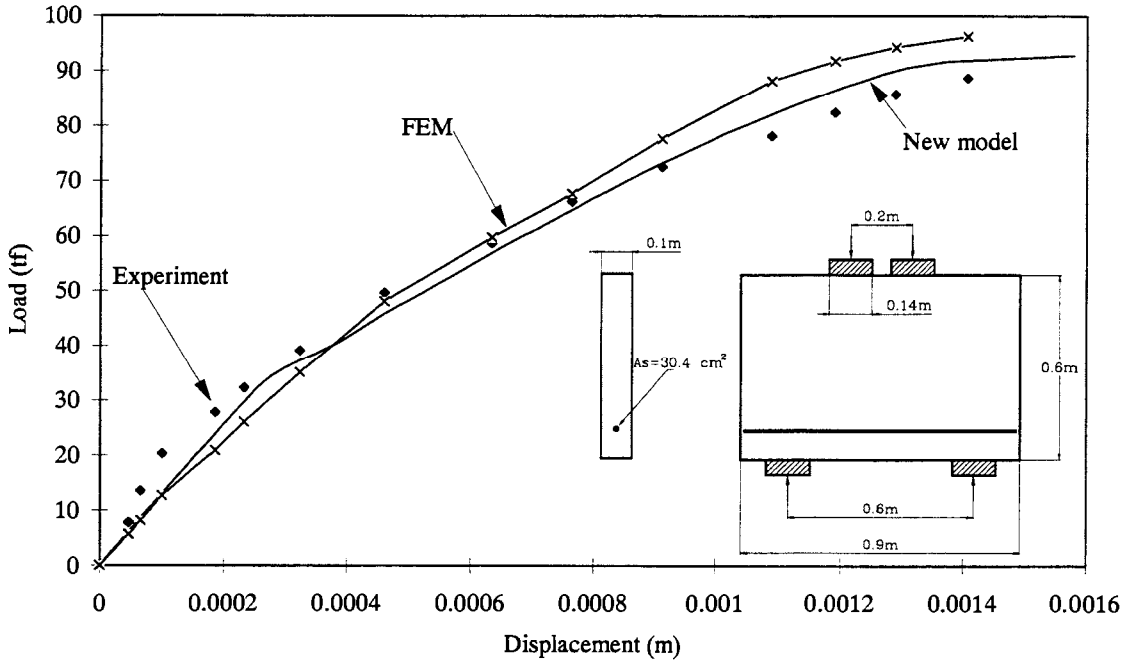

Fig. (10) Relation between load and displacement under the constant rate load for RC deep beam

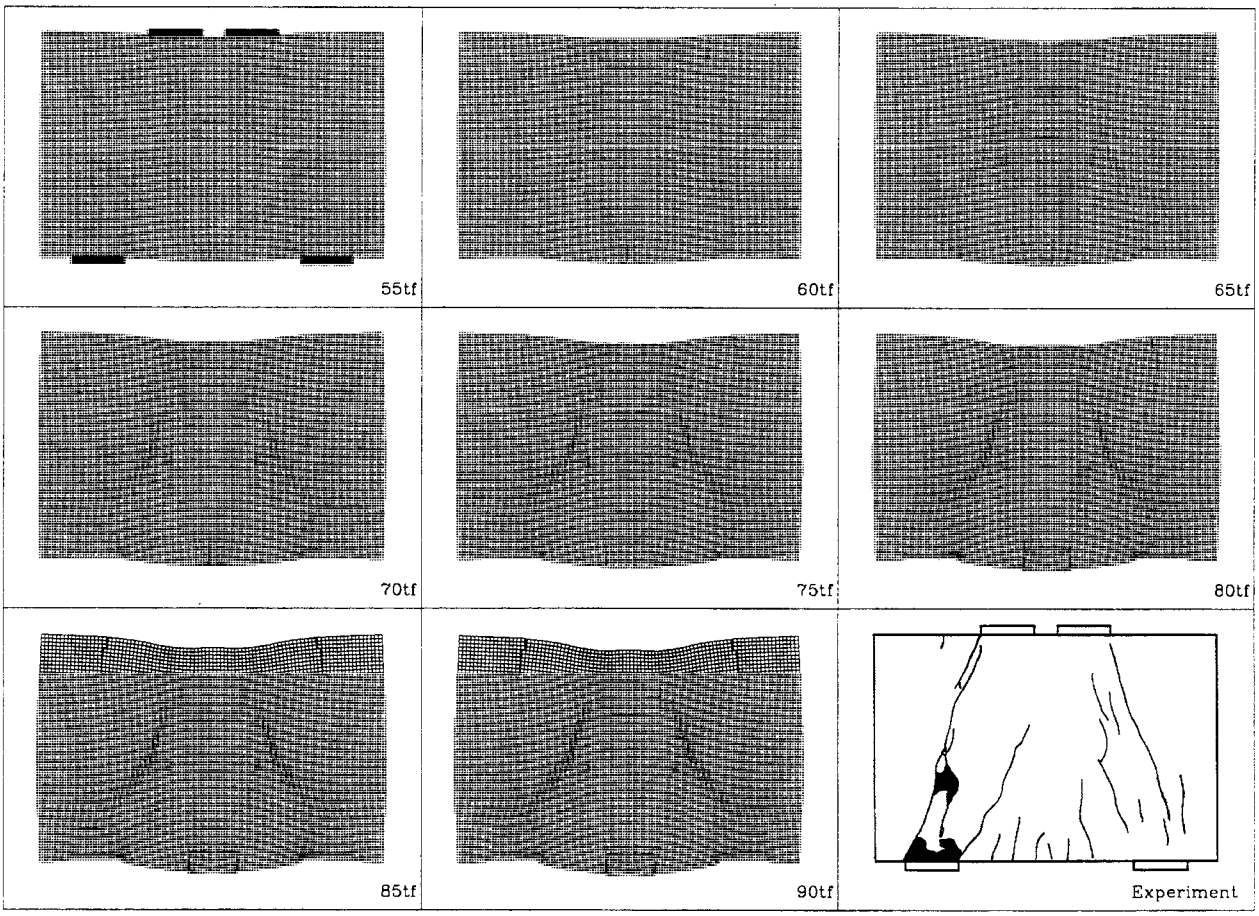

Fig. (11) Deformed shape of deep beam. (Simulation Scale Factor=40)

RC Frame

The third verification example is an RC frame structure. Dimensions, loading conditions and reinforcement details[6] are shown in Figure (12). This frame is modeled using 1880 elements with 10 connecting springs. The maximum load is applied in 200 increments at the shown location. It should be noted also that all reinforcement details, including stirrups location and diameters, were taken into account. Figure (12) shows also the relation between load and deformation calculated from our simulation and measured from the experiment. It can be noticed that excellent agreement between the two results has been achieved. Figure (13) shows the deformed shape and crack location at the final stage of our result and experiment. Good agreement between the measured and calculated crack locations, crack inclination and crack length can also be obtained. In both experiment and numerical simulation, failure occurs near the base and at connections.

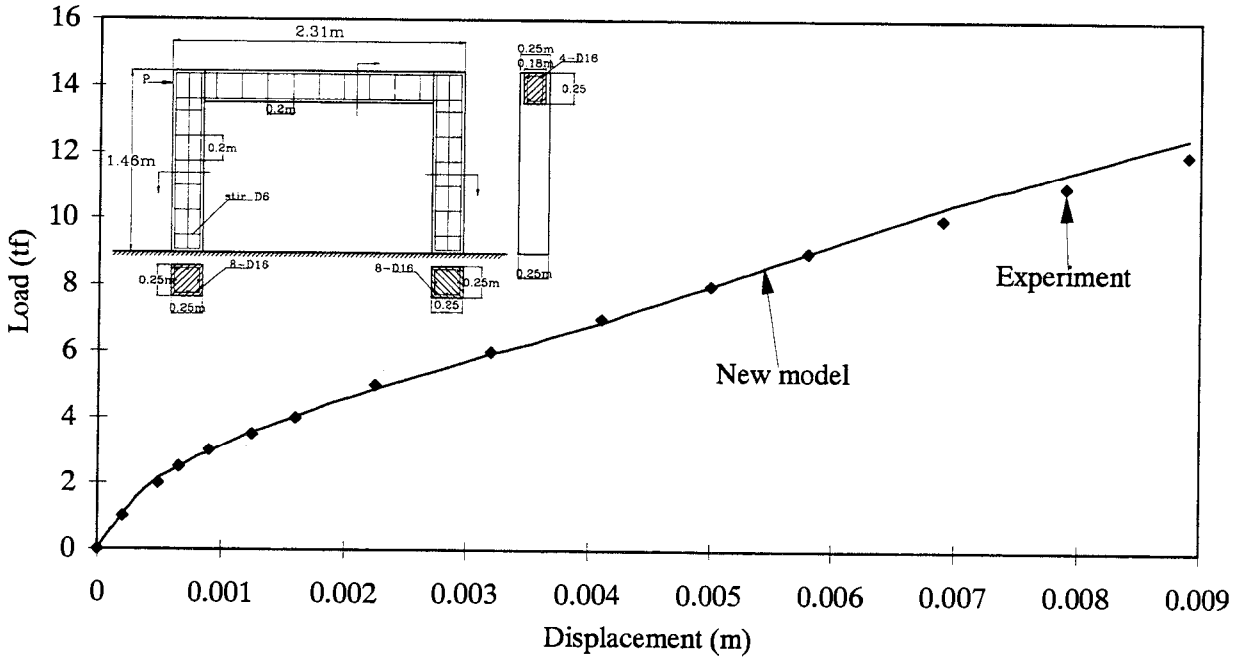

Fig. (12) Relation between load and maximum displacement at the loading point of RC frame

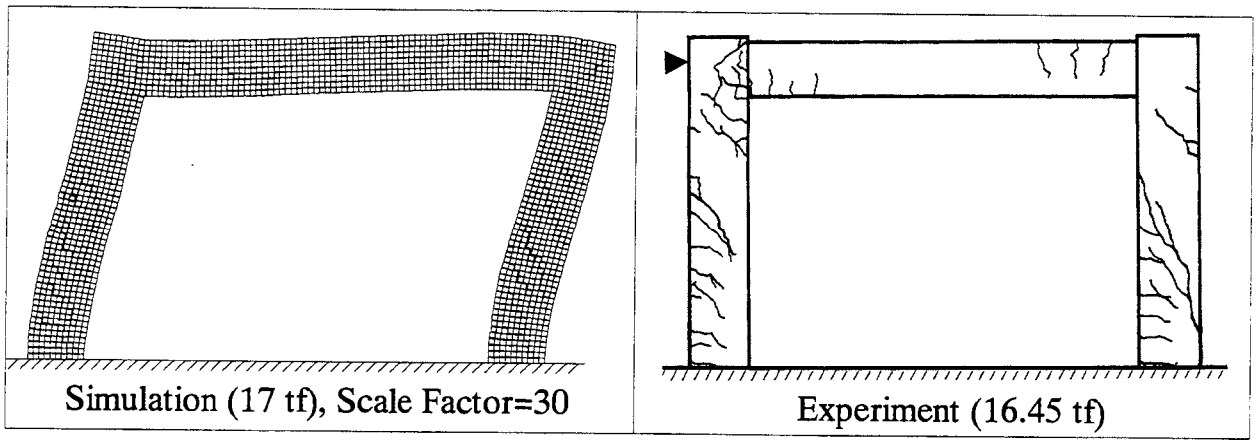

Fig. (13) Deformed shape of RC frame

RC Deep Beams Without Shear Reinforcement Bars

In this section, simulation results of three deep beams[7] which do not have shear reinforcement in the shear zone are introduced. This type of analysis is generally difficult because of excessive cracking which occurs during loading. The results obtained through our model are compared with the experimental results and FEM results as shown in Figures (14) to (16). The shape, loading conditions, reinforcement and deformed shape are also shown in these figures. In general, the results of the proposed model are more accurate than those obtained with the FEM. The accuracy of the FEM decreases and finally becomes impossible to apply the FEM when the ratio between shear zone length and the total beam length increases. The reason is simply because no reinforcement is used in the shear zone and hence, the sensitivity of the concrete to cracking increases. This effect can not be accurately followed using the FEM.

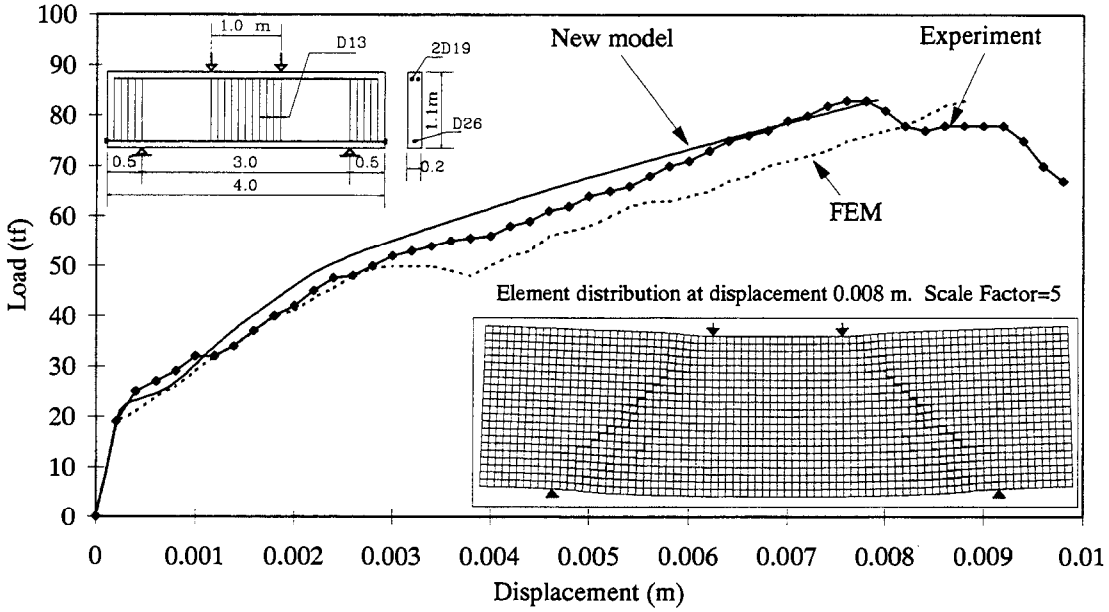

Fig. (14) Shape and results of a two point loading deep beam without shear reinforcement

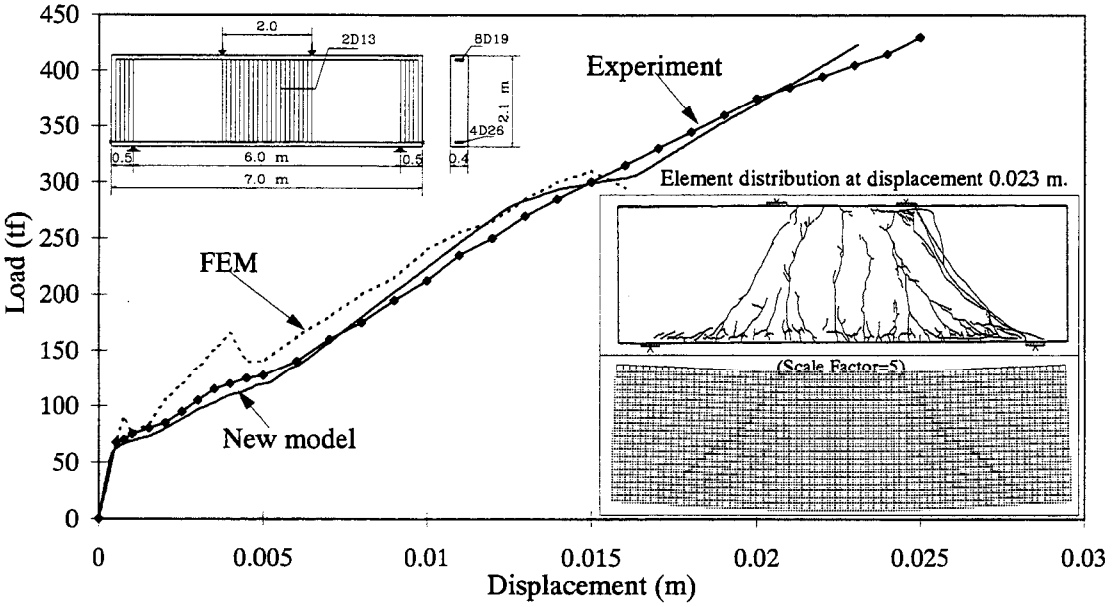

Fig. (15) Shape and results of a two point loading deep beam without shear reinforcement

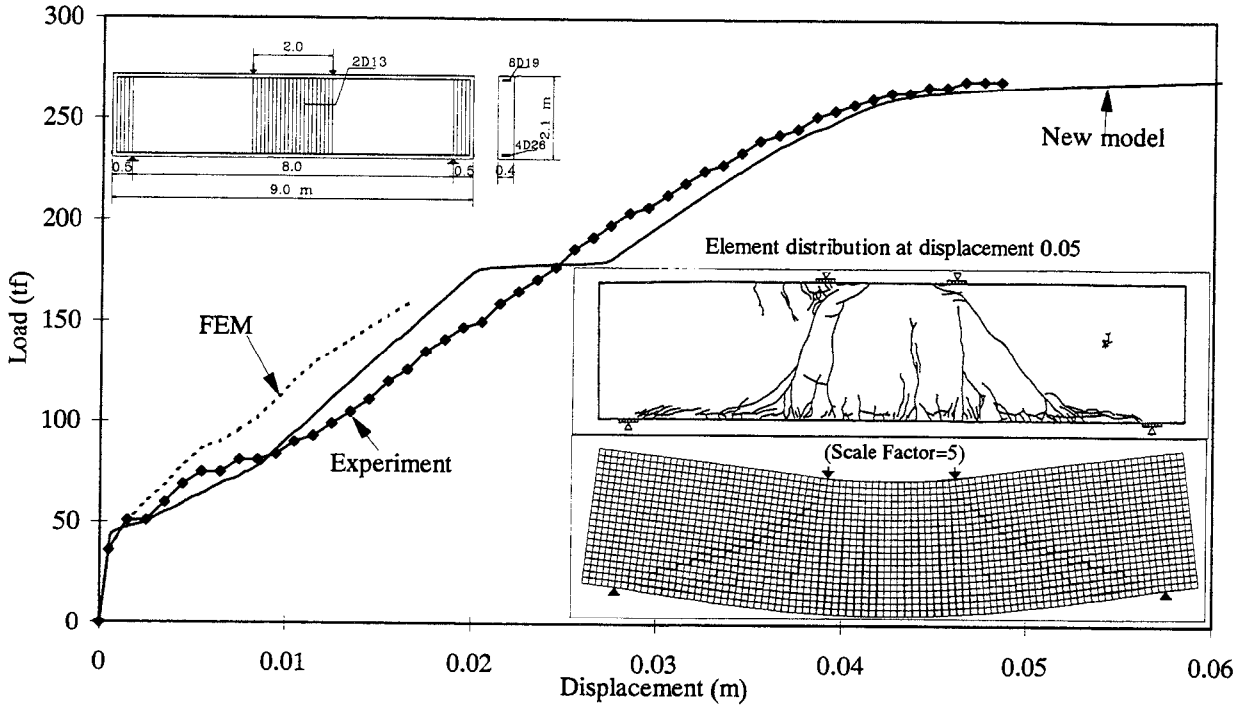

Fig. (16) Shape and results of a two point loading deep beam without shear reinforcement

NUMERICAL RESULTS IN CYCLIC LOADING

Material Modeling

For concrete springs subjected to cyclic loading, Maekawa's compression model[8] shown in Figure 17(a) is adopted to simulate cyclic stress-strain relation. On the other hand, for reinforcement, the steel model shown in Figure 17(b) is used[9]. The main advantage of these models are that they incorporate only one equation for the simulation of behavior in loading, unloading, reloading and post peak behaviors. Stress-strain relation for concrete springs subjected to tension is assumed linear till reaching the cracking point and then the stiffness is assumed zero.

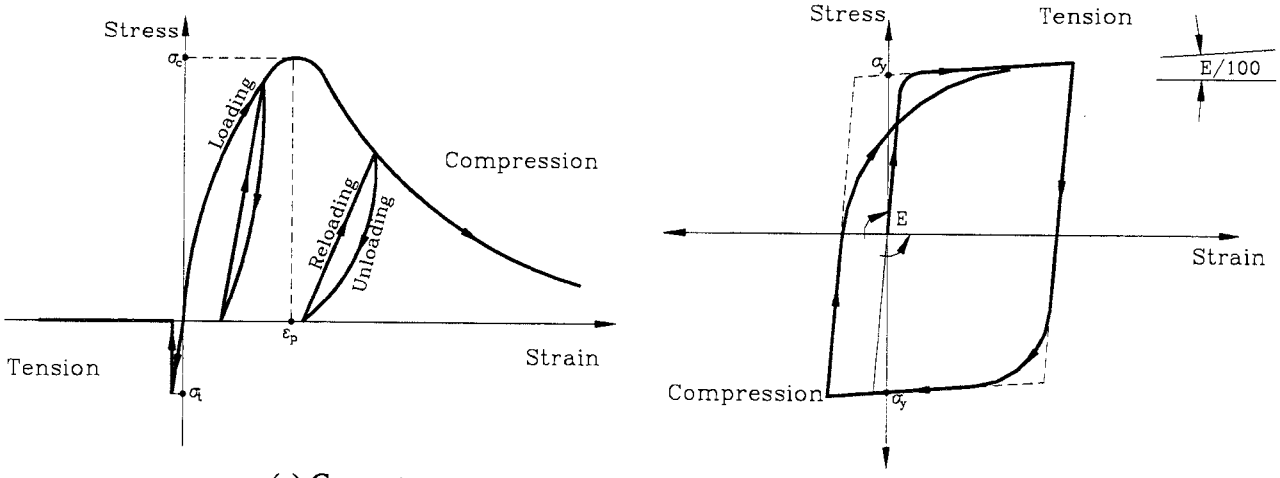

(a) Concrete (b) Steel

Fig. (17) Material models for steel and concrete

Two-Storied RC Wall Structure Subjected to Cyclic Loading

To verify the accuracy of the model under cyclic loading, the simulation results are compared with the experimental results of the two-storied RC wall structure in cyclic loading conditions. The applied cyclic load is shown in Figure (18). The wall shape, reinforcement and loading point were shown in Figure (7). Figure (19) shows the number of failed springs during loading. It is obvious that this number always has a peak when the applied load is maximum and then decreases in the unloading stage. Figure (20) shows the relation between load and angle of rotation (θ) during the loading. It seems from the relation shown in Figure (20) that the value of plastic strain and unloading behavior are not so accurate because of element dislocations during loading process. This leads to incomplete cracking closure and hence the unloading stiffness becomes less than the measured one. Figure (21) shows the stress-strain relation for steel bars located at point "A". It can be noticed that the value of tensile strain is larger than that of compressive strains. The reason is crack closure in compression. It should be emphasized that it is very easy to follow all reinforcement details and any stress-strain relation at any point for the studied structure. With the FEM, it is practically impossible to follow all reinforcement details in the analysis. Figure (22) shows the deformed shape and crack locations in the specimen. It is clear that the crack locations are very near to those from the experiment. The generated cracks open and close in such a way which is similar to what happens in the experiment. These cracks are generated without use of any special techniques, such as joint elements in FEM, and without assuming the crack location and direction of propagation before the analysis.

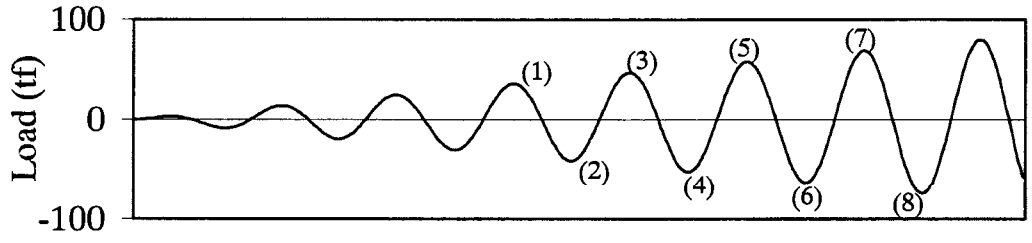

Fig. (18) Load pattern

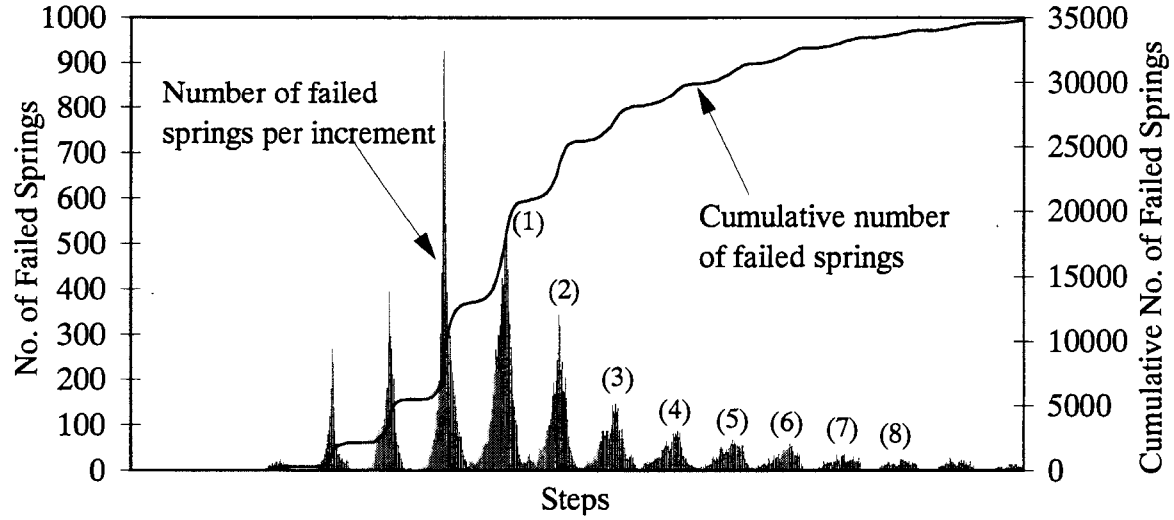

Fig. (19) Number of failed springs for each step

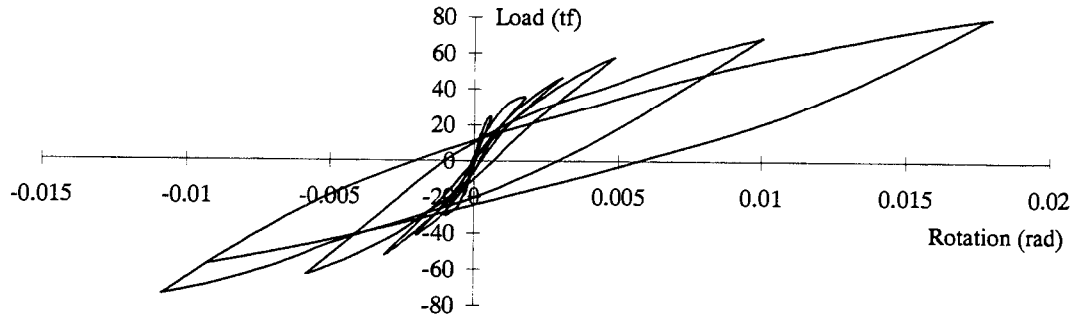

Fig. (20) Relation between load and rotation (θ)

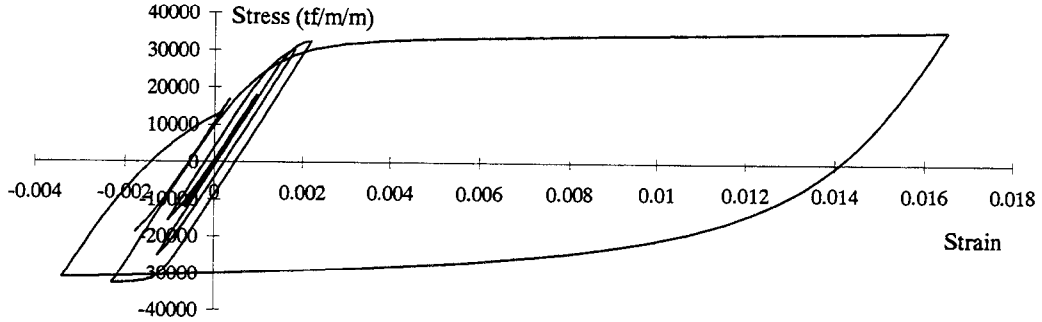

Fig. (21) Stress-strain relation at point "A" at the base of left column

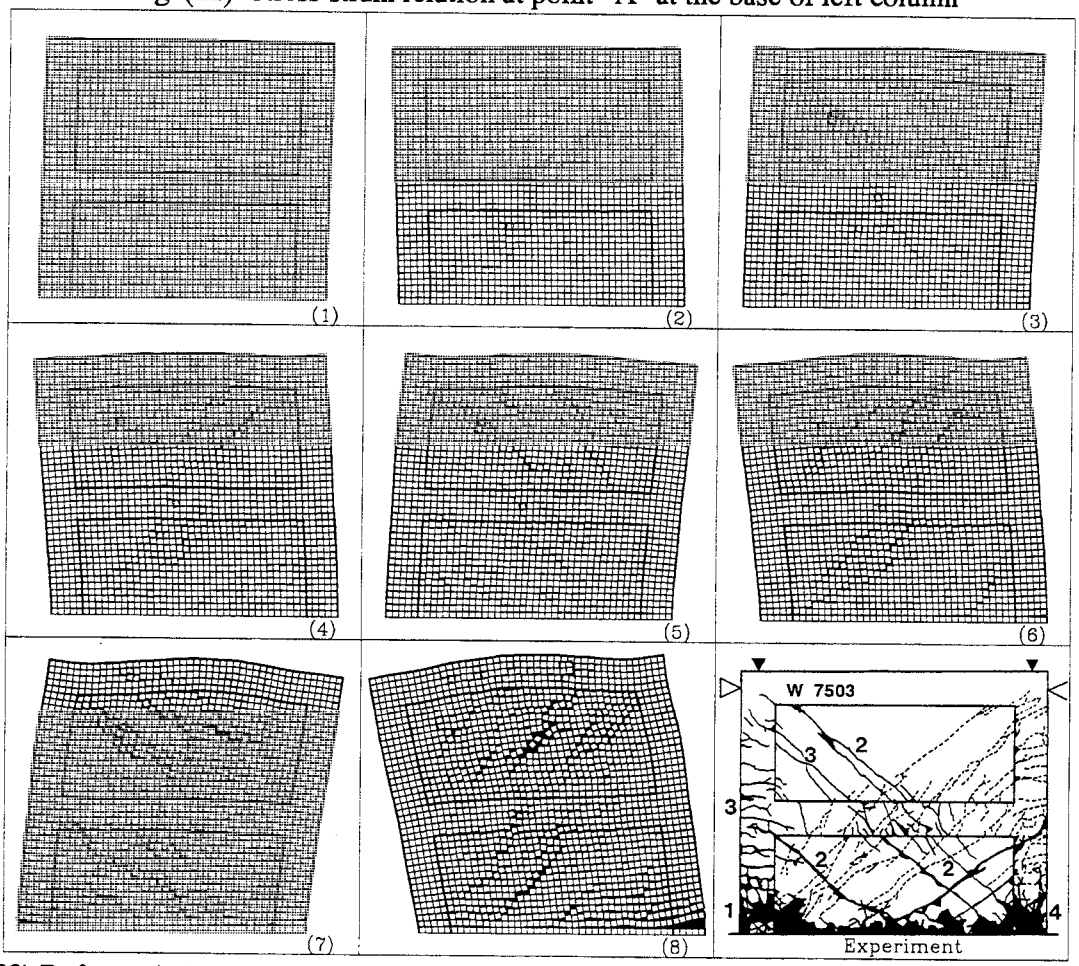

Fig. (22) Deformed shape and crack location at different loading stages (Simulation Scale Factor=30)

CONCLUSIONS

Through numerical simulations of reinforced concrete structures, it is confirmed that the new proposed model is capable of simulating the fracture behavior of concrete structures. The results of load and displacements in monotonic loading almost coincide with the experimental results by at least 95% accuracy. The expected failure mode is also very close to the measured one. Through this new model, stresses, strains, deformations, crack initiation and propagation of cracks can be calculated with high accuracy and relatively simple techniques. In addition, all reinforcement details, such as bar location and shear reinforcement details, can be taken into account without any additional complications to the analysis. Also, it is very easy to follow the mechanical behavior of steel and concrete at any point. Although the shape of the element used was square, it did not affect the crack propagation in the material. Even though the formulations used for the material properties were relatively simple, the results obtained are better or of the same accuracy of the FE analysis. This method does not require any complicated models for the representation of cracking or special elements, such as joint elements, to follow the crack propagation, the results obtained by the proposed method in monotonic loading condition agree well with experimental results. However, for cyclic loading, further research may improve the accuracy of unloading behavior. This model can be easily combined with the EDEM to simulate the total behavior of structure till complete failure. The proposed model is expected to give high accuracy to wide applications where FEM does not give reliable accuracy.

REFERENCES

1. Okamura H. and Maekawa K.: Nonlinear analysis and constitutive models of reinforced concrete, Gihodo Co. Ltd., Tokyo, 1991.
2. Kawai T.: Some considerations on the finite element method, Int. J. for Numerical Methods in Engineering, Vol. 16, pp. 81-120, 1980.
3. Meguro K. and Hakuno M.: Fracture analyses of concrete structures by the modified distinct element method, Structural Eng./Earthquake Eng., Japan Society of Civil Engineers, Vol. 6., No. 2, pp. 283s-294s, October, 1989.
4. Hajime Ono et al.: Study on seismic capacity of reinforced concrete shear wall, Part 7, Relation between load history and horizontal reinforcement, Proc. of annual conference of Architectural Institute of Japan (AIJ), pp. 1601-1602, 1976. (in Japanese)
5. Niwa J., Maekawa K. and Okamura H.: Nonlinear finite element analysis of deep beams, 10th annual lecture on "FEM Analysis of Reinforced Concrete Structures", Civil Engineering Department, The University of Tokyo, 1995.
6. Muto K.: Strength and deformations of structures, Maruzen Co. Ltd., 1965. (in Japanese)
7. Railroad Research Institute and Research Institute of Tekken Co. Ltd.: Study on shear capacity of RC members based on fracture mechanics, Internal report, 1997. (in Japanese)
8. Okamura H., Maekawa K. and Izumo J.: Reinforced concrete plate element subjected to cyclic loading, 10th annual lecture on "FEM Analysis of Reinforced Concrete Structures", Civil Engineering Department, The University of Tokyo, 1995.
9. Ristic D., Yamada Y., and Iemura H.: Stress-strain based modeling of hystertic structures under earthquake induced bending and varying axial loads, Research report, No. 86-ST-01, School of Civil Engineering, Kyoto University, March, 1986.

To Isolate or Not to Isolate: Insights from Field and Laboratory Experiments

S.S. Chen, J.B. Mander, D.A. Wendichansky, and D. K. Kim
Department of Civil Engineering
State University of New York at Buffalo

Abstract

The principal objective of this research is to investigate, both experimentally and analytically, the seismic performance of slab-on-steel-girder bridges before and after rehabilitating them with elastomeric bearings. The original bearings used in this class of bridge (that is typical of bridges constructed in the central and eastern United States prior to the 1980's) generally consist of a variety of low (sliding) and high (rocker) steel bearings. According to the recently published FHWA Seismic Retrofitting Manual [Buckle and Friedland, 1995], such bearings are considered prime candidates for replacement due to their historically poor performance in earthquakes. The three main objectives of this research are: (i) to determine the level of seismic excitation at which the steel bearings perform satisfactorily; (ii) to investigate whether simple retrofits to the steel bearings themselves markedly improve overall seismic resistance; and (iii) to assess the performance effectiveness of different types of elastomeric bearings with and without supplemental energy dissipation capabilities.

Background and Objectives

The fundamental options confronting a bridge engineer charged with determining a suitable seismic retrofit strategy for a bridge seated on bearings are the following (excluding foundation rehabilitation):

a) do nothing
b) let the superstructure move (i.e., seismic isolation)
   i) using standard low-damping elastomeric bearings, or
   ii) using such bearings or sliding bearings in conjunction with supplemental damping devices, or
   iii) using high-damping bearings such as lead-rubber seismic isolation bearings,
c) strengthen applicable load-path elements to transfer inertial loads reliably to the foundation, where such elements in slab-on-girder bridges include the following:
   i) cross frames at supports,
   ii) bearings and their anchorages,
   iii) bearing pedestals, and
   iv) substructures (columns).

With the soon-to-be-revised AASHTO Guide Specifications on Seismic Isolation Design (AASHTO 91), lead cores are often added to laminated elastomeric bearings installed in bridges to provide additional seismic protection when option b is chosen. The relative paucity of information available on the in-situ efficacy of such bridge bearing retrofits motivates the use of full-scale, large-amplitude field vibration tests. Other such tests are described in Douglas (1976), Lam (1990), Kawashima et al. (1992) and Robson (1996).

It is reasonable, however, to question whether the existing steel bearings in common use on thousands of slab-on-girder bridges in low to moderate seismic zones really need to be replaced.

That is, either option a (do nothing) or option c (strengthen the load path) may be more viable in certain situations than option b (seismic isolation). The present work addresses this question by comparing before- and after-retrofit field behavior along with corresponding analytical modeling studies informed by companion laboratory experiments (Kim et al. 1997, Mander et al. 1996) on the strength and hysteretic characteristics of actual bearings which were either retrieved from, or installed in, the bridges being field-tested.

In this investigation, the principal objectives of the field experiments, laboratory experiments on bearings, and companion analytical studies are intended to aid seismic vulnerability assessment via:

(1) Measurement and assessment of in-situ dynamic behavior and performance of a typical slab-on-girder bridge subjected to transverse quick-release loading and supported on the three different types of bearings, and

(2) Quantification of the in-situ dynamic performance change attributable to:
   a) bearing replacement using standard laminated elastomeric bearings,
   b) bearing replacement using lead-core seismic isolation bearings, and
   c) simple retrofits of the steel bearings themselves.

Bridge Description

Figure 1 shows a side elevation view of the bridges carrying Route 400 over the Cazenovia Creek some *50 km* southeast of Buffalo, N.Y. The abutments and two-column reinforced concrete pier bents are supported by a concrete pile cap and battered steel H-piles extending *15 m* to *21 m* into the soil. Constructed in 1967 and supported on high-type fixed and rocker steel bearings over the piers and low-type steel-bronze sliding expansion bearings over the abutments, bearings were replaced following rehabilitation work on the reinforced concrete decks. The northbound bridge was rehabilitated during October-December 1993 with circular laminated elastomeric bearings. The southbound bridge was seismically retrofitted during December 1993 to June 1994 with square laminated elastomeric lead-rubber bearings on each abutment and standard square laminated elastomeric bearings on each pier.

Research Approach

Quick-release (snap-back) techniques employed in the field on the pre-retrofitted and post-retrofitted bridges were complemented by ambient vibration tests. Response results were examined to infer in-situ frequencies, mode shapes, damping ratios, and higher mode effects. Static (pre-snap) data also provides insight into in-situ pier, diaphragm and bearing flexibility, which are of use in calibrating analytical models and evaluating design approaches.

The field quick-release experimentation was complemented by laboratory tests performed on actual bearings from the bridges (both old steel bearings salvaged from the pre-retrofit bridges and new bearings used in the aseismic retrofits) along with finite element analysis informed by these bearing test results at several levels of modeling detail. These global and component-based experimental studies, combined with the analytical studies, enable an assessment of suitable analytical modeling approaches as well as quantification of the in-situ dynamic performance changes attributable to the bearing retrofits of the two subject bridges.

Recent efforts on this project have focused on the following: i) construction and deployment of a new under-bridge loading scheme shown in Fig. 2b on the south pier of the soutbound bridge and use of this new setup alongside the previously used over-deck test setup [Zhang 96], ii) completion of a draft report that combines the pre-retrofit and post-retrofit experimental and analytical studies performed on both bridges [Wendichansky et al. 96], (iii) conduct of seismic vulnerability assessments of the subject bridges using analytical models developed in (ii) [Wendichansky 96], (iv) conduct of an initial cold-weather experiment using the new under-deck test setup, (v) publication of a report on the analytical modeling and experimental behavior (capacity) of the salvaged steel bearings under reversed cyclic loading [Mander et al. 96], and (vi) analysis of loads (demands) on the same steel bearings.

Field Experimental Plan And Setup

Figure 2a shows the quick-release loading scheme initially employed to test the southbound bridge. The tension bars straddle the near column of the anchor pier and pass through holes cored into both curbs of the tested bridge, anchored on the far side of the deck. In order to avoid the difficulties of interfering with traffic, the under-deck setup shown in Fig. 2b was developed. A mechanical fuse device was constructed which is electrically triggered to release the tendon's tensile load suddenly.

The instruments used consist of linear motion potentiometers and accelerometers with a response of $\pm 25\ g$ at *0-100 Hz*, the latter connected to a model 2310 Micro Measurements signal conditioner. The signal was filtered by the conditioners with a low pass band of *25 Hz*. Two 486 computers with ADAC 12 and 16 bit A/D boards handling up to 32 channels each were used for data acquisition. A *140 Hz* dynamic sampling rate was used to record 20 second post-snap data sets. The loading bars themselves were instrumented with strain gauges to determine the applied load before and after release for the over-deck test setup. A load cell is used in the under-deck test setup. Table 1 summarizes tests conducted on the southbound post-retrofitted bridge. The "under-deck 96" test was conducted in cold temperatures ($-12°C$).

Analytical Modeling and System Identification: Global Bridge

Analytical models of the investigated bridges, both pre-retrofit (on original steel bearings) and post-retrofit (on elastomeric and seismic isolation bearings) were developed at several levels of detail in order to investigate the degree of detail needed to reliably predict observed experimental behavior. The linearized 3D SAP90 model developed earlier was complemented by several 2D nonlinear DRAIN-2DX models which were able to match field-measured observations quite closely.

Pre-Retrofit (on Steel Bearings)

The frequencies and mode shapes for the snap-back test of the pre-retrofitted bridges were computed using two different methods. Method 1 was the common "peak picking" method using Frequency Domain analysis techniques. Method 2 was a time domain curve fitting procedure. For the first method the time histories were augmented by 8192 zeroes in order to reduce potential inaccuracies (Veletsos, 1985) and others' suggestions (Hogue, 1987; Harris, 1978) were considered in order to reduce leakage and errors. For the purpose of determining the natural frequencies and mode shapes, the Fourier amplitude spectra and the phase spectra were computed for each digital record. Natural frequencies were estimated from the Fourier spectra whose magnitude was used to construct a normalized vector dividing the values of each

accelerometer station for a given frequency by the largest value. The phase spectra were used to identify the arithmetic sign of the modes. The vertical modes were constructed using the quick-release test data augmented by model information obtained from ambient vibration tests which oriented deck-level accelerometers in the vertical direction. Method 2, an alternate method in the time domain based on a least squares curve fitting, was developed due to the existence of closely spaced modes. Foundation stiffnesses were initially based on results of a companion study [Douglas et al. 94].

Figure 3 shows the principal transverse mode shapes and frequencies for the pre-retrofitted southbound bridge. The mode shapes and frequencies are taken as the average of the results for different tests and different system identification techniques (time domain or frequency domain). Reasonable agreement, including the two closely-spaced modes in Figs. 3a and 3b, was obtained between the transverse accelerations in the field and those of 3D analytical models.

Post-Retrofit (Seismically Isolated)

For the post-retrofitted southbound bridge where nonlinear behavior is expected, it was decided to divide the time history of the quick-release tests into two portions. The first portion corresponds to larger deformations and the second to the remaining data. Inelastic behavior can be assumed initially since it occurs in the first cycle. Elastic behavior is assumed in the remaining portion of the time history. Frequencies and mode shapes were extracted from the elastic portion of the time history using the procedure described for the pre-retrofitted bridges. The approximate damping values were obtained from Fourier spectra using the half power method.

With the frequencies and mode shapes extracted from the elastic portion of the time history and with the data from the static test, an optimization procedure was used in order to extract the initial stiffness of the bearings in the transverse direction of the bridge. The optimization process (Masri, 1985) starts with the assumption of a simplified model of the bridge. In this model the only assumed unknowns are the bearing characteristics; all the other values (mass, stiffness, etc.) were extracted from the model of the pre-retrofitted bridge. The stiffness values of the bearings that minimize the error between the predicted frequencies, mode shape and displacements from static test at low load level and the experimental results are taken as the initial stiffness value of the bearings. The initial stiffness values for the lead rubber bearings were *6255 kN/m, 6672 kN/m* for the north and south abutment, respectively, and *788 kN/m* for the rubber bearings located in the pier bents. With the initial stiffness value and assuming that the laminated rubber bearings located over the piers behave linearly by the reactions from basic equilibrium, equations were computed for each interval using the relative displacement measured at the bearings locations and the load time history from the static test. Figure 4 compares the load vs. deformation obtained from the procedure described above with the laboratory experimental test performed over the bearings. For a nonlinear prediction of the field test and using the curve defined for the lead rubber bearings, a "yield force" of *21 kN* and a post-yielding stiffness of *867 kN/m* were proposed. Also, for an equivalent elastic analysis, a stiffness defined between the origin and the maximum displacements in each abutment was extracted from the graph. Table 2 compares the results of bearing property identification from the above as well as from laboratory experiments conducted on the bearings [Mander et al. 96] and from a simplified method used on results from subsequent field tests [Zhang 96]. Values of identified bearing properties appear to depend on the identification method used more than on the test method or temperature (down to $-12°C$). An alternate approach is being developed by Douglas and Maragakis at the University of Nevada-Reno.

Representative Behavior Results: Global Bridge

Examination of acceleration time histories and corresponding Fourier spectra of the post-retrofitted southbound bridge indicate that none of the modes include a high participation of the pier bent. The deck system is indeed "isolated" from the supports. Figure 5 compares the experimental frequencies and mode shapes for both bridges and those predicted using the initial stiffness values for the bearings (SAP90 and DRAIN-2DX), where the second mode is only weakly indicated. It can be inferred that the first two modes correspond closely to a rigid body motion of the deck and that the third (*14.03 Hz*) resembles the shape of a free-free long beam mode. This behavior is in apparent agreement with the findings from other researchers (Skinner, 1993) who suggest that the bearings properties control the lower modes and the structure characteristics the higher modes. The results for subsequent (over-deck vs. under-deck) tests are similar, as shown in Fig. 6. Cold temperatures (under-deck 1996 test) result in some stiffening, as reflected in the frequency shift shown in Fig. 7.

By comparing Fig. 3 with Fig. 5, it can be seen that the replacement of the original steel bearings with elastomeric isolation bearings produced a significant change in the transverse dynamic characteristics of the bridge. The initial transverse frequency of the Southbound bridge was around 5.5 Hz (with 6% damping). This dropped to less than 2 Hz (an upper bound based on the elastic stiffness) and frequencies as low as 1.08 Hz (22% equivalent viscous damping) were observed due to nonlinear seismic response. This latter result was obtained with a deformation of 38 mm or around 33% of the maximum bearing displacement. Even lower frequencies (and higher damping) can be expected for higher deformations that would occur under large seismic loading conditions. For the Northbound bridge, the first transverse frequency dropped from a value of 5.8 Hz (6% damping) for the steel bearings to less than 1.8 Hz (9% damping) for the neoprene elastomeric bearings. Also, new rubber expansion joints were installed a few weeks before testing the rehabilitated bridges. Due to frictional restraint, these joints provided a noticeable contribution to the overall transverse stiffness of the rehabilitated bridges.

This change in dynamic properties does not imply, however, that the actual seismic resistance of either bridge is necessarily improved by the seismic isolation retrofit. The following sections outline the reasons for this somewhat surprising caveat.

Analytical Investigation of Seismic Vulnerability

The analytical studies have focused on conducting nonlinear dynamic time history analyses of the two bridges supported on the different types of steel and elastomeric bearings. To enable such analyses to be conducted, it was first necessary to make accurate force-displacement models of the steel and elastomeric bearings to capture the highly nonlinear behavior of these elements. Various combinations of nonlinear truss and link elements (that include gap effects) have been used for the steel bearings to capture sliding, prying, and keeper plate and/or anchor bolt fracture. The properties of these models are inferred directly from laboratory experiments on the bearings used on both the pre- and post-retrofit bridges.

Role of Companion Laboratory Experiments

During the course of bridge rehabilitation, steel bearings were retrieved from the field and destructively tested in the laboratory under simulated constant axial gravity load and simulated reversed cyclic lateral earthquake loading. The bearings were first tested with strong anchorages to investigate

stability and strength issues pertaining to the bearings themselves. The bearings were tested on reinforced concrete pedestals using swedged anchor bolts (also retrieved from the field) to investigate the steel bearing-anchorage-concrete pedestal system interaction. NYSDOT replaced the Northbound bridge steel bearings with conventional elastomeric bearing pads and the Southbound bridge steel bearings with seismic isolation bearings. All of the different types of elastomeric bearing systems were tested in the laboratory to characterize their performance under large displacements.

Figure 8 compares experimental observations with the analytical model prediction under transverse loading for a low type sliding bearing. A new thermo-visco-elasto-plastic model has also been developed for modeling elastomeric bearing behavior both with and without a lead core. With these primary sources of nonlinear bridge performance modeled, the next step was to develop overall nonlinear mathematical/structural models of the bridges. For this purpose, the experimental quick release test time histories were used to validate the computational models. Once validated, the computational models were used to predict expected performance for a large range of strong earthquake ground motions – not only motions that may be expected in low to medium seismic zones, but also very strong near-field motions that include fling effects observed in high seismic zones. In addition to investigating seismic behavior using nonlinear time history analysis, simplified analysis techniques were advanced that use: linearized elastic capacity-demand spectra, and nonlinear inelastic capacity-demand spectra.

Steel Bearings and Pedestals

Bearing behavior can be largely described by rigid body kinematics (i.e., sliding and rocking) with some yielding of critical parts such as anchor bolts, pintles and guide plates. For each type of steel bearing where sliding is possible, the laws of Coulomb friction are obeyed. Results show that by retrofitting the existing high type steel bridge bearings it is possible to provide sufficient strength and displacement capability to withstand substantial ground shaking. The weak link in the chain of force transmission may thus become the anchor bolts and/or the reinforced concrete pedestal. Experimental results demonstrate the importance of considering the flexibility of the concrete pedestal-anchor bolt system (Fig. 9). The bearing assembly elastic stiffness may be determined by assessing the flexural and shear flexibility of each of the constituent bearing parts. Ultimate lateral strength may be determined using either rigid body kinematics or upper bound plastic mechanism analysis.

Elastomeric Bearings

At extremely cold temperatures, rubber glass-hardens with the bearing behaving in a significantly nonlinear fashion. The hysteretic performance of elastomeric bearings may be characterized by a temperature dependent nonlinear Kelvin model – that is a bi-linear spring and velocity dependent nonlinear viscous dashpot. The cold temperature effects of lead-rubber bearings may also be obtained by similarly adding the visco-elasto-plastic effects of lead to the model of the rubber bearing.

Synthesis of Results

Due to the reserve strength of the columns and of the original steel bearings [Mander et al. 96], subjecting the calibrated analytical models to various ground motion scenarios demonstrates that the actual seismic resistance of the retrofitted southbound bridge is not greatly increased by the seismic isolation retrofit [Wendichansky 96]. As summarized in Fig. 10, the analytical portion of this study has shown that when seated on the original steel bearings, the bridges were capable of sustaining earthquakes with peak

ground accelerations of at least 0.65 g. If for reasons other than seismic retrofitting steel bearings are rehabilitated using traditional elastomeric/neoprene bearings while also pinning one abutment to provide some anchorage for thermal expansion (as for the northbound bridge in this study), then a torsional imbalance may be expected. Predictions show a seismic resistance of PGA = 0.6 g for this class of rehabilitation of the Northbound bridge. This indicates that the bearing rehabilitation of the Northbound bridge did not improve the seismic resistance of that bridge beyond the expectations of the original steel bearings. The use of the proposed methodology to evaluate the capacity/demand (C/D) ratio based on an inelastic response spectrum approach provides a rational basis for studying systems where the overall structural behavior is governed by different types of hysteretic response. The results obtained using this methodology show good agreement with the results obtained from rigorous inelastic time history analysis.

On the other hand, if the steel bearings are replaced with a well-conceived and designed seismic isolation system, the seismic resistance may be improved; predictive results for the Southbound bridge show an improvement in seismic capacity to PGA = 0.9 g for lead-rubber isolation bearings from 0.75g for the steel bearings. These results show that current seismic evaluation techniques, recommended in the recently published FHWA Seismic Retrofitting Manual (Buckle and Friedland, 1995), underestimate the real resistance capacity of slab-on-girder bridges seated on steel bearings. This is largely because simplistic elastic analysis models, when used, ignore the beneficial effects of friction in steel bearings. Also, current retrofit techniques generally recommend conventional retrofitting or the use of protective systems. This study has demonstrated that existing bridges designed using the provisions of the 1960's and 70's can sustain the design earthquakes forces. Therefore, by performing a detailed engineering analysis of the structure, unnecessary retrofitting may be avoided in some cases.

For bridges located in low to moderate seismic zones such as those in the eastern and central United States, the use of lead rubber bearings may not be necessary. Partial isolation can be achieved by replacing steel bearings with regular laminated elastomeric bearings. If extra damping or a torsionally imbalanced condition exists, then the behavior of these less expensive bearings can be augmented by using shock absorbing devices.

Acknowledgements

Funding for this project has been provided by NCEER under FHWA Contract DTFH61-92-C-00106 on the Seismic Vulnerability of Existing Highway Construction. The New York State Department of Transportation has provided site access and field coordination along with steel bearing salvage, the latter in conjunction with Union Concrete and Construction Corp. Dynamic Isolation Systems provided elastomeric and lead-core bearings for the laboratory studies. The help of Professor B. M. Douglas, who provided the loading jacks used initially in the study, is gratefully acknowledged, as is the subsequent effort of Mr. Mark Drotar in constructing the under-bridge setup. Mr. Gary Majewski, Mr. Mark Pitman, Mr. Paul Pattarroyo, Mr. Richard Cizdziel, Dr. Joel From, Mr. Gokhan Pekcan, Mr. Lijia Zhang, Mr. Gang Hu and numerous other graduate and undergraduate students assisted with various aspects of the field preparations and experiments.

Table 1 Southbound Bridge Quick-Release Tests Conducted

Load Cell	Location	Test Name	Type of Test	Load (kN)	Release System
L1 + L2	North Pier	SBPOST-T1-TP	Two Piers	384	Mechanical Fuse
L3 + L4	South Pier	SBPOST-T1-TP	Two Piers	290	Mechanical Fuse
L1 + L2	North Pier	SBPOST-T2-TP	Two Piers	555	Mechanical Fuse
L3 + L4	South Pier	SBPOST-T2-TP	Two Piers	520	Mechanical Fuse
L1 + L2	North Pier	SBPOST-T3-OP		0	
L3 + L4	South Pier	SBPOST-T3-OP	One Pier	604	Mechanical Fuse
L1 + L2	North Pier	SBPOST-T4-OP		0	
L3 + L4	South Pier	SBPOST-T4-OP	One Pier	679	Fuse Bar-South Pier
L3 + L4	South Pier	Over-Deck: OD 95	One Pier	658 kN	Mechanical Fuse
Load Cell	South Pier	Under-Deck: UD 95	One Pier	667 kN	Mechanical Fuse
Load Cell	South Pier	Under-Deck: UD 96 (cold)	One Pier	660 kN	Mechanical Fuse

Note: Location: North Pier = The force was applied at the deck level over the pier mentioned.
Test Name: SBPOST = Southbound Bridge Post-Retrofitted Bridge
T3 = Test #3
OP = One Pier (Pulling Condition)

Table 2 Comparison of Bearing Parameters

Identification Method	Test Type	K_1 *kN/mm*	K_2 *kN/mm*	K_{p1} *kN/mm*	F_y *kN*	C *kNs/mm*
Lab test (Kim et al., 1996)	static	10.9	0.726	0.708	31.2	
Monotonic 1995 under-deck (Zhang 96)	static	6.91	0.96	1.08	26.9	
Monotonic 1995 over-deck (Zhang 96)	static	10.1	1.78	2.35	27.6	
Quasi-structural 1995 under-deck	dynamic	10.6	1.0	0.73	28.5	908
Optimization (Wendichansky, 1996)	static	6.67	0.867	0.78	21	
Monotonic 1996 under-deck (cold)	static	9.18	1.28	0.56	29.3	

References

AASHTO Guide Specifications for Seismic Isolation Design, American Association of State Highway and Transportation Officials, June 1991.

Buckle, I.G., and Friedland, I.M., (1995), "Seismic Retrofitting Manual for Highway Bridges," Federal Highway Administration, Report No. FHWA-RD-94-052, 309 pp.

Douglas, B. M., "Quick-Release Pullback Testing and Analytical Seismic Analysis of a Six-Span Composite Girder Bridge", Technical Report No. FHWA-RD-76-173, 1976.

Douglas, B. M., Maragakis, E. M., and Feng, S., "Stiffness Evaluation of Pile Foundation of Cazenovia Creek Overpass", Report No. CCEER-94-2, University of Nevada, Reno, 1994.

Harris, F. J., "On the Use of Windows for Harmonic Analysis with the Discrete Fourier Transform", Proceedings of the IEEE, Vol. 66, No. 1, Jan. 1978, pp. 51-83.

Hogue, T. D., "Concept and Application of Frequency Domain Analysis in Structural Dynamics", M.S. Thesis in Civil Engineering, Louisiana State University, August 1987.

Kawashima, K., Nagashima, H., Masumoto, S., and Hara, K., "Response Analysis of Miyagawa Bridge Based on a Measured Acceleration Record", in Proceedings of the Second US-Japan Workshop on Earthquake Protective Systems for Bridges, Technical Memorandum of PWRI No. 3196, Public Works Research Institute of Japan, December 7-8,1992, pp. 467-476.

Kim, D. K., Mander, J. B., and Chen, S. S., "Experimental Study and Thermo-Visco-Elasto-Plastic Modeling of Elastomeric Seismic Isolation Bearings", Technical Report NCEER-97-XXXX, to be published.

Lam, V., "The System Identification of a Nonlinearly Responding Base-Isolated Bridge", Ph.D. Thesis, Dept. of Civil Engineering, University of Auckland, New Zealand, Feb. 1990.

Mander, J. B., Kim, D. K., Chen, S. S., and Premus, G. J., "Response of Steel Bridge Bearings to Reversed Cyclic Loading", Technical Report No. NCEER-96-0014, November 1996.

Powell, G. H., et al., "DRAIN-2DX Version 1.03 User's Guide, Report No. UCB/SEMM-92/29, Dept. of Civil Engineering, University of California at Berkeley, 1992.

Robson, B., "Field Testing of a Seismically Isolated Skewed P/C Girder Bridge", Proceedings of the 13th Annual International Bridge Conference, June 1996.

Veletsos, A. S., and Ventura, C. M., "Dynamic Analysis of Structures by the DFT Method", Journal of Structural Engineering, ASCE, Vol. 111, No. 12, December, 1985, pp. 2625-2643.

Wendichansky, D. A., "Experimental Investigation of the Dynamic Response of Two Bridges Before and After Retrofitting with Elastomeric Bearings," Ph.D. Thesis, Dept. of Civil Engineering, State University of New York at Buffalo, April 1996.

Wendichansky, D. A., Chen, S. S., and Mander, J. B., "Experimental Investigation of the Dynamic Response of Two Bridges Before and After Retrofitting with Elastomeric Bearings", Technical Report NCEER-96-XXXX, to be published.

Zhang, L., "Field Testing and Modeling of a Seismically Isolated Slab-on-Girder Birdge under Quick-Release Loading", M.S. Thesis, Dept. of Civil Engineering, State University of New York at Buffalo, February 1996.

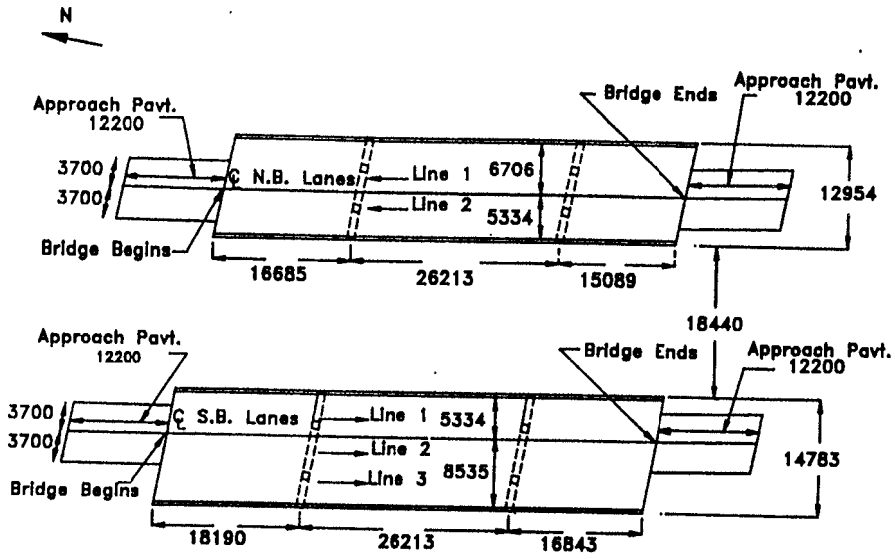

(a)

	BEARING TYPE		
	PRE-RETROFIT	POST-RETROFIT	
	S. BOUND & N. BOUND	S. BOUND	N. BOUND
N. ABUT.	LOW STL. EXP.	LEAD CORE ELAST.	STD. ELAST. (With Pin)
PIER #1	HIGH STL. FIXED	STD. ELAST.	STD. ELAST.
PIER #2	HIGH STL. EXP.	STD. ELAST.	STD. ELAST.
S. ABUT.	LOW STL. EXP.	LEAD CORE ELAST.	STD. ELAST.

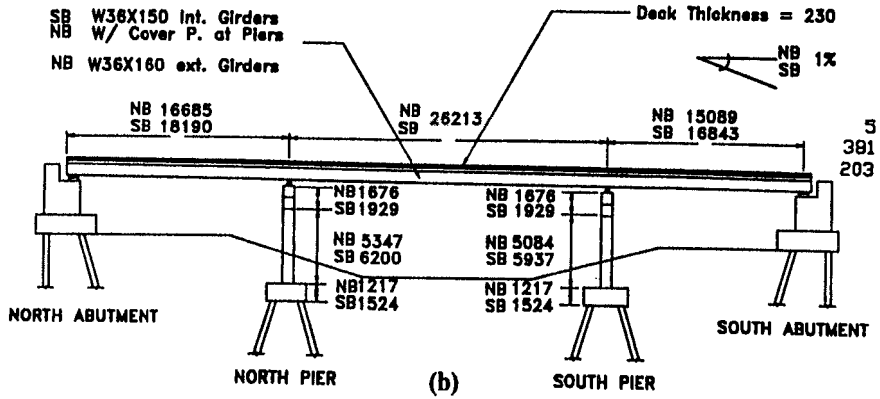

(b)

FIGURE 1 Plan and Longitudinal View of the Bridges Over the Cazenovia Creek

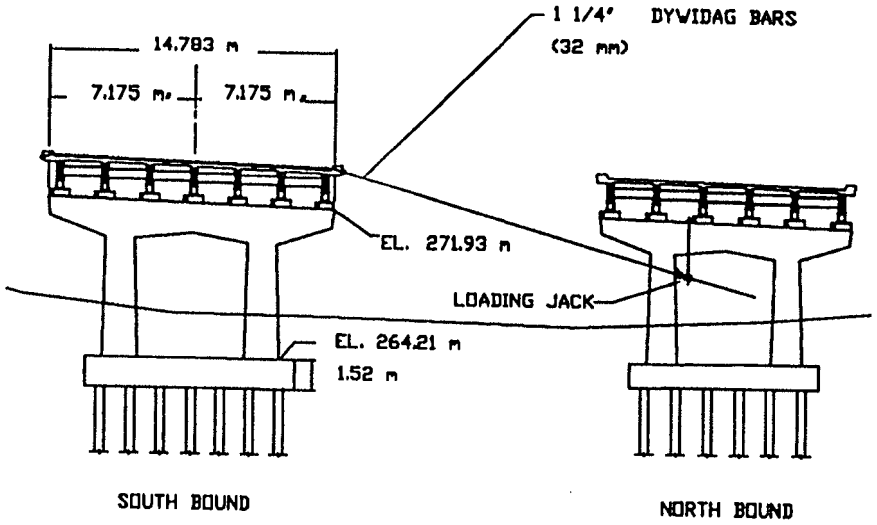

Fig. 2a Over bridge loading set-up

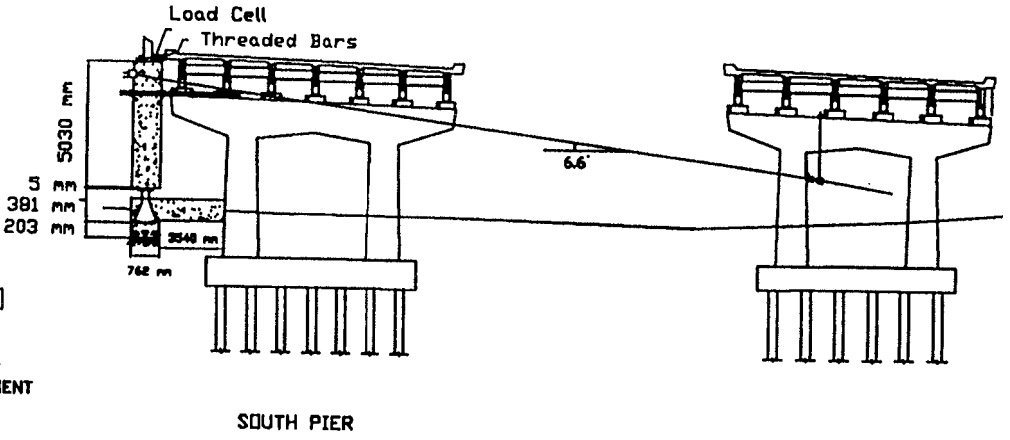

Fig. 2b Under bridge loading setup

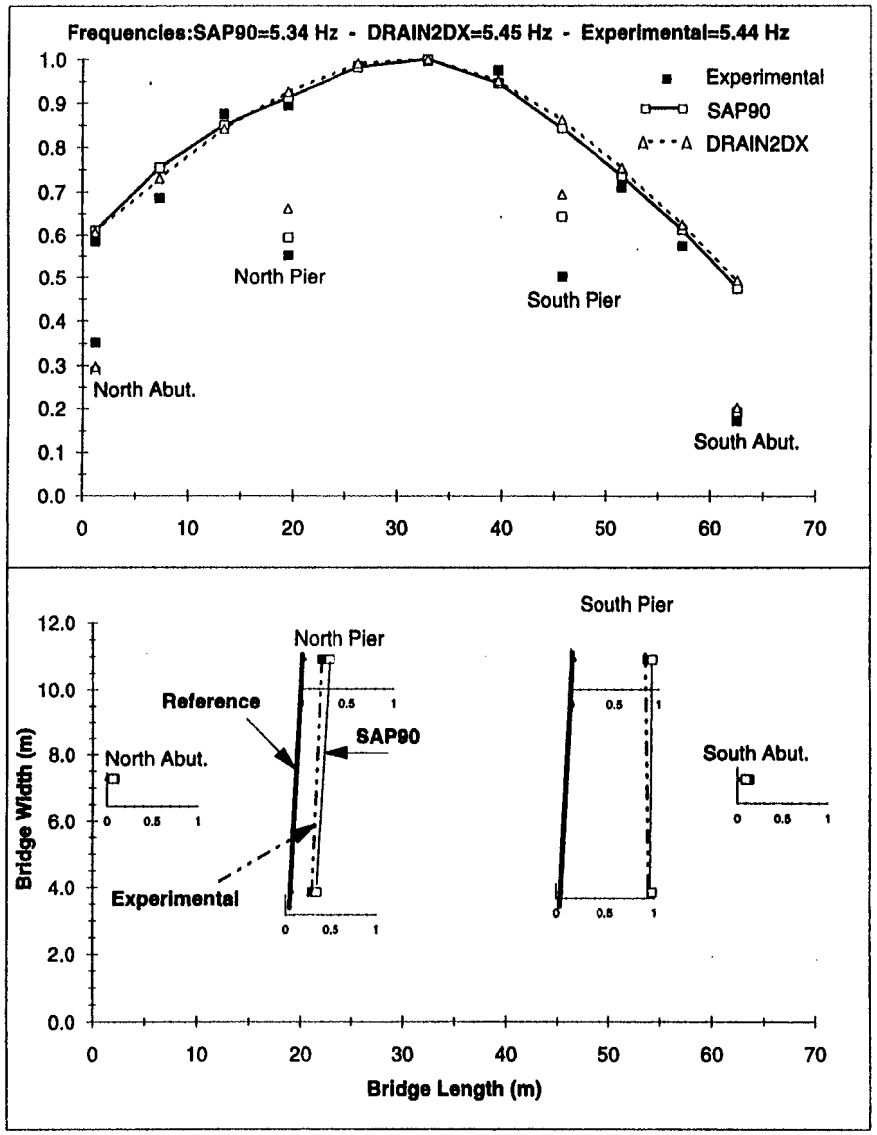

FIGURE 3a Southbound Bridge - First Transverse - Longitudinal Mode

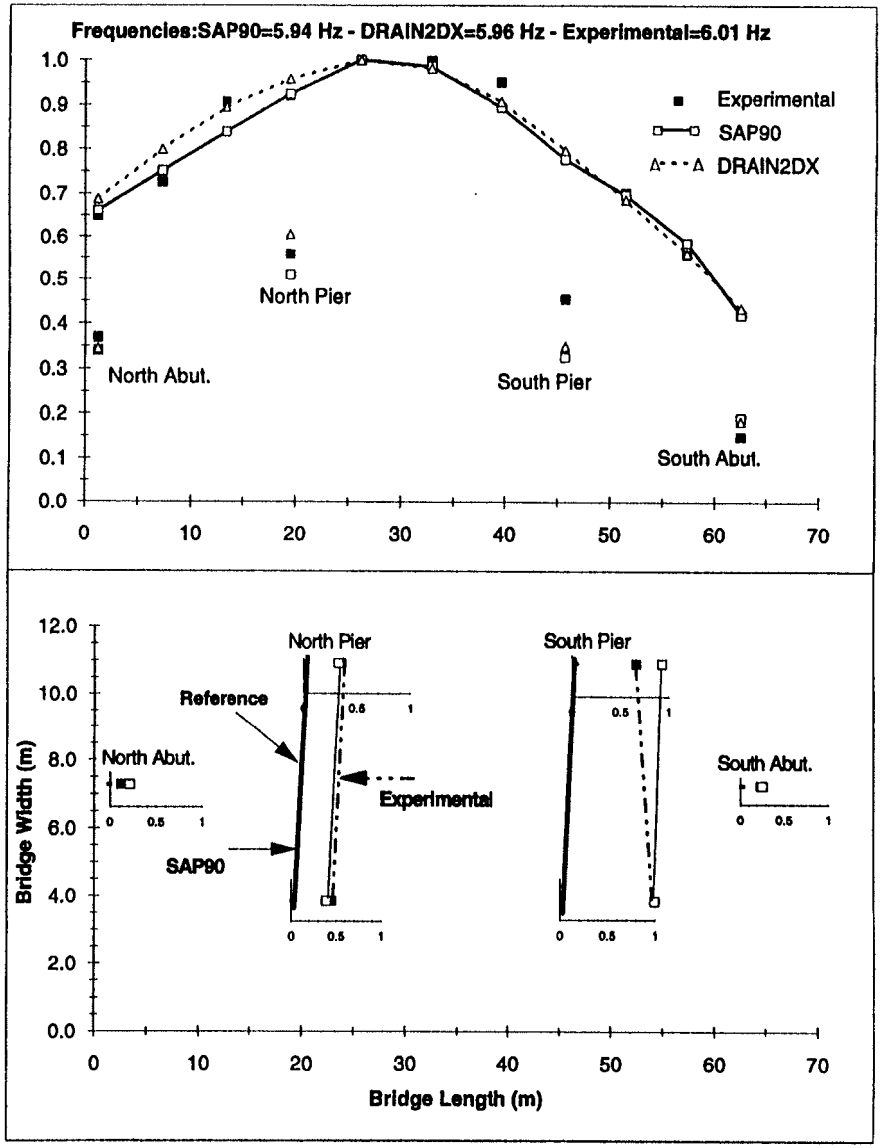

FIGURE 3b Southbound Bridge - Second Transverse - Longitudinal Mode

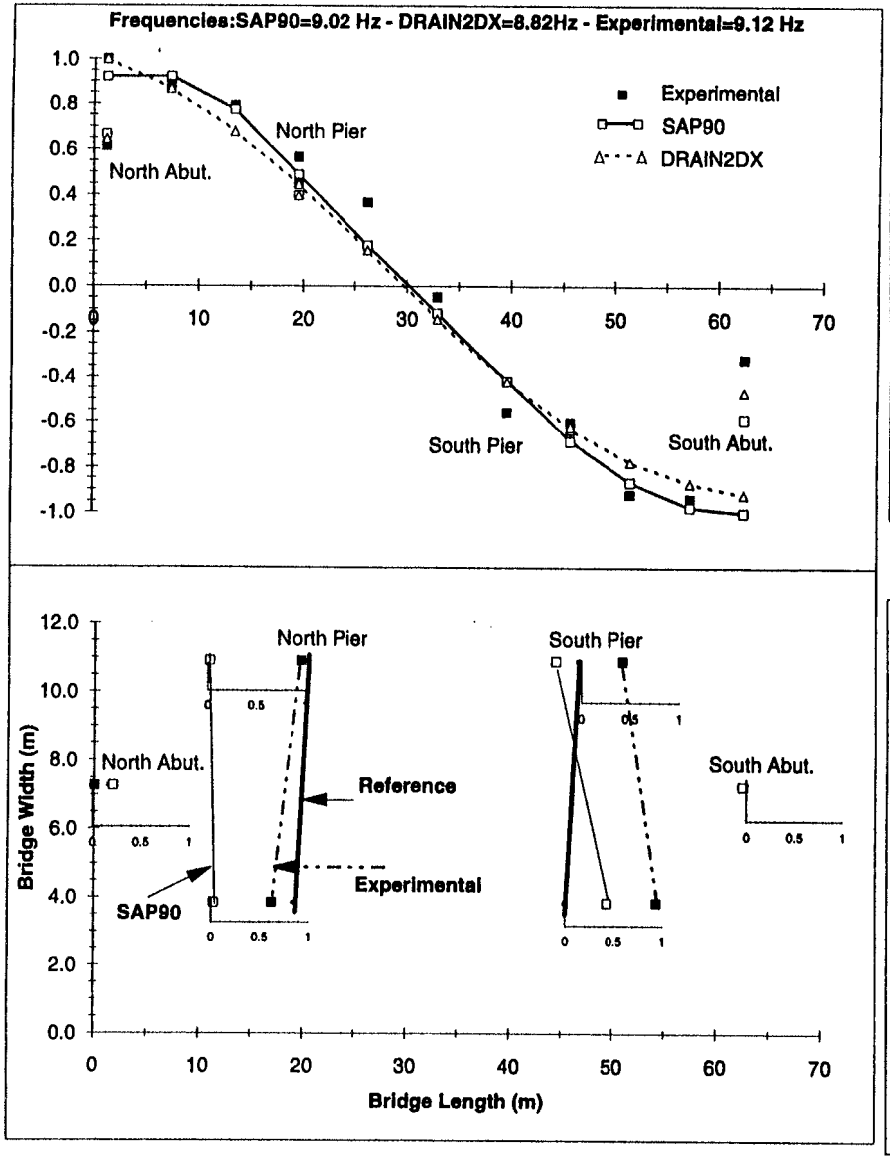

FIGURE 3c Southbound Bridge - Third Transverse Mode

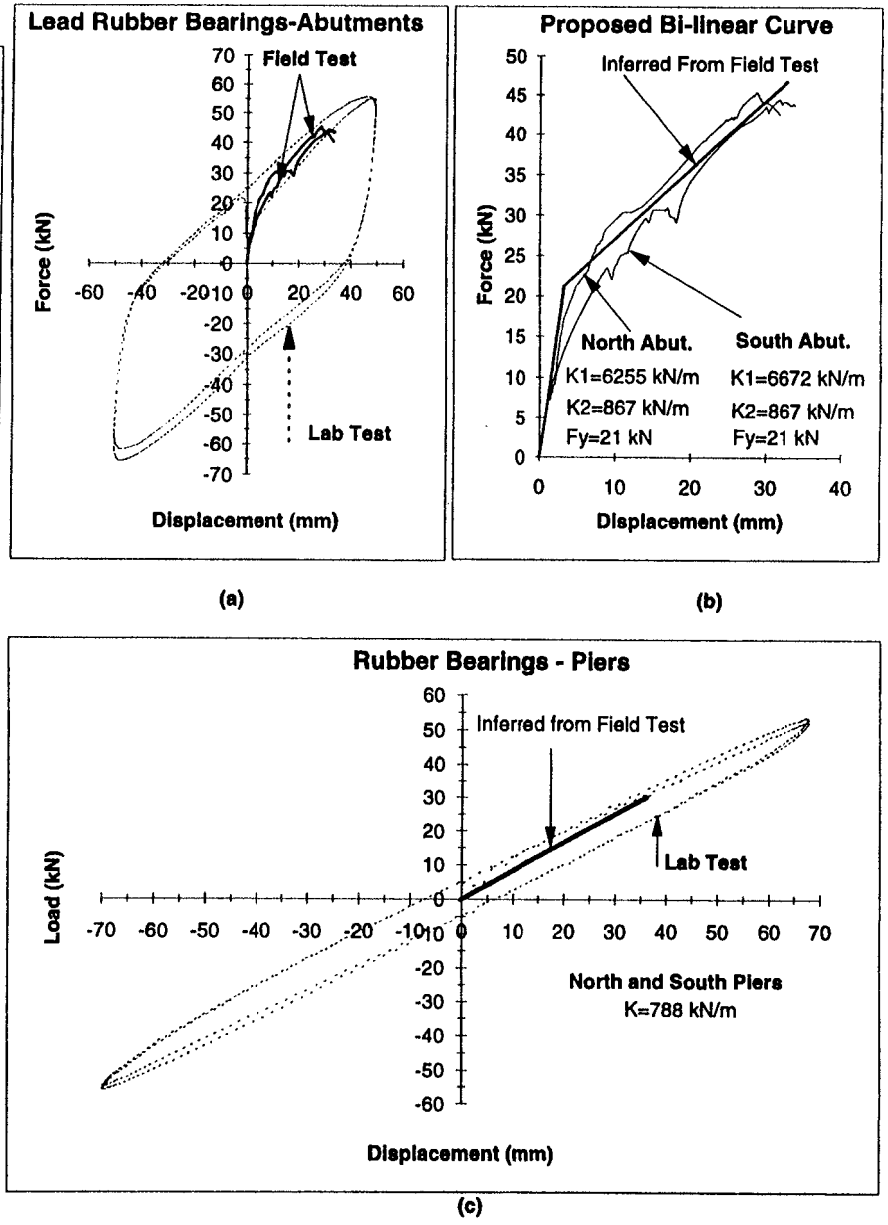

FIGURE 4 Lab Test vs Field Test Behavior - Two Piers Static Test

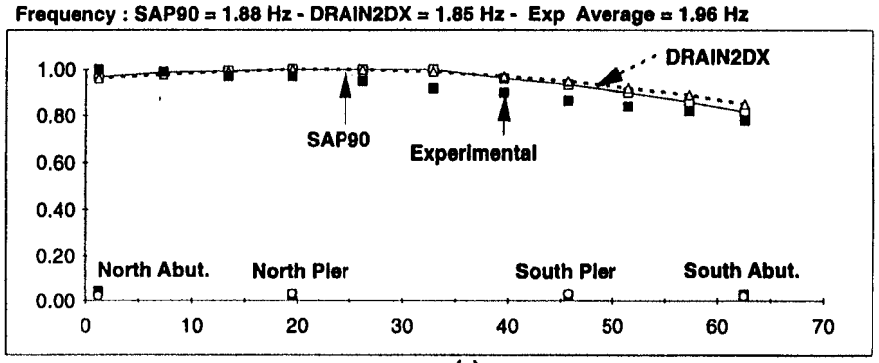

(a)

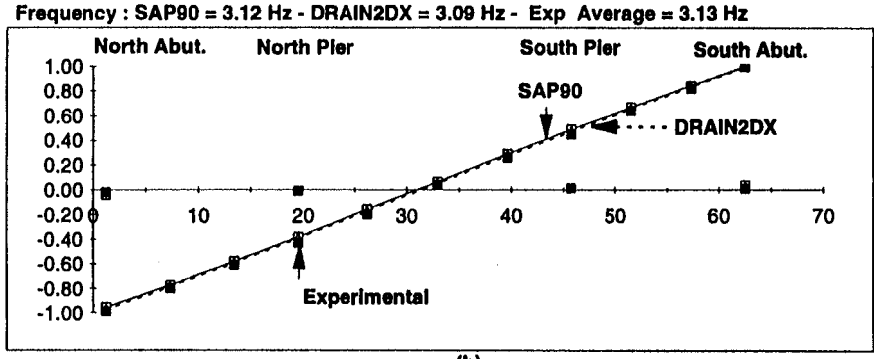

(b)

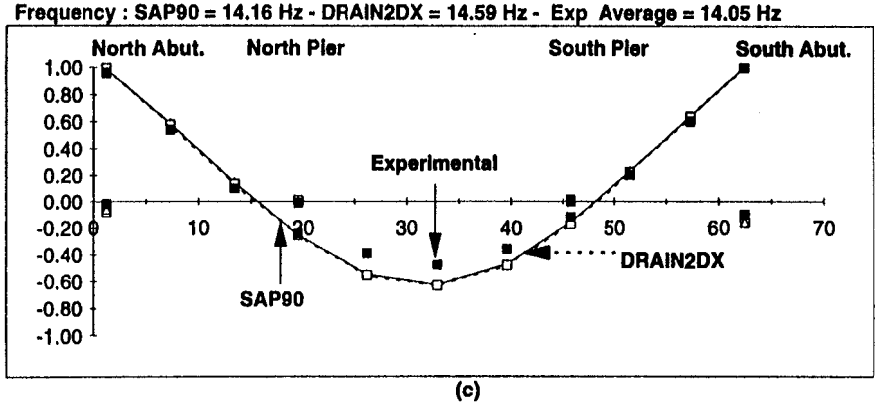

(c)

FIGURE 5 Post-Retrofitted Southbound Bridge - Transverse Modes

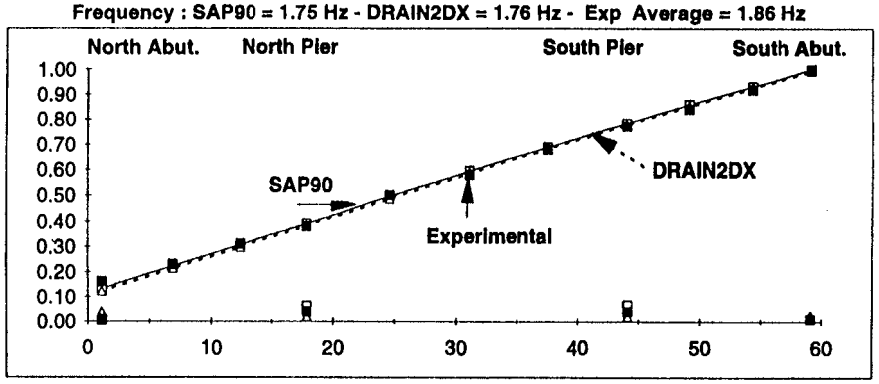

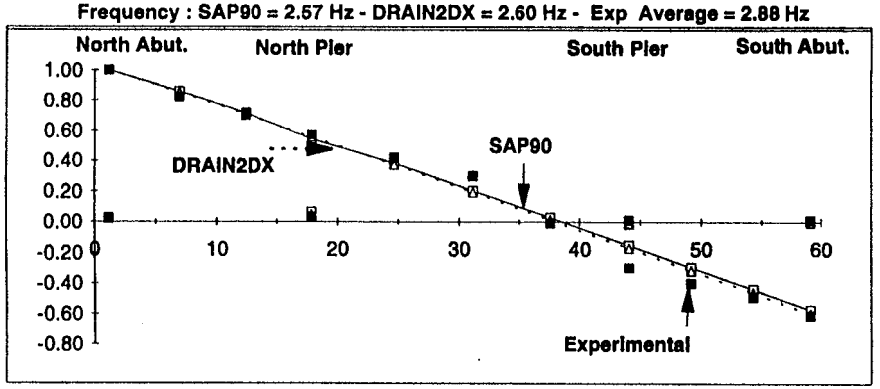

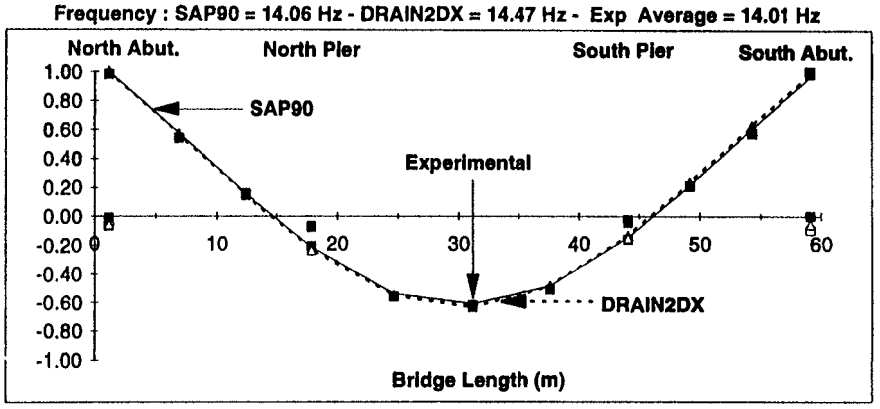

FIGURE 5 Post-Retrofitted Northbound Bridge - Transverse Modes
cont'd

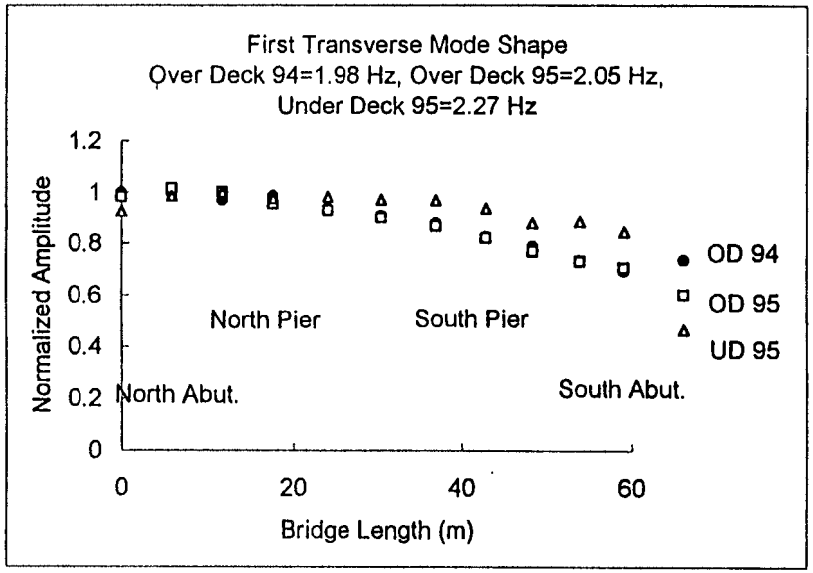

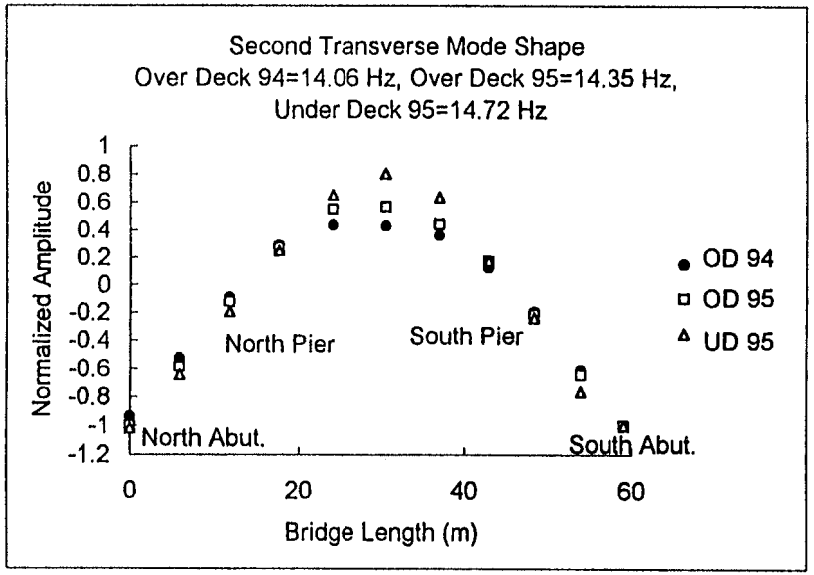

Fig. 6 Transverse mode shapes on deck

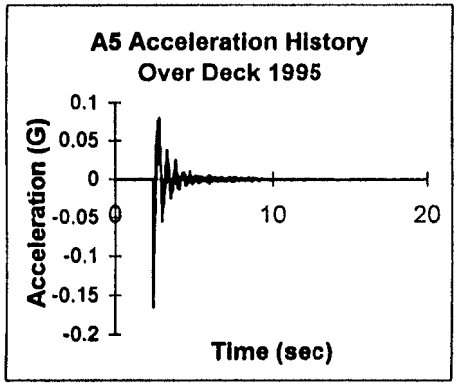

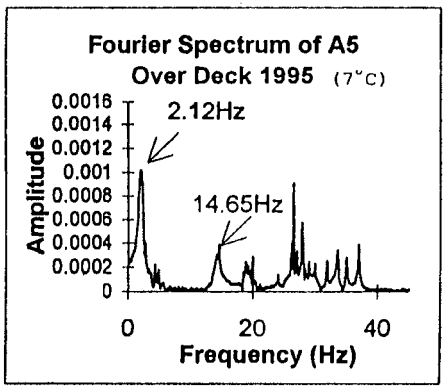

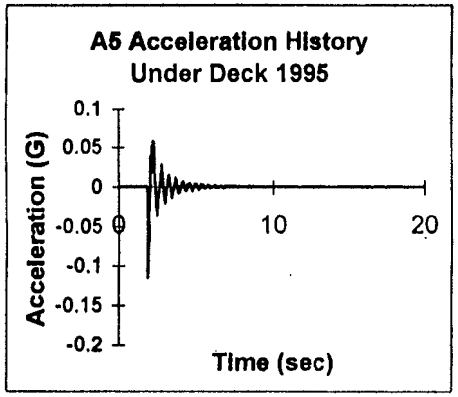

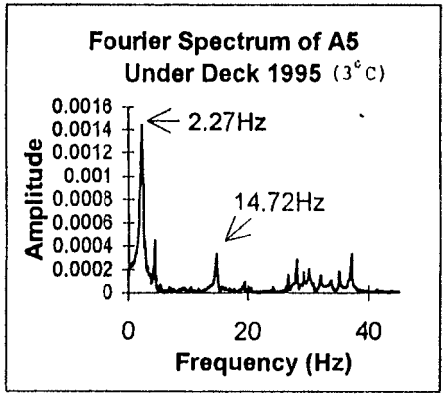

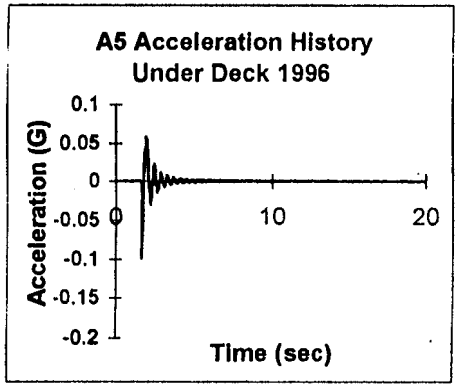

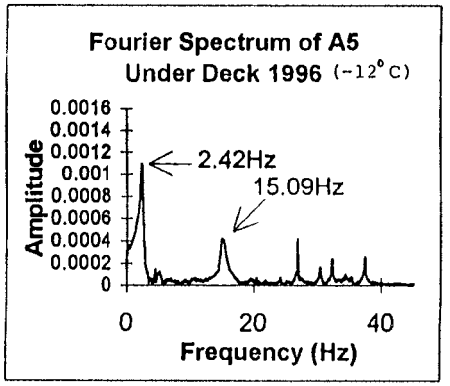

Fig. 7 Transverse Deck-Level Accelerations and Fourier Spectra

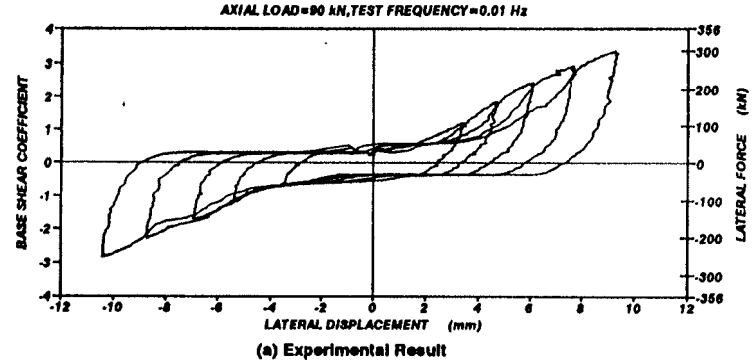

(a) Experimental Result

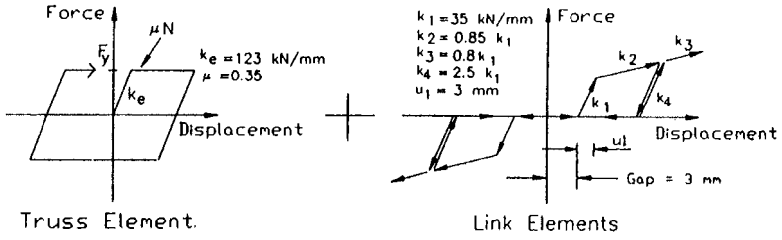

(b) Combination of DRAIN-2DX Elements

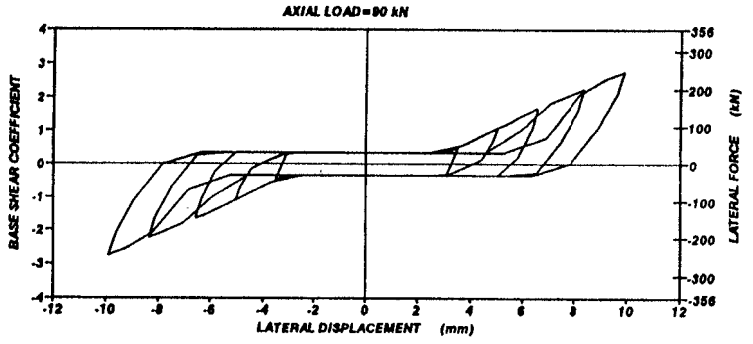

(c) Analytical Result

Figure 8 Hysteresis loop for the low type sliding bearing - transverse direction.

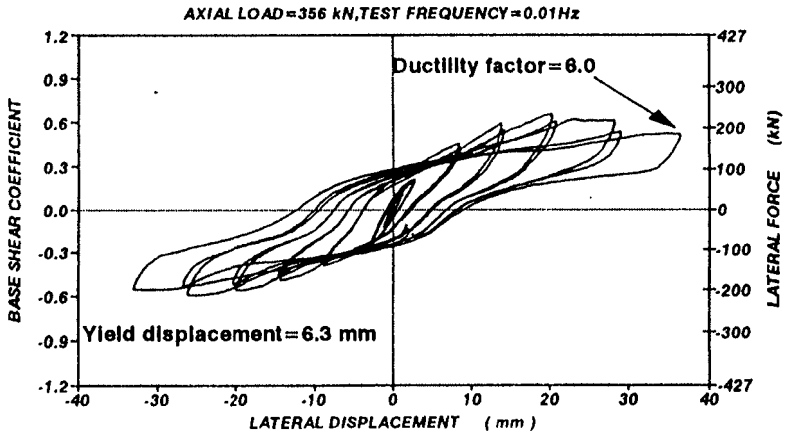

(a) Mounted on Concrete Pedestal with Swedged Anchor Bolts

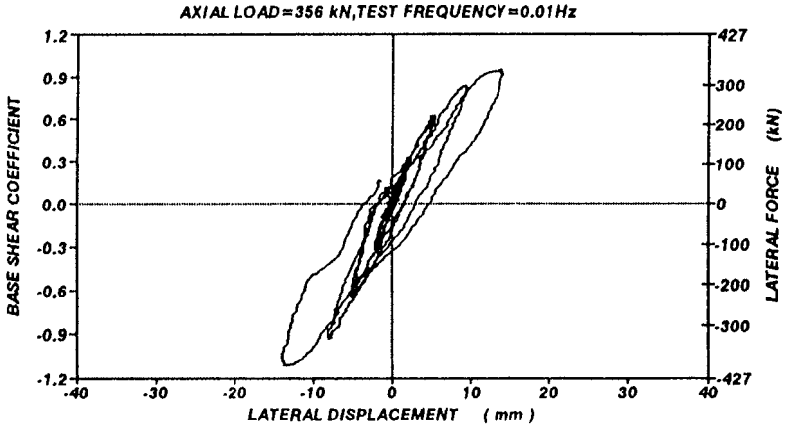

(b) Mounted on Steel Base with Strong Anchor Bolts

Figure 9 Response of the high type fixed steel bearing in longitudinal direction test.

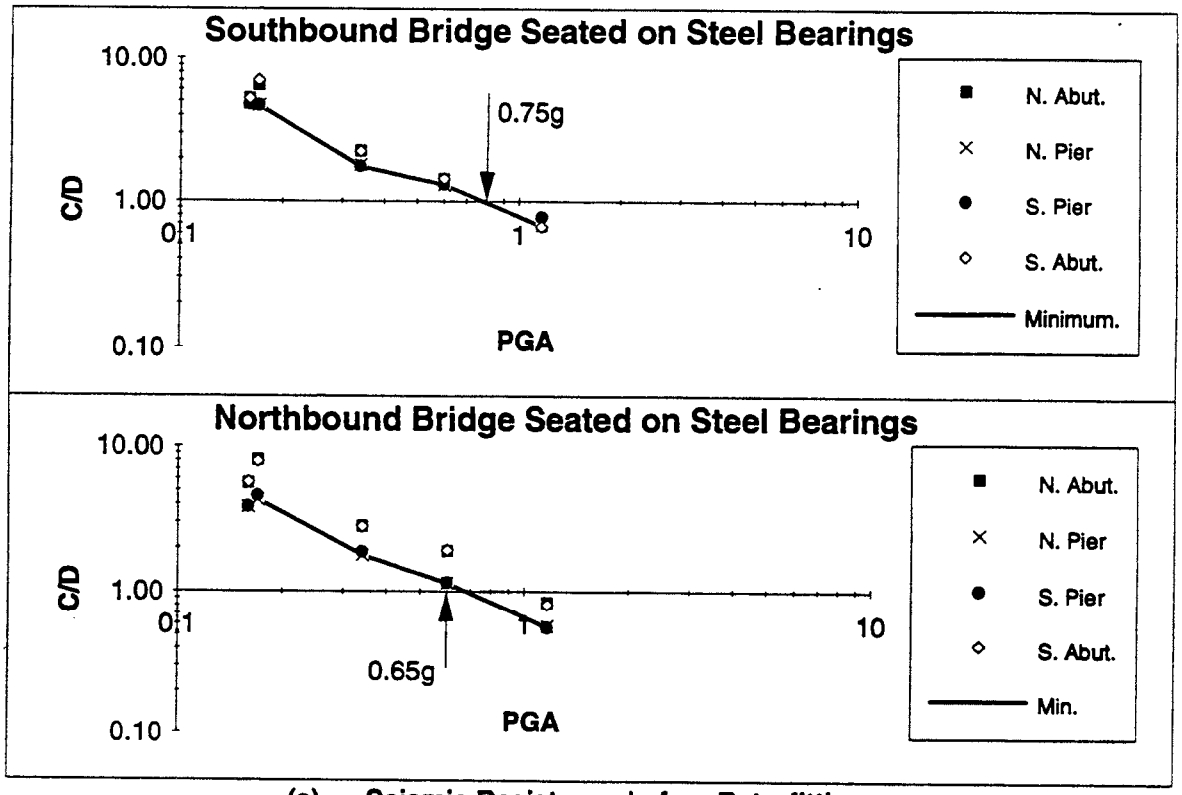

(a) Seismic Resistance before Retrofitting

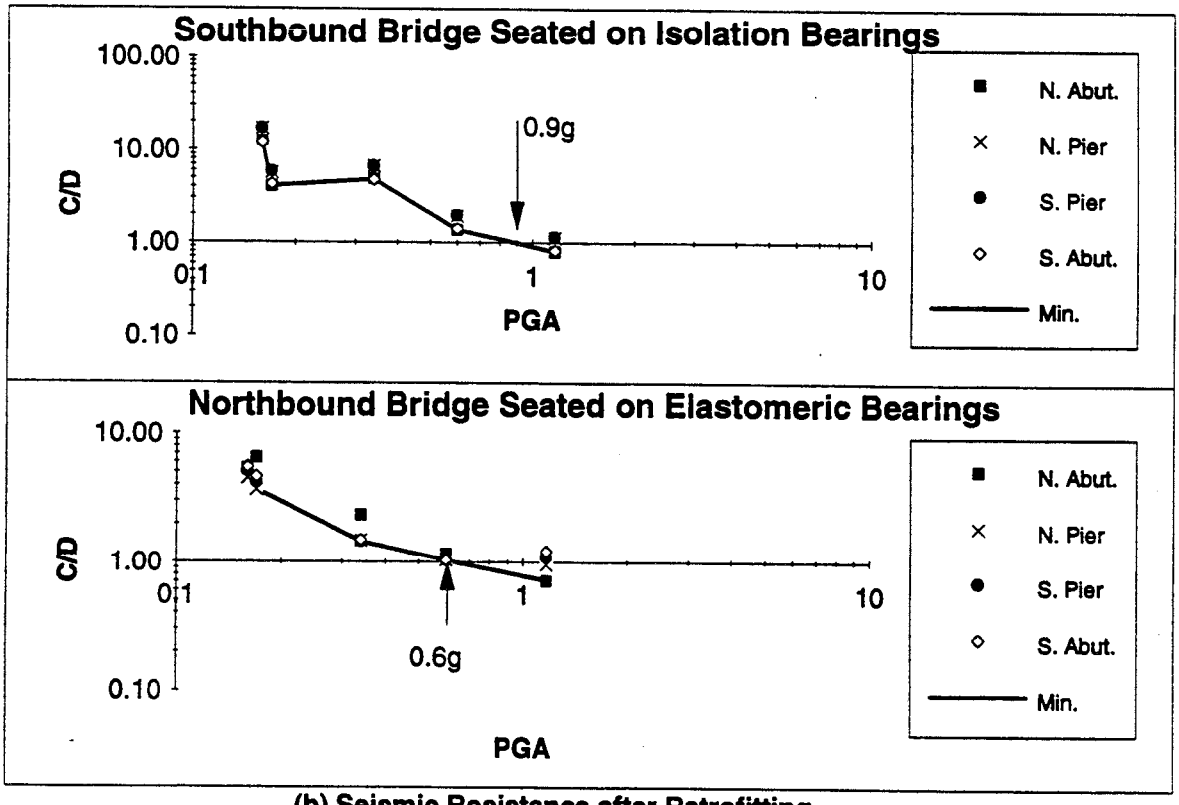

(b) Seismic Resistance after Retrofitting

FIGURE 10 Comparison of C/D ratio With PGA Before and After Retrofitting

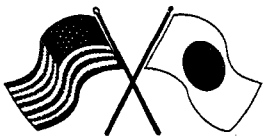

Session 5
Design and Retrofitting

Session Co-chairs: Michael Kreger and Hiroshi Mutsuyoshi

THE 1996 SEISMIC DESIGN SPECIFICATIONS OF HIGHWAY BRIDGES

by
Kazuhiko Kawashima
Tokyo Institute of Technology, Tokyo, Japan
and
Shigeki Unjoh
Public Works Research Institute, Tsukuba, Japan

Abstract

This paper describes the revised Seismic Design Specifications of Highway Bridges in 1996 as well as the background of the revision. Damage features of bridges in the 1995 Hyogo-ken Nanbu Earthquake is first described with an emphasis on the lessons learned from the earthquake. Seismic performance levels and design method as well as the seismic design force introduced in the 1996 Design Specifications are then described.

Keywords: Seismic Design, Bridge, Design Codes, Hyogo-ken Nanbu Earthquake

INTRODUCTION

Highway bridges in Japan had been considered safe even against extreme earthquakes such as the Great Kanto Earthquake (M7.9) in 1923, because various past bitter experiences have been accumulated to formulate the seismic design method (Kawashima (1995)). Large seismic lateral force ranging from 0.2g to 0.3g has been adopted in the allowable stress design approach. Various provisions for preventing damage due to instability of soils such as soil liquefaction have been adopted. Furthermore, design detailings including the unseating prevention devices have been implemented.

In fact, reflecting those provisions, number of highway bridges which suffered complete collapse of superstructures was only 15 since the 1923 Great Kanto Earthquake. Based on such evidence, it had been regarded that the seismic damage of highway bridges has been decreasing in recent year.

However the Hyogo-ken nanbu earthquake of January 17, 1995, exactly one year after the Northridge, California, USA, earthquake caused destructive damage to highway bridges. Collapse and nearly collapse of superstructures occurred at 9 sites, and other destructive damage occurred at 16

sites (Ministry of Construction, 1995a). The earthquake revealed that there are a number of critical issues to be revised in the seismic design and seismic strengthening of bridges in urban areas.

After the earthquake, the "Committee for Investigation on the Damage of Highway Bridges Caused by the Hyogo-ken Nanbu Earthquake" (chairman: Toshio Iwasaki, Executive Director, Civil Engineering Research Laboratory) was formulated in the Ministry of Construction to survey the damage and clarify the factors which contributed to the damage. On February 27, 1995, the Committee approved the " Guide Specifications for Reconstruction and Repair of Highway Bridges which Suffered Damage due to the Hyogo-ken Nanbu Earthquake," (Ministry of Construction 1995b) and the Ministry of Construction noticed on the same day that the reconstruction and repair of the highway bridges which suffered damage in the Hyogo-ken nanbu earthquake should be made by the Guide Specifications. It was decided by the Ministry of Construction on May 25, 1995 that the Guide Specifications should be tentatively used in all sections of Japan as an emergency measure for seismic design of new highway bridges and seismic strengthening of existing highway bridges until the Design Specifications of Highway Bridges was revised.

In May, 1995, the " Special Sub-Committee for Seismic Countermeasures for Highway Bridges" (chairman: Kazuhiko Kawashima, Tokyo Institute of Technology) was formulated in the " Bridge Committee" (chairman: Nobuyuki Narita, Tokyo Metropolitan University), Japan Road Association to draft the revision of the Design Specifications of Highway Bridges. The Special Sub-Committee drafted the new Design Specifications of Highway Bridges, and after the approval of the Bridge Committee, the Ministry of Construction released it on November 1, 1996.

This paper summarizes the damage feature of highway bridges by the Hyogo-ken nanbu earthquake and the new Design Specifications of Highway Bridges issued in November 1996.

DAMAGE FEATURES OF BRIDGES IN THE HYOGO-KEN NANBU EARTHQUAKE

Hyogo-ken nanbu earthquake was the first earthquake which hit an urban area in Japan since the 1948 Fukui earthquake. Although the magnitude of earthquake was moderate (M7.2), the ground motion was much larger than anticipated in the codes. It occurred very close to the Kobe City with shallow focal depth.

Damage was developed at highway bridges on Routes 2, 43, 171 and 176 of the National Highway, Route 3 (Kobe Line) and Route 5 (Bay Shore Line) of the Hanshin Expressway, and Meishin and Chugoku Expressway. Damage was surveyed for all bridges on National Highways, Hanshin Expressways and Expressways in the area where destructive damage occurred. Total number of piers

surveyed reached 3,396 (Ministry of Construction, 1995a). Fig. 1 shows the Design Specifications referred to in design of the 3,396 piers. Most of piers (bridges) which suffered damage were designed according to the 1964 Design Specifications or older Design Specifications. Although the seismic design methods have been improved and amended several times since 1926 based on damage experience and progress of bridge earthquake engineering, only a requirement for lateral force coefficient was provided in the 1964 Design Specifications or older Specifications.

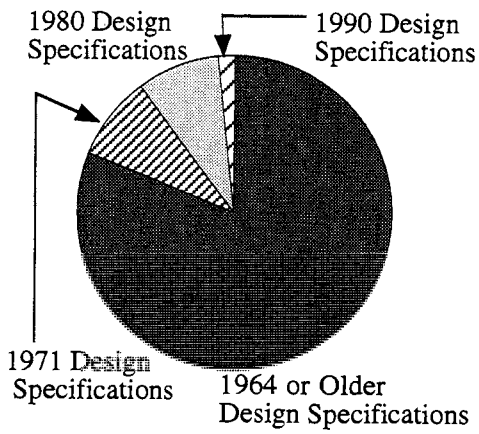

Fig. 1 Design Specifications Referred to in Design of Hanshin Expressway

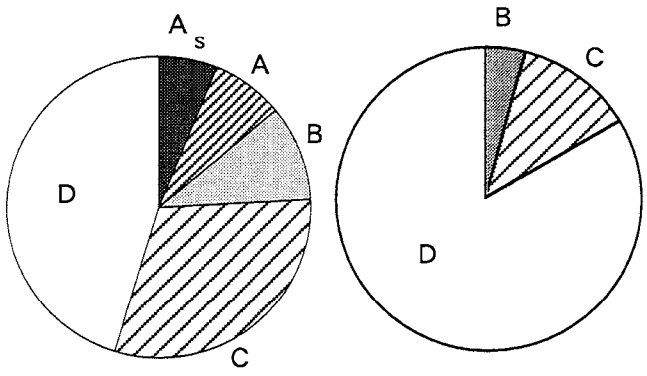

(a) Route 3 (b) Route 5

Fig. 2 Comparison of Damage Degree between Route 3 and Route 5 (As: Collapse, A: Nearly Collapse B: Moderate Damage, C: Damage of Secondary Members, D: Minor or No Damage)

Fig. 2 compares damage of piers on the Route 3, Kobe Line, and Route 5, Bay Shore Line, of the Hanshin Expressway. Damage degree was classified as A_S (collapse), A (nearly collapse), B (moderate damage), C (damage of secondary members) and D (minor or no damage). Substructures of the Route 3 and Route 5 were designed with the 1964 Design Specifications and 1980 Design Specifications, respectively. It should be noted in this comparison that the intensity of ground shaking in terms of response spectra was smaller at the Bay Area than the narrow rectangular area where JMA Seismic Intensity was VII (equivalent to the Modified Mercalli Intensity of X-XI). The Route 3 was located in the narrow rectangular area while the Route 5 was located in the Bay Area. Keeping in mind such difference of ground motion, it is apparent in Fig. 2 that about 14 % of the piers on Route 3 suffered A_S or A damage while no such damage was developed in the piers on the Route 5.

Although damage concentrated on the bridges designed with the older Design Specifications, it was thought that essential revision was required even in the recent Design Specifications to prevent damage against destructive earthquakes such as the Hyogo-ken nanbu earthquake. The main points requiring modifications were;

(1) it was required to increase lateral capacity and ductility of all structural components in which seismic force is predominan t so that ductility of a total bridge system be enhanced. For such purpose, it was required to upgrade the " Check of Ductility of Reinforced Concrete Piers," which has been used since 1990, to a " Ductility Design Method," and to apply the Ductility Design Method to all structural components. It should be noted here that " check" and " design" is different; the check is only to verify the safety of a structural member designed by other design method, and is effective only to increase the size or reinforcements if required, while the design is an essential procedure to determine the size and reinforcements,

(2) it was required to include the ground motion developed at Kobe in the earthquake as a design force in the Ductility Design Method,

(3)it was required to specify input ground motions in terms of acceleration response spectra for dynamic response analysis more actively,

(4) it was required to increase tie reinforcements and to introduce intermediate ties for increasing ductility of piers. It was decided not to terminate main reinforcements at mid-height for preventing premature shear failure, in principle,

(5) it was suggested to adopt multi-span continuous bridge for increasing number of indeterminate of a total bridge system,

(6) it was suggested to adopt rubber bearings for absorbing lateral displacement between a superstructure and substructures. It was important to consider correct mechanism of force transfer from a superstructure to substructures,

(7) it was suggested to include the Menshin design (seismic isolation),

(8) it was required to increase strength, ductility and energy dissipation capacity of unseating prevention devices, and

(9) it was required to consider the effect of lateral spreading associated with soil liquefaction in design of foundati ons at the site vulnerable to lateral spreading.

BASIC PRINCIPLE OF SEISMIC DESIGN

Table 1 shows the seismic performance level provided in the revised Design Specifications in 1996. The bridges are categorized into two groups depending on their importanc e; standard bridges (Type-A bridges) and important bridges (Type-B bridges). Seismic performance level depends on the importance of bridges. For moderate ground motions induced in the earthquakes with high probability to occur, both A and B bridges should behave in an elastic manner without essential structural damage. For extreme ground motions induced in the earthquakes with low probability to occur, the Type-A bridges should prevent critical failure, while the Type-B bridges should perform with limited damage.

In the Ductility Design Method, two types of ground motions must be considered. The first is the ground motion which could be induced in the plate boundary-type earthquakes with magnitude of about 8. The ground motion at Tokyo in the 1923 Kanto earthquake is a typical target of this type of ground motion. The second is the ground motion developed in earthquakes with magnitude of about 7-7.2 at very short distance. Obviously the ground motion at Kobe in the Hyogo-ken nanbu earthquake is a typical target of this type of ground motion. The first and the second ground motions are called as Type-I and Type-II ground motions, respectively. The recurrence time of the Type-II ground motion may be longer than that of the Type-I ground motion, although the estimation is very difficult.

Table 1. Seismic Performance Levels

<table>
<tr><td colspan="2" rowspan="2">Type of Design Ground Motions</td><td colspan="2">Importance</td><td colspan="2">Design Methods</td></tr>
<tr><td>Type-A Bridges (Standard Bridges)</td><td>Type-B Bridges (Important Bridges)</td><td>Equivalent Static Lateral Force Methods</td><td>Dynamic Analysis</td></tr>
<tr><td colspan="2">Ground Motions with High Probability to Occur</td><td colspan="2">Prevent damage</td><td>Seismic Coefficient Method</td><td rowspan="3">Step by Step Analysis or Response Spectrum Analysis</td></tr>
<tr><td rowspan="2">Ground Motions with Low Probability to Occur</td><td>Type-I (Plate-boundary type Earthquakes)</td><td rowspan="2">Prevent Critical Failure</td><td rowspan="2">Limited Damage</td><td rowspan="2">Ductility Design Method</td></tr>
<tr><td>Type-II (Inland Earthquakes)</td></tr>
</table>

DESIGN METHODS

Bridges are designed by both the Seismic Coefficient Method and the Ductility Design Method as shown in Fig. 3. In the Seismic Coefficient Method, a lateral force coefficient ranging from 0.2 to 0.3 has been used based on the allowable stress design approach. No change was introduced since the 1990 Specifications in the Seismic Coefficient Method.

In the Ductility Design method, assuming a principal plastic hinge formed at the bottom of pier as shown in Fig. 4 (a) and the equal energy assumption, a bridge is designed so that the following requirement is satisfied.

$$P_a \geq k_{he} W \tag{1}$$

where

$$k_{he} = \frac{k_{hc}}{\sqrt{2\mu_a - 1}} \tag{2}$$

$$W = W_U + c_P W_P \tag{3}$$

in which P_a= lateral capacity of a pier, k_{he}= equivalent lateral force coefficient, W= equivalent weight, k_{hc}= lateral force coefficient, μ_a= allowable displacement ductility factor of a pier, W_U= weight of a part of superstructure supported by the pier, W_P= weight of a pier, and c_P=coefficient depending on the type of failure mode. The c_P is 0.5 for a pier in which either flexural failure or shear failure after flexural cracks are developed, and 1.0 for a pier in which shear failure is developed. The lateral capacity of a pier P_a is defined as a lateral force at the gravity center of a superstructure.

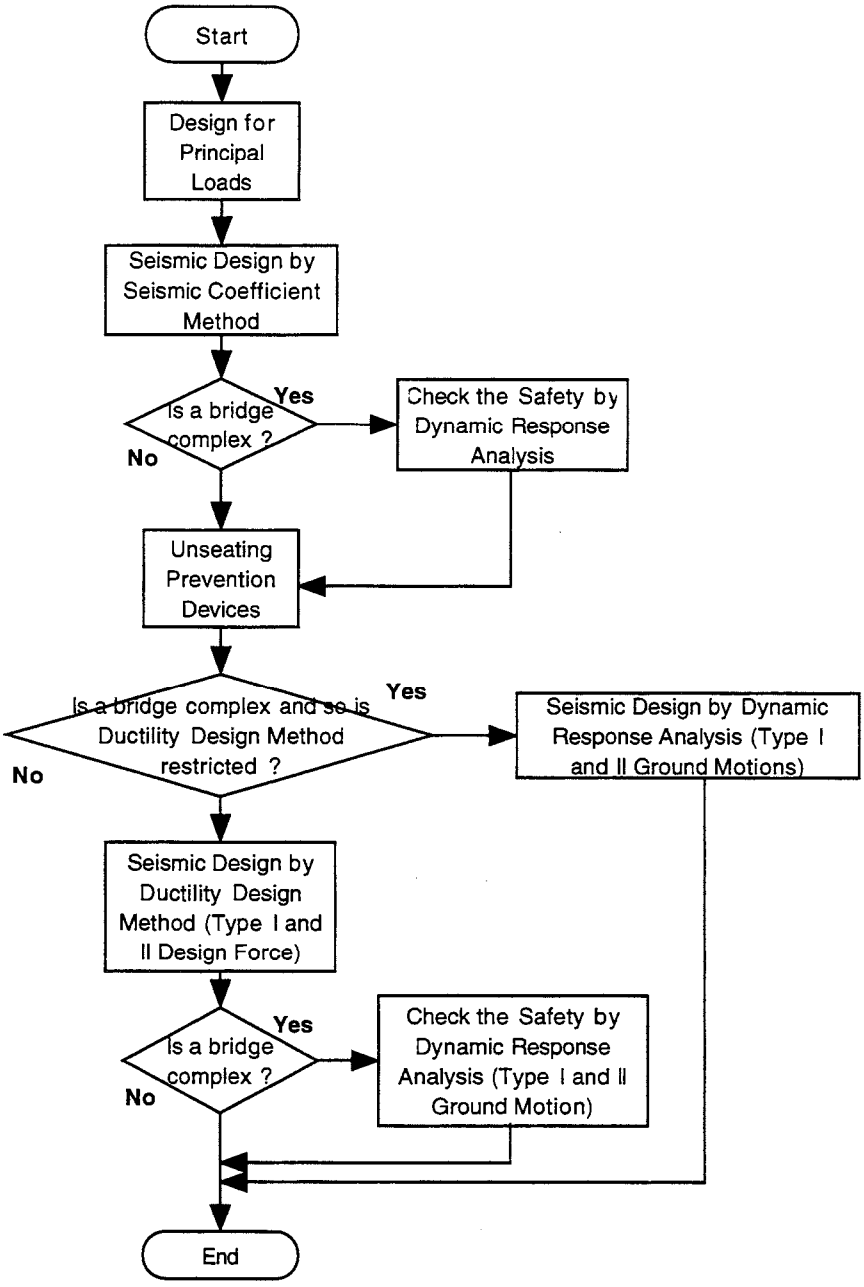

Fig. 3 Flowchart of Seismic Design

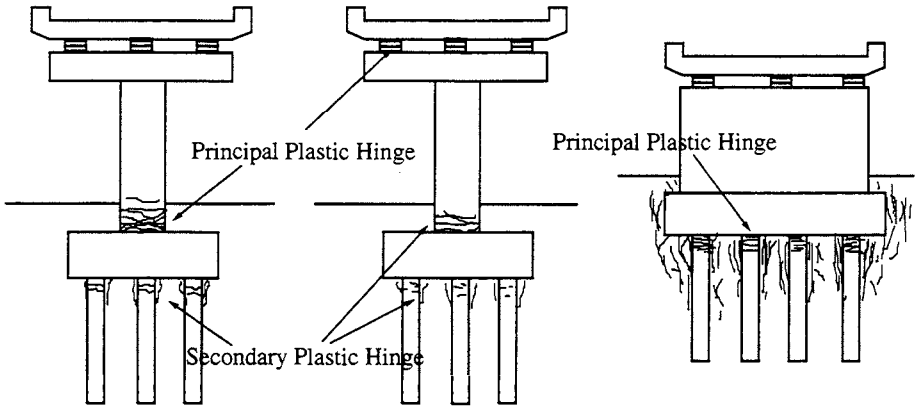

(a) Conventional Design (b) Menshin Design (c) Bridge Supported by a Wall Pier

Fig. 4 Location of Primary Plastic Hinge

In the Type-B bridges, residual displacement developed at a pier after an earthquake must be checked as

$$\delta_R \le \delta_{Ra} \tag{4}$$

where

$$\delta_R = c_R(\mu_R - 1)(1 - r)\delta_y \tag{5}$$

$$\mu_R = \frac{1}{2}\left\{\left(\frac{k_{hc}W}{P_a}\right)^2 + 1\right\} \tag{6}$$

in which δ_R= residual displacement of a pier after an earthquake, δ_{Ra}= allowable residual displacement of a pier, r= bilinear factor defined as a ratio between the first stiffness (yield stiffness) and the second stiffness (post-yield stiffness) of a pier, c_R= factor depending on the bilinear factor r, μ_R= response ductility factor of a pier, and δ_y= yield displacement of a pier. The δ_{Ra} should be 1/100 of a distance between the bottom of a pier and a gravity center of a superstructure.

In a bridge with complex dynamic response, the dynamic response analysis is required to check the safety of a bridge after it is designed by the Seismic Coefficient Method and the Ductility Design Method. Because this is only for a check of the design, the size and reinforcements of structural members once determined by the Seismic Coefficient Method and the Ductility Design Method can only be increased if necessary. It should be noted however that under the following conditions in which the Ductility Design Method is not directly applied, the size and reinforcements can be determined based on the results of a dynamic response analysis as shown in Fig. 3. The conditions when the Ductility Design Method should not be directly used include

(1) principal mode shapes which contribute to bridge response are different from the ones assumed in the Ductility Design Method,

(2) more than two modes significantly contribute to bridge response,

(3) principal plastic hinges form at more than two locations, or principal plastic hinges are not known where to be formed, and

(4)response modes for which the equal energy assumption are not applied.

In the seismic design of a foundation, a lateral force equivalent to the ultimate lateral capacity of a pier P_u is assumed to be a design force as

$$k_{hp} = c_{df} P_u / W \tag{7}$$

in which k_{hp}= lateral force coefficient for a foundation, c_{df} = modification coefficient (=1.1), and W =equivalent weight by Eq. (3). Because the lateral capacity of a wall-type pier is very large in transverse direction, the lateral seismic force evaluated by Eq. (7) becomes in most cases excessive. Therefore if a foundation has sufficiently large lateral capacity compared with the lateral seismic force, the foundation is designed assuming a plastic hinge at the foundation and the surrounding soils as shown in Fig. 4 (c).

DESIGN SEISMIC FORCE

The lateral force coefficient k_{hc} in Eq. (2) is given as

$$k_{hc} = c_Z \cdot k_{hc0} \tag{8}$$

in which c_Z= modification coefficient for zone, and is 0.7, 0.85 and 1.0 depending on zone, and k_{hc0}= standard modification coefficient. Table 2 and Fig. 5 show the standard lateral force coefficients k_{hc0} for the Type-I and the Type-II ground motions. The Type-I ground motions have been used since 1990 (1990 Specifications), while the Type-II ground motions were introduced in the 1996 Specifications. It should be noted here that the k_{hc0} at stiff site (Group I) has been assumed smaller than the k_{hc0} at moderate (Group II) and soft soil (Group III) sites in the Type-I ground motions as well as the seismic coefficients for the Seismic Coefficient Method. The Type-I ground motions were essentially estimated from an attenuation equation for response spectra that was derived from a statistical analysis of 394 components of strong motion records. Although the response spectral accelerations at short natural period are larger at stiff sites than at soft soil sites, the tendency had not been explicitly included in the past. This was because damage has been more developed at soft sites than at stiff sites. To consider such fact, the design force at stiff sites has been assumed smaller than that at soft sites even at short natural period. However being different from such a traditional consideration, the Type II ground motions were determined by simply taking envelops of response accelerations of major strong motions recorded at Kobe in the Hyogo-ken Nanbu earthquake. It was considered appropriate to set realistic ground motions.

Although the acceleration response spectral intensity at short natural period is higher in the Type-II ground motions than in the Type-I ground motions, the duration of extreme acceleration excursion

is longer in the Type-I ground motions than the Type-II ground motions. As will be described later, such a difference of the duration has been taken into account to evaluate the allowable displacement ductility factor of a pier.

Table 2 Lateral Force Coefficient k_{hc0} in the Ductility Design Method

(a) Type-I Ground Motions

Soil Condition	Lateral Force Coefficient k_{hc0}		
Group I (stiff)	$k_{hc0}=0.7$ for $T \leqq 1.4$		$k_{hc0}=0.876\ T^{-2/3}$ for $1.4 < T$
Group II (moderate)	$k_{hc0}=1.51\ T^{1/3} \geqq 0.7$ for $T < 0.18$	$k_{hc0}=0.85$ for $0.18 \leqq T \leqq 1.6$	$k_{hc0}=1.16\ T^{-2/3}$ for $1.6 < T$
Group III (soft)	$k_{hc0}=1.51\ T^{1/3} \geqq 0.7$ for $T < 0.29$	$k_{hc0}=1.0$ for $0.29 \leqq T \leqq 2.0$	$k_{hc0}=1.59\ T^{-2/3}$ for $2.0 < T$

(b) Type-II Ground d Motions

Soil Condition	Lateral Force Coefficient k_{hc0}		
Group I (stiff)	$k_{hc0}=4.46\ T^{2/3}$ for $T < 0.3$	$k_{hc0}=2.0$ for $0.3 \leqq T \leqq 0.7$	$k_{hc0}=1.24\ T^{-4/3}$ for $0.7 < T$
Group II (moderate)	$k_{hc0}=3.22\ T^{2/3}$ for $T < 0.4$	$k_{hc0}=1.75$ for $0.4 \leqq T \leqq 1.2$	$k_{hc0}=2.23\ T^{-4/3}$ for $1.2 < T$
Group III (soft)	$k_{hc0}=2.38\ T^{2/3}$ for $T < 0.5$	$k_{hc0}=1.50$ for $0.5 \leqq T \leqq 1.5$	$k_{hc0}=2.57\ T^{-4/3}$ for $1.5 < T$

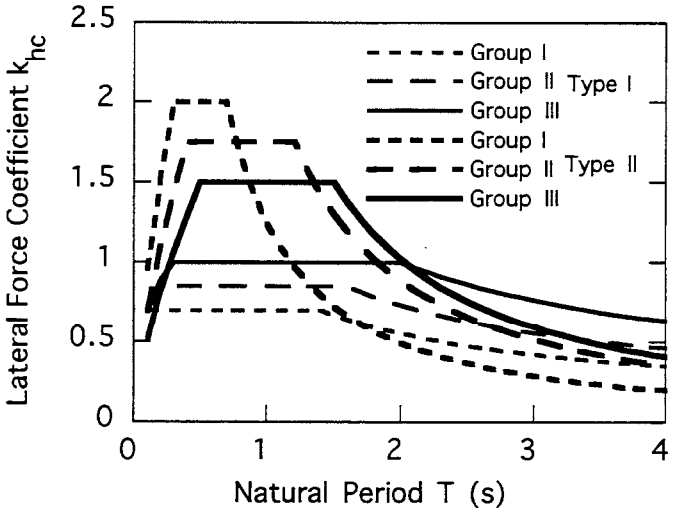

Fig. 5 Type I and Type II Lateral Force Coefficients in the Ductility Design Method

EVALUATION OF DISPLACEMENT DUCTILITY FACTOR OF A PIER

Reinforced concrete pier

The allowable displacement ductility factor of a pier μ_a in Eq. (2) is evaluated as

$$\mu_a = 1 + \frac{\delta_u - \delta_y}{\alpha \cdot \delta_y} \tag{9}$$

in which α= safety factor, δ_y= yield displacement of a pier, and δ_u= ultimate displacement of a pier. As well as the lateral capacity of a pier P_a in Eq. (1), the δ_y and δ_u are defined at the gravity center of a superstructure. In a reinforced concrete single pier as shown in Fig. 4 (a), the ultimate displacement δ_u is evaluated as

$$\delta_u = \delta_y + (\phi_u - \phi_y)(h - L_p/2)L_p \tag{10}$$

in which ϕ_y= yield curvature of a pier at a plastic hinge zone, ϕ_u= ultimate curvature of a pier at a plastic hinge zone, h= height of a pier, and L_p= plastic hinge length of a pier. The plastic hinge length is given as

$$L_p = 0.2h - 0.1D \qquad (0.1D \le L_p \le 0.5D) \tag{11}$$

in which D is a width or a diameter of a pier.

The yield curvature ϕ_y and the ultimate curvature ϕ_u in Eq. (10) are evaluated assuming a stress-strain relation of reinforcements and concrete as shown in Fig. 6. The stress σ_c - strain ε_c relation of concrete with lateral confinement is assumed as

$$\sigma_c = \begin{cases} E_c\varepsilon_c\left\{1 - \frac{1}{n}\left(\frac{\varepsilon_c}{\varepsilon_{cc}}\right)^{n-1}\right\} & (0 \le \varepsilon_c \le \varepsilon_{cc}) \\ \sigma_{cc} - E_{des}(\varepsilon_c - \varepsilon_{cc}) & (\varepsilon_{cc} \le \varepsilon_c \le \varepsilon_{cu}) \end{cases} \tag{12}$$

$$n = \frac{E_c\varepsilon_{cc}}{E_c\varepsilon_{cc} - \sigma_{cc}} \tag{13}$$

in which σ_{cc}= strength of confined concrete, E_c= elastic modulus of concrete, ε_{cc}= strain at maximum strength, and E_{des}= gradient at descending branch. In Eq. (12), the σ_{cc}, ε_{cc} and E_{des} are determined as

$$\sigma_{cc} = \sigma_{ck} + 3.8\alpha\rho_s\sigma_{sy} \tag{14}$$

$$\varepsilon_{cc} = 0.002 + 0.033\beta\frac{\rho_s\sigma_{sy}}{\sigma_{ck}} \tag{15}$$

$$E_{des} = 11.2\frac{\sigma_{ck}^{\,2}}{\rho_s\sigma_{sy}} \tag{16}$$

in which σ_{ck}= design strength of concrete, σ_{sy}= yield strength of reinforcements, α and β= coefficients depending on the shape of a pier (α=1.0 and β=1.0 for a circular pier, and α=0.2 and β=0.4 for a rectangular pier), and ρ_s= tie reinforcement ratio defined as

$$\rho_s = \frac{4A_h}{s \cdot d} \tag{17}$$

in which A_h= area of tie reinforcements, s= space of tie reinforcements, and d= effective width of tie reinforcements.

The ultimate curvature ϕ_u is defined as a curvature when concrete strain at longitudinal reinforcing bars in compression reaches an ultimate strain ε_{cu} defined as

$$\varepsilon_{cu} = \begin{cases} \varepsilon_{cc} & \text{for Type I ground motions} \\ \varepsilon_{cc} + \dfrac{0.2\sigma_{cc}}{E_{des}} & \text{for Type II ground motions} \end{cases} \tag{18}$$

It is important to note here that the ultimate strain ε_{cu} depends on the types of ground motions; the ε_{cu} for the Type-II ground motions is larger than that for the Type-I ground motions. Based on a loading test, it is known that a certain level of failure in a pier such as a sudden decrease of lateral capacity occurs at smaller lateral displacement in a pier subjected to a loading hysteresis with more number of load reversals. To reflect such a fact, it was decided that the ultimate strain ε_{cu} should be evaluated by Eq. (18), depending on the type of ground motions. Therefore, the allowable ductility factor μ_a also depends on the type of ground motions; the μ_a is larger in a pier subjected to the Type-II ground motions than a pier subjected to the Type-I ground motions.

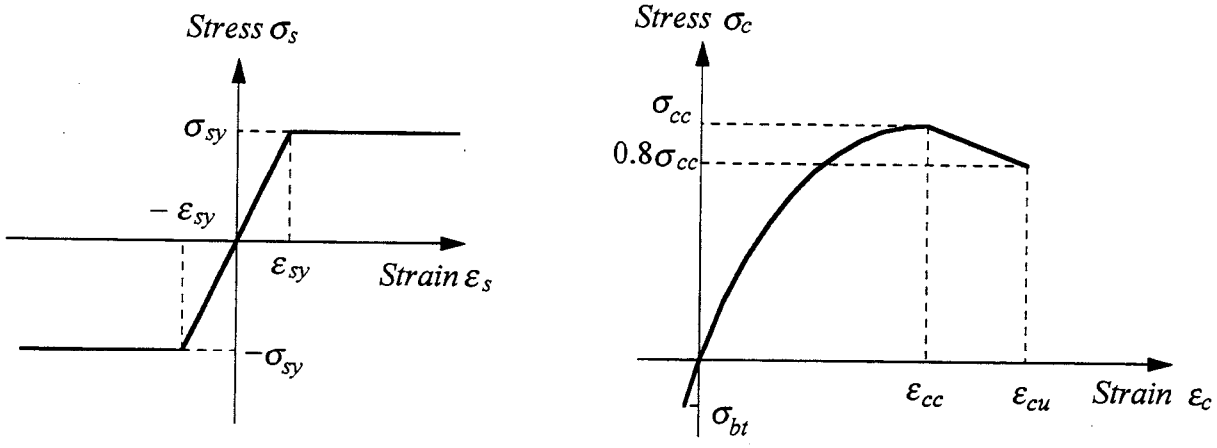

(a) Reinforcing Bars (b) Confined Concrete

Fig. 6 Stress and Strain Relation of Confined Concrete and Reinforcing Bars

It should be noted that the safety factor α in Eq. (9) depends on the type of bridges as well as the type of ground motions as shown in Table 3. This is to preserve higher seismic safety in the important bridges, and to take account of the difference of recurrent time between the Type-I and the Type-II ground motions.

Table 3 Safety Factor α in Eq. (9)

Type of Bridges	Type-I Ground Motions	Type-II Ground Motions
Type-B	3.0	1.5
Type-A	2.4	1.2

Fig. 7 shows suggested arrangement of tie reinforcement. Tie reinforcement should be deformed bars with a diameter larger than 13 mm, and it should be placed in most bridges at a distance of no longer than 150 mm. In special cases such as the bridges with pier height taller than 30m, the distance of tie reinforcement may be increased as large as 300 mm, but special attention should be paid not to suddenly increase the distance at a height so that pier strength should not be sharply decreased at the section. Intermediate ties should be also provided with the same distance with the ties to confine the concrete. Space of the intermediate ties should be less than 1m.

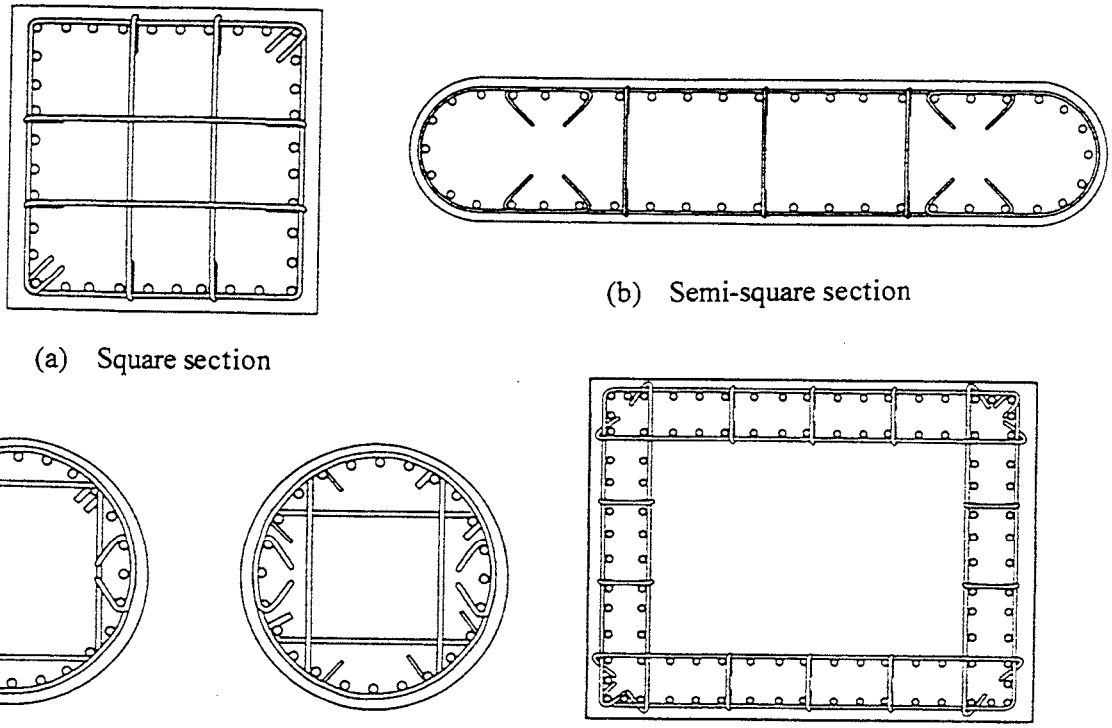

(a) Square section

(b) Semi-square section

(c) Circular section

(d) Hollow section

Fig. 7 Confinement of Core-concrete by Tie Reinforcement

Steel pier

In a concrete infilled steel pier, the lateral capacity P_a and the allowable displacement ductility factor μ_a in Eqs. (1) and (2) are evaluated as

$$P_a = P_y + \frac{P_u - P_y}{\alpha} \tag{19}$$

$$\mu_a = \left(1 + \frac{\delta_u - \delta_y}{\alpha \delta_y}\right) \frac{P_y}{P_a} \tag{20}$$

in which P_y and P_u = yield and ultimate lateral capacity of a pier, δ_y and δ_u = yield and ultimate displacement of a pier, and α = safety factor (refer to Table 3). The P_a and the μ_a are evaluated idealizing that a concrete infilled steel pier resists flexural moment and shear force as a reinforced concrete pier. It is assumed in this evaluation that the steel section be idealized as reinforcing bars and that only steel section resists axial force. A stress vs. strain relation of steel and concrete as shown in Fig. 7 is assumed. The height of infilled concrete has to be decided so that buckling is not developed above the infilled concrete.

A steel pier without infilled concrete must be designed with the dynamic response analysis. Properties of the pier need to be decided based on a cyclic loading test. Arrangement of stiffeners and welding at corner must be precisely evaluated so that brittle failure could be avoided.

DYNAMIC RESPONSE ANALYSIS

Dynamic response analysis is required in the bridges with complex dynamic response to check the seismic safety of the static design. Dynamic response analysis is also required as a " design" tool in the bridges for which the Ductility Design Method is not directly applied. In dynamic response analysis, ground motions which are spectral fitted to the following response spectra are used;

$$S_I = c_Z \cdot c_D \cdot S_{I0} \tag{21}$$

$$S_{II} = c_Z \cdot c_D \cdot S_{II0} \tag{22}$$

in which S_I and S_{II} = acceleration response spectrum for Type-I and Type-II ground motions, S_{I0} and S_{II0} = standard acceleration response spectrum for Type-I and Type-II ground motions, respectively, c_Z = modification coefficient for zone (refer to Eq. (5)), and c_D = modification coefficient for damping ratio given as

$$c_D = \frac{1.5}{40h + 1} + 0.5 \tag{23}$$

Table 4 and Fig. 8 show the standard acceleration response spectra for the Type-I and Type-II ground motions.

Table 4 Standard Acceleration Response Spectra

(a) Type-I Response Spectra S_{I0}

Soil Condition	Response Acceleration S_{I0} (gal=cm/sec^2)		
Group I	S_{I0}=700 for $T_i \leqq 1.4$		S_{I0}=980/ T_i for $T_i > 1.4$
Group II	S_{I0}=1,505 $T_i^{1/3}$ for $T_i < 0.18$	S_{I0}=850 for $0.18 \leqq T_i \leqq 1.6$	S_{I0}=1,360/ T_i for $T_i > 1.6$
Group III	S_{I0}=1,511 $T_i^{1/3}$ for $T_i < 0.29$	S_{I0}=1,000 for $0.29 \leqq T_i \leqq 2.0$	S_{I0}=2,000/ T_i for $T_i > 2.0$

(b) Type-II Response Spectra S_{II0}

Soil Condition	Response Acceleration S_{II0} (gal=cm/sec^2)		
Group I	S_{II0}=4,463 $T_i^{2/3}$ for $T_i \leqq 0.3$	S_{II0}=2,000 for $0.3 \leqq T_i \leqq 0.7$	S_{II0}=1,104 $T_i^{5/3}$ for $T_i > 0.7$
Group II	S_{II0}=3,224 $T_i^{2/3}$ for $T_i < 0.4$	S_{II0}=1,750 for $0.4 \leqq T_i \leqq 1.2$	S_{II0}=2,371 $T_i^{5/3}$ for $T_i > 1.2$
Group III	S_{II0}=2,381 $T_i^{2/3}$ for $T_i < 0.5$	S_{II0}= 1,500 for $0.5 \leqq T_i \leqq 1.5$	S_{II0}=2,948 $T_i^{5/3}$ for $T_i > 1.5$

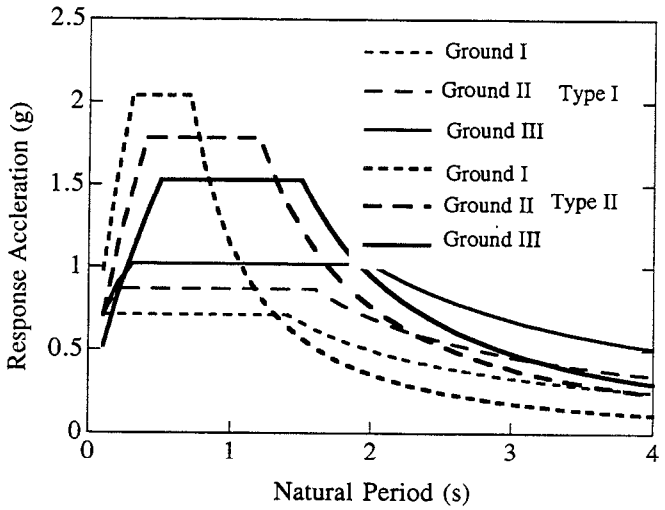

Fig. 8 Type I and Type II Standard Acceleration Response Spectra

It is recommended to use at least three ground motions per analysis, and take an average to evaluate the response.

In the dynamic response analysis, modal damping ratios have to be carefully evaluated. To determine the modal damping ratios, a bridge may be divided into several sub-structures in which energy dissipating mechanism is essentially the same. If one can specify a damping ratio of each sub-structure for a given mode shape, the modal damping ratio for i-th mode h_i may be evaluated as

$$h_i = \frac{\sum \phi_{ij}^T \cdot h_{ij} \cdot k_j \cdot \phi_{ij}}{\Phi_i^T \cdot K \cdot \Phi_i} \tag{24}$$

in which h_{ij}= damping ratio of j-th substructure in i-th mode, ϕ_{ij}=mode vector of j-th substructure in i-th mode, k_j=stiffness matrix of j-th substructure, K=stiffness matrix of a bridge, and Φ_i=mode vector of a bridge in i-th mode, and is given as

$$\Phi_i^T = \left\{\phi_{i1}^T,\ \phi_{i2}^T,\ \cdots\cdots,\ \phi_{in}^T\right\} \tag{25}$$

Table 5 shows recommended damping ratios for major structural components.

Table 5 Recommended Damping Ratios for Major Structural Components

Structural Components	Elastic Response		Nonlinear Response	
	Steel	Concrete	Steel	Concrete
Deck	0.02-0.03	0.03-0.05	0.02-0.03	0.03-0.05
Rubber Bearings	0.02		0.02	
Menshin Bearings	Equivalent damping ratio by Eq. (26)		Equivalent damping ratio by Eq.(26)	
Substructures	0.03-0.05	0.05-0.1	0.1-0.2	0.12-0.2
Foundations	0.1-0.3		0.2-0.4	

MENSHIN DESIGN

Basic principle

Implementation of the menshin bridges should be carefully decided, from not only seismic performance but function for traffic and maintenance point of view, based on the advantage and disadvantage of increasing natural period. The menshin design should not be adopted at the following conditions;

(a) sites vulnerable to lose bearing capacity due to the soil liquefaction and the lateral spreading,
(b) bridges supported by flexible columns,
(c) soft soil sites where potential resonance with surrounding soils could be developed by increasing the fundamental natural period, and
(d) bridges with uplift force at bearings.

It is suggested that the design should be made with an emphasis on an increase of energy dissipating capability and a distribution of lateral force to as many substructures as possible. To concentrate the hysteretic deformation at not piers but bearings, the fundamental natural period of a menshin bridge should be about 2 times or longer than the fundamental natural period of the same bridge supported by the conventional bearings. However, elongation of natural period aiming to decrease the lateral force should not be attempted.

Design procedure

Menshin bridges are designed by both the Seismic Coefficient Method and the Ductility Design Method. In the Seismic Coefficient Method, no reduction of lateral force from the conventional design is made.

In the Ductility Design Method, the equivalent lateral force coefficient k_{hem} in the menshin design is evaluated as

$$k_{hem} = \frac{k_{hcm}}{\sqrt{2\mu_m - 1}} \tag{26}$$

$$k_{hcm} = c_E \cdot k_{hc} \tag{27}$$

in which k_{hcm}= lateral force coefficient in menshin design, μ_m= allowable ductility factor of a pier, c_E= modification coefficient for energy dissipating capability (refer to Table 6), and k_{hc}= lateral force coefficient by Eq. (8). Because the k_{hc} is the lateral force coefficient for a bridge supported by the conventional bearings, Eq. (27) means that the lateral force in the menshin design can be reduced, as large as 30 %, by the modification coefficient c_E depending on the modal damping ratio for the fundamental mode of a bridge.

Table 6 Modification Coefficient for Energy Dissipation Capability

Damping Ratio for 1st Mode h	Coefficient c_E
h<0.1	1.0
0.1≦h<0.12	0.9
0.12≦h<0.15	0.8
h≧0.15	0.7

Modal damping ratio of a menshin bridge h for the fundamental mode is computed as

$$h = \frac{\sum K_{Bi} \cdot u_{Bi}^2 \cdot \left\{ h_{Bi} + \frac{h_{Pi} \cdot K_{Bi}}{K_{Pi}} + \frac{h_{Fui} \cdot K_{Bi}}{K_{Fui}} + \frac{h_{F\theta i} \cdot K_{Bi} \cdot H^2}{K_{F\theta i}} \right\}}{\sum K_{Bi} \cdot u_{Bi}^2 \cdot \left\{ 1 + \frac{K_{Bi}}{K_{Pi}} + \frac{K_{Bi}}{K_{Fui}} + \frac{K_{Bi} \cdot H^2}{K_{F\theta i}} \right\}} \tag{28}$$

in which h_{Bi}= damping ratio of i-th damper, h_{Pi}= damping ratio of i-th pier or abutment, h_{Fui}= damping ratio of i-th foundation associated with translational displacement, $h_{F\theta i}$= damping ratio of i-th foundation associated with rotational displacement, K_{Pi}= equivalent stiffness of i-th pier or abutment, K_{Fui}= translational stiffness of i-th foundation, $K_{F\theta i}$= rotational stiffness of i-th foundation, u_{Bi}= design displacement of i-th menshin device, and H= distance from a bottom of pier to a gravity center of a deck.

In the menshin design, the allowable displacement ductility factor of a pier μ_m in Eq. (26) is evaluated by

$$\mu_m = 1 + \frac{\delta_u - \delta_y}{\alpha_m \cdot \delta_y} \tag{29}$$

in which α_m is a safety factor used in menshin design, and is given as

$$\alpha_m = 2\alpha \tag{30}$$

where α is the safety factor in the conventional design (refer to Table 3). Eq. (30) means that the allowable displacement ductility factor in the menshin design μ_m should be smaller than the allowable displacement ductility factor μ_a by Eq. (2) in the conventional design. The reason for the smaller allowable ductility factor in the menshin design is to limit the hysteretic behavior of a pier at the plastic hinge zone so that principal hysteretic behavior occurs at the menshin device as shown in Fig. 4 (b).

Design of menshin devices

Simple devices stable against extreme earthquakes have to be used. The bearings have to be anchored to a deck and substructures with bolts, and should be replaceable. The clearance has to be provided between a deck and an abutment or between two adjacent decks.

The bearings are classified into two group; the first is the bearings which resist the seismic force of Eq. (2), and the second is the bearings which resist the seismic force in the Seismic Coefficient Method. The first and the second bearings are called as the Type-B bearings and the Type-A bearings, respectively. Seismic performance of the Type-B bearings is, of course, much higher than the Type-A bearings. In the Type-A bearings, a displacement limiting device, which will be described later, has to be co-installed in both longitudinal and transverse directions, while it is not required in the Type-B bearings. Because of the importance of bearings as one of the main structural components, the Type-B bearings should be used in the menshin bridges.

Isolators and dampers must be designed for a desired design displacement u_B. The design displacement u_B is evaluated as

$$u_B = \frac{k_{hem} \cdot W_u}{K_B} \tag{31}$$

in which k_{hem}= equivalent lateral force coefficient by Eq. (27), K_B= equivalent stiffness, and W_u= dead weight of a superstructure. It should be noted that because the equivalent lateral force coefficient k_{hem} depends on the type of ground motions, the design displacement u_B also depends on it.

The equivalent stiffness K_B and equivalent damping ratio h_B of a device are evaluated as

$$K_B = \frac{F(u_{Be}) - F(-u_{Be})}{2u_{Be}} \tag{32}$$

$$h_B = \frac{\Delta W}{2\pi W} \tag{33}$$

$$u_{Be} = c_B \cdot u_B \tag{34}$$

in which $F(u)$= restoring force of a device at a displacement u, u_{Be}=effective design displacement, ΔW= energy dissipaion of a device per cycle, W= elastic strain energy, and c_B= coefficient to evaluate effective displacement (=0.7).

In design of menshin devices, the following requirements have to be satisfied:

1) The displacement computed by Eq. (31) should be within $\pm 10\%$ from the assumed design displacement u_B, and the equivalent damping ratio evaluated by Eq. (33) should not be less than the equivalent damping ratio assumed in design.
2) Shear strain induced in a laminated rubber bearing γ subjected to a lateral force equivalent to the equivalent lateral force coefficient k_{hem} by Eq. (26) are evaluated as

$$\gamma = \frac{u_B}{\sum_{i=1}^{n} t_{ei}} \tag{35}$$

in which u_B= design displacement of a rubber bearing by Eq. (31), t_{ei}=thickness of i-th rubber, and n= number of layers of rubber. The shear strain by Eq. (35) should be less than 250 %.
3) Local shear strain should be less than the rupture strain divided by a safety factor of 1.2. Recommended rupture strains are presented in Table 7.

Table 7 Recommended Rupture Strain of Rubber

Type of Rubbers	Shear Modulus (N/mm^2)	Rupture Strain (%)
Natural Rubbers	80	500
	100	500
	120	400
Chloroplane Rubbers	80	400
	100	400

4) The devices have to be designed and fabricated so that scatter of the equivalent stiffness K_B and the equivalent damping ratio h_B be within $\pm 10\%$ of the design values.
5) The devices have to be stable against at least 50 and 15 load reversals, for the Type-I and Type-II ground motions, respectively, with the design displacement u_B by Eq. (31) under a vertical force equivalent to the dead weight of a superstructure.
6) Tangential stiffness of a device should be positive at any displacement within the design displacement. This is to prevent a possible shake-down of the devices in one side, when they are subjected to large cyclic load reversals.
7) A deck should return to the rest position even after it is subjected to an large earthquake. The residual displacement u_{BR} developed in a device after it is smoothly released from a deformed displacement equivalent to the design displacement u_B by Eq. (31) should be less than 10% of the design displacement u_B.

8) The equivalent stiffness K_B and the equivalent damping ratio h_B of a device shall be stable against a change of load condition and natural environment such as the temperature change.

In addition to the above requirements, a special provision which will be described in the following section should be adopted in the unseating prevention systems.

UNSEATING PREVENTION SYSTEMS

Unseating prevention measures are required for the highway bridges. The measures required for the highway bridges are as:

1) the unseating prevention systems have to be so designed that unseating of a superstructure from their supports can be prevented even if unpredictable failures of the structural members occur,
2) the unseating prevention systems are consisted of providing enough seat length, a falling-down prevention device, a displacement limiting device, and a device for preventing settlement of a superstructure,
3) enough seat length must be provided and a falling-down prevention device must be installed at the ends of a superstructures against longitudinal response. If the Type-A bearings are to be used, a displacement limiting device has to be further installed at not only the ends of a superstructure but each intermediate support in a continuous bridge, and
4) If the Typr-A bearings are used, a displacement limiting device is requested at each support against transverse response. The displacement limiting device is not generally required if the Type-B bearings are used. But, even if the Type-B bearing is adopted, it is required in skewed bridges, curved bridges, bridges supported by columns with narrow crest, bridges supported by few bearings per piers, and bridges constructed at the sites vulnerable to lateral spreading associated with soil liquefaction.

The seat length S_E is evaluated as

$$S_E = u_R + u_G \geq S_{EM} \tag{36}$$

$$S_{EM} = 0.7 + 0.005l \tag{37}$$

$$u_G = \varepsilon_G \cdot L \tag{38}$$

in which u_R= relative displacement (m) developed between a superstructure and a substructure subjected to a seismic force equivalent to the equivalent lateral force coefficient k_{hem} by Eq. (26), u_G= relative displacement of ground along the bridge axis, S_{EM}= minimum seat length (m), ε_G= ground strain induced during an earthquake along the bridge axis, and is 0.0025, 0.00375, and 0.005 for Group-I, II and III sites, respectively, L= distance which contributes to the relative displacement of ground (m), and l= span length (m). If two adjacent decks are supported by a pier, the lager span length should be l in evaluating the seat length in Eq. (37).

In the menshin design, in addition to the above requirements, following considerations have to be made.

1) To prevent collisions between a deck and an abutment or between two adjacent decks, enough clearance must be provided. The clearance between those structural components S_B shall be evaluated as

$$S_B = \begin{cases} u_B + L_A & \text{between a deck and an abutment} \\ c_B \cdot u_B + L_A & \text{between two adjacent decks} \end{cases} \tag{39}$$

in which u_B= design displacement of a device in Eq. (31), L_A=redundancy of a clearance (generally $\pm$15mm), and c_B= modification coefficient for clearance (refer to Table 8). The modification coefficient c_B was determined based on an analysis of the relative displacement response spectra. It depends on a difference of natural periods $\Delta T = T_2 - T_1$ ($T_1 \geq T_2$), in which T_1 and T_2 represent the natural period of the two adjacent bridge systems.

Table 8 Modification Coefficient for Clearance c_B

$\Delta T / T_1$	c_B
$0 \leqq \Delta T / T_1 < 0.1$	1
$0.1 \leqq \Delta T / T_1 < 0.8$	$\sqrt{2}$
$0.8 \leqq \Delta T / T_1 \leqq 1.0$	1

2) The clearance at an expansion joint L_E is evaluated as

$$L_E = u_B + L_A \tag{40}$$

in which u_B= design displacement of a device in Eq. (31), and L_A= redundancy of a clearance (generally $\pm$15mm).

CONCLUDING REMARKS

The preceding pages presented an outline of the new Seismic Design Specifications of Highway Bridges issued in 1996 as well as the damage features of highway bridges in the 1995 Hyogo-ken nanbu earthquake. The Hyogo-ken nanbu earthquake was the first earthquake which developed destructive damage in an urban area since the 1948 Fukui earthquake. Because it had been considered that such destructive damage could be prevented due to the progress of construction technology in recent years, it provided a large impact on the earthquake disaster prevention measures in various fields. The "Part V Seismic Design" of the "Design Specifications of Highway Bridges" (JRA) was totally revised in 1996, and the design procedure moved from the traditional Seismic Coefficient Method to the

Ductility Design Method. The revision was so comprehensive that the past revisions in the last 30 years look minor.

Major point of the revision was the introduction of explicit two-level seismic design consisting of the Seismic Coefficient Method and the Ductility Design Method. Because the Type-I and the Type-II ground motions are considered in the Ductility Design Method, three design seismic forces are totally used in design. Seismic performance for each design force was clearly stated in the Specifications.

The fact that lack of near-field strong motion records prevented to seriously evaluate the validity of recent seismic design codes is important. The Hyogo-ken nanbu earthquake revealed that history of strong motion recording is very short, and that no near-field records have yet been measured by an earthquake with magnitude on the order of 8. It is therefore essential to have enough redundancy and ductility in a total bridge system. It is hoped that the revised Seismic Design Specifications of Highway Bridges contributes to enhance seismic safety of highway bridges.

REFERENCES

Japan Road Association (1996) Design Specifications of Highway Bridges, Part I Common Part, Part II Steel Bridges, Part III Concrete Bridges, Part IV Foundations, and Part V Seismic Design.

Kawashima, K. (1996) Impact of Hanshin/Awaji Earthquake on Seismic Design and Seismic Strengthening of Highway Bridges, Report No. TIT/EERG 95-2, Tokyo Institute of Technology.

Ministry of Construction (1995a) Report on the Damage of Highway Bridges by the Hyogo-ken Nanbu Earthquake, Committee for Investigation on the Damage of Highway Bridges Caused by the Hyogo-ken Nanbu Earthquake.

Ministry of Construction (1995b) Guide Specifications for Reconstruction and Repair of Highway Bridges Which Suffered Damage due to the Hyogo-ken Nanbu Earthquake.

APPENDIX TABLE OF CONTENTS OF "PART V SEISMIC DESIGN" OF "DESIGN SPECIFICATIONS OF HIGHWAY BRIDGES," JAPAN ROAD ASSOCIATION, 1996

RECOMMENDED SEISMIC DESIGN CRITERIA FOR THE NATION'S HIGHWAY BRIDGES

Christopher Rojahn, Ronald L. Mayes, and Richard V. Nutt
Applied Technology Council
Redwood City, California

ABSTRACT

Applied Technology Council (ATC), with funding from the Federal Highway Administration (FHWA) and the California Department of Transportation (Caltrans), has recently completed two projects that provide recommendations for improved seismic design criteria and specifications. The ATC-32 project report provides provisional recommendations for Caltrans *Bridge Design Specifications*. The ATC-18 project report reviews currently available seismic design criteria and specifications for highway structures worldwide and provides recommendations for improved national seismic design specifications for highway bridges. These recommendations embody significant changes to current specifications.

INTRODUCTION

Prior to the 1971 San Fernando, California earthquake, which severely damaged bridges in the Los Angeles region, the American Association of State Highway and Transportation Officials (AASHTO) specifications for the seismic design of bridges were based in part on the lateral force requirements for buildings developed by the Structural Engineers Association of California. In 1973, prompted by the 1971 San Fernando earthquake, the California Department of Transportation (Caltrans) introduced new seismic design criteria for bridges, which included the relationship of the site to active faults, the seismic response of the soils at the site, and the dynamic response characteristics of bridges. In 1975 AASHTO adopted Interim Specifications, which were a slightly modified version of the 1973 Caltrans provisions, and made them applicable to all regions of the United States. At about the same time, FHWA awarded Applied Technology Council a contract to develop nationally applicable guidelines for the seismic design of bridges. These guidelines were completed in 1981 and are known as ATC-6 (ATC, 1981).

AASHTO subsequently adopted the ATC-6 guidelines, first as a set of Guide Specifications in 1983 and later by incorporating them into the *Standard Specifications for Highway Bridges* in 1991. (At the same time, the 1981 map of acceleration coefficients was replaced with a revised version prepared by the U.S. Geological Survey in 1988.) The 16th edition of AASHTO's Standard Specifications for Highway Bridges was published in 1995.

In the fifteen years since the original ATC-6 report was prepared, there have been numerous advances in earthquake engineering. Also, a considerable body of experience has been accumulated both through the use of the 1983 Guide Specifications and the performance of bridges during the 1989 Loma Prieta, California earthquake, the 1990 and 1991 Costa Rica and Philippine earthquakes, and the 1994 Northridge, California earthquake.

Summarized in this paper are recommendations from two recently completed Applied Technology Council (ATC) projects carried out to develop improved specifications for the seismic design of highway bridges. The ATC-32 project, funded by the California Department of Transportation (Caltrans), focused on bridge design specifications for California (ATC, 1996a). The ATC-18 project, funded by the Federal Highway Administration and carried out as part of a larger project conducted by the National Center for Earthquake Engineering Research (NCEER), focused on national bridge design specifications but also considered other highway structures (ATC, 1996b).

AT-32 RECOMMENDATIONS FOR IMPROVED CALIFORNIA BRIDGE DESIGN SPECIFICATIONS

Bridge failures during the October 17, 1989 Loma Prieta, California, earthquake demonstrated a clear need for review and revision, as necessary, of the existing seismic design standards and specifications for bridge structures in California. Thirteen bridges sustained structural damage severe enough to cause closure for extended periods of time and 78 other bridges sustained major damage. Damage included collapsed and partially collapsed concrete bents; spalled concrete columns; shifted superstructures; anchor bolt and expansion joint damage; damage to bearings, caps, and earthquake restrainers; large cracks in concrete box culvert walls and ceilings; and failure of steel rocker bearings. In addition, the month-long closure of the San Francisco-Oakland Bay Bridge, where a link span collapsed, and the brief closure of the San Mateo-Hayward Bridge, which sustained rocker bearing damage, underscored the need for establishing and implementing seismic design standards and criteria that will enable critical structures to remain serviceable following severe earthquake-induced ground motions.

As a result of the effects of the 1989 Loma Prieta earthquake on bridge structures, the Governor of California appointed a Board of Inquiry to investigate damage resulting from this earthquake and to develop recommendations as to appropriate, necessary actions. The Board made 52 specific findings and eight recommendations. Recommendation 6 calls for ensuring "that Caltrans seismic design policies and construction practice meet the seismic safety policy and goals established by the Governor". Part A reads:

> "Review and revise standards, performance criteria, specifications, and practices to ensure that they meet the seismic safety goal established by the Governor and apply them to the design of new structures and rehabilitation of existing transportation structures. These standards, criteria, and specifications are to be updated and periodically revised with the assistance of external technical expertise."

Concurrent with the development of the Board of Inquiry's recommendations, Applied Technology Council (ATC) submitted a proposal to Caltrans to review and revise as necessary the existing standards, performance criteria, specifications, and practices for the design and construction of new bridge structures and the rehabilitation of existing structures. The intent of the proposed project was to provide criteria and methodology that will ensure that California bridge structures of all types perform well in earthquakes and meet the seismic safety goals established by the Governor. When ATC's proposed project was funded by Caltrans in 1991 (ATC-32 project), the portion of the proposed project pertaining to rehabilitation of existing

structures was excluded from the contract and deferred until a later date.

Project Scope

The current Caltrans *Bridge Design Specifications* (BDS) (Caltrans, 1993) are comprehensive provisions covering all aspects of bridge design. They are based on the 1983 AASHTO Bridge Specifications (AASHTO, 1983) and subsequent interim modifications. Caltrans has further modified these AASHTO specifications to suit its specific needs, particularly in the area of seismic design.

The recommended changes to the Caltrans *Bridge Design Specifications* that were developed as part of the ATC-32 project deal only with those portions of the current BDS that are related to seismic design. This involved a complete revision of Article 3.21 dealing with seismic loads; the addition of Article 4.5, which covers the seismic design of bridge foundations; and the modification and/or addition of several articles in Sections 8 and 10 that deal respectively with the seismic design of reinforced concrete and steel bridge components. In addition, the specifications were revised to more accurately consider displacements in order to better meet the new performance criteria that Caltrans adopted during the course of the ATC-32 project (see below).

Several issues pertaining to earthquake ground motions were considered outside the scope of the project. Caltrans currently has hazard maps that are consistent with safety evaluation under the newly established performance criteria. These maps are based on the concept of a maximum credible earthquake, which is determined by the location, type, and extent of known active faults. Seismic hazard is defined in terms of expected peak rock acceleration values derived from an average attenuation of the resulting rock and stiff soil motions (determined from published attenuation relationships). New maps that will consider the effects of thrust faults, added faults, and spectral accelerations are currently under development by Caltrans, as a separate effort.

Similarly, it was not within the scope of ATC-32 to develop seismic hazard maps for functional-evaluation earthquakes. Although the established seismic performance criteria propose that functional-evaluation earthquakes be established on probabilistic principles (e.g., a 60-percent chance of not being exceeded during the life of the bridge), the absence of statewide site-dependent seismic hazard maps that are consistent with the proposed performance criteria was a factor in the development of the ATC-32 recommendations.

Seismic Performance Criteria

Recently, Caltrans, with the support of an external Seismic Advisory Board and the ATC-32 project team, has developed a set of seismic performance criteria for new bridges. These criteria, which are the basis for the recommended revisions to the BDS, are summarized in Table 1.

In these criteria, both safety-evaluation and functional-evaluation design earthquakes are defined. The safety-evaluation earthquake, which Caltrans currently defines deterministically as the Maximum Credible Earthquake (MCE), has only a small probability of occurring during the

useful life of the bridge. A statewide hazard map given in terms of the peak bedrock acceleration generated by this level of earthquake has been available for some time (CDMG, 1992). In the newly defined performance criteria, the safety-evaluation earthquake may alternately be defined probabilistically as an earthquake with a 1000- to 2000-year return period. The probabilistic safety-evaluation ground motion must be determined on a site-specific basis.

The functional-evaluation earthquake is intended to represent an event that has a reasonable probability of not being exceeded (approximately 60%) during the life of the bridge. Because no statewide hazard map for these earthquakes has been developed at this time, the functional-evaluation ground motion must also be determined on a case by case basis through site-specific studies.

Performance is defined in terms of two criteria: the service level of the structure immediately following the earthquake and the extent (or repairability) of physical damage. Although performance is defined qualitatively, the recommended revisions to the BDS are based on a more quantitative definition established by the ATC-32 project. Required performance varies for each of the two earthquake loadings defined above. Required performance also depends on whether a bridge is classified as Important or Ordinary.

Table 1. Caltrans Seismic Performance Criteria

Ground Motion at Site	Ordinary Bridges	Important Bridges
Functional-Evaluation Ground Motion	Service Level—Immediate Repairable Damage	Service Level—Immediate Minimal Damage
Safety-Evaluation Ground Motion	Service Level—Limited Significant Damage	Service Level—Immediate Repairable Damage

Structural Action

A new requirement of the recommended ATC-32 BDS is that the designer identify the type of structural action desired. Fully ductile behavior assumes that the designer will take maximum advantage of plastic hinging while ensuring structural safety. This type of action implies considerable damage and is reserved for Ordinary Bridges only. Structural action consistent with limited ductility is recommended for Important Bridges and certain critical foundation components. This type of structural action is intended to limit inelastic response to levels consistent with reduced structural damage. Elastic structures carry seismically induced loads elastically and thus remain undamaged. Finally, the proposed specifications recognize the potential use of protective systems that incorporate base isolation, passive energy dissipation, and other mechanical devices intended to control seismic response, although no specific design guidelines are given for these systems.

Seismic Loading

Recent studies of strong motion instrumentation results have yielded information that makes it possible to refine the current Caltrans design spectra. Therefore, new design spectra for three earthquake magnitude ranges were developed as part of the ATC-32 project. Because some California sites can be adversely affected by Maximum Credible Earthquakes on a number of different faults, it may be necessary to design for multiple spectra in some cases.

The proposed family of site-dependent design spectra, which vary from the current Caltrans curves, are based on four of the six standard sites defined in a 1994 ground motion workshop sponsored by NCEER. These standard sites are primarily characterized by the typical shear wave velocity of the upper 100 feet of the soil profile, as shown in Table 2. Spectra for type A (hard rock) and F (poor soils) sites as well as type E sites with peak rock accelerations over 0.4 *g* must be determined on a site-specific basis.

Table 2. Proposed ATC-32 Site Characteristics for Standard Design Spectra

Site Designation	Site Description	Shear Wave Velocity Range
B	Medium rock	2500 to 5000 ft/sec
C	Soft rock/Dense soil	1200 to 2500 ft/sec
D	Soft soil	600 to 1200 ft/sec
E	Soft soil	<600 ft/sec

The standard design spectra may also not be appropriate for sites adjacent to active faults. At these sites, the standard spectra may account for the high spectral accelerations, but may not adequately account for the pulse-type motion or the differences between fault-normal and fault-parallel motions observed in past earthquakes. The effect of these motions on structural response is most accurately determined from an inelastic dynamic analysis using spectrum-compatible motions that contain the appropriate velocity pulses. The ATC-32 recommendations give some guidance for selecting appropriate time history input motions.

The nature of vertical earthquake loading is complex: it depends on rupture mechanism, proximity of the earthquake source, local soil conditions, and other factors. The ATC-32 revisions recommend that vertical earthquake design loading may be taken as two-thirds of the horizontal loading spectra for typical sites not adjacent to active faults. When available, site-specific vertical loading spectra are preferred.

Analysis

Although the ATC-32 recommendations retain a force-based design approach, some of the inherent shortcomings of this approach have been overcome. This is done through the use of new response modification factors and modeling techniques for analysis that more accurately consider seismic displacement. The ATC-32 procedures also provide specific means for directly

considering geometric and material nonlinearity in special cases.

As shown in Table 3, the ATC-32 project has developed recommended requirements for the minimum type of analysis that should be used under various circumstances. The type of analysis depends on whether or not the bridge is classified as Important and on the complexity of the structural configuration (Type I = simple and Type II = complex). These analysis types include Equivalent Static Analysis, Elastic Dynamic Analysis, and Inelastic Static Analysis. Basic requirements for each of these analysis types are also included.

Table 3. ATC-32 Recommended Minimum Required Analysis

Bridge Type	Functional Evaluation	Safety Evaluation
Ordinary Bridge, Type I	None Required	Equivalent Static Analysis, or Elastic Dynamic Analysis
Ordinary Bridge, Type II	None Required	Elastic Dynamic Analysis
Important Bridge, Type I	Equivalent Static Analysis, or Elastic Dynamic Analysis	Equivalent Static Analysis, or Elastic Dynamic Analysis
Important Bridge, Type II	Elastic Dynamic Analysis	Elastic Dynamic Analysis, and Inelastic Static Analysis (Substitution of Inelastic Dynamic Analysis is Acceptable)

Equivalent Static Analysis allows an equivalent static force to be applied to the structure. The magnitude of this force is determined from the value of the design spectra at the structure's fundamental period of vibration. This force is applied at the vertical center of mass and distributed in the horizontal plane based on the distribution of mass in the structure or on the product of mass distribution and displacement.

Elastic Dynamic Analysis is required when the distribution of stiffness and/or mass within the structure and/or the configuration is complex enough to preclude the reliable prediction of response without such an analysis. In most cases a multi-modal response spectrum analysis using a lumped-mass "stick" model will satisfy these requirements. It is Caltrans practice to use this type of analysis for most bridges, since the analytical capabilities are readily available to most designers. Member stiffness values that account for cracking of reinforced concrete members are to be used in both Equivalent Static Analysis and Elastic Dynamic Analysis. This differs from the current Caltrans practice of using gross section properties for force demands.

Inelastic Static Analysis is required only when the bridge is classified as Important and it is not simple in configuration. The analysis, commonly referred to as a "push-over" analysis, is done in conjunction with Elastic Dynamic Analysis, and requires a preliminary determination of the strength and stiffness of critical members. Loads are applied incrementally until the structure has reached ultimate displacements. At each step, changes in the structure's characteristics due to

geometric and material nonlinearity are considered. The effects of gravity loads including dead load and a portion of the live load are also considered. Results of this analysis are used to confirm that the structure is capable of accommodating the displacement demands determined from an Elastic Dynamic Analysis. A factor of safety of 1.5 for displacement capacity versus displacement demand is recommended. In general, results of this analysis cannot be used to reduce design quantities determined from an Elastic Dynamic Analysis.

Although Inelastic Dynamic Analysis is not required for any structure type, the ATC-32 criteria provide guidelines for conducting such an analysis. This type of analysis may be substituted for Inelastic Static Analysis. Because member strength and stiffness values are a prerequisite, this analysis is used primarily for verifying a completed design, although its results may be used to reduce design quantities to 80 percent of those determined from elastic analysis. Both geometric and material nonlinearity should be considered. In general a lumped-mass "stick" model with five percent of critical damping is appropriate. The maximum response to three representative input motions or the average response to seven such input motions is recommended.

As with current Caltrans practice, the results from Equivalent Static Analysis or Elastic Dynamic Analysis for orthogonal response spectrum loadings must be combined to obtain design forces and displacements. The results for each orthogonal loading are first obtained by combining the maximum modal responses according to the complete quadratic combination (CQC) rule. The ATC-32 recommendations then prescribe the "40 percent rule," as opposed to the "30 percent rule" currently used by Caltrans for combining the results for orthogonal loadings. In addition, vertical motion is included when it is critical. Therefore, three design load cases may be considered, each of which includes 100 percent of the actions for loading in one of the orthogonal directions plus 40 percent of the actions for each of the remaining two orthogonal loadings. Alternately, 100 percent of all three orthogonal loadings may be applied simultaneously, and the modal results combined using the square root of the sum of the squares (SRSS) method. When either elastic or inelastic time-history analysis is used, 100 percent of the loadings in each of the orthogonal directions is applied simultaneously, and the resulting maximum actions are taken directly from the analysis results.

The ATC-32 recommendations also provide a method for adjusting the displacement results from an Elastic Dynamic Analysis to better reflect the actual maximum inelastic displacements that are likely to occur during an earthquake. The adjustment factor, R_d, is given by the following formula:

$$R_d = (1-1/Z)(T^*/T) + 1/Z \geq 1$$

where

T = natural period of the structure
T* = predominant period of ground motion
Z = response modification factor

This adjustment factor was derived empirically for typical ground motions and may not be appropriate for near-fault sites where pulse-type motions are likely. Although several simplified methods have been suggested for assessing the impact of pulse-type motion on structural response, Inelastic Dynamic Analysis is still the most accurate method currently available for this purpose.

Caltrans currently determines component design forces by dividing the forces obtained from elastic analysis by Z factors to account for ductility and risk. Revised Z factors have been developed as part of the ATC-32 project. Nonlinear dynamic analysis studies demonstrated that very little, if anything, was lost in using a simplified Z factor, as opposed to a more complicated factor based on column aspect ratios. Therefore, the ATC-32 recommendations include simplified Z factors for columns and other components. The full value of Z applies at a structural period of T*, and the value of Z decreases linearly with period. Z reaches a minimum value of 1.0 at a period of zero. Charts showing new Z factors, which are typically lower than those defined in the current Caltrans Bridge Design Specifications, are included in Figure 1.

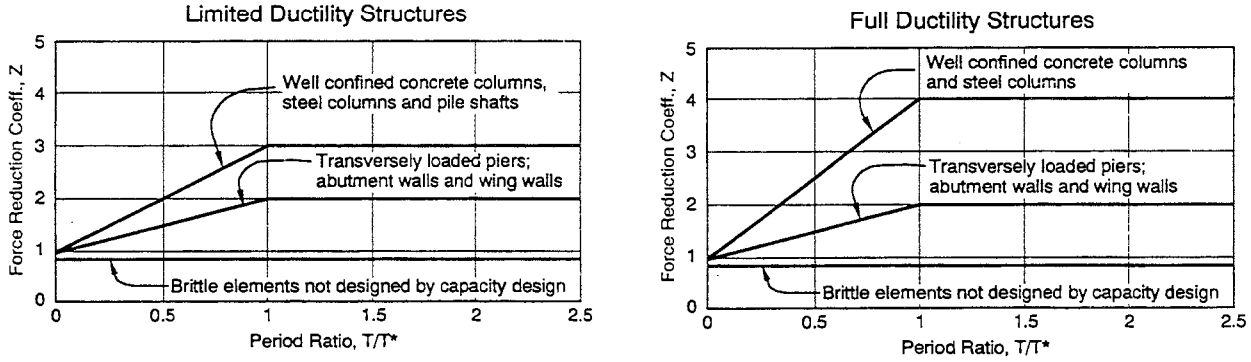

Figure 1. ATC-32 Recommended Response Modification Factor, Z

Design

The ATC-32 recommendations contain several provisions that address design issues for reinforced concrete and structural steel components, and for foundations.

Proposed modifications for reinforced concrete design pertain to the design of ductile elements, the design of nonductile elements and actions using capacity design, and detailing of reinforced concrete for seismic resistance. Included are recommended revised column shear design criteria; new reinforcing steel anchorage provisions for columns; and new design requirements for shear and bending within footing and superstructure joints.

Steel seismic design guidelines, which are absent from the current Caltrans BDS, have been developed that pertain to construction and detailing requirements for steel framing and various types of steel joints likely to be used in bridge work. These requirements are directed toward moment-resisting beam-to-column connections, diaphragms and cross-bracing, slip-critical bolted connections, concentrically braced steel frames, and stiffened as well as unstiffened box sections. In addition, recommendations for the seismic design of conventional bridge bearings

have been developed.

Foundation design guidelines that have been developed include provisions for site investigation; determination of site stability; and modeling and designing of abutments and wingwalls, pile and spread footing foundations, drilled shafts, and earth-retaining structures. For the most part, these recommendations tend to validate current Caltrans practice although there are suggested refinements in some cases.

ATC-18 RECOMMENDATIONS FOR IMPROVED AASHTO BRIDGE DESIGN SPECIFICATIONS

The ATC-18 project to review and evaluate current seismic design criteria and specifications for highway structures was one of several projects carried out under the NCEER project to identify ways to reduce the seismic vulnerability of new highway construction (FHWA Project DTFH61-92-C-00112). The objective of the NCEER project, which commenced in 1992, is to perform a comprehensive study of the seismic vulnerability of highways, tunnels, retaining structures, and highway bridges in order to develop technical information on which new seismic design specifications can be founded. It is anticipated that current guidelines for bridges will be revised and that new seismic design guidelines will be prepared for other highway system components.

ATC-18 Project Scope

While the overall scope of work on the ATC-18 project pertained to all types of highway structures, particular attention was given to bridge structures and foundations. The ATC-18 project team initially focused on a review of current design practice and criteria for new bridge design, as well as the philosophies on which they are based. This involved a review of existing U.S. standards along with the latest codes of Japan, New Zealand, and Europe. Guidelines developed for the Transportation Corridor Agencies (TCA) for Orange County, California, and in-progress work such as the new AASHTO Load Resistance Factor Design (LRFD) Bridge Specifications and information emanating from the ATC-32 project were also reviewed. The final phase of the ATC-18 project focused on the development of recommendations for the future direction of seismic code requirements for bridge structures in the United States. An important part of the recommendations is a two-level design approach.

Following are specific recommendations for future development of bridge seismic design codes. The organization of the recommendations is intended to suggest proposed elements for a future seismic code.

Performance Criteria

ATC-18 recommends that the performance criteria to be included in any future code should be approved by a group that includes legislative policy makers. In order for this review to be effective, a significant amount of cost and technical data will need to be developed before the performance criteria can be intelligently discussed by a non-technical panel. The other key

requirement for the recommended performance criteria is a specific and unambiguous definition of *Important* and *Ordinary* bridges. Future codes may have significantly different design requirements for these two bridge categories.

Two-level Design Approach. The recommended performance criteria for a two-level design approach is the same as that shown in Table 1. Both the functional- and safety-evaluation earthquakes should have specific definitions in terms of probabilistic return periods; i.e., 72, 150, or 250 years for a functional evaluation design event and 950 or 2475 years for a safety-evaluation event. The expected performance of Ordinary bridges should be similar to those of the typical one-level procedure; i.e., collapse will be prevented, but significant damage may occur. Bridges should be designed so that damage occurs in visible locations.

One-level Design Approach. The performance criteria for a one-level design approach cannot be as specific as for a two-level design approach, because the performance in the lower level events can only be implied from the design requirements of the upper-level event. (This is consistent with current design philosophies). A suggested philosophy follows:

1. For a low level earthquake there should be only minimal damage.

2. For a significant earthquake, collapse should be prevented but significant damage may occur. Damage should occur in visible locations.

3. An addition to Item 2 is required if different response modification (*R* or *Z)* factors are used for Important and Ordinary bridges in a one-level design procedure. Item 2 as it stands would apply to Ordinary bridges. The following would be added to Item 2 for Important bridges:

   For a significant earthquake, only repairable damage would be expected for Important bridges, and full access to the bridge should be possible within three days after the earthquake.

Two-levels Of Design Earthquakes. Two-levels of design earthquakes are required if a two-level procedure is developed.

Functional-evaluation ground motion. This is an event that is determined to have a reasonable (approximately 30 percent to 50 percent) probability of occurring during the useful life of a bridge. (Note that this may eventually become a 72-, 150-,or 250-year return-period event, depending on the chosen probability of exceedance and the definition of useful life of the bridge.) This definition may also result in more than one design return period since some bridges will have longer useful lives.

Safety-evaluation ground motion. This is an event with only a small probability of occurring during the useful life of the bridge (i.e., 10 percent probability of exceedance for a design life of 100 or 250 years. This results in a return period of 950 years or 2475 years, respectively). Note: The current AASHTO specifications use a 10 percent probability of exceedance in 50 years or

475-year return period event as the design earthquake.

Service Levels. Two definitions of service levels are recommended for the two-level design approach.

Service Level — Immediate. Full access to normal traffic is available almost immediately (e.g., within hours) following the earthquake. (It may be necessary to allow 24 hours or so for inspection of the bridge.)

Service Level — Limited. Limited access (reduced lanes, light emergency traffic) is possible within three days of the earthquake. Full service can be restored within months.

Damage Levels. A significant amount of work is required to develop reasonably specific definitions for levels of damage to columns, caissons, abutments and retaining walls. The following definitions are based on the ATC-32 criteria. It is recommended that they be augmented wherever possible with closure time frames, ductility levels, and, if feasible, allowable steel and concrete strain levels.

- *Minimal Damage*. Although minor inelastic response may occur, postearthquake damage is limited to narrow flexural cracking in concrete. Permanent deformations are not apparent. Criteria for abutments, wing walls, and steel members need to be developed.

- *Repairable Damage*. Inelastic response may occur, resulting in concrete cracking, reinforcement yield, and minor spalling of cover concrete. The extent of damage should be sufficiently limited that the structure can be essentially restored to its pre-earthquake condition without replacing reinforcement or structural members. Repair should not require closure. Permanent offsets are small and there is no collapse.

- *Significant Damage*. Although there is no collapse, permanent offsets may occur and damage consisting of cracking, reinforcement yield, and major spalling of concrete may require closure to repair. Partial or complete replacement may be required in some cases. Criteria need to be developed for abutments, wing walls, and steel members.

Design Approach

It is recommended that the current AASHTO Seismic Performance Category approach be continued in future codes, since it is a good method of varying design requirements in different seismic zones. It is also recommended that a two-level design approach be adopted at least for Important Bridges in higher seismic zones. The lower-level design requirements should be based on elastic design principles to ensure that there is no damage. The upper-level analysis should be deformation-based using nonlinear static (pushover) analysis procedures with strength and stiffness requirements being derived from appropriate nonlinear response spectra.

If a single-level design procedure is adopted for *Ordinary* bridges, it is recommended that

the design approach include a nonlinear static analysis as part of the design procedure.

Seismic Loading

Two-level Design Approach. The upper-level design event is recommended to be a 2475-year return-period event. (Note: It may be necessary to have different return periods for the eastern and western portions of the United States; 2475 years and 950 years, respectively). The lower-level design event would be in the range of a 72-year to 250-year return-period earthquake. The return period would be based on the same probability of exceedance (e.g., 30 to 50 percent) and may be different for Ordinary and Important Bridges because Important Bridges would have a longer design life (i.e., 200 years versus 50 years).

One-level Design Approach. It is recommended that a single level design procedure be based on 2475-year return-period risk maps if they are available. (Note: It may be necessary to have different return periods for the eastern and western portions of the United States of 2475 years and 950 years, respectively.)

Site Effects

It is recommended that the 1994 NEHRP (BSSC, 1994) soil factors or their derivatives be the basis for the response spectra used for design.

Damping

Current practice is to use a five-percent damped response spectra for design. If nonlinear static analysis is adopted for the upper-level design event, then nonlinear spectra will have to be derived from the elastic spectra. The nonlinear spectra will incorporate whatever levels of energy dissipation (hysteretic and viscous) are deemed appropriate. If nonlinear static analysis is not adopted, higher damping levels in combination with elastic response spectra may be appropriate for the upper-level design event.

Analysis

Two-level Design Approach. Current elastic analysis procedures (equivalent static and multi-modal) are appropriate for the lower-level event. It is envisioned that the lower-level design procedures would use component stiffness values consistent with "little or no" damage. The recommended procedure for the upper-level event should include a nonlinear static analysis. However, this analysis method requires additional development work before it can be used as a standard office procedure.

One-level Approach. There is no consensus on the best method of implementing a one-level procedure. It is desirable for nonlinear static analysis to be a part of any analysis requirements. At a minimum, nonlinear static analysis should be required for Important Bridges. Current elastic design and analysis procedures may be sufficient for smaller Ordinary Bridges. It is possible that the analysis procedure in a one-level design approach could incorporate both the current R-Factor

elastic procedure and nonlinear static analysis. Nevertheless, requiring different analysis procedures for different seismic input levels in a two-level approach seems more rational than requiring two analysis procedures for the same seismic input level in a single-level design approach.

Design Forces

Following are recommendations pertaining to a two-level design approach:

1. *Ductile components.* These should be sized to remain undamaged for the lower-level event and to have adequate ductility to meet the performance criteria for the upper-level event. A definition is required for undamaged; e.g., elastic response and uncracked, or cracked with limited inelastic response but no spalling. Concrete and steel strains and ductility levels for minimal, repairable, and significant damage need to be developed.

2. *Non-ductile components.* These should be sized to remain undamaged for the lower-level event. The design requirement for the upper-level event would depend on whether or not the element was sacrificial. For sacrificial elements, the ultimate strength should be close to but larger than that required for the lower-level event. The actual capacity of sacrificial elements must be low enough to ensure that these elements will fail in the upper-level event. If they do not, they may make the consequences of the upper-level event worse. Nonsacrificial essential elements should be designed either for elastic demands from the upper-level event or by the use of capacity design procedures.

3. *Foundations.* A capacity design procedure should be used for all foundation designs to ensure there is no damage in either design event. Special studies are required for pile bents, drilled shafts, and caissons to determine appropriate design criteria. As with the evaluation of the columns and abutments, more attention is required of the deformation capacities and demands in foundations.

Following are recommendations pertaining to a one-level design approach:

1. *Ductile components.* These should be sized by the *R*-Factor elastic design procedure or by nonlinear static analysis. The R Factors or permissible ductility levels in a nonlinear static analysis may vary depending on the desired performance for the upper-level event.

2. *Non-ductile components.* Nonsacrificial elements should be designed for elastic demands from the upper-level event or by the use of capacity design procedures. Sacrificial elements would have to be designed using a guideline that would somewhat correspond to the design level of an unspecified lower-level event. For example, the sacrificial elements could be designed to withstand one-half or one-third of the force required for the upper-level event.

3. *Foundations.* A capacity design procedure should be used for all foundation designs to ensure that there is no damage. Special studies are required for pile bents, drilled shafts, and caissons

to determine appropriate design criteria.

Design Displacements

Design displacement values should be determined from the upper-level design event, using stiffness properties appropriate to the expected level of displacement. These values could be determined directly from a nonlinear static analysis, but in a one-level elastic approach, an iterative analysis procedure may be needed to ensure that the appropriate stiffness values are used. It is recommended that the current minimum seat width requirements remain since it is not considered practical in a design office environment to accurately calculate the relative displacement for all applicable parameters (e.g., surface wave effects). It is also recommended that overall drift limits be incorporated to avoid *P-Delta* effects on long period structures.

Concrete And Steel Design

It is recommended that capacity design procedures be used to prevent brittle modes of failure in all critical members. Confinement, shear, joint shear, torsion, anchorage, and splice reinforcement requirements will be improved as research progresses over the next several years. It is recommended that the requirements be updated to reflect new research findings.

Foundation Design

Two-level Design Approach. Geotechnical analyses should be conducted for both levels of design acceleration to confirm that response of the soil will not adversely affect the performance of structures supported on or within the soil. These analyses should include assessments of the potential for liquefaction, lateral spreading, and slope instability; dynamic earth pressures on buried walls; soil-structure interaction; and uplift and rocking of the foundation. Since some of the analyses depend on the magnitude of the earthquake causing the design acceleration, care must be used in selecting an earthquake magnitude that is compatible with the seismo-tectonics in the area, both in terms of source mechanism and source distance. Where partial or total liquefaction of saturated, cohesionless soil layers is predicted, the effects of loss in soil strength on the stability of sloping ground, in particular, and the vertical and horizontal bearing capacity of the soil, must be addressed to confirm that structures supported on or within the soil can tolerate these effects. The evaluation should also consider the amount and effects of settlement resulting from liquefaction or densification of granular soil and the increased soil downdrag forces on pile foundations resulting from liquefaction or densification of the soil.

It is critical that geotechnical analyses be completed for both levels of design, rather than just the higher level. The implications of soil response at both design levels should be considered in light of bridge performance criteria. In all cases, soil behavior that degrades the structural capacity of the foundations must be prevented at the lower-level event; soil behavior that leads to damage in the upper-level event may be permissible as long as it does not lead to catastrophic failure of the foundation. For pile-supported and spread footing foundations, this generally means that permanent vertical or horizontal foundation movement should not occur during the lower-level event and that movement should be less than a maximum acceptable amount during the upper-

level event. For the lower-level event, uncertainties in soil and soil-structure performance should be incorporated in the evaluation by incorporating a factor of safety when estimating soil strength. For the upper-level event, best-estimate soil properties and a factor of safety of 1.0 should be used, given the low probability of this event.

One-level Design Approach. Procedures identified for the two-level design approach should be applicable to the one-level design approach. Given that the design event in the single level approach generally corresponds to the upper-level event in the two-level approach, it is likely that liquefaction, soil spreading, and slope instabilities would be common. These ground failure problems can often be corrected through ground improvement technologies or by avoiding susceptible areas. In many cases, thorough corrective measures would be economically unrealistic. For bridges that are not considered essential, a lower level of ground motion might be appropriate for the geotechnical analyses. It is suggested that this lower level be 50 percent of the design acceleration. Under this lower acceleration level, large ground movement should not occur.

References

AASHTO, 1995, *Standard Specifications for Highway Bridges*, 16th Edition, American Association of State Highway and Transportation Officials.

ATC, 1981, *Seismic Design Guidelines for Highway Bridges*, Report No. ATC-6, Applied Technology Council, Redwood City. Also published by Federal Highway Administration as FHWA/RD-81/081, Washington, D.C.

ATC, 1996a, *Improved Seismic Design Criteria for California Bridges: Provisional Recommendations*, Report No. ATC-32, Applied Technology Council, Redwood City

ATC, 1996b, *Seismic Design Criteria for Highway Structures: Current and Future*, Report No. ATC-18, Applied Technology Council, Redwood City

Caltrans, 1993, *Bridge Design Specifications Manual*, California Department of Transportation, Division of Structures, Sacramento, California.

CDMG, 1992, "Peak Acceleration from Maximum Credible Earthquakes in California (Rock and Stiff-Soil Sites)," Open-File Report 92-01, California Department of Conservation, Division of Mines and Geology, Sacramento, California.

BSSC, 1994, *NEHRP Recommended Provisions for the Development of Seismic Regulations for New Buildings*, Building Seismic Safety Council, Washington, DC.

POUNDING IN ELEVATED BRIDGES DURING EARTHQUAKES AND REDUCTION OF ITS EFFECTS

ROBERT JANKOWSKI, KRZYSZTOF WILDE AND YOZO FUJINO

Department of Civil Engineering, University of Tokyo, Hongo 7-3-1, Bunkyo-ku, Tokyo 113, Japan

SUMMARY

Records after severe earthquakes indicate that pounding may cause a considerable damage or even lead to collapse of colliding structures. The aim of this paper is to analyze pounding between superstructure segments of elevated isolated bridge induced by the traveling seismic wave and to propose possible methods for minimizing the effects of collisions. In the analysis, the isolation of high damping rubber bearings (HDRBs) is modeled by proposed nonlinear formulation. The results show that pounding have considerable influence on the structural response and may lead to the increase of pier reaction forces. The reduction of pounding effects can be achieved by either increasing the gap between superstructure segments, in order to avoid collisions, or by decreasing it to the smallest possible size. Further analysis indicates that placing additional devices between deck elements with high damping or stiffness properties can prevent collisions and improve the bridge behavior.

INTRODUCTION

Pounding between superstructure segments and abutments as well as between adjacent superstructure segments was observed in elevated bridges during severe earthquakes.[1,2] It may result in a damage of the deck ends and in some cases can be the reason of a collapse of the structure. Pounding is caused by a phase shift in vibration of neighboring parts of the structure separated by expansion joints. The higher possibility of collisions exists in isolated bridges where, due to extension of the natural period, the superstructure displacements are larger.

The earthquake induced pounding has been intensively studied within the latest years. Most of research work, however, deals with collisions of buildings with different dynamic characteristics which have inadequate gap between.[3-5] The interest grows as records after earthquakes show that pounding can be the reason of considerable damage or collapse of many structures.[6-7] It usually amplifies the response and thus should be treated as a more severe load condition. It was noticed that in some cases, when interior structures are analyzed, pounding can play a positive role reducing the overall response.[8] Even then, however, it can cause a local damage to points of collisions and thus should be minimized or avoided at all.

The most natural way to prevent pounding of buildings is by ensuring sufficiently large spacing between them. The necessary seismic gap is specified in several codes for earthquake resistant design and is usually obtained using the spectral difference method.[9] To enhance the performance of existing buildings without sufficient space between, a number of pounding mitigation techniques have also been proposed. One of the suggested methods is applying link elements between buildings which transmit axial forces.[10] Such connections, however, benefit usually more flexible structure while the response of the stiffer one increases. Another technique is using bumper-damper devices[11] or viscoelastic materials which fill the gap. They lead to reduction of local damage in points of contact but can increase the overall structural response. The alternative to the seismic separation might be also to provide strong shear walls to act as bumper elements protecting the rest of the building.[8]

On the contrary to the collisions between buildings, problem of pounding in bridges has not been so intensively studied. Few results are available from the analysis of contact between superstructure segment and abutment in single-span bridges.[12,13] Although there are many similarities between pounding of buildings and bridge elements, causes of collisions can be different. In case of longer bridge structures, the seismic wave traveling effect can be the dominant factor leading to contact between superstructure segments.[14] When the wave travels, supports of long bridges receive different input loads and thus parts of superstructure are subjected to different excitations. This effect is usually negligible in buildings which are not so extended in length. Another reason leading to pounding may result from the difference in the natural frequencies of adjacent segments due to the difference in ground conditions or stiffness of piers along the structure. Pounding can also occur after failing of the bearing support what changes the dynamic behavior of the bridge.

MODELING OF POUNDING IN ISOLATED ELEVATED BRIDGE

The structure used in the analysis is a base-isolated highway elevated bridge which is assumed to be of infinite length. It has a three-span-continuous, prestressed concrete deck with a mass of $2 \cdot 10^4$ kg/m. The span length and the width of the superstructure are 40 m and 14 m, respectively. A substructure consists of reinforced concrete piers of equal height 11.5 m. Two high damping rubber bearings (HDRBs) support the superstructure at every pier. The cross section area and the height of rubber layers in a single bearing are 0.7921 m and 0.082 m, respectively. Exact dimensions and cross section properties of the structural members are specified according to the "Manual for Menshin Design of Highway Bridges".[15] The schematic model of the bridge is presented in Fig. 1.

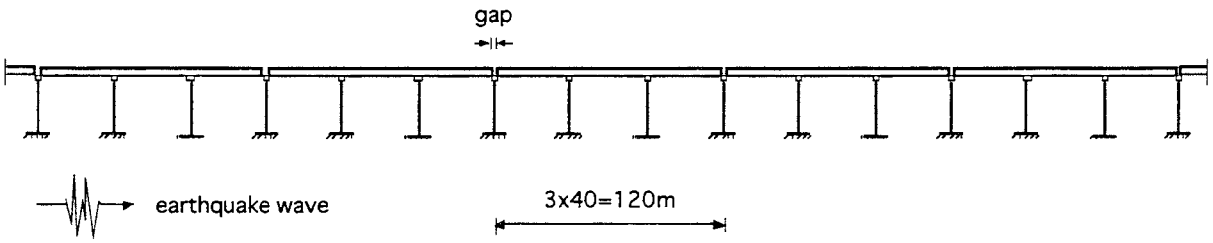

Fig. 1. Full model of the bridge

In order to obtain a better performance of the isolated bridge, the natural period of the superstructure is extended, whereas piers are constructed possibly rigid. In the modeled structure, the ratio between natural frequencies for modes corresponding to the response of piers and deck is equal to 11.[15] Thus, the contribution of dynamics of piers to the total response of the structure is relatively small and can be neglected in the analysis. Under this simplification, every superstructure segment can be treated as one degree-of-freedom system (Fig. 2) with lumped mass $m_i = 2.4 \cdot 10^6$ kg. All HDRBs supporting the segment are modeled by single spring-dashpot element with stiffness K_i and damping C_i,

It is usually the common procedure to model the seismic isolation devices using the equivalent linear model for the simplicity of design.[16] Although, it may not be accurate in case of pounding involved analysis, as will be shown later, the linear model of HDRB was used for the preliminary calculations. The effective stiffness and the equivalent damping ratio for a pair of bearings for the design displacement of 0.185 m is $K_b = 2.3298 \cdot 10^7$ N/m and ξ_b = 0.14, respectively.[15]

The NS component of EL Centro earthquake (May 18, 1940) with peak acceleration value of the record scaled to 800 gal was applied as the design one in the analysis. Under this ground motion excitation, the response of the free vibrating single superstructure segment gives the maximum displacement equal to the specified design one.

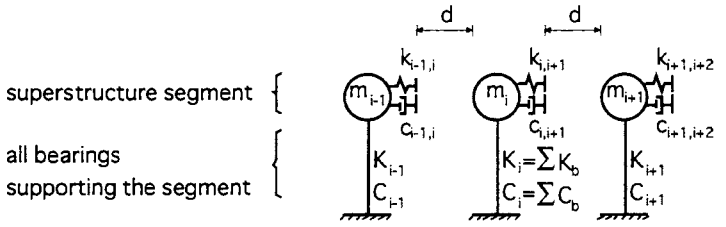

Fig. 2. Model of adjacent superstructure segments

In the analysis, pounding between adjacent superstructure segments in the longitudinal direction of the bridge was modeled by linear viscoelastic impact elements with stiffness $k_{i,i+1}$ and damping $c_{i,i+1}$ (Fig. 2). These elements become active when the relative displacement between discretized masses is smaller than the initial gap d. Therefore, the problem of collisions is described by two sets of linear differential equations. First set is applied when two masses vibrate separately and the second one when contact occurs. Changing from one stage to the other simulates the boundary nonlinearity of pounding phenomenon.

Stiffness of the impact element $k_{i,i+1}$, when contact occurs, can be calculated as an axial stiffness of the superstructure segment. For the analyzed structure, this value has been computed equal to: $k_{i,i+1} = 3.4751 \cdot 10^9$ N/m. The impact element damping $c_{i,i+1}$ is connected with a coefficient of restitution e which accounts for nonlinearities and energy dissipation during pounding. Coefficients of restitution correspond to different damping ratios ξ. This relation is described in the form:[3]

$$\xi = \frac{-\ln e}{\sqrt{\pi^2 + (\ln e)^2}} \tag{1}$$

Value of $e = 1$ ($\xi = 0$) deals with the case of fully elastic collision, value of $e = 0$ ($\xi = 1$) with fully plastic one. The most common range of coefficient of restitution used to simulate real collision[4] is somewhere between 0.5 and 0.75. In the presented in the paper analysis, value of $e = 0.65$ was applied. The damping $c_{i,i+1}$ of impact element between two equal masses m_i can be obtained from formula:

$$c_{i,i+1} = 2\xi\sqrt{k_{i,i+1}\frac{m_i}{2}} \tag{2}$$

The dynamic equation of motion for a discretized superstructure segment m_i including pounding with adjacent deck elements can be written in the form:[3]

$$m_i\ddot{u}_i(t) + C_i\dot{u}_i(t) + K_i u_i(t) - F_{i-1,i}(t) + F_{i,i+1}(t) = -m_i\ddot{u}_{gi}(t) \tag{3}$$

where $\ddot{u}_i(t)$, $\dot{u}_i(t)$, $u_i(t)$ are an acceleration, velocity and displacement of mass m_i, $\ddot{u}_{gi}(t)$ is an acceleration input ground motion and $F_{i,i+1}(t)$ is an impact force due to pounding of mass m_i with m_{i+1}. Its value is equal to:

$$\left.\begin{aligned} F_{i,i+1}(t) &= 0 && \text{for } \delta_{i,i+1}(t) \le 0 \quad \text{(no contact)} \\ F_{i,i+1}(t) &= k_{i,i+1}\delta_{i,i+1}(t) + c_{i,i+1}\dot{\delta}_{i,i+1}(t) && \text{for } \delta_{i,i+1}(t) > 0 \quad \text{(contact)} \end{aligned}\right\} \tag{4}$$

where $\delta_{i,i+1}(t)$ is defined as:

$$\delta_{i,i+1}(t) = u_i(t) - u_{i+1}(t) - d \tag{5}$$

In the analysis, pounding was induced due to the seismic wave traveling effect. Therefore, the input acceleration excitation $\ddot{u}_{gi}(t)$ acting on every degree of freedom was shifted by the time-delay parameter. This parameter depends on the mean earthquake wave velocity and the distance between masses.

It was noticed that because of pounding, the response of a given superstructure element depends much on the displacement histories of few adjacent segments from both sides. It is obvious that the contribution of deck elements located far from the analyzed one decreases with the distance. Although, the theoretical derivation of the edge conditions for a given segment seems to be impossible due to the randomness of pounding for different earthquakes. Numerical simulations were carried out under design El Centro ground motion excitation using different models of the bridge. The results of the analysis for models consisting of 3, 5 and 7 superstructure segments for different gap sizes with constant apparent seismic wave velocity v = 1000 m/s are presented in Fig. 3.

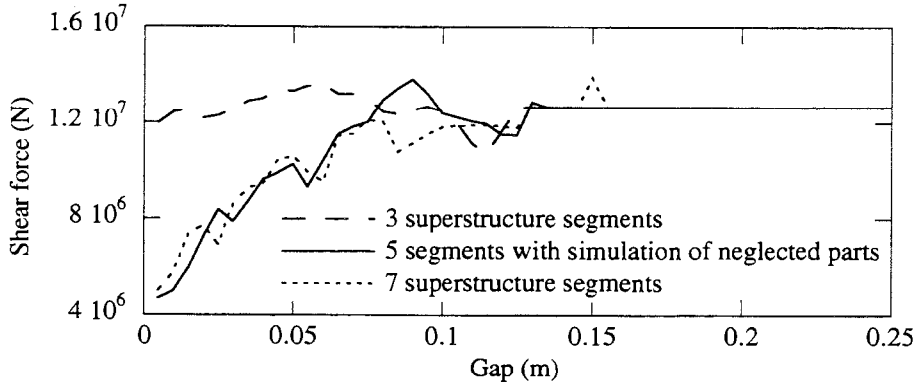

Fig. 3. Maximum shear forces of middle segment with respect to gap size for different bridge models

By decreasing the number of segments taken into account, it was found that at least five of them should be analyzed with neglected parts of the bridge simulated as spring-dashpot elements. It can be seen from Fig. 3 that for such configuration the influence of boundary conditions is minimized and more accurate response of the middle superstructure segment for different gaps can be obtained. Therefore, the model of the bridge from Fig. 1 could be simplified as 5 degree-of-freedom system as shown in Fig. 4.

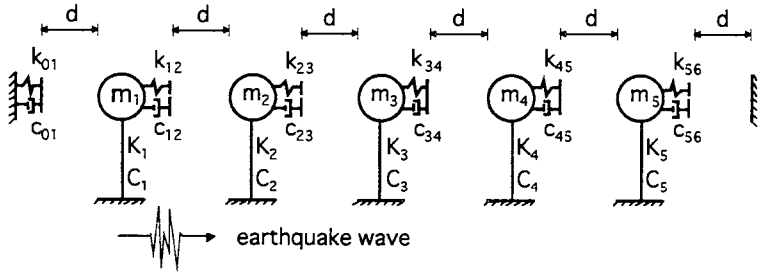

Fig. 4 Simplified model of the bridge

The equation of motion for 5 degree-of-freedom model of the bridge (Fig. 4) can be written in the matrix form as:

$$\mathbf{M}\ddot{\mathbf{u}}(t) + \mathbf{C}\dot{\mathbf{u}}(t) + \mathbf{K}\mathbf{u}(t) + \mathbf{D} = -\mathbf{M}\ddot{\mathbf{u}}_g(t) \tag{6}$$

where:

$$\mathbf{u}(t)=\begin{bmatrix}u_1(t)\\u_2(t)\\u_3(t)\\u_4(t)\\u_5(t)\end{bmatrix} \qquad \ddot{\mathbf{u}}_g(t)=\begin{bmatrix}\ddot{u}_{g1}(t)\\\ddot{u}_{g2}(t)\\\ddot{u}_{g3}(t)\\\ddot{u}_{g4}(t)\\\ddot{u}_{g5}(t)\end{bmatrix} \qquad \mathbf{M}=\begin{bmatrix}m_1&&&&\\&m_2&&&\\&&m_3&&\\&&&m_4&\\&&&&m_5\end{bmatrix} \qquad \mathbf{D}=\begin{bmatrix}(k_{01}-k_{12})d\\(k_{12}-k_{23})d\\(k_{23}-k_{34})d\\(k_{34}-k_{45})d\\(k_{45}-k_{56})d\end{bmatrix} \tag{7a}$$

$$\mathbf{C}=\begin{bmatrix}C_1&&&&\\&C_2&&&\\&&C_3&&\\&&&C_4&\\&&&&C_5\end{bmatrix}+\begin{bmatrix}c_{01}+c_{12}&-c_{12}&&&\\-c_{12}&c_{12}+c_{23}&-c_{23}&&\\&-c_{23}&c_{23}+c_{34}&-c_{34}&\\&&-c_{34}&c_{34}+c_{45}&-c_{45}\\&&&-c_{45}&c_{45}+c_{56}\end{bmatrix} \tag{7b}$$

$$\mathbf{K}=\begin{bmatrix}K_1&&&&\\&K_2&&&\\&&K_3&&\\&&&K_4&\\&&&&K_5\end{bmatrix}+\begin{bmatrix}k_{01}+k_{12}&-k_{12}&&&\\-k_{12}&k_{12}+k_{23}&-k_{23}&&\\&-k_{23}&k_{23}+k_{34}&-k_{34}&\\&&-k_{34}&k_{34}+k_{45}&-k_{45}\\&&&-k_{45}&k_{45}+k_{56}\end{bmatrix} \tag{7c}$$

To satisfy the pounding conditions from equation (4), if there is no contact between masses m_i and m_{i+1} at time t, values of $k_{i,i+1}$ and $c_{i,i+1}$ are set to zero.

NONLINEAR MODEL OF HIGH DAMPING RUBBER BEARING

The linear Kelvin model of HDRB is usually quite accurate for calculation of maximum response of the free vibrating structure.[16] The peak displacement and reaction forces are obtained assuming constant values of equivalent stiffness K_b and damping ratio ξ_b during the whole time of earthquake. These linearized parameters are computed from the hysteresis loop of the bearing specified for the design displacement.[17] HDRB, however, shows strongly nonlinear behavior depending much on the shear strain. It can also be influenced by the axial pressure, loading history or increase of internal temperature. The dependence of equivalent stiffness and damping ratio on the shear strain for a pair of analyzed bearings[15] is presented in Fig. 5.

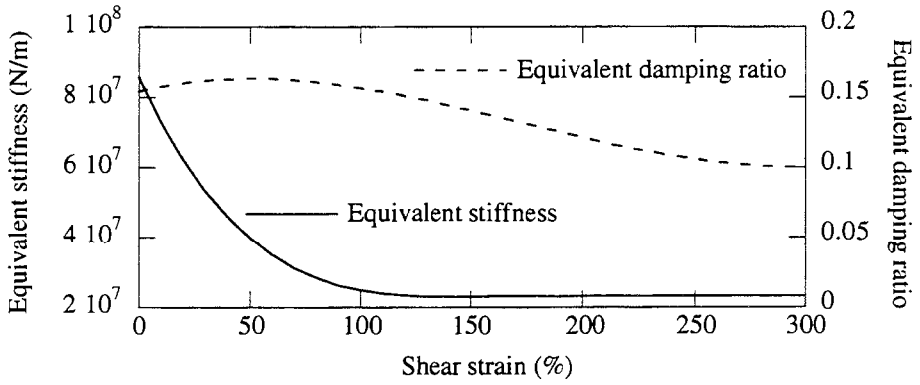

Fig. 5 Equivalent stiffness and damping ratio for HDRB with respect to shear strain

It seems, that in case of pounding analysis, more accurate model of HDRB should be applied. The need arises as a careful simulation of displacement histories for colliding superstructure segments may be essential for correct results. Used in the further analysis shear strain dependent model of HDRB is a modification of a formulation proposed by Pan et al.[18] The horizontal response of the bearing under specified axial load is simulated by nonlinear spring-dashpot element. The shear stiffness and damping coefficients at a given time t are computed from the actual values of displacement and velocity using formulas:

$$K_b(t) = a_1 + a_2 u^2(t) + a_3 u^4(t) + \frac{a_4}{\cosh^2(a_5 \dot{u}(t))} + \frac{a_6}{\cosh(a_7 \dot{u}(t))\cosh(a_8 u(t))} \tag{8}$$

$$C_b(t) = \frac{a_9 + a_{10} u^2(t)}{\sqrt{a_{11}^2 + \dot{u}^2(t)}} \tag{9}$$

where a_1 - a_{11} are parameters of the model which are obtained by fitting the experimental data using the least squares optimization method. The specified hysteresis loops for analyzed pair of bearings together with the simulated ones for the set of parameters:

$$\begin{aligned} a_1 &= 1.6074 \cdot 10^7 & a_7 &= 7.7280 \\ a_2 &= -3.7000 \cdot 10^7 & a_8 &= 48.013 \\ a_3 &= 8.8153 \cdot 10^8 & a_9 &= 9.7679 \cdot 10^5 \\ a_4 &= 5.9956 \cdot 10^6 & a_{10} &= 5.1964 \cdot 10^6 \\ a_5 &= 1.5753 & a_{11} &= 0.59601 \\ a_6 &= 6.0450 \cdot 10^7 \end{aligned} \tag{10}$$

are shown in Fig. 6. In can be seen from the graph that the proposed model fits the experimental data quite well over a wide range of shear strains.

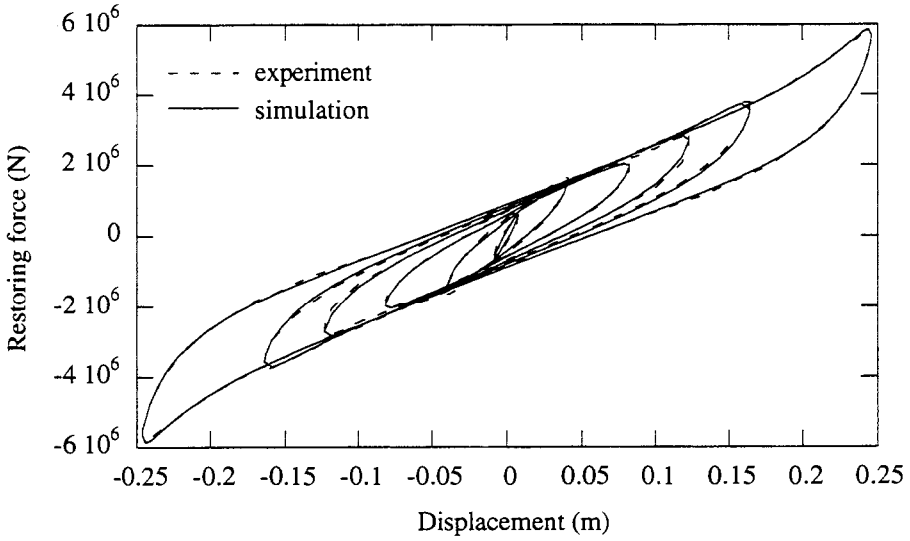

Fig. 6 Specified and simulated hysteresis loops for HDRB

NUMERICAL SIMULATIONS

The simplified 5 degree-of-freedom lumped mass model from Fig. 4 was used for the numerical simulations of the bridge response. It was observed that the pattern of pounding is determined by the input record and depends much on the gap size between superstructure segments. To check this influence, the analysis was carried out using the nonlinear model of HDRB for the design El Centro earthquake with constant apparent seismic wave velocity v = 1000 m/s. The displacement time histories of the middle deck element, m_3, for gaps d = 0.01 m and d = 0.11 m together with the response when no pounding occurs are presented in Fig. 7. For these values of the separation width, the relative velocities and the pounding forces between mass m_3 and m_4 are also shown in Fig. 8 and Fig. 9. The graphs indicate that pounding mechanism can strongly modify the behavior of the structure. It can either increases the response of the bridge or play a positive role depending on the collision history between adjacent segments. It can be seen from Fig. 8 and Fig. 9 that the pounding forces and the relative velocity values increase as the separation width becomes bigger, whereas the number of collisions is reduced.

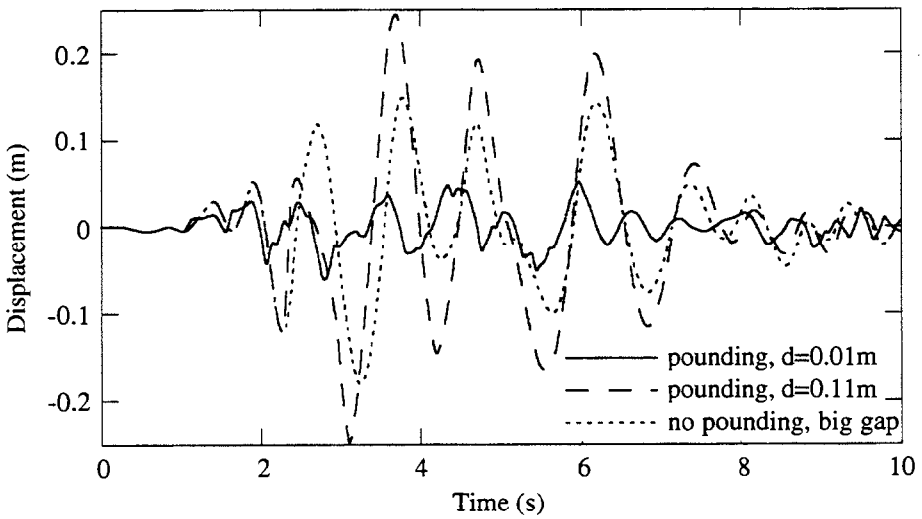

Fig. 7 Displacement time histories of middle segment for different gap sizes.

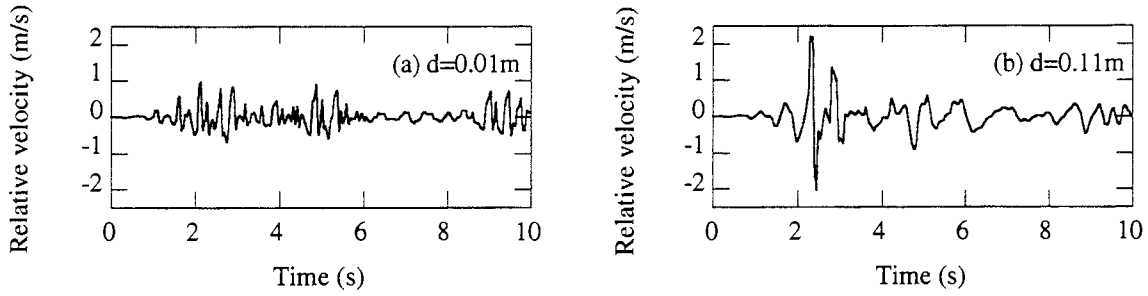

Fig. 8 Relative velocity history for: (a) gap d = 0.01 m; (b) gap d = 0.11 m

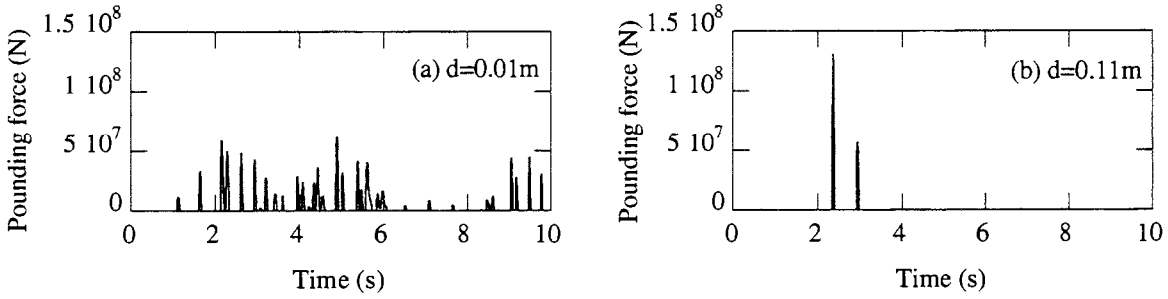

Fig. 9 Pounding time history for: (a) gap d = 0.01 m; (b) gap d = 0.11 m

The further parametric study was conducted for different values of the gap size between deck elements applying linear and nonlinear models of rubber bearing. The results of the analysis in means of the maximum shear forces for the middle segment are shown in Figure 10. It can be seen from the graph that when the gap between superstructure segments becomes bigger, the bridge response increases. The trend is maintained till the moment of fall of peak reaction forces for gaps big enough that pounding effects are minimized. The comparison between two HDRB models shows that both of them give similar results for smaller gap values for which displacements of segments are lower than the design one specified for linear model. On the other hand, maximum shear forces are larger using nonlinear model for the range of gap sizes where displacements are higher than the design value. This is due to the fact that both equivalent stiffness and damping ratio decreases with increase of shear strain (Fig. 5) leading to larger displacements and shear forces for deck elements. It can be also seen from Fig. 10 that the accurate response of the superstructure segment can be obtained using linear model if pounding does not occur.

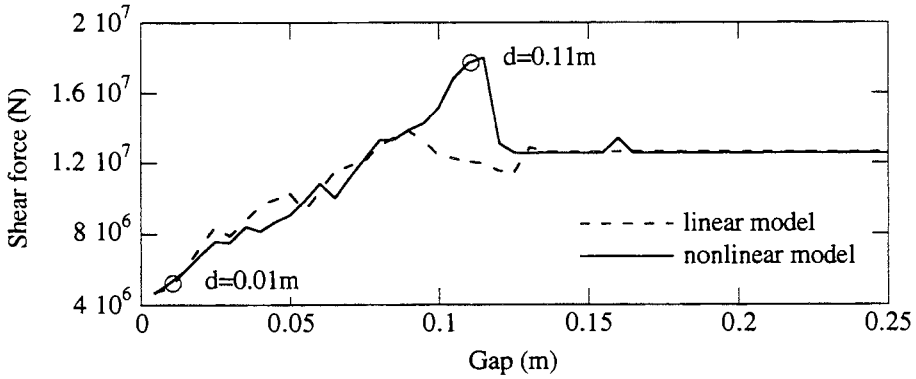

Fig. 10 Maximum shear forces with respect to gap size for linear and nonlinear models of HDRB

The analysis for different values of gap size and apparent seismic wave velocity was carried out for several ground motions. Together with used so far El Centro excitation, acceleration records of Kobe (January 17, 1995) and Kushiro (January 15, 1993) earthquakes were also applied. The records of the events were scaled to give the response with the maximum shear strain of HDRB not exceeding 300% (Fig. 5). Original and scaled peak acceleration values (PGA) for used in the analysis input ground motions are shown in Table I. The maximum shear forces for the middle mass, m_3, with respect to the analyzed parameters under different earthquakes are presented in Fig. 11-13. The maximum pounding forces versus the separation width for the apparent seismic wave velocity v = 1000 m/s are also shown in Fig. 14.

Table I. Ground motions used in the analysis

Earthquake	Original PGA (gal)	Scale factor	PGA after scaling (gal)
El Centro NS	340.2	2.3516	800.0
Kobe NS	817.8	0.6725	550.0
Kushiro NS	814.7	1.2274	1000.0

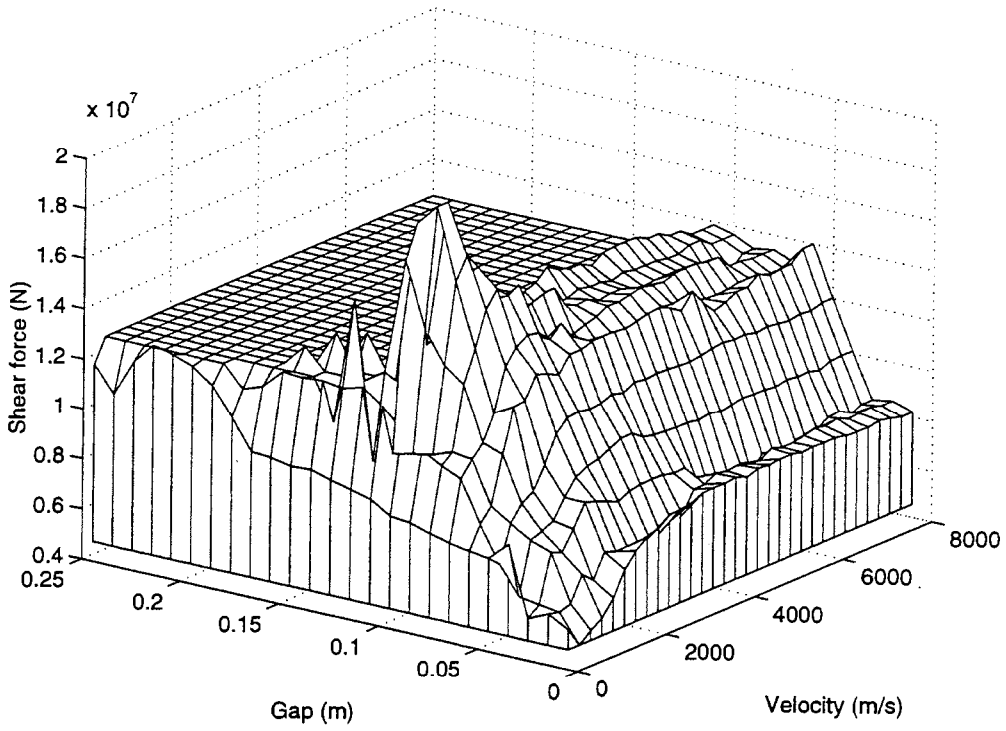

Fig. 11 Maximum shear forces with respect to gap size and seismic wave velocity under El Centro earthquake

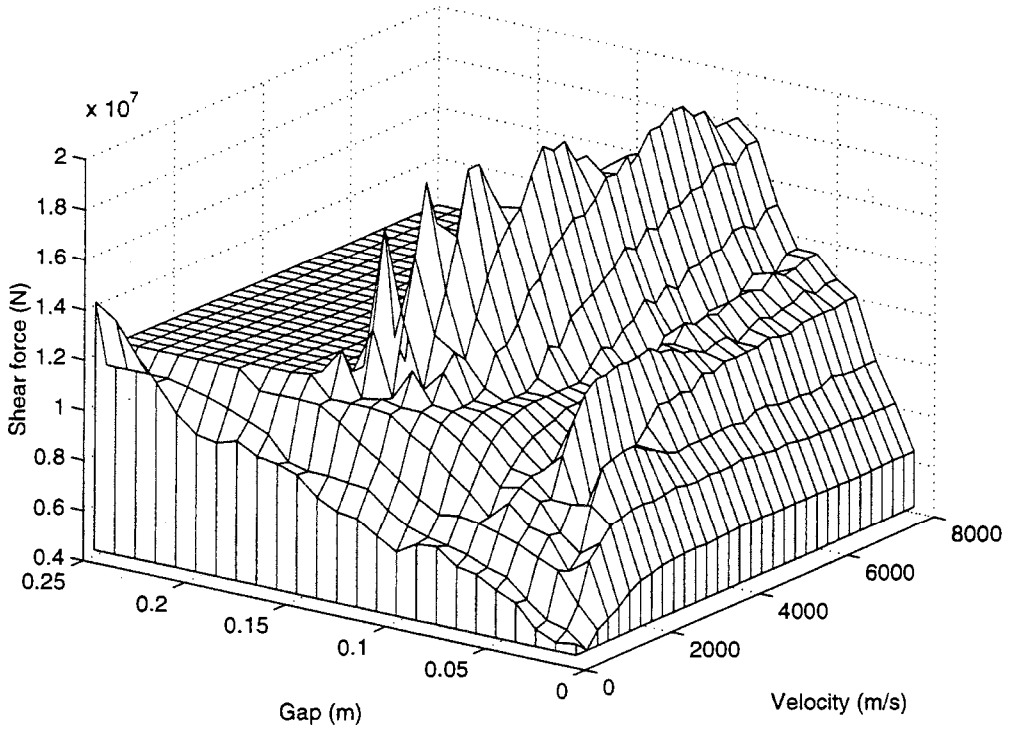

Fig. 12 Maximum shear forces with respect to gap size and seismic wave velocity under Kobe earthquake

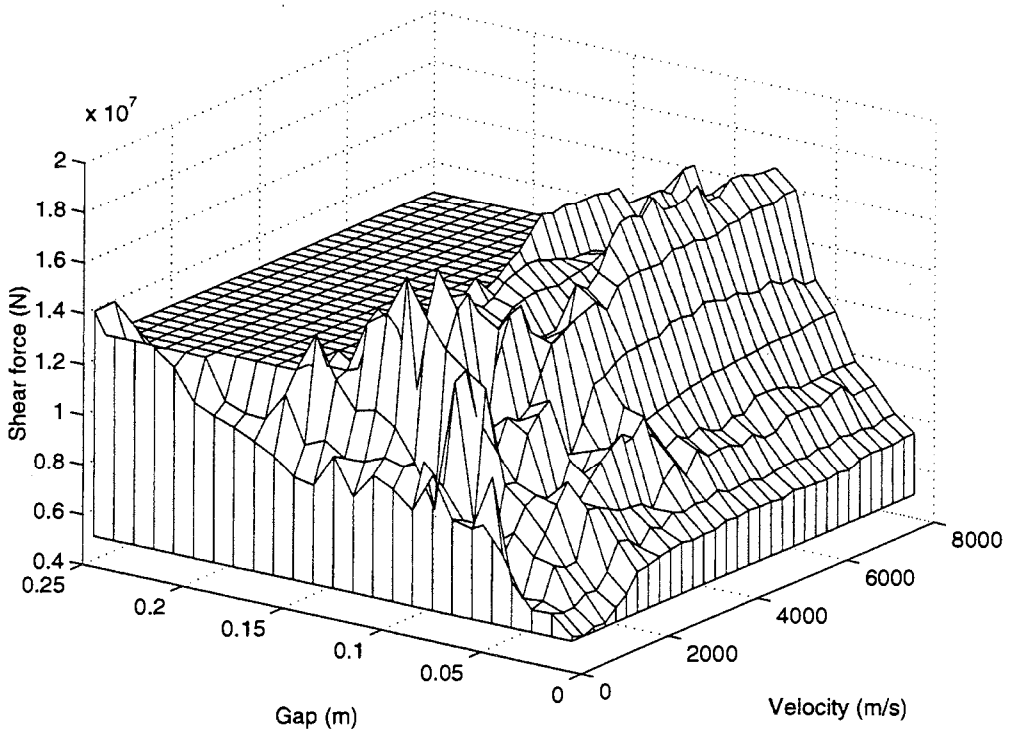

Fig. 13 Maximum shear forces with respect to gap size and seismic wave velocity under Kushiro earthquake

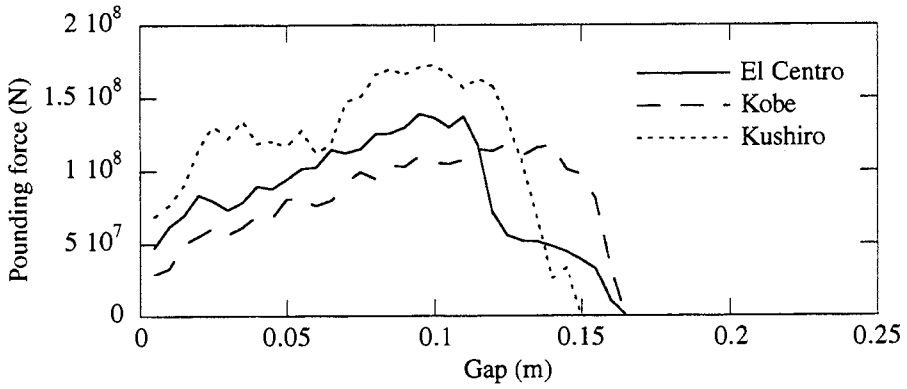

Fig. 14 Maximum pounding forces with respect to gap size

It can be seen from Fig. 11-13 that the structural response is similar for all used in the analysis ground motions. The results confirm the significant influence of the gap size on the bridge behavior as described previously. They indicate that, in case of pounding involved analysis, the largest shear forces can be expected for bigger gaps. Fig. 11-13 show also the dependence of the seismic wave velocity on the response of the bridge. It can be seen that for smaller velocity values, maximum shear forces are lower but bigger gap is needed to prevent pounding. On the other hand, for higher seismic wave velocities, shear forces are larger although smaller gap can be applied to avoid collisions.

Fig. 14 shows a similar tendency of maximum pounding forces with respect to gap for different earthquakes. For all events, with the increase of separation width, forces due to collisions become initially bigger and then fall sharply to zero for gaps big enough to prevent pounding.

REDUCTION OF POUNDING EFFECTS

The results of the analysis indicate the existence of two gap intervals between adjacent deck elements for which the smallest structural response can be obtained. The optimal separation width seems to be a small one or big enough to avoid contact at all.

The interval of small gap size stands for the case of nearly fully continuous deck. When seismic wave travels along the bridge, long continuous superstructure is subjected in different places to excitations shifted in time. That makes them act in opposite direction at the same time and smaller response is possible. Expansion joints applied in bridges should be designed to accommodate length changes of the superstructure due to thermal, creep and shrinkage effects. They should also allow some space for placement of bridge decks. That requires usually the minimum separation width specified in the bridge design codes[19] of about 2.5 cm. It can be seen from Fig. 14, however, that for this value of gap size, the pounding forces can be already relatively large with values much higher than shear forces. Therefore, the application of such gap size may lead to some extensive damage of deck ends during pounding.

On the other hand, in case of big gap size, every superstructure segment vibrates separately and the negative effects of pounding such as the increase of displacement after contact or damage to deck ends is prevented. However, in order to avoid collisions, a substantial increase of the separation width would be required, especially if the seismic wave velocity is expected to be small. It can be seen from Fig. 14 that for the velocity value v = 1000 m/s at least 17 cm would be needed and even that may not be enough for severe earthquakes, such as Kobe, which record was scaled down in the analysis. Such enlarging of the gap between adjacent superstructure segments may be difficult as heavy traffic loads moving on the deck are to be carried over expansion joints. Therefore, some bridge design codes[19] specify the maximum roadway surface gap as about 10 cm for straight bridges.

Since none of the theoretically optimal gap sizes can be practically applied in bridge structures, other methods which can minimize the pounding effects were considered. It seems that preventing

the destructive collisions without enlarging the separation width can be obtained by applying additional dampers or stiffeners between superstructure and substructure or between adjacent deck elements. The increase of damping or stiffness characteristics between deck and piers can be done by changing the properties of bearings. To test the structural response under different values of bearing parameters the analysis was conducted for design El Centro earthquake with constant gap size $d = 0.05$ m and the apparent seismic wave velocity $v = 1000$ m/s. The maximum shear forces of the middle segment of the bridge model from Fig. 4 as the results of the analysis are shown in Fig. 15. It can be seen from the graph that the increase of both damping and stiffness between superstructure and substructure leads to elimination of pounding but at the same time the reaction forces become significantly bigger. This is due to the fact that the increase of bearing parameters makes the structure stiffer and thus less isolated from the ground motion excitation.

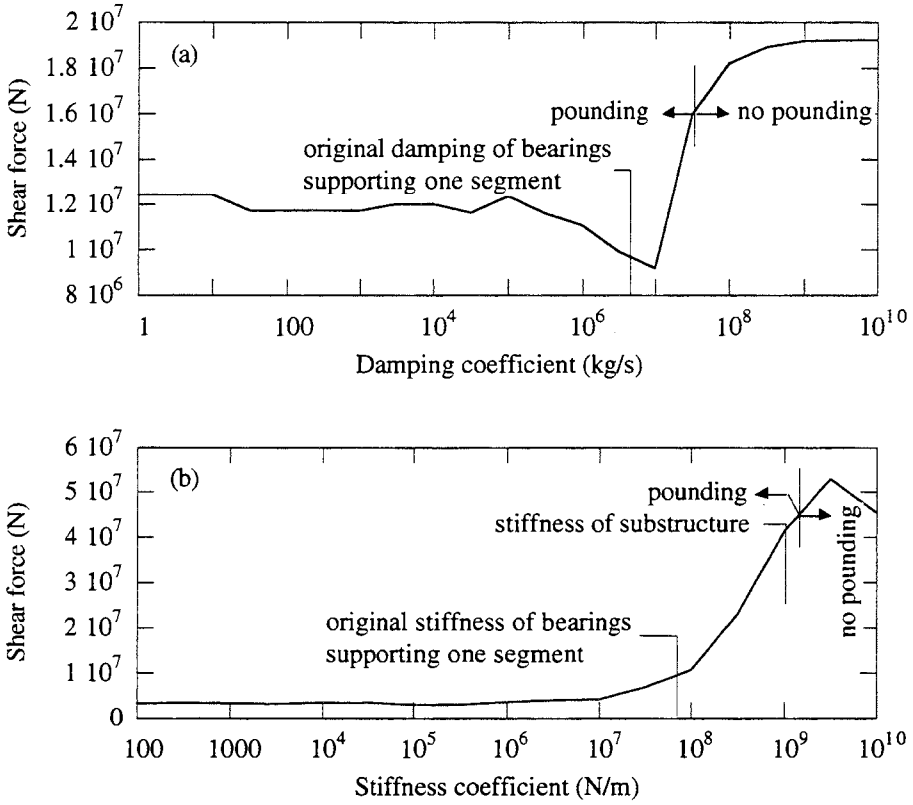

Fig. 15 Maximum shear forces with respect to: (a) damping of bearings; (b) stiffness of bearings

The reduction of collision forces can be also obtained if additional dampers or stiffeners are placed between deck elements. The results of the analysis carried out for different parametric values of such devices are presented in Fig. 16. The graph shows that collisions can be eliminated and the bridge behavior substantially improved (reduction of shear forces up to nearly 40%) for large damping and stiffness coefficients. These values, however, stand for the case when adjacent segments are nearly fixed one with another. Smaller values do not prevent pounding and moreover may change the pattern of collisions between segments. That can even lead to the increase of reaction forces as can be observed in Fig. 16(a) for the range of damping coefficient: $10^6 < C < 10^7$ kg/s. In this case, the dissipation of energy mechanism does not seem to be effective as the relative velocities between deck elements are rather low as shown in Fig. 8.

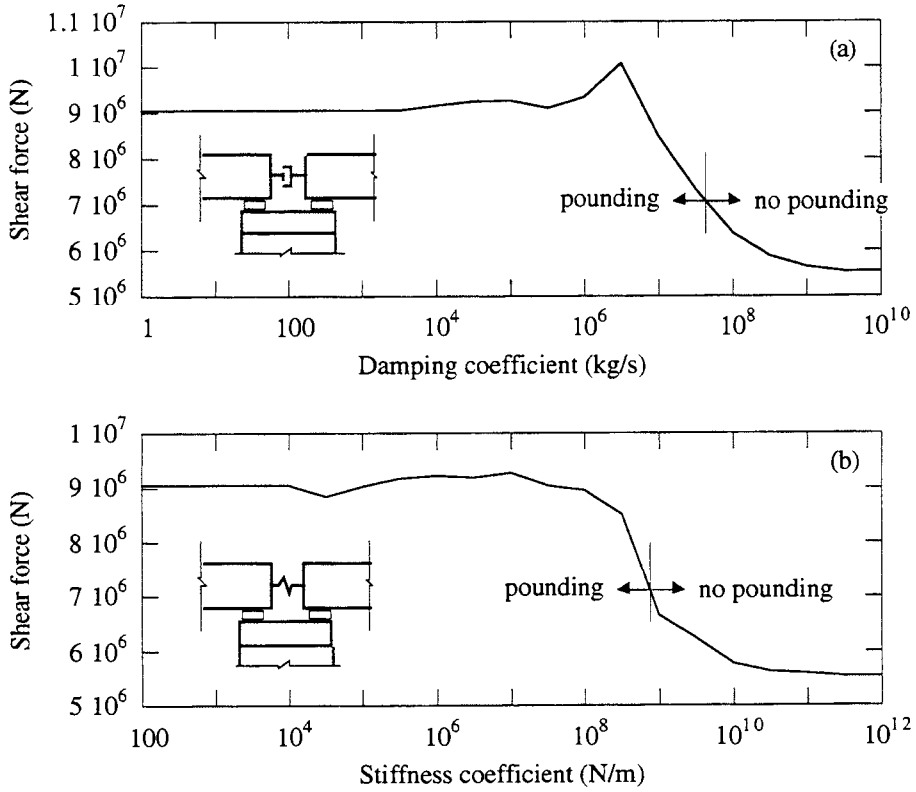

Fig. 16 Maximum shear forces with respect to: (a) damping of additional devices; (b) stiffness of additional devices

The application of additional devices with high damping or stiffness properties which nearly fix adjacent deck elements makes the superstructure long and continuous. This may result in the increase of internal forces in the deck due to its length changes caused by thermal, creep or shrinkage effects. It seems, however, that the use of recently developed shock transmission units (STU)[20,21] can solve the problem. The device shown schematically in Fig. 17 is similar to a standard damper with difference of special silicone putty used instead of oil. The putty has such properties that STU shows minor resistance under slow movements of deck resulting from change of its length. On the other hand, the device becomes very stiff if the shock impact is applied. Therefore, shock transmission units allow the connection between segments to be fixed during earthquake preventing from damage of deck and leading to smaller reaction forces.

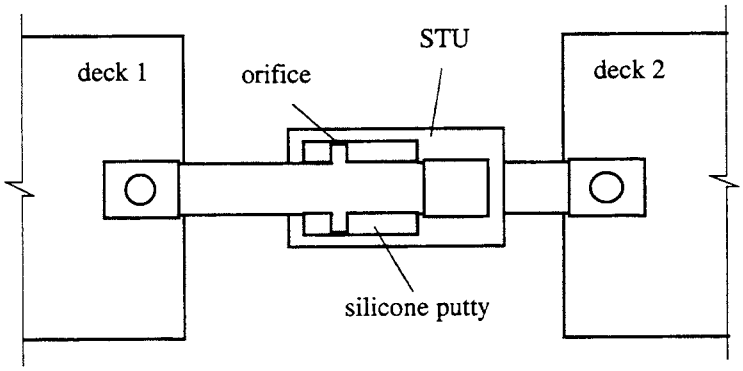

Fig. 17 Shock transmission unit

CONCLUSIONS

In this paper, pounding between superstructure segments of elevated isolated bridge induced by the seismic wave propagation effect has been analyzed. The results show that collisions have considerable influence on the structural response and may increase the forces exerted on the bridge. It is therefore suggested, that the possibility of pounding should be taken into consideration at the design stage of the structure.

It was found that in case of pounding involved analysis in isolated bridges, more accurate results can be obtained using precise model of isolation devices. Proposed herein the nonlinear formulation for high damping rubber bearing appears to be suitable for that purpose.

The results of the analysis show that the response of the bridge depends on the gap size between deck elements. The smallest response was observed for very small separation width and big enough to prevent collisions. Both intervals, however, seem not to be practically applicable as the minimum and maximum value of the surface gap is often restricted. It was also shown that the structural behavior may depend on the seismic wave velocity. Generally, for smaller velocity values, maximum shear forces are lower but bigger gap is needed to avoid collisions. On the other hand, for higher seismic wave velocities, shear forces are larger although smaller separation width can be applied to prevent pounding.

Further studies indicate that contact can be avoided and the bridge behavior much improved if additional devices with high damping or stiffness properties are placed between deck elements. To overcome the difficulties connected with increase of internal forces in superstructure due to its length changes, shock transmission units are suggested to be used. They show minor resistance in case of slow movements and act as stiff connectors during impact loading. Nevertheless, the practical application of the devices requires further investigation.

REFERENCES

1. M. J. N. Priestley, F. Seible and G. M. Calvi, *Seismic Design and Retrofit of Bridges*, John Wiley & Sons, New York, 1996.
2. P. K. Malhotra, M. J. Huang and A. F. Shakal, 'Seismic interaction at separation joints of an instrumented concrete bridge', *Earthquake eng. struct. dyn.*, **24**, 1055-1067 (1995).
3. S. A. Anagnostopoulos, 'Pounding of buildings in series during earthquakes', *Earthquake eng. struct. dyn.*, **16**, 443-456 (1988).
4. S. A. Anagnostopoulos and K. V. Spiliopoulos, 'An investigation of earthquake induced pounding between adjacent buildings', *Earthquake eng. struct. dyn.*, **21**, 289-302 (1992).
5. M. Papadrakakis, C. Apostolopoulou, A. Zacharopoulos and S. Bitzarakis, 'Three-dimensional simulation of structural pounding during earthquakes', *J. eng. mech.*, **122**(5), 423-431 (1996).
6. E. Rosenblueth and R. Meli, 'The 1985 earthquake: causes and effects in Mexico City', *Concrete international*, **8**(5), 23-34 (1986).
7. K. Kasai and B. F. Maison, 'Structural pounding', *Reflections on the Loma Prieta Earthquake of October 17, 1989*, Chapter 6, Structural Engineers Association of California (SEAOC), 1991.
8. S. A. Anagnostopoulos, 'Building pounding re-examined: how serious a problem is it?', *Eleventh world conf. on earthquake eng.*, Acapulco, Mexico, June 23-28, 1996, paper no. 2108.
9. K. Kasai, A. R. Jagiasi and V. Jeng, 'Inelastic vibration phase theory for seismic pounding mitigation', *J. struct. eng.*, **122**(10), 1136-1159 (1996).
10. B. D. Westermo, 'The dynamics of interstructural connection to prevent pounding', *Earthquake eng. struct. dyn.*, **18**, 687-699 (1989).
11. T. Kobori, T. Yamada, Y. Takenaka, Y. Maeda and I. Nishimura, 'Effect of dynamic tuned connector on reduction of seismic response - application to adjacent office buildings -', *Proc. of ninth world conf. on earthquake eng.*, Vol.V, Tokyo - Kyoto, August 2-9, 1988, pp.773-778.
12. X. Ma and C. P. Pantelides, 'Nonlinear pounding of bridges in earthquakes', *Structures Congress ASCE*, Chicago, April 17-19, 1996, pp.1180-1204.

13. K. Kawashima and M. Yabe, 'Effectiveness of unseating prevention device with energy dissipation', *Fourth U.S.-Japan workshop on earthquake protective systems for bridges*, Osaka, Japan, December 10-11, 1996.
14. V. Jeng and K. Kasai, 'Spectral relative motion of two structures due to seismic travel waves, *J. struct. eng.*, **122**(10), 1128-1135 (1996).
15. K. Kawashima, M. Okado and M. Horikawa, 'Design example of a highway bridge based on the Manual for Menshin Design of Highway Bridges', *Recent Selected Publications at Earthquake Engineering Division, Public Works Research Institute (No.2)*, May, 1993, pp.191-208.
16. E. Mele, A. De Luca and R. Ramasco, 'The effect of using different device numerical models on the global nonlinear behaviour of base isolated structures', *Eleventh world conf. on earthquake eng.*, Acapulco, Mexico, June 23-28, 1996, paper no. 1541.
17. H. Sugita and S. A. Mahin, 'Manual for Menshin Design of Highway Bridges: Ministry of Construction, Japan', *EERC Report No. 94/10*, Earthquake Engineering Research Center, University of California at Berkeley, CA, 1994.
18. T. C. Pan and G. Yang, 'Nonlinear analysis of base-isolated MDOF structures', *Eleventh world conf. on earthquake eng.*, Acapulco, Mexico, June 23-28, 1996, paper no. 1534.
19. American Association of State Highway and Transportation Officials, *AASHTO LRFD Bridge Design Specifications*, AASHTO, Washington, 1994.
20. B. P. Pritchard, 'The use of shock transmission units in bridging', *Proc. Instn Civ. Engrs Structs & Bldgs*, **116**, 82-95 (1996).
21. W. Tanzo and A. Tsuzuki, 'Enhanced seismic lateral load distribution in continuous span bridges fitted with viscoelastic devices', *Eleventh world conf. on earthquake eng.*, Acapulco, Mexico, June 23-28, 1996, paper no. 1528.

STANDARD AND INNOVATIVE RETROFIT DETAILS AND NEW CONSTRUCTION DETAILS FOR HIGHWAY BRIDGES

James L Foster Jr., P.E.
California Department of Transportation
Engineering Service Center
Sacramento, California

ABSTRACT

This paper presents standard and innovative retrofit details which have been used by Caltrans to retrofit existing highway bridges and also discusses some innovative seismic details currently being used for new construction of highway bridges resulting from lessons learned from the San Fernando (1971) , Loma Prieta (1989), Northridge (1994) and Kobe (1995) earthquakes.

INTRODUCTION

As stated in the 1995 publication entitled " Improved Seismic Retrofit Details for Highway Bridges" by James E. Roberts, Director, Engineering Services, Chief Structures Engineer, California Department of Transportation, "The California Department of Transportation staff engineers, Consulting firms, Independent Peer Review Teams, and University Researchers have cooperated in an unprecedented, accelerated program of research based Bridge Seismic Design and Retrofit Strengthening..." He continued to state, "Performance of highway bridges in the January 1994 Northridge earthquake provided reasonable assurance that those bridges which were designed or retrofitted to the new criteria and with the improved structural details can withstand expected earthquakes without collapse or serious damage."

This paper describes common failure mechanisms, common and innovative retrofit solutions and some innovative construction seismic details which are currently being constructed to prevent major damage and/or collapse of highway bridges in California.

This paper is not intended to cover all retrofit and new construction details developed to date. It merely provides a summary of construction details which have been used for most common seismic retrofits in a production environment and also shows some of the new innovative details used in some of the more unique situations.

FAILURE MECHANISMS

The major failure mechanisms which have been identified can be placed into three main categories:

Longitudinal Displacement.

The longitudinal displacement of highway bridges during a seismic event has resulted in the pull off and collapse of the superstructure due to relatively narrow support seats at thermal expansion joints.

Differential Transverse Displacement

The differential transverse displacement of skewed highway bridges during a seismic event has resulted in the pull off and collapse of the superstructure from relatively narrow support seats at thermal expansion joints.

Lack of Ductility

The lack of ductility in intermediate highway bridge supports during a seismic event has resulted in the collapse of the superstructure due to the loss of the supporting capacity of the columns, either due to the loss of bond between the column reinforcing steel and the footing or inadequate confinement of the column reinforcing steel.

RETROFIT SOLUTIONS

The retrofit solutions which have been developed to address the failure mechanisms stated above are:

Longitudinal Displacement Retrofit

The longitudinal displacement retrofit of the highway bridge superstructure is handled slightly differently for each superstructure type as follows:

Steel Girder Superstructure

Typically restrainer cables or rods are attached across a thermal expansion joint to the bottom flange of the steel girders and to the supporting element or to the adjacent steel girders with brackets. This prevents large differential longitudinal displacements from occurring which would result in the pull off of the seat. (Figure 1)

Restrainer brackets are also attached to the bottom flange of the steel girder to engage the substructure in compression to minimize the longitudinal displacement of the superstructure. (Figure 2)

In some cases continuity plates are bolted to the webs of each girder across the expansion joint to prevent the large differential longitudinal movements.

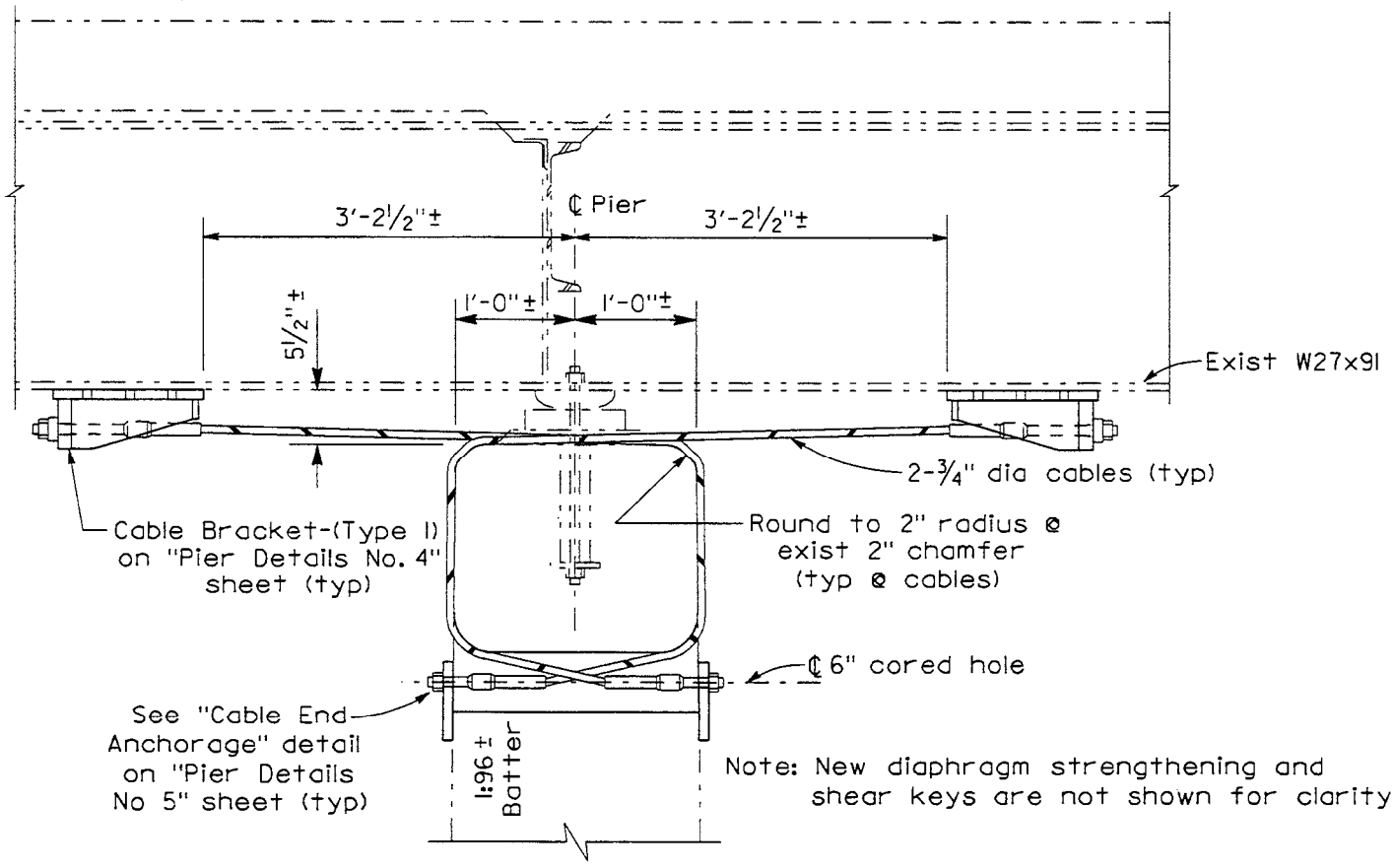

Figure 1 - Steel Girder Restrainer Cables

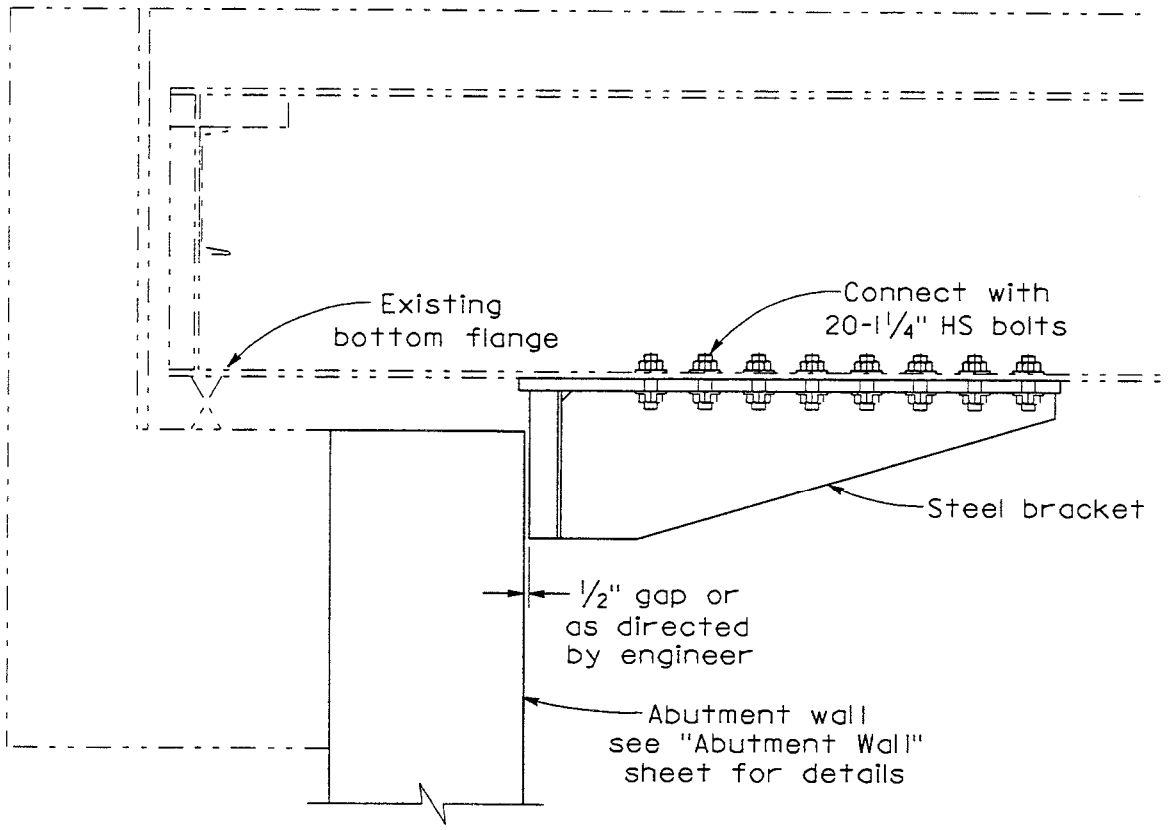

Figure 2 - Steel Girder Restrainer Bracket

T Beam, Precast I Girder and Concrete Box Girder Superstructure

Restrainer cables or rods are usually placed across a thermal expansion joint to prevent large differential longitudinal displacements from occurring which would result in the pull off of the seat. A standard Drawing for cable restrainers has been developed by Caltrans (Figure 4)

Pipe seat extenders are also added to allow for a larger longitudinal displacement and prevent the loss of vertical support. (Figure 3)

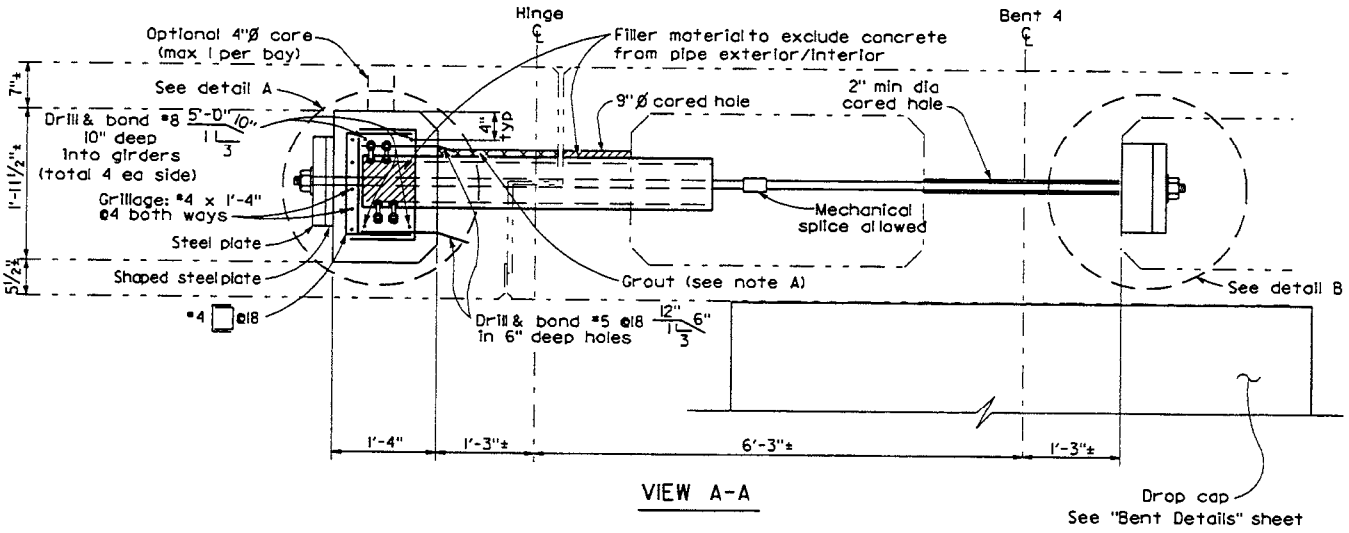

Figure 3 - Concrete Box Girder Pipe Seat Extenders with Restrainer Rods.

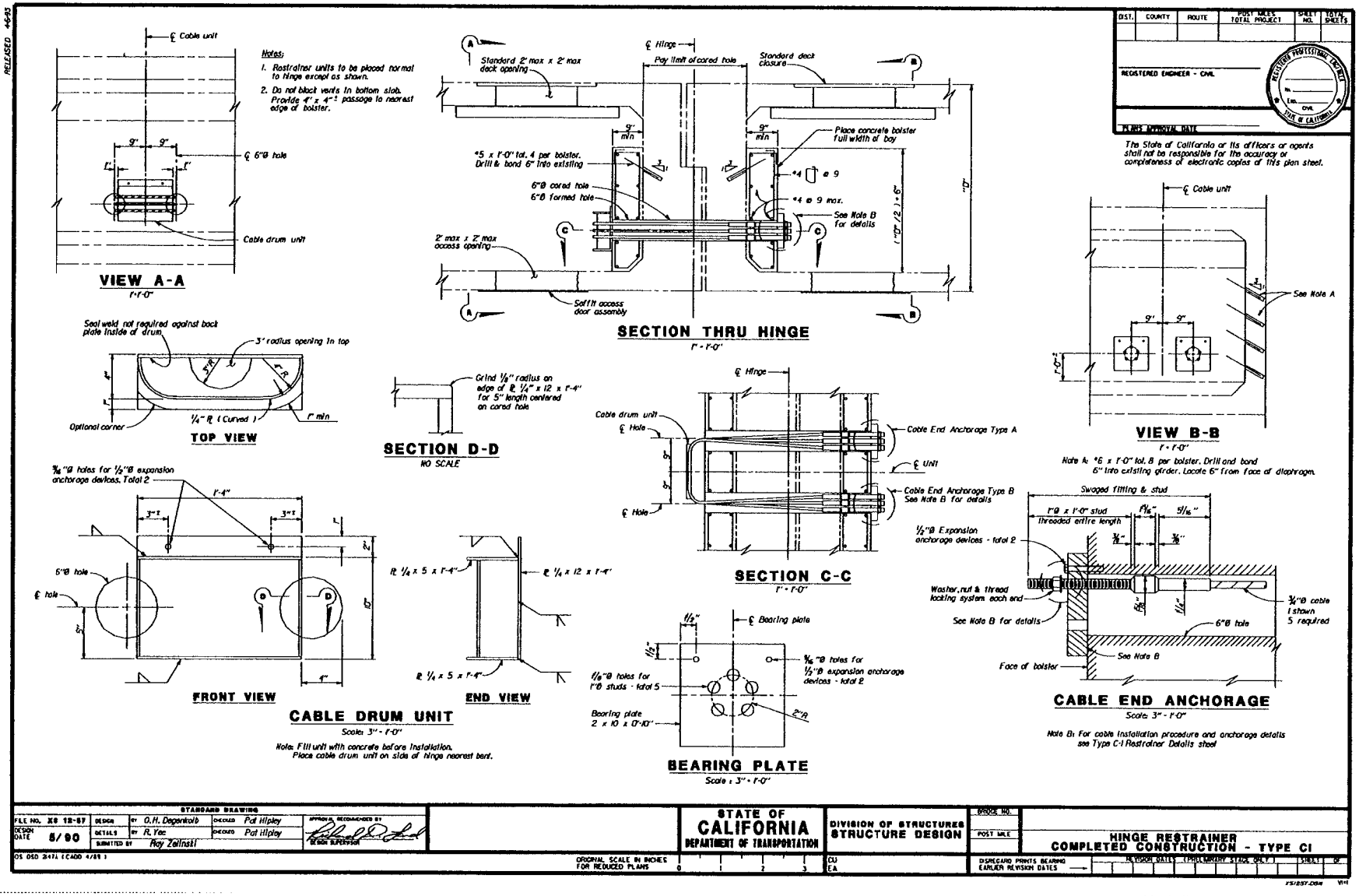

Figure 4 - Standard Drawing for Concrete Box Girder Cable Restrainers

Abutments

Typically a large amount of longitudinal force is required to be resisted by the abutments to limit the longitudinal deflections of the superstructure.

On seat type abutments, timber blocking between the end of the superstructure and the back wall of the abutment provides for the early engagement of the soil behind the back wall and is approximately equal the depth of the superstructure. (Figure 5)

In order to engage more soil on seat type abutments, the restrainer brackets are used for steel girder superstructures. (Figure 2) For concrete box girder superstructures a longitudinal shear key is used. (Figure 6)

On diaphragm type abutments, the diaphragm can be strengthened either by coring and bonding high strength rods into the existing diaphragm or by adding concrete to the face of the abutment.

When more longitudinal abutment force is required to restrain the superstructure displacement then anchor slabs or large diameter shafts are used. (Figure 7 & 8)

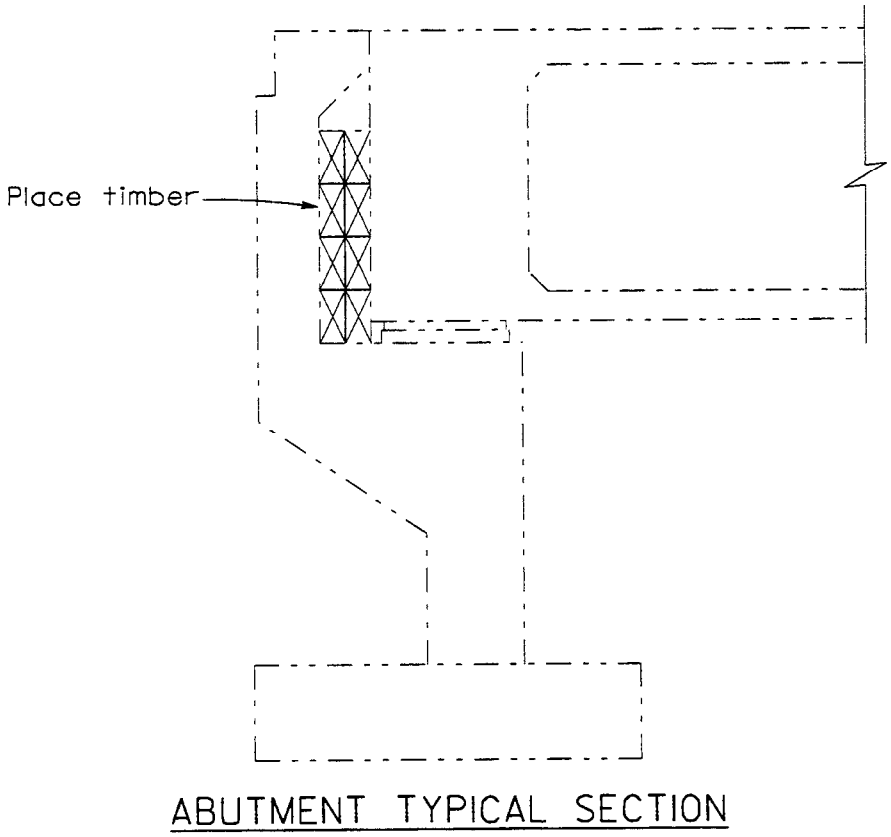

Figure 5 - Timber Blocking

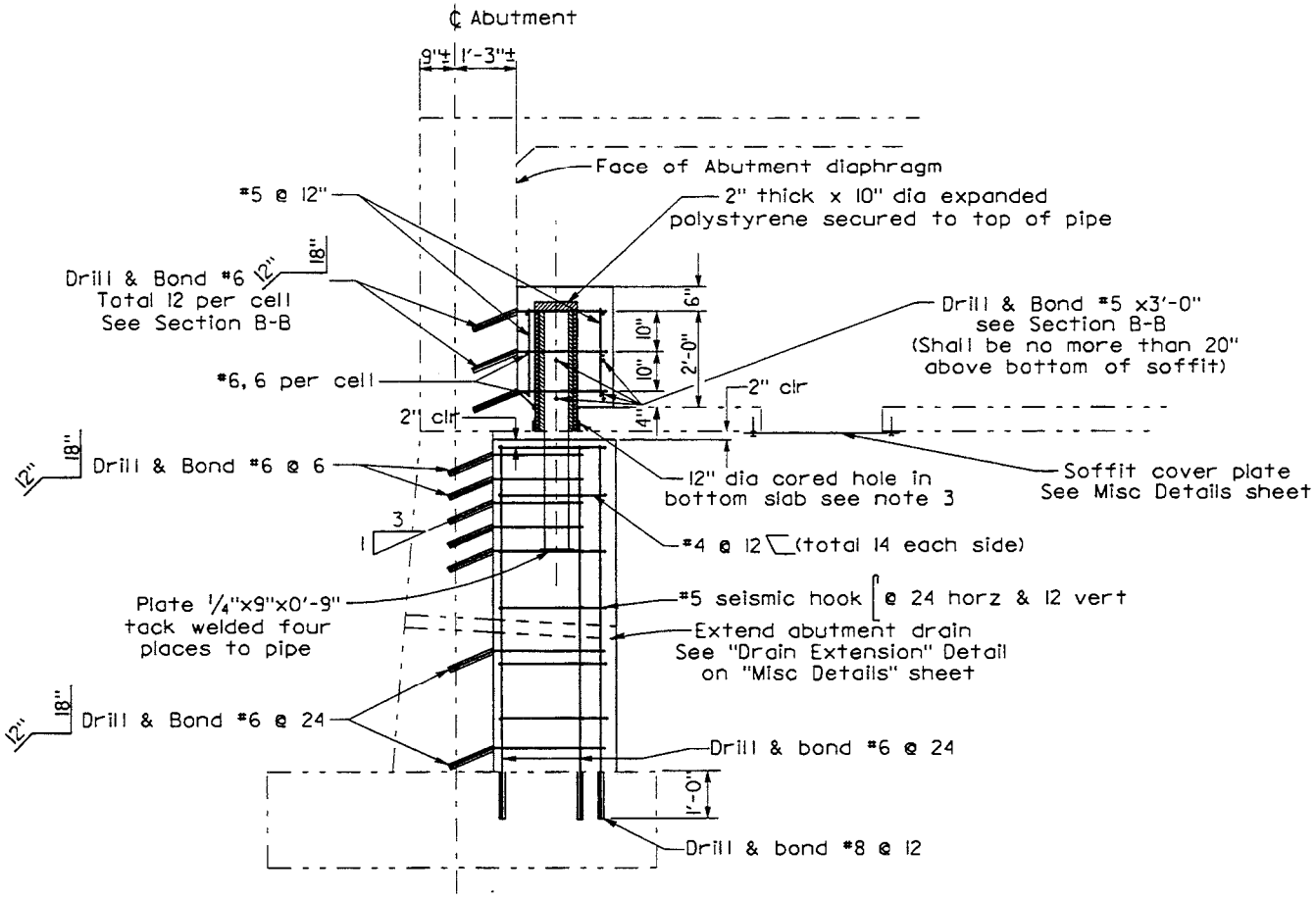

SECTION A-A

Figure 6 - Box Girder Longitudinal Shear Key

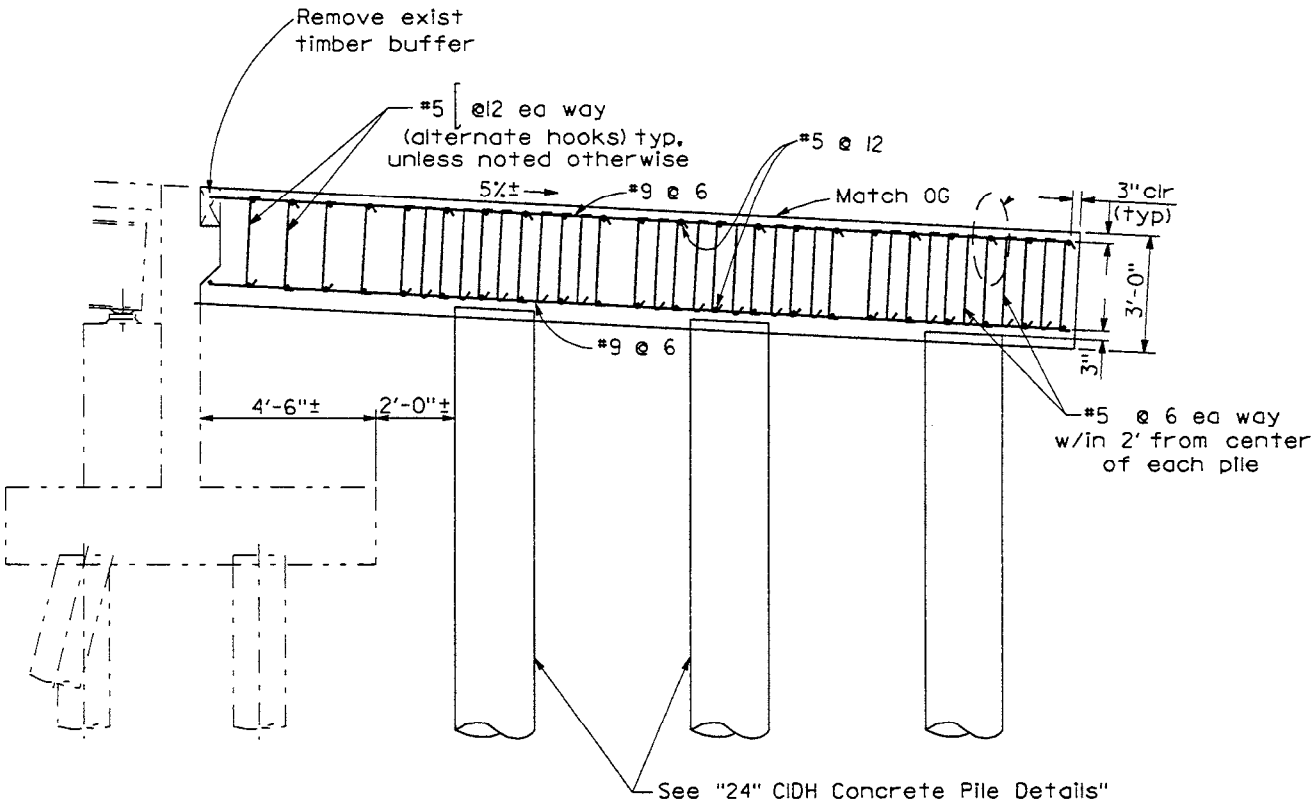

SECTION B-B

Figure 7 - Anchor Slab

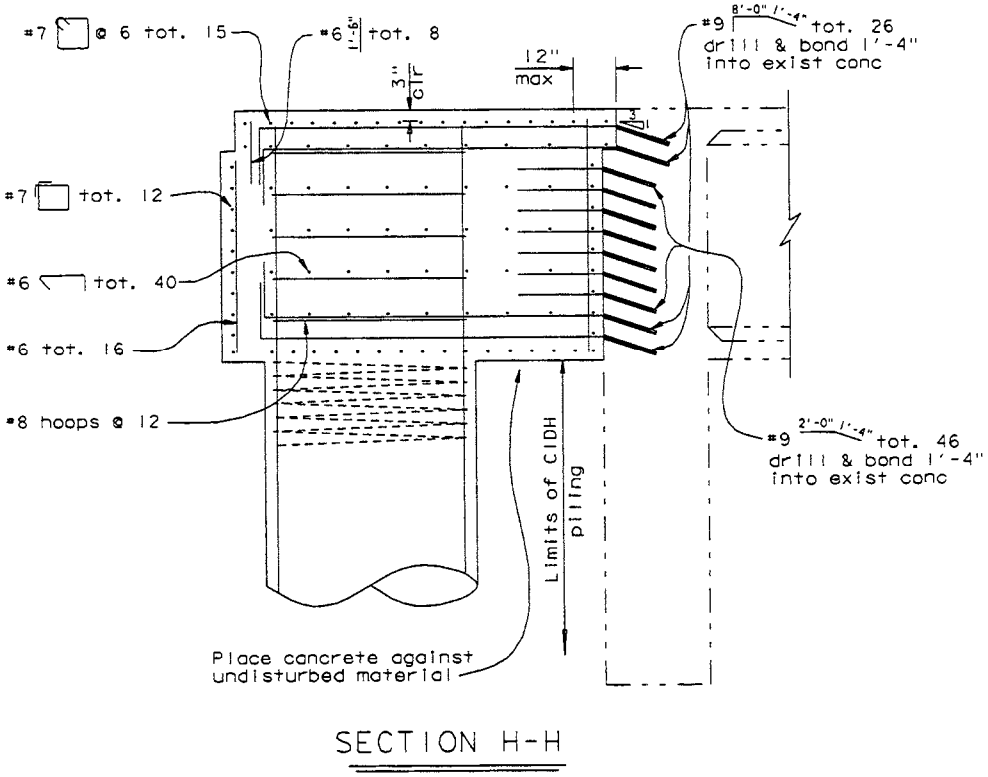

Figure 8 - Large Diameter Shafts

Differential Transverse Displacement Retrofit

The differential transverse displacement retrofit of highway bridge superstructures is handled differently for each superstructure type as follows:

Steel Girder Superstructure

Shear keys are usually attached to the top or sides of the substructure element between the girders which restrain the superstructure transversely and also prevent large vertical displacements in case the rocker bearings fail. (Figure 9)

Where excessive vertical displacements will not occur , the end diaphragms are strengthened with braces and the superstructure is allowed to slide on the supporting element.

Another solution is to replace the rocker bearings with elastomeric bearing pads or isolation bearings. (Figure 10)

When hinges in steel girder superstructures are to be restrained, the end diaphragms are strengthened and the transverse keys are strengthened or replaced. (Figure 11) In some cases the addition of restrainer brackets can be placed on the end diaphragms and/or pipe elements can be placed in the sidewalk on the bridge deck. (Figure 12 & 13)

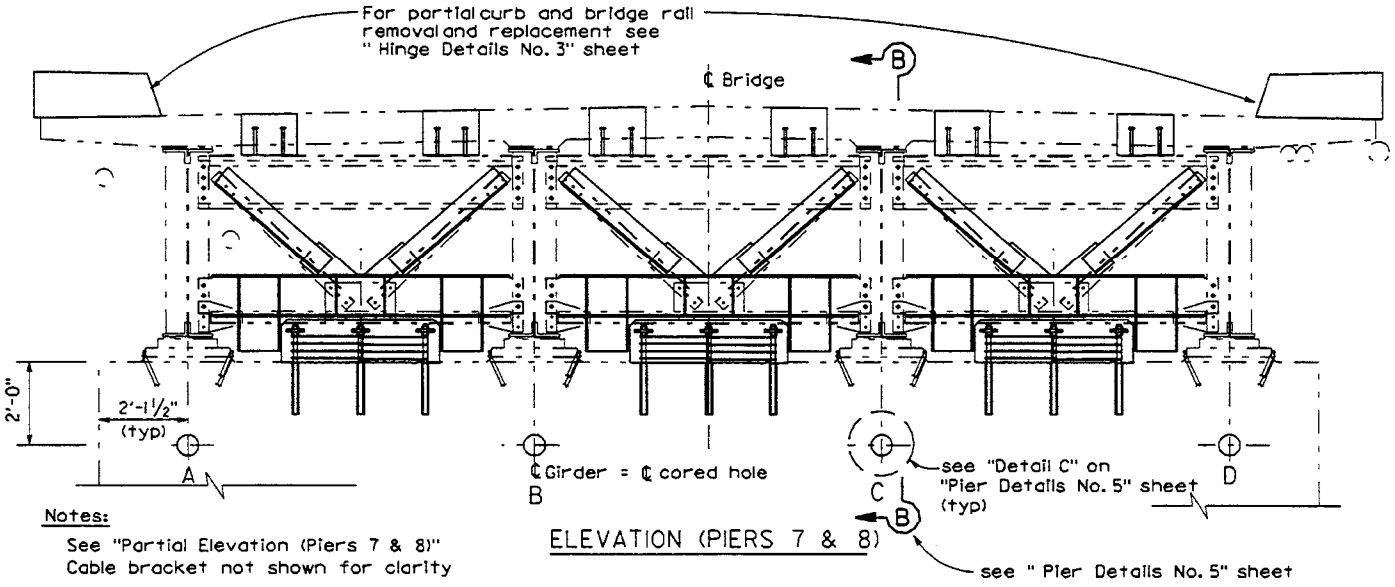

Figure 9 - Steel Girder Transverse Shear Keys with End Diaphragm Strengthening

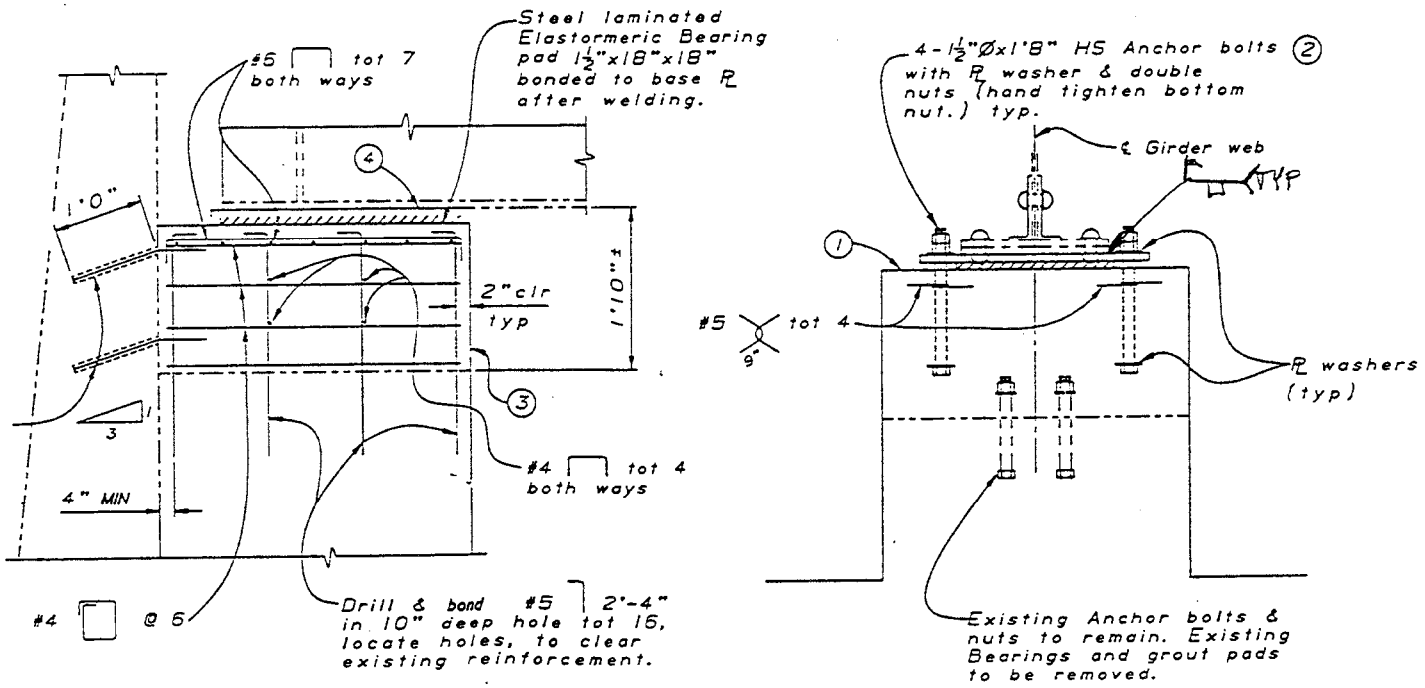

Figure 10 - Steel Girder Bearing Replacement.

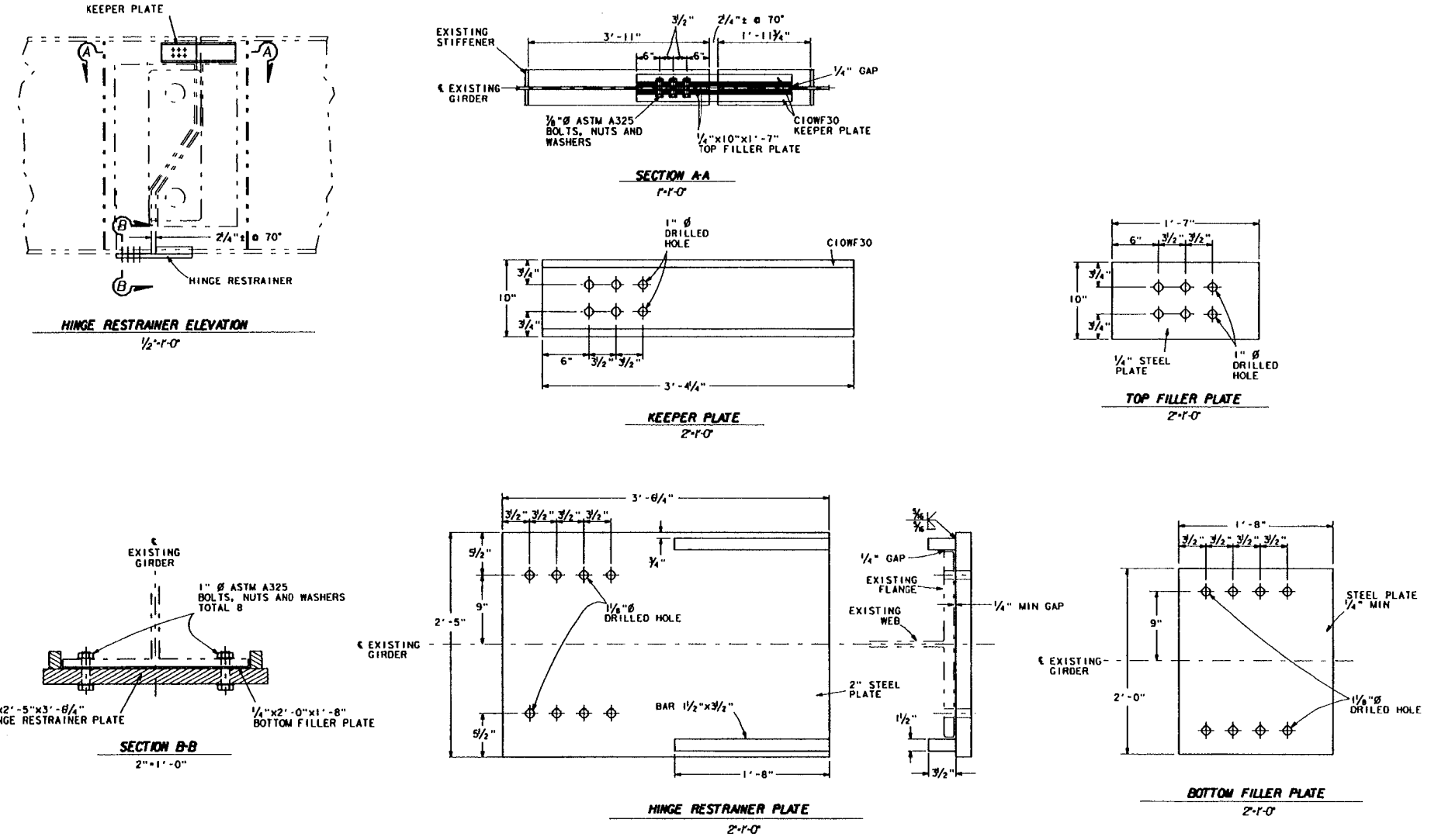

Figure 11 - Steel Girder Hinge Key Strengthening

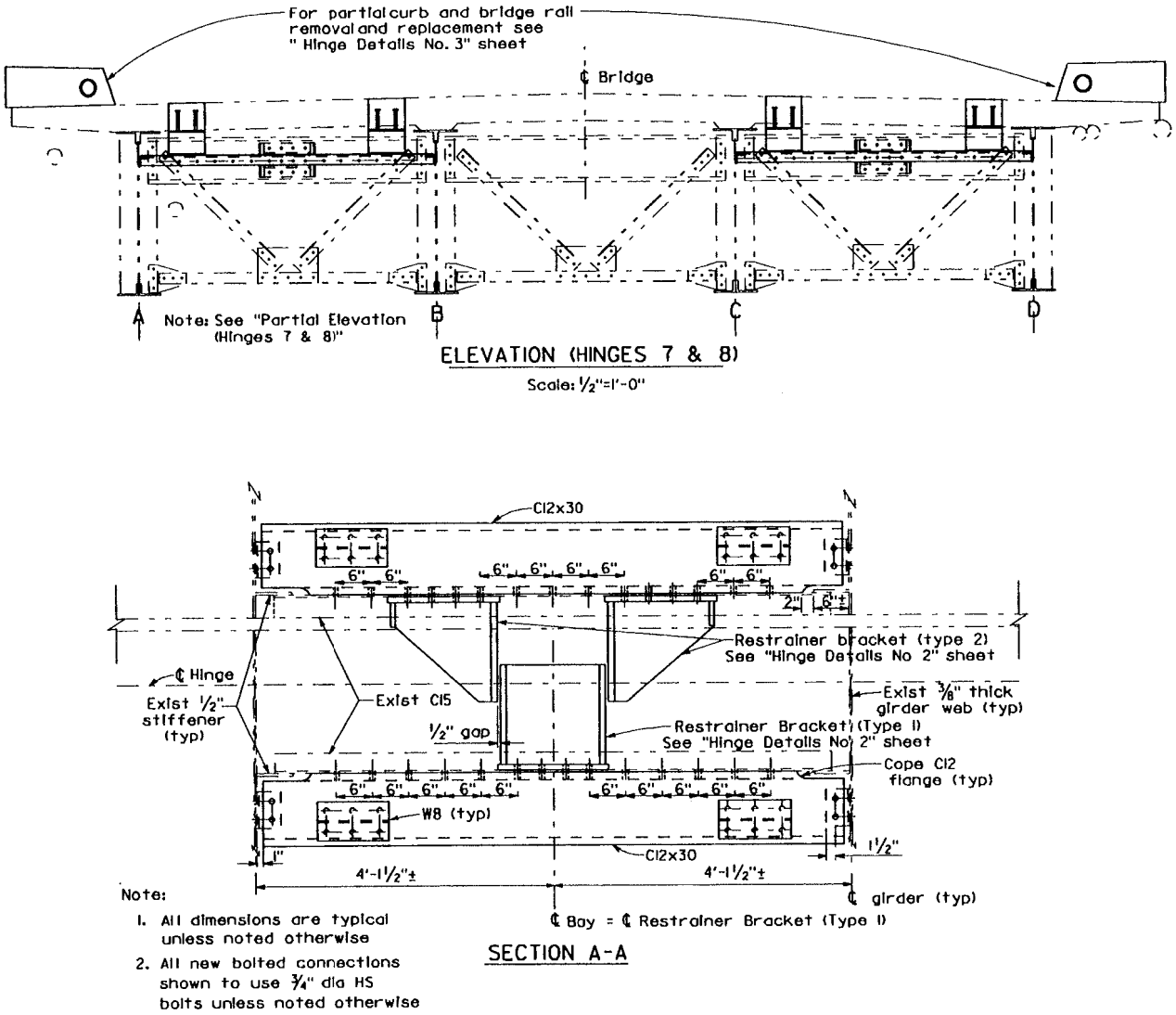

Figure 12 - Steel Girder Hinge End Diaphragm Shear Keys

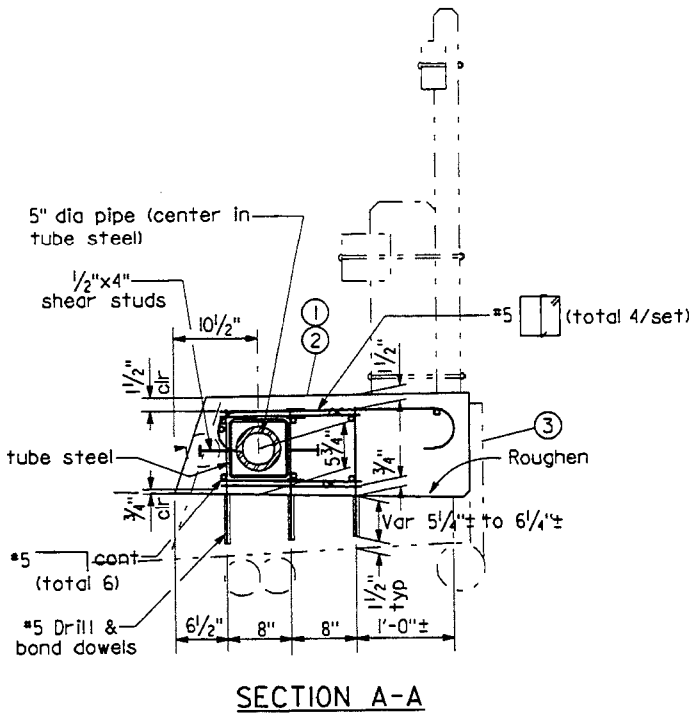

Figure 13 - Steel Girder Hinge Shear key in Sidewalk on Concrete Deck

Precast I Girder

Pipe seat extenders are typically used as transverse shear keys and/or the end diaphragm attachment to the substructure is strengthened. (Figure 14) Extending the support width and adding shear keys between the girders are also common retrofits.

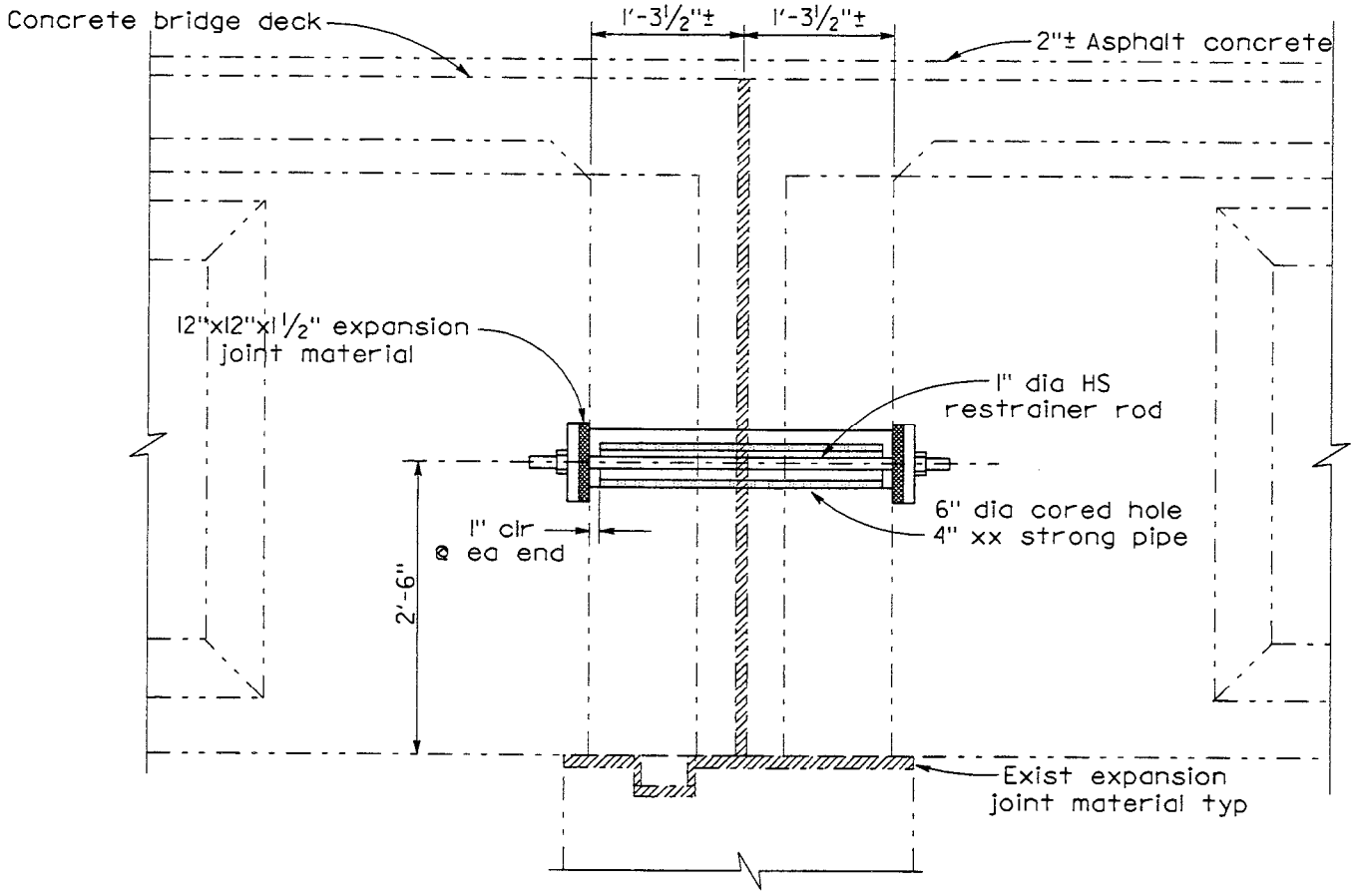

Figure 14 - Precast I Girder Shear Key

Concrete Box Girder Superstructure

Pipe seat extenders are typically used as transverse shear keys. In some cases the end diaphragm is strengthened. (Figure 15)

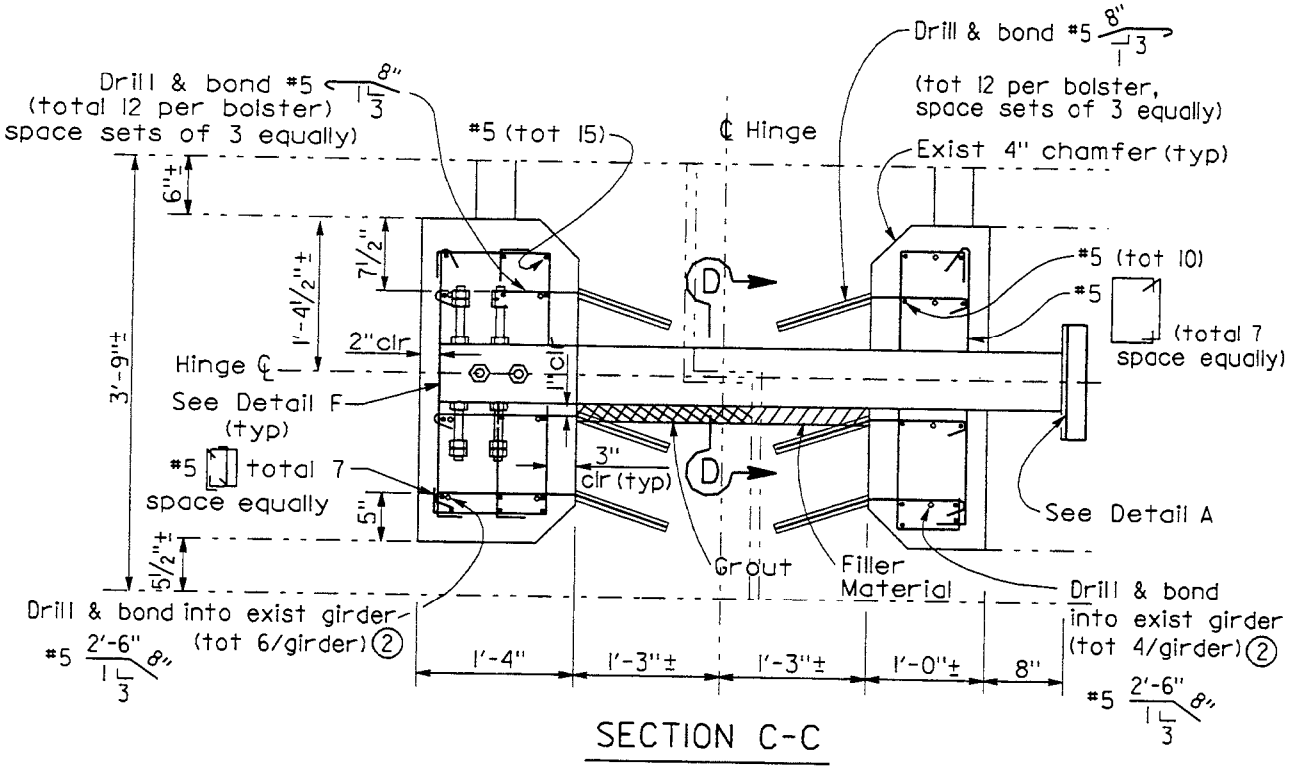

Figure 15 - Concrete Box Girder Shear Key

Abutments

Usually, a large amount of transverse force is required to be resisted by the abutments to limit the transverse deflections of the superstructure.

Strengthening the seat abutment transverse shear keys is often accomplished by drilling and bonding into the existing abutment and casting additional shear keys. The wing walls on diaphragm and seat abutments are also strengthened to engage more soil. (Figure 16)

In some cases a restraint wall is added to resist the transverse forces. (Figure 17)

For box girder superstructures where force demands may be relatively high, anchor slabs are used and pipe seat extenders installed as transverse shear keys between the anchor slab and the superstructure. (Figure 18) Large diameter shafts have also been used with the pipe seat extenders to accomplish the same goal. (Figures 19 & 20)

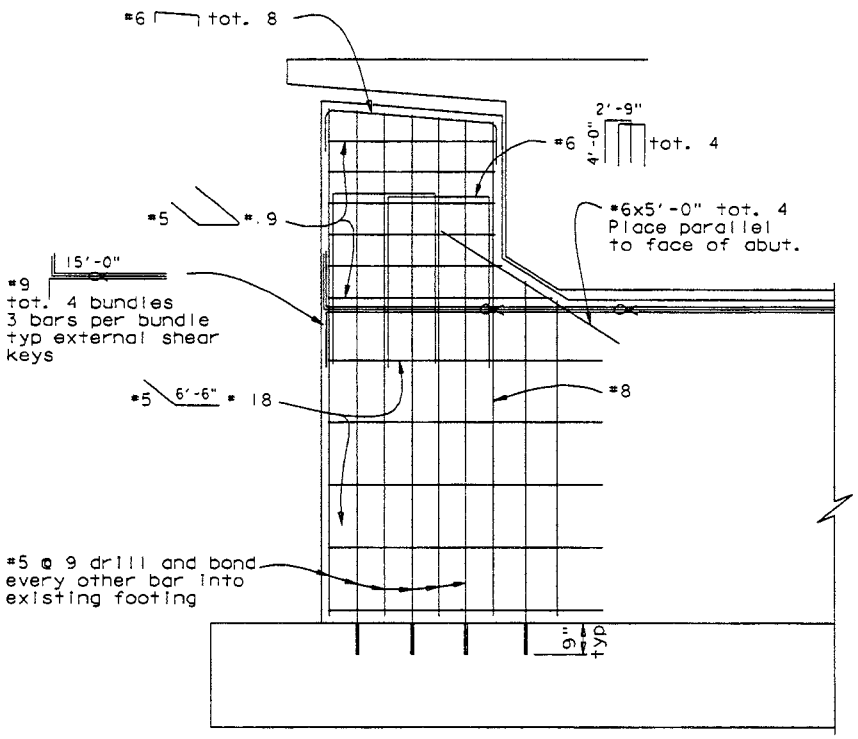

Figure 16 - Seat Abutment Shear Key Strengthening

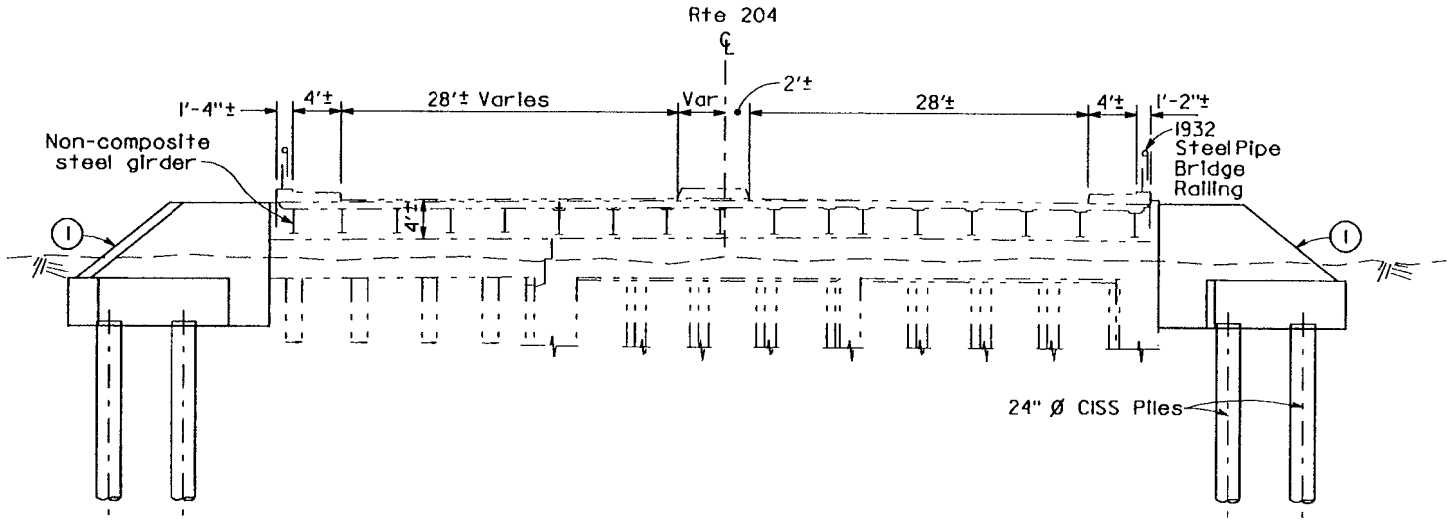

Figure17 - Transverse Restraint Wall

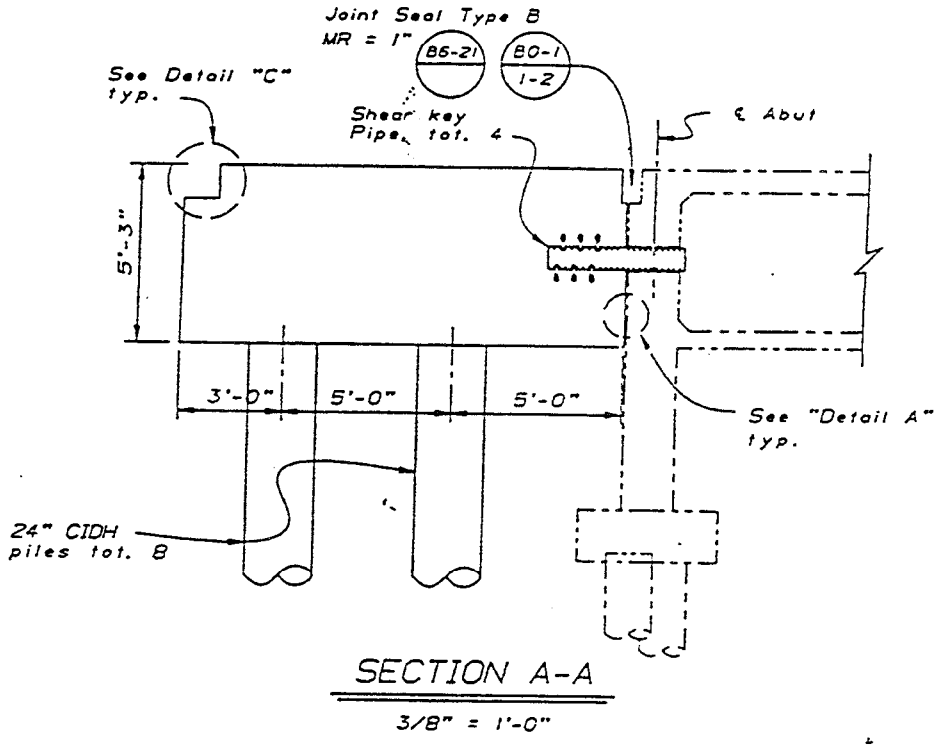

Figure 18 - Anchor Slab

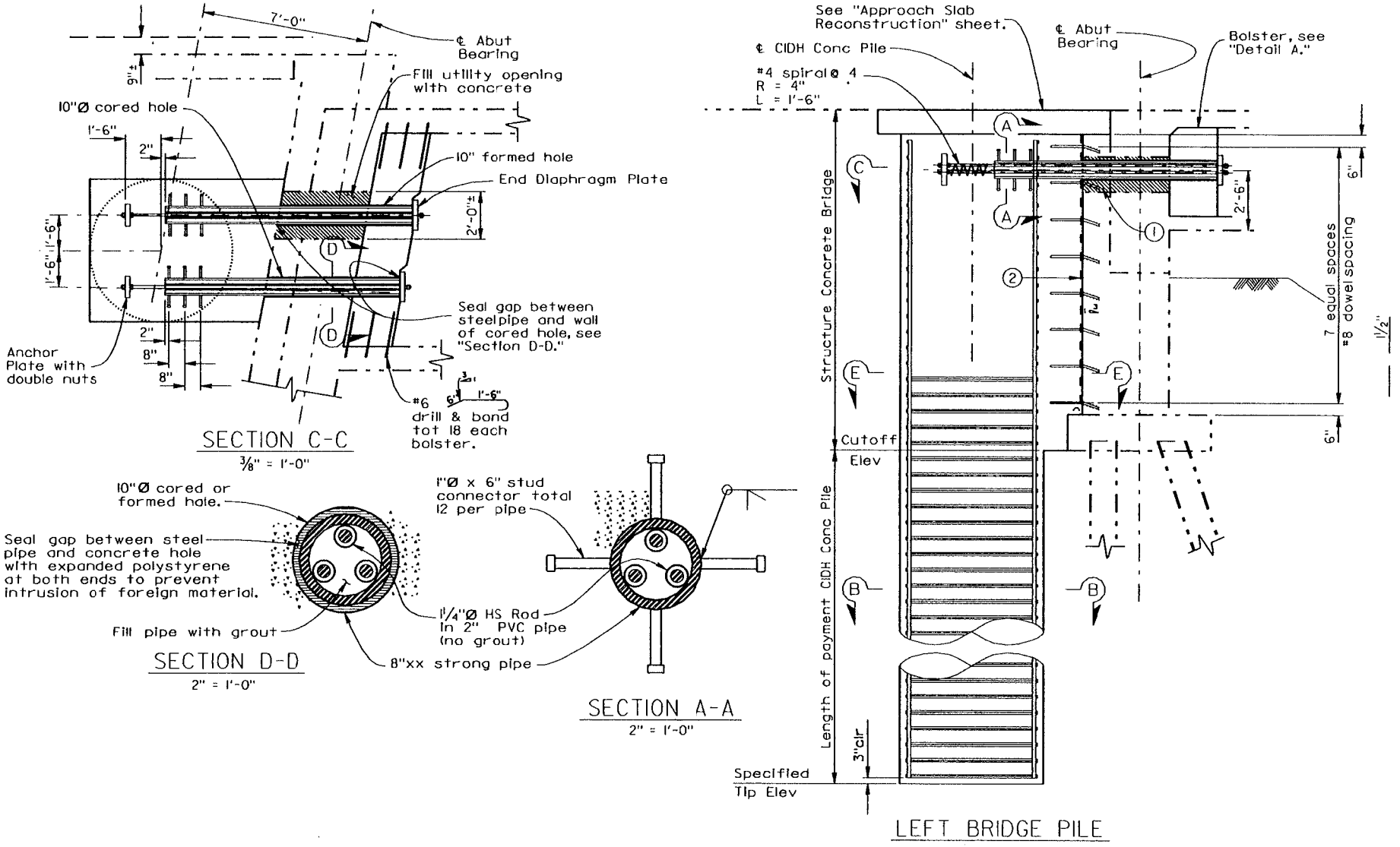

Figure 19 - Large Diameter Shafts Behind Abutment

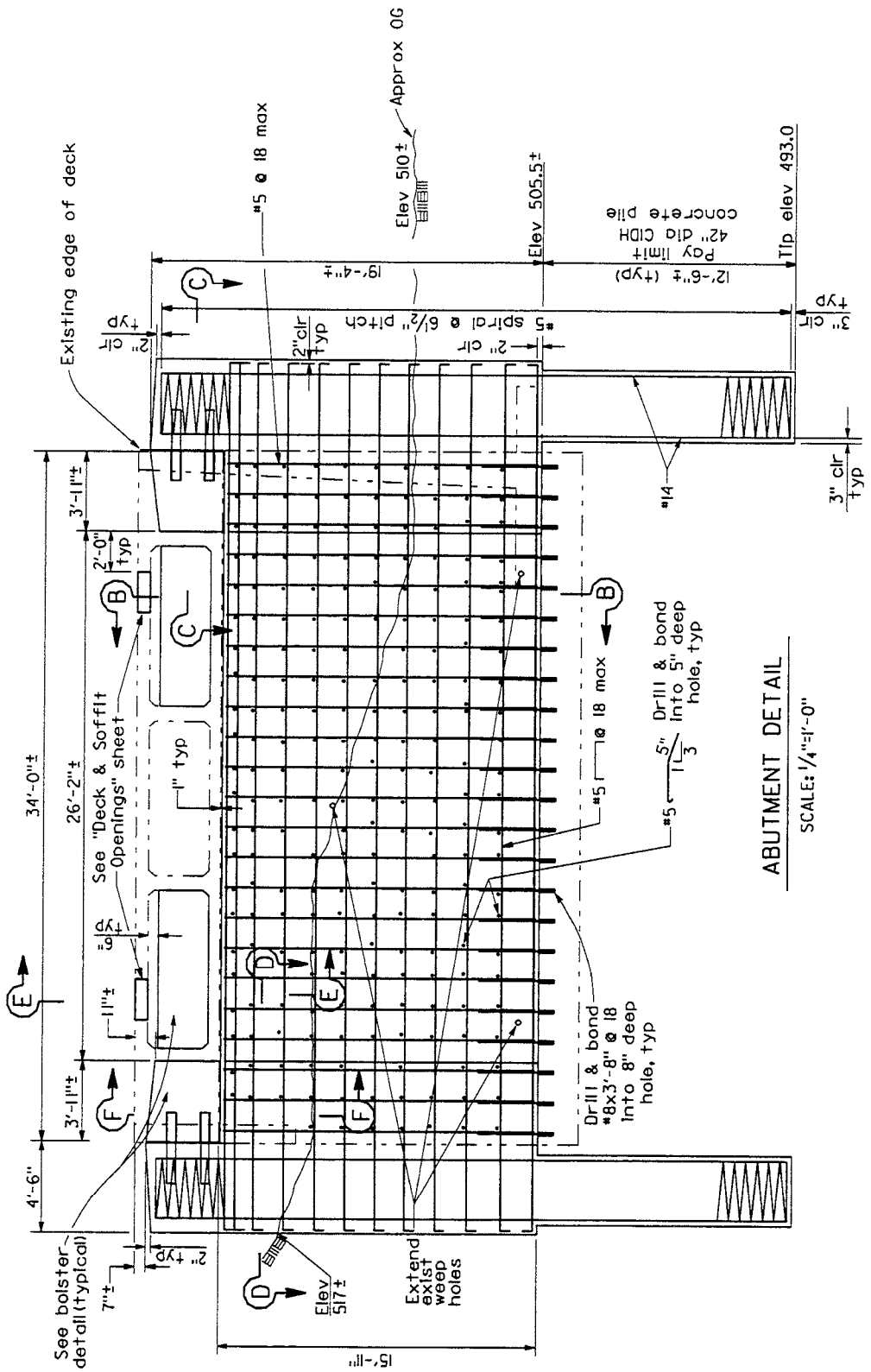

Figure 20 - Large Diameter Shafts Outside Abutment

Improving Substructure Ductility and Strength

The ductility of substructure elements which support the various superstructure types has proven to be a very important consideration in a highway bridge to prevent major damage or collapse. The improvement of the substructure ductility and strength is commonly accomplished by several methods:

Column and Pier Encasement and Strengthening

Typically columns and piers constructed prior to 1971, lack sufficient confinement to provide the shear strength and/or moment ductility needed to accommodate the large cyclic displacements induced during a seismic event. The existing confinement is also typically not adequate to develop the lap splices which may exist within the plastic hinge region. In order to provide adequate confinement, the columns are encased with steel casings or concrete shells. Caltrans has developed a standard drawing for steel column casings. (Figure 25)

Some columns can have inadequate strength even with adequate confinement and require strengthening. (Figure 21 & 22) In these cases, additional longitudinal reinforcement is added within the encasement. The longitudinal reinforcement is bonded in a drilled hole in the footing and bent cap and a footing overlay added and/or the bent cap is strengthened as described later.

In some cases the columns and footings can be replaced. (Figure 23)

Another approach is to place an infill wall. Although this does not improve the ductility of the columns, the infill wall can add ductility for longitudinal displacements and eliminate the need to increase the strength of the bent cap and column. (Figure 24)

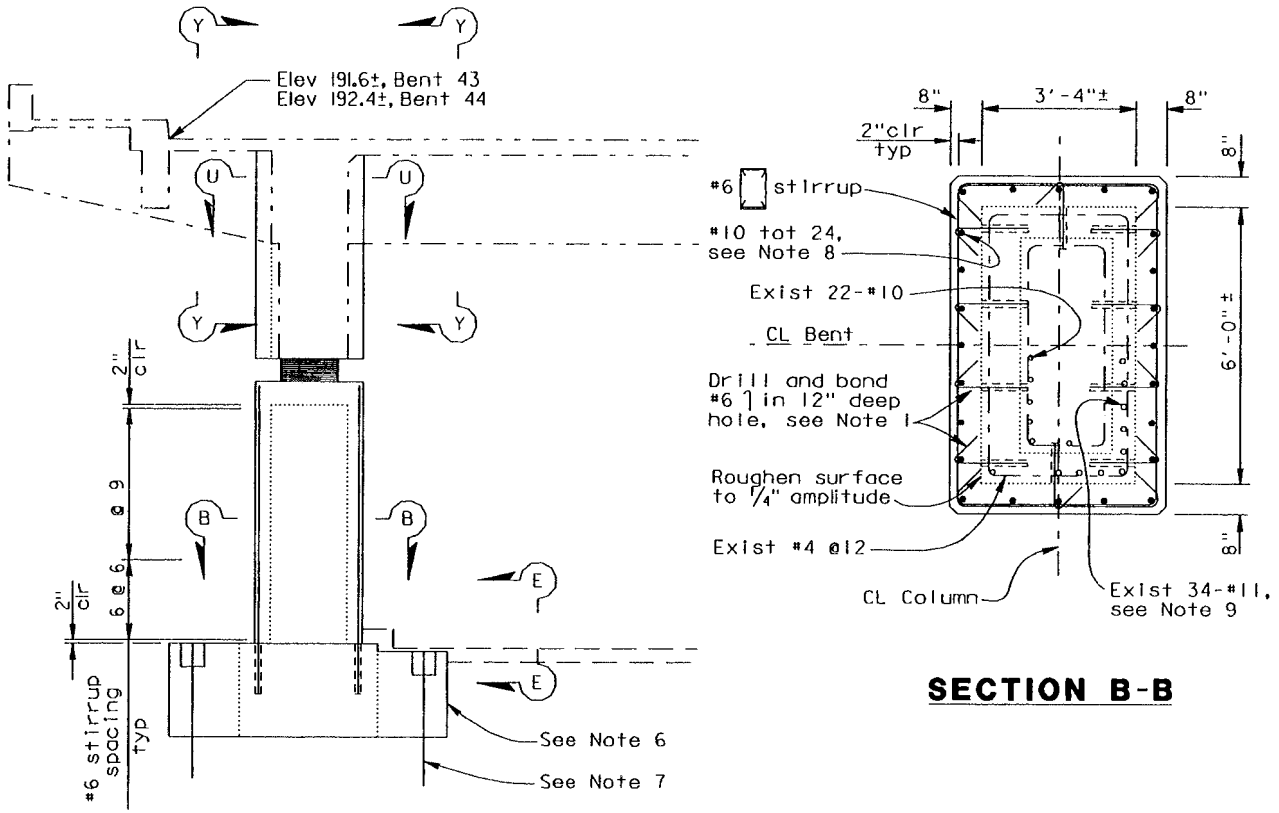

Figure 21 - Concrete Encasement of Column with Strengthening and Isolation Bearings.

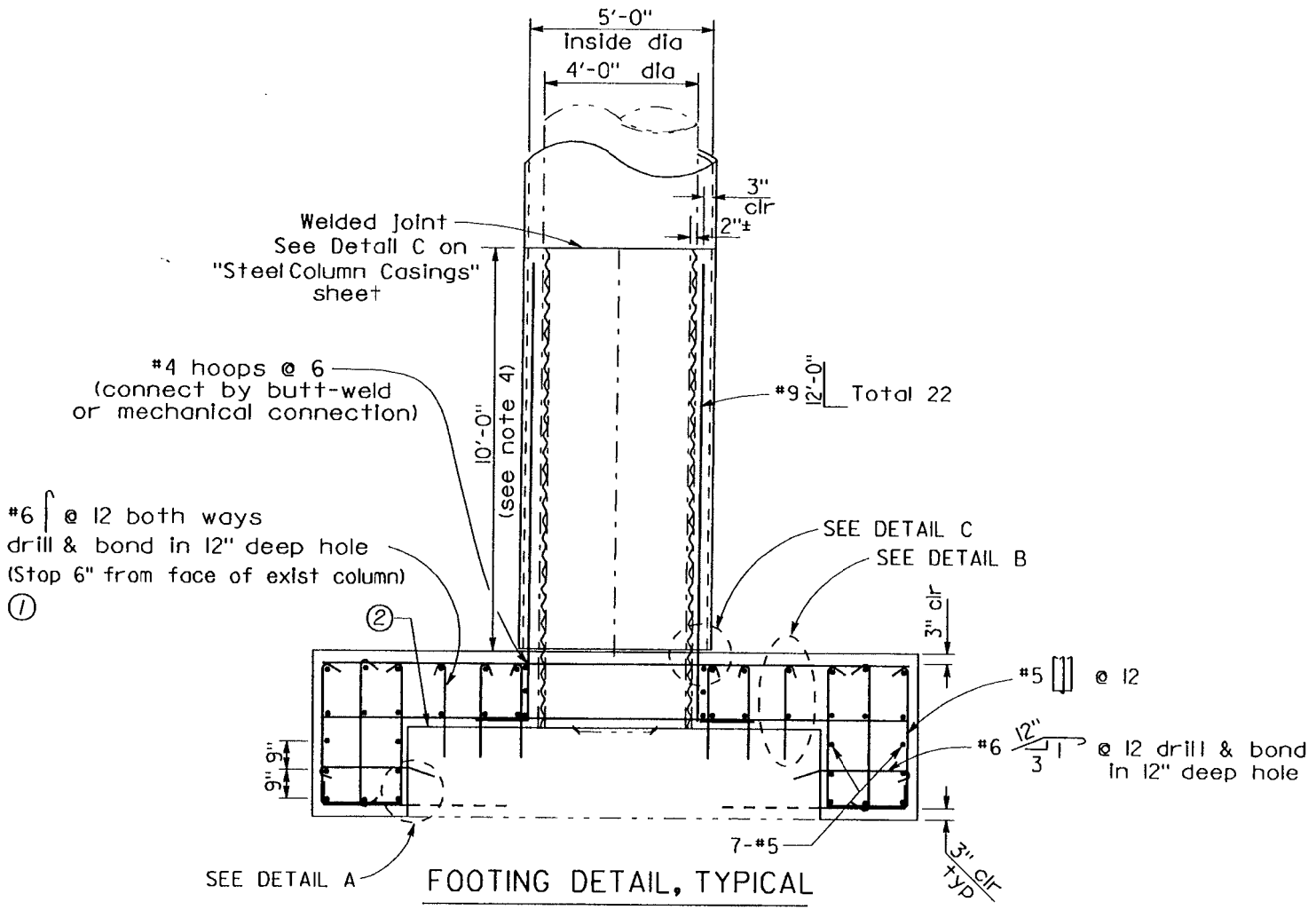

Figure 22 - Steel Casing with Column Strengthening

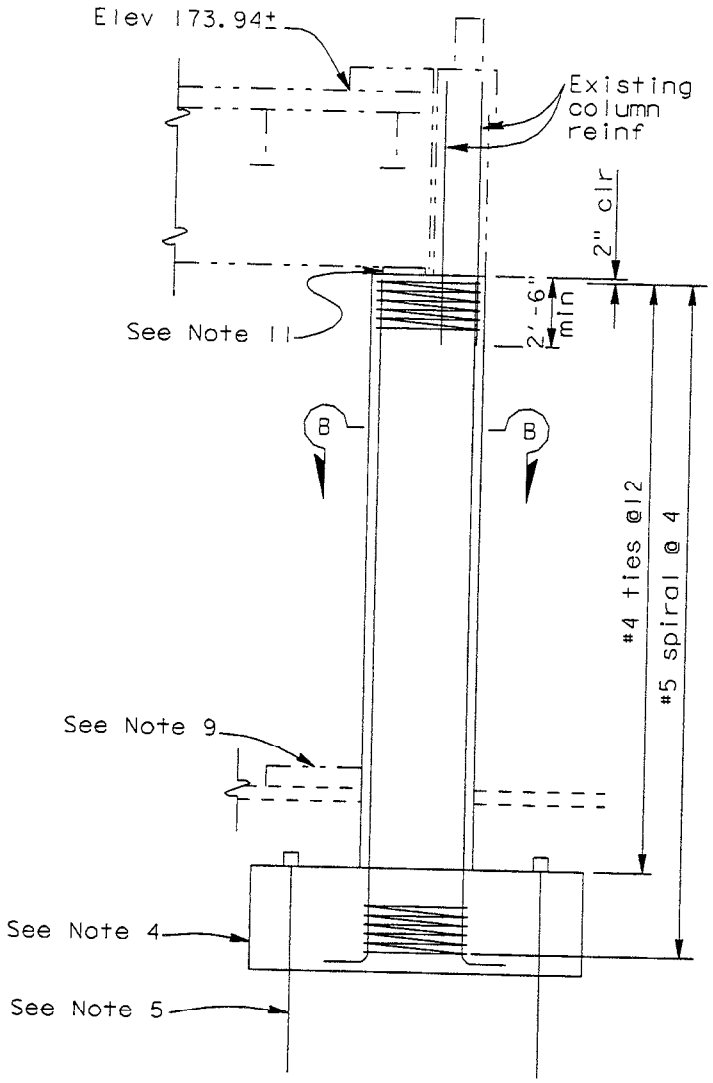

Figure 23 - Column and Footing Replacement

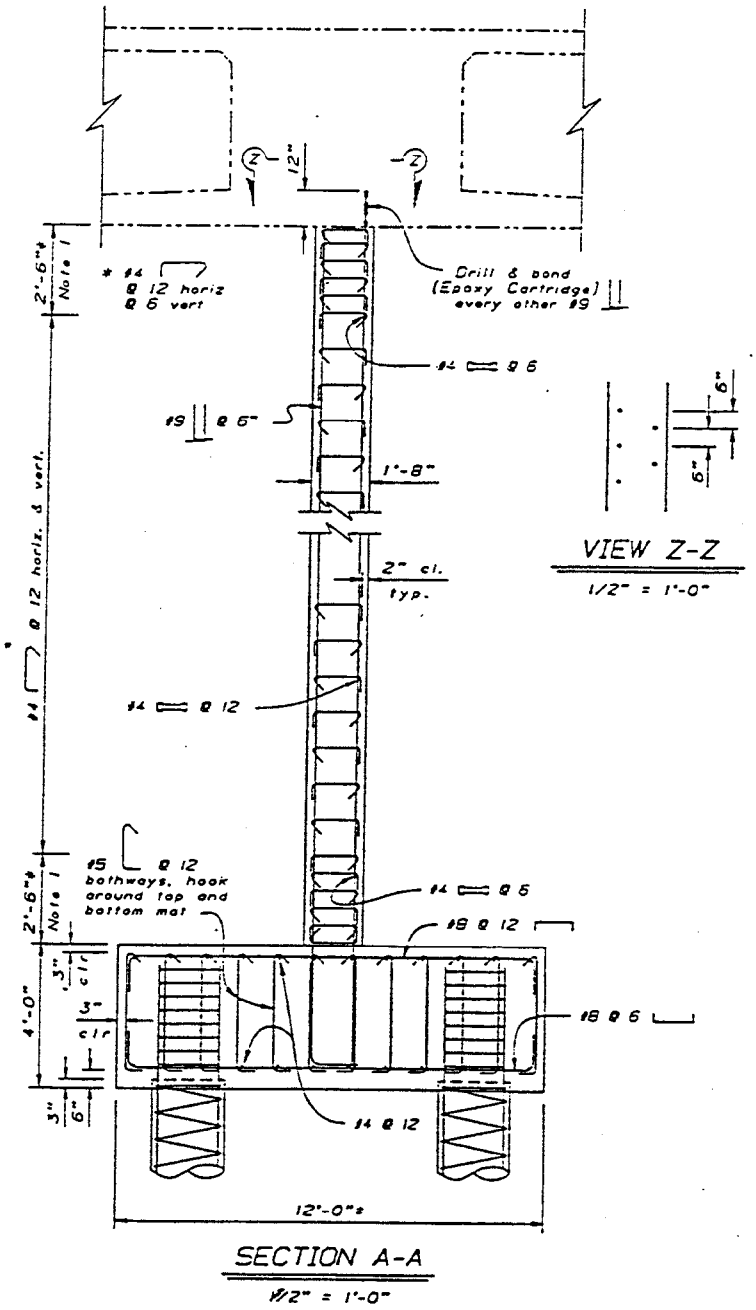

Figure 24 - Infill Wall

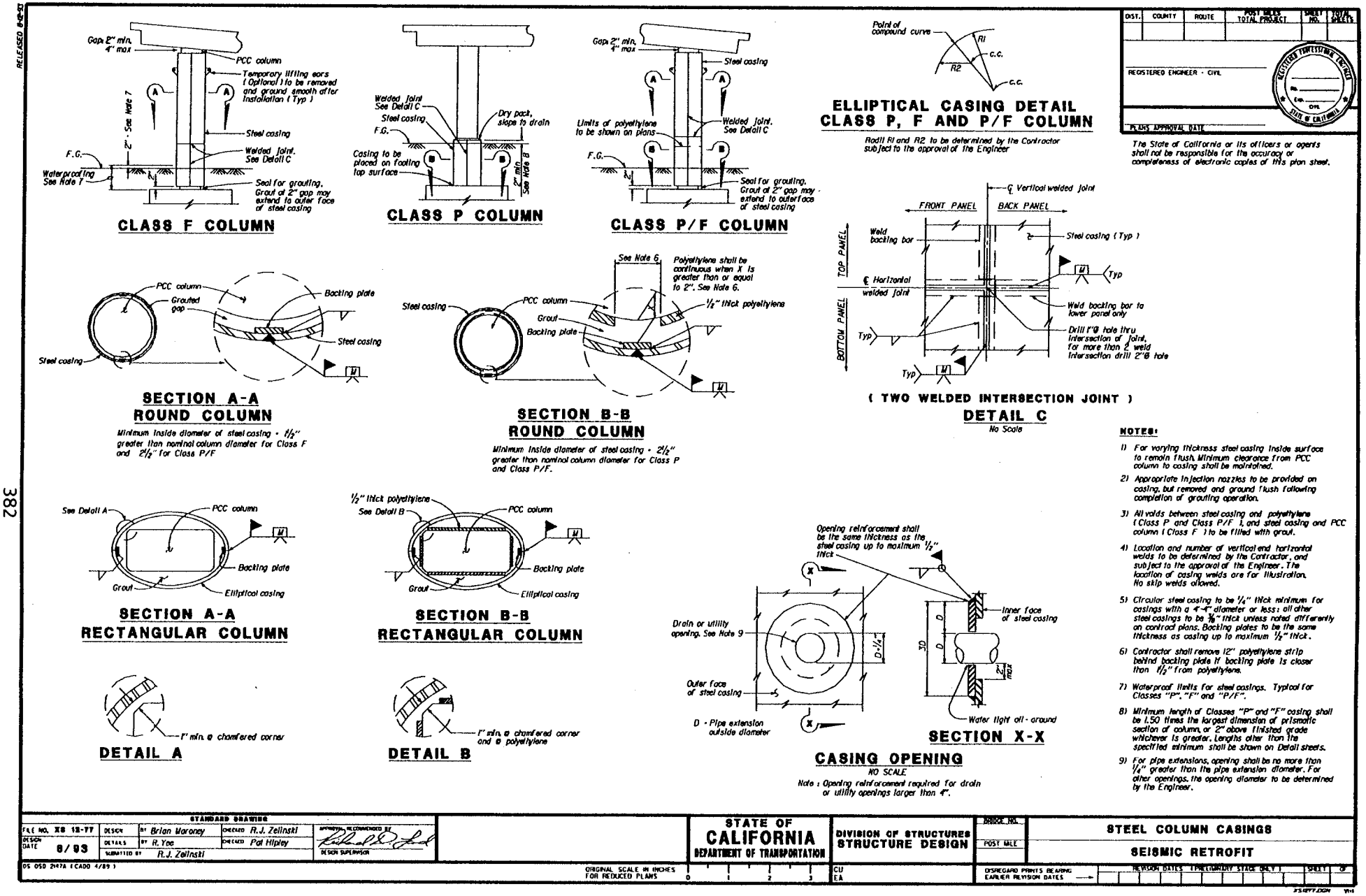

382

Figure 25 - Steel Casing Standard Drawing

Column/Superstructure Isolation

Another alternative to strengthening the superstructure and substructure is to isolate them from each other by using isolation bearings. This approach allows for a response period increase which reduces the seismic demand on the highway bridge. In some cases both strengthening and isolation may be necessary. (Figure 26)

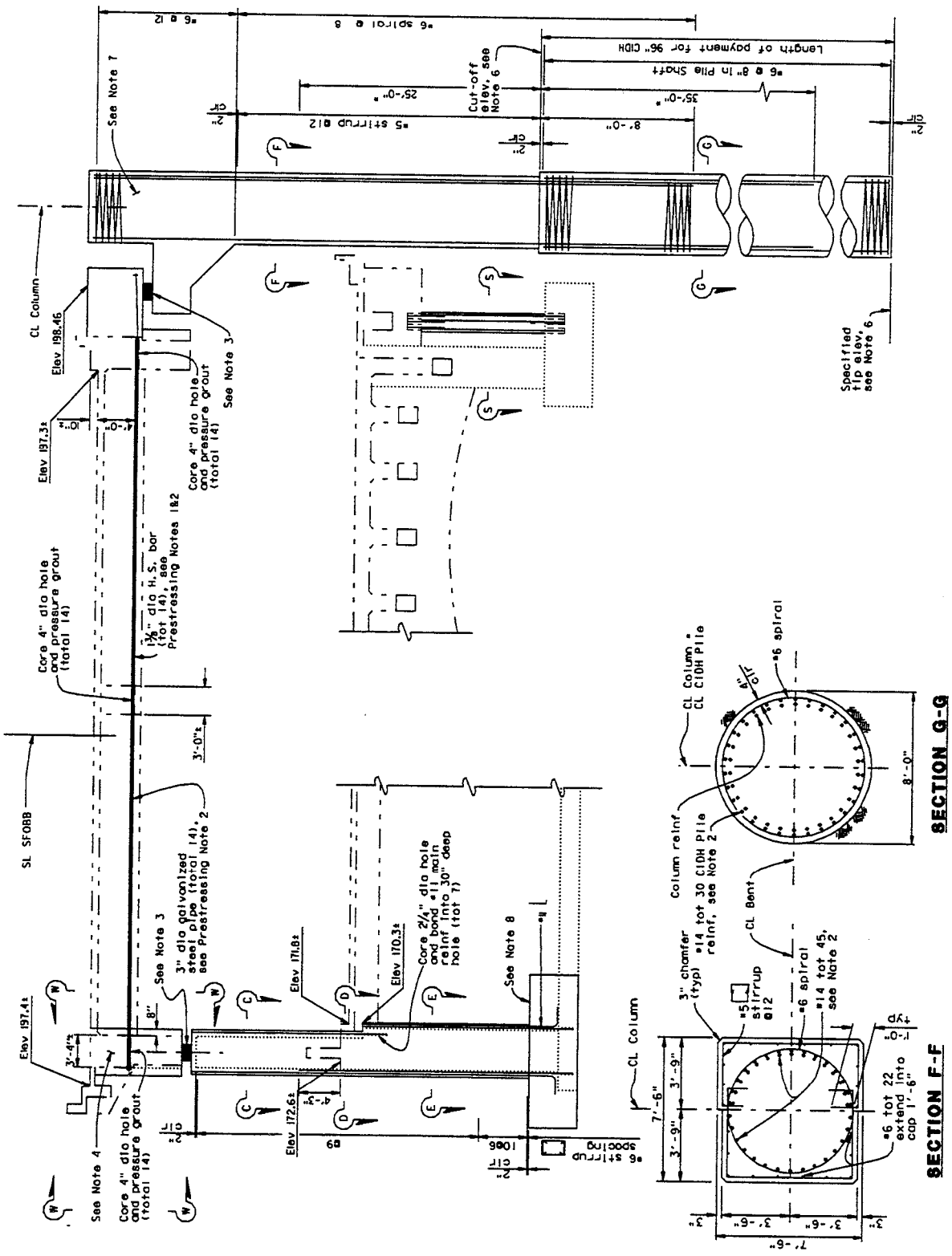

Figure 26 - Superstructure Isolation

Bent Cap Strengthening

In some cases the bent cap does not have adequate capacity to force the plastic hinge to occur within the column. The bent cap is then strengthened by encasing it with concrete and adding longitudinal reinforcement or high strength rods. (Figure 27)

When the bent cap does not have adequate capacity to resist the joint shear stresses and force the plastic hinge to occur within the column, the bent cap is strengthened by encasing it with concrete and adding transverse reinforcement or high strength rods.

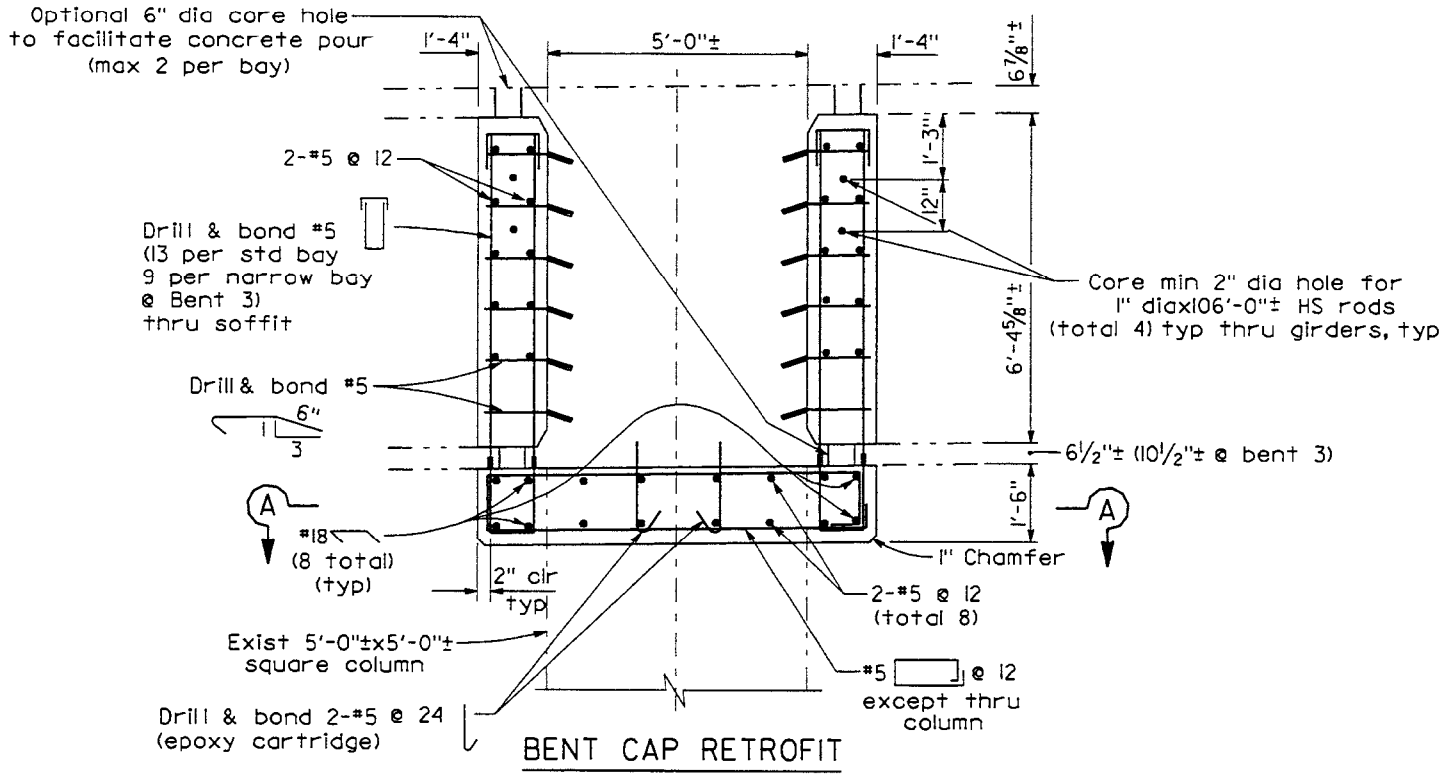

Figure 27 - Concrete Box Girder Bent Cap Strengthening

Footing & Footing/Pile Connection Strengthening

When the footing does not have adequate shear and/or flexural capacity to force the plastic hinge to occur within the column, a footing overlay with additional reinforcement is installed, additional piles are placed, and the footing size is increased. (Figure 28) Typically the connection of the existing piles to the footing is inadequate to develop the tensile capacity of the piles. In some cases, the footing can be allowed to rock on the piles. When the tensile capacity is needed, it is possible to excavate below the footing and add reinforcement to the piles and then encase it in concrete.

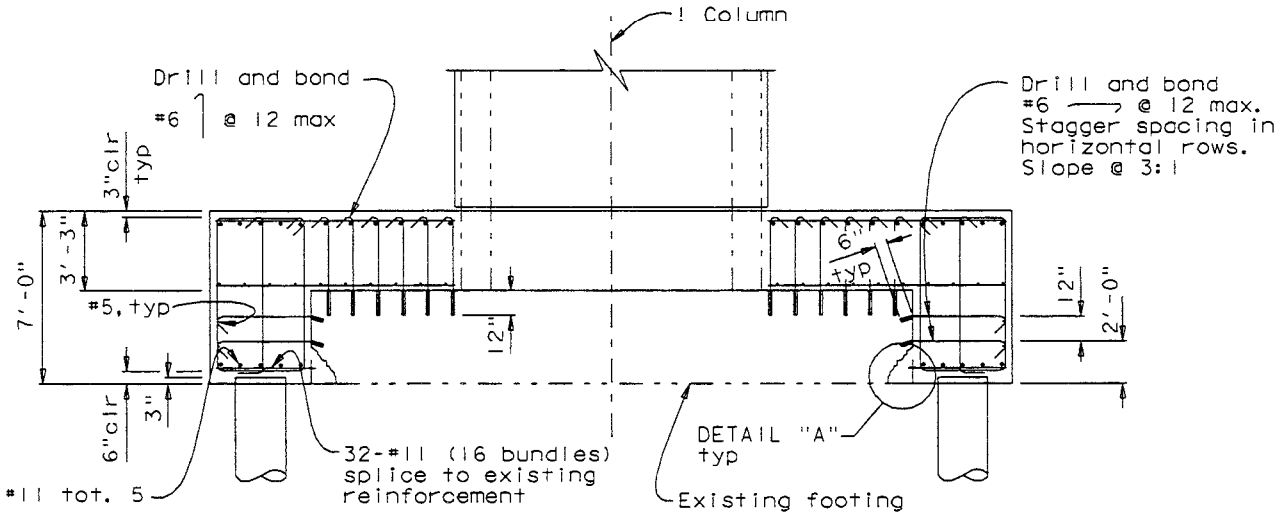

Figure 28 - Footing Strengthening

Retrofit Detail Example

An extensive retrofit which provides for full serviceability after the maximum credible earthquake can become very complex and relatively costly. (Figure 29)

NEW CONSTRUCTION SEISMIC DETAILS

From the observations made and lessons learned from the recent Loma Prieta (1989), Northridge (1994) and Kobe (1995) earthquakes we have improved the seismic details used in the construction of new highway bridges.

Longitudinal and Differential Transverse Displacement

Hinges

To prevent the unseating of hinges in regions of high seismic activity and large displacements, the hinge been located such that each side of the hinge is cantilevered from the adjacent span. (Figure 30)

Abutments

To prevent large longitudinal and differential transverse displacements, the abutments can be designed with integral anchor slabs or large diameter shafts. (Figure 31 & 32)

Substructure Ductility and Strength Improvements

Columns

To provide adequate confinement in columns the confinement steel has been significantly increased. (Figure 33)

In cases where the column stiffness is significantly different among the supports in a structure, isolation casings have been installed to balance the stiffness i.e. increase the effective length of the short column. This has been accomplished in both dry and wet (below ground water level) construction conditions. (Figure 34 & 35)

To prevent external elements and architectural elements from adversely affecting the column stiffness, gaps between barrier rails and walls which intersect the columns are now required and gaps are formed into the column flares at the soffit. (Figure 36)

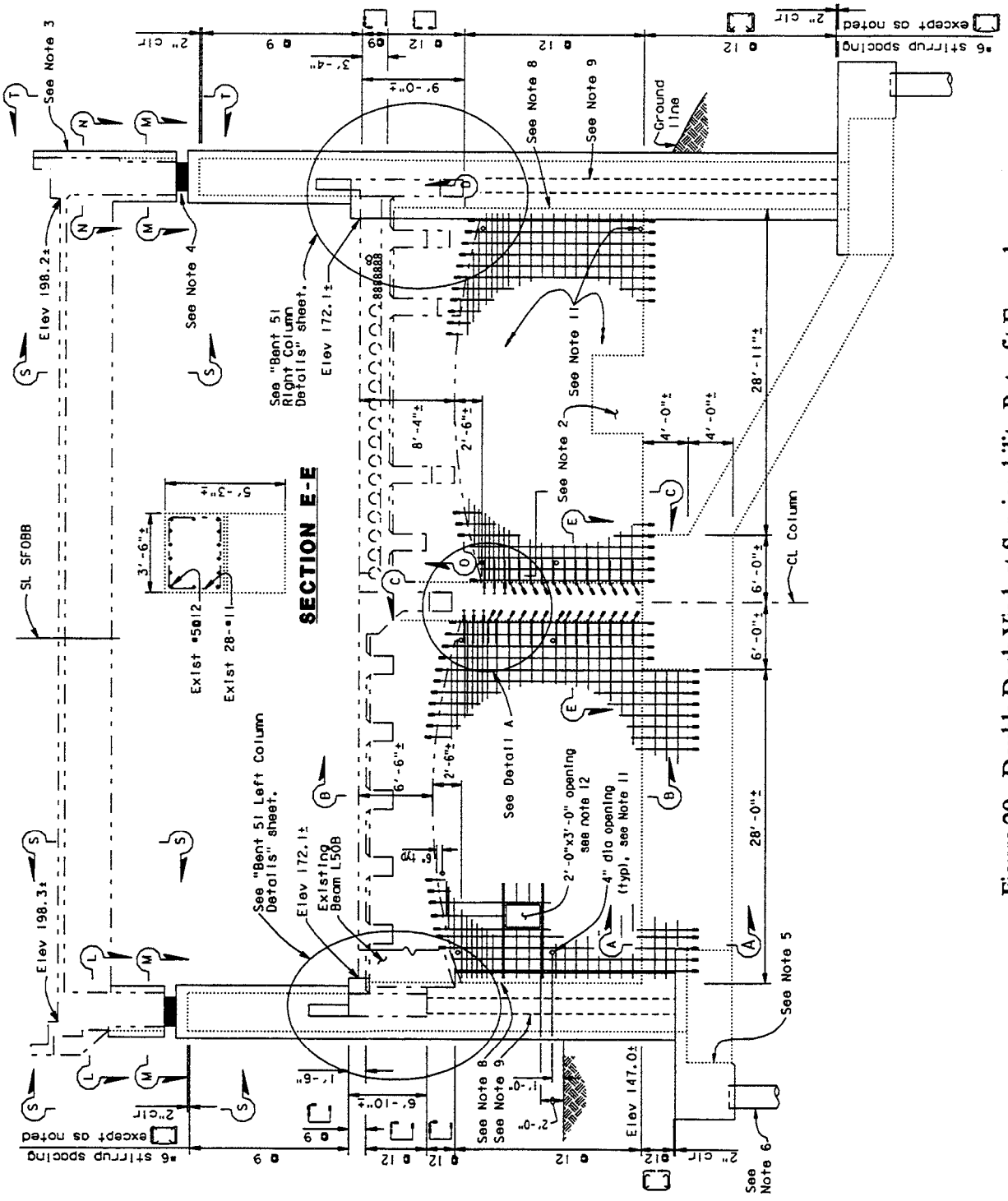

Figure 29 - Double Deck Viaduct Serviceability Retrofit Example

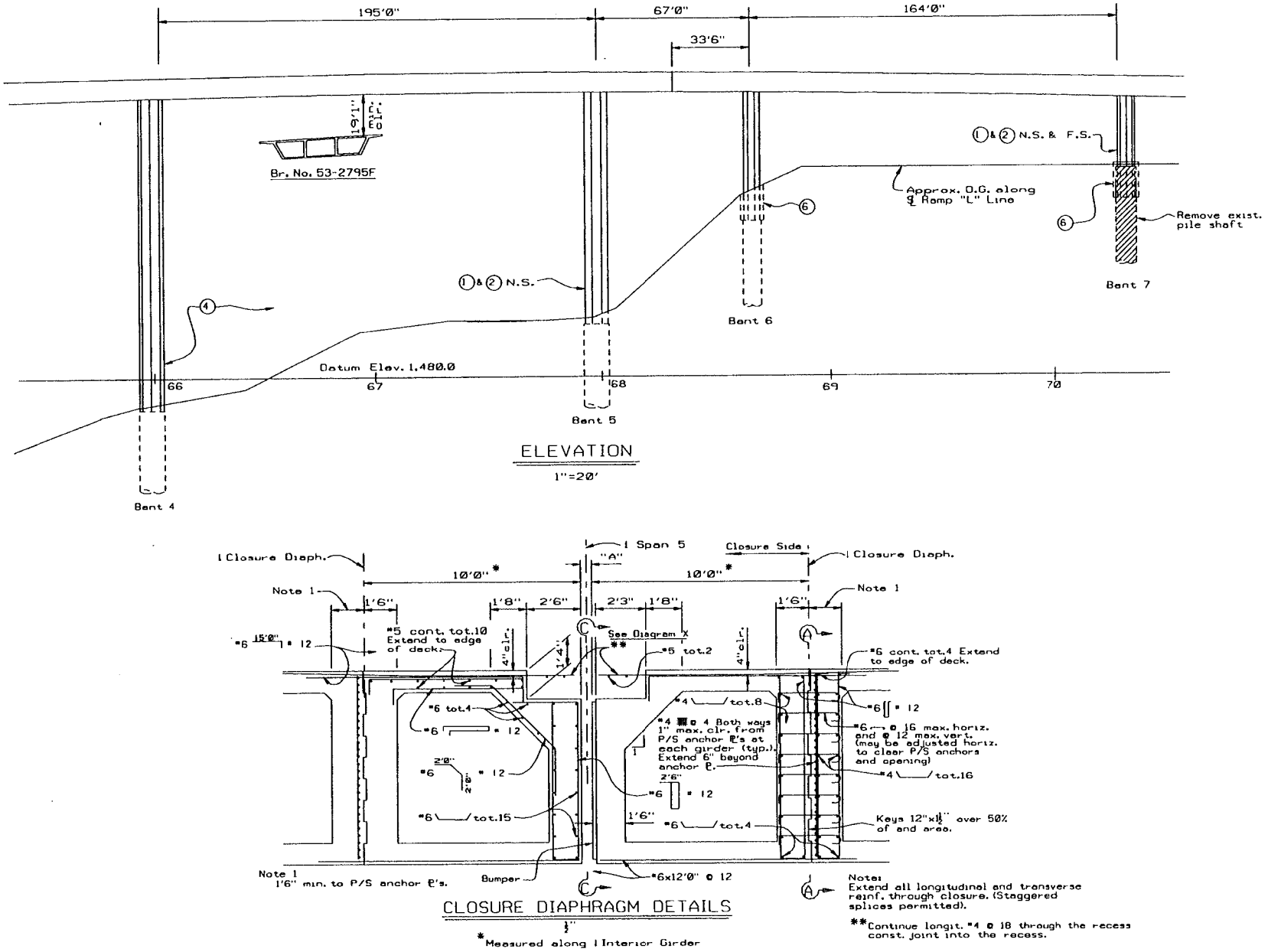

Figure 30 - Concrete Box Girder Double Cantilever Hinge

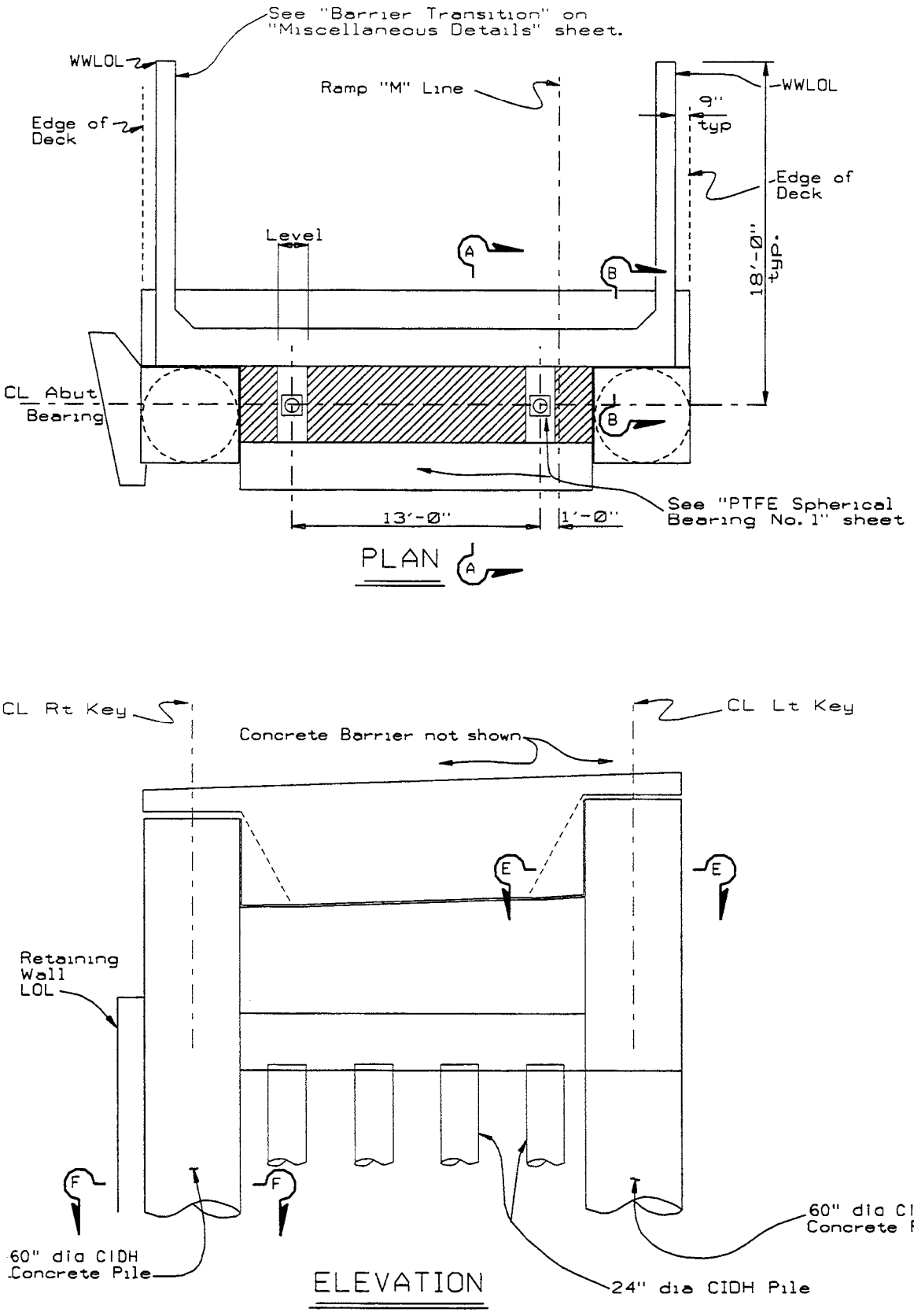

Figure 31 - Large Diameter Shafts for Transverse Restraint

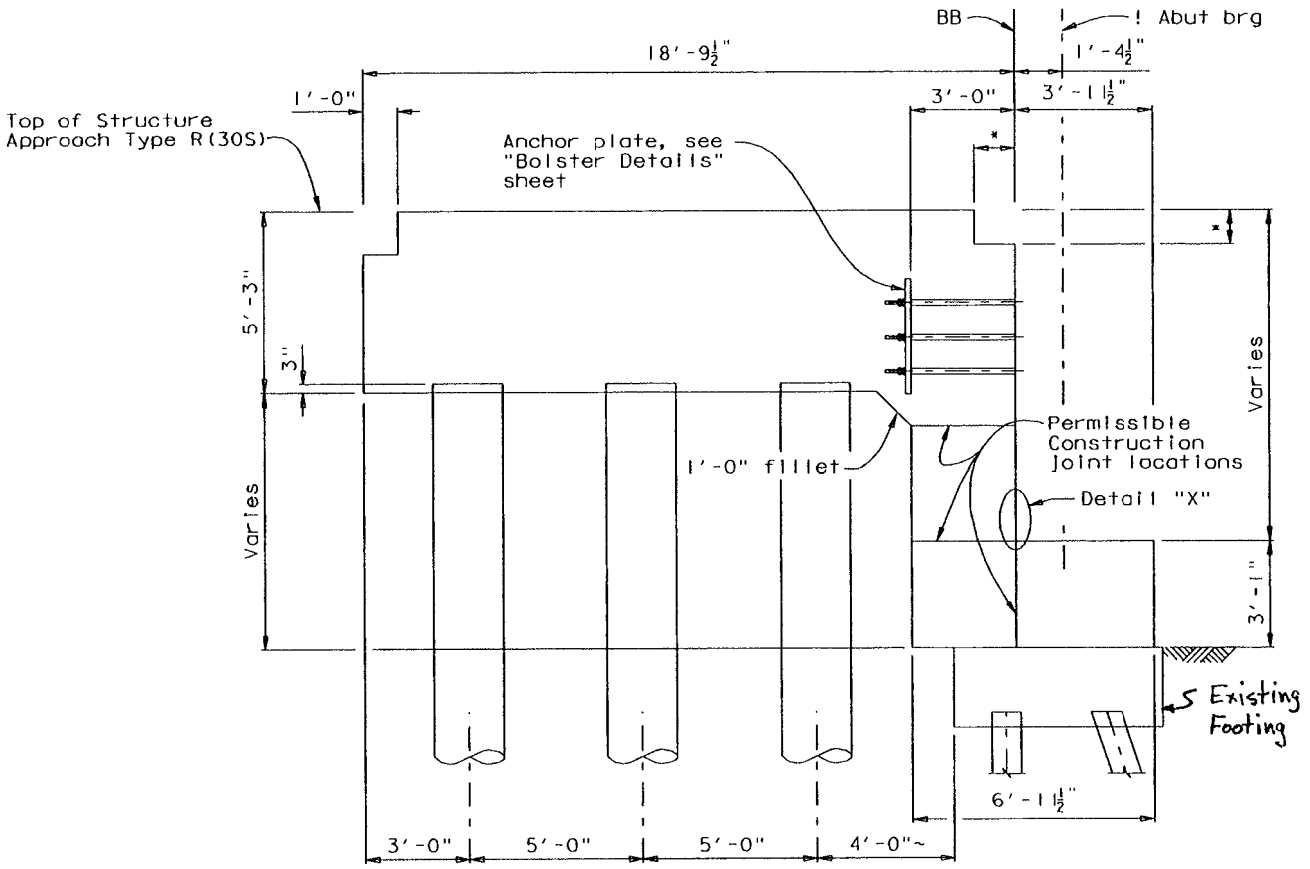

Figure 32 - Damaged Abutment Replacement with Integral Anchor Slab Retrofit

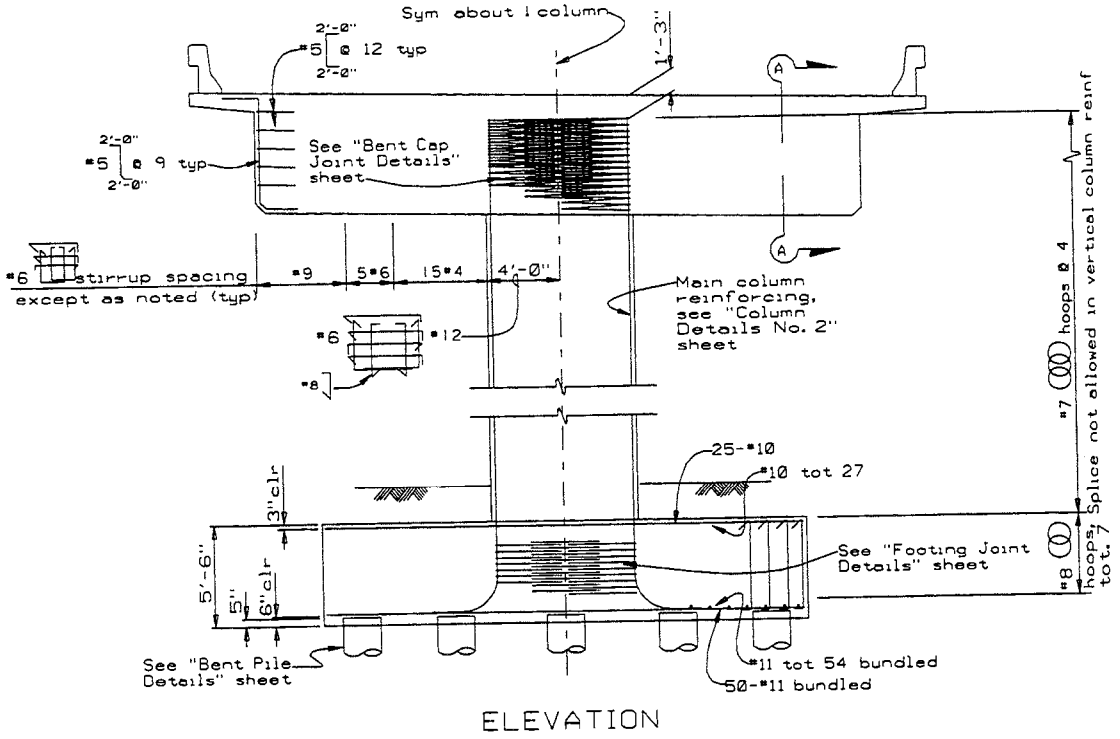

ELEVATION

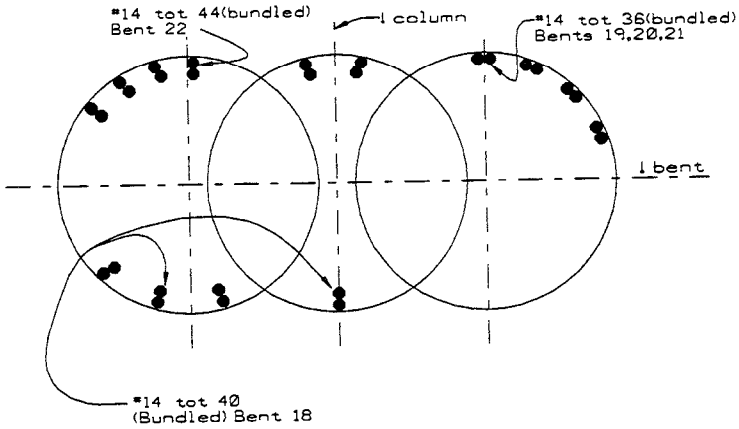

MAIN COLUMN REINFORCEMENT

Figure 33 - Column Reinforcement

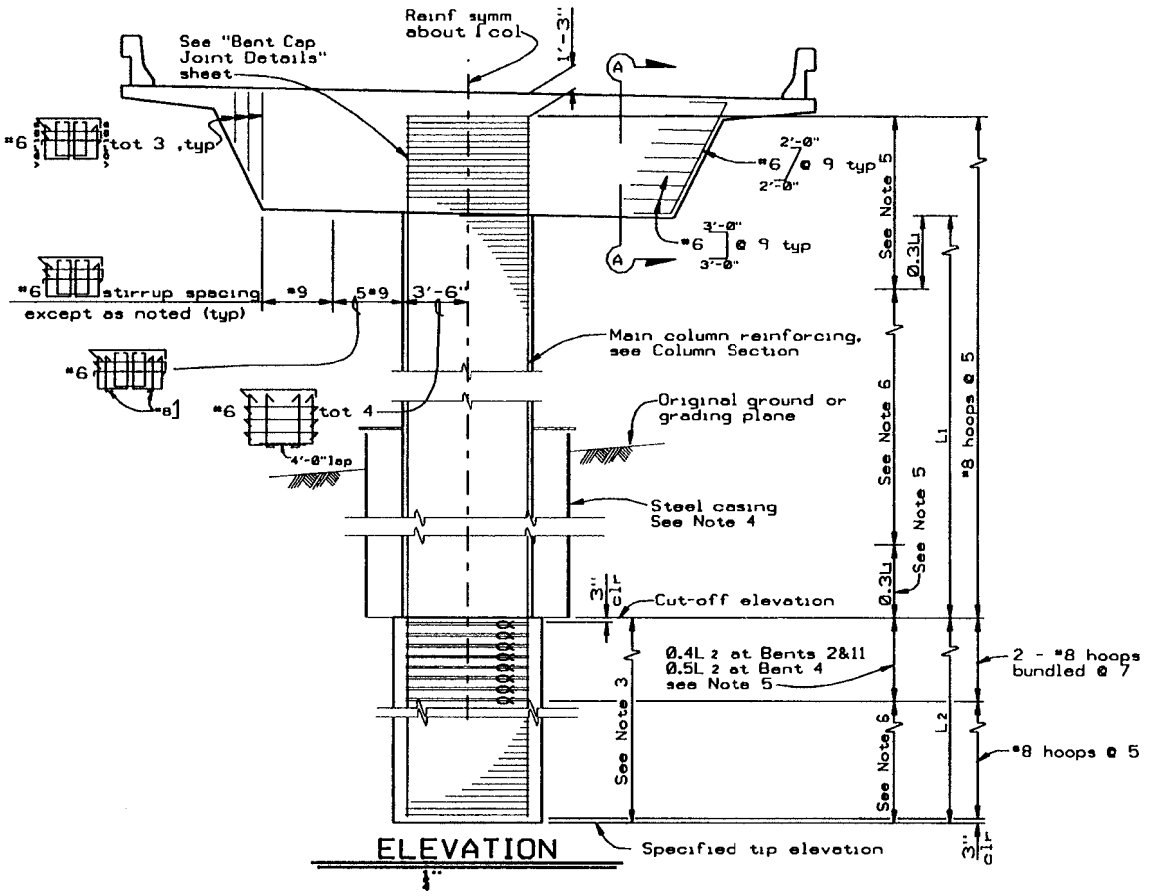

Figure 34 - Isolation Casing Installed in Dry Conditions

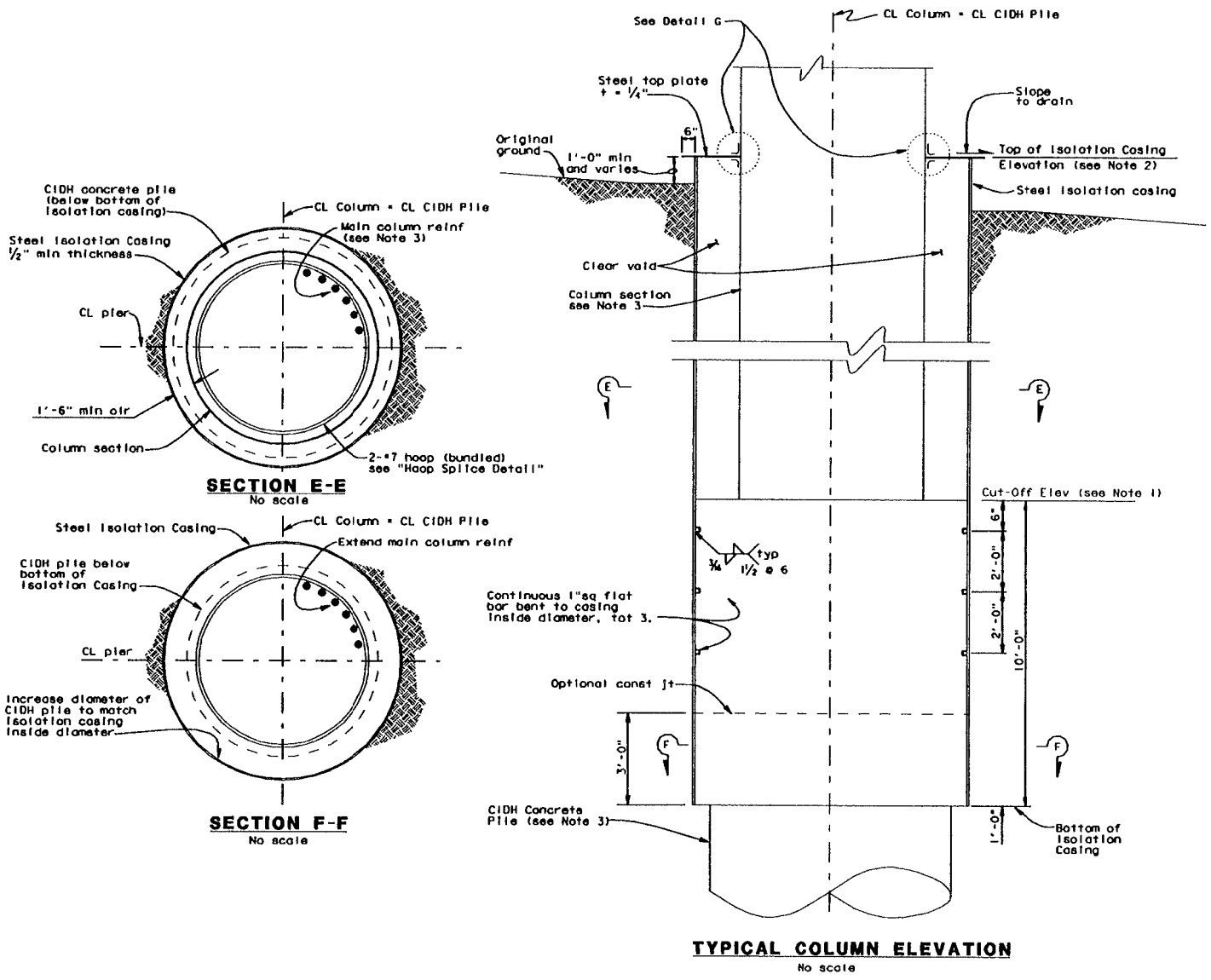

Figure 35 - Isolation Casing Installed in Wet Conditions

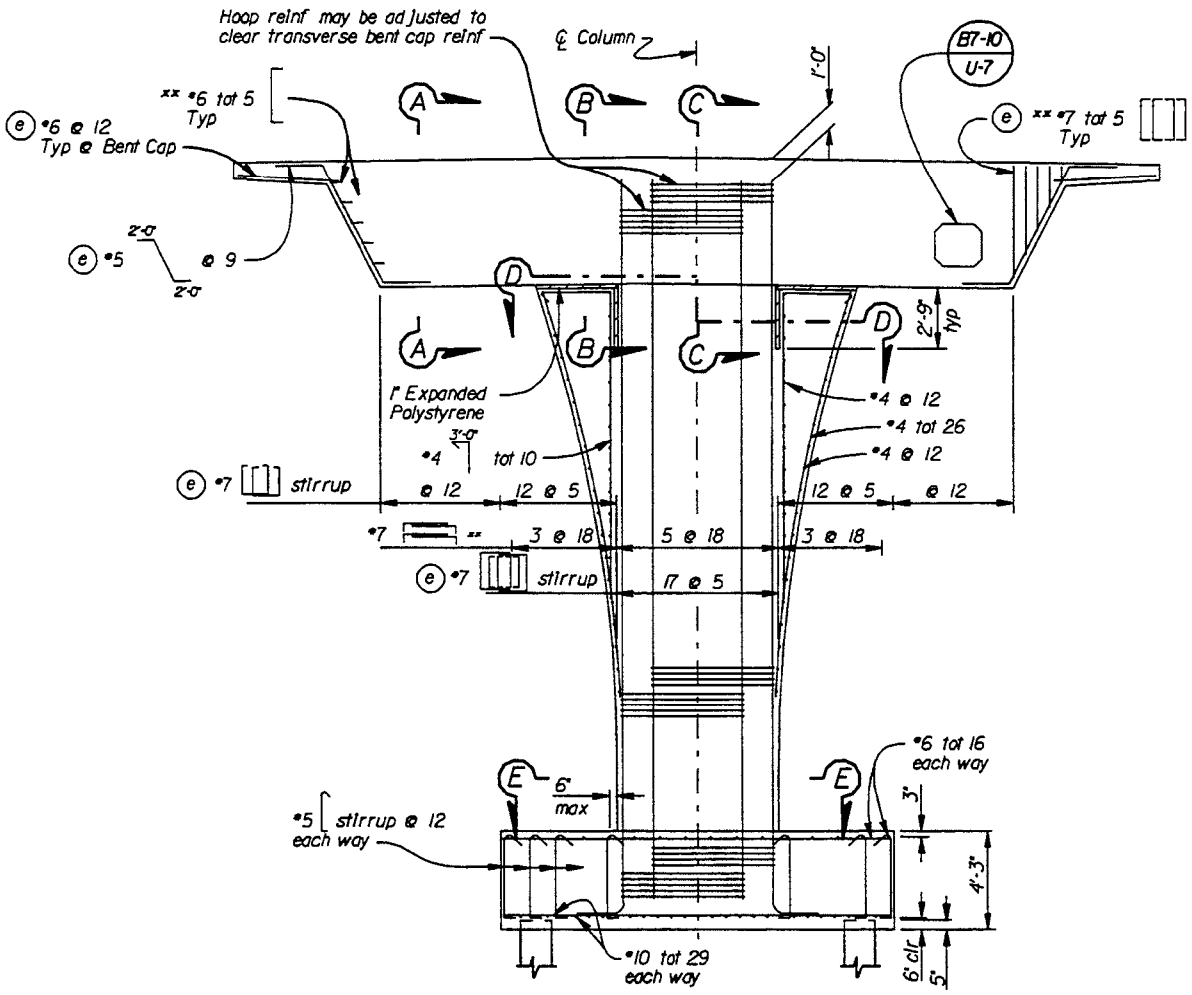

Figure 36 - Architectural Treatment Detail

Footings

In soft soils, cast-in-steel shell piles have been used. A reinforced cage is inserted into the steel shell and filled with concrete. These piles have the connection strength and ductility needed to sustain the large seismic cyclic displacements. (Figure 37)

Post Earthquake Inspection and Repair Improvements

Hinges

One area which needed improvement that was identified after 1989 Loma Prieta and 1994 Northridge earthquakes was the inspection of the concrete box girder hinges and restrainer cables. As a result of needing to quickly determine damage, indicator bushings are now commonly installed on cable restrainers. These bushings are designed to collapse when the yield strength of the cable is reached. This will quickly indicate to the post earthquake inspector whether or not the cable restrainer(s) need to be replaced. (Figure 38)

An accessible hinge detail has also been developed. This detail modifies the current standard hinge detail by providing an access opening to expose the hinge bearings for easy inspection and replacement if necessary. (Figure 39)

Providing soffit access openings on each side of the hinge in box girder bridges is now standard.

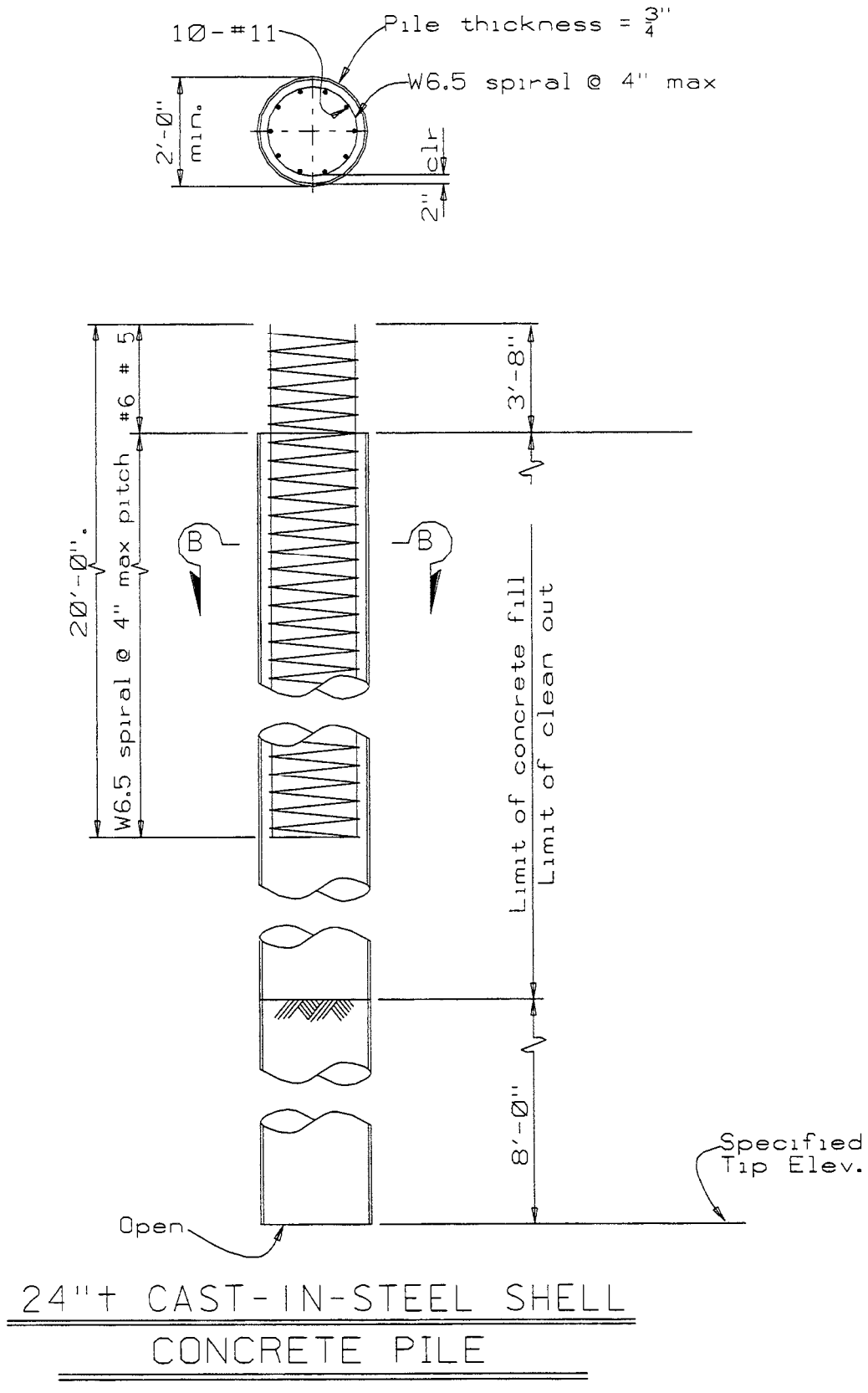

Figure 37 - Piles used in Soft Soil Locations.

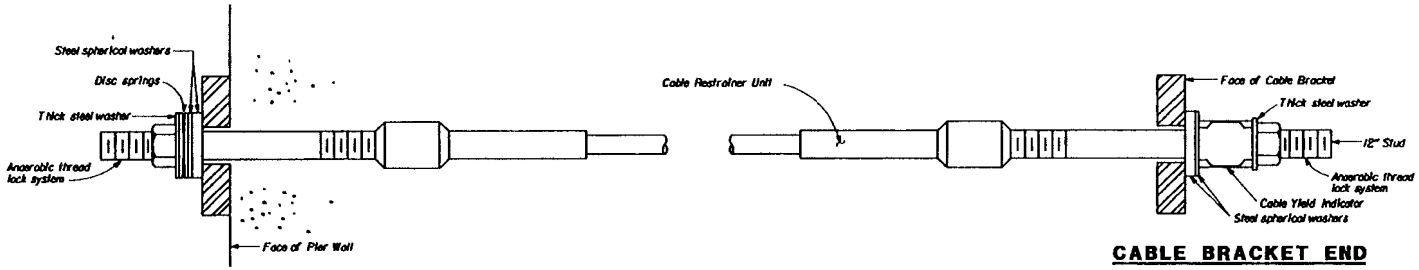

PIER END **CABLE UNIT** **CABLE BRACKET END**

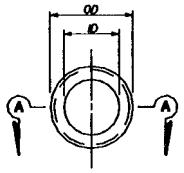

END VIEW

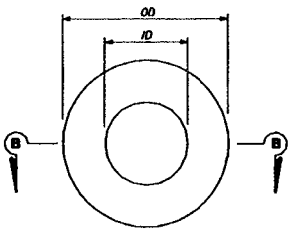

PLAN

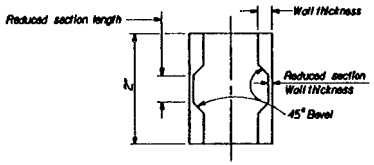

SECTION A-A

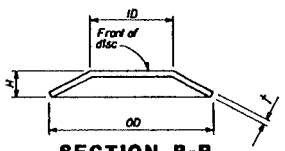

SECTION B-B
(Single spring)

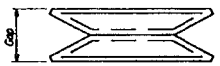

AS INSTALLED ON STUD

DISC SPRING
Note: For dimensions not shown see table

ASTM	GRADE	CLASS
A-543 TYPE 5	1020	DDM

DIMENSIONS: ± 0.005"

OD	WALL	ID (After Galv.)
1.500"	0.250"	1.000"

REDUCED SECTION:

Length	Wall Thickness
0.500" ± 0.001"	0.073" ± 0.0005"

" All dimensions are before galvanizing except as noted "

CABLE YIELD INDICATOR

DISC SPRINGS AND WASHERS

" All dimensions in inches, except as noted "

	DISC SPRING				SPHERICAL WASHER			THICK WASHER		
L*	ID	OD	t	H	ID	OD	Nom. thick.	ID	OD	t
10.0 - 25.0	1.000	2.000	0.065	0.130	1.1875	2.250	0.500	1.030	2.000	0.312
25.1 - 31.9	1.000	2.000	0.084	0.136	1.1875	2.250	0.500	1.030	2.000	0.312
32.0 - 37.9	1.000	2.000	0.097	0.145	1.1875	2.250	0.500	1.030	2.000	0.312
38.0 - 45.0	1.250	2.500	0.120	0.180	1.3120	2.500	0.500	1.156	2.250	0.312

*For length L (ft), see " Cable Restrainer Unit - Type 2 " sheet

RESTRAINER UNIT INSTALLATION PROCEDURE

1. Place anaerobic thread locking system on pier end stud prior to tightening the cable. If a nut needs to be removed after compound sets, the stud must be cleaned with manufacturer's solvent before thread locking system can be reapplied.
2. Install disc springs on pier end of cable system using spherical washers to align discs to stud. Discs shall be installed front to front as shown in " Disc Spring " detail. Install Cable Yield Indicator and Spherical Washers on the cable bracket end of restrainers as shown in " Cable Unit " detail. Use 12" stud for cable yield indicator end.
3. Tighten the cable from pier end of restrainer until the disc springs collapse and there is no gap remaining between the discs. The cable should be approximately straight with no sag.
4. Place thread locking system on pier side stud after tightening the cable, but before backing off the nut. Back off the nut at pier side equal to the "d" distance shown in the table on this sheet.
5. If existing retrofit cables are being reused, 12" studs shall be installed.

NOTE: If the cable needs to be secured from turning while tightening, use double nut locking technique on the stud to protect the threads.

SEASON	"d" DISTANCE
Summer	1/4"
Spring / Fall	1/2"
Winter	3/4"

Figure 38 - Cable Restrainer Indicator Bushings.

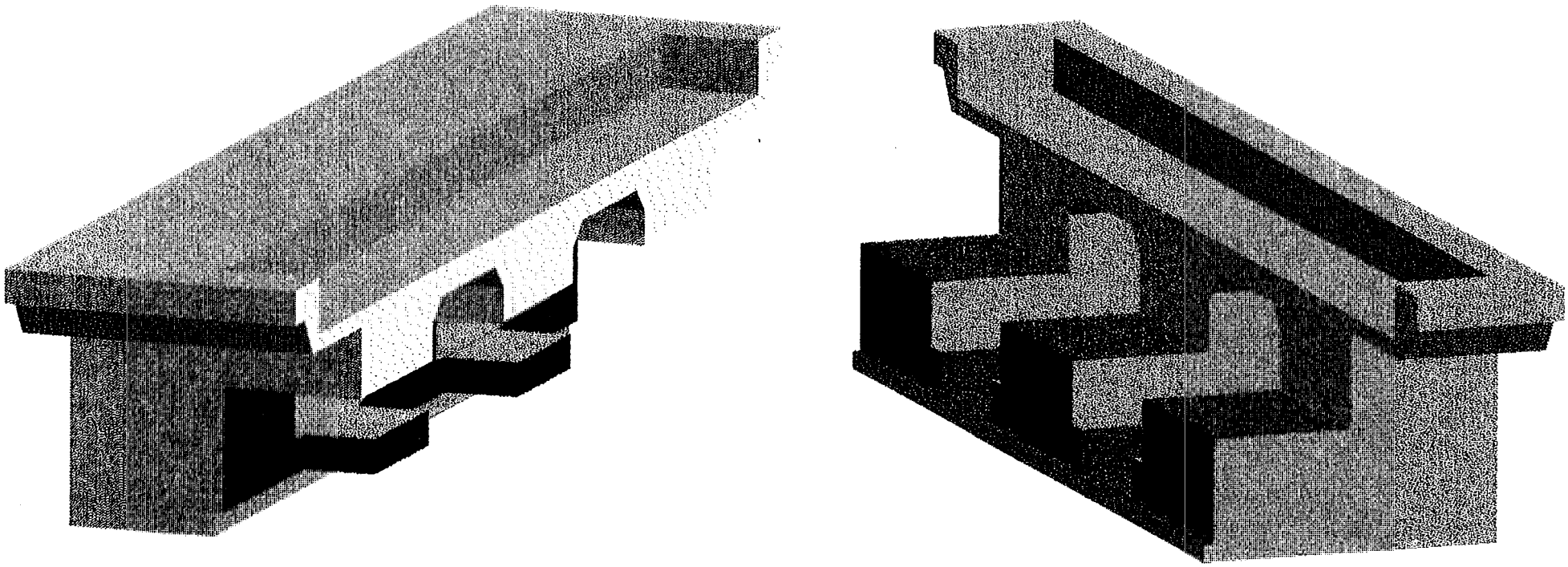

Figure 39 - Accessible Hinge View.

SUMMARY

Caltrans has almost completed the seismic retrofit design for approximately 2200 existing State highway bridges which have been identified as needing seismic retrofitting. Most of these designs will be constructed by December of this year (1997).

As stated in the 1995 publication entitled " Improved Seismic Retrofit Details for Highway Bridges" by James E. Roberts, Director, Engineering Services, Chief Structures Engineer, California Department of Transportation, " The success of (the seismic retrofit) program has been due to dedicated staff and consultants, both of whom have developed innovative retrofit details to accomplish the seismic safety that is required for these bridges."

Although all of the seismic retrofit details and new construction details were not covered in this paper, a majority of the failure mechanisms and retrofit solutions as well as some of the new construction details have been presented. Hopefully the details discussed will prove useful to other engineers who are engaged in the seismic retrofit and/or new design of seismically safe highway bridges.

BIBLIOGRAPHY AND REFERENCES

1. Caltrans Division of Structures. "Field Tests of Large Diameter Drilled Shafts", Report of Lateral Load Tests, Sacramento, California, March, 1990

2. Caltrans Division of Structures. "The Northridge Earthquake-Post Earthquake Investigation Report. Sacramento, California, February, 1994

3. Chai, Y.H., Priestley, M.J., Seible, F. University of California at San Diego. "Seismic Retrofit of Bridge Columns by Steel Jacketing", Third Bridge Engineering Conference at Denver, Colorado, March, 1991. Report: Transportation Research Board Record 1290. TRB, National Research Council, Washington,DC

4. Division of New Technology, Materials and Research, Office of Geotechnical Engineering, Caltrans.
"Caltrans Procedures for Development of Site-Specific Acceleration Response Spectra", Seismic Design and Retrofit of Bridges, Seminar Proceedings, Earthquake Engineering Research Center, University of California at Berkeley and California Department of Transportation, Division of Structures, Sacramento, California, 1992

5. Filippou, F. C., Cheng,C., University of California at Berkeley. "Anchorage of Large Diameter Reinforcing Bars", Seismic Design and Retrofit of Bridges, Seminar Proceedings, Earthquake Engineering Research Center, University of California at Berkeley and California Department of Transportation, Division of Structures, Sacramento, California, 1992

6. Idriss, I.M., University of California at Davis. "Response of Soft Soil Sites During Earthquakes", Proceedings of the Memorial Symposium to Honor Professor Harry Bolton Seed, Berkeley, California, May, 1990

7. Maroney, B., Gates, J., Caltrans. "Seismic Risk Identification and Prioritization in the Caltrans Seismic Retrofit Program", Proceedings of the 4th U.S.-Japan Workshop on Earthquake Disaster Prevention for Lifeline Systems, Los Angeles, California, 1991

8. Maroney, B, Romstad, K., Kutter, B., University of California at Davis. "Experimental Testing of Laterally Loaded Large Scale Bridge Abutments", Proceedings: ASCE Structures Congress XI, Irvine, California, April1993

9. Mayes, R. L., Dynamic Isolation Systems. "Seismic Isolation Design of Bridges", Seismic Design and Retrofit of Bridges, Seminar Proceedings, Earthquake Engineering Research Center, University of California at Berkeley and California Department of Transportation, Division of Structures, Sacramento, California, 1992

10. Mellon, S., et al., Caltrans. "Post Earthquake Investigation Team Report of Bridge Damage in the Loma Prieta Earthquake", Proceedings: ASCE Structures Congress XI, Irvine, California, April1993

11. Mualchin, L., Caltrans. "Seismic Hazards of Caltrans Facilities After the Loma Prieta Earthquake and the Implications for Caltrans Seismic Programs", International Symposium on Safety of Urban Life and Facilities: Lessons learned from the 1989 Loma Prieta Earthquake, November 1-2, 1990, Tokyo Department of Environmental Engineering, Graduate School at Nagatsuta, Tokyo Institute of Technology, Yokohama, Japan, 1990

12. Roberts, J. E., Caltrans. "Bridge Seismic Retrofit Program For California Highway System" Proceedings: US-Japan Workshop on Lifeline Earthquake Engineering, Public Works Research Institute, Tsukuba Science City, Japan, May, 1989

13. Roberts, J. E., Caltrans. "Theory of California Seismic Bridge Design And Analysis For The Beginner "California Department of Transportation, Division of Structures, Training Course for Entry Level Engineers, July, 1989

14. Roberts, J. E., Caltrans. "Recent Advances in Seismic Design and Retrofit of Highway Bridges", Proceedings of the Third U.S. Conference, Report:Technical Council on Lifeline Earthquake Engineering, Monograph 4, American Society of Civil Engineers, New York, August, 1991

15. Roberts, J.E., Caltrans. "Seismic Design of Bridge Foundations", Proceedings Transportation Research Board Annual Meeting, Washington, D.C., January, 1992

16. Roberts, J.E., Caltrans. "Research Based Bridge Seismic Design and Retrofit Program, Criteria, Standards and Status", Proceedings: Fifth U.S.-Japan Workshop on Earthquake Disaster Prevention for Lifeline Systems, Tsukuba Science City, Japan, October 26, 1992

17. Roberts, J.E., Caltrans. "Effect of Foundation Soil Response on Bridge Seismic Performance", Proceedings: Fifth U.S.-Japan Workshop on Earthquake Disaster Prevention for Lifeline Systems, Tsukuba Science City, Japan, October 26, 1992

18. Roberts, J.E., Caltrans. " Improved Seismic Retrofit Details for Highway Bridges ", Structural Engineering Review, Vol. 7, No.3, pp. 195-206, 1995 Elsevier Science Ltd. , Pergamon (0952-5807(95)00019-4)

19. Seed, R. B., Dicksenson, S. E., Mok, C. M., University of California at Berkeley. "Recent Lessons Regarding Seismic Response Analyses of Soft And Deep Clay Sites", Seismic Design and Retrofit of Bridges, Seminar Proceedings, Earthquake Engineering Research Center, University of California at Berkeley and California Department of Transportation, Division of Structures, Sacramento, CA, 1992

20. Yashinsky, M., Caltrans. "Performance of Retrofit Measures on Existing Older Bridges", Proceedings: 59th Annual Convention, Structural Engineers Association of California, Sacramento, California, September, 1990

21. Zelinski, R., Caltrans. "California Highway Bridge Retrofit Strategy and Details", Proceedings: 59th Annual Convention, Structural Engineers Association of California, Sacramento, CA, September, 1990

22. Zelinski, R., Caltrans. "California Highway Bridge Retrofit Strategy and Details", Proceedings: Second Workshop on Bridge Engineering Research in Progress, University of Nevada at Reno, 1990

23. Zelinski, R., Dubovik, A. K., Caltrans. "Seismic Retrofit of Highway Bridge Structures", Lifeline Earthquake Engineering: Proceedings of the Third U.S. Conference, Report: Technical Council on Lifeline Earthquake Engineering, Monograph 4, ASCE, New York, August, 1991

A MODEL FOR CONFINEMENT EFFECT FOR CONCRETE CYLINDERS CONFINED BY CARBON FIBER SHEETS

Hosotani, Manabu[1], Kawashima, Kazuhiko[2] and Hoshikuma, Jun-ichi[3]

1) Research Student, Tokyo Institute of Technology (Taisei Corporation), O-okayama, Meguro-ku, Tokyo, 152, Japan
2) Professor, Department of Civil Engineering, Tokyo Institute of Technology, O-okayama, Meguro-ku, Tokyo, 152, Japan
3) Research Engineer, Earthquake Engineering Division, Public Works research Institute, Ministry of Construction, Tsukuba Science City, 305, Japan

ABSTRACT

Most of reinforced concrete bridge piers which suffered damage in the 1995 Hyogoken-Nanbu Earthquake were designed with the seismic standards in 1960s in which the importance of ductility of structural components was not considereds. Consequently, existing reinforced concrete columns which were designed with the seismic standards in 1960s and are vulnerable to seismic disturbance require to be strengthened urgently. As one of the seismic strengthening methods of reinforced concrete columns, carbon fiber sheet (CFS) jacketing is an attractive method because of the superior workability. To reflect the confinement effecst by the CFS in seismic strengthening, a series of compressive loading tests of concrete cylinders were conducted and a stress-strain model of concrete confined by CFS is proposed.

INTRODUCTION

The Hyogo-ken Nanbu earthquake of January 17, 1995 caused destructive damage in various structures. Bridges which were designed and constructed by the Design Specifications issued in 1960s suffered extensive damage[9]. At those days, the importance of confinement of core-concrete by tie reinforcements[1)6)7)8)10)11)] was not recognized at all. Because there are a number of bridges which were designed based on the similar design concept, it is obvious that seismic retrofit is required for those bridges which are vulnerable to the extreme earthquakes.

Seismic retrofit has been extensively conducted throughout the country for reinforced concrete piers which were designed by the pre-1980 Design Specifications. The steel jacketing with controlled increase of flexural strength has been widely adopted for seismic retrofit of

reinforced concrete pier[2)3)4)5)]. Although the steel jacketing is effective from various points such as the effective confinement, the enhancement of shear / flexural strength and cost, it is unable to adopt at the sites where enough space to set the steel jacket is not available and where restriction of traffic is significant.

Various new technical developments with use of advanced and high performance materials have been conducted to provide an adequate solution for the limitation of the steel jacketing method. One of the most interesting methods may be the strengthening with use of CFS. It is light, easy to handle, strong in tension and is favorable in workability. For example, the CFS has a tensile strength of 3,000MPa which is about ten times higher than steel. The weight is only 18 kN/m^3, and it is only 1/5 of steel. It takes only 30 minutes to place a sheet on surface of a reinforced concrete pier. Thus, it has been considered effective to use the CFS to confine concrete of a pier. It has been found that the carbon fiber jacketing is effective to enhance the shear capacity of a reinforced concrete pier at a termination point of longitudinal reinforcements with inadequate anchoring length[12)]. It has been also recognized that the CFS is effective to enhance the flexural capacity of a reinforced concrete pier at the plastic hinge zone. Although cyclic loading tests have been conducted at various organizations, few information is available on how much increase of strength and strain can be obtained by the confinement by CFS. This is due to the lack of information on the lateral confinement effect of CFS.

To develop an appropriate stress vs. strain relation of concrete confined by the CFS, a series of compressive loading tests for concrete cylinders were conducted. Based on the test result, this papers proposes a model of stress vs. strain relation under the confinement by the CFS.

TEST SPECIMENS AND TEST PROCEDURE

Table 1 shows the test specimens. The parameters considered in the test were shape (circular and square of concrete cylinder), and volume and elastic modulus of CFS. The specimens were 600 mm high, 200 mm wide or diameter. The design strength of concrete was 30MPa. A total of 10 (circular cylinders) and 12 (square cylinders) 6mm deformed reinforcements with a yield strength of 295 MPa (SD295) were provided in the longitudinal direction, while no reinforcements were provided in the hoop direction. This was to isolate the effect of CFS from the confinement by hoop reinforcements. Axial reinforcement ratio was 1 % in both circular and square cylinders.

There were three series of specimens; first, specimens without confinement by the CFS (N-series) ; second, specimens confined by the CFS with a normal elastic modulus of 2.30×10^5MPa (S-series); and third, specimens confined by the CFS with a high elastic modulus of 3.92×10^5MPa (H-series). Table 2 compares the mechanical properties of the two types of CFS. While tensile strength was almost the same between the normal-modulus type and high-modulus type CFS, rupture strain was smaller in the high-modulus type (1.0%) than in the normal-modulus type (1.5%).

Volumetric ratio of CFS (carbon fiber ratio) was defined as

$$\rho_{CF} = 4 \times N \times t_{CF} / d \qquad (1)$$

where t_{CF} = thickness of a layer of CFS(mm), N = number of layers of CFS, d = diameter (circular) or width (square) of a concrete cylinder.

The carbon fiber ratio ρ_{CF} was varied in the range of 0.05~1.5% in S-series and 0.15~1.5% in H-series. This corresponds to confine a reinforced concrete column with a diameter of 3m by 2~60 layers of normal modulus CFS (S-series) and 7~60 layers of high modulus CFS (H-series). Because it is feasible to wrap as large as 10~15 layers around a reinforced concrete column based on the current technique, ρ_{CF} of 1.5% is obviously very high for implementation.

Fig.1 shows the adhesion of a CFS. The CFS was wrapped in the hoop direction. The lap splice length was 10cm. While 10cm is too short for implementation, it was selected in the test because long lap splice increases the carbon fiber ratio; thus the lap splice length was made as short as possible. As will be results presented later, no failure occurred in CFS at the spliced zone. Corners in the square specimens were rounded with a radium of 30mm to prevent rupture of CFS due to the stress concentration.

The specimens were loaded in axial direction under the displacement control with the loading rate of 0.2mm/min. Relative displacement of the specimens between the top and the bottom surface was measured by four displacement sensors to compute axial strain.

STRESS VS. STRAIN RELATION OF UNCONFINED CONCRETE CYLINDERS

Fig.2 shows an axial stress vs. axial strain relation of six unconfined concrete cylinders. The initial stiffness E_C was about 2.0×10^5MPa, with the axial strain corresponding to the peak axial stress being about 3,000~3,500 μ. The concrete cylinders failed when the CFS strain

reached about 4,000 μ.

Fig.3 shows an axial stress of concrete vs. circumferential CFS strain relation. At the initial stage, the circumferential CFS strain increases as the axial stress of concrete cylinder increases. The circumferential CFS strain then increases sharply after it reached about 500 μ, and becomes almost stable at an circumferential concrete strain of 1,200~1,700 μ. That is due to the dilation of the concrete cylinder; hoop expansion of concrete cylinder becomes predominant at the circumferential concrete strain of about 500 μ and concrete cylinders initiated to fail at the circumferential concrete strain of about 1,200~1,700 μ. The circumferential strain of concrete cylinder at its failure is designated as ε_{pf} (ε_{pf} = 1,200~1,700 μ).

EFFECT OF CARBON FIBER RATIO ρ_{CF}

Fig.4 shows an axial stress f_c vs. axial strain ε_c relation of concrete cylinders confined by the CFS. The axial concrete strain increases with the initial stiffness E_c at small axial concrete strain, and as soon as the CFS ruptured, the concrete cylinders failed. A close examination of the test results in Fig.4 reveals the followings:

(a) At ρ_{CF} in the range of 0.056~0.167%, the peak axial concrete stress f_{cc} is about 37~41MPa with a strain corresponding to the peak stress ε_{cc} being about 2,500~3,000 μ regardless of the carbon fiber ratio ρ_{CF} and the cross sectional shape of specimens. As the carbon fiber ratio ρ_{CF} increases, the deteriorating rate of the axial stress over the peak stress f_{cc} decreases and the ultimate strain of concrete at rupture of CFS increases; and

(b) At ρ_{CF} of 1.336%, the axial concrete stress continues to increase without deterioration until the CFS fails. However, at an axial strain of concrete around 3,000~3,500 μ, the increasing rate of the axial concrete stress becomes smaller. This axial concrete strain is designated hereinafter as ε_t. The second gradient E_g is larger in the circular cylinders than the square cylinders.

Fig.5 shows an axial stress of concrete vs. the circumferential strain of CFS relation. The following characteristics may be pointed out:

(a) At the carbon fiber ratio of 0.056 ~ 0.167%, the axial concrete stress reaches its peak value at the circumferential CFS strain, ε_{CFC}, of about 1,100~2,500 μ. It means that because the elastic modulus of the CFS, E_{CF}, is 2.43×10^5MPa, the hoop stress induced in the CFS is only

250~550MPa at ε_{CFC} of 1,100~2,500 μ, which is only 1/10~1/5 of the rupture strength of the CFS (about 3,500MPa); and

(b) At the carbon fiber ratio ρ_{CF} of 1.336% (S-4 and S-12), the axial concrete stress keeps increasing as the circumferential strain of CFS increases, while the gradient becomes smaller over a certain strain. The strain of the CFS at the transition zone where the gradient changes from the initial value to the second value, ε_{CFt}, is about 1,800~1,900 μ. The concrete stress at ε_{CFt} is about 47~55MPa , and this is designated herein as f_t.

Fig.6 shows the general characteristics of the axial concrete stress - the axial concrete strain - the circumferential CFS strain relation which were presented in Figs. 2~5. It is interesting to note that ε_{CFt} (=1.800~1,900 μ) and ε_{CFC} (=1,100~2,500 μ) are in the same order with ε_{pf} (=1,200~1,700 μ) .This may be interpreted that regardless to the degree of lateral confinement, the concrete cylinders initiate to fail when the circumferential concrete strains reaches ε_{pf}. Consequently, if ρ_{CF} is in the order of 0.05~0.15%, the axial concrete stress decreases over ε_{pf}, resulting that the axial concrete stress decreases over ε_{cc}. And if ρ_{CF} is in the order 1%, while the axial concrete stress continues to increase over ε_{pf}, the gradient of axial concrete strain vs. circumferential CFS strain relation changes at around ε_{pf} resulting that the gradient of axial concrete stress vs. axial concrete strain relation also changes from E_C to E_g at about ε_{pf}.

EFFECT OF HIGH ELASTIC MODULUS CFS

Fig.7 compares the axial stress vs. axial strain relation of concrete cylinders confined by the high-modulus type CFS to that confined by the normal-modulus type. Test data for the concrete cylinders with similar carbon fiber ratio ρ_{CF} are presented here. The axial concrete stress at transition zone f_t and the second gradient E_g are larger in the concrete cylinders confined by the normal-modulus type CFS than those confined by the high-modulus type CFS in both circular and square specimens.

Fig.8 compares the circumferential CFS strain vs. the axial concrete stress relation between the concrete cylinders confined by the normal-modulus type CFS and those confined by the high-modulus type CFS. The gradient changes at the circumferential CFS strain of 1,600~2,500 μ, which is again quite close to ε_{pf}.

MODELING OF THE STRESS-STRAIN RELATION

From Fig.6, the axial concrete stress vs. axial concrete strain relation may be idealized as shown in Fig.9. When the gradient E_g is negative, the axial concrete stress vs. axial concrete strain relation in the first region and the second region may be modeled by a second order parabola and a straight line, respectively, as[1];

$$f_c = \begin{cases} E_c \varepsilon_c \left\{ 1 - \frac{1}{n} \left(\frac{\varepsilon_c}{\varepsilon_{cc}} \right)^{n-1} \right\} & \left(0 \le \varepsilon_c \le \varepsilon_{cc} \right) \\ f_{cc} + E_g \left(\varepsilon_c - \varepsilon_{cc} \right) & \left(\varepsilon_{cc} \le \varepsilon_c \le \varepsilon_{cu} \right) \end{cases} \tag{1}$$

where f_c = axial stress of a concrete cylinder, ε_c = axial strain of a concrete cylinder, f_{cc} = peak axial stress of a concrete cylinders (MPa), ε_{cc} = concrete strain at f_{cc}, E_c = initial stiffness of a concrete cylinder (MPa) and n = a coefficient defined as

$$n = \frac{E_c \varepsilon_{cc}}{E_c \varepsilon_{cc} - f_{cc}} \tag{2}$$

Eq.(1) was derived to represent the confinement effect of tie reinforcements, and satisfies the following four boundary conditions:

1)initial condition: ε_c=0 at f_c=0,
2)initial stiffness: ε_c=0 at $\partial f_c / \partial \varepsilon_c = E_c$, (3)
3)compatibility condition(1): $\varepsilon_c = \varepsilon_{cc}$ at $f_c = f_{cc}$, and
4)compatibility condition(2): $\varepsilon_c = \varepsilon_{cc}$ at $\partial f_c / \partial \varepsilon_c$=0.

To expand Eq.(1) for the concrete cylinders with positive E_g, the fourth condition in Eq.(3) is changed as

$$\varepsilon_c = \varepsilon_t \text{ at } \partial f_c / \partial \varepsilon_c = E_g \tag{4}$$

where ε_t = axial strain of a concrete cylinder at f_t. Thus, Eq.(1) is rewritten as

$$f_c = \begin{cases} E_c \varepsilon_c \left\{ 1 - \frac{1}{n} \left(1 - \frac{E_g}{E_c} \right) \left(\frac{\varepsilon_c}{\varepsilon_t} \right)^{n-1} \right\} & \left(0 \le \varepsilon_c \le \varepsilon_t \right) \\ f_t + E_g \left(\varepsilon_c - \varepsilon_t \right) & \left(\varepsilon_t \le \varepsilon_c \le \varepsilon_{cu} \right) \end{cases} \tag{5}$$

where

$$n = \frac{\left(E_c - E_g \right) \varepsilon_t}{E_c \varepsilon_t - f_t} \tag{6}$$

Because ε_{cc} (f_{cc}) in Eq.(1) and ε_t (f_t) in Eq.(5) are a controlling parameter of the

transition zone which reflects the initiation of concrete failure, they may be analyzed as a same parameter; Hence, in Eq.(1) ε_{cc} and f_{cc} were replaced with ε_t and f_t, respectively, in the following analysis.

EVALUATION OF PARAMETERS OF THE PROPOSED MODEL

In the model of Eqs.(1) and (5), the factors of controlling the stress-strain relation of concrete confined by CFS are f_t, ε_t, E_s and ε_{cu}. They must be properly determined as follows.

Strength at Transition Zone f_t

Fig.10 shows the confinement effect vs. the axial concrete stress f_t relation. At a CFS hoop strain of ε_{CF}, the CFS hoop stress is $\varepsilon_{CF} \times E_{CF}$. Thus, the axial concrete stress f_t was assumed in the form of

$$\frac{f_t}{f_{co}} = \alpha + \beta \frac{\rho_{CF} \varepsilon_{CF} E_{CF}}{f_{co}} \tag{7}$$

where f_{co} = strength of unconfined concrete (MPa), and α and β are the coefficients to be determined from the test results. Because the strain at the transition zone (ε_{CFc} and ε_{CFt}) is approximately 1,500 μ, ε_{CF} was assumed here 1,500 μ. By regressing the test data, the following relations are obtained.

$$\frac{f_t}{f_{co}} = 1.0 + 1.93 \frac{\rho_{CF} \varepsilon_{CF} E_{CF}}{f_{co}} \quad \text{(circular specimens)} \tag{8}$$

$$\frac{f_t}{f_{co}} = 1.0 + 1.53 \frac{\rho_{CF} \varepsilon_{CF} E_{CF}}{f_{co}} \quad \text{(square specimens)} \tag{9}$$

Comparison of Eqs.(8) and (9) with the experiment results are presented in Fig.10. It is seen that Eqs.(8) and (9) provide acceptable approximation to the test results.

Strain at Transition Zone ε_t

In the similar way, expressing the confinement effect by CFS by $\varepsilon_{CF} E_{CF} \times \rho_{CF}$, the axial strain of a concrete cylinder ε_t vs. $\rho_{CF} \varepsilon_{CF} E_{CF} / f_{co}$ relation was obtained as shown in Fig.11. Again, ε_{CF} was assumed here as 1,500 μ. By regressing the data, the following relations were obtained

$$\varepsilon_t = 0.00343 + 0.00939 \frac{\rho_{CF} \varepsilon_{CF} E_{CF}}{f_{co}} \quad \text{(circular specimens)} \tag{10}$$

$$\varepsilon_t = 0.00330 + 0.00995 \frac{\rho_{CF} \varepsilon_{CF} E_{CF}}{f_{co}} \quad \text{(square specimens)} \tag{11}$$

Eqs.(10) and Eq.(11) represent the experiment results in a satisfactory manner as shown in

Fig.11.

Second Gradient E_g

To systematically evaluate E_g, it was defined as an averaged modulus between ε_t and ε_{cu} for $E_g \leqq 0$, and between ε_t and ε_{cu} for $E_g \geqq 0$, as shown in Fig.12. In Figs.4 and 6, it is seen that the second gradient E_g becomes larger as ρ_{CF} and E_{CF} increase. Therefore, by expressing the effect of the confining pressure in terms of $\sqrt{\rho_{CF}}E_{CF}$, the second gradient E_g was assumed as

$$E_g = \alpha \frac{f_{co}^{\ 2}}{\rho_{CF} f_{CF}} + \beta \sqrt{\rho_{CF}} E_{CF} \tag{12}$$

By determining α and β from a regression analysis, Eq.(12) may be written as

$$E_g = -7.427 \frac{f_{co}^{\ 2}}{\rho_{CF} f_{CF}} + 0.086 \sqrt{\rho_{CF}} E_{CF} \quad \text{(circular specimens)} \tag{13}$$

$$E_g = -13.726 \frac{f_{co}^{\ 2}}{\rho_{CF} f_{CF}} + 0.023 \sqrt{\rho_{CF}} E_{CF} \quad \text{(square specimens)} \tag{14}$$

Ultimate Strain ε_{cu}

As was presented in the previous sections (Figs.4 and 6), the ultimate strain ε_{cu} of concrete cylinders confined by the CFS increases as ρ_{CF} increases, however it does not necessarily increase in the confinement by the high-modulus type CFS. Thus ε_{cu} was correlated with $\rho_{CF} f_{CF} / E_{CF}$ as shown in Fig.13, and by regressing the data, the following relations were obtained

$$\varepsilon_{cu} = 1.384 \sqrt{\rho_{CF} \left(\frac{f_{CF}}{E_{CF}} \right)} \quad \text{(circular specimens)} \tag{15}$$

$$\varepsilon_{cu} = 1.212 \sqrt{\rho_{CF} \left(\frac{f_{CF}}{E_{CF}} \right)} \quad \text{(square specimens)} \tag{16}$$

EVALUATION OF PROPOSED MODEL

To show an effectiveness of the proposed model, the stress-strain relation evaluated by the proposed model was compared with the test results as shown in Fig. 14. It is observed in the comparison that the proposed model provides acceptable agreement with the test results.

CONCLUSIONS

To propose a stress-strain model of concrete confined by CFS, a series of uniaxial compression

tests were conducted. The conclusions from the study presented herein may be deduced as:

1) At ρ_{CF} in the range of about 0.05~0.15%, the peak axial stress of concrete, f_{cc}, and the axial strain of concrete corresponding to the peak stress, ε_{cc}, do not necessarily increase as the carbon fiber ratio increases, and they are almost independent of the cross sectional shape of specimens. However, the deteriorating rate of the axial concrete stress after the peak stress decreases and the axial strain of concrete at rupture of the CFS increases as the carbon fiber ratio ρ_{CF} increases.

2) At ρ_{CF} larger than about 1%, the axial stress of concrete continues to increase with a change of gradient at the axial concrete strain of 3,000~3,500 μ until the CFS fails.

3)The circumferential strain of the CFS at the peak axial stress of concrete, ε_{CFc}, is 1,100~2,500 μ at the carbon fiber ratio of 0.056 ~ 0.167%, while the circumferential strain of the CFS where the gradient changes from the initial value to the second gradient, ε_{CFt}, is 1,800~1,900 μ at the carbon fiber ratio of 1.336%; thus, ε_{CFc} is quite close to ε_{CFt}. This may be due to the fact that the concrete cylinders initiate to fail at the circumferential strain over 1,100~2,500 μ.

4)Considering f_t, ε_t, E_s and ε_{cu} as parameters, a model of axial stress vs. axial strain of concrete confined by the CFS is proposed as shown in Eqs.(1) and (5).

5)The proposed model provides good agreement with the test results.

REFERENCES

1) Hoshikuma, J., Kawashima, K. and Nagaya, K.: A Stress-Strain Model for Reinforced Concrete Columns Confined by Lateral Reinforcement, Journal of Materials, Concrete Structures and Pavements, Japan Society of Civil Engineers, No.520, V-28, pp.1-11, 1995.8

2) Japan Road Association: Guide Specifications for Earthquake Hazard Mitigation for Road Transportation Facilities, Pre-Earthquake Countermeasures, 1987

3) Japan Road Association: Guide Specifications for Reconstruction and Repair of Highway Bridges which suffered Damage due to the Hyogo-ken Nanbu Earthquake, 1995

4) Kawashima, K.: Impact of Hanshin/Awaji Earthquake on Seismic Design and Seismic Strengthening of Highway Bridges, Report No. TIT/EERG 95-2, Department of Civil Engineering, Tokyo Institute of Technology, 1996

5) Kawashima, K., Nishikawa, K., Nakano, M., Unjoh, S., Kimura, Y. and Hoshikuma, J.: Guide Specifications for Reconstruction and Repair of Highway Bridges which suffered damage due to the Hyogo-ken Nanbu Earthquake, Proc. 28th Joint Meeting of the UJNR Panel on Wind and Seismic Effects, NIST Special Publication SP 904, pp. 159-174, 1996

6) Kent, D.C. and Park, R.: Flexural members with confined concrete, Journal of the Structural Division, ASCE, Vol.97, No.ST7, pp.1969-1990, Jul. 1971
7) Mander, J.B., Priestley, M.J.N. and Park, R.: Theoretical stress-strain model for confined concrete, Journal of the Structural Division, ASCE, Vol.14, No.ST8, pp.1804-1826, Aug. 1988
8) Mander, J.B., Priestley, M.J.N. and Park, R.: Observed stress-strain behavior of confined concrete, Journal of the Structural Division, ASCE, Vol.114, No.ST8, pp.1827-1849, Aug. 1988
9) Ministry of Construction: Report on the Damage of Highway Bridges by the Hyogo-ken Nanbu Earthquake, Committee for Investigation on the Damage of Highway Bridges Caused by the Hyogo-ken Nanbu Earthquake, 1995
10) Park, R. et al.: Ductility of square-confined concrete columns, Journal of the Structural Division, ASCE, Vol.108, No.ST4, pp.929-950, Apr. 1982
11) Priestley, M.J.N., Seible, F. and Calvi, G.M.: Seismic Design and Retrofit of Bridges, John Wiley & Sons, Inc., 1996
12) Uji, K., Yokota, K. and Ikeda, S.: Property of RC Structure Reinforced with Sheet Type Carbon Fiber, Proceedings, Japan Concrete Institute, Vol.148, No.2, pp695-700, 1992

NOTATIONS

d = diameter (circular) or width (square) of a concrete cylinder
E_C = initial stiffness of concrete
E_{CF} = elastic modulus of CFS
E_g = second gradient of axial stress f_c vs. axial strain ε_c relation of a concrete cylinder
f_c = axial stress of a concrete cylinder
f_{cc} = peak axial stress (strength) of a concrete cylinder
f_{CF} = tensile strength of CFS
f_{co} = strength of unconfined concrete
f_t = strength of transition zone of a concrete cylinder
f_{yh} = yield strength of hoop reinforcement
N = number of layers of CFS
n = a coefficient defined by Eqs.(2) and (6).
t_{CF} = thickness of a layer of CFS
ε_c = axial strain of a concrete cylinder
ε_{cc} = axial strain of a concrete cylinder at f_{cc}

ε_{CF} = a CFS hoop strain (ε_{CF} is assumed here 1,500 μ)

ε_{CFC} = circumferential strain of CFS at f_{cc}

ε_{CFt} = circumferential strain of CFS where the gradient of axial stress of concrete vs. circumferential strain of CFS changes from the initial value to the second value

ε_{cu} = ultimate strain of a concrete cylinder

ε_{pf} = circumferential strain of a concrete cylinder at its failure

ε_t = axial strain of a concrete cylinder at f_t

ρ_{CF} = carbon fiber ratio

ρ_s = the volumetric ratio of hoop reinforcement

Table 1 Test Specimens

Series		Section	Size	Strength of Concrete (MPa)	Carbon Fiber Sheet		
					Nominal Elastic Modulus (MPa)	Weight of Carbon per Unit Area (g/m²)	ρ_{CF} (%)
N	N-1	Circular	φ200mm ×h 600mm	30	—	—	—
	N-2						
	N-3						
	N-6	Square	□200mm ×h 600mm				
	N-7						
	N-8						
S	S-1	Circular	φ200mm ×h 600mm	30	2.30×10^5	200	0.056
	S-2						0.111
	S-3						0.167
	S-4					300	1.336
	S-9	Square	□200mm ×h 600mm			200	0.056
	S-10						0.111
	S-11						0.167
	S-12					300	1.336
H	H-1	Circular	φ200mm ×h 600mm	30	3.92×10^5	300	0.169
	H-2						0.338
	H-3						0.676
	H-4						1.352
	H-5	Square	□200mm ×h 600mm				0.169
	H-6						0.338
	H-7						0.676
	H-8						1.352

Table 2 Mechanical Properties of Carbon Fiber Sheet

		Normal Elastic Modulus Type		High Elastic Modulus Type
Design Value	Weight of Carbon per Unit Area (g/m²)	200	300	300
	Thickness (mm)	0.111	0.167	0.163
	Tensile Strength (MPa)	3,481		2,942
	Elastic Modulus (MPa)	2.30×10^5		3.92×10^5
	Rupture Strain (%)	1.5	1.5	1.0
Measured	Weight of Carbon per Unit Area (g/m²)	200	300	309.5
	Thickness (mm)	0.110	0.167	0.169
	Tensile Strength (MPa)	4,227	4,433	3,972
	Elastic Modulus (MPa)	2.43×10^5	2.52×10^5	4.39×10^5
	Rupture Strain (%)	1.74	1.76	0.90

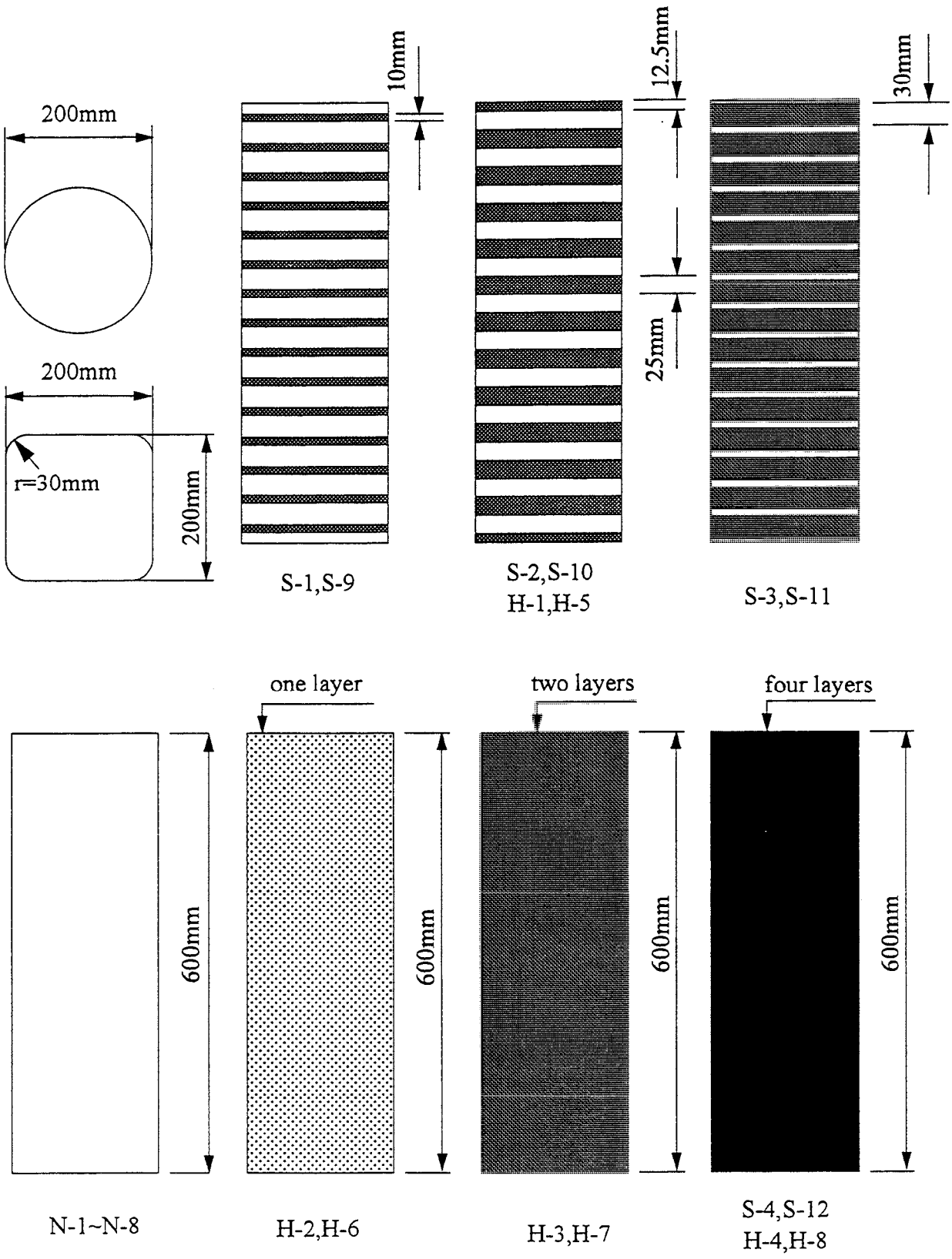

Fig.1 Adhesion of Carbon Fiber Sheet

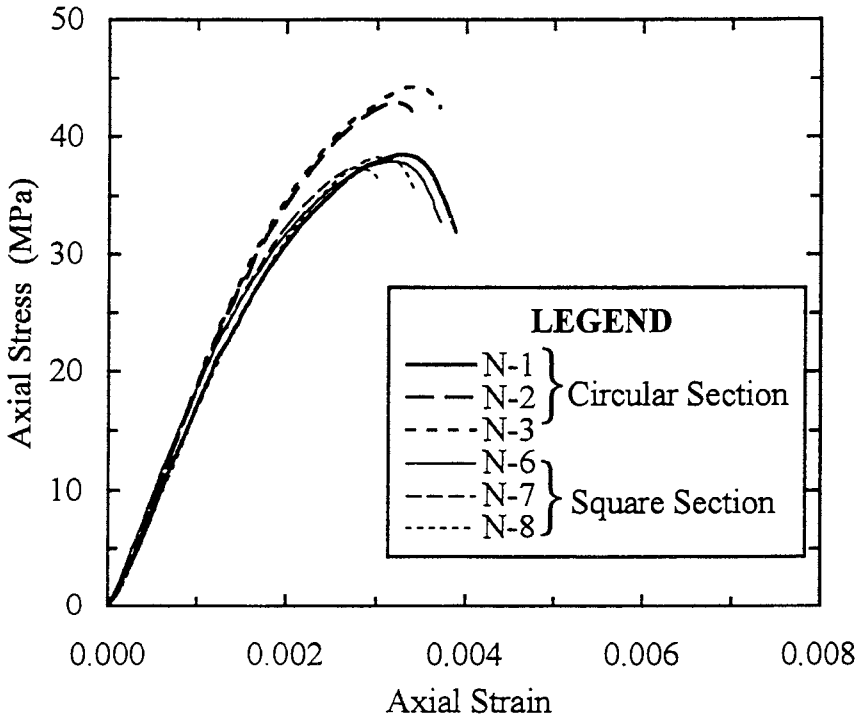

Fig.2 Stress vs.Strain Relation of Unconfined Concrete Cylinders

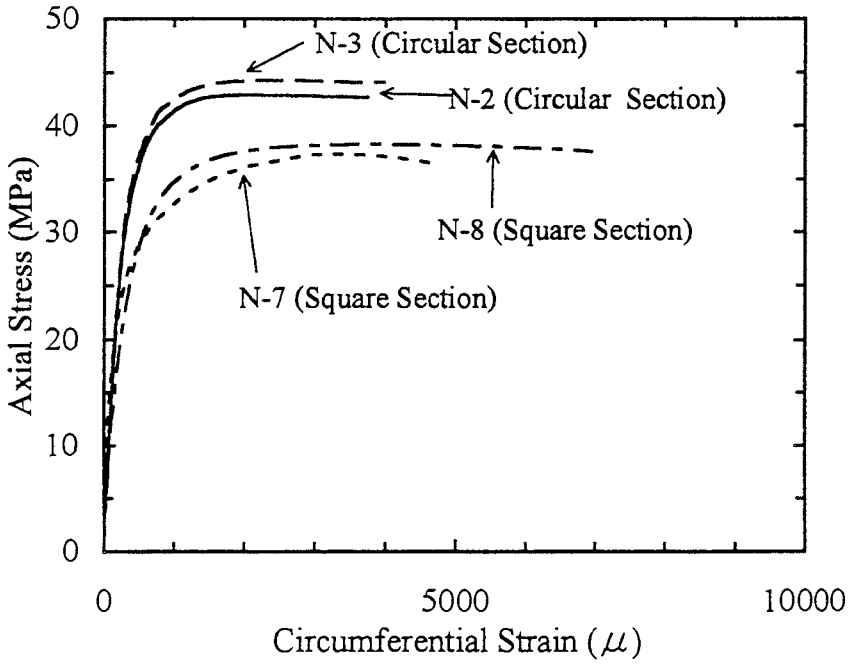

Fig.3 Axial Stress vs. Circumferential Strain of Unconfined Concrete Cylinders

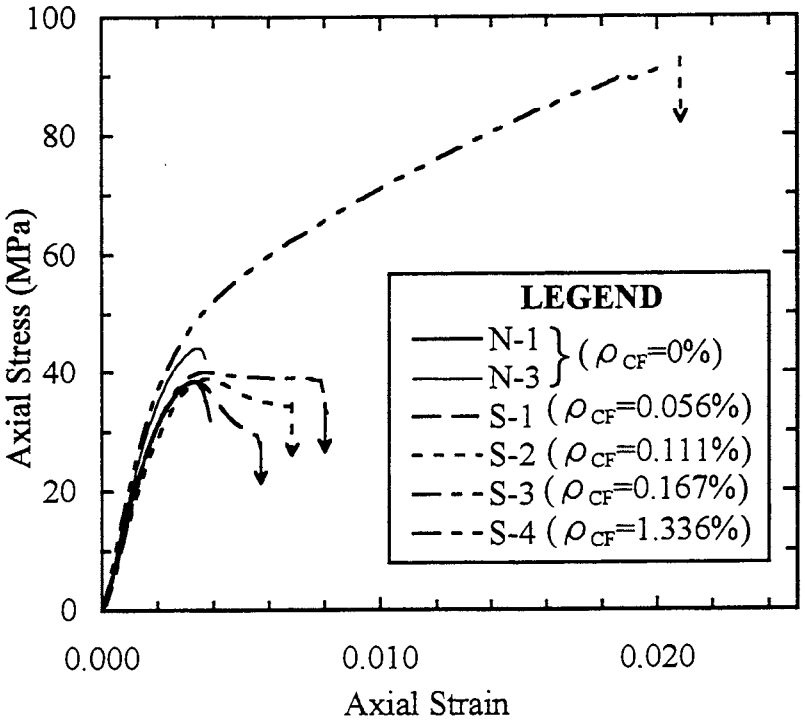

(a) Circular Section

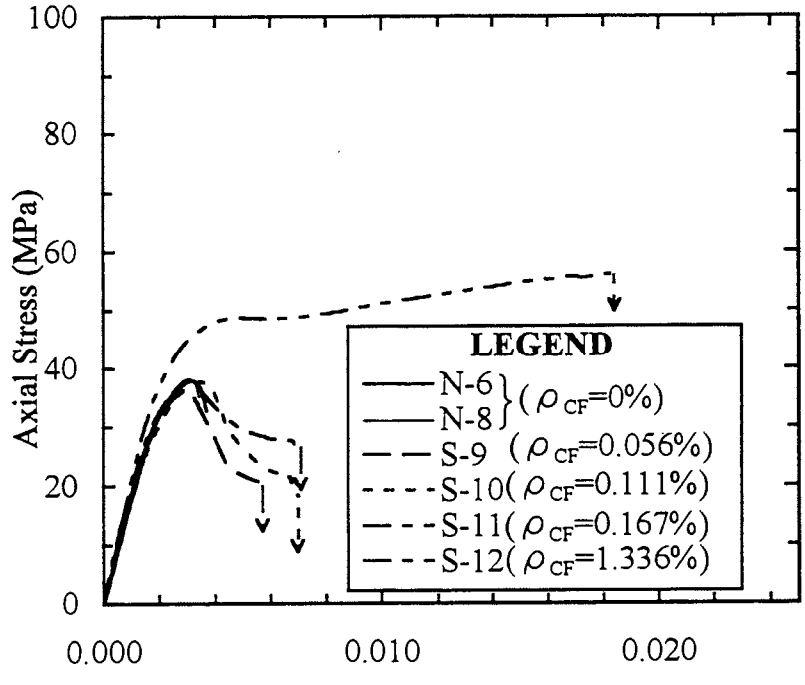

(b) Square Section

Fig.4 Axial Stress vs. Axial Strain Relation of Concrete Confined by CFS

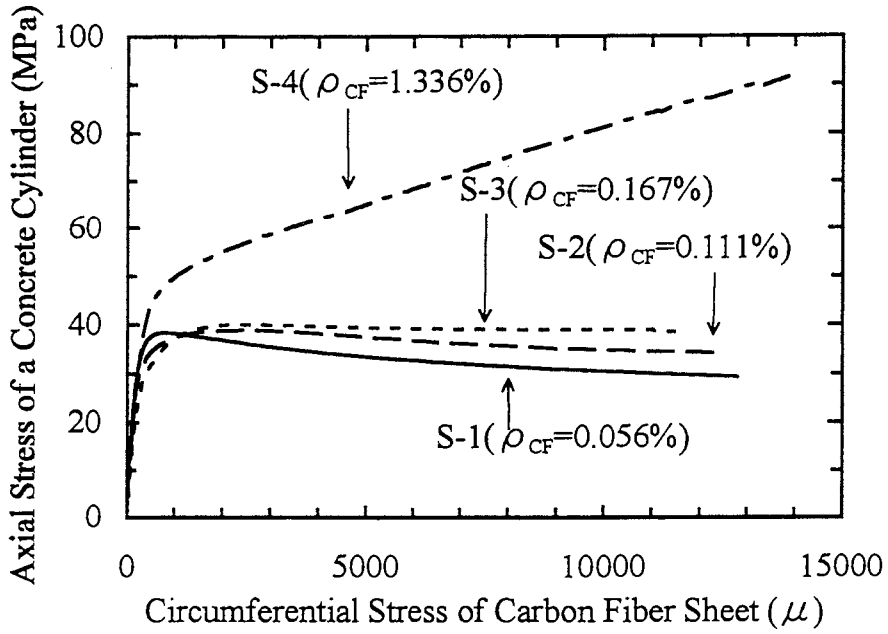

(a) Circular Section

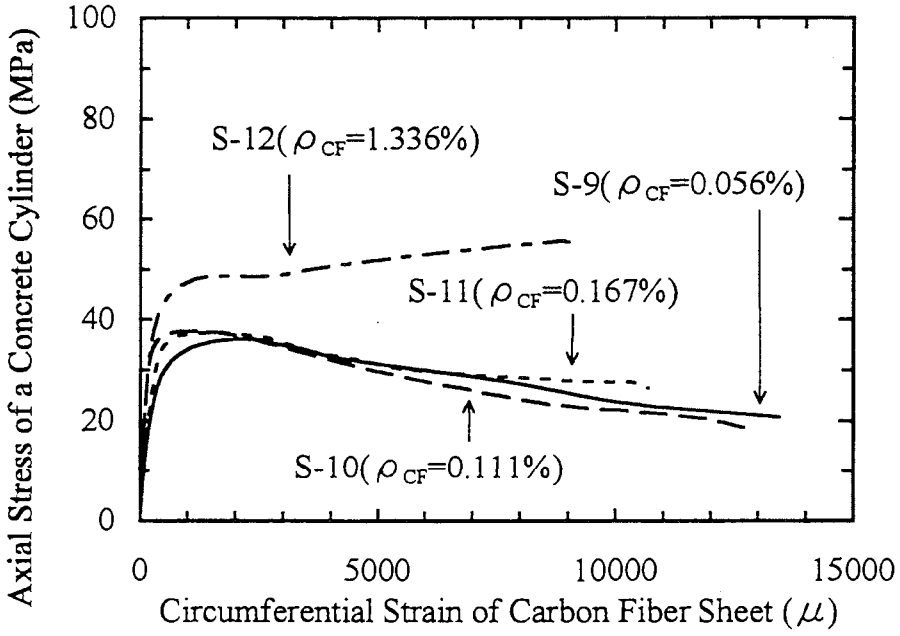

(b) Square Section

Fig.5 Relation between Axial Stress of Concrete and Circumferential Strain of CFS

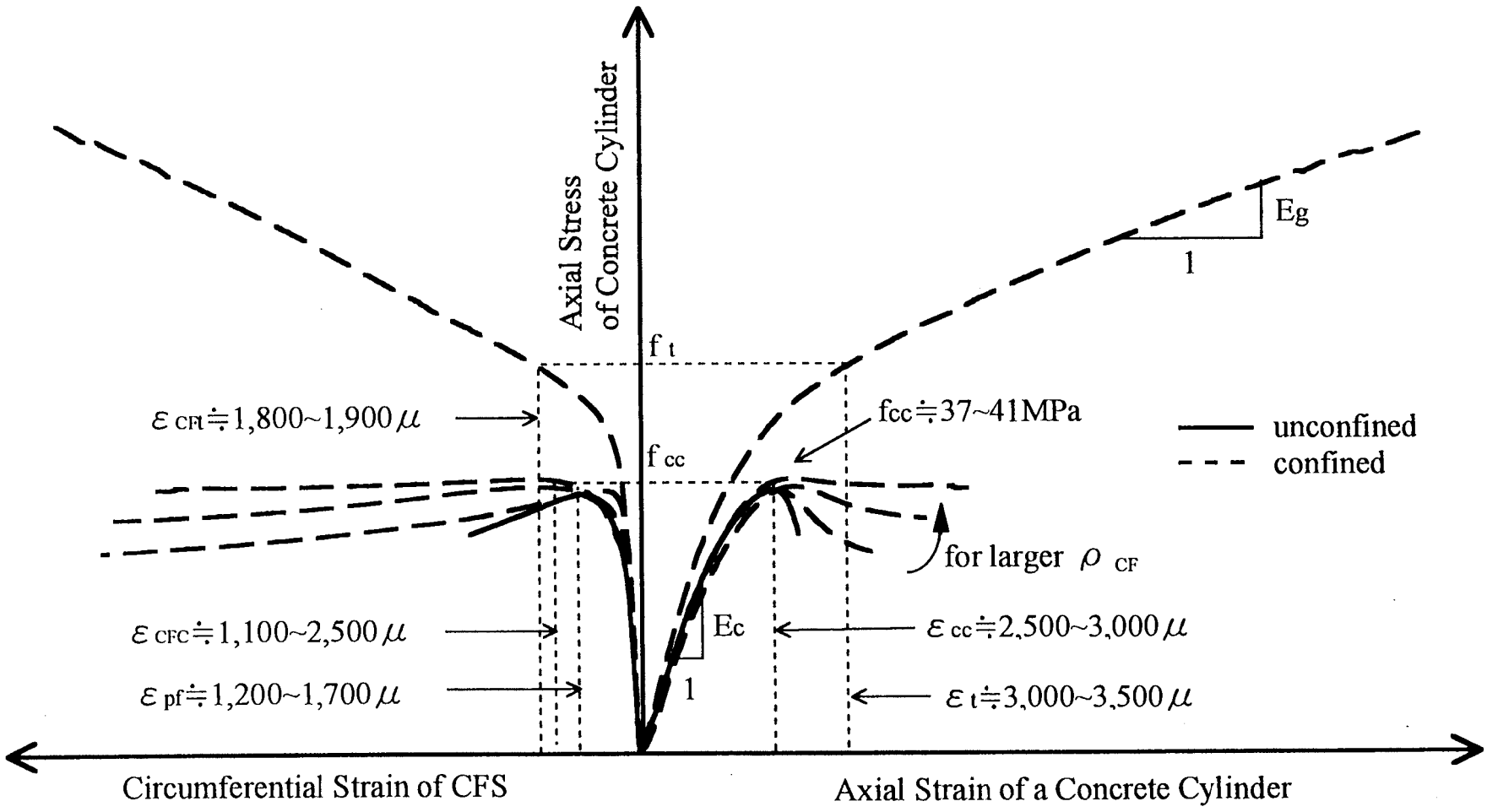

Fig.6 General Characteristics of Stress vs. Strain Relation of Concrete Cylinder with and without Confined by CFS

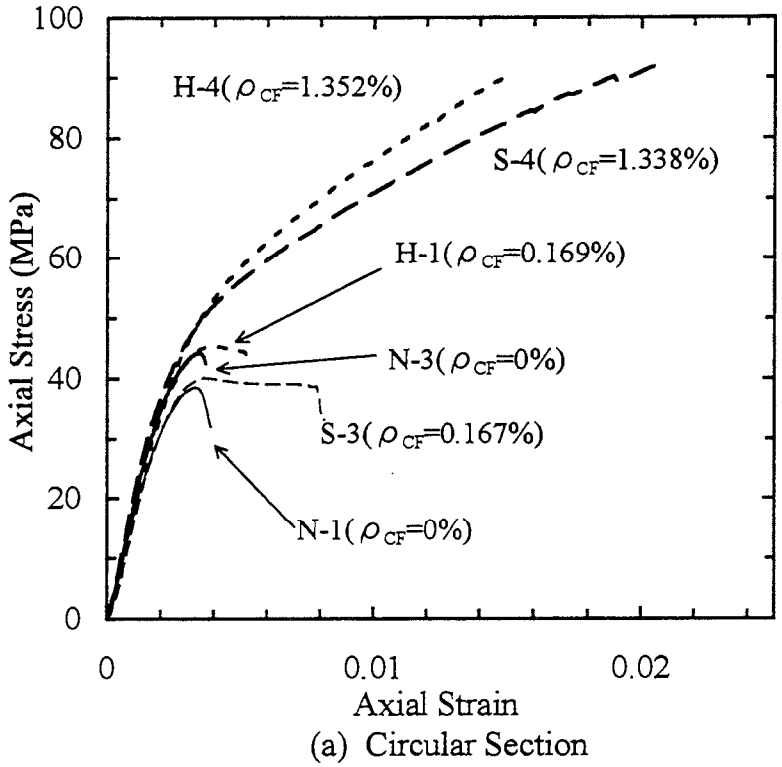

(a) Circular Section

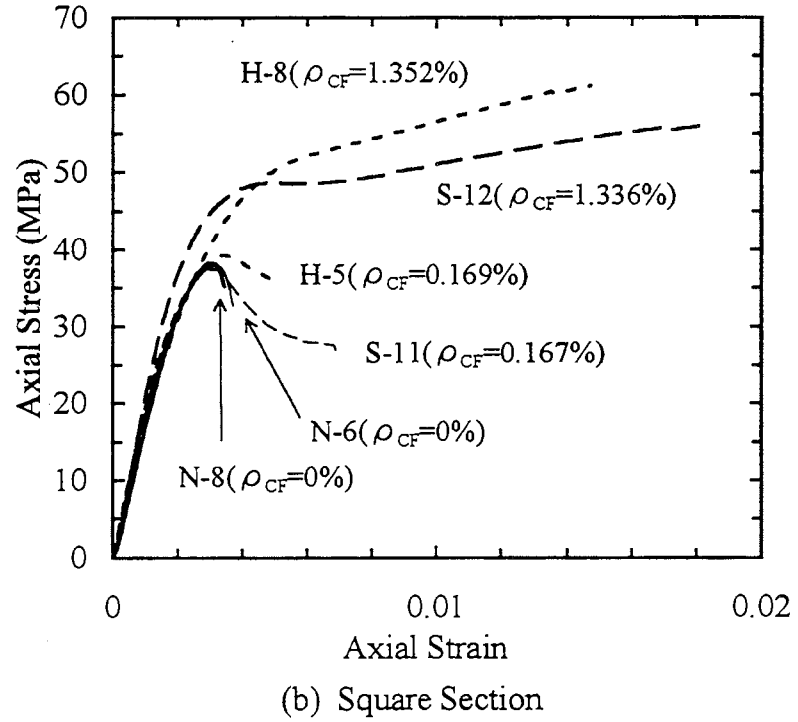

(b) Square Section

Fig.7 Effect of High-Modulus Type CFS for Axial Stress vs. Axial Strain relation of Concrete cylinder

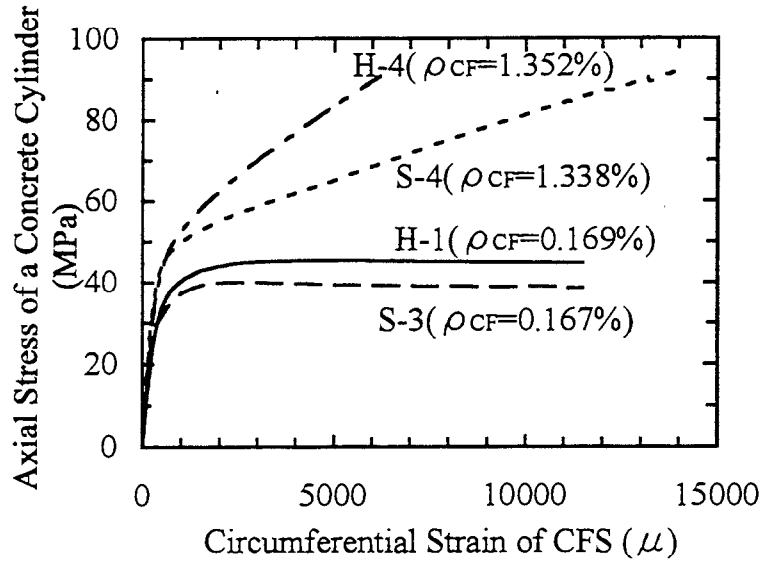

(a) Circular Section

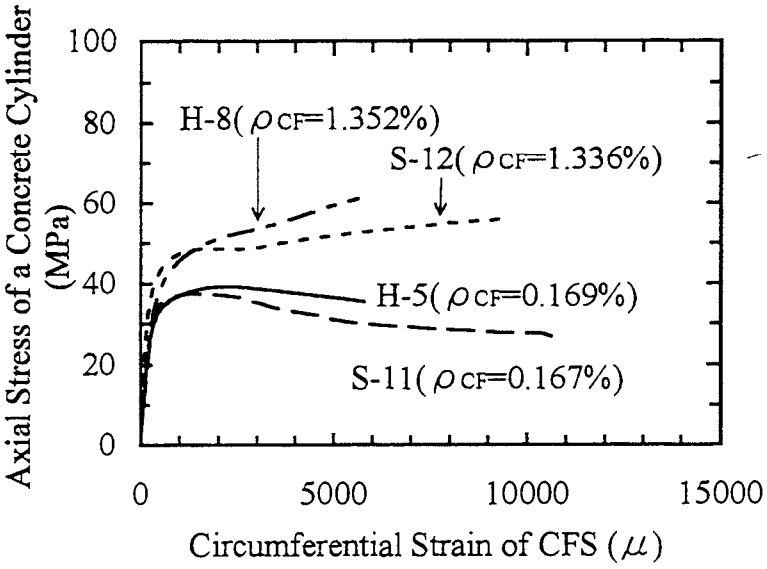

(b) Square Section

Fig.8 Effect of High-Modulus Type CFS for Axial ConcreteStress vs. Circumferential Strain of CFS

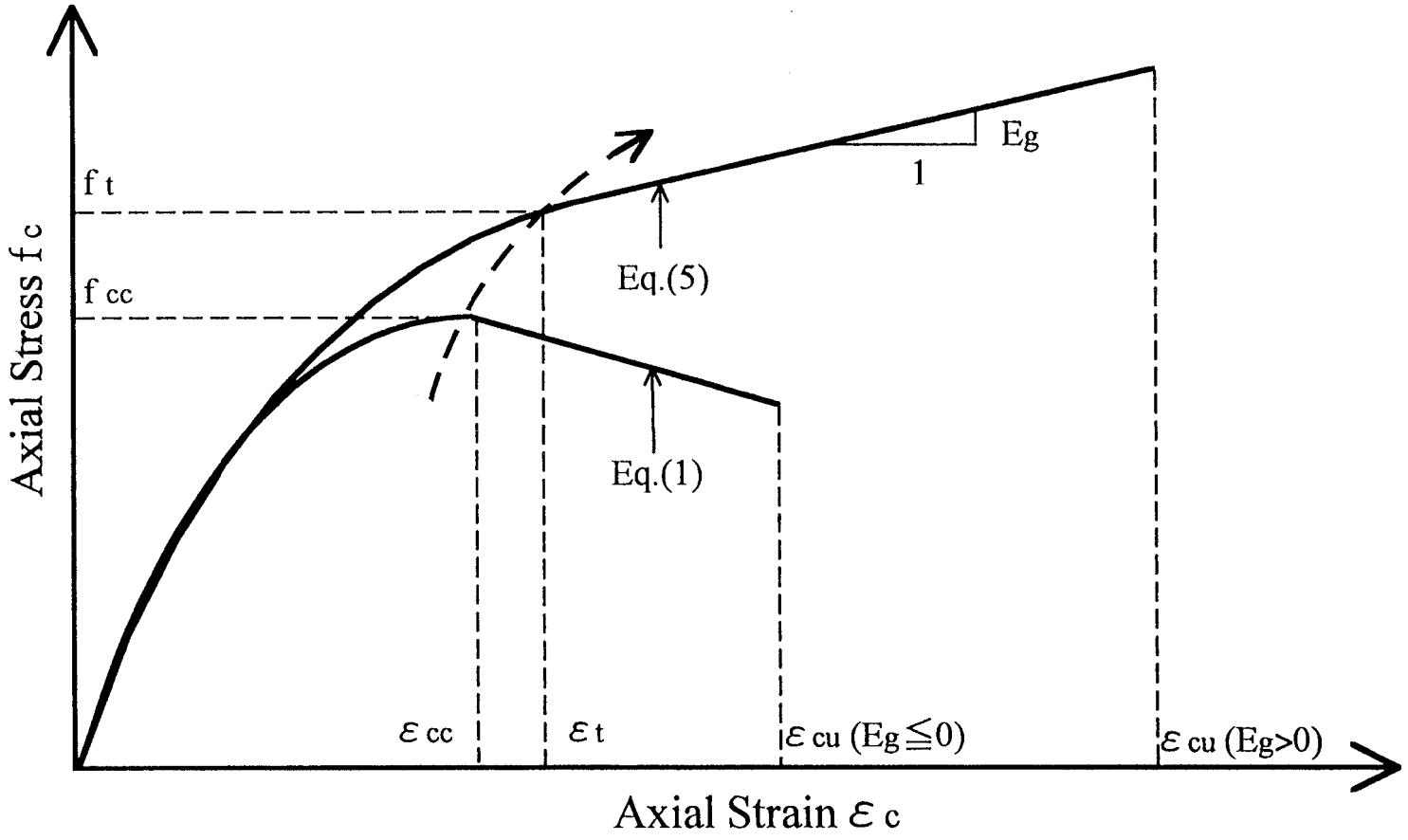

Fig.9 Axial Stress-Axial Strain Relation Proposed for Concrete Cylinders Confined by CFS

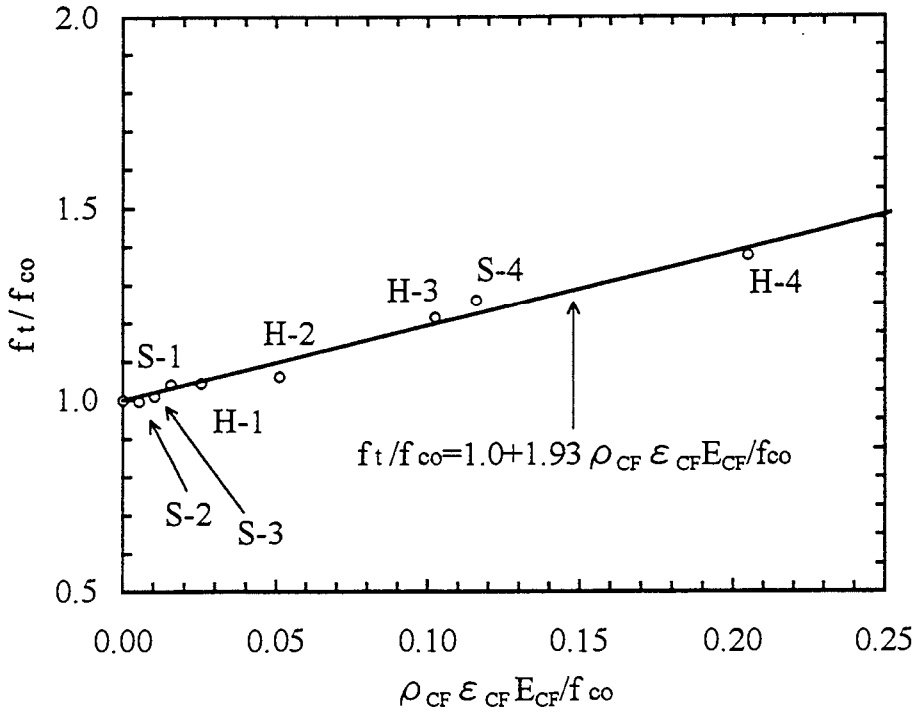

(a) Circular Section

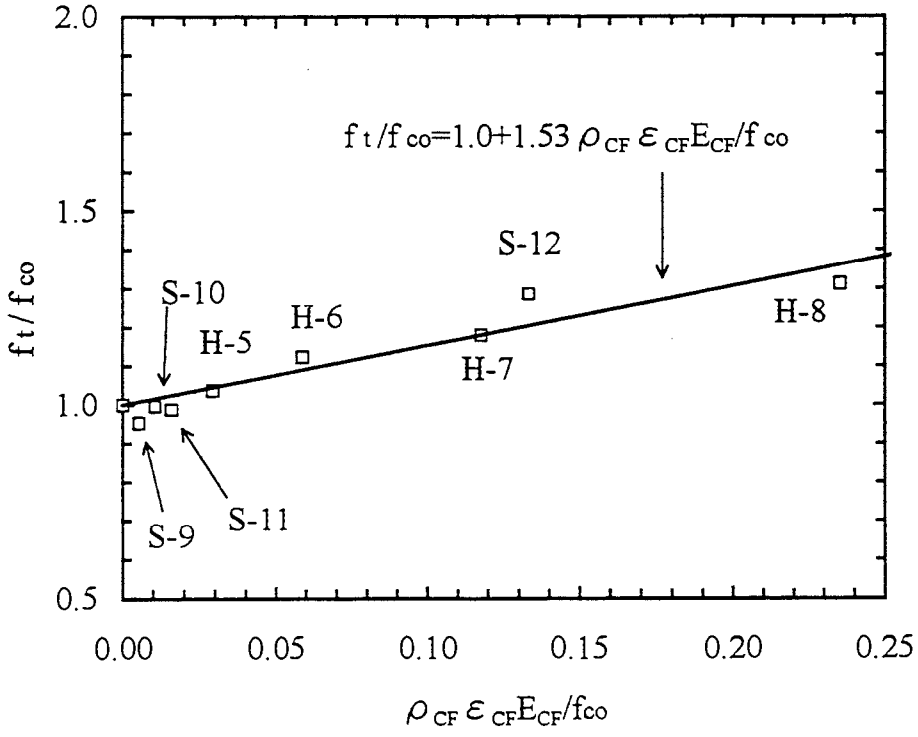

(b) Square Section

Fig.10 Evaluation of Strength at Transition Zone ft

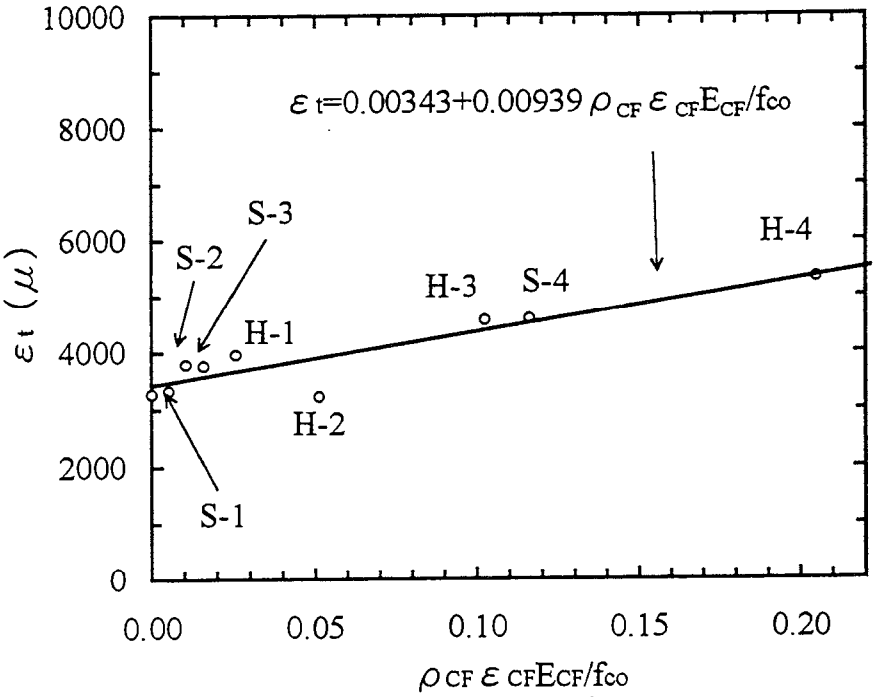

(a) Circular Section

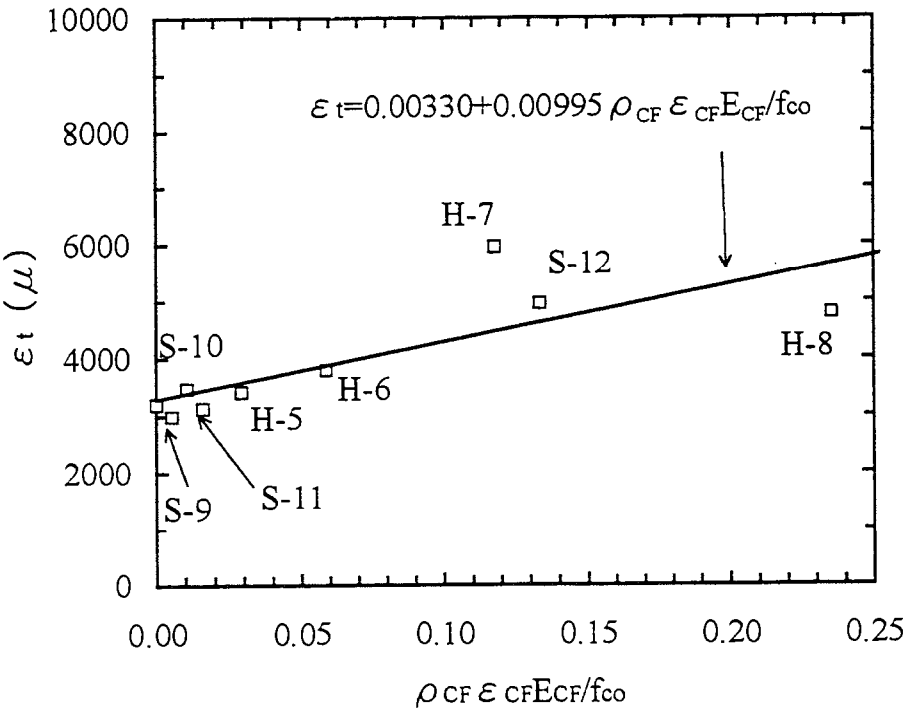

(b) Square Section

Fig.11 Evaluation of Axial Concrete Strain εt

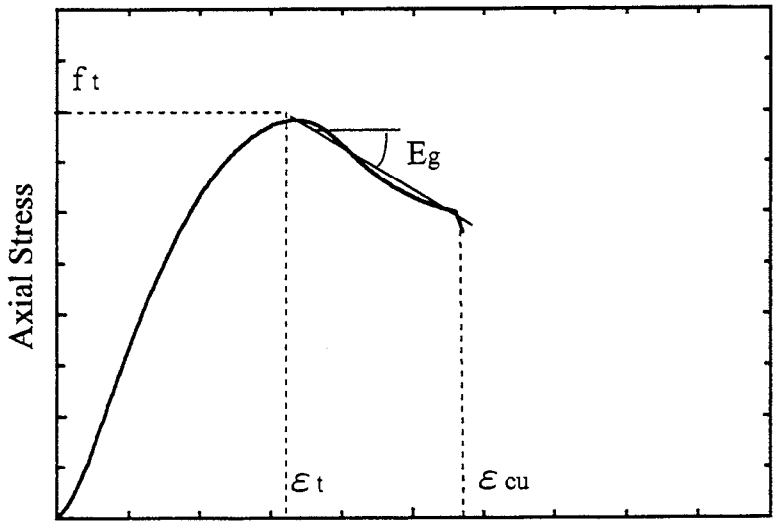

(a) Eg<0

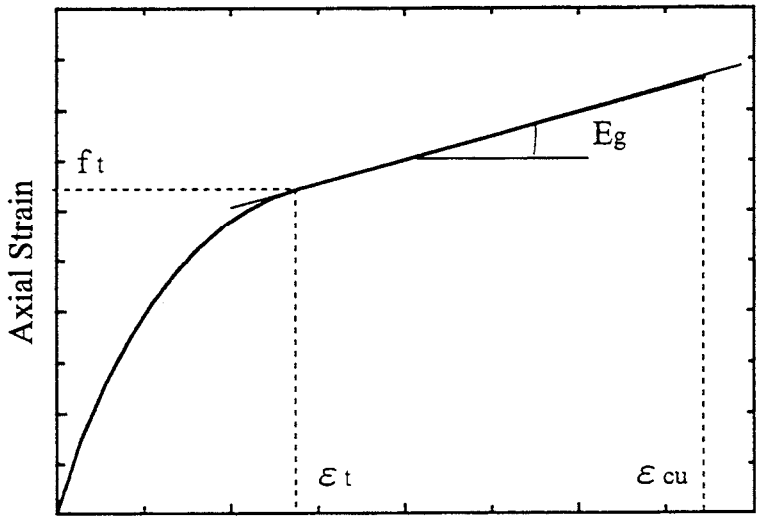

(b) Eg≧0

Fig.12 Definition of Second Gradient Eg

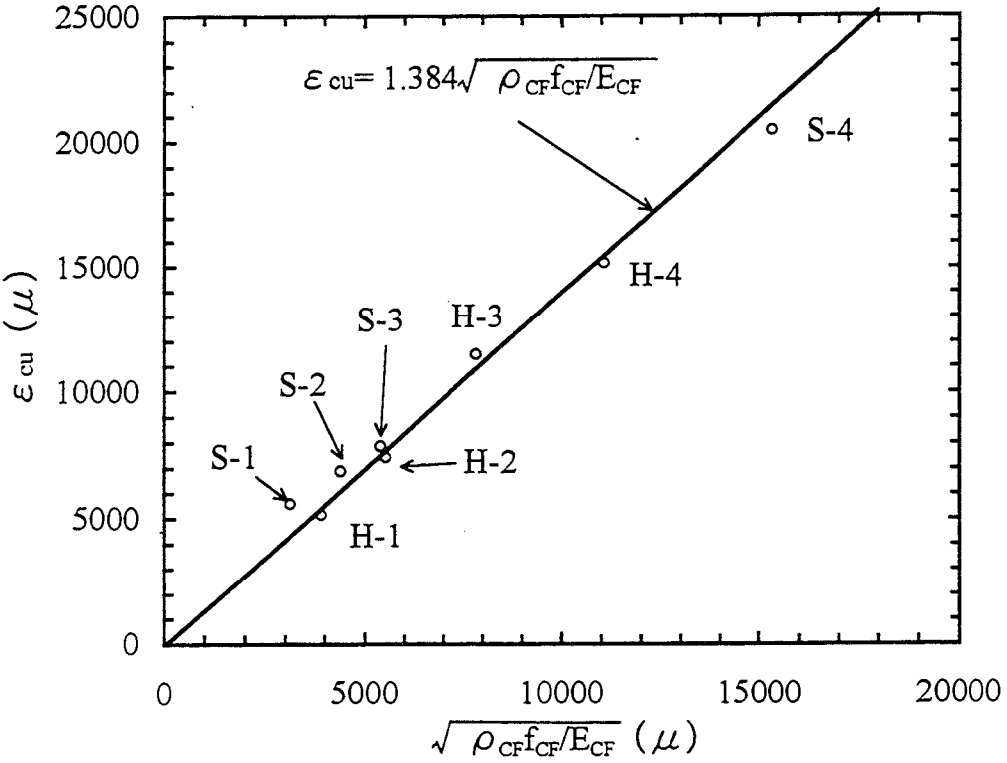

(a) Circular Section

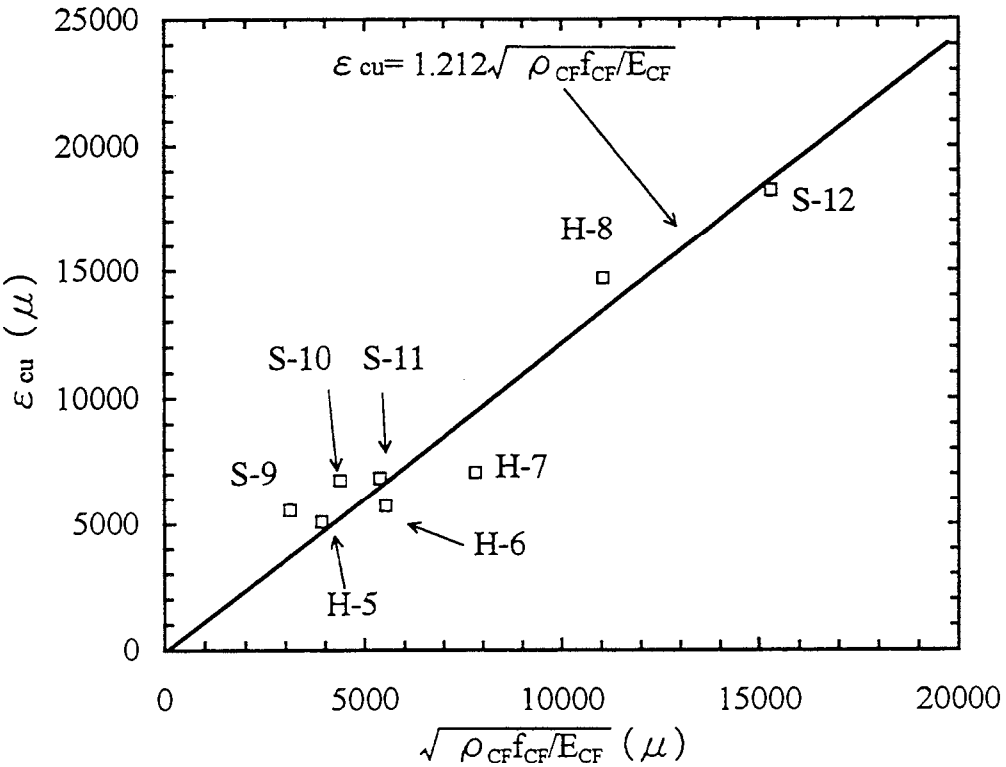

(b) Square Section

Fig.13 Evaluation of Ultimate Strain ε_{cu}

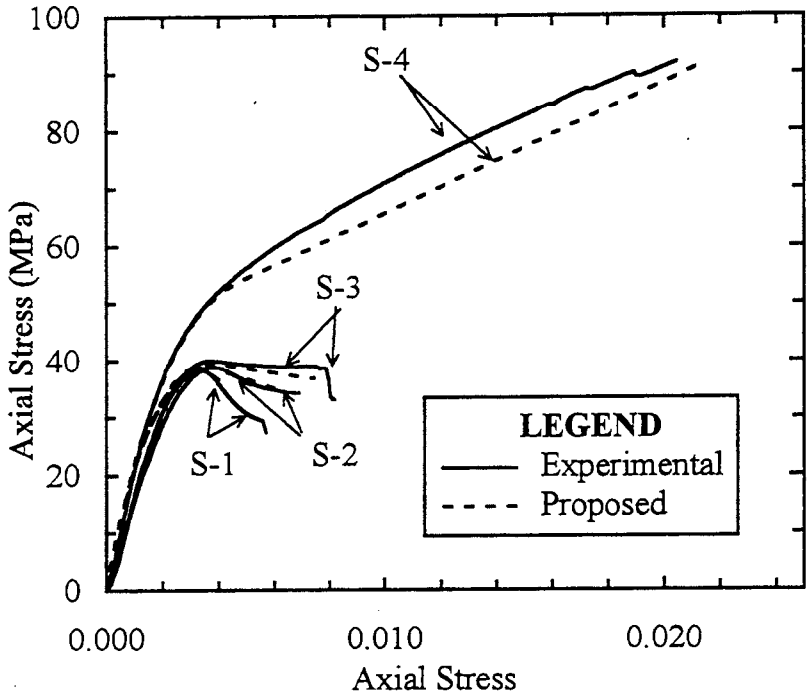

(a) Circular S-Series Specimens

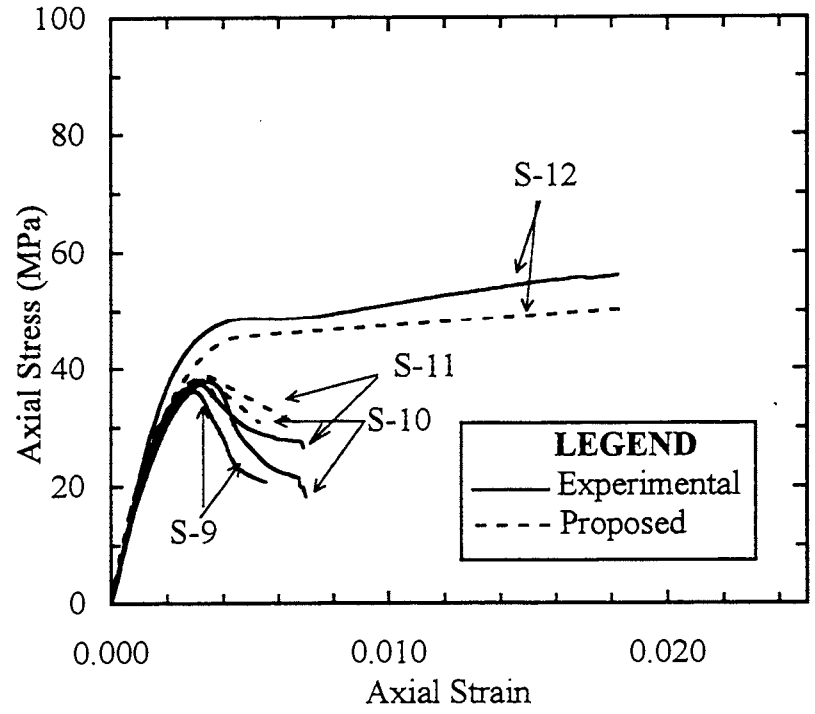

(b) Square S-Series Specimens

Fig.14(1) Comparison of Axial Stress vs. Axial Strain Relation between Test Results and Proposed Model

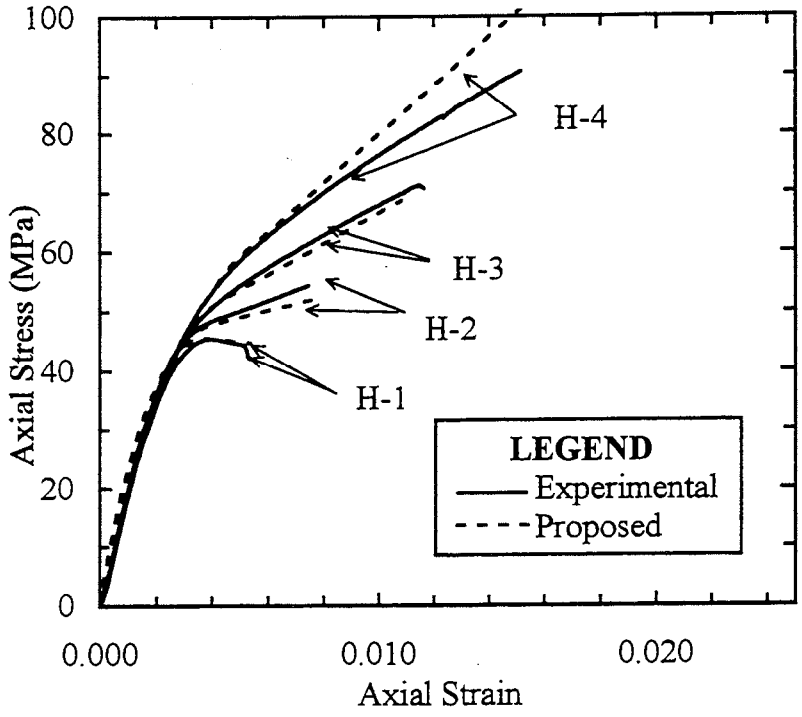

(c) Circular H-Series Specimens

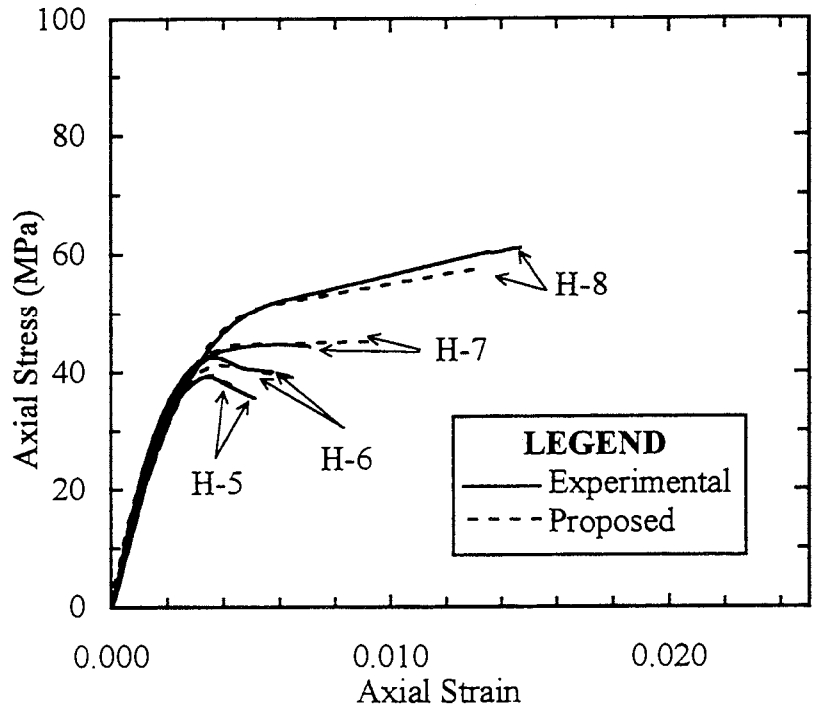

(d) Square H-Series Specimens

Fig.14(2) Comparison of Axial Stress vs. Axial Strain Relation between Test Results and Proposed Model

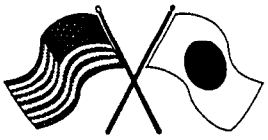

Session 6
Earthquake Protective Systems

Session Co-chairs: Christopher Rojahn and Masato Abe

NATIONAL CENTER FOR EARTHQUAKE ENGINEERING RESEARCH
Headquartered at the State University of New York at Buffalo

INSTITUTE OF INDUSTRIAL SCIENCE INCEDE UNIVERSITY OF TOKYO

OPTIMAL DESIGN PARAMETERS OF BRIDGE BEARINGS FOR SEISMIC PROTECTION

Masato Abé and Yozo Fujino

Department of Civil Engineering, The University of Tokyo,

Hongo 7-3-1, Bunkyo-ku, Tokyo 113, Japan.

ABSTRACT

In this paper, optimization of bearings and dampers to improve seismic performance of bridges is studied. At the first half of the paper, general optimization procedure for seismic response reduction is constructed. The seismic excitation is modeled by stationary gaussian white noise for the convenience of the analysis, and the expected peak response is expressed in terms of the response spectra by applying simple approximation on peak factors. Then, optimal design values are derived by minimizing mean square responses of interest. Following the construction of the general method, optimal design of deck connections and bearings are demonstrated using simple linear two-degree-of-freedom structural models. Analytical expressions for optimal design values are also developed for these devices. The validity of the proposed optimization procedure and design values are studied using the observed ground motions of 1941 El Centro earthquake, and 1995 Kobe earthquake.

1. INTRODUCTION

Recent earthquakes, such as 1994 Northridge earthquake and 1995 Kobe earthquake caused considerable damage to elevated highway bridges in urban area, which lead to not only direct loss of human lives but also economic loss due to disruption of the urban transportation system. Energy dissipation devices and base-isolation are often installed to improve seismic performance of bridges. These energy dissipation devices are placed at connections of each structural element where relative motion is possible.

Figure 1 shows a possible application of dampers to bridge structures (Shinozuka, 1996). By placing dampers at gaps between decks, unseating of decks and impact due to pounding of decks can be greatly reduced. Commonly used base-isolation system is shown in Figure 2. The bearings of decks are now replaced by elastomeric rubber to make natural period longer and increase damping. Various devices to achieve high damping in bridges have been developed (Skinner, et. al., 1993): e.g., lead rubber bearing, lead extrusion damper, hydraulic damper, steel damper, e.t.c.

Addition of more damping to connections appear to improve the seismic performance of bridges, because it will reduce relative displacement. However, this observation is not entirely correct when the seismic performance of the total structural system of bridges is considered. For example, addition of too much damping to deck connections makes the decks approximately continuous and the energy dissipation effect due to relative displacement will be lost. Also, bearings with very high damping would increase the transmission of inertia force from the deck to the pier and make the pier more vulnerable to seismic force. Therefore, a bridge must be treated as a structural system which consisit of several elements, and energy dissipation devices must be designed to optimize the seismic performance of the system, not only for each element.

In this paper, optimization of dampers at gaps of decks and bearings to improve seismic performance of elevated highway bridge system is studied. At the first half of the paper, general optimization procedure for seismic response reduction is constructed. The seismic excitation is modeled by stationary gaussian white noise for the convenience of the analysis, and the expected peak response is expressed in terms of the response spectra by applying simple approximation on peak factors. Then, optimal design values are derived by minimizing responses of interest. Following the construction of the general optimization theory, optimal design parameters of dampers and bearings is derived for simple linear two-degree-of-freedom structural model. Analytical expressions for optimal design values are also developed for these devices. The validity of the proposed optimization procedure and design values are numerically demonstrated using the ground motion records of 1941 El Centro earthquake, and 1995 Kobe earthquake, whose accelerograms and response spectra are shown in Figures 3 and 4.

2. OPTIMIZATION PROCEDURE

In this section, general optimization procedure for structures subject to earthquake excitation is developed. Peak responses which are usually used to evaluate the seismic performance are expressed in terms of mean square responses and peak factors assuming the excitation is stationary gaussian white noise. Then, normalized response is obtained by dividing expected response with response spectra of the nominal structure. With the approximation that peak factors are approximately the same for nominal and objective structures, the reduction rate can be calculated without any information on ground motion and solely depends upon the structural parameters.

Two simplifications are made in the following analysis: (i) ground excitation is assumed to be stationary gaussian white noise, (ii) the structure is linear elastic. Validity and restriction of the first simplification are discussed by numerical simulations in the next section which use ground motion records. Although the second simplification appears to be unrealistic because structural responses undergo inelastic region in severe earthquakes, the method shown here could be extended to inelastic structures using the equivalent linearization technique (Caughey, 1960).

Equations of motion of linear structures subject to earthquake excitation can be expressed as,

$$\mathbf{M}\ddot{\mathbf{x}} + \mathbf{C}\dot{\mathbf{x}} + \mathbf{K}\mathbf{x} = -\mathbf{M}\mathbf{r}\ddot{x}_g, \tag{1}$$

where $\mathbf{x}$: displacement vector, $\mathbf{M}$: mass matrix, $\mathbf{C}$: damping matrix, $\mathbf{K}$: stiffness matrix, $\mathbf{r}$: influence coefficient vector, and $\ddot{x}_g$: ground acceleration. Equation (1) can be rewritten as

$$\mathbf{M}\ddot{\mathbf{x}} + (\mathbf{C}_0 + \mathbf{C}_1)\dot{\mathbf{x}} + (\mathbf{K}_0 + \mathbf{K}_1)\mathbf{x} = -\mathbf{M}\mathbf{r}\ddot{x}_g \tag{1a}$$

by expanding $\mathbf{C}$ and $\mathbf{K}$ into two parts: i.e., damping and stiffness without energy dissipation devices ($\mathbf{C}_0$ and $\mathbf{K}_0$), and contribution of energy dissipation devices ($\mathbf{C}_1$ and $\mathbf{K}_1$). Here, the design parameters for energy dissipation devices are expressed by $\mathbf{C}_1$ and $\mathbf{K}_1$.

This equation can be rewritten in the first order form:

$$\dot{\mathbf{z}} = (\mathbf{F}_0 + \mathbf{F}_1)\mathbf{z} + \mathbf{G}\ddot{x}_g \tag{2}$$

where,

$$\dot{\mathbf{z}} = \begin{bmatrix} \dot{\mathbf{x}} \\ \mathbf{x} \end{bmatrix}, \quad \mathbf{F}_0 = \begin{bmatrix} -\mathbf{M}^{-1}\mathbf{C}_0 & -\mathbf{M}^{-1}\mathbf{K}_0 \\ \mathbf{I} & \mathbf{0} \end{bmatrix}, \quad \mathbf{F}_1 = \begin{bmatrix} -\mathbf{M}^{-1}\mathbf{C}_1 & -\mathbf{M}^{-1}\mathbf{K}_1 \\ \mathbf{I} & \mathbf{0} \end{bmatrix}, \quad \mathbf{G} = \begin{bmatrix} -\mathbf{r} \\ \mathbf{0} \end{bmatrix}. \tag{2a,b,c}$$

Response values of design interests can be expressed by linear combination of the state vector $\mathbf{z}$:

$$\mathbf{y} = \mathbf{H}\mathbf{z}. \tag{3}$$

Then, the covariance matrix whose diagonal elements correspond to mean square responses of $\mathbf{y}$ can be expressed by,

$$E[\mathbf{y}\mathbf{y}^T] = E[\mathbf{H}\mathbf{z}(\mathbf{H}\mathbf{z})^T] = E[\mathbf{H}\mathbf{z}\mathbf{z}^T\mathbf{H}^T] = \mathbf{H}E[\mathbf{z}\mathbf{z}^T]\mathbf{H}^T. \tag{4}$$

Assuming seismic excitation $\ddot{x}_g$ is stationary gaussian white noise, i.e., one obtains autocorrelation of $\ddot{x}_g$ as

$$E[\ddot{x}_g(t)\ddot{x}_g(\tau)] = Q\delta(t-\tau), \tag{5}$$

where Q is a time invariant constant. Its power spectral density S_g can be obtained by applying Wiener-Khintchine relationship as,

$$S_g = \frac{1}{2\pi}\int_{-\infty}^{\infty} E[\ddot{x}_g(t)\ddot{x}_g(t-\tau)]e^{-i\omega\tau}d\tau = \frac{1}{2\pi}\int_{-\infty}^{\infty} Q\delta(\tau)e^{-i\omega\tau}d\tau = \frac{Q}{2\pi}. \tag{6a}$$

or

$$Q\delta(t-\tau) = E[\ddot{x}_g(t)\ddot{x}_g(t-\tau)] = \int_{-\infty}^{\infty} S_g e^{i\omega\tau}d\omega = 2\pi S_g\delta(\tau) \tag{6b}$$

Response $\mathbf{z}$ is expressed by,

$$\mathbf{z}(t) = \int_{-\infty}^{\infty} e^{\mathbf{F}(t-t_0)}H(t-t_0)\mathbf{G}\ddot{x}_g(t_0)dt_0 = \int_0^{\infty} e^{\mathbf{F}(\tau)}\mathbf{G}\ddot{x}_g(t-\tau)d\tau, \tag{7}$$

where $\mathbf{F} = \mathbf{F}_0 + \mathbf{F}_1$, and $H(t)$ is the Heaviside step function. Then, the covariance matrix is calculated as,

$$
\begin{aligned}
E[\mathbf{z}\mathbf{z}^T] &= E\left[\int_0^\infty e^{\mathbf{F}(\tau_1)}\mathbf{G}\ddot{x}_g(t-\tau_1)d\tau_1\left(\int_0^\infty e^{\mathbf{F}(\tau_2)}\mathbf{G}\ddot{x}_g(t-\tau_2)d\tau_2\right)^T\right] \\
&= \int_0^\infty\int_0^\infty e^{\mathbf{F}(\tau_1)}\mathbf{G}E\left[\ddot{x}_g(t-\tau_1)\ddot{x}_g(t-\tau_2)\right]\mathbf{G}^T e^{\mathbf{F}^T(\tau_2)}d\tau_1 d\tau_2 \\
&= \int_0^\infty\int_0^\infty e^{\mathbf{F}(\tau_1)}\mathbf{G}Q\delta(\tau_1-\tau_2)\mathbf{G}^T e^{\mathbf{F}^T(\tau_2)}d\tau_1 d\tau_2 \\
&= \int_0^\infty e^{\mathbf{F}(\tau)}\mathbf{G}Q\mathbf{G}^T e^{\mathbf{F}^T(\tau)}d\tau
\end{aligned}
\tag{8}
$$

When all the eigenvalues of $\mathbf{F}$ have negative real parts and the system is stable, the final integral value exists and can be calculated by solving the following Lyapunov equation (Bellman, 1995, Bryson and Ho, 1975).

$$\mathbf{F}\mathbf{Z}+\mathbf{Z}\mathbf{F}^T+\mathbf{G}Q\mathbf{G}^T=\mathbf{0} \tag{9}$$

where $\mathbf{Z}=E[\mathbf{z}\mathbf{z}^T]$. A powerful numerical procedure has been developed to solve this matrix equation(Bartels and Stewart, 1972), and it is employed in the numerical analyses in the next section.

The covariance matrix $E[\mathbf{z}\mathbf{z}^T]$ can also be calculated in frequency domain by,

$$E[\mathbf{z}\mathbf{z}^T]=\int_{-\infty}^{\infty}\mathbf{S}_z(\omega)d\omega \tag{10a}$$

$$\mathbf{S}_z(\omega)=[i\omega\mathbf{I}-\mathbf{F}]^{-1}\mathbf{G}S_g\mathbf{G}^T[-i\omega\mathbf{I}-\mathbf{F}]^{-T}. \tag{10b}$$

Evaluation of Eq.(10a) involves integration of infinite domain, which is not effective in numerical computation. Nevertheless, this method is also used in the next section, because Eq.(10a) is analytically integrated by looking at Cauchy principal values and tables for formulas can be found in literature (Crandall and Mark, 1963).

For stationary gaussian excitation, the mean value for peak response is given by multiplication of peak factor to root mean square response, as,

$$E[R_j]=p_j\sqrt{E[y_j^2]} \tag{11}$$

where y_j is the j-th response in y, R_j is its peak response value, and p_j is the corresponding peak factor. In Davenport (1964), the peak factor is obtained as a function of duration of excitation and mean zero crossing rate.

In seismic design, response spectra, which is the spectra of maximum response values for single degree of freedom structure, are usually defined according to the seismicity and other site conditions. This design response value can also be expressed as,

$$E[R_\xi]=p_\xi\sqrt{E[\xi^2]}, \tag{12}$$

using the peak factor. Then, the fraction of response R_j with respect to R_ξ can be written as,

$$\gamma=\frac{E[R_j]}{E[R_\xi]}=\frac{p_j\sqrt{E[y_j^2]}}{p_\xi\sqrt{E[\xi^2]}}. \tag{13}$$

The parameter γ is called normalized response in this paper. It represents the response reduction due to energy dissipation devices when R_j is the response of the structure with them and R_ξ is the response of structure without them. To simplify the analysis, the ratio p_j/p_ξ is approximated to be close to unity, because in practical range of natural frequencies and duration of excitation in earthquake engineering, the peak factor changes only within the range of 3 to 4. The same approximation is successfully applied in calculating seismic response of structures with multiple degree of freedom from the response spectra (Der Kiureghian, 1981). Hence, Eq. (13) is simplified to:

$$\gamma\approx\frac{\sqrt{E[y_j^2]}}{\sqrt{E[\xi^2]}}. \tag{14}$$

It can clearly be seen from the calculation of $E[\mathbf{z}\mathbf{z}^T]$, that mean square response is linearly proportional to the value of Q. Therefore the response reduction rate defined by (14) is independent of the strength of excitation and solely depends upon the system parameters. By minimizing this normalized response within the feasible range of stiffness and damping, the seismic response of structures are expected to be minimized, and the expected reduction of response spectra can be found by evaluating Eq. (14).

Because seismic response is evaluated by Eq. (14), seismic performance of the system can be defined by the summation of mean square responses as,

$$J = tr\left(E\left[\mathbf{y}\mathbf{y}^T\right]\right), \tag{15}$$

where, $tr()$ denotes the trace of matrix. Derivative of J with respect to $\mathbf{F}_1$ can be obtained by applying Bellman's expansion and Kleinman's lemma following the procedure presented in Levine and Athans(1970) and Xu, et. al. (1994):

$$\frac{dJ}{d\mathbf{F}_1} = 2\mathbf{HLZH}^T, \tag{16}$$

where

$$\mathbf{L} = \int_0^\infty e^{\mathbf{F}(\tau)} e^{\mathbf{F}^T(\tau)} d\tau, \tag{16a}$$

which can be calculated by

$$\mathbf{FL} + \mathbf{LF}^T + \mathbf{I} = \mathbf{0} \tag{16b}$$

The performance index J can be efficiently minimized by applying standard numerical optimization procedure such as steepest descent method or Davidon-Fletcher-Powell method along with derivative of Eq.(16)

3. APPLICATION TO SIMPLE BRIDGE STRUCTURES

The optimization method developed in the previous section is applied to simple structures and its validity is studied by numerical simulations using observed ground motion records at 1941 El Centro earthquake and 1995 Kobe earthquake. Two example structural systems are considered herein: (i) two oscillators connected by a damper, which can be considered as a simple model for deck connections, and (ii) bridge deck/pier system with base-isolation modeled by a two degree of freedom. Simple analytical formulas for optimal design values are also developed, which may be practically used in preliminary structural design.

3.1. DAMPERS AT DECK CONNECTIONS

Decks connected by a damper in Figure 1 are modeled by a 2 degrees of freedom system with equal masses in Figure 4, which can be considered as two consecutive spans in Figure 1 with fixed support bearings on one side and moving supports on the other. The equations of motion is :

$$\begin{bmatrix} m & 0 \\ 0 & m \end{bmatrix}\begin{bmatrix} \ddot{x}_1 \\ \ddot{x}_2 \end{bmatrix} + \begin{bmatrix} 2m\zeta_1\omega_1 + 2m\zeta_c\omega_1 & -2m\zeta_c\omega_1 \\ -2m\zeta_c\omega_1 & 2m\zeta_2\omega_2 + 2m\zeta_c\omega_1 \end{bmatrix}\begin{bmatrix} \dot{x}_1 \\ \dot{x}_2 \end{bmatrix} + \begin{bmatrix} m\omega_1^2 & 0 \\ 0 & m\omega_2^2 \end{bmatrix}\begin{bmatrix} x_1 \\ x_2 \end{bmatrix} = -\begin{bmatrix} m \\ m \end{bmatrix}\ddot{x}_g, \tag{17}$$

where x_1 and x_2 are the displacement of each deck, m is the mass of each deck, and $_{w1}$, ω_2 and ζ_1, ζ_2 are the natural frequencies and damping ratios of each pier. The damping coefficient of the connection is expressed as $2m\zeta_c\omega_1$, and hence, ζ_c is the design value of the connection damper.

One of the problems of interest for neighboring spans in earthquakes is the relative displacement between them, because the pounding between decks depends on it, and besides, moving supports need to allow expected relative displacement to prevent unseating of the deck (Kawashima and Sato, 1996, Jeng and Kasai, 1996). The maximum relative displacement x_2- x_1 when ζ_c =0 is shown in Figure 6. The response is normalized by displacement response spectrum with ω_1 and ζ_1, Three values of ω_1, i.e., 4π, 2π, and $4\pi/3$ are chosen, which corresponds to natural periods of 0.5[sec], 1[sec], and 1.5 [sec]. Both damping ratios ζ_1 and ζ_2 are set to 0.05. When the frequency ratio ω_2/ω_1 is equal to 1, no relative displacement is observed because both oscillators vibrates identically. As ω_2/ω_1 increases, the normalized displacement approaches to 1, because the second deck becomes much more rigid than the first deck. Solid line shows the normalized displacement predicted by Eq. (9). It can be seen that the value obtained by Eq. (9) predicts average tendency of the response.

Figure 7 (a) shows the relative displacement with respect to connection damping ζ_c when ω_2/ω_1=1.5. The relative displacement decreases by increasing ζ_c. However, smaller relative displacement means smaller energy dissipation, and the absolute displacement of each deck may increase. To observe this effect, square root of the sum of maximum displacement of each deck is plotted in Figure 7(b). The normalized displacement takes minimum value at small value of ζ_c and gradually increases with ζ_c. This optimal value of ζ_c to minimize response can be calculated by minimizing the value of Eq.(14) using Eq. (9). In this case, the optimal value is computed as ζ_c =0.217. Although responses subject to seismic records have large variation, the value ζ_c =0.217 gives good estimate of optimal values even for seismic excitation.

Simple analytical forms for the mean square response of relative and absolute displacements can be obtained when ζ_1 and ζ_2 are negligibly small.

$$E\left[(x_1 - x_2)^2\right] = \frac{\omega_1^2 + \omega_2^2}{2\zeta_c \omega_1^3 \omega_2^2} \tag{18a}$$

$$E\left[x_1^2\right] = \frac{\left(1+32\zeta_c^2\right)\omega_1^4 - 2\omega_1^2\omega_2^2 + \omega_2^4}{2\zeta_c \omega_1^3 \left(-\omega_1^2 + \omega_2^2\right)^2} \tag{18b}$$

$$E\left[x_2^2\right] = \frac{\omega_1^4 - 2\omega_1^2\omega_2^2 + 32\zeta_c^2\omega_1^2\omega_2^2 + \omega_2^4}{2\zeta_c \omega_1 \omega_2^2 \left(-\omega_1^2 + \omega_2^2\right)^2} \tag{18c}$$

Eq. (18a) clearly shows the inversely proportional relationship between relative displacement and the connection damping. Hence, increasing ζ_c always reduces relative displacement. Design formula for optimal damping to reduce square root of sum of absolute displacements can also derived by minimizing J=E[x_1^2]+E[x_2^2] as,

$$\zeta_c = \frac{\sqrt{-\omega_1^4\omega_2^2 + \omega_1^6 - \omega_1^2\omega_2^4 + \omega_2^6}}{8\omega_1^2\omega_2} \tag{19}$$

Design value obtained by Eq. (19) is 0.188, which is close to the optimal value 0.217.

3.2. BEARINGS

Bridge pier/deck system is modeled by a two degrees of freedom structure shown in Figure 8.

$$\begin{bmatrix} m_1 & 0 \\ m_2 & m_2 \end{bmatrix}\begin{bmatrix} \ddot{x}_1 \\ \ddot{x}_2 \end{bmatrix} + \begin{bmatrix} 2m_1\zeta_1\omega_1 & -2m_2\zeta_b\omega_1 \\ 0 & 2m_2\zeta_b\omega_1 \end{bmatrix}\begin{bmatrix} \dot{x}_1 \\ \dot{x}_2 \end{bmatrix} + \begin{bmatrix} m_1\omega_1^2 & -m_2\omega_b^2 \\ 0 & m_2\omega_b^2 \end{bmatrix}\begin{bmatrix} x_1 \\ x_2 \end{bmatrix} = -\begin{bmatrix} m_1 \\ m_2 \end{bmatrix}\ddot{x}_g \tag{20}$$

where x_1 is the displacement of the pier relative to the ground and x_2 is the displacement the deck relative to the pier. Masses of the pier and the deck are denoted by m_1 and m_1, andω_1, and ζ_1 are the natural frequency and the damping ratio of the pier. Design values of bearings are the spring and damping constants between the pier and the deck, i.e., ω_b and ζ_b.

Figure 9 shows the effects of bearing damping ratio ζ_b to the responses of the pier x_1 and deck x_2, where frequency ratio is set to ω_2/ω_1=0.1. This frequency ratio is taken to simulate the effect of base-isolation. Again, three values of ω_1, i.e., 4π, 2π, and $4\pi/3$ are used. Damping ratio of the pier ζ_1 is 0.05, and the deck mass m_2 = $5m_1$, which reflects the values for typical urban elevated highway bridges. The response is normalized by response of single degree of freedom structure with natural frequency $\omega_1/\sqrt{1+\mu}$ and damping ratio $\zeta_1/\sqrt{1+\mu}$, which corresponds to the response of the pier when the deck is not base-isolated but fixed. Both responses x_1 and x_2 are decreasing for smaller values of ζ_b, but response of the pier increases with excessive damping. When ζ_b is large, transmission of inertia force from the deck to the pier increases although deck displacement relative to the pier is suppressed naturally. The value of ζ_b to minimize the pier response can be found through minimization of Eq. (14) as 0.0481.

Analytical expressions for mean square response can be developed when the damping of the pier ζ_1 is neglected:

$$E\left[x_1^2\right] = \frac{Q}{\omega_1^3}\left\{\frac{1-(1+\mu)^2(2-\mu)f^2 + (1+\mu)^4 f^4}{4\mu\zeta_b} + \frac{\zeta_b(1+\mu)^3}{\mu}\right\}, \tag{21a}$$

$$E\left[x_2^2\right] = \frac{Q}{4\mu\zeta_b\omega_1^3}\left\{(1+\mu)^2 + \frac{\mu}{f^2}\right\}, \tag{21b}$$

where f=ω_2/ω_1, and μ= m_2/m_1. The deck response of Eq.(21b) is monotonically decreasing with respect to f and ζ_b. The pier response of Eq.(21a) can be minimized by taking the values of

$$\omega_2 = \frac{\sqrt{1-\mu/2}}{1+\mu}\omega_1 \tag{22a}$$

$$\zeta_b = \frac{1}{2}\sqrt{\frac{\mu(1-\mu/4)}{(1+\mu)^3}} \tag{22b}$$

when $\mu \le 2$, and

$$\omega_2 = 0 \tag{23a}$$

$$\zeta_b = \frac{1}{2\sqrt{(1+\mu)^3}} \tag{23b}$$

when $\mu \geq 2$. Because $\mu \geq 2$ for ordinary elevated highway bridges, the latter set of formulas will be applied in most cases. Eq. (22) is known as the optimal parameters of dynamic vibration absorber (Warburton, 1981).

Sensitivity of responses with respect to f is shown in Figure 10. The same parameters of the calculation of Figure 9 is used except for f and ζ_b of Eq.(26) is used. The pier displacement is monotonically increasing while the deck displacement is monotonically decreasing. The optimal value for f could be obtained by specifying certain weights on both the pier and the deck displacements.

Figure 11 shows the pier response normalized by response of single degree of freedom structure with natural frequency ω_1 and damping ratio ζ_1, which corresponds to the response of the pier when the deck is perfectly sliding and no inertia force is transmitted. Here, the frequency ratio f is set to 0, while all other values are the same as the previous computation. The optimal damping ζ_b is numerically found to be 0.0245, while the design value obtained by Eq. (23b) is 0.0340. For small values of ζ_b, the response is smaller than unity. It implies that the weak connection between the deck and the pier is more desirable than perfect isolation of the deck. This is because the deck behaves as a dynamic absorber and dissipates energy.

4. SUMMARY

Simple method for optimization of passive systems subject to seismic excitation is constructed, and is applied to design of gap dampers and bearings of bridges.

Major conclusions are summarized as follows:

1. Simple optimization method where ground motion is assumed to be stationary gaussian white noise is proposed and its validity is studied by numerical simulations using observed ground motion records. Numerical results show that the prediction by the current method gives average tendency of seismic response and can be used to obtain optimal design values.
2. The proposed method is applied to two simple but important problems in seismic design of bridges, i.e., dampers attached at gaps of decks and bearings. Design values to minimize responses in the decks and piers are found and trade-off between them are discussed.
3. Simple formulas which can be used in preliminary design are derived by analytically finding the minimum point of the mean square response.

Analysis in this paper is based upon the assumption that ground motion is stationary gaussian white noise and the structure is linear elastic. Validity and restriction of the first assumption are discussed by numerical simulations using ground motion records. Although applicability of the second assumption is not discussed in this paper, the proposed optimization may be extended to nonlinear elasto-plastic structures by applying appropriate equivalent linearization.

ACKNOWLEDGMENT

The research work in this paper is supported by the Scientific Research Grant (Fundamental Research B, No. 08455209) of the Ministry of Education, Science and Culture of Japan. This support is gratefully acknowledged.

REFERENCES

Bartels, R. H. and Stewart, G. W., 1972, "Solution of the matrix equation AX+XB=C," Communications of the ACM, **15**, 820-826.

Bellman, R., 1995, *Introduction to Matrix Analysis*, Society for Industrial and Applied Mathematics, Philadelphia.

Bryson, A. E., Jr. and Ho, Y-C, 1975, *Applied Optimal Control*, Hemisphere, New York.

Caughey, T. K., 1960 "Random excitation of a system with bilinear hysteresis," *J. Applied Mech.*, ASME, **27**, 649-652.

Crandall, S. H. and Mark, W. D., 1963, *Random Vibrations in Mechanical Systems*, Academic Press, New York.

Davenport, A. G., 1964, "Note on the distribution of the largest value of a random function with application to gust loading," *Proceedings of the Institute of Civil Engineers*, **28**, 187-196.

Der Kiureghian, A., 1981, "A response spectrum method for random vibration analysis of MDF systems," *Earthquake Engineering and Structural Dynamics*, **9**, pp.419-435.

Jeng, V. and Kasai, K., 1996, "Spectral relative motion of two structures due to seismic travel waves," *Journal of Structural Engineering*, ASCE, **122**, pp.1128-1135.

Kawashima, K., and Sato, T., 1996, "Relative displacement response spectrum and its application," *Journal of Structural Engineering*, JSCE, **42A**, pp.645-652 (in Japanese).

Levine, W. S., and Athans, M, 1970, "On the determination of the optimal constant output feedback gains for linear multivariable systems," IEEE Transactions on Automatic Control, **AC-15**, pp.44-48.

Shinozuka, M., 1996, "Use of visco-elastic dampers to suppress seismic vibration of bridges," *Fourth U.S.-Japan Workshop on Earthquake Protective Systems for Bridges*, Osaka, Japan.

Skinner, R. I., Robinson, W. H., and McVerry, G. H., 1993, *An Introduction to Seismic Isolation*, John Wiley & Sons.

Warburton, G. B., 1981, "Optimum absorber parameters for minimizing vibration response," *Earthquake Engineering and Structural Dynamics*, **9**, pp.251-262.

Xu, K., Warnitchai, P., and Igusa, T., 1994, "Optimal placement and gains of sensors and actuators for feedback control," *Journal of Guidance, Control and Dynamics*, AIAA, **17**, pp.929-934.

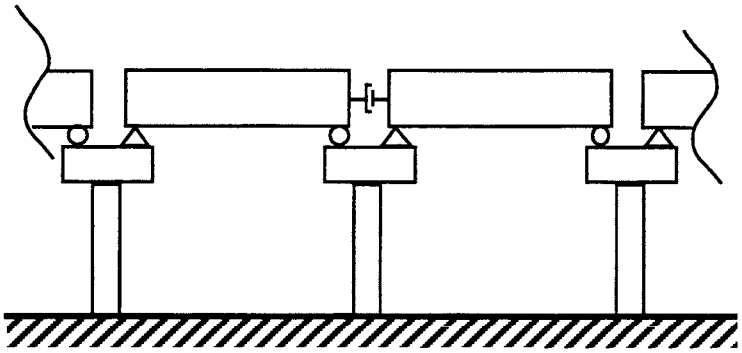

Figure 1 Simply supported bridges with deck connection dampers.

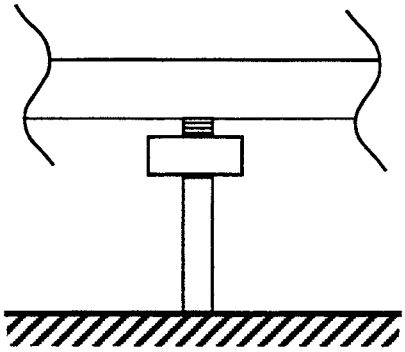

Figure 2 Bridge with elastomeric bearings.

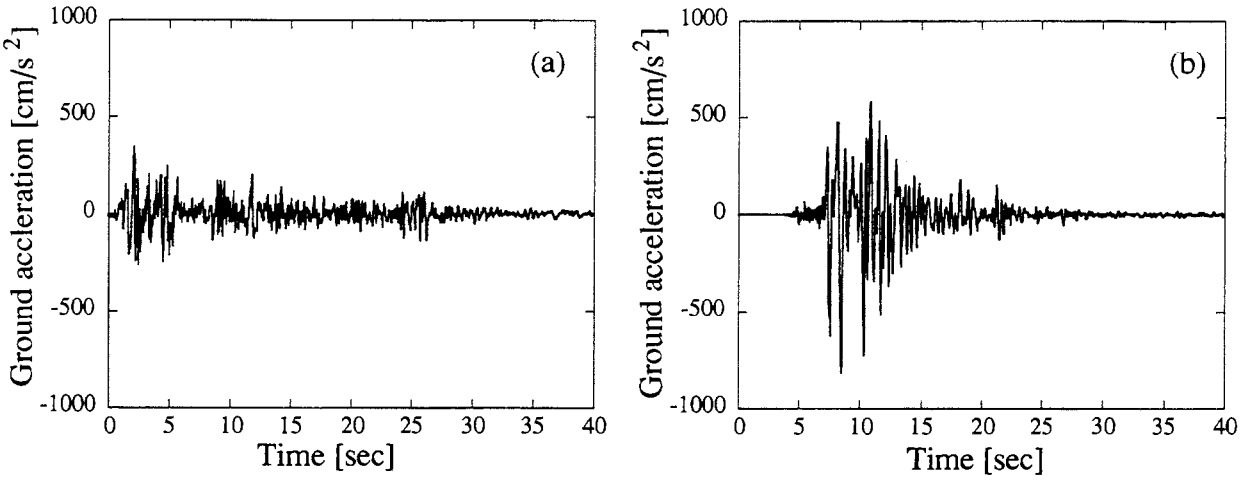

Figure 3. Accelerograms of (a) 1941 Elcentro and (b) 1995 Kobe earthquakes.

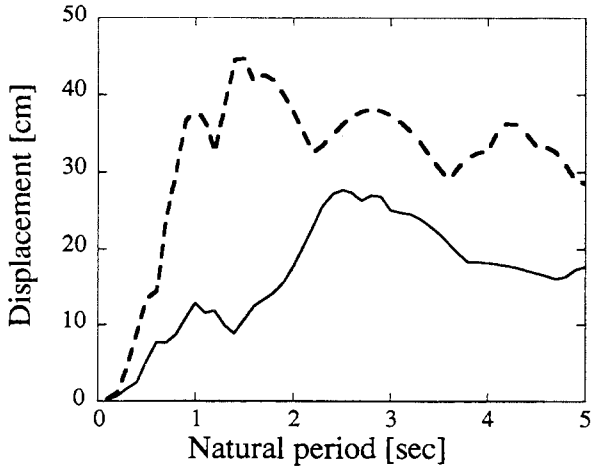

Figure 4. Displacement response spectra of 1941 Elcentro (———) and 1995 Kobe (- - - - - -) earthquakes.

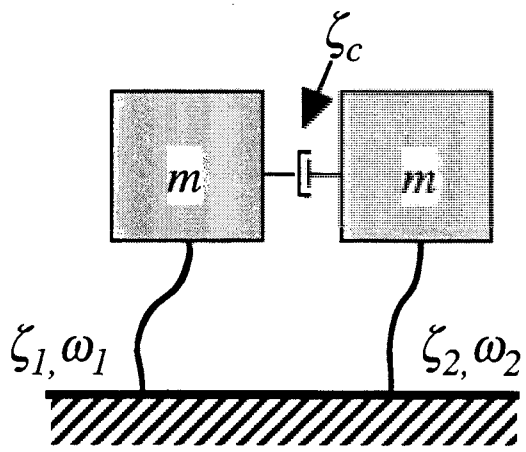

Figure 5. Two degree of freedom model for simply supported bridges with dampers at deck connection.

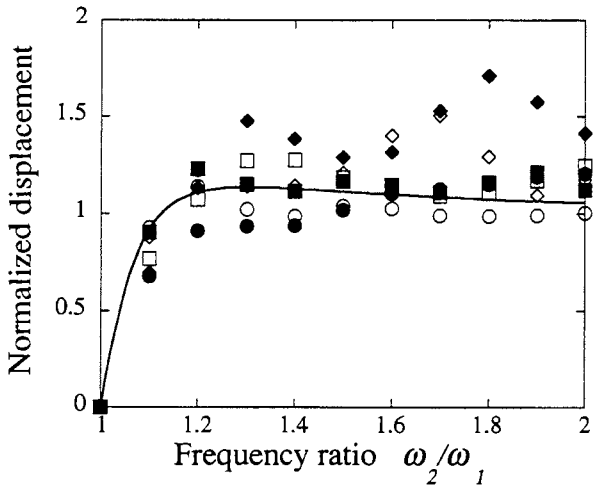

Figure 6. Normalized relative displacement between decks.

———: theory,

● : El Centro with $\omega_1=4\pi$, ■ : El Centro with $\omega_1=2\pi$, ◆ : El Centro with $\omega_1=4\pi/3$,

○ : Kobe with $\omega_1=4\pi$, □ : Kobe with $\omega_1=2\pi$, ◇ : Kobe with $\omega_1=4\pi/3$.

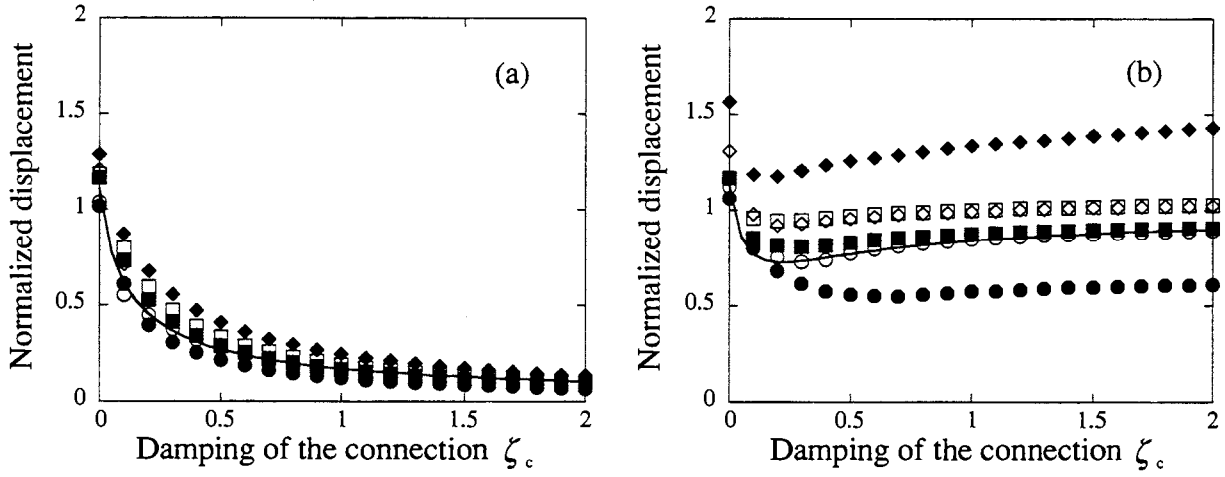

Figure 7. Normalized displacement with deck connection damper, (a) relative displacement between decks, (b) square root of sum of absolute displacement of both decks.

———: theory,

● : El Centro with $\omega_1=4\pi$, ■ : El Centro with $\omega_1=2\pi$, ◆ : El Centro with $\omega_1=4\pi/3$,

○ : Kobe with $\omega_1=4\pi$, □ : Kobe with $\omega_1=2\pi$, ◇ : Kobe with $\omega_1=4\pi/3$.

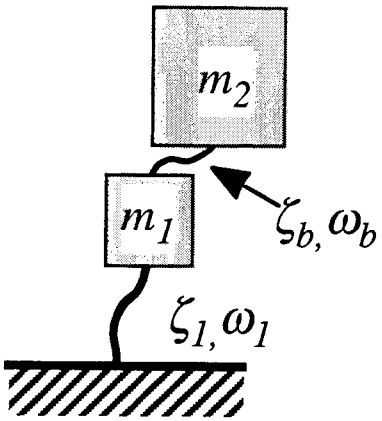

Figure 8. Two degree of freedom model for a bridge supported by elastomeric bearing.

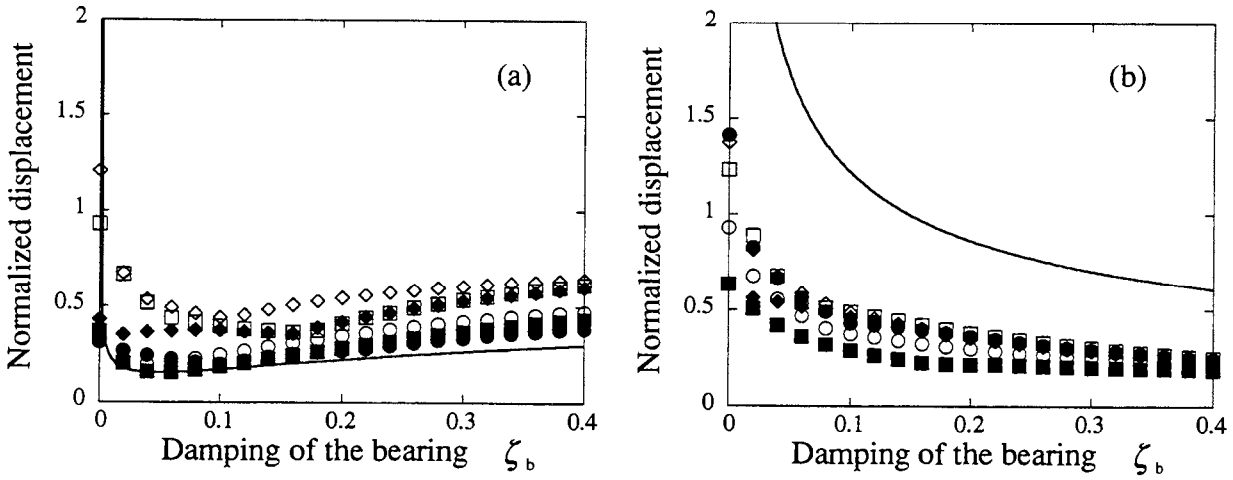

Figure 9. Normalized displacement with elastomeric support (μ=5, f=0.1, ζ_1=0.05), (a) pier displacement, (b) deck displacement.

———: theory,

●: El Centro with $\omega_1=4\pi$, ■: El Centro with $\omega_1=2\pi$, ◆: El Centro with $\omega_1=4\pi/3$,

○: Kobe with $\omega_1=4\pi$, □: Kobe with $\omega_1=2\pi$, ◇: Kobe with $\omega_1=4\pi/3$.

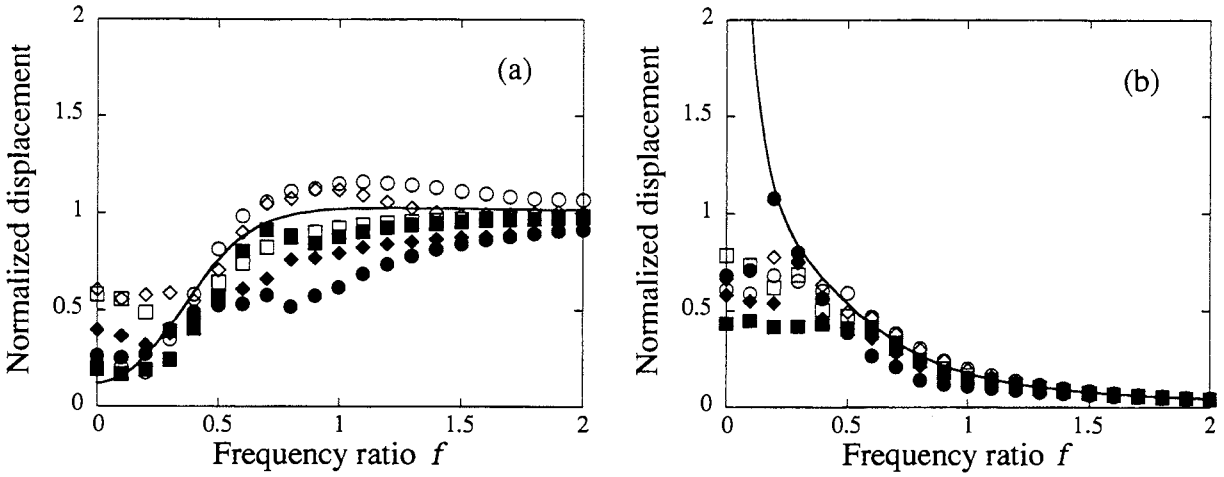

Figure 10. Normalized displacement with elastomeric support (μ=5, $\zeta_b = 0.5/\sqrt{(1+\mu)^3} = 0.340$, ζ_1=0.05), (a) pier displacement, (b) deck displacement.

———: theory,

●: El Centro with $\omega_1=4\pi$, ■: El Centro with $\omega_1=2\pi$, ◆: El Centro with $\omega_1=4\pi/3$,

○: Kobe with $\omega_1=4\pi$, □: Kobe with $\omega_1=2\pi$, ◇: Kobe with $\omega_1=4\pi/3$.

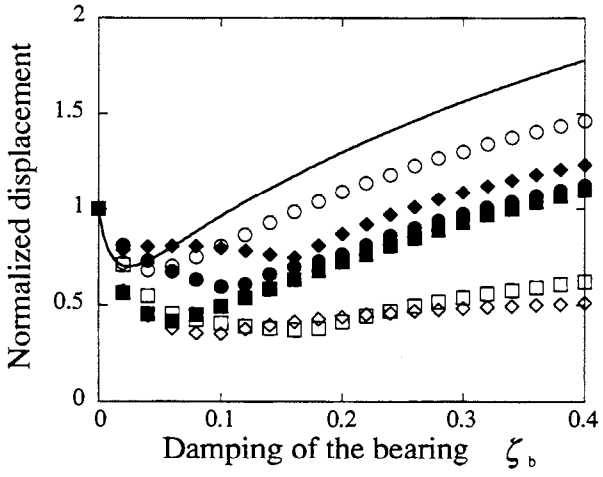

Figure 11. Pier displacement normalized by response of perfectly isolated condition (μ=5, f=0, ζ_1=0.05).

———: theory,

●: El Centro with $\omega_1=4\pi$, ■: El Centro with $\omega_1=2\pi$, ◆: El Centro with $\omega_1=4\pi/3$,

○: Kobe with $\omega_1=4\pi$, □: Kobe with $\omega_1=2\pi$, ◇: Kobe with $\omega_1=4\pi/3$.

PROPERTY MODIFICATION FACTORS AND RESPONSE MODIFICATION FACTORS FOR SEISMICALLY ISOLATED HIGHWAY BRIDGES

M.C. Constantinou, P. Tsopelas and J. Quarshie
Department of Civil Engineering, State University of New York
Buffalo, New York

ABSTRACT

The ballot version of the 1997 AASHTO Guide Specifications for Seismic Isolation Design (March 1997) [1] contains a number of modifications and improvements over its predecessor, the 1991 AASHTO Guide Specification [2]. Of these, two major changes are (a) the introduction of isolator Property Modification Factors, and (b) the specification of substructure Response Modification Factors that are lower than those of non-isolated bridges. This paper presents the rationale behind these modifications and some research results that led to the establishment of the aforementioned factors.

INTRODUCTION

The design of seismically isolated highway bridges is based on the prediction of isolator displacements and forces, and of forces acting on the bridge substructure. This prediction is primarily dependent on the force-displacement characteristics of the isolation system and on the characteristics of the seismic excitation.

The force-displacement characteristics of isolation systems are affected by the environment (e.g., temperature), history of loading, variability in properties and aging. This leads to the requirement for consideration of bounding values of isolator parameters based on a rational analysis of the effects of environment, aging, etc. For this purpose, the 1997 AASHTO Guide Specifications (ballot version) introduce Property Modification Factors (or λ-factors). These factors apply on isolator properties (which are established by testing) to produce maximum and minimum nominal values of properties for bounding analysis.

The design of highway bridges in the United States is based on the calculation of forces resulting from the assumption of elastic substructure response, and subsequently dividing these forces by appropriate Response Modification Factors (R-factors) which account for substructure inelastic behavior. It is argued and demonstrated in this paper that R-factors for isolated bridges should be lower than R-factors for non-isolated bridges. The underlying reasons for this are: (a) elastic or nearly elastic substructure behavior is required for proper behavior of the isolation system, and (b) seismically isolated bridges exhibit more sensitivity of the substructure response to the variability in the seismic input.

PROCEDURES FOR ESTABLISHING BOUNDING VALUES OF PROPERTIES OF SEISMIC ISOLATION HARDWARE

Seismic isolation hardware exhibits behavior that may be typified for the lateral force-displacement loop of Fig. 1. The important properties that describe this behavior are the characteristic strength Q_b and the stiffness K_b. Both of these properties may be affected by the environmental conditions, aging, etc.

The developed procedures establishes maximum and minimum nominal values of a property, P_{max} and P_{min} respectively, based on a value of property P (e.g., strength Q_b or stiffness K_b) which is established by testing of new specimens at normal temperature and at the relevant conditions of axial load, amplitude of motion, and frequency or velocity of motion. The nominal values are

$$P_{max} = \lambda_{max} P \ , \ P_{min} = \lambda_{min} P \tag{1}$$

where λ_{max} and λ_{min} are factors (respectively larger and less than unity) to account for the aforementioned effects of environment, aging, etc.

The λ_{max} and λ_{min} factors consist of the product of several λ-factors, each one of which accounts for a specific effect. For example,

$$\lambda_{max} = \lambda_{max,t} \cdot \lambda_{max,a} \cdot \lambda_{max,c} \cdots \tag{2}$$

where $\lambda_{max,t}$ is the factor for temperature effect and so on. The establishment of the λ-factors is based on experimental results, engineering judgment and considerations of likelihood of simultaneous occurrence of several extreme events (i.e., lowest temperature, design basis earthquake, etc.). On the latter, the use of adjustment factors that reflect the importance of the bridge has been proposed. That is, adjustment factors of 1.0 for critical bridges, 0.75 for essential bridges and 0.66 for all other bridges have been proposed. The adjustment factors apply to that portion of a λ-factor that deviates from unity. For example, if $\lambda_{max,t} = 1.20$ before adjustment, the adjusted factor will be $1 + 0.75 \times 0.20 = 1.15$ for an essential bridge.

λ-FACTORS FOR SLIDING ISOLATION SYSTEMS

A research project at the University at Buffalo under the Highway Program at the National Center for Earthquake Engineering Research concentrated on the establishment of bounding values of frictional properties of sliding isolation systems. The project resulted in the proposition of the λ-factor approach as described in the previous section, which was incorporated in the 1997 AASHTO Guide Specifications for Seismic Isolation Design.

Sliding isolation systems exhibit, in general, the behavior illustrated in Fig. 1. The characteristic strength Q_b is the product of the coefficient of friction and axial load. Stiffness K_b may be provided by various means, such as elastomeric bearings or the use of a spherical sliding surface (Friction Pendulum or FPS Bearings). In general, both properties Q_b and K_b are affected by the environment, aging, etc., with exception of the FPS system for which the stiffness cannot change. However, the most important property of sliding isolation systems is the coefficient of friction.

It is recognized that the coefficient of friction of sliding bearings is affected by parameters such as composition of sliding interface, bearing pressure, velocity of sliding, temperature, contamination, travel (that is, cumulative distance traveled due to thermal changes and traffic) and aging. Herein, aging is defined as the process of changing frictional properties with time that may be affected by a variety of phenomena, such as a corrosion, change of the true area of contact due to viscoelastic effects, etc.

A number of researchers have studied the effects of temperature, contamination and travel on the coefficient of friction of selected sliding interfaces [3-5]. While these studies provide valuable information on the behavior of sliding bearings, the reported results are restricted to quasi-static conditions, that is, they do not necessarily apply for the conditions of high velocity motion encountered in an earthquake. Accordingly, tests under dynamic conditions were conducted on a number of sliding interfaces to evaluate the effects of temperature, surface roughness (in an attempt to quantify the effects of corrosion) and short cumulative travel.

Fig. 2 shows results on the effect of surface roughness on the sliding coefficient of friction of unfilled PTFE at pressure of 20.7 MPa (3000 psi). Stainless steel of grade 304 has been used at surface roughness of 0.03 μm R_a (mirror finish), 0.30 μm R_a (unpolished) and 0.5 μm R_a. Measurements of friction force were obtained under harmonic motion and in the first half cycle of movement, following travel of less than 25 mm. That is, the stainless steel surface was not allowed to be coated with a film of PTFE prior to measurement of friction. The results indicate a minor effect of roughness on the high velocity coefficient of friction (say, velocities above 25 mm/s). This may be explained by the presumption that at high velocities of sliding, friction is primarily the result of shearing of PTFE in its bulk.

Relating surface roughness to surface corrosion is, of course, difficult. The tested surface was uniformly rough but not corroded. Corrosion is, typically, non-uniform and part of corroded particles can be rather easily removed by the moving PTFE sheet. That is, it is believed that the effects of corrosion are not as severe as those of uniform surface roughness. Nevertheless, conservatism has been exercised in preparing Table 1 which presents values of factor $\lambda_{max,\,a}$, that is, for aging, of unlubricated unfilled PTFE-stainless steel interfaces. Distinction is made between sealed and unsealed conditions and normal and severe environments. It has been assumed that unsealed conditions will allow

exposure to water and salt, thus promoting corrosion. Moreover, environments such as industrial and marine (severe) are assumed to further promote corrosion [6].

Fig. 3 presents results on the coefficient of friction of unfilled PTFE in contact with polished stainless steel at pressure of 20.7 MPa (3000 psi) and temperature in the range of 50°C (122°F) to -40°C (-40°F). Interfaces were maintained at the indicated temperatures within the testing arrangement for a period not more than about 3 hours. Testing was conducted by moving the slider to a displacement of not more than 25 mm under very low speed (this allowed measurement of breakaway friction [7]) and subjecting the interface to cyclic harmonic motion. Measurement of the friction coefficient under dynamic conditions was made following one quarter cycle or travel of not more than 25 mm. That is, the interfaces were not subjected to significant movement that would have allowed increase of temperature due to frictional hearing.

Of interest in Fig. 3 is to observe the substantial effect of temperature on the breakaway coefficient of friction (these results are in very good agreement with those reported by Campbell [4]). However, the effect of temperature in the high velocity region is substantially less, due, apparently, to the effects of frictional heating. Table 2 presents $\lambda_{max,\,t}$ factors that reflects this observation. Note that the table is based on the presumption that the reference coefficient of friction is established at the temperature of 70°F (21°C). Moreover, the lowest considered temperature is -22°F (-30°C), which is 75% of the extreme temperature specified in the AASHTO Standard Specifications.

Table 2 presents also $\lambda_{max,\,t}$ factors for other isolation bearings as they will appear in the 1997 AASHTO Guide Specifications. These factors apply for the determination of bounding values of the characteristic strength Q_b.

λ-factors for the coefficient of friction of sliding bearings have been also developed for the effects of travel (cumulative travel due to traffic and thermal movement) and contamination. Particularly with respect to travel, test data at high velocities of sliding are limited to travel of less than about 2 km. For example, Fig. 4 presents values of the coefficient of friction of an unfilled PTFE-polished stainless steel interface at pressure of 20.7 MPa (3000 psi) and travel of up to 500 m. The interface was subjected to low velocity motion of either 0.8 or 2.4 mm/s, and periodically subjected to higher velocity cycling to obtain measurements of friction. It is observed that the high velocity friction coefficient (f_{max}) reduces and then shows a small tendency to increase with increasing travel. It is likely that f_{max} will remain below the initial, first cycle value for travel of over 1 km. Accordingly, $\lambda_{max,\,tr}$ for this interface is specified as 1.0 when travel is less than 1 km, as 1.2 when travel is less than 2 km, while testing would be required for longer travel.

RESPONSE MODIFICATION FACTORS FOR ISOLATED BRIDGES

The 1991 AASHTO Guide Specifications [2] specify Response Modification Factors (R-factors) for substructures that are the same as those for non-isolated bridges.

Accordingly, it would have been possible to arrive at designs in which the substructure strength is lesser than the characteristic strength of the isolation system. This would have resulted in excessive inelastic action in the substructure, with the isolation system rendered ineffective.

Recognizing this potential problem, the 1997 AASHTO Guide Specifications [1] specify R-factors for isolated bridges that are in the range of 1.5 to 2.5, that is, R-factors are about one half of those used for non-isolated bridges (which are in the range of 2 to 5).

The R-factor consists of three multiplied components, namely a portion related to material overstrength (value of 1.5), a portion related to redundancy and a portion related to ductility [8]. The latter portion is the one of concern in the design of isolated bridges. It may be shown that an R-factor of 1.5 to 2.5 for isolated bridges corresponds to a ductility-based portion in the range of 1.0 to about 1.5. The corresponding range of the ductility-based portion of R-factor for non-isolated bridges is 1.0 to 3.0.

A study has been conducted to investigate the ductility demand in substructures of non-isolated and isolated bridges designed with ductility-based R-factor in the range of 1.0 to 3.0 and 1.0 to 1.5, respectively. Fig. 5 illustrates the simple model utilized in the case of the isolated bridge. For the non-isolated bridge, the isolation system was simply rigid.

In both cases the redundancy-based R-factor is unity, whereas material overstrength has not been considered. The pier is considered to have perfect bilinear hysteretic behavior with post-yielding stiffness equal to 0.05 (parameter α in Fig. 5) times the elastic stiffness.

Analysis of the studied bridges was performed by the single-mode spectral method in the case of the non-isolated bridge and by the uniform load method in the case of the non-isolated bridge. The design basis earthquake was the one for A = 0.4, soil profile type II per AASHTO. The analysis resulted in a value for the statically equivalent seismic force under elastic substructure conditions. This value was subsequently divided by the ductility-based portion of the R-factor to obtain the actual strength of the substructure. The bridge model with the actual pier strength was then analyzed by the time-history method giving due account for the nonlinear behavior of the isolation system and pier. The input excitation consisted of 20 components which have been consistently scaled to represent the response spectrum in an average sense.

Fig. 6 presents the calculated average pier ductility ratio (defined as the pier maximum displacement divided by the pier yield displacement) for the non-isolated bridge. Period T is the elastic period of the bridge. Values of the average ductility ratio range between 1.0 and 4.5 for ductility-based R-factor in the range of 1.0 to 3.0.

For the isolated bridge, there is a wide range of parameters to consider. In the results presented herein, the ratio of tributary deck weight to effective pier weight W_d/W_p

has been 10 and the pier elastic period T_p has been either 0.1 or 0.5 sec. Note that period T_p is defined as

$$T_p = 2\pi\left(\frac{W_p}{gK_p}\right)^{1/2} \tag{3}$$

where K_p is the pier elastic stiffness. That is, a value of $T_p = 0.1$ sec represents the case of a stiff, but not excessively stiff, pier. Moreover, the characteristic strength of the isolation system, Q_b, was varied in the range of 0.04 to 0.10 W_d and the period of the isolation system, as represented by quantity T_b, was varied in the range of 1.5 to 3.0 sec. Quantity T_b is defined as

$$T_b = 2\pi\left(\frac{W_d}{gK_b}\right)^{1/2} \tag{4}$$

That is, T_b represents the period based on the post-yielding stiffness.

Fig. 7 presents average pier ductility ratios for the isolated bridge in the four cases of combination of T_p (=0.1 and 0.5 sec) and ductility-based R-factor (=1.0 and 1.5). It may be observed that average ductility ratios are in the same range as those of the non-isolated bridge (Fig. 6) except for the case of the stiff pier and R-factor of 1.5. In this case, the ductility ratio for the very flexible isolation systems may reach large values.

The presented results clearly demonstrate the need for lower R-factors in isolated bridges than in non-isolated bridges. Moreover, it is worthy of noting in Figures 6 and 7 the difference in the ductility ratio between non-isolated and isolated bridges in the case of ductility-based R-factor of 1.0. This represents the case of elastic substructure design. Nevertheless, inelastic action in the substructure may occur due to variability in the characteristics of earthquake excitation. The effect of this variability appears to be significant in the case of isolated bridges. It is believed that the use of overall R-factors in the range of 1.5 to 2.5 for isolated bridges would result in substructure ductility demands which are comparable to those in non-isolated bridges designed with overall R-factors in the range of 2.0 to 5.0.

ACKNOWLEDGEMENTS

Financial support for this work has been provided by the National Center for Earthquake Engineering Research, Highway Project.

REFERENCES

1. American Association of State Highway and Transportation Officials (AASHTO), Guide Specifications for Seismic Isolation Design, March 1997 (ballot version).

2. American Association of State Highway and Transportation Officials (AASHTO), Guide Specifications for Seismic Isolation Design, 1991.

3. Campbell, T.I., Fatemi, M.J. and Manning, D.G. "Friction in Bridge Bearings with Contaminated TFE Slide Surface". *J. Struct. Engng., ASCE,* 119 (11), 3169-3177, 1993.

4. Campbell, T.I., Pucchio, J.B., Roeder, C.W. and J.F. Stanton, "Frictional Characteristics of PTFE Used in Slide Surfaces of Bridge Bearings." Proc., 3rd World Congress on Joint Sealing and Bearing Systems for Concrete Structures, Toronto, Canada, 1991 (available in Preprint form from National Center for Earthquake Engineering Research, Buffalo, NY).

5. Kauschke, W. and Baigent, M. "Improvements in the Long Term Durability of Bearings in Bridges, Especially of PTFE Slide Bearings." Proc., 2nd World Congress on Joint Sealing and Bearing Systems for Concrete Structures, San Antonio, Texas, 1986 (publication SP-94 of American Concrete Institute).

6. American Society of Metals. Corrosion, Vol. 13 of Metals Handbook, 9th Edition, 1987.

7. Mokha, A., Constantinou, M.C. and Reinhorn, A.M. Teflon Bearings in Aseismic Base Isolation: Experimental Studies and Mathematical Modeling. Report No. NCEER-88-0038, National Center for Earthquake Engineering Research, Buffalo, NY.

8. Uang, C-M. "Establishing R (or R_w) and C_d Factors for Building Seismic Provisions". *J. Struct. Engng.*, ASCE, 117 (1), 19-28, 1991.

Table 1: λ_{max} - Factor for Aging of Unlubricated PTFE Sliding Bearings

	Condition	
Environment	Sealed	Unsealed
Normal	1.1	1.2
Severe	1.2	1.5

Values are for 30 year exposure of stainless steel. For chrome-plated carbon steel multiply values by 3.0.

Table 2: λ_{max} - Factor for Temperature Effect on Characteristic Strength

Minimum Temp for Design °F (°C)	Unlubricated PTFE Sliding Bearings	Lead-rubber Bearings	High Damping Rubber Bearings
70 (21)	1.0	1.0	1.0
32 (0)	1.1	1.3	1.1-1.2*
14 (-10)	1.2	1.4	1.2-1.4*
-22 (-30)	1.5	1.5	1.4-2.0*

*Lowest value is for bearings with small difference between scragged and unscragged properties. Highest value is for bearings with at least 25 percent difference between unscragged and scragged properties.

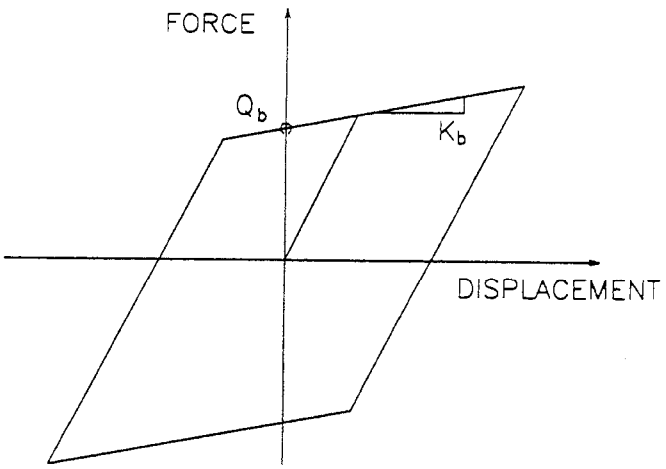

Fig. 1 Idealized Force-Displacement Relation of Isolation Bearings.

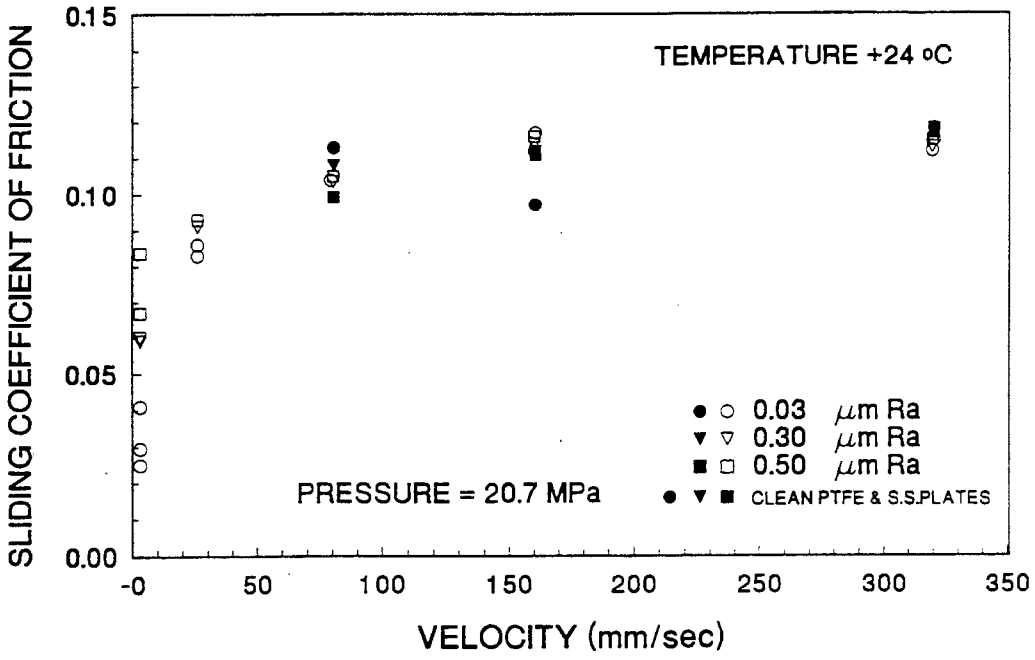

Fig. 2 Effect of Surface Roughness on Coefficient of Friction of Unfilled PTFE Sliding Bearings.

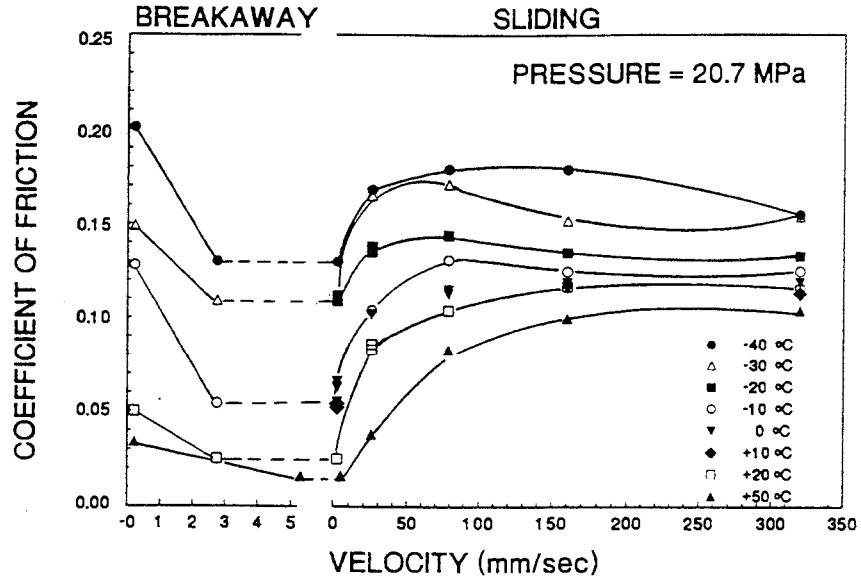

Fig. 3 Effect of Temperature on Coefficient of Friction of Unfilled PTFE Sliding Bearings.

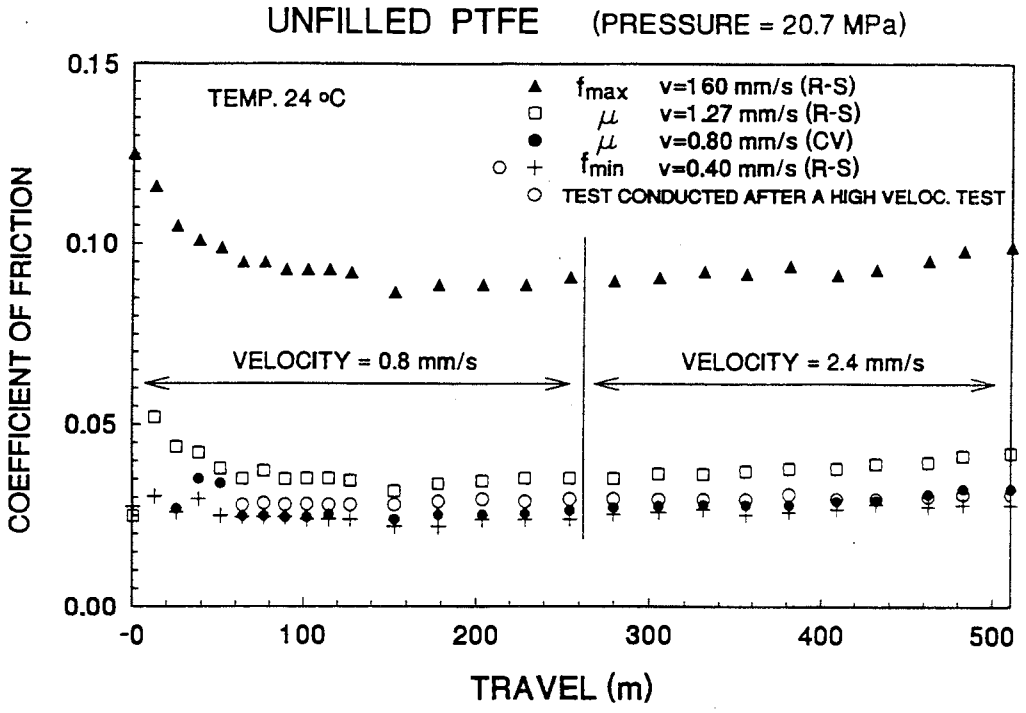

Fig. 4. Effect of Cumulative Travel on Coefficient of Friction of Unfilled PTFE Sliding Bearings.

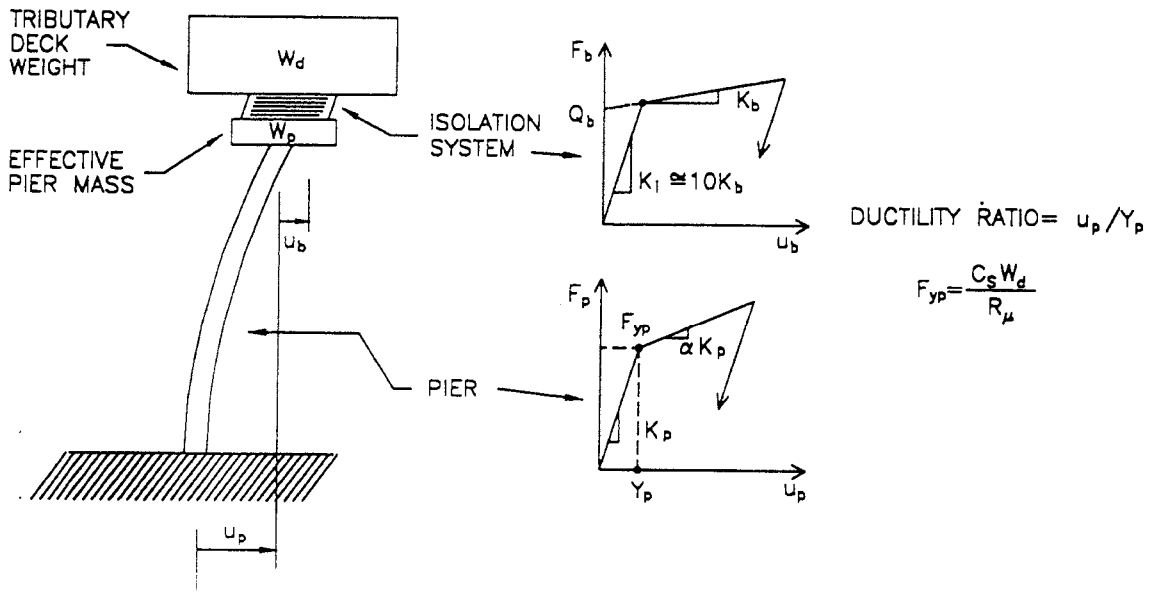

Fig. 5 Model of Isolated Bridge Used in Analysis of Substructure Inelastic Response.

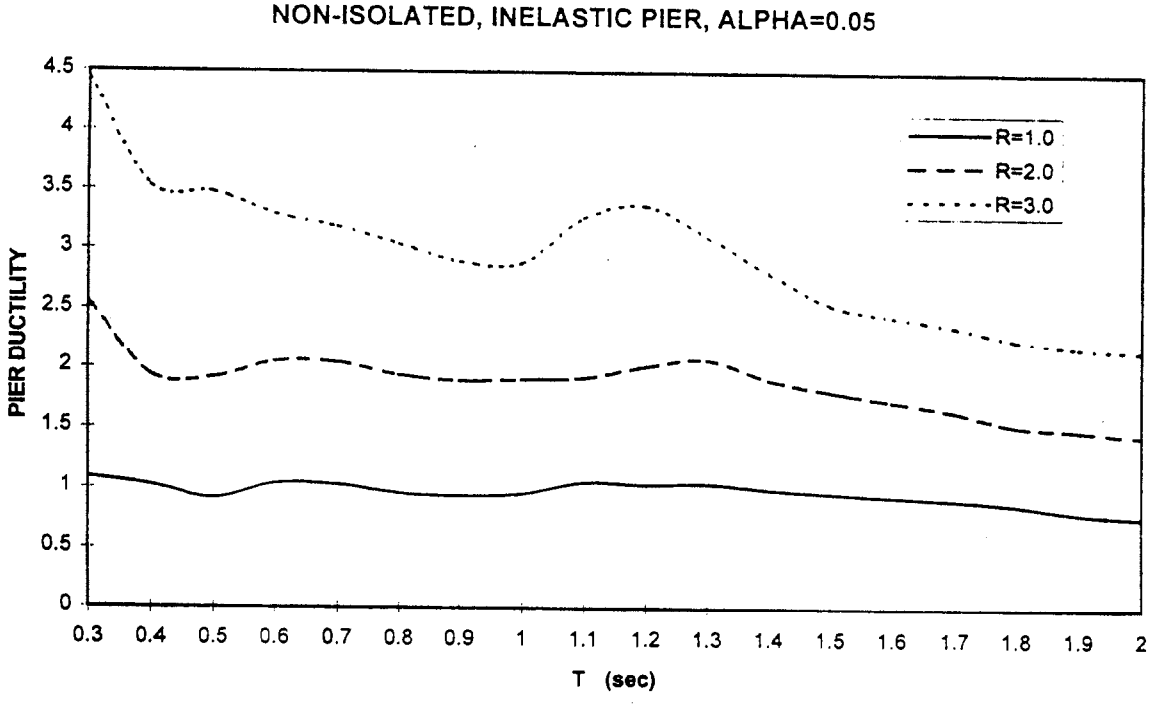

Fig. 6 Average Ductility Ratio in Substructure of Non-Isolated Bridge.

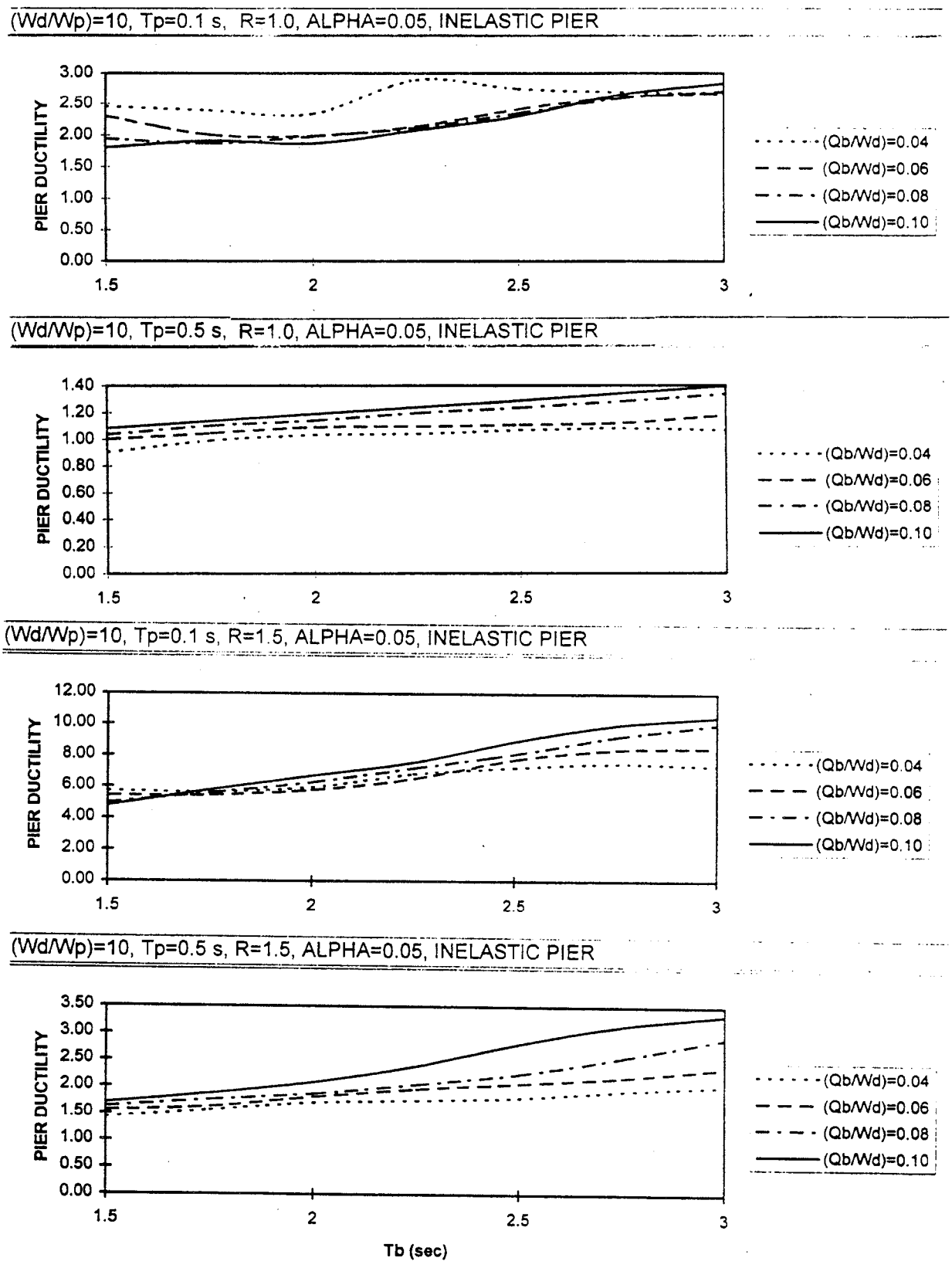

Fig. 7 Average Ductility Ratio in Substructure of Isolated Bridge.

THE RESTORING FORCE CHARACTERISTICS OF LRB UNDER THE INFLUENCE OF VARIABLE AXIAL LOADS AND ROTATIONAL DEFORMATION

H. Iemura[1], A. Igarashi[1], Y.Z. Chen[2] and H. Nakazima[3]

[1] Dept. of Civil Engineering Systems, Kyoto University

[2] Dept. of Civil Engineering, Kyoto University

[3] Hanshin Expressway Public Corporation

Abstract

In the application of base isolation devices to bridge structures, in most cases the base isolation bearings are installed between the girders and the piers' top where conventional bearings have been installed. However, in the restoration of the Hanshin Expressway No.3 in Benten District, base isolation bearings (LRB) are installed at the bottom of the columns of the framed bridge structure because of space limitation for conventional type of bridge. For this type of bridge structure, not only the horizontal deformation, but also the variable axial load and rotaional deformation of the LRB take place in the event of strong earthquakes. It is of great importance to experimentally assess the influence of these effects to ensure the safety of the seismic isolator implementation of this type. The horizontal restoring force characteristics of LRB-type isolator were investigated by means of triaxial loading tests. It is shown that the effect of variable axial load is more significant than that of the rotational deformation.

1 INTRODUCTION

Recently, especially after the Hyogoken-Nanbu Earthquake, base isolated structures are becoming popular. The principle of the base isolation is "the elongation of the natural period of structures to reduce the inertia force acting on structures and the enhancement of energy dissipation capacity to reduce large displacements".

In the application of base isolation bearings to bridge structures, the bearings are mostly installed between the girders and the piers' top as shown in Fig. 1 (a), where conventional bearings have been installed.

However, in the restoration of the Hanshin Expressway No.3 in Benten District, base isolation bearings are installed at the bottom of the columns of the framed bridge structure as shown in Fig. 1 (b). This type of configuration is employed since the size of the space for the construction of the viaduct in a densely populated urban area is tightly limited, and excessive seismic loading to the foundation needs to be avoided.

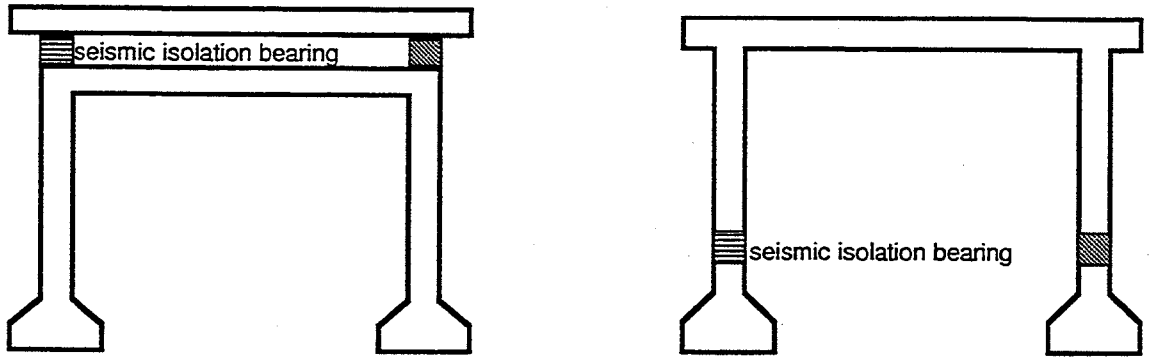

(a) Typical Seismic Isolation for Bridge Structures

(b) Hanshin Expressway No.3 in Benten District

Figure 1 Implementation of Seismic Isolation Bearings

The base isolation bearings implemented as shown in Fig. 1 (b) is expected to undergo not only horizontal deformation, but also variable axial load and rotational deformation, due to the dynamic response of the framed structure. Effects of variable axial load and rotational deformation on the performance of the base isolation bearings have to be experimentally examined in order to use this unconventional implementation in practice.

In this paper, the verification test results conducted at the earthquake engineering laboratory of Kyoto University, using the newly developed test equipment for the triaxial loading of seismic isolatiors are presented.

2 EXPERIMENTAL SYSTEM

The schematic of the experimental system used in this study is shown in Fig. 2. Three actuators are digitally controlled to apply the specified horizonatial, rotational deformation and axial force. The digital controller allows a high accuracy of loading through the actuators.

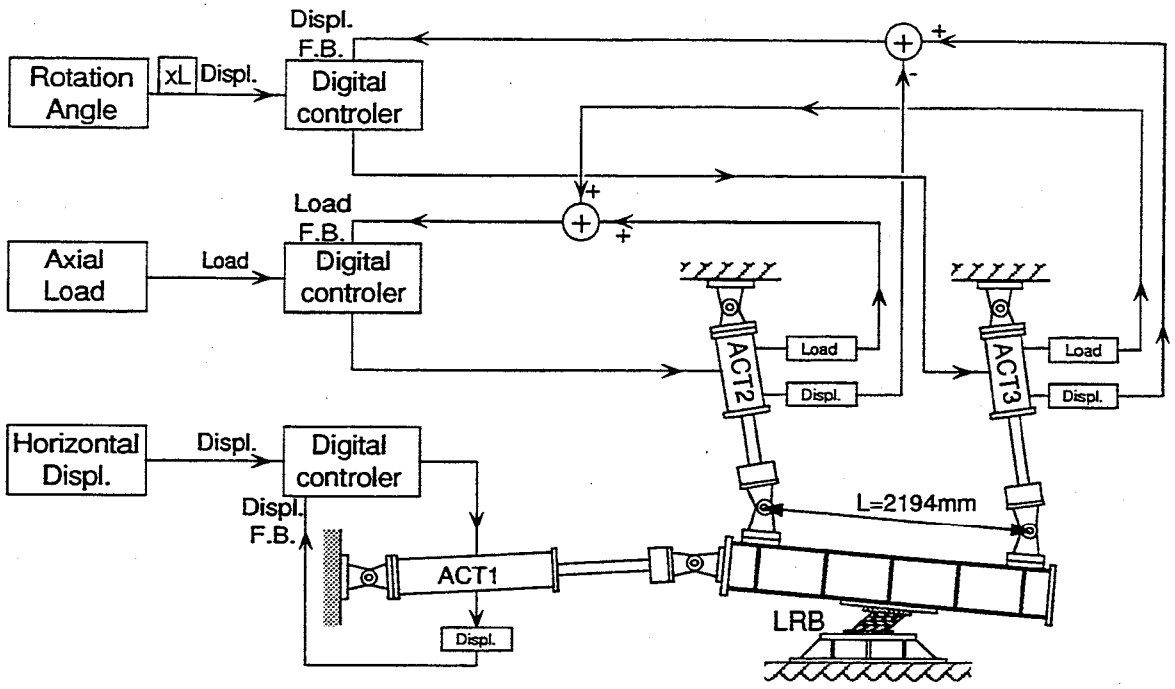

Figure 2 The Test System

2.1 Loading System

As shown in Fig. 2, the actuator No.1 (ACT1, hereafter) imposes the horizontal displacement on the loading beam and the specimen. The vertically hunged ACT2 and ACT3 apply the axial force and rotational deformation through the horizontal rigid beam.

2.2 Control System

ACT1 is operated in the displacement control mode. ACT2 is operated in the force control mode to apply the axial load, which is the sum of reaction forces of ACT2 and ACT3. ACT3 is operated in the displacement control mode to impose the angle of rotation on the loading beam, see Fig. 2.

2.3 Instrumentation

In addition to displacement and load transducers installed in ACT1, 2 and 3, external displacement transducers and sensors are set to the beam for the more accurate measurement. All the measured data are recorded on the hard disk of the computer.

3 LOADING EXPERIMENTS

In this study, Lead Rubber Bearing(LRB) are tested. There are four specimens(A1, A2, B1, B2) with two types(A, B). Both types of the specimens are one third models of the actual bearings used in the Hanshin Expressway restoration. The difference between the types A and B is the thickness of the steel plates. Dimensions of the bearings are shown in Fig. 3.

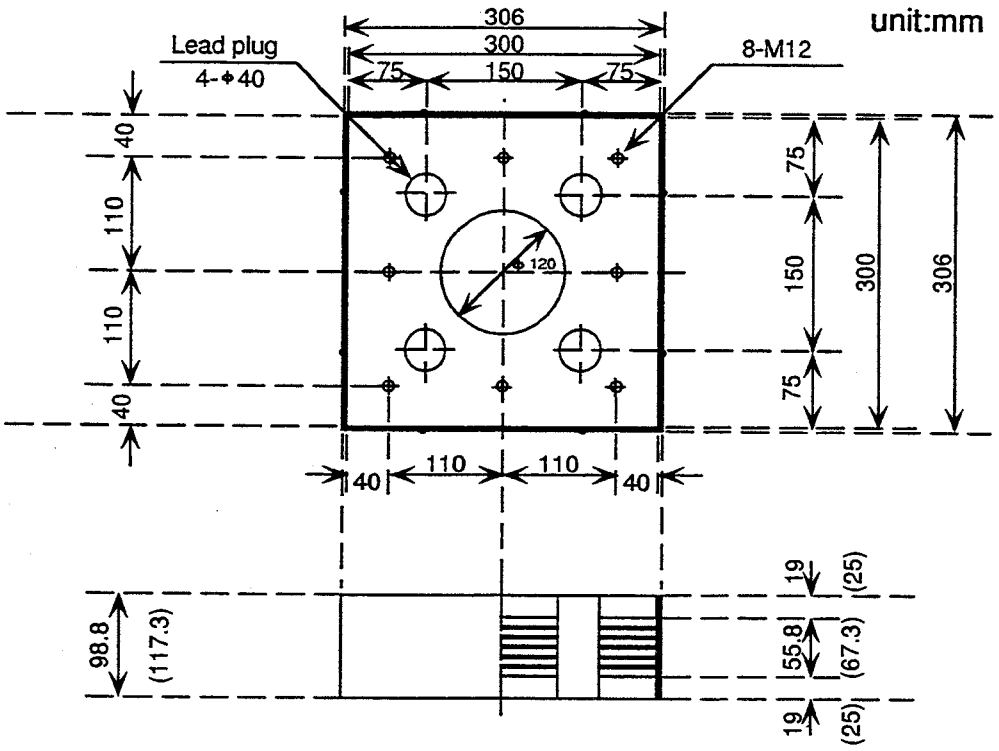

Figure 3 Dimensions of Specimens (Inside parenthesis: type B)

Since the purpose of the experiments is to verify the performance of the bearing under the triaxial loading for the application of Benten District reconstruction, the test scheme is devised to subject the seicmic isolator specimen to simulated horizontal displacements, variable axial loads, and rotation. The loading condition is first calculated by a dynamic response analysis of the framed bridge of the Benten section, modelled as in Fig. 4, in which the NS component of the acceleration record of the Hyogoken-Nanbu Earthquake at JR Takatori Station is used as the input.

Calculated horizontal displacement, axial load and rotational angle working on the bearing are shown in Figs. 6, 7 and 8. All of the three time histories have a similar shape, since the first mode is predominant in the response of the structure.

The following four types of tests were conducted.

Test 1: Under the constant axial load, forced rotation of which time history is shown in Fig. 5 is applied to examine rotational restoring force characteristics of the bearing.

Test 2: Under the constant axial force and without rotational deformation, a series of horizontal displacements shown in Fig. 6 is imposed on the specimen.

Test 3: Without rotational deformation, a series of horizontal displacements shown in Fig. 6 and the variable axial force shown in Fig. 7 are applied

Test 4: Horizontal displacement(Fig. 6) and variable axial force (Fig. 7) are applied while the rotational deformation shown in Fig. 8 is imposed on the specimen.

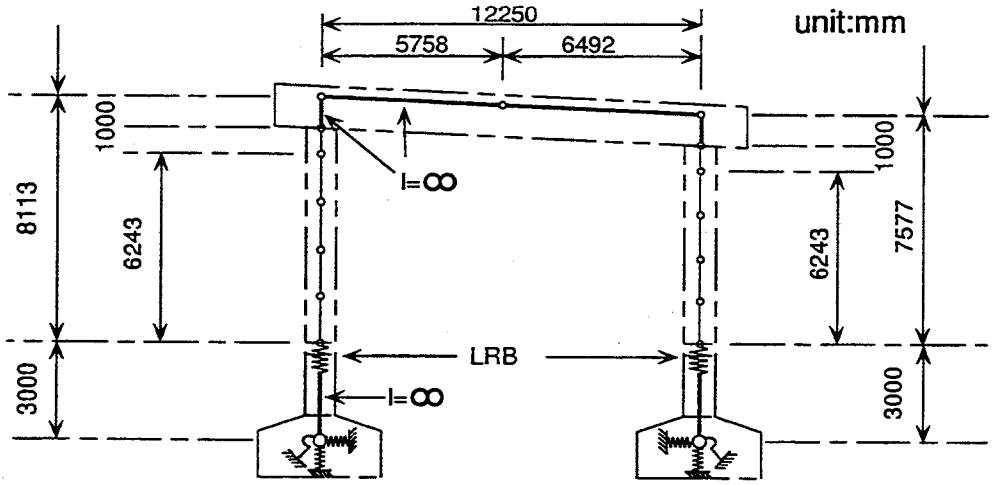

Figure 4 Transverse Model of The Viaduct

In Tests 2, 3 and 4, the horizontal displacement, axial load and rotational deformation as shown in Figs. 6, 7 and 8 are scaled down to 1/3, 1/9, 1, respectively, to fit the reduced scale of the specimen, and futhermore, scaled down to 80%, due to the loading capacity of the test equipment. The time history of 16 second as shown in Figs. 6, 7, 8 are divided into a series of 800 target values for the loading steps. The initial axial load for each test is $27.3tonf(267.3kN)$, which is equivalent to the weight of the upper part (the upper structure including the bent columns) of the viaduct.

Left direction, upper direction and counterclockwise rotation in the Fig. 2 are defined as the positive direction for horizontal displacement, axial load and rotational angle, respectively.

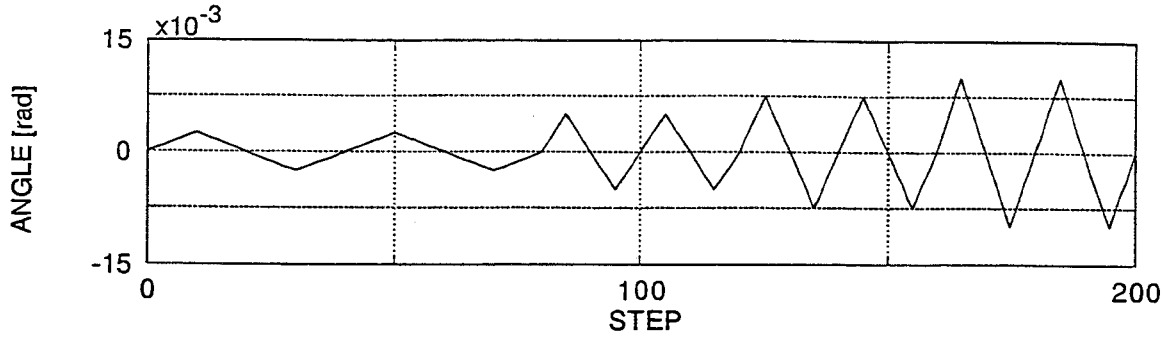

Figure 5 Rotational Angle Sequence for Test 1

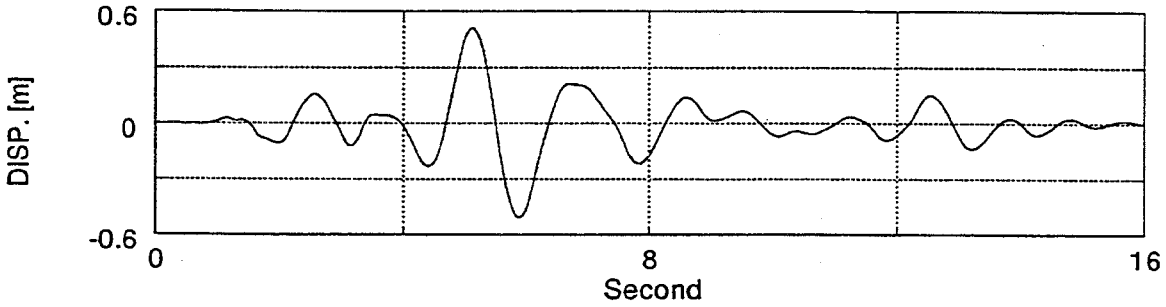

Figure 6 Horizontal Displacement Time Hisitory Obtained from Numerical Calculation

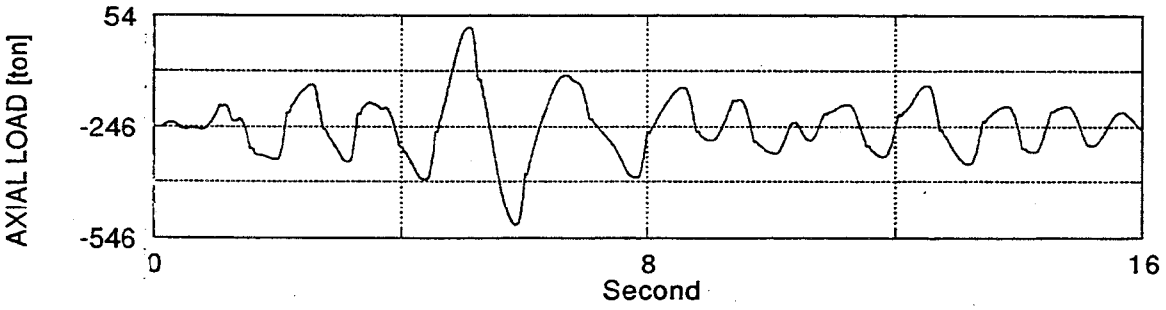

Figure 7 Variable Axial Load Hisitory Obtained from Numerical Calculation

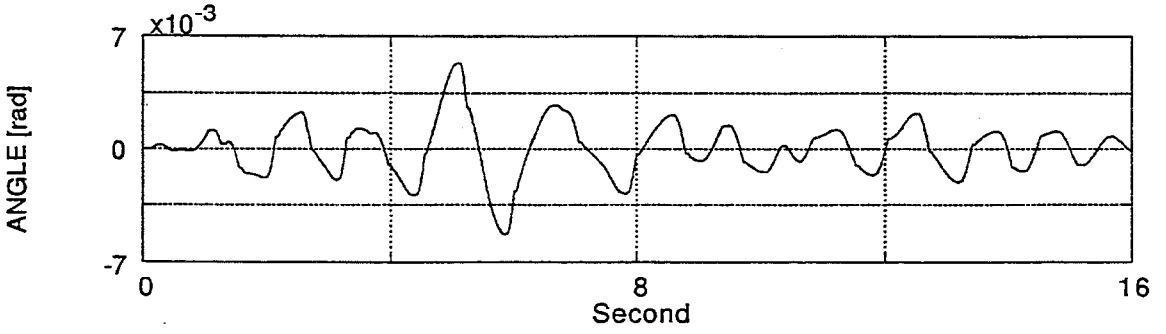

Figure 8 Rotational Angle Time Hisitory Obtained from Numerical Calculation

4 TEST RESULTS

In this section, the test results, namely the angle of rotation-resistance moment hysteretic response and equivalent rotational stiffness versus rotation angles obtained from Test 1, horizontal displacement-horizontal restoring force hysteresis loops, equivalent stiffness versus shear strain, equivalent damping ratio versus shear strain, and horizontal displacement-resistance moment hysteresis loops obtained from Tests 2, 3, and 4 are shown to verify the influence of the effects of variable axial load and rotational deformation.

Control errors of ACT 1, 2, and 3 throughout all the experiments were approximately $0.5mm$, $0.2tonf(2kN)$, and $0.1mm$, respectively.

4.1 Angle of Rotation and Resistance Moment

Rotational angle-resistance moment hysteresis loop obtained from Test 1 shows bilinear behavior as shown in Fig. 9 (a). Within the angle range of this experiments, so called hardening and deteriorarion of elastomer were not obserbed.

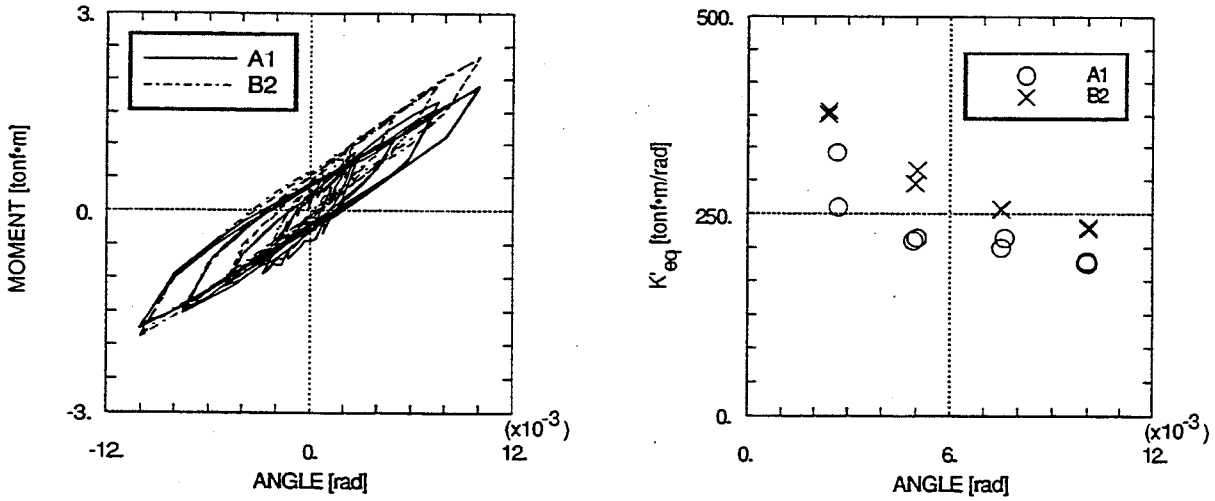

(a) Rotational Angle-Resistace Moment Hysteretic Response

(b) Angle of Rotation-Equivalent Rotational Stiffness

Figure 9 Test Result Obtaind from Test 1

The resistance moments at $10 \times 10^{-3}rad$ (the maximum angle of rotation for Test 1) were approximately $1.6tonf \cdot m$ (type A) and $1.8tonf \cdot m$ (type B), and at $5 \times 10^{-3}rad$ (the maximum angle of rotation for Test 4) the moments were about $1.3tonf \cdot m$ (type A) and $1.5tonf \cdot m$ (type B).

4.2 Equivalent Rotational Stiffness

As shown in Fig. 9 (a), rotational angle-resistance moment hysteresis loops obtained from Test 1 of all specimens show that the maximum angle of rotation and maximum resistance moment are achieved at the same loading steps. Hence the equivalent bending stiffness(K'_{eq}) can be defined by the following expression.

$$K'_{eq} = \frac{M_{max}}{\theta_{max}} \tag{1}$$

M_{max} : maximum resistance moment for each cycle
θ_{max} : maximum angle rotation for each cycle

Figure 9 (b) shows a plot of the equivalent rotational stiffness versus the angle of rotation. It shows that K'_{eq} decreases as the rotational angle becomes larger.

The value of K'_{eq} of specimen type B is slightly larger than that of type A.

4.3 Horizontal Displacement and Horizontal Restoring Force

Figure 10 shows the horizontal displacement-horizontal restoring force hysteresis response obtained from Tests 2, 3 and 4. The response curves within the deformation range of $\pm 100mm$ can be approximately described as bilinear hysteresis loops. However, hardening can be obserbed outside the displacement range of $\pm 100mm$, hence the hysteretic response develops the loops of a reverse S shape.

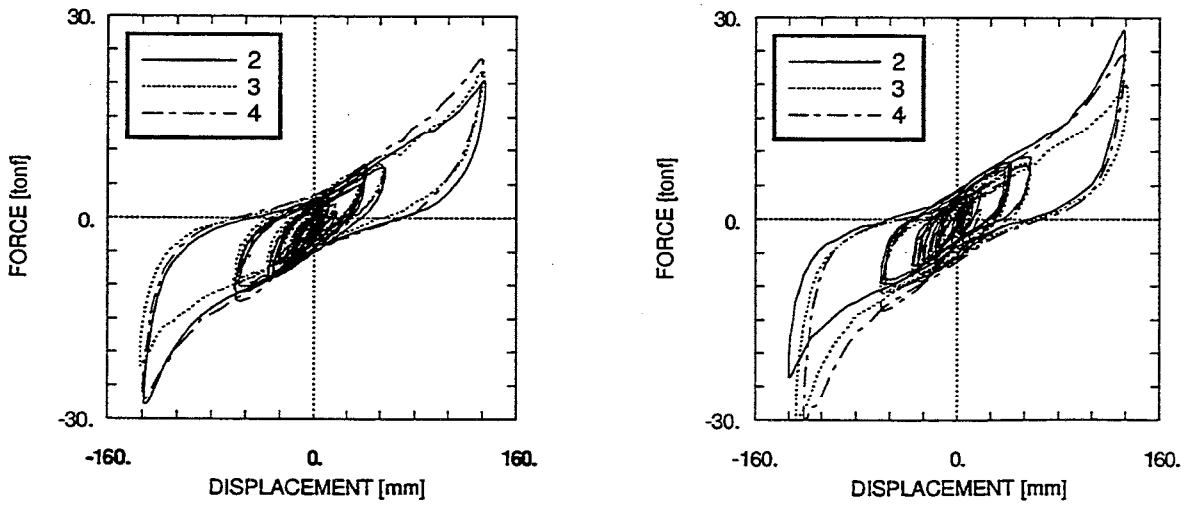

(a) Specimen A1 (b) Specimen B1

Figure 10 Horizontal Displacement-Restoring Force Hysteresis Loop

It should be noted that, at most of the loading steps, positeve horizontal displacement in Fig. 6 and the increase of axial load toward the positive direction take place simultaneously,

and vice versa. This implies that axial load vary to tension in the positive deformation range, and it to compression in the negative deformation range in the hysteresis loop shown in Fig. 10

The results of Tests 2 and 3 indicate that the variable axial loads cause an increase in the horizontal restoring force of the type A bearings in the positive deformation range and reduce the restoring force in the negative deformation range. However, specimen type B has the opposite tendency.

The horizontal restoring force of both specimens types takes approximetely similar or slightly larger value with the rotational loading, according to the results of Tests 3 and 4.

4.4 Equivalent Stiffness

The equivalent stifness is defined by the following expression.

$$K_{eq+} = \frac{F_{max}}{D_{max}} \tag{2}$$

$$K_{eq-} = \frac{F_{min}}{D_{min}} \tag{3}$$

F_{max}, F_{min} : maximum and minimum restoring forces for each cycle
D_{max}, D_{min} : maximum and minimum horizontal displacements

The two types of equivalent stiffnesses are defined in order to evaluate the influence of the effect of variable axial load. K_{eq+} is the equivalent stiffness of the positive deformation range, where axial loads vary to tension. K_{eq-} is the equivalent stiffness of the negative deformation range, where axial loads vary to compression. The shear strain γ is defined as follows.

$$\gamma = \frac{Horizontal\ Displacement}{Total\ Rubber\ Thickness} \tag{4}$$

Figure 11 shows the equivalent stiffness versus shear strain plot obtained from Tests 2, 3, and 4. In the figure, test numbers with symbols '+' and '−' correspond to K_{eq+} and K_{eq-}, respectively.

Within a shear strain range up to 120%, a steep reduction of the equivalent stiffness with the development of shear strain can be seen. The eqivalent stiffness at 240% strain is slightly larger than the values at 120% strain. Although there are no data where the shear strain range between 120% and 240% (the deformation at the cycle reaching the peak amplitude is remarkably larger than that of the other cycles, see Fig. 6), it is possible to infer that the minimum value of the equivalent stiffness exists within this shear strain range. This tendency is common in all specimens and all Test types, and little difference can be seen in terms of the rate of increase and decrease among the test types.

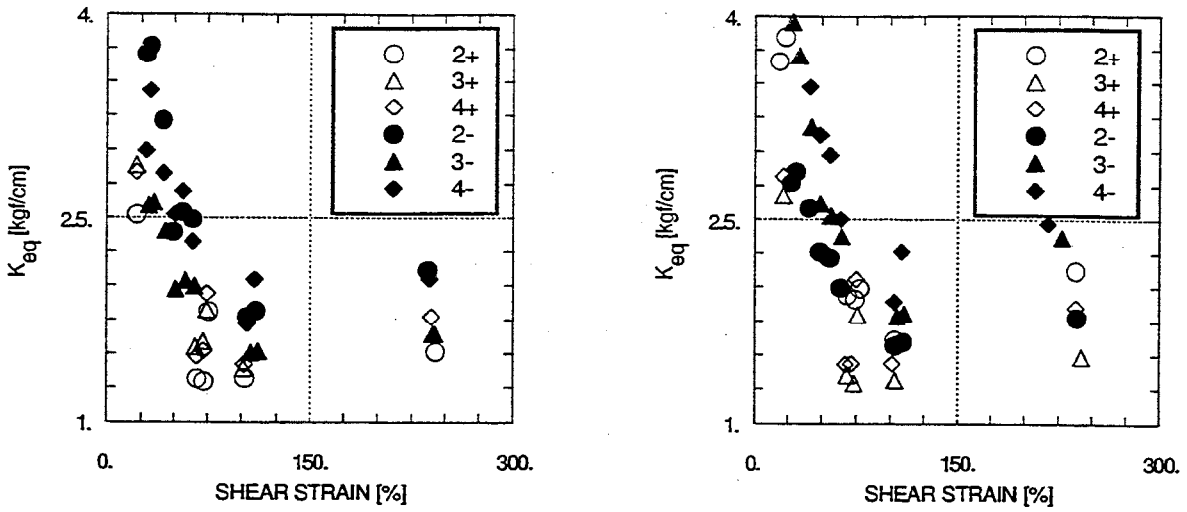

(a) Specimen A1 (b) Specimen B1

Figure 11 Shear Strain-Equivalent Stiffness

Comparison of Test 2 with Test 3 reveals that the equivalent stiffness of type A is larger in the positive deformation range(K_{eq+}), and shows the smaller value in the negative deformation range(K_{eq-}) under variable axial loads. However, specimen of type B shows the opposite tendency.

From the results of Tests 3 and 4, no significant difference is induced by the rotational deformation in the equivalent stiffness, K_{eq+} and K_{eq-}, with the exception of the 240% shear strain case.

4.5 Equivalent Damping Ratio

The equivalent damping ratio is defined by the following expression.

$$h_{eq+} = \frac{1}{4\pi} \cdot \frac{\Delta W_+}{W_+} \tag{5}$$

$$h_{eq-} = \frac{1}{4\pi} \cdot \frac{\Delta W_-}{W_-} \tag{6}$$

ΔW_+ : hysteretic enegy absorbed in the positive deformation range
ΔW_- : hysteretic enegy absorbed in the negative deformation range
W_+ : elastic strain enegy in the positive deformation range
W_- : elastic strain enegy in the positive deformaiton range

The two types of equivalent damping ratio, h_{eq+} and h_{eq-}, are defined in order to assess the influence of the effect of variable axial load.

Figure 12 shows the equivalent damping ratio versus shear strain obtained from Tests 2, 3, and 4. In the figures, test numbers with symbols '+' and '−' correspond to h_{eq-} and h_{eq-}, respectively.

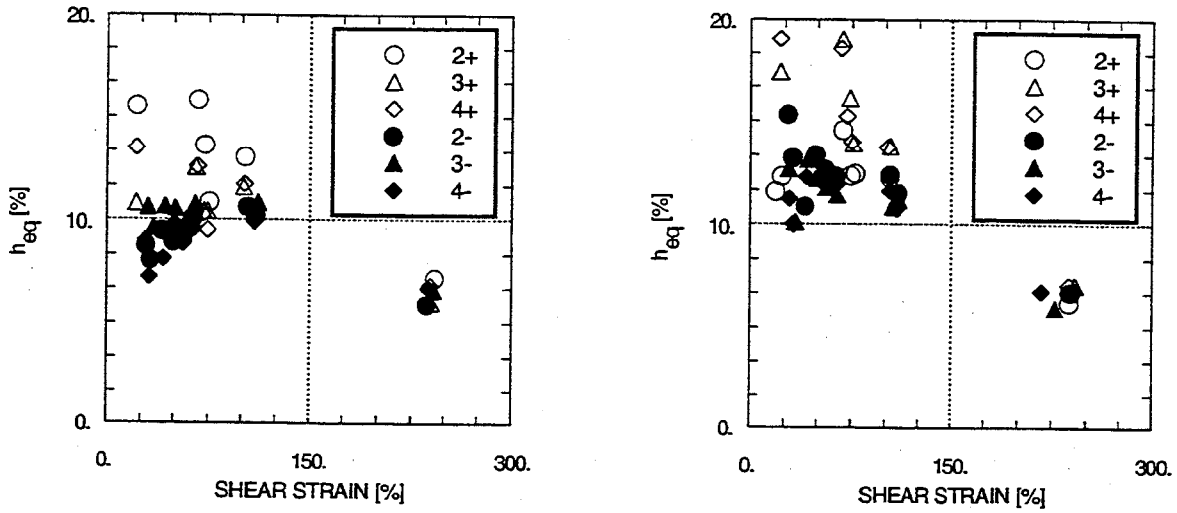

(a) Specimen A1 (b) Specimen B1

Figure 12 Shear Strain-Equivalent Damping Ratio

In general, it is found that the equivalent damping ratio increases as shear strain becomes larger within 50%, and decreases in the shear strains exceeding 50%. The reduction of damping for type B is greater than that for type A.

Comparison of Test 2 with Test 3 in Fig. 12 indecates that the equivalent damping ratio is smaller under variable axial loads, while that of type B takes a larger value. The difference of both types of specimens between Test 2 and Test 3 reduces as the shear strain increases, and there exists little difference at the maximum deformation points. The equivalent damping h_{eq-} of type A takes larger values in almost all the shear strain range and type B takes smallr values. The magnitude of the difference of h_{eq-} between Test 2 and Test 3 is relatively small, hence h_{eq-} is less affected by the variable axial loads than h_{eq+}.

The test results of Test 3 with Test 4 indicate that the equivalent damping is smaller when the rotational deformaiton is induced for both specimens. However, at a number of points, the difference is rather negligible.

4.6 Horizontal Displacement-Resistance Moment Hysteresis Loop

Figure 13 shows the horizontal displacement-resistance moment hysteretic response obtaind from Tests 2, 3 and 4.

Comparing Test 2 with Test 3, the shape of the hysteresis loop obtained from Test 2 is alomost a straight line, and no residual horizontal displacement is observed. Whereas the

hysteresis loop of Test 3 deviates toward the positive direction of the resistance moment as the greater horizontal displacements. The resistance moment tends to decrease in the positive deformation range and increases in the negative deformation range under the variable axial loading. The resistance moments with variable axial loads decrease by 70% at the maximum positive deformation points and increase by 20% to 40% at the maximum negative deformation points with constant axial loads.

The hysteresis loops of both specimens in Tests 3 and 4 follow an almost similar pattern, indicating that the influence of the rotational deformation is smaller than that of the variable axial loads.

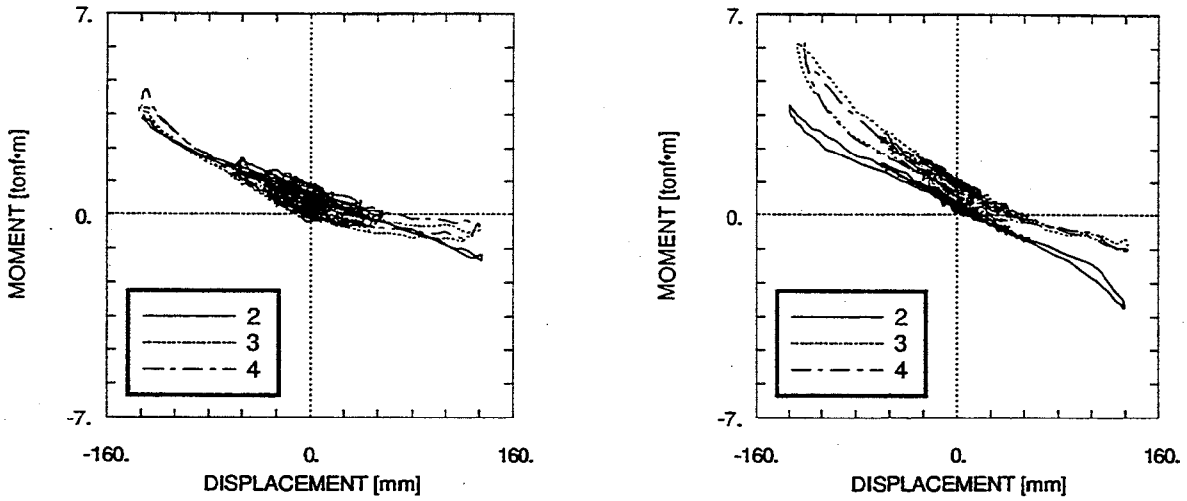

(a) Specimen A1 (b) Specimen B1

Figure 13 Horizontal Displacement-Resistance Moment Hysteresis Loop

Considering the angle of rotation-resistance moment hysteresis loop shown earlier, it is expected that the resistance moment under rotational deformation will vary to the negative direction in the negative deformation range. The for the opposite result of the tests may be explained by the larger magnitude of resistance moment by horizontal deformation than that by the rotational deformation, or greater influence of the effect on the loading history.

5 CONCLUSION

A series of tests of Lead Rubber Bearings (LRB) using a triaxial loading system is conducted in order to validate the preformance of LRB used in a section of Hanshin Expressway where variable axial loads and rotational deformation of the bearings are expected in the event of strong earthquakes. The hysteretic restoring force characteristics of scaled models under the simulated variable axial loads and the rotational deformation are experimentally investigated.

Based on the test results, the following conclusions have been reached.

1. In the cyclic rotational loading tests of LRB, the angle of rotation-resistance moment hysteresis loop shows the typical bileanear behavior, and equivalent rotational stiffness decreases as the rotational angle becomes larger.

2. The influence of the variable axial loads on the horizontal restoring force, equivalent stiffness, and equivalent damping ratio differs depending on the specimen type. Resistance moment increases when the axial load increases in compression. The influence of axial loads is considerably more significant than that of the rotational deformation.

3. The tests, which modelled Hanshin Expressway No.3 in Benten District, did not indicate any significant influence nor negarive influence of variable axial load and rotational deformation on the effectiveness of seismic base isolation.

ACKNOWLEDGMENTS

The authors wish to thank the engineers of Yokokawa Technology Information, Inc., Yokokawa Bridge, Inc., and OILES Industrial, Inc. for their supports and cooperation in conducting the experiments.

REFERENCES

[1] M.Hakuno, T.Okada, K.Takanashi, K.Toki, S.Ikeda, H.Iemura and T.Kitada, *Application Manual for Hybrid Experiments*, 1990 (in Japanease).

[2] Technology Center for National Land Development and Hanshin Expressway Public Corp., *Guidelines for Seismic Isolation Design of Highway Bridges*, 1989 (in Japanese).

[3] Public Works Research Institute Ministry of Construction, *Manuals for Seismic Isolation Design of Highway Bridges*, 1992 (in Japanese).

[4] Japan Road Association, *Specification for Highway Bridges (Part V Seismic Design)*, 1990 (in Japanese).

[5] Disaster Prevention Research Association, *Review of Seismic Isolation Design of Highway Bridges*, 1992 (in Japanese).

[6] Japan Construction Society, *Guidelines for Seismic Isolation Structure Design*, 1989 (in Japanese).

SEISMIC VIBRATION REDUCTION OF HIGHWAY BRIDGE BY REAL-TIME STRUCTURAL PARAMETER MODIFICATION (RSPM)

M. Tong[(1)], Y.H. Wu[(2)], and G.C. Lee[(3)]

National Center for Earthquake Engineering Research
State University of New York at Buffalo
Buffalo, New York

ABSTRACT

A new semi-active control system is considered for a three-span highway bridge seismic retrofitting. The bridge model is based on the design information of Memphis bridge 502-11D #124/125. The performance criterion includes the relative displacement between superstructure and cap beam and the column base moments. Numerical analysis results show that, with the added RSPM control system, both the relative displacement and the base moment could be considerably reduced.

INTRODUCTION

In the United States, many highway bridges constructed in the 50s and 60s were designed without seismic protection. Some of these bridges are located in moderate to high earthquake risk zones. Retrofitting of these bridges has been a continued effort. In recent years, since many new technologies and devices are available for civil infrastructure applications, it has become practical to use vibration reduction devices as an alternative approach in seismic retrofit.

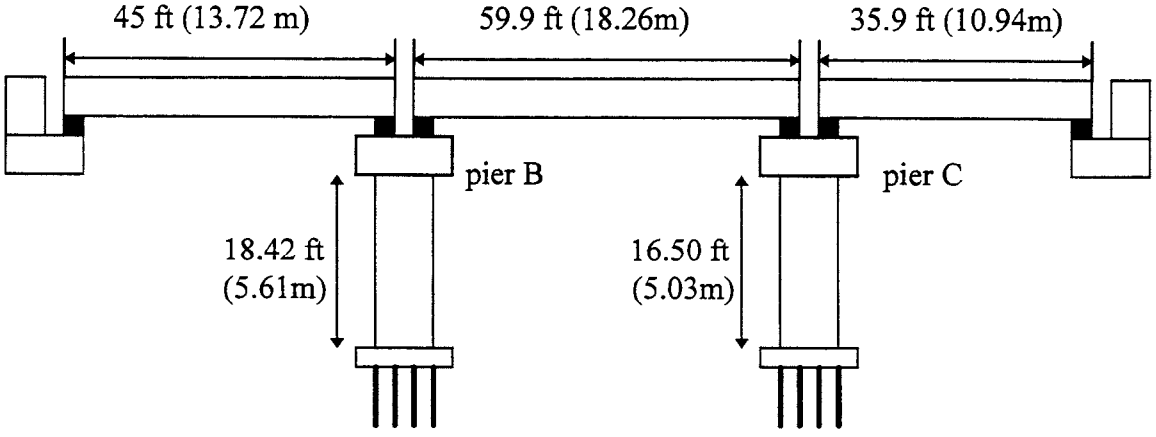

Figure 1. Elevation of the 3-span highway bridge

---

1. Research Scientist, 2. Visiting Scholar, 3. Professor and Director

The three-span highway bridge, Memphis bridge 502-11D#124/125, was designed and constructed in 1965. The design complied with the standard road and bridge specifications of Tennessee Department of Highways. Currently, there is no extra seismic protective treatments applied to the bridge. Figures 1 and 2 provide simplified sketches of the profiles of the bridge.

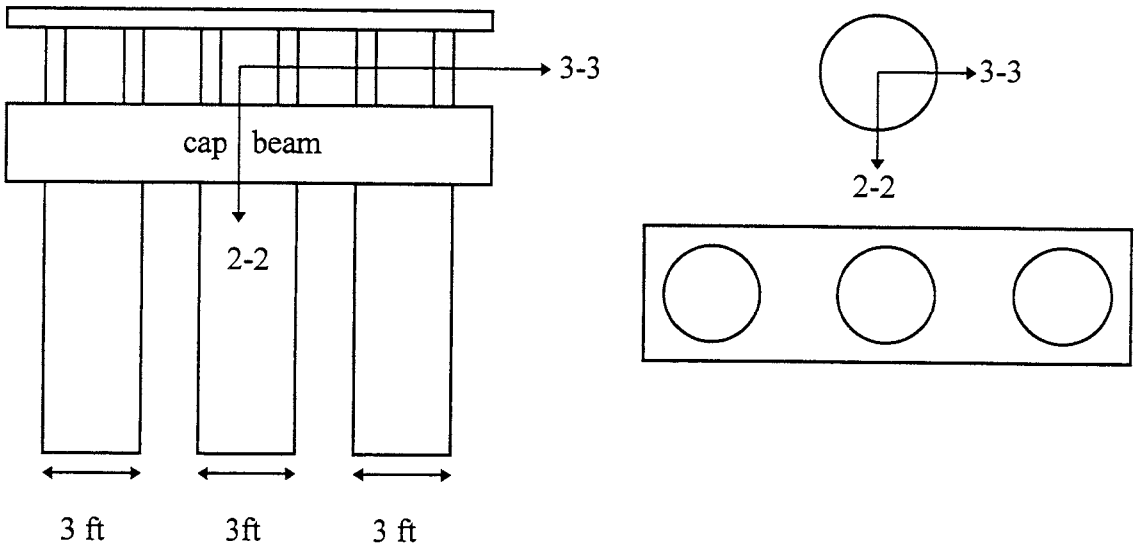

Figure 2. Cross sectional and top view of a bridge pier

The bridge is being evaluated for potential damages. Since it is a typical highway bridge, we are attempting to establish a hypothetical bench model for highway bridge response calculations, based on this reinforced concrete bridge.

The material properties of the structure elements are combined and simplified by Dr. J.H. Kim of the University at Buffalo. We list in the following some of the main items:

	Weight	EA	EI_{22}	EI_{33}
circular column (pier B):	19 kips	1.93×10^{6} kips	9.4×10^{7} kips-in^2	same as EI_{22}
(pier C):	17 kips	same as above		
cap beam:	95 kips	3.35×10^{6}kips	2.96×10^{7}kips-in^2	same as EI_{22}
superstructures (span 1):	366 kips	3.02×10^{7}kips	1.08×10^{12}kips-in^2	6.18×10^{9}kips-in^2
(span 2):	585 kips	3.79×10^{7}kips	1.29×10^{12}kips-in^2	8.44×10^{9}kips-in^2
(span 3):	295 kips	3.02×10^{7}kips	1.1×10^{12}kips-in^2	6.18×10^{9}kips-in^2
rubber bearing pads (fixed):	NA	9.02×10^{2}kips	NA	NA
(expansion):	NA	4.50×10^{2}kips	NA	NA

The horizontal stiffness of the neoprene rubber bearing pads are mainly due to their shear resistance capacities; therefore, the bending rigidities, EI, are neglected. The calculated horizontal stiffness of the pads are 19.04 kips/in and 18.71 kips/in for fixed and expansion bearings respectively.

THE BRIDGE RESPONSES UNDER EARTHQUAKE LOADING

Based on the design information of the bridge, a FEM model is formed in SAP90. There are total of 254 beam elements used in the model. The mesh of the model is given in Figure 3. The mass of the superstructure is represented as distributed mass in the six main girders. As it is seen from Figure 3, the three spans are fixed from the left side, which correspond to the rubber bearing pads with dowel bars in the center to prevent horizontal movement. Since the problem of interest is seismic damage, the static analysis of the bridge was not pursued.

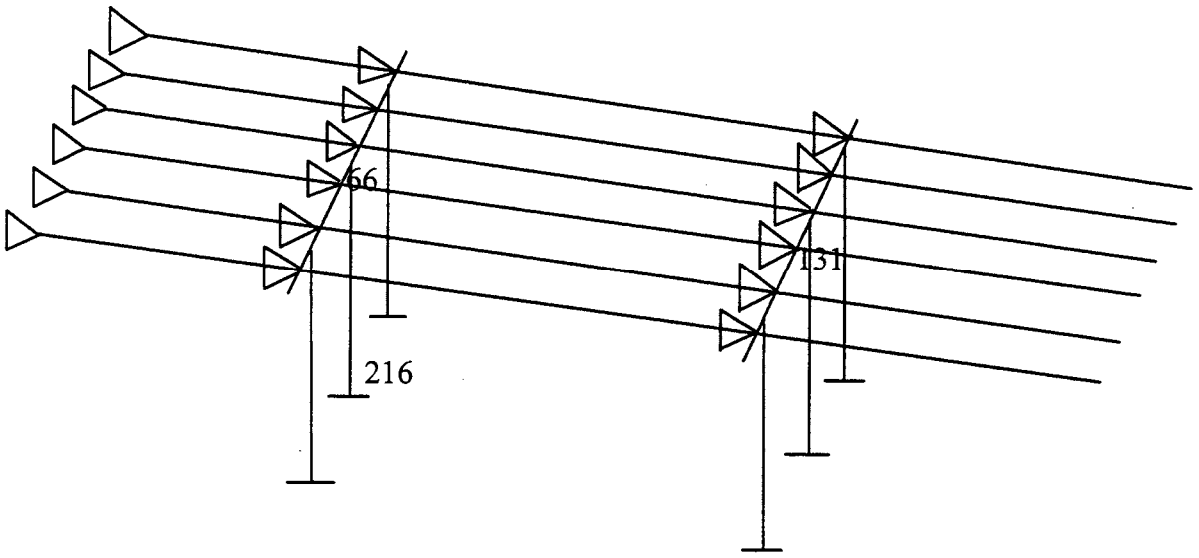

Figure 3. FEM mesh of bridge model

The profile of the bridge pier shows that it is weak in the longitudinal direction. The calculated modal parameters of the structure contain two translation modes in this direction. The frequencies of these two modes are 1.22 and 1.60 Hz., which correspond to the two lowest frequencies of the entire bridge structure. Since these frequencies are within the range of dominant earthquake ground motion frequency, we applied the El Centro earthquake record as the input in the longitudinal direction, and computed the bridge dynamic responses. Figure 4 shows the time history of the displacements at the cap beams of piers B and C, which represent the relative displacements between the decks and the piers. Figure 5 shows the dynamic moment and base shear force of the center column in pier B.

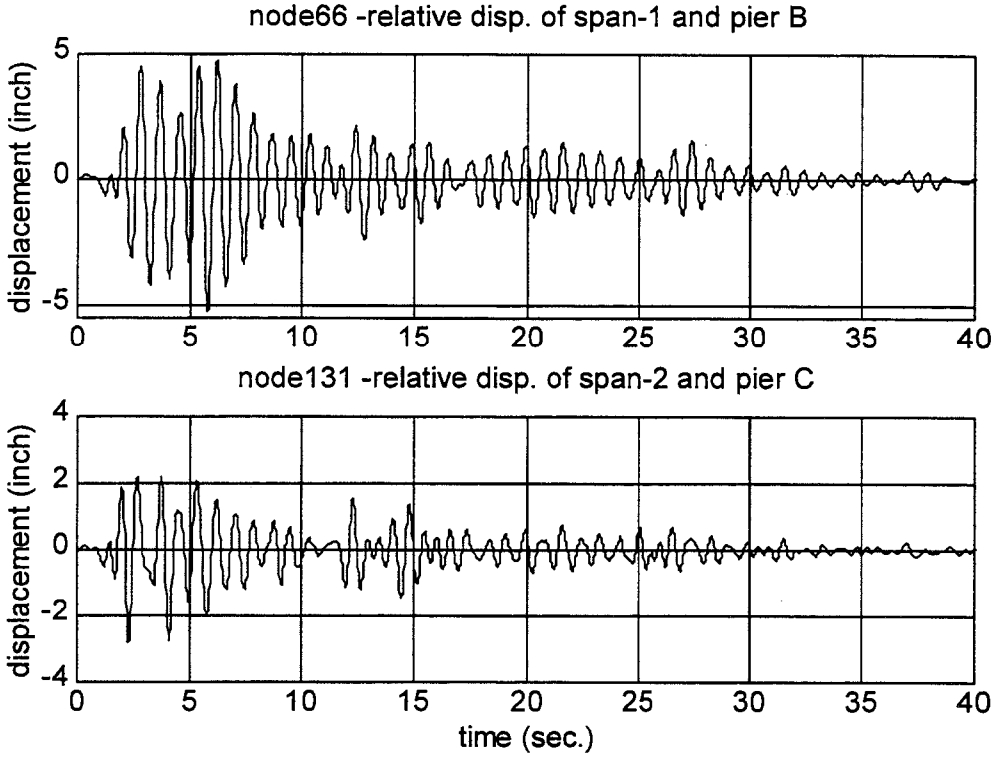

Figure 4 . Relative displacements of decks and piers

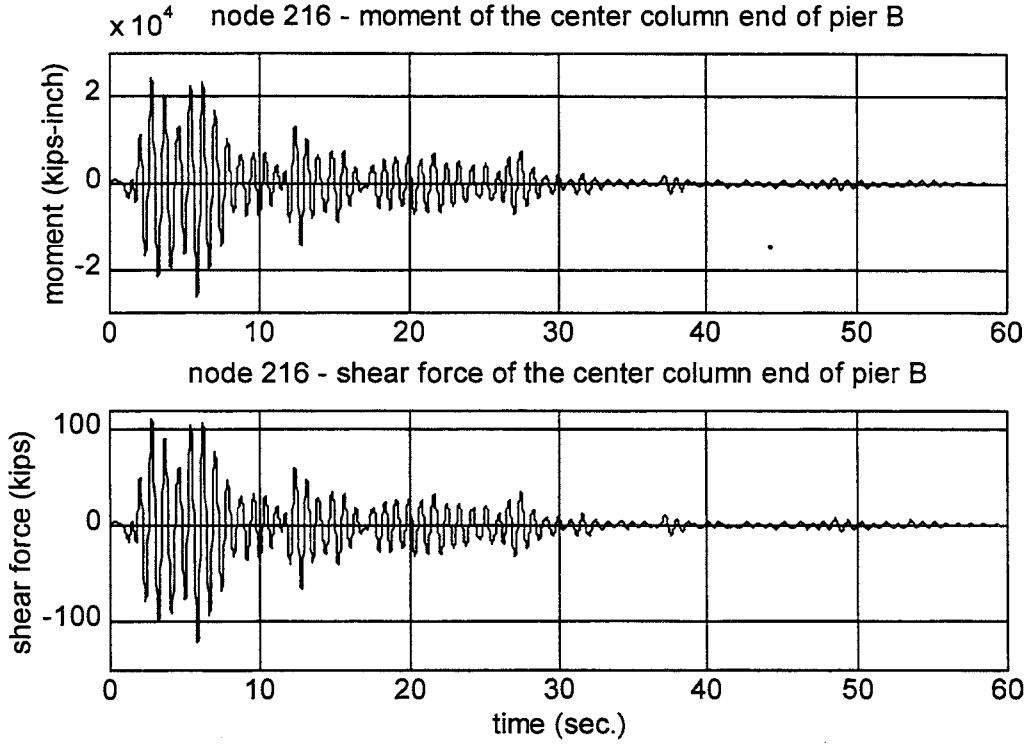

Figure 5. Dynamic moment and shear force

The maximal relative displacements at node 66 of Figure 4, which corresponds to displacement between the cap beam of pier B and the deck of the first span, are -5.2 inches and +4.7 inches. The maximal displacements at node 131, which corresponds to the relative displacement between the cap beam in pier C and the deck of the second span, are +3.1 inches and -2.4 inches (3% damping is assumed in the model for all the response calculations). The large relative displacements indicate that there is a potential risk for the decks to fall off from the bearings. Also, by checking the strength of each structural members, it is identified that the dowel bar is at great risk for excessive lateral force due to the large dynamic displacement. The plastic strength of the dowel bar in lateral direction is 4.75 kip, the calculated maximal forces on the dowel bars from left to right are 17.1 kips, 62.2 kips and 23.6 kips.

The maximal base moment of the center column in pier B is 2.9 Mlbf-in. The maximal base shear force of this column is 135 kips. Since the columns are ecentrically loaded, to determine the allowable moment, an axial loading vs. moment relation is formulated according to ACI nominal strength. For the calculated peak axial loading of 180 kips, the nominal moment is 10 Mlbf-in. In comparing with the peak moment value, it is seen that the base moment is only 30% of the nominal level. We will show in the following that an improvement of reduced displacement can be achieved by adding an RSPM control system. This benefit does not sacrifice the moment or shear force capacities.

USING RSPM AS AN ALTERNATIVE SEISMIC RETROFIT OF THE BRIDGE

According to the calculated responses, the column moments of the two piers have not exceeded the allowable value. In contrast, the relative displacement between the superstructure and pier B is considerably large. To lower the level of the displacement without sacrificing the moment and shear capacities of the columns, we consider to add an RSPM system between the deck and the cap beam. Assume a set of 12 RSPM devices to be placed between cap beams and the deck girders. On each cap beam in piers B and C, we use four RSPM devices to enhance the first, third, fourth and sixth expansion rubber bearings. These added devices will be pinned to the cap beam and the girder over the original rubber expansion bearings. We assume that each device has a stiffness of 7.5 kips/in and stroke of 10 inches.

The RSPM control is realized through the semi-active hydraulic devices. By adaptively opening and closing the orifice according to the control algorithm described in the Appendix, the devices could provide variable damping and stiffness to the bridge system.

Since the RSPM system is a highly non-linear control system, to evaluate its effect on the bridge system with a finite element model will require a large amount of computation. To reduce the calculation, we first simplify the finite element model by reducing it into a one direction 16 DOF model, which represents the column as a 4 element bending model and the superstructure as a rigid mass. The simplified model is

illustrated in Figure 6. The modal parameters of the simplified model are checked against the original finite element model. The natural frequencies of the first two modes of the simplified model are 1.2 and 1.8 Hz, which are relatively close to the corresponding frequencies identified in the finite element model. In the 16 DOF model, since M_1 has combined the mass of cap beam of pier B and the deck mass of the second span, the displacement of M_1 represents the relative displacement of the deck of the first span and pier B. Also, this is the displacement of the cap beam of pier B. Similarly, the difference between the

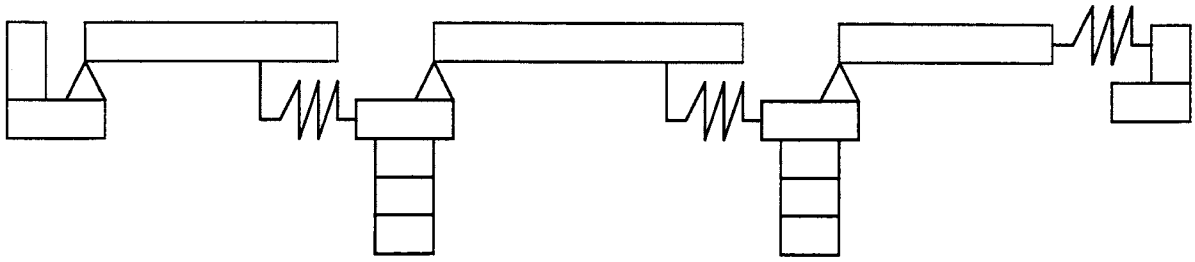

A simplified bridge model

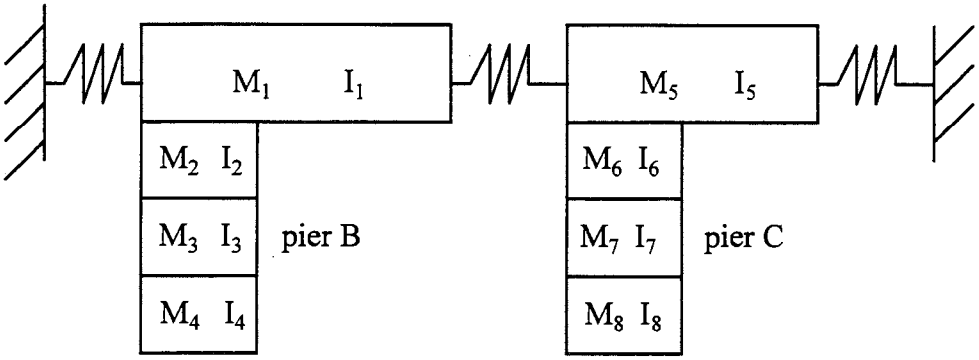

Figure 6. 16 DOF consistent mass bridge model

displacements of M_1 and M_5 represents the relative displacement between the deck of the second span and pier C. The displacement of M_5 itself represents the relative displacement of the deck of the third span to the supporting abutment.

Figure 7 compared the relative displacements of the two cap beam responses obtained from the 16 DOF model and the FEM model. It is seen that the differences are reasonably small. In particular, the maximal response of the 16 DOF model is 5.7 inches at the time point of 5.8 seconds. The corresponding peak response of the FEM model is 5.2 inches at 5.76 seconds.

Using the 16 DOF consistent mass model and representing RSPM devices as special control elements connected between M_1 and the ground, M_2 and M_5, M_5 and the ground, the response of the controlled bridge system is numerically simulated.

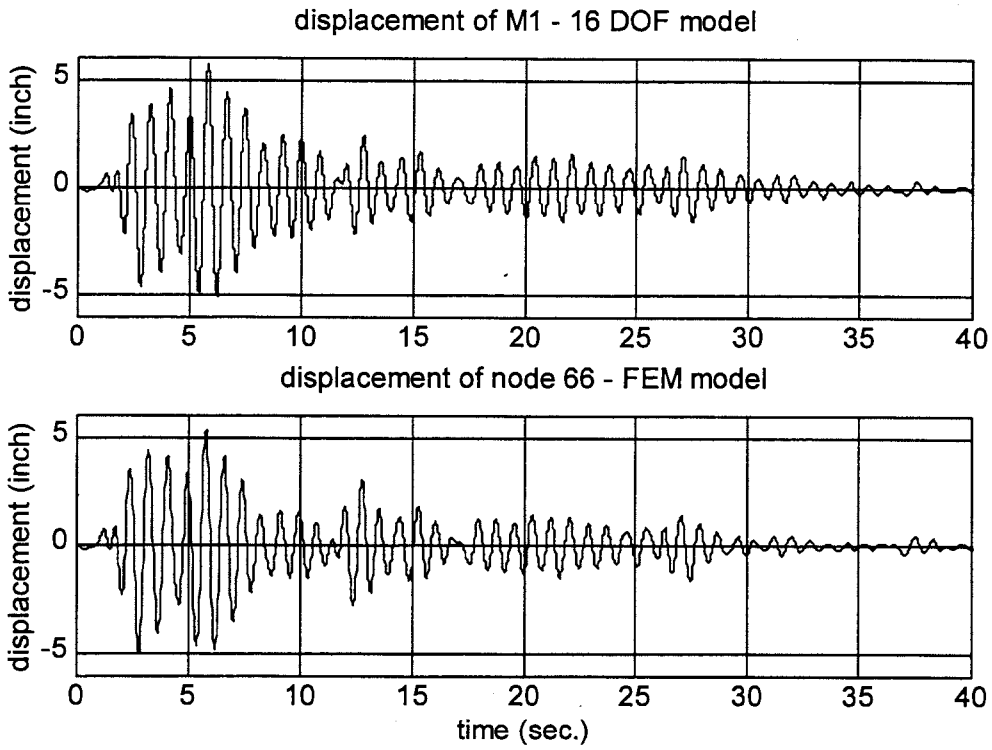

Figure 7. Displacement responses 16 DOF vs. FEM

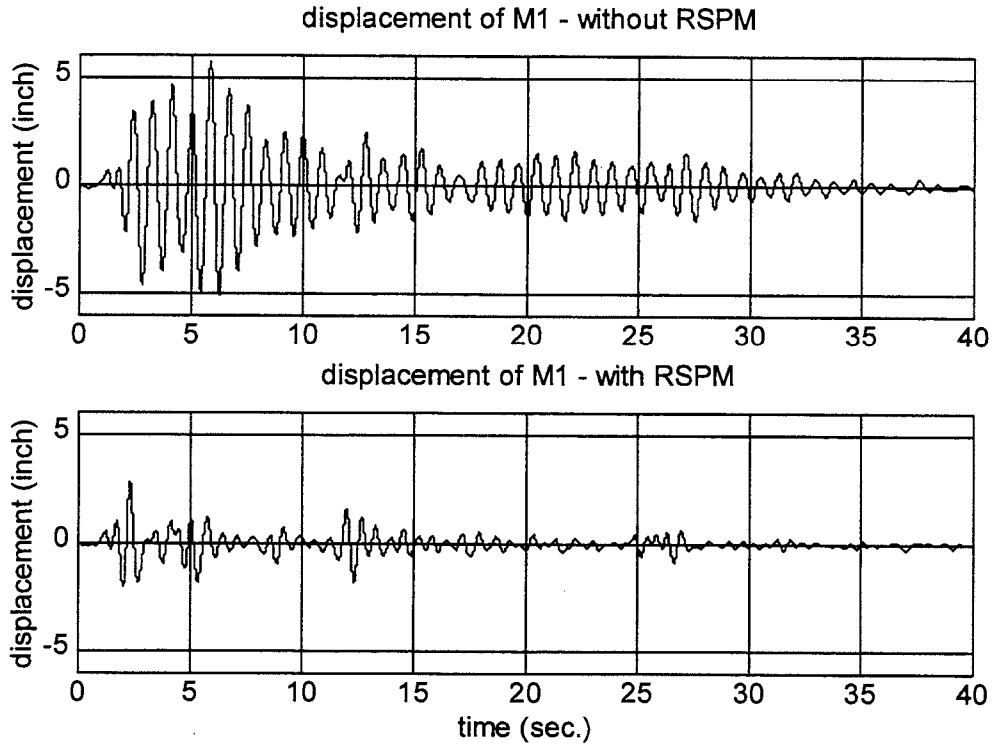

Figure 8. Responses without/with RSPM control

Figure 9 shows the relative displacements of M_1 without/with RSPM control system. It is seen that this displacement has been reduced significantly. The peak displacements with the RSPM system are +2.02 and -2.7 inches. Comparing with the corresponding displacements from FEM model, there is about 50% reduction achieved.

Figures 9 and 10 show the base shear force and moment of the center column in pier B. The comparisons indicate that, for the base shear force, the peak values without/with RSPM are 137 kips and 117 kips, respectively; for the dynamic moments, the peak values without/with RSPM are 3.0 mlbf-in and 2.2 mlbf-in, respectively. The reductions are 15% and 25%. Note that, without RSPM control, the calculated peak shear force and base moment from the 16 DOF model is within less than 5% of those from the FEM model. This confirms the validity of the model reduction.

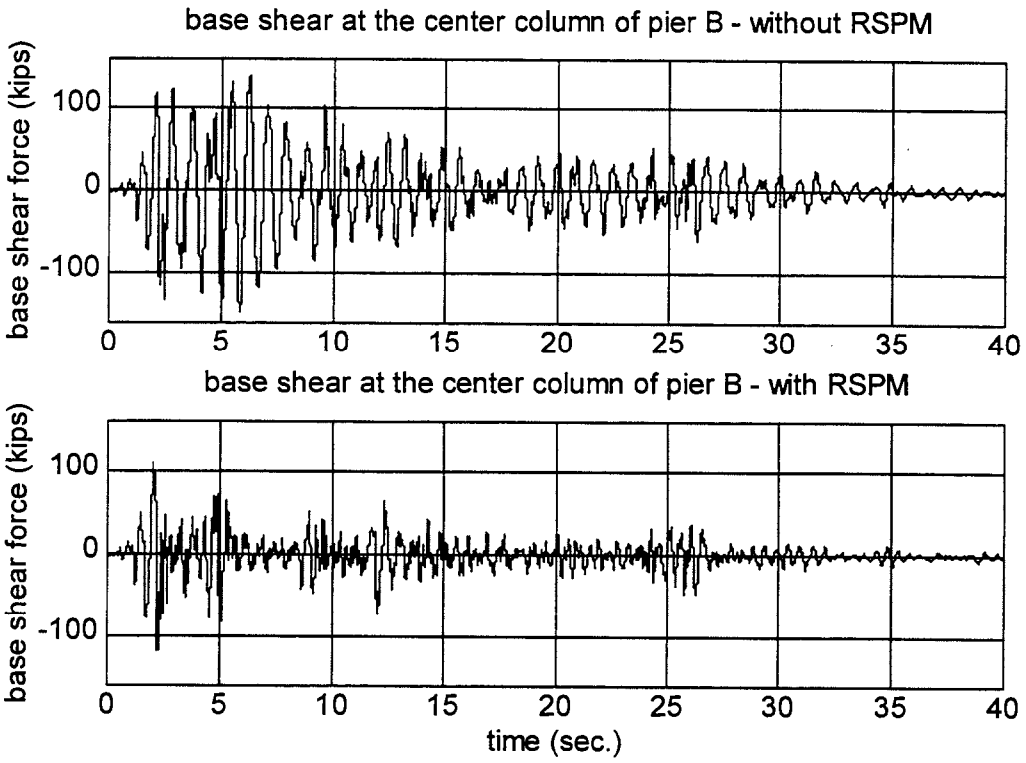

Figure 9. Base shear of the center column in pier B

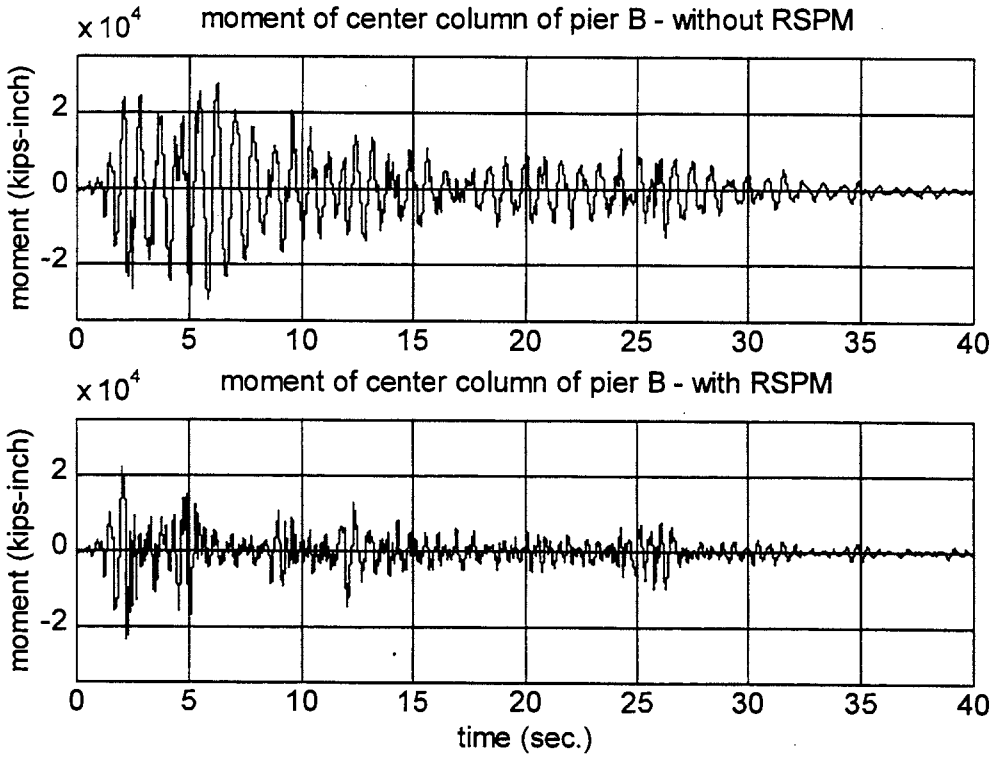

Figure 10. Base moment of the center column in pier B

CONCLUDING REMARKS

In this paper, we have evaluated a potential case of applying a new semi-active control system (RSPM) to highway bridge seismic retrofitting. The analytical and numerical analysis results indicate that the control system could effectively reduce both the base moment of pier columns and the relative displacement between the superstructure and the pier support. Although these results are subject to the theoretical assumption of the elastic material properties for the load carrying members, we believe that the generality of the assumption and the accuracy of the results are acceptable to standard bridge design practice. In particular, the reduction of the FEM model to the 16 DOF model has been validated by the dominant frequencies and displacement, shear force and moment time responses, which implies that this approach could be generally applicable to other non-linear structural control analysis.

APPENDIX: THE RSPM SYSTEM

RSPM is a semi-active control system. It was originally developed with partial support from the National Center for Earthquake Engineering Research (NCEER), State University of New York at Buffalo. After a series of analyses and experiments on a prototype model, it has been demonstrated that the system is potentially capable to control low frequency structural dynamic problems. A TRP project is being jointly carried out at present by The State University of New York at Buffalo, Enidine Inc., and The Caderak Division of Office of Naval Research to further evaluate and develop the RSPM system.

The main function of RSPM control system is to provide variable physical parameters to the control object. In this regard, there are many different control methods available. They may be generally classified into three types: varying damping, varying stiffness, and redistribution of mass. The current RSPM system is based on varying stiffness.

Consider first the following dynamic system

$$MZ'' + C(Z'-x') + K(Z-x) + k_d(Z-y_d) = 0$$

$$m_d y_d'' + k_d (y_d - Z) + c_d(y_d'-x') = 0 \qquad (1)$$

where M, C and K are the mass, damping and stiffness of control object, respectively. Z is the system's displacement. m_d, c_d and k_d are the mass, damping and stiffness of a serial spring-damper assembly connected to the system. y_d is the corresponding device displacement. x and x' are the external motion input.

For this single DOF system, we may denote the control unit as a scalar function R(Z,Z',Z",f). Thus, the dynamic equation can be expressed as

$$MZ'' + CZ' + KZ + R(Z,Z',Z'',f) = f(t) \tag{2}$$

If R(Z,Z',Z",f) represents a switching type of control, and there is no excessive internal power supply for the control device, R can only provide limited control capabilities. The prominent characteristics of such control is adaptive modification of the physical parameters of the spring-damper assembly.

To analyze the effect of R, we may separate the following equation for the serially connected viscous damper and linear spring assembly from the above system of equations (1)

$$m_d y_d'' + c_d y_d' + k_d y_d = kx_1 + cx_2' \tag{3}$$

where x_1 and x_2' are the displacement of the end of spring side and velocity of the end of the damper side, respectively. Depending upon which side of the device is connected to the main system mass, the force acting to the control object is expressed by

$$R_1 = k_d(y_d - x_1)$$

or (4)

$$R_2 = c_d(y_d' - x_2')$$

To correctly carry out parameter control algorithms, the m_d, c_d, and k_d parameters should be chosen carefully, and the interaction of these parameters should be treated properly as well. Some of the issues in this regard may be important to the control device design, but we shall only consider a simple case which will help to describe the RSPM control algorithm.

Consider the dynamic stiffness and impedance of the spring-damper unit (all notations are defined in conjunction with equations (1), (2), (3), and (4))

$$DS_{spring} = \frac{k_d m_d \omega^2 - k_d c_d \omega i}{-m_d \omega^2 + c_d \omega i + k_d}, \qquad DS_{damper} = \frac{k_d c_d \omega i}{-m_d \omega^2 + c_d \omega i + k_d} \tag{5}$$

$$IM_{spring} = \frac{k_d c_d}{-m_d \omega^2 + c_d \omega i + k_d}, \qquad IM_{damper} = \frac{c_d m_d \omega^2 - k_d c_d}{-m_d \omega^2 + c_d \omega i + k_d} \tag{6}$$

If the driving frequency ω is close to or above the natural frequency of the device assembly, R1 and R2 will be largely different. For low driving frequency ω, the mass vs. damping and stiffness ratio become influential.

It is easy to see from the above formulas that the forces at the two ends of the assembly will be the same if mass is neglected. In this case (if the mass is negligible), the device will behave as a spring element when damping is very large; the device will

behave as a damping element when the spring is very stiff; the device can be considered as disconnected when either one of these parameters is very weak. This implies that by controlling either damping or stiffness of the device, we can actually realize a stiffness or damping dominated control algorithms.

The RSPM algorithm is of stiffness dominated type. However, the realization of the algorithm is via controlling of damping parameter in the spring-damper device. In a simplified formulation, the control force is given by

$$R = \begin{cases} k_d(S_d(t) - S_d(\underline{t}_i)) & \underline{t}_i < t < \underline{t}_{i+1} \\ 0 & t = \underline{t}_{i+1} \end{cases} \qquad (7)$$

where $S_d = (y_d - x)$; $\underline{t}_i$ is the i^{th} control point at which a switching command is executed and the device force is released. The control point is determined by a feedback signal. One of the effective algorithms is to maximize the total energy dissipation over the complete course of motion. Namely,

$$E = \max \{ \Sigma dE_i \} \qquad (8)$$

Note that $\{[\underline{t}_i, \underline{t}_{i+1}] \}$ is a finite partition of the interested time segment. The end points of the intervals in the partition correspond to the control points. Substitute equation (7) into (8), we have

$$E = \max_{\Delta} \{ \frac{1}{2} \Sigma k_d \Delta S_i^2 \} \qquad (9)$$

where $\Delta S_i = S(\underline{t}_i) - S(\underline{t}_{i+1})$. The maximum is taken with respect to all finite partitions of the interested time segment. It can be shown that the general result depends on the frequencies and the corresponding amplitudes involved in S. In the simple case of one frequency vibration, the partition for maximal E consists of a finite sequence of time intervals $[\underline{t}_i, \underline{t}_{i+1}]$ such that $S(\underline{t}_i)$ is in one-to-one correspondence with the local maximal points of S.

In simple terms, the RSPM system will take maximal relative displacement as the control points for loading and unloading of the control device. The device is locked in high stiffness mode between the loading and unloading points, and unlocked in low stiffness mode between the unloading point and the next loading point. Thus, in each cycle of motion, the control system will only execute one pair of on/off commands. The control command is derived from the maximal displacement signal, which is independent of the zero-displacement reference. Also, the displacement peak information can be obtained from relative velocity signal, which, in many cases, is more convenient to handle than the displacement information itself.

RSPM control, in general, is most effective for control of displacement related vibration problems. It is equivalent to an adaptive friction damper, which automatically adjusts the "friction force" in proportion to the maximal displacement at each cycle of motion. Such a feature is directly beneficial to seismic applications since most structural

damages are due to large deformation developed in major load carrying members. Thus, reducing the deformation in these members will largely protect structures from earthquake damages. In base isolation applications, the situation is not as straightforward as the seismic ones. It is known that increasing stiffness does not help in reducing the acceleration transmission; however, by maximizing the energy dissipation from the control object, the overall energy transmission will be decreased. In particular, if the control object has strong low frequency vibration in addition to the problem of high frequency motion being not effectively isolated, the solution may be found from using RSPM control along with softer isolator mounts.

ACKNOWLEDGMENTS

The research results reported herein have been partially funded by the National Science Foundation (NCEER contract No. BCS 90-25010) and Office of Naval Research / Advanced Research Projects Agency (ARPA) Cooperative Agreement N00014-96-0007.

Retrofit of Existing Reinforced Concrete Bridges Using VE Dampers

Nishith GUPTA
Graduate School of Engineering
Saitama University JAPAN

Hiroshi MUTSUYOSHI
Dept. of Civil Engineering
Saitama University Japan

William TANZO
Dept. of Civil Engineering
Saitama University Japan

Abstract

The extensive damage caused by the Hyogo-Ken Nanbu earthquake has given sufficient warning of the need for enhancement of seismic resistance of existing RC bridge piers through retrofitting. In this study, a new type of viscoelastic(VE) device was developed to increase the seismic resistance of existing RC bridge piers which typically support the continuous girder. The effectiveness of such a device was proved clearly. Firstly, dynamic properties of a VE device were examined. Secondly, using such a VE device, the response behavior of RC bridge pier under severe earthquakes was investigated taking the nonlinear stiffness degrading behavior of reinforced concrete and the frequency dependent behavior of VE device into account. Furthermore a parametric study was conducted to clarify the influence of moment capacity of RC pier, VE device parameters and different earthquake acceleration levels on the ductility factor of the RC bridge pier. It was found that VE devices are able to reduce the ductility demand of existing RC bridge piers.

1 Introduction

In order to reduce the damage of existing RC pier under severe earthquakes, retrofitting or strengthening of RC piers has been conducted in Japan after the Hyogo-ken-nanbu Earthquake. Most of the methods for retrofit or strengthening of bridge piers aim to increase the strength and ductility by externally reinforcing them with steel plates. The means to reduce earthquake force by some device have hardly been developed and applied to existing RC piers. Generally continuous girders have both movable and fixed bearings. While large earthquake forces act on the piers with fixed bearings, little force is applied to the piers with movable bearings. Therefore there is a need to redistribute these forces among the piers. A VE device consisting of silicone putty has been developed to redistribute forces among piers. In this paper, dynamic properties of the VE device were investigated and response behavior of bridge piers equipped with VE devices was clarified.

2 Characteristics of Viscoelastic Device

A typical VE device shown Fig.1 is composed of a viscoelastic material such as silicone putty, which is vacuum packed between its housing and the movable shaft. The surface of the shaft

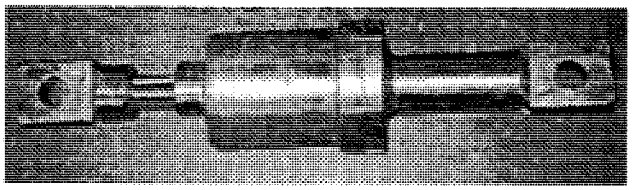

Fig.1 Overview of Viscoelastic Device

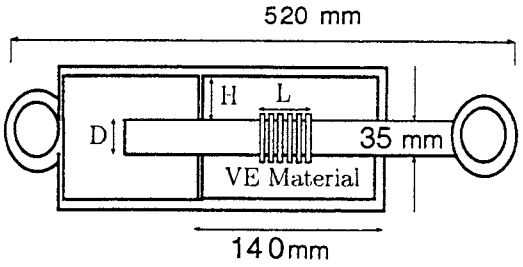

Fig.2 Dimensions of VE Device

has been roughened to provide effective bond between the shaft and the material. This device allows a uniaxial shearing of VE material. The energy dissipation is mainly due to the shear deformation of the material trapped between the shaft and the housing as shown schematically in Fig.2. As shown is Fig.2, D is diameter of shaft, L is the length of shaft roughened and H is VE layer thickness. The effective area(A) in shear becomes A= πDL.

Dynamic tests of the VE devices were conducted under different sinusoidal frequencies. The recorded force displacement loops (Fig.3 and Fig.4) show an almost precise elliptical shape. The equivalent damping factor is 111.0% at 1.0 hz, while it is 51.0% at 3.0 hz. This shows a decrease in damping with increase in frequency. Comparing Fig.3 and Fig.4, it is clear that the inclination of the major axis of the ellipitical loops rotates towards force axis, indicating that the stiffness of VE device becomes larger with the increase of the frequency.

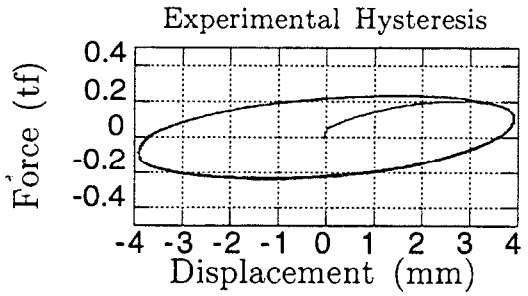

Fig.3 1Hz Hysteresis

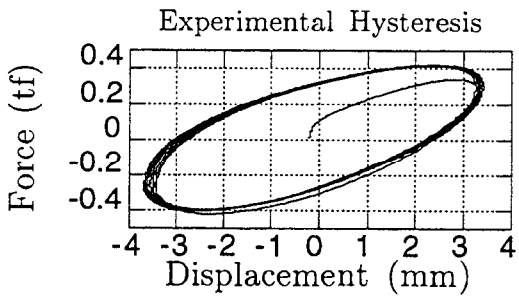

Fig.4 3Hz Hysteresis

3 RC Bridge Used for Analysis

A typical 4-span RC continuous bridge was taken for response analysis. A 2-span, continuous girder bridge, which consists of a middle pier connected to the other two piers by VE devices as shown in Fig.5 was used for the analysis.

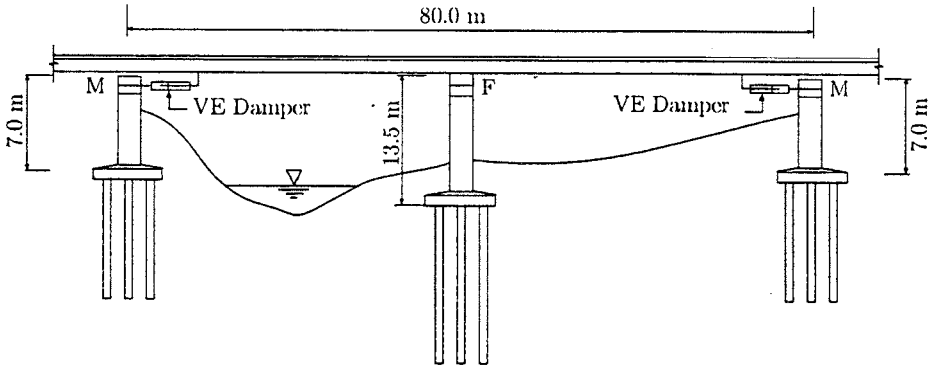

Fig.5 Model of RC Bridge for Analysis

3.1 Numerical Example

The numerical values of the structural properties for the RC bridge (Fig.5.) are given in Table 1. Based on the optimal design method [1], the following values were obtained for VE device

Table 1: Numerical Values

Parameter	Middle Pier	Left Pier	Right Pier
Weight(tons)	916	56	56
Stiffness(tf/m)	12699.0	17766.0	17766.0
Time Period	0.537	0.112	0.112
Moment Capacity (tf-m)	3000	3000	3000

which are as follows: A combination of (i) spring(K_p = 327tf/m) and (ii) dashpot(C_p = 1050 tf-sec/m) in parallel, connected to a (iii) series spring (K_s = 14000.0 tf/m).

4 Response Behavior of RC bridge Structures

The main focus of this paper is on the reduction of the ductility demand of the RC pier with the VE devices, particularly the middle pier because of its high ductility demand. For all the response analyses Takeda's model was used for modeling of the restoring force of the RC piers and Kobe Earthquake with maximum acceleration of 617.0 gals was used as shown in the Fig.6.

4.1 Analytical Results

Fig.7 shows the time history of the displacement response of the middle pier. The maximum displacement response without the VE device is about 20 cm at the time 4.25 sec, while with VE device the maximum one is about 6 cm occurring at the time 8.25 sec. It should be noted that with the installation of the VE devices, the maximum displacement decreases by 14 cm.

Fig.8 shows the time history of the velocity response of the middle pier. The maximum value of velocity without VE device is about 100 cm/sec at time 4.5 sec, while with the VE device the maximum value is about 70 cm/sec at the time 8.5 sec. It is also noted that the maximum velocity reduces from 100 cm/sec to 70 cm/sec with the installation of the VE devices.

Fig.9 shows the time history of the acceleration response of the middle pier. The maximum value of acceleration without VE device is about 750 gals at the time 4.75 sec, while with the VE device the maximum one is about 1100 gals at the time 8.75 sec. Contrary to the trend of displacement and velocity, the maximum value of response acceleration increases by installing the VE device. The maximum inertia force of the pier with the VE device is much larger than that without VE device though the load carrying capacity is the same. The reason for this is that the inertia force was transferred to the other two piers by the VE devices. This is a very important role of the VE device.

4.1.1 Restoring force-displacement curve of the Middle Pier

The Restoring force-displacement curves of the middle pier without and with device are shown in Fig.10 and Fig.11 respectively. It is evident that the use of VE device reduces the damage to the RC pier. Fig.12 shows the relationship between the restoring force and the displacement of the VE device. It is also clear that a VE device absorbs much energy.

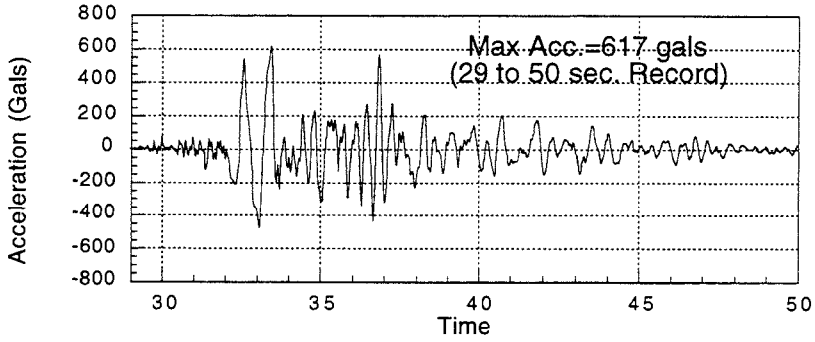

Fig. 6 KOBE (E-W Component)

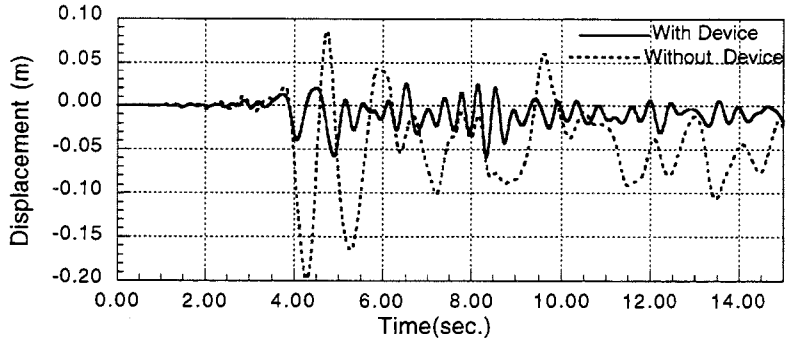

Fig.7 Middle Pier Displacement Response

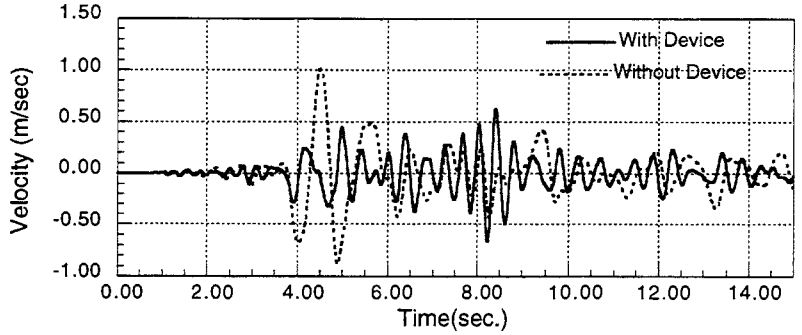

Fig.8 Middle Pier Velocity Response

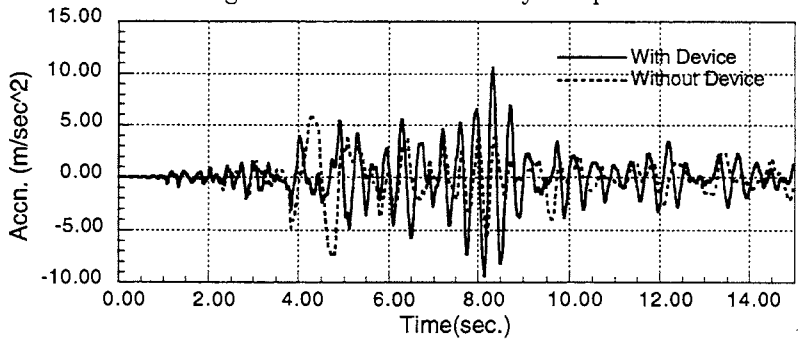

Fig.9 Middle Pier Accn. Response

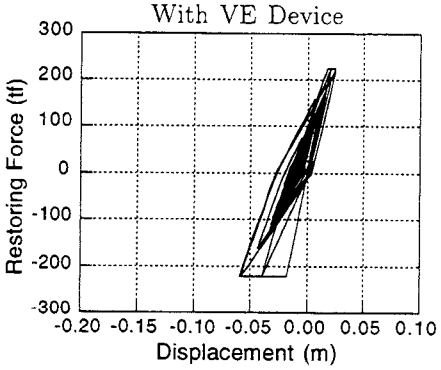

Fig.11 Middle Pier Hysteresis

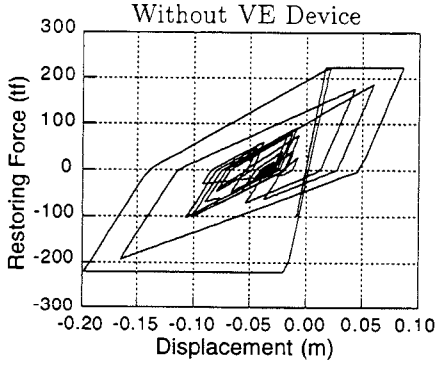

Fig.10 Middle Pier Hysteresis

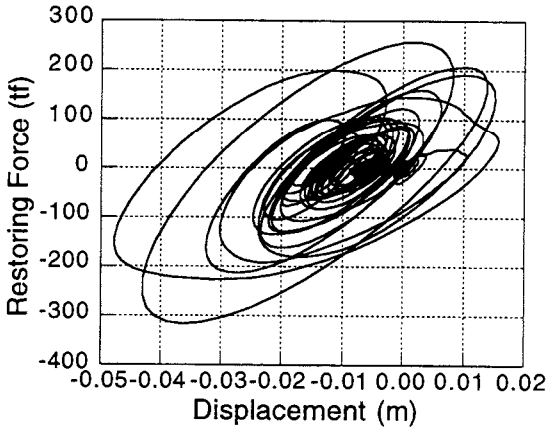

Fig.12 VE Device Hysteresis

4.2 Parametric Study

The numerical analysis was conducted using the same bridge configuration as shown in Fig.5 for different values of the variables given in Table 2. Fig.13 shows the relationship between moment capacity and ductility demand for the middle pier. It is clear that the VE devices can reduce the ductility demand significantly and the A/H ratio (shaft area/viscoelastic layer thickness) over 1.0 reduces the ductility demand effectively. As a result the other piers have to withstand larger forces transferred through the VE device.

Table 2: Variables for Parametric Study

Variables	Range	Remarks
Earthquake Loading	KOBE(E-W):400;800 gals	PGA=617 gals
Moment Capacity(tf-m)	2197.0 (0.6 %); 2945.0(0.95 %); 3496.0(1.20 %); 3924.0(1.40 %)	Moment-capacity (%Reinforcement)
$(A/H)_{prototype}$	$0.1(A/H)_{opt}$, $1(A/H)_{opt}$, $10(A/H)_{opt}$	$(A/H)_{opt}$ is optimal ratio

A/H = The ratio of effective area of shaft in shear to the thickness of VE layer

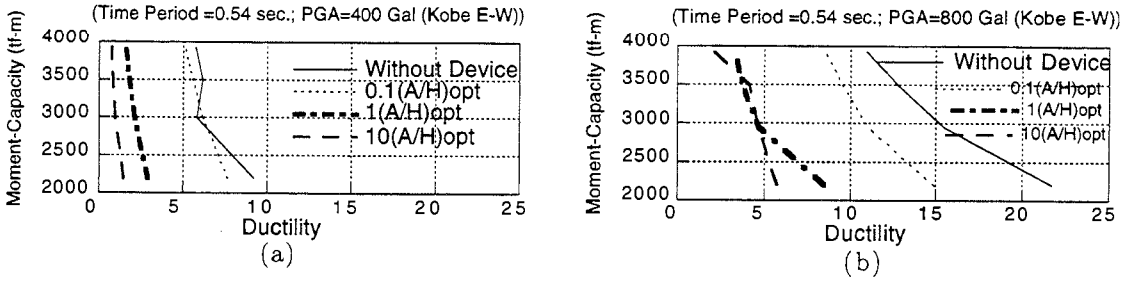

Fig.13: Variation of ductility demand of middle pier for different devices

5 Conclusion

In this study the various aspects of response behavior of RC bridge piers with VE devices have been investigated. It is found that the VE devices can reduce the ductility demand of the reinforced concrete pier significantly by dissipating the vibration energy. It can be concluded that the VE device can be applied to retrofit of the actual existing RC piers in order to enhance their seismic resistance.

References

[1] Gupta, N. " Analysis and Design of Viscoelastic Damper for Earthquake Resistant Bridges". Ph.D Thesis (March 1997), Dept. of Civil and Enviromental Engg. Saitama University, Japan.

[2] Gupta, N., Mutsuyoshi, H., Tanzo, W., Machida, A. " Optimal Design of Viscoelastic Damper for Earthquake Resistant Bridge". Third International Conference on Motion and Vibration Control, Vol.2, pg. 65-71 September, 1-6, 1996 Chiba Japan.

[3] Tanzo, W., Hernandez, J., Mutsuyoshi, H., Tsuzuki, A. " Enhancement of Lateral Sesimic Load Distribution in continuous girder bridges: Test of stiffening and damping component of a new device". Proceedings of Fourth U.S. Japan workshop on earthquake protective systems for bridges. Dec. 1996 Osaka Japan.

ANALYTICAL STUDIES OF SHAPE MEMORY ALLOY DAMPERS FOR STRUCTURAL CONTROL OF BASE ISOLATED BRIDGES

KRZYSZTOF WILDE, PAOLO GARDONI, YOZO FUJINO

Department of Civil Engineering, University of Tokyo, Hongo 7-3-1, Bunkyo-ku, Tokyo 113, Japan

SUMMARY

Base isolation provides a very effective passive method of protecting bridges from the hazard of earthquakes. The proposed smart isolation system combines the laminated rubber bearing with the device made of shape memory alloy (SMA). The constitutive law for superelastic material is extended to describe a hardening of the stress-strain relation of SMA at large strain levels. The smart base isolation utilizes the different responses of the SMA at different levels of strain to control the displacements of the rubber bearing at various excitation levels. At the same time the hysteresis of the alloy is used to increase the energy dissipation capacity. The performance of the smart base isolation is compared with the responses of laminated rubber bearing with lead core to quantify the benefits of applying SMA for isolation of elevated highway bridge.

INTRODUCTION

In recent years, base isolation has become an accepted design alternative for earthquake hazard mitigation for various structures. Extensive reviews on historical developments and recent literature on isolation systems are provided by Kelly[1] and Buckle[2]. Various designs of base isolation were proposed and many concepts were incorporated into seismic isolation framework. The most important common features of such systems are shift of the natural frequency of the structure to a lower value and energy dissipation capacity. In the wake of recent damaging earthquakes in Japan and other countries this passive way of enhancing the performance of the structures becomes particularly attractive due to its simplicity and effectiveness.

Innovative techniques, for controlling structural response, are reaching for smart materials which can introduce new possibilities in earthquake protection methods. One class of such materials is metallic alloys known as shape memory alloys (SMAs). SMA displays a thermoplastic martensitic phase transformation. As SMA is cooled through its transformation temperature range its parent state (austenite) transforms to the lower temperature martensite phase. Such transformation also occurs when the stress is applied to the material. Since stress induced martensite is not thermally stable, as soon as the stress is removed the alloy can revert to the austenite. The inverse transformation recovers the induced strain and such effect is referred to as pseudoelasticity. The pseudoelastic behavior of SMA is observed only when the material is strained above the transformation temperature range, namely, above the austenite finish temperature usually denoted by A_f. The variety of available SMA[3,4] like Nickel Titanium (NiTi), copper based alloys: CuZnAl and CuAlNi, or alloys with Fe, Mn or Sn posses different characteristics of their martensitic transformation. Furthermore, their hysteretic behavior can be controlled by the selection of material and heat treatment. Their usable strain range is much longer than that of the ordinary metals and for some alloys can reach even strain of 70% which is comparable to the allowable strain of mild steel[5]. The pseudoelasticity, freedom of shaping the hysteresis and large ductility of SMAs make them particularly attractive material for applications as an additional damper.

Greasser and Cozzarelli[6] considered Nitinol (NiTi alloy) as a damping material. They proposed a one-dimensional constitutive law for superelastic behavior and verified the applicability of the mathematical model experimentally. The feasible application of a damping device for Nitinol has been investigated by Clark et al.[7] and Higashino et al.[8] The damper proposed by them, was built of

multiple loops of NiTi wire wrapped around cylindrical support posts. The device was experimentally tested over a range of strain amplitudes, loading frequencies and temperatures. Analytical study of the damper, used as a bracing element, were performed on a two-dimensional computer model of 6 story building. The obtained response reduction of displacements was of order 1/2, and the energy absorbed in a frame was 1/8 compared to the frame without SMA device. It was found that the acceleration response was increased. However, the analytical model of SMA, used in the simulations, was a bi-linear law in which neither the superelastic effect nor hardening of Nitinol after the completeness of transformation to martensite could be incorporated.

The seismic isolation of highway bridges by laminated rubber bearing with lead core has been extensively studied[9,10] and the most commonly used procedures for design of bridge with such system are summarize in design guide of the New Zealand Ministry of Works[11] and California code[12]. The ordinary elastomeric bearing with lead core increases the damping of the structure due to the hysteretic properties of the inelastic deformation of lead. Such isolation method gives a significant reduction of pier shear force and pier displacement comparing to monolithic bridge, especially when piers are low and have high rigidity[9]. However, the behavior of lead rubber bearings under strong ground motion result in large deformations of the superstructure and additional displacement restraining device is necessary. The most suitable device for isolation of the bridge deck from seismic input should have variable properties with respect to the intensity of external excitation. For loading caused by stopping of cars, wind action or small earthquake, the bearing should behave as rigid connector, so that the minor external force are not damaging the expansion joints or other auxiliary elements of the bridge. Since, at this level of excitation, the pier shear force is small, the isolation of the superstructure form pier vibration is not essential. For medium intensity loading the isolation system should be fully utilized, i.e., it has to be flexible and provide adequately high damping. At very large ground motions the isolation device should be able to restrain the motion of the superstructure within the design range. Excessive motion of the deck can lead to pounding of the adjacent superstructures which can significantly increase the pier shear force as well as maximum displacements of the deck. Large relative displacements between the superstructure and substructure may cause falling down of the deck. At this excitation level the primary objective is prevention from the total destruction of the bridge and the some potential damage to piers due to increased shear force form stiffer isolation must be accepted. The combination to the ordinary isolation system with the displacement restraining system of stopper can be one direction of varying the isolation property. The variable properties can be also provided by active or semi-active device [13], however, such systems are relatively complex since they require special hardware, sensors, and constant maintenance. A simple bar of SMA inserted into laminated rubber bearing can provide a damper with the desired variable characteristics based solely on the material properties of alloys. (SMAs have high stiffness for small strain levels - elastic modulus of austenite, reduced stiffness for intermediate levels of strain - transformation from austenite to martensite, and high stiffness at high strain - elastic modulus of pure martensite) Furthermore, the proposed device has the inherent centering ability due to pseudoelastic behavior of SMA.

In this paper performance of the SMA device combined with ordinary laminated rubber bearing is presented. Since the proposed device utilizes the SMA "plastic" range as well as elastic response of pure martensite, the constitutive model of Graesser and Cozzarelli[6] is extended to describe hardening at higher strain levels. The simulations are conducted on two degree of freedom model of elevated highway bridge subjected to harmonic excitation of different intensities. The comparison of the performance of proposed smart base isolation and conventional laminated rubber bearing with lead core is presented.

EXTENDED SUPERELASTIC MODEL OF SHAPE MEMORY ALLOYS

A comprehensive constitutive law for Shape Memory Alloys (SMAs) in a thermodynamic formulation has been proposed by Achenbach[14]. The model, derived for the case of plane strain, defines the inelastic strain rate in terms of stress, phase fractions, and several internal variables in a manner analogous to inelastic formulation for creep and viscoplasticity. However, for the preliminary

verification of engineering application of SMA, such a model is far too complex, thus a relatively simple law proposed by Graesser and Cozzarelli[6] is herein adopted.

The model suggested by Graesser and Cozzarelli[6] describes the uniaxial behavior of superelastic material and is a direct modification of rate independent Ozdemir's model[15] for the hysteretic behavior. . The schematic plot of the $\sigma - \varepsilon$ curve of the superelastic material is given in Figure 1.

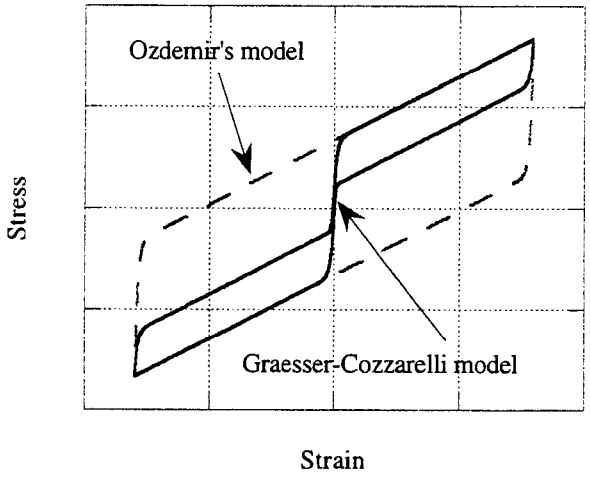

Figure 1. Schematic stress-strain relations due to Ozdemir's and Graesser-Cozzarelli model

The constitutive law due to Graesser et al. modifies the expression of the backstress such that the twinning hysteretic and/or superelastic behavior can be modeled. The stress, σ and strain, ε, are given as follows:

$$\dot{\sigma} = E \cdot \left[\dot{\varepsilon} - |\dot{\varepsilon}| \cdot \left(\frac{\sigma - \beta}{Y} \right)^n \right] \tag{1a}$$

$$\beta = E \cdot \alpha \cdot \left\{ \varepsilon^{in} + f_t \cdot |\varepsilon|^c \cdot erf(a \cdot \varepsilon) \cdot \left[u(-\dot{\varepsilon} \cdot \varepsilon) \right] \right\} \tag{1b}$$

where β denotes one-dimensional backstress, Y is the "yield" stress, or in case of SMA the beginning of the stress induced transition from austenite state to martensite, n is the overstress power and $\dot{(\cdot)}$ is the ordinary time derivative. $\alpha = E_y/(E - E_y)$ is a constant controlling the slope of $\sigma - \varepsilon$, where E is the elastic modulus of austenite and E_y is the slope after yielding. Inelastic strain, ε^{in}, is given by:

$$\varepsilon^{in} = \varepsilon - \frac{\sigma}{E}. \tag{2}$$

Error function, *erf*, and unit step function, $u(x)$, are defined as:

$$erf(x) = \frac{2}{\sqrt{\pi}} \cdot \int_0^x e^{-t^2} dt \tag{3}$$

$$u(x) = \begin{bmatrix} 1 & x \geq 0 \\ 0 & x < 0 \end{bmatrix} \tag{4}$$

Coefficients f_t, c, a are material constants controlling the recovery of the elastic strain during unloading.

When the coefficient f_t is zero, the constitutive law (1) degenerates into a classic viscoplastic behavior show in Figure 1. The superelastic type of response is obtained by modification of the backstress β by the term $f_t \cdot |\varepsilon|^c \cdot erf(a \cdot \varepsilon) \cdot [u(-\dot{\varepsilon} \cdot \varepsilon)]$. For the onset of unloading, the term is activated by the unit step function and the backstress is suddenly increased which simultaneously decreases the inelastic strain. As unloading continues and strain moves closer to zero, the error function (3) is approaches zero, as a result the backstress decreases. The backstress at the point of zero stress is zero and the reverse loading begins with no inelastic strain

Since in this paper, SMA is intended to be used in a wide strain range, the Graesser-Cozzarelli model is extended to represent the hardening of the SMA after the transition to martensite state is completed. As the load increases, the pure martensite follows elastic response with modulus E_m. The modified model is of the form:

$$\dot{\sigma} = E \cdot \left[\dot{\varepsilon} - |\dot{\varepsilon}| \cdot \left(\frac{\sigma - \beta}{Y} \right)^n \right] \cdot u_I(\varepsilon) + E_m \cdot \dot{\varepsilon} \cdot u_{II}(\varepsilon) + \left(3a_1 \cdot \dot{\varepsilon}\varepsilon^2 + 2 \cdot a_2 \cdot sign(\varepsilon) \cdot \dot{\varepsilon}\varepsilon + a_3 \cdot \dot{\varepsilon} \right) \cdot u_{III}(\varepsilon) \qquad (5a)$$

$$\beta = E \cdot \alpha \cdot \left\{ \varepsilon^{in} + f_t \cdot |\varepsilon|^c \cdot erf(a \cdot \varepsilon) \cdot [u(-\dot{\varepsilon} \cdot \varepsilon)] \right\} \qquad (5b)$$

where the functions $u_I(\varepsilon)$, $u_{II}(\varepsilon)$ and $u_{III}(\varepsilon)$ are:

$$u_I(\varepsilon) = \left(1 - u_{II}(\varepsilon) - u_{III}(\varepsilon)\right)$$

$$u_{II}(\varepsilon) = \begin{bmatrix} 1 & |\varepsilon| \geq \varepsilon_m \\ 0 & otherwise \end{bmatrix} \qquad (6)$$

$$u_{III}(\varepsilon) = \begin{bmatrix} 1 & \varepsilon\dot{\varepsilon} > 0 \ and \ \varepsilon_1 < |\varepsilon| < \varepsilon_m \\ 0 & otherwise \end{bmatrix}$$

The term $E_m \cdot \dot{\varepsilon} \cdot u_{II}(\varepsilon)$ in equation (5a) describes the elastic behavior of martensite. It is activated when the strain is higher then ε_m. Strain, ε_m, defines the point when the transformation of SMA from austenite to martensite is completed. The smooth transition from the curve of slope E_y to the slope E_m is obtained by adding the last term in equation (5a) which is evaluated only during loading and for strain $\varepsilon_1 < |\varepsilon| < \varepsilon_m$. The limits are selected from the experimental data[3] for the given shape memory alloy. The constants a_1, a_2 and a_3 are controlling the curvature of the transition. The constants are selected so as the slopes of the function defined by the last term at points ε_1 and ε_m are consistent with the slopes of SMA "plastic" behavior and martensite elastic response. The smoothness of the transition is governed by the selection of slope at strain ε_2. Figure 2 explains the introduced constants in a graphical form.

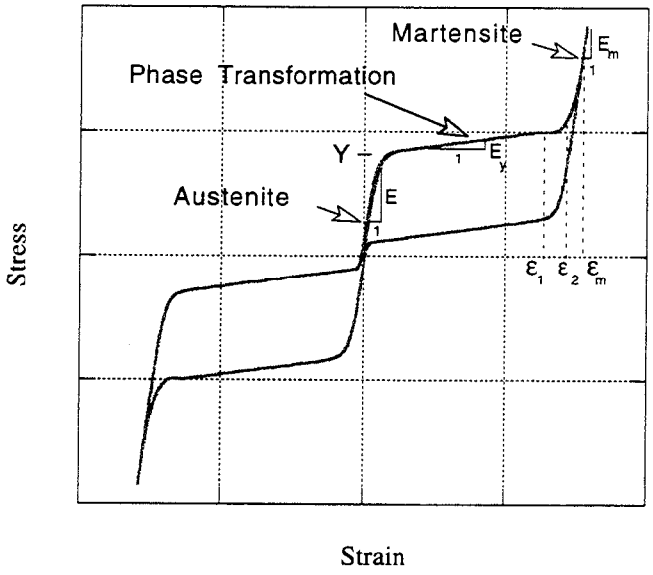

Figure 2. Schematic stress-strain relations of the extended hysteretic model

MODEL OF THE ELEVATED HIGHWAY BRIDGE WITH DAMPING DEVICES

The considered elevated highway bridge, shown in Figure 3, is a three-span-continuous concrete box girder of 14 m width. The reinforced concrete piers have height of 11.5 m and the distance between them is 40 m. The isolation between the pier and the superstructure is achieved by two laminated rubber bearing with lead core or bearings with SMA. The cross sectional area and the height of rubber layers in a single bearing are 0.8881 m and 0.154 m, respectively. Exact dimensions and cross section properties of the structural members are determined after "Manual for Menshin Design of Highway Bridges"[10].

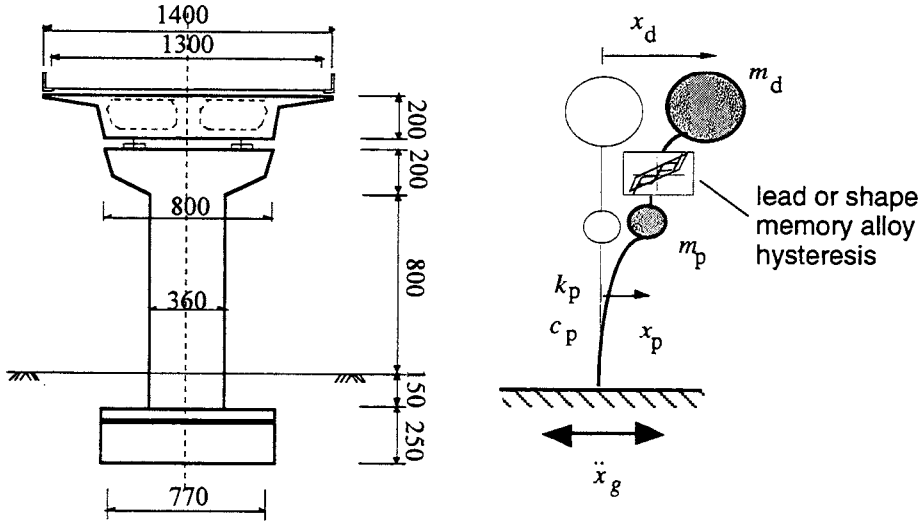

Note: All dimensions are in cm

Figure 3. Structural model of elevated highway bridge with isolation system

The equations of motion of two degree of freedom model bridge are:

$$\begin{aligned} m_d\ddot{x}_d(t) - N \cdot F(x_d, \dot{x}_d, x_p, \dot{x}_p, t) &= -m_d\ddot{x}_g(t) \\ m_p\ddot{x}_p(t) + c_p\dot{x}_p(t) + k_p x_p(t) - N \cdot F_{NZ/SMA}(x_d, \dot{x}_d, x_p, \dot{x}_p, t) &= -m_p\ddot{x}_g(t) \end{aligned} \tag{7}$$

where x_d, x_p and m_d, m_p are displacements and masses of the deck and pier, respectively, and $\ddot{x}_g$ is the ground acceleration. The coefficient of damping and stiffness of the pier are denoted by c_b and k_b. $F_{NZ/SMA}(x_d, \dot{x}_d, x_p, \dot{x}_p, t)$ is the hysteretic force generated by the isolation system and N the number of bearings supporting the deck. The parameters of the two degree of freedom model were estimated by the method given in reference[10] and are given as follows

$$\begin{aligned} m_d &= 8 \cdot 10^5 kg \\ m_p &= 1.4 \cdot 10^5 kg \\ k_p &= 3.2256 \cdot 10^8 N/m \\ \xi_p &= 5\% \end{aligned} \tag{8}$$

Laminated rubber bearing (LRB) with lead core was proposed by Robinson[16] which is often referred to as NZ system. The hysteretic restoring force F_{NZ} is modeled by Wen's model[17] as

$$F_{NZ}(x_b, \dot{x}_b) = \alpha \frac{F_y}{Y} \cdot x_b + (1-\alpha) F_y Z \tag{9}$$

where the relative displacement, s, is

$$s = x_d - x_p \tag{10}$$

Z is the dimensionless displacement governed by first-order differential equation of the form

$$Y\dot{Z} = -\gamma|\dot{x}_b|Z|Z|^{\eta-1} - \lambda\dot{x}_b|Z|^{\eta} + \theta\dot{x}_b \tag{11}$$

Where F_y and Y are the force and the yield displacement and γ, β, θ are dimensionless parameters. The smoothness of transition from elastic to plastic region is governed by η, and α is the ratio of the stiffness of plastic and elastic responses. For the simulations, the parameters are selected as follows: F_y=143,590 kN, Y=0.007 m, α=0.22, β=-0.9, γ = 1.4, θ=1.0 and η=1.

The equation of motion of the bridge with shape memory alloy device is analogous to equation (7) . The additional restoring force $F_{SMA}(x_d, \dot{x}_d, x_p, \dot{x}_p, t)$ is computed from the extended model of SMA defined by equation (5). The elastic modulus of SMA austenite state is $E = 9.66 \cdot 10^{10}$ N/m^2. The elastic modulus of pure martensite, for most of shape memory alloys, is lower than E. However, in this simulations E_m is identical to E. The "yield" stress is assumed to be $Y = 7.245 \cdot 10^7$ N/m^2. The constraints controlling the shape of the superelastic loop are: $n = 1, \alpha = 0.019$, $c = 0.001, a = 900$ and $f_t = 0.02$. The limit of the superelastic range is $\varepsilon_m = 0.11$ and the points defining the transition from the slope E_y to elastic response of pure martensite are $\varepsilon_1 = \varepsilon_m - 0.01$ and $\varepsilon_2 = (\varepsilon_m + \varepsilon_1)/2$. The volume of the alloy is optimized so that the stress in the alloy during the largest considered acceleration level reaches the elastic response of pure martensite. For this condition the total area of the alloy was found to be $A = 0.0185$m^2.

RESPONSE ANALYSIS

The proposed base isolation system has the potential ability of dissipating energy and controlling the maximum displacements of the deck at different levels of external excitation. The main focus in the following analysis is placed on the displacement and acceleration of the deck, on the relative displacement between deck and pier, on the shear force of the pier, and on the amount of damaging energy absorbed by the structure. The advantages and disadvantages of smart base isolation are presented by comparing with the performance of the structure isolated by rubber bearings with lead core. For easy understanding and interpretation, the earthquake excitation is assumed to be a simple harmonic function.

a) Deck displacement and relative displacement between deck and pier

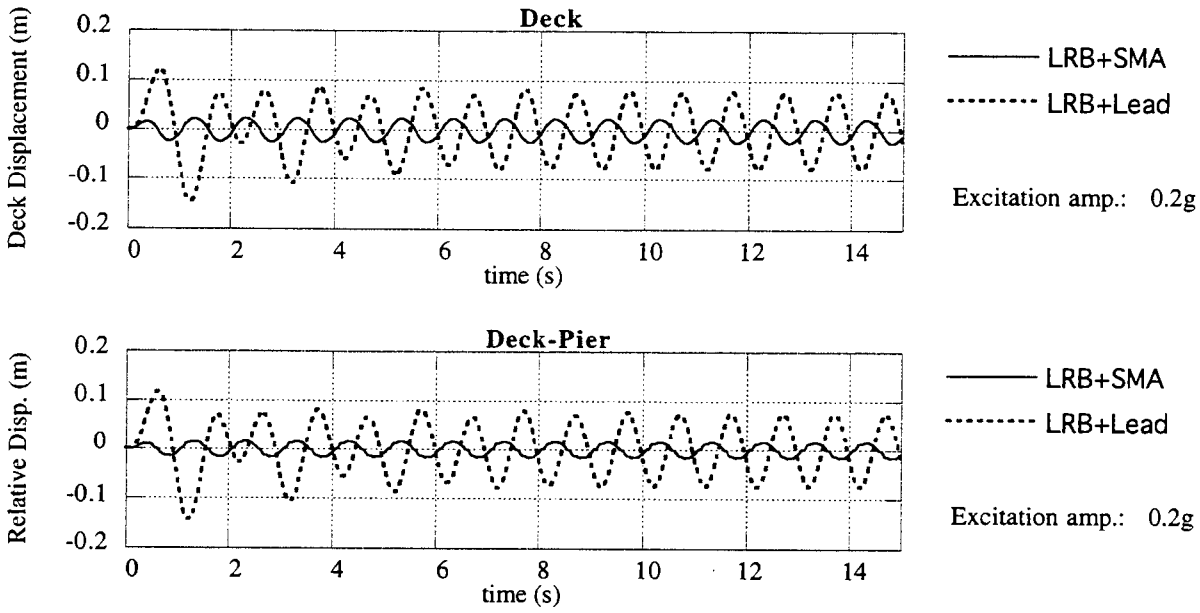

Figure 4. Response of structure with NZ system and SMA base isolation to harmonic excitation with amplitude 0.2g

The preliminary simulations are conducted for a sinusoidal ground motion with frequency $\omega_g = 6.28$ rad/s ($T_g = 2\pi/\omega_g = 1$) and for three acceleration amplitudes: 0.2g, 0.4g and 0.6g.

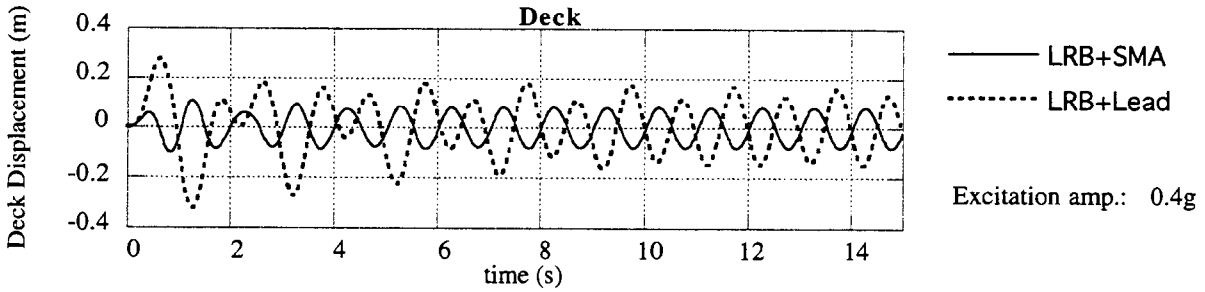

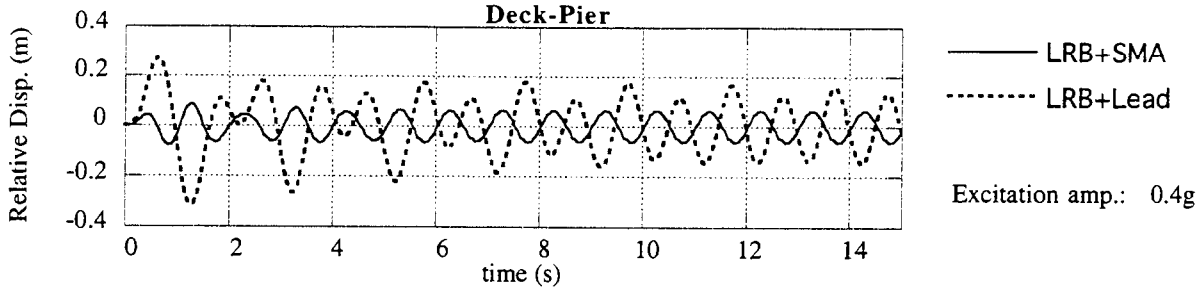

Figure 5. Response of structure with NZ system and SMA base isolation to harmonic excitation with amplitude 0.4g

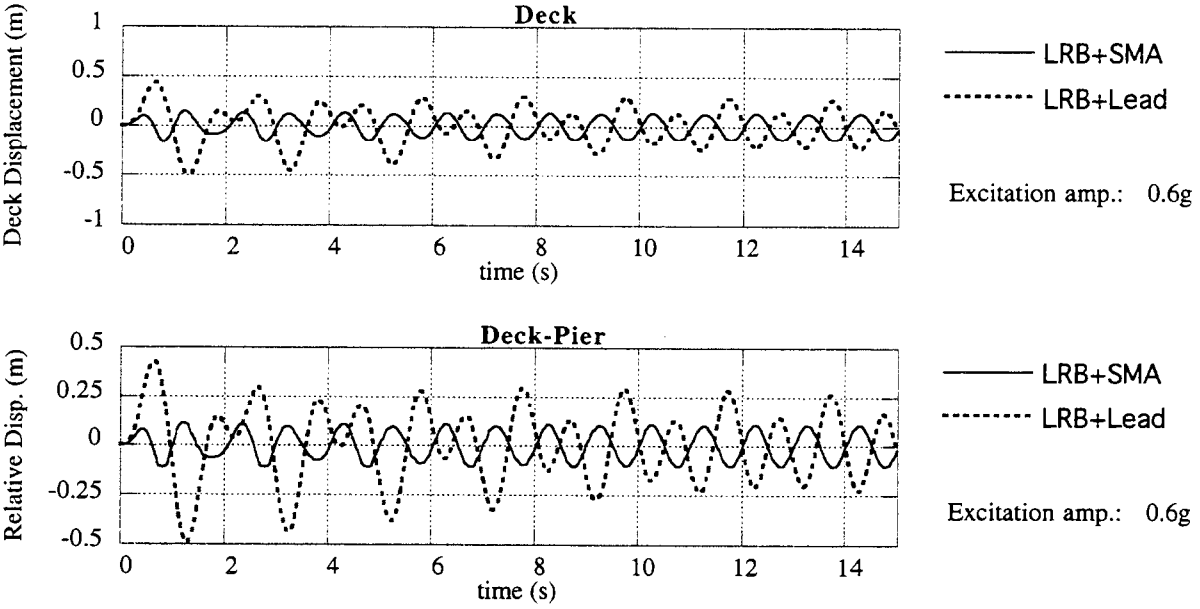

Figure 6. Response of structure with NZ system and SMA base isolation to harmonic excitation with amplitude 0.6g

Selected responses of the structure with NZ system (LRB+Lead) and smart base isolation (LRB+SMA) are plotted in Figure 4, 5 and 6. Relative displacement between deck and pier of the system with SMA device under 0.2g excitation amplitude is very small compared to the NZ system, since the alloy almost remains in its elastic range, going only into the very beginning of the formation of stress-induced martensite (SIM) phase. For this excitation amplitude, the steady-state relative displacement in case of NZ system is six times the steady-state relative displacement in case of LRB+SMA, and the absolute steady-state displacement of the deck is around five times the one for LRB+SMA. For the excitation amplitude 0.4g and 0.6g the steady-state relative displacement in case of NZ system is, in both cases, around two times the steady-state relative displacement for LRB+SMA. The same proportion is found for the steady state absolute displacements of the deck of the two hysteretic system. Displacement of the pier, for LRB+SMA, was found to be four times the NZ system for all excitation amplitudes, Figure 7 shows the pier displacement for the excitation amplitude 0.6g.

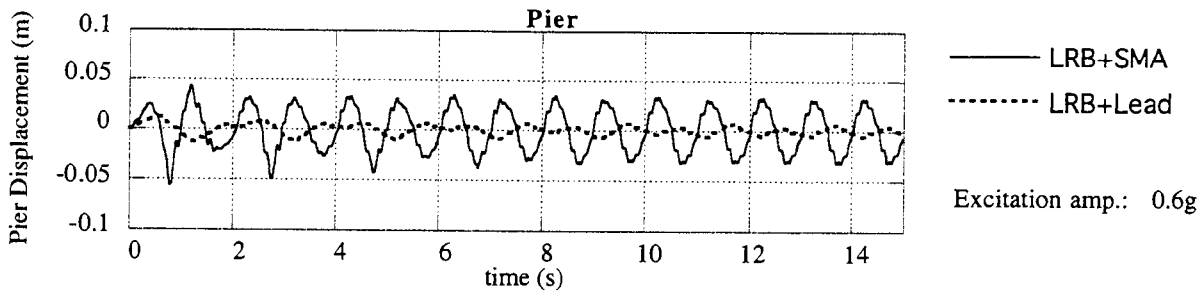

Figure 7. Response of structure with NZ system and SMA base isolation to harmonic excitation with amplitude 0.6g

b) Hysteretic force-displacement relations of LRB+lead core and LRB+SMA

Figure 8 compares the force-displacement relations in the additional dampers of NZ and LRB+SMA systems for different loading levels.

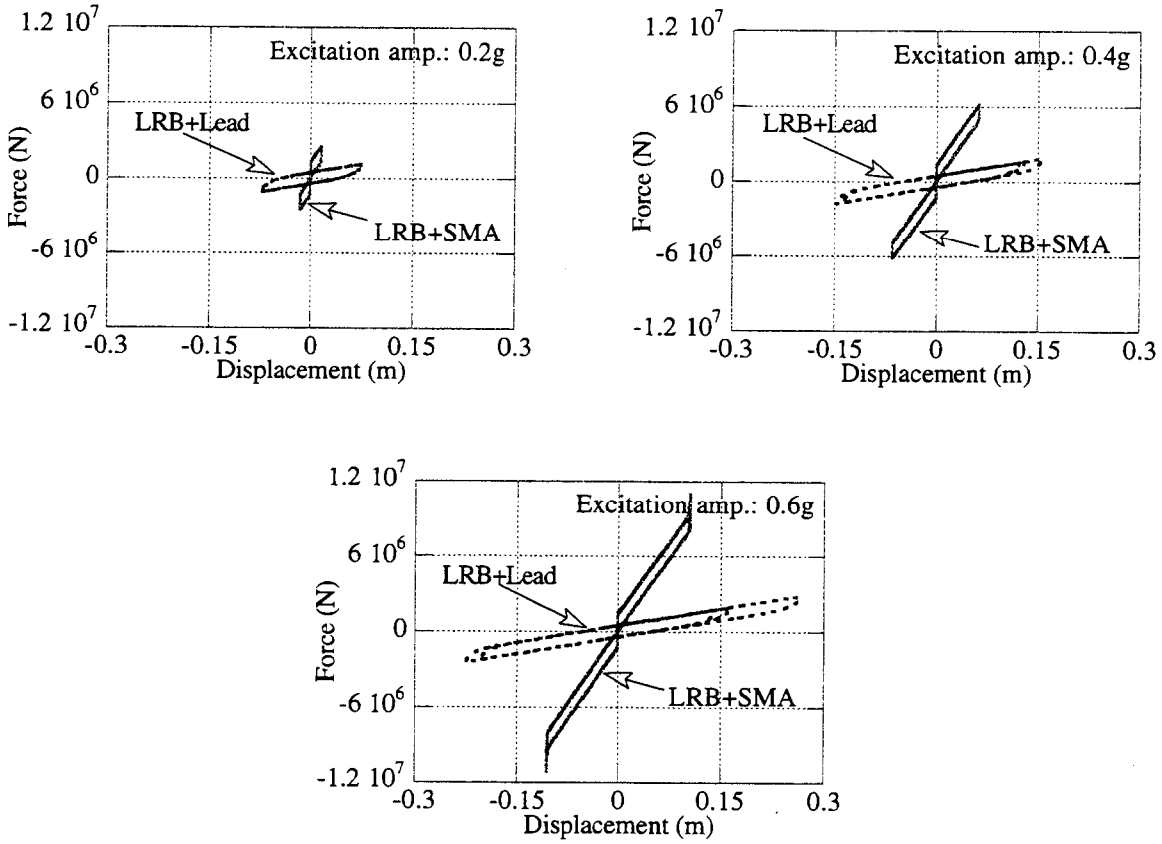

Figure 8. Hysteretic force-displacement relations of LRB+lead core and LRB+SMA under harmonic excitation of different intensity

c) Deck acceleraiotn and pier shear force

A drawback of adding a damper (lead or SMA) to LRB system is the increase of acceleration response. The change of stiffness of the SMA, particularly during the transition from "plastic" response to the elastic one, results in sudden jump of acceleration. For all the loading levels the steady-state peak acceleration of the deck with SMA device is larger by a factor ranging between 2 and 3 as compared to the acceleration response of NZ system. This difference is most pronounced under 0.6g amplitude excitation and is shown in Figure 9

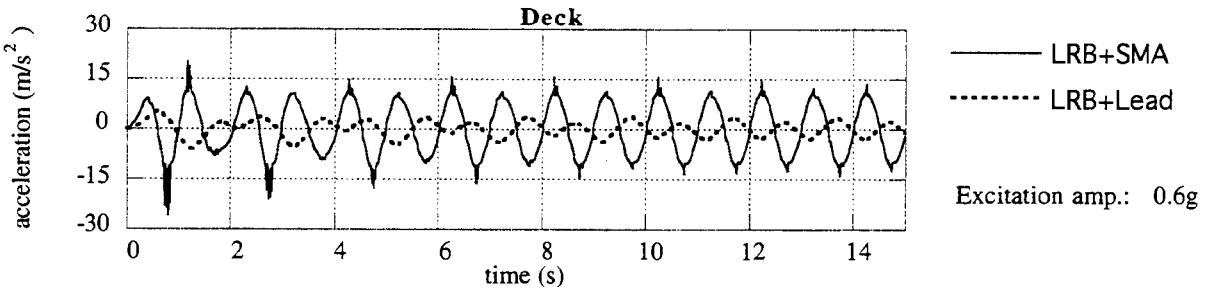

Figure 9. Acceleration response of the deck with NZ system and SMA base isolation to harmonic excitation with amplitude 0.6g

It was found that the shear force at the base of the pier also increases in LRB+SMA system with respect to the NZ system. The most negative case of shear force response is under 0.6g excitation and it is shown in figure 10.

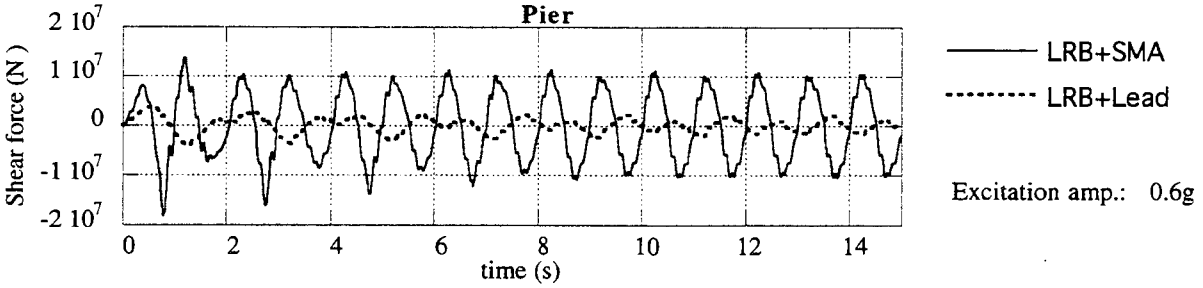

Figure 10. Shear force response of the deck with NZ system and SMA base isolation to harmonic excitation with amplitude 0.6g

d) Energy time histories

The performance of proposed base isolation system is analyzed by comparing the time histories of energy of the structure with NZ system. The input energy is the total energy related to inertia forces included by the ground motion, i.e., the summation of all the right hand side terms in equation (7). The kinetic energy of pier and deck plus the elastic energy of pier and LRB is referred here as the structure damage energy. The time history of energy of the structure with NZ system for the three different excitation amplitude is shown in Figure 11. While the same for SMA system is shown in Figure 12.

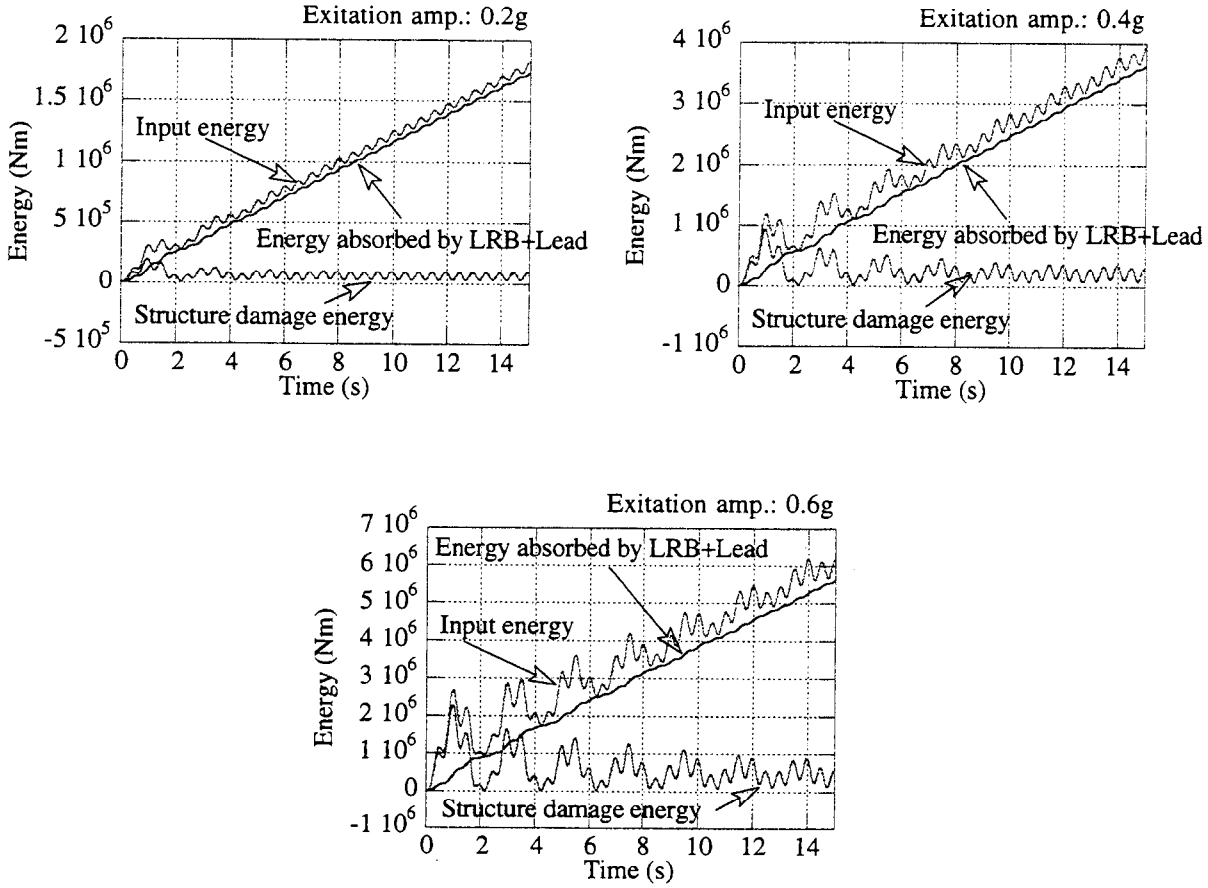

Figure 11. Energy time histories for bridge with NZ

In LRB+SMA system, the input energy for all cases of loading is smaller than the NZ system. At the ground acceleration amplitude of 0.2g; the input energy for NZ system is three times bigger than LRB+SMA and the damage energy is eight times larger. Under excitation level of 0.4g input energy and damage energy, for the NZ system, are respectively 1.5 and 2.7 times bigger than for LRB+SMA. While the same indices are 1.2 and 2.5 for 0.6g acceleration..

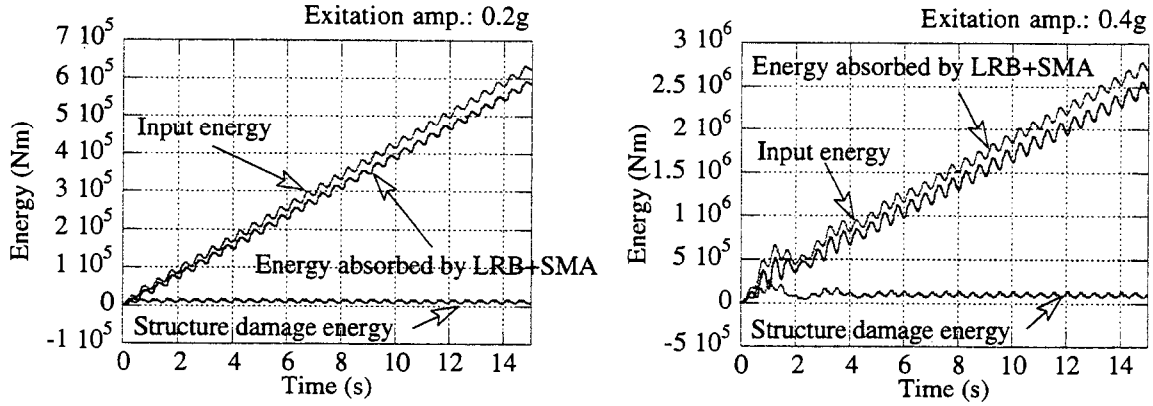

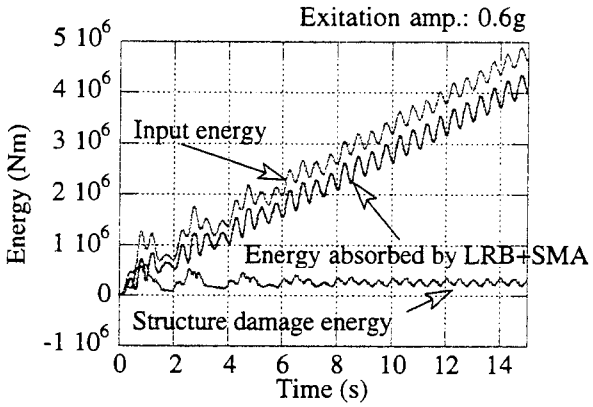

Figure 12. Energy time histories for bridge with LRB with SMA

e) Spectral analysis

Using a ground acceleration with an amplitude of 0.5g and Tg ranging from 0.3s to 1.5s, the performances of NZ system and LRB+SMA are evaluated and the resulting response spectra are described in this section. The variations of the steady-state peak relative displacement versus period of external excitation Tg for the two base-isolation systems are shown in Figure 12. It must be noted that the SMA device was designed for Tg=1, at which value the maximum relative displacement of LRB+SMA system is half as compared to the NZ system. Therefore the proposed system achieves of avoiding span fall-off or pounding with the adjacent superstructures. Figure 12 shows also that for all the periods of external excitation the maximum relative displacement is never going to exceed ε_m, which is due to the hardening of Nitinol, giving a plateau from Tg=0.6 to Tg=0.9.

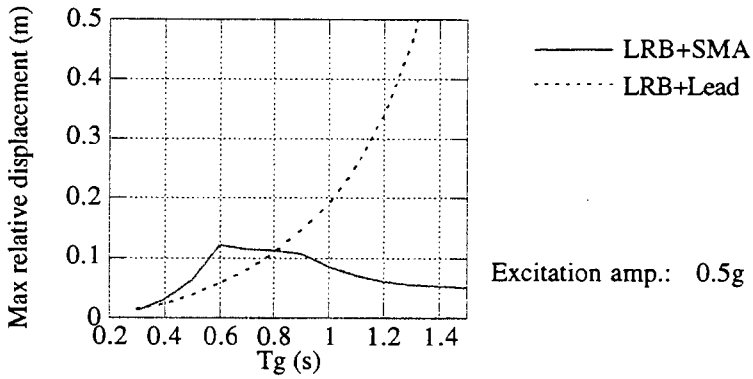

Figure 13. Variation of peak relative displacement with the period of the sinusoidal excitation Tg

CONCLUDING REMARKS

The work presented in this paper is a beginning of the analytical and experimental study of a possible application of SMA as an additional damping device for base isolation system. The potential advantages of an additional damper of SMA are the possibility of varying the base isolation properties at different levels of excitation, restoring force provided by the superelasticity effect, large ductility and large energy dissipating capacity. Although the mechanical properties of alloys other

then Nitinol are not well understood, the variety of available SMA and the possibility of controlling their properties through material selection and applied heat treatment makes them potential candidates for further base isolation applications.

The uniaxial model of superelastic material is extended to incorporate the SMA behavior after the completeness of the transformation from austenite to martensite. The model is used to simulate the restoring hysteretic force generated in SMA device under harmonic ground motion with different intensities. Although, the configuration of the device is not explicitly specified, the desired force-displacement relationship is determined. For selected parameters of SMA the proposed smart base isolation system reduces the relative displacements between deck and pier in all the considered levels of external loads. Under small excitations, e.g. small earthquakes or wind forces, the isolation with SMA behaves like rigid member. At medium size loads, SMA enters the transformation and due to hysteretic behavior dissipates energy. The maximum relative displacements due to strong ground motion can be limited by the additional hardening of martensite state. The attachment of SMA to the LRB system reduces the damage energy which enters the structure comparing to the LRB system with a lead core up to eight times. However, the acceleration response of the deck and the shear force at the base of the pier are increased. The peak responses are also studied, changing the external excitation period, and it is shown the effectiveness of SMA device in the smart limitation of the relative displacement between deck and pier.

ACKNOWLEDGMENTS

The authors would like to thank Stefano Besseghini from ITM-CNR, Italy, and Robert Jankowski and Muhammad T.A. Chaudhary from the Department of Civil Engineering, University of Tokyo, Japan, for discussions and valuable comments.

REFERENCES

1. J. M. Kelly, "A seismic base isolation : a review and bibliography", *Soil Dynamics & Earthquake Engineering*, **5**, pp. 202-216. 1986.
2. J. G. Buckle and R. L. Mayes, "Seismic isolation: history, application and performance-a world overview", *Earthquake Spectra*, **6**, No. 2, pp. 161-202. 1990.
3. T. W. Duerig, K. N. Melton, D. Stockel, and C. M. Wayman, *Engineering aspects of shape memory alloys,* Butterworth-Heinemann, 1990.
4. S. Besseghini, L. Mirri, and A. Tuissi, "Production and functional characterization of TiNiCu based shape memory alloys", *Proceedings of 7-th International Conference on Adaptive Structures and Technologies*, Rome, Italy, 1996.
5. M. Nakashima, "Strain-hardening behavior of shear panels made of low-yield steel. I: Test", *Journal of Structural Engineering ASCE*, Vol. **121**, No. 12, pp. 1742-1757, 1995.
6. E. J. Graesser and F. A. Cozzarelli, "Shape Memory Alloys as New Materials for Aseismic Isolation", J. Eng. Mech. ASCE, Vol. **117**, No. 11, pp. 2590-2608, 1991.
7. P. W. Clark, I. D. Aiken, J. M. Kelly, M. Higashino, and R. C. Krumme, "Experimental and analytical studies of shape memory alloy damper for structural control", *Proceedings of Passive Damping*, San Diego, California, 1995.
8. M. Higashino, S. Aizawa, P. W. Clark, A. S. Whittaker, I. D. Aiken and J. M. Kelly, "Experimental and analytical studies of structural control system using shape memory alloy", *Proceedings of 2nd International Workshop on Structural Control*, Hong Kong, December, 1996.
9. D. H. Turkington, A. J. Carr, N. Cooke, and P. J. Moss, "Seismic design of bridges on lead-rubber bearings", *Journal of Structural Engineering ASCE*, Vol. **115**, No. 12, pp. 3000-3016, 1989.
10. K. Kawashima, M. Okado and M. Horikawa, 'Design example of a highway bridge based on the Manual for Menshin Design of Highway Bridges', *Recent Selected Publications at Earthquake Engineering Division, Public Works Research Institute (No.2)*, May, 1993, pp.191-208.

11. New Zealand Ministry of Work and Development. (1983). "Design of lead-rubber bridges bearings" *Civil Division Publication 818/A*. New Zealand Ministry of Works and Development, Wellington, New Zealand.
12. Dynamic Isolation Systems. (1984). *Seismic base isolation using lead-rubber bearing-Design procedures for bridges*. Dynamic Isolation Systems, Berkeley, California.
13. K. Kawashima, S. Unjoh, H. Iida, and H. Mukai, "Effectiveness of the variable damper for reducing seismic response of highway bridges", *Recent Selected Publications at Earthquake Engineering Division, Public Works Research Institute (No.2)*, May, 1993, pp.133-148.
14. M. Achenbach, T. Atanochovic, and I. Muller, " A model for memory alloys in plane strain", *International Journal of Solids and Structures,* **22(2)**, pp. 171-193, 1986.
15. H. Ozdemir, "Nonlinear transient dynamic analysis of yielding structures", Doctoral thesis, University of Berkeley California, 1976.
16. W. H. Robinson and A. G. Tucker, "A lead-rubber shear damper", *Bulletin of New Zealand National Soci. for Earthquake Eng.* **10**, No. 3, pp. 151-153, 1977.
17. M. C. Constantinou, and I. G. Tadjbakhsh, "Hysteretic dampers in base isolation: random approach", *Journal of Structural Engineering ASCE*, Vol. **111**, No. 4, pp. 705-721, 1985.

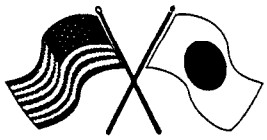

Session 7
Reconstruction Strategies, Social & Economic Impacts

Session Co-chairs: James Foster and Akira Igarashi

Rapid Disaster Recovery: A Case Study for Bridge Replacement
Earl Seaberg

An Integrated Model of Bridge Performance, Highway Networks, and the Spatial Metropolitan Economy: Towards a General Model of How Losses due to Earthquake Impacts on Lifelines Affect the Economy
Peter Gordon, James E. Moore II, H. W. Richardson and Masanobu Shinozuka

Rapid Disaster Recovery:
A Case Study for Bridge Replacement

By

Earl Seaberg, P.E. [1]

Abstract

On January 17, 1994, the northern region of the Los Angeles basin was rocked by a magnitude 6.8 earthquake. This paper presents a case study of the California Department of Transportation's response to the January 17, 1994, Northridge Earthquake for the replacement of Gavin Canyon Overcrossing. The replacement bridge was redesigned in 20 days and it opened to traffic after 120 days.

This paper is from the perspective of a structural design engineer and may not discuss other important aspects that could play a significant role in the recovery process.

Introduction

Disasters that affect our human environment happen with great regularity around the world. Lives are lost due to the event itself or due to circumstances that follow. Facilities of many types suffer substantial damage and loss of use for a considerable time following the event. The economic losses can have a greater impact than the event itself.

Transportation facilities are subject to the same forces of nature and have suffered significant damage and a similar loss of use. The response to this event and others like it has demonstrated that these facilities can be rapidly repaired or replaced. It is important to understand how this was accomplished and what actions are necessary that allow this to happen.

Events of January 17, 1994

On January 17, 1994, at 4:31 AM, a magnitude 6.8 (Richter) shook the San Fernando Valley area of Southern California. Damage to the region was extensive and over fifty people lost their lives.

[1] Senior Bridge Engineer
Office of Structure Design
California Department of Transportation
P.O. Box 942874
Sacramento, CA 94274-0001

The region's freeway corridors suffered extensive damage. Seven bridges had suffered partial collapse rendering four freeways unusable and created a transportation nightmare for commuters and commerce until partial service was restored through the use of detours.

The original Gavin Canyon Undercrossing were twin parallel bridges that crossed the old state highway. Built in 1965, the original concrete box girder bridges were 741 feet in length, each having five spans. The earthquake caused the superstructure to unseat at the expansion joints causing a flexural failure in the superstructure.

Reconnaissance and Assessment

The recovery process began immediately. Caltran's Engineering and Maintenance Staff who live in the area reported to work and began reconnaissance and assessment of the damage.

Additional teams of Bridge Maintenance Engineers and Design Engineers from Sacramento assembled and left for Southern California later the same morning. Their primary responsibilities were reconnaissance, performing a detailed damage assessment of the affected structures, and preparing recommendations for repair or replacement. This effort is crucial for developing an effective strategy for recovery.

Only a few people were called in to work on January 17. Even though it was an official state holiday, many arrived in the Sacramento office with bags packed, ready for several days of field assignment. All of those who arrived in the office that day were utilized in some fashion.

Once the teams arrived in the Los Angeles area later in the evening, they reconvened at a pre-designated hotel that became the operation's headquarters for the next several weeks. Each day the teams met at breakfast to receive route assignments and then began inspecting there assigned routes from the area closet to the epicenter, working radially outward, until no further damage was found. They met back at the hotel every evening and prepared Supplemental Bridge Reports of the day's activities before retiring for the night.

Preliminary Recovery Planning.

While the reconnaissance and damage assessment operations were in progress, other engineering staff remained in the Sacramento office to begin the process of the planning the reconstruction.

The preliminary information that was available on the day of the earthquake was very poor. Some of the best information came from television news reports. It was quite

obvious that several bridge replacements were essential, although it was necessary to precisely identify these bridges before any work could begin.

The detailed damage assessments started to arrive in Sacramento on the evening of the 17th, as the local reconnaissance teams returned from the field. The influx of damage assessments continued every evening for several days. Engineering staff were camping out in the Sacramento office for several days receiving these reports or assisting with any needs of the teams in the Los Angeles area.

It is imperative that accurate damage information from trained and experienced staff be obtained quickly. Reliable, meaningful information is one of the most important parts of the recovery process. Only when this information is available can a legitimate recovery strategy be created.

This strategy must consider the importance of the routes served and the availability of detours, as well as the ease of repair or replacement.

Designing the Replacement

The detailed planning and design process begins after determining the specific locations and the extent of the damage. The starting point for the design is assembling the readily available knowledge that the organization has already gathered.

There are several areas of critical information that should be gathered as a part of the normal practice of doing business. Gathering this information before a catastrophic event will greatly enhance the ability to recover rapidly.

- Gather, maintain, and make readily available as-built plans for all projects. These must include original project and any subsequent modifications or repairs. This is probably the single most important element when faced with an emergency replacement project.

- Original soil boring logs are of great importance when determining the foundation type for the new structure.

- Current utility information is essential to properly locate the new foundations of the replacement structure. Facility owners in hazardous areas should maintain current and accurate utility mapping for any utility that encroaches on their right-of-way. This information becomes invaluable during a crisis.

- Record all obstructions that could interfere with a replacement or repair project and make these records readily accessible. These may include buildings or other facilities

that occupy the area below or are immediately adjacent to elevated structures. In urban areas it is common practice to lease the airspace under bridges for commercial enterprise. If a replacement becomes necessary these facilities could suffer a great disruption until the construction is complete.

Even though an organization has established a database of information, it may be necessary to obtain additional information to complete the contract documents for the new project.

- Given advances in geotechnical engineering, additional foundation studies may be necessary, which could include more soil borings. Carefully consider how this will affect the design and the project schedule.

- Current utility information must be available. This is necessary for determining the locations of the new foundations.

- Other information may be required depending specific conditions at a particular site. The presence of waterways, railroads, environmentally sensitive areas, or other special conditions may have a significant impact on the direction and schedule of the project. The Management and Design Teams should be sensitive to these conditions and be prepared to respond accordingly.

Assign the project to staff that have demonstrated considerable experience and judgment. Many decisions based on solid engineering judgment with few calculations will be necessary to complete the project in a timely fashion.

There are several important points that are somewhat unique to emergency replacement projects.

- It is important to understand that the adversary is usually time and not the project costs. The total cost of the project must include the economic losses that are occurring while operating without the facility. In urban areas these costs are often very high and, depending on the facility and the availability of quality detours, could be lower in rural areas. Adding the design duration to this cost makes it necessary to find ways to reduce this time. This rational allows a design that may be somewhat more expensive, while reducing the design and construction time.

- Replace the structure to the same alignment and elevations of the previous structure. This is another important use for the as-built information. Realize that the replacement project will need to tie into the existing facilities and elevations at some location.

- Keep the design as simple as possible. This will allow for faster design and construction while minimizing construction problems. It also allows for the use of conservative judgement in making design decisions.

- It is important to focus the efforts on the most important part of the design package, the plans. Subsequent portions of the project often require the use of the plans. Experienced structural drafting technicians can draw plans for many bridge types without the engineering being complete.

- The method used for the replacement of Gavin Canyon was a "team double component design" using a large staff, as opposed to a more traditional finish-to-start process for design, detail, check, method that is performed by a few people. This operation occurred simultaneously with the plan preparation.

After resolving the differences, the "double design" method in effect serves to check the engineering and all that remains is a plan check. This method allowed for the design, detailing, and checking to occur simultaneously. However, this method is very inefficient and increases design costs 20% to 50%. It does make a drastic cut in the time required to complete the project documents. After the final plans were completed and delivered one engineer performed a final check on the project.

The plans for the Gavin Canyon project were 80% complete and were finished 5 ½ days after the project assignment was made, only 9 days after the earthquake. These plans were more than adequate to Advertise and begin construction. The project was Advertised on January 26, 10 days after the earthquake. The final plans were completed 17 days after the project assignment, on February 5. The total time from the earthquake to delivery of the final contract plans was 20 days.

Other very important and noteworthy efforts were made by the staff who were responsible for the foundation studies and site plans. The drilling and surveying operations occurred during the demolition operations, other staff who prepared the specifications and estimate, completed this task using very preliminary information. The final bid package was assembled in a few hours and hand carried to pre-selected contractors around the state.

These techniques allowed for the project development process to take a few weeks as opposed to one to two years for the normal process.

Design Features

Several noteworthy features were incorporated into the designs to allow for ease of adjustment should field conditions warrant.

The piles at the abutment and bents are the concrete, cast-in-drilled-hole type. This allowed for adjustments in length using readily available onsite materials.

This became necessary for the Gavin Canyon project as the final foundation study was not completed until February 3. This study showed that the soil assumptions made using the as-built plans were in error and the CIDH piles at the bents needed to be about 25 feet longer than originally planned. Because this foundation system is fabricated onsite, it was very easy to extend the length of the pile.

All of the abutments were designed for the single worst case for the maximum height of the fills, even though some savings could have been realized by using the actual heights at the various locations. Although conservative, it proved to be a good choice as one of the abutment slopes were cut back further than we had planned, thus exposing the footing. The abutment footing was lowered without a costly redesign.

Reconstruction

Immediately after the earthquake, contracts were issued to demolish the existing bridges. This began the evening of January 17 and continued until the replacement contract started on January 30. The existing bridge was demolished and a temporary detour was established through the site using the lower roadway, which was the original highway. This complicated the foundation studies, site survey, and the construction efforts.

The contract documents were based on the Preliminary Plans that were 80% complete. The contract was Advertised to pre-selected contractors on January 26th and the bids were opened on January 29th.

The contract contained several features designed to speed construction. The successful bid was determined based on the value of contract items plus the number of working days. The number of working days were multiplied by the daily incentive/disincentive value of $150,000 per calendar day. No non-working days were granted for any reason, including inclement weather.

This contract method allows the contractor a bonus for early completion or a penalty for completing the work after the time that was bid. This allowed the contractor to become very creative in resolving problems normally associated with this type of work.

Fortunately the weather cooperated and it only rained a few times with minimal impact to the contract. A contractor on another project even leased a train to bring supplies to the Los Angles area. This is an example of the creativity that the contractors displayed in completing these projects.

The worked progressed around the clock until traffic was fully restored on May 18.

Despite the accelerated schedule, only a few problems were encountered. Design staff were available on an around the clock basis to resolve any questions or conflicts. However, a higher than normal number of conflicts should be expected when preparing and constructing projects in this fashion.

Conclusions

This effort and others like it demonstrated that a rapid and successful recovery can occur after natural disasters. Within six months most of the key bridges had been repaired or replaced. By years end work on the remaining structures was completed and full service had been restored to all the freeways that were affected by the earthquake.

The recovery effort demonstrates that the way an organization conducts its business under normal circumstances has a major impact on how it is able to respond during a crisis.

Information that is considered vital for the recovery effort that can easily be obtained, should be gathered and maintained as a normal part of conducting business. In this case as-built plans, utility information, and foundation information were crucial. Other important information regarding railroads, land use, or hydrology information may be necessary and should be gathered in a centralized location.

Recovery plans should be made and updated regularly. Inform all staff in critical areas of these plans and review these plans on an annual basis. Other agencies or commercial entities that are a part of a recovery process should be involved with the planning and review process.

A thorough review of these plans should be made after any disaster to assess the performance of the plan, discover any weak areas, and modify the plan based on the lessons learned.

Critical staff should be told what could be expected of them when such events occur. Management teams and recovery teams need to work together to determine needs and the appropriate course of action.

Whether they be hurricanes, earthquakes, floods, fires, extreme weather conditions, or other disasters, the recovery from these events can be successfully planned. Although prevention is the best strategy, and should be implemented whenever possible, we can not plan for every contingency in our complex societies. Recovery from these disasters can be accomplished through appropriate planning that has enough foresight to anticipate the needs and enough flexibility to allow those who are responsible to take the necessary action. This has been demonstrated in this case as well as in other crisis events. We must keep in mind that we are serving the needs of society and their welfare depends on it.

Bibliography

Department of Transportation, 1994, "The Northridge Earthquake," Post-Earthquake Investigation Report, Caltrans, Division of Structures, February 8, 1994.

Housner, G., 1990, "Competing Against Time: Report to Governor George Deukmejian from the Governor's Board of Inquiry on the 1989 Loma Prieta Earthquake," George W. Housner, Chairman, C.C. Thiel Editor. State of California, Office of Planning and Research, Sacramento, California.

Housner, G., 1994, "The Continuing Challenge: The Northridge Earthquake of January 17, 1994", Report to the Director, California Department of Transportation. Seismic Advisory Board, George W. Housner, Chairman.

LeBeau, R., Fung, G., Goldschmidt, A., Belvedere, J., 1971, Caltrans, "Post Earthquake Investigation of Bridge Damage in the San Fernando Earthquake of February 9, 1971", Report to the State Highway Engineer.

Roberts, J. E., 1995, "Improved Seismic Details for Highway Bridges"

Zelinski, R., Seaberg, E., 1991, "Post Earthquake Investigation Team" Lifeline Earthquake Engineering, Proceedings of the Third U.S. Conference,

AN INTEGRATED MODEL OF BRIDGE PERFORMANCE, HIGHWAY NETWORKS, AND THE SPATIAL METROPOLITAN ECONOMY: TOWARDS A GENERAL MODEL OF HOW LOSSES DUE TO EARTHQUAKE IMPACTS ON LIFELINES AFFECT THE ECONOMY

Peter Gordon, Professor of Urban Planning and Economics
James E. Moore II, Associate Professor of Urban Planning and Civil Engineering
H. W. Richardson, Professor of Urban Planning and Economics, and
M. Shinozuka, Professor of Civil Engineering

with

K. Y. Cho, S. B. Cho, B. S. Kim, and G. Y. Kim.

School of Urban Planning and Development
University of Southern California
Los Angeles, California 90089-0042
USA

ABSTRACT

We summarize an integrated model of losses due to earthquake impacts on transportation and industrial capactiy affect the urban economy. The procedure advances transportation and activity system analysis techniques in ways that help capture the most important economic implications of earthquakes. Network costs and origin/ destination requirements are endogenous and consistent. Indirect and induced losses associated with direct impacts on transportation and industrial capacity are distributed across zones and economic sectors. This study of the transportation network is suggested as a template for studying the full range of losses associated with other lifeline impacts.

INTRODUCTION

1. Objective

This is an effort to trace the effects of an earthquake on the metropolitan economy, including its impact on the highway network. To do this, we integrate

a. bridge and other structure performance models,

b. highway network models,

c. spatial allocation (of economic activity) models, and

d. interindustry (input/output) models.

In this document, we take **1a.** as given, and discuss the integration of points **1b.**, **1c.**, and **1d.**

2. Data

We have available

a. baseline 1990 census data describing the spatial distribution (by traffic analysis zone) of residences and workplaces by major economic sector;

b. a 515 sector Regional Science Research Institute (RSRI) input output model of the Los Angeles metropolitan (five-county) economy based on 1992 economic census data;

c. the 1994 transportation planning network equilibrium model constructed by the Southern California Association of Governments (SCAG);

d. and a spatial allocation model of the same area that has been used to distribute aggregate input-output results (in $ and/or jobs) to 308 zones (political jurisdictions) across 17 economic sectors.

The model we have used in our previous work is the Southern California Planning Model (SCPM). SCPM aggregates the 515 sectors represented in the RSRI model to 17. Each sector uses the other sectors' outputs as inputs, and each sector supplies the other sectors with inputs. The input/output perspective implies accounting assumptions.

Total Gross Regional Product = Total Value Added
= Total Final Demand. (1.)

Total Regional Production > Total Gross Regional Product (2.)

due to interindustry linkages.

The difference between Total Regional Production and Total Final Demand is Total Intermediate Use.

Total Regional Production = Total Intermediate Use
+ Total Final Demand (3.)

In matrix terms,

$$\mathbf{X} = \mathbf{AX} + \mathbf{Y}; \quad \text{(3a.)}$$

where

$\mathbf{X}$ = a vector describing Total Regional Production by economic sector

$\mathbf{Y}$ = a vector describing Total Final Demand by economic sector, and

$\mathbf{A}$ = a matrix of fixed value coefficients describing in $ terms the quantities of the various outputs from each economic sector needed as inputs to produce $ 1 of output in each sector.

Final Demand is separated into a household component $\mathbf{Y}_1$, which is intraregional; a governmental component $\mathbf{Y}_2$, which is intraregional; and an external, interregional component $\mathbf{Y}_3$. This gives

$$\mathbf{X} = \mathbf{AX} + \mathbf{Y}_1 + \mathbf{Y}_2 + \mathbf{Y}_3. \quad \textbf{(3b.)}$$

This research extends SCPM, endogenizing otherwise exogenous matrices describing the travel behavior of households, achieving consistency across network costs and origin/destination requirements, and better allocating indirect and induced economic losses over zones in response to direct earthquake losses to industrial and transportation capacity.

PROCEDURE

3. Establishing a Baseline

We want to model effects of earthquakes on industrial capacity and system-wide transportation demand and supply. We also want to measure the full economic impact associated with both of these effects. Our first step is to create a transportation baseline that is consistent with respect to equilibrium network costs, network flows, interzonal flows and origin/destination requirements.

a. The existing version of SCPM treats work and shopping trips, but not other nonwork travel and freight. The SCAG network model includes origin/destination requirements for work and nonwork trips, but not freight flows. We use Nationwide Personal Transportation Study (NPTS) data to determine the proportion of total trips allocated to work trips and shopping trips, and use these proportions to scale the interzonal flows associated with the loaded SCAG network.

b. We map the five county, 1,527 zone SCAG transportation network to the five county, 308 zone SCPM activity system. This expresses the scaled interzonal flows associated with the loaded SCAG transportation network in terms of flows between SCPM zones.

c. The scaled SCPM interzonal flows extracted from the NPTS proportions applied to SCAG's data are aggregated into row sums and column sums defining origins and destinations for SCPM zones.

d. The scaled origin/destination requirements from step **3c.** are disaggregated into separate pairs of origin/destination vectors describing work (journey-to-work, JTW) and shopping (journey-to-shop, JTS) trip ends. Each element in the SCPM JTW matrix describes the proportion of workers residing in zone i who work in zone j. Each element of the SPCM JTS matrix describes the proportion of shoppers residing in zone i who shop in zone j. The relative magnitudes of the zone to zone flows on which these proportions are based are used to separate the scaled origin/destination requirements from step **3c.** into new JTW and JTS matrices. The marginal sums of these matrices provide new JTW and JTS trip ends.

SCPM's journey-to-work (JTW) matrix is based on spatial distributions extracted from 1990 census data. SCPM's journey-to-shop matrix is the result of a doubly constrained gravity model estimation. Trip productions are residential population in each zone multiplied by NPTS proportions describing shopping trips per person per day. Trip attractions are the sum of retail and service employment from SCAG's 1990 census transportation planning package (CTPP) data.

e. SCPM's 17 economic sectors include four involving freight. The RSRI model provides information describing total $ per unit output per worker. This is not the wage. The wage measures $ of value added per worker.

Freight flows include intermediate flows to production facilties, as well as flows to final demand sites inside and outside the system. This includes import and export flows, but not flows to and from residential sites. These latter sets correspond to shopping and work trips, respectively. Export flows satisfy final demand outside the region. Some import flows satisfy final demand within the region, and some are inputs to production processes. Import and export flows may also appear as throughputs.

Given the SCPM input/output relationships describing input requirements per unit of output, and given baseline jobs by economic sector and zone from the census, compute interindustry shipments out of zone z by each of four sectors,

$$O^z_i = \sum_j a_{ij} \bullet X^z_i + \text{sector i shipments out of zone z to nonhousehold final demand sectors located everywhere;} \quad (4.)$$

where X^z_i = the total output of commodity i in zone z given base year employment in sector i and zone z, and

a_{ij} = is the i, jth element of A, the matrix of technical coefficients for the

(open) input/output model. This is the flow from i to j per unit output of j.

Thus O^z_i excludes shipments to households everywhere. These shipments are treated as shopping trips.

f. Given baseline jobs by economic sector and zone from the census, compute interindustry shipments into zone z by sector,

$D^z_j = \sum_i a_{ij} \bullet X^z_j$ + sector j shipments from everywhere to nonhousehold final demand sectors in zone z; **(5.)**

where X^z_j = the total output of commodity j in zone z given base year employment in sector j and zone z, and

a_{ij} = is the i, jth element of A, the matrix of technical coefficients for the (open) input/output model. This is the flow from i to j per unit output of j.

Thus D^z_j excludes shipments to households residing in zone z. These are also shopping trips.

Equations **(4.)** and **(5.)** both presume application of an input/output processing sector that is open with respect to labor. the SCPM solution includes all equilibrium journey-to-work and journey-to-shop flows for 17 sectors. These shopping flows are excluded from the right hand sides of equations **(4.)** and **(5.)**.

g. Using factors from the 1993 Commodity Flow Survey (CFS), convert all O^z_i and D^z_j $ values to truckload equivalents. The CFS describes freight flows in terms of $/ton for the major industrial sectors. The 1992 census of transportation describes (we think) tons/truck.

h. Based on SCAG's network equilibrium costs $c^{SCAG}_{i,j}$ and the O/D vectors determined in steps **3d.** and **3g.**, calibrate separate JTW, JTS, and sectoral commodity flow spatial interaction models. Each of the six (JTW, JTW, and four commodity) matrices of interzonal flows is estimated separately given common measure of network cost. This provides a set of separately calibrated gravity models providing interzonal flows by work trip, shopping trip, and commodity.

The objective of these singly constrained gravity model calibrations is the estimation of distance decay parameters. These paramaters are calibrated based on the following criteria.

$$\underset{ß}{\text{Minimize}} \quad \sum_i S_i(ß) \bullet ln(S^{I/O}{}_i) - \sum_i S_i(ß) \bullet ln(S_i(ß)), \tag{6.}$$

where ß = distance decay coefficient,

$S_i(ß)$= estimated amount of commodity supplied in zone i,

$$= \sum_j D_j \bullet [A_i \bullet exp(-ß \bullet c_{i,j}) / \sum_i A_i \bullet exp(-ß \bullet c_{i,j})], \tag{7.}$$

$c_{i,j}$ = generalized cost of transportation from origin zone i to destination zone j,

A_i = constant specific to zone i,

D_j = trips attracted to destination zone j, and

$S^{I/O}{}_i$ = input/output estimate of the quantity of commodity supplied to zone i.

i. Endogenizing journey-to-work flows estimates the following matrix.

Home O(rigin)$_i$	Zone 1	Zone 2		Zone 307	Zone 308
Zone 1	$T_{i,j} = T(O_i, D_j, c^{SCAG}{}_{i,j}, ß)$				
Zone 2					
Zone 307					
Zone 308					
	Zone 1	Zone 2		Zone 307	Zone 308
	Work D(estination)$_j$				

ii. Endogenizing journey-to-shop flows estimates the following matrix.

Home O(rigin)$_i$	Zone 1	Zone 2		Zone 307	Zone 308
Zone 1	$T_{i,j} = T(O_i, D_j, c^{SCAG}{}_{i,j}, ß)$				
Zone 2					
Zone 307					
Zone 308					
	Zone 1	Zone 2		Zone 307	Zone 308
	Shopping D(estination)$_j$				

iii. Endogenizing commodity flows estimates the following set of four matrices.

Production O(rigin)$_i$	Zone 1					
	Zone 2					
			$T_{i,j} = T\ (O_i, D_j, c^{SCAG}{}_{i,j}, ß)$			
	Zone 307					
	Zone 308					
		Zone 1	Zone 2		Zone 307	Zone 308
		Use in Production D(estination)$_j$				

i. Sum interzonal work, shopping, and shipping flows to create a single matrix of interzonal requirements expressed in passenger car equivalents (PCEs).

j. Given the matrix constructed in step **3i.**, model network equilibrium flows to obtain new matrix of interzonal costs. If interzonal costs match the costs applied in steps **3hi-iii.**, stop with equilibrium link costs $c^*_{i,j}$.

Home, Home, Production O(rigin)$_i$	Zone 1					
	Zone 2					
			$T_{i,j} = T\ (O_i, D_j, c^*_{i,j}, ß)$			
	Zone 307					
	Zone 308					
		Zone 1	Zone 2		Zone 307	Zone 308
		Work, Shopping, Use in Production D(estination)$_j$				

If not, return to step **3h.** and continue.

Alternatively, iteration between the network equilibrium model and the spatial allocation model might be replaced by a unified formulation.

$$\text{Minimize} \quad \sum_a \int_0^{x_a} t_a(w)\, dw, \qquad \textbf{(8.)}$$

$$\text{subject to} \quad \sum_k f^{i,j}{}_k = v_{i,j} \quad \text{for all zones i and j;} \qquad \textbf{(9.)}$$

$$\sum f^{i,j}{}_k \bullet \delta^{i,j}{}_{a,k} = x_a \quad \text{for all links a;} \qquad \textbf{(10.)}$$

$$\underset{i,j,k}{}$$

$$f^{i,j}_{k} \geq 0 \qquad \text{for all zones i and j, and paths k;} \qquad \textbf{(11.)}$$

$$(A_i \bullet B_j \bullet O_i \bullet D_j) / exp(\beta \bullet c^*_{i,j}) = v_{i,j} \qquad \text{for all zones i and j;} \qquad \textbf{(12.)}$$

$$\sum_i v_{i,j} = D_j \qquad \text{for all destination zones j;} \qquad \textbf{(13.)}$$

$$\sum_j v_{i,j} = O_i \qquad \text{for all origin zones i;} \qquad \textbf{(14.)}$$

$$\underset{k}{\text{minimum}} \left[\sum_a \delta^{i,j}_{a,k} \bullet t_a(x_a)\right] = c^*_{i,j}; \qquad \textbf{(15.)}$$

where $t_a(x_a)$ = generalized cost function for link a;

$v_{i,j}$ = trip interchange from zone i to zone j;

$f^{i,j}_{k}$ = commodity flow from zone i to zone j on path k;

$\delta^{i,j}_{a,k}$ = 1 if link a is in path k for flows origininating in zone i and terminating in zone j,
0 otherwise;

A_i, B_j = constants corresponding to origin zone i and destination zone j, respectively;

O_i, D_j = trips produced in origin zone i and attracted to destination zone j, respectively;

$c^*_{i,j}$ = equilibrium generalized cost of transportation between orign zone i and destination zone j; and

β = distance decay coefficient.

Equations **(8.)** to **(11.)** represent the user equilibrium assignment model. Equations **(12.)** to **(14.)** denote a doubly constrained gravity model. These two otherwise separable models are connected by Equation **(15.)**, which requires that the transportation costs used to estimate the gravity model be rational, minimum path costs.

k. In either case, matrices describing work, shop, and commodity flows between zones remain distinct. Each matrix's spatial interaction parameters is estimated separately in response to a single set of common network costs. Each matrix is exogenous to step **3j.** and the determination of equilibrium network costs. Each new set of matrices is an update to an otherwise static application of SCPM.

4. Modeling Final Demand and Transportation Cost Impacts on Origin/Destination Requirements.

Our objective is to model demand and network impacts on origins and destinations due to earthquakes. The state of information needed to model the base line with the degree of internal consistency described here is sufficient to treat changes in configuration of the network and the activity system. Following an earthquake, there will losses of network capacity and simultaneous losses of industrial capacity. The former reduces transportation capacity and raises costs. The latter will reduce demands imposed on the network. Results from models identified in step **1a.** provide scenarios ascribing consistent losses of both types to particular events. The spatial interaction elements of our approach make it possible to capture the changes in transportation requirements associated with changes in network performance. These changes and changes resulting from earthquake damage to industrial facilities are treated simultaneously and consistently.

a. Earthquakes induce changes in industrial production due to effects on building stocks. Using loss-of-function curves (available from EQE), we convert damage to building stocks to loss of production by zone and sector. A vector consisting of inverses of 515 RSRI multipliers is used to reduce output losses to corresponding reductions in final demands. This change in final demands drives SCPM, providing changes in output for 17 sectors and 308 zones. These changes modify the values O^z_i and D^z_i generated in step 3e.

b. Earthquakes also eliminate bridges and other transportation structures. Changes in network configuration will produce changes in network equilibrium costs and interzonal requirements. These latter changes are endogenous. Modify baseline cij's by increasing costs for missing links to large numbers.

c. Given steps **4a.** and **4b.**, re-estimate the separate sectoral commodity flow spatial interaction models in step **3h.** At present, this procedure excludes effects on housing stocks.

d. Re-estimate network flows and costs in light of new interzonal requirements from **4c.**

e. These new costs will not be consistent with the interzonal requirements computed in **4a.** and imposed in **4d.** Update the cost data used to estimate the JTW, JTS and

commodity flow matrices, and recompute. If interzonal costs match the costs applied in step **4c.**, stop with costs $c^*_{i,j}$. If not, return to step **4c.** and continue.

f. Once consistency across network costs and origin/destination requirements is achieved, apply SCPM to reallocate changes in output over 17 sectors and 308 zones. SCPM computes indirect and induced economic impacts associated with direct changes in final demand, and allocates these changes to zones. Economic activity induced by household consumption is treated with special attention. Outputs from two versions of the RSRI input/output model are computed and aggregated. In the first version of the model, household demand is exogenous. The formulation is open with respect to labor. Labor is outside the processing sector. In the second version of the model, labor is treated as an economic activity, making household demand endogenous. In the second case the formulation is closed with respect to labor. Labor is inside the processing sector, and is treated as a production activity. The input/output requirements associated with the production of labor are described by household consumption functions. The difference between the solutions to these open and closed models identifies the system wide impacts associated with household consumption.

The total economic impact associated with exogenous constraints on final demand is thus separable as follows.

$$\text{Total economic impact} = \text{Total direct impact} + \text{Total indirect impact} + \text{Total induced impact.} \quad \textbf{(16.)}$$

where

- Total direct impact = reduction in final demand accounted for by earthquake losses to industrial capacity (exogenous);
- Total indirect impact = additional reductions in production of commodities other than labor due to interindustry linkages inthe economy (endogenous to the open model); and
- Total induced impact = additional reductions in production driven by endogenous changes in labor requirements (the difference between the solutions to the open and closed versions of the model).

g. We can execute this procedure for any relevant scenario. The procedure is summarized in Figure 1.

CONCLUSION

Our integration of seismic, highway, spatial allocation, and input/output models permits the study of how the economic impacts of industrial and transportation structure loss are distributed over metropolitan space. Some of this loss is produced directly by

the earthquake, which destroys industrial capacity. The procedure accounts for the impact of industrial structure losses on final demand. The model computes further indirect and induced losses, and makes the spatial distribution of these losses sensitive to increases in network costs resulting from transportation structure losses. The procedure does not yet account for the impact of transportation structure losses on final demand. However, the model does achieve consistency across transportation supply, transportation demand and post-event production.

Our approach combines the indirect and induced impacts associated with direct losses in transportation capacity with direct losses in industrial capacity. However, transportation systems are only one example of urban lifelines. Other networks perform according to other physical rules, but all are subject to modeling. This approach can be extended by formulating models that account for post event performance of other networks. The economic losses associated with earthquake impacts on other lifeline capacities can be incorporated into this framework as readily as impacts on transportation networks, in some cases, more readily.

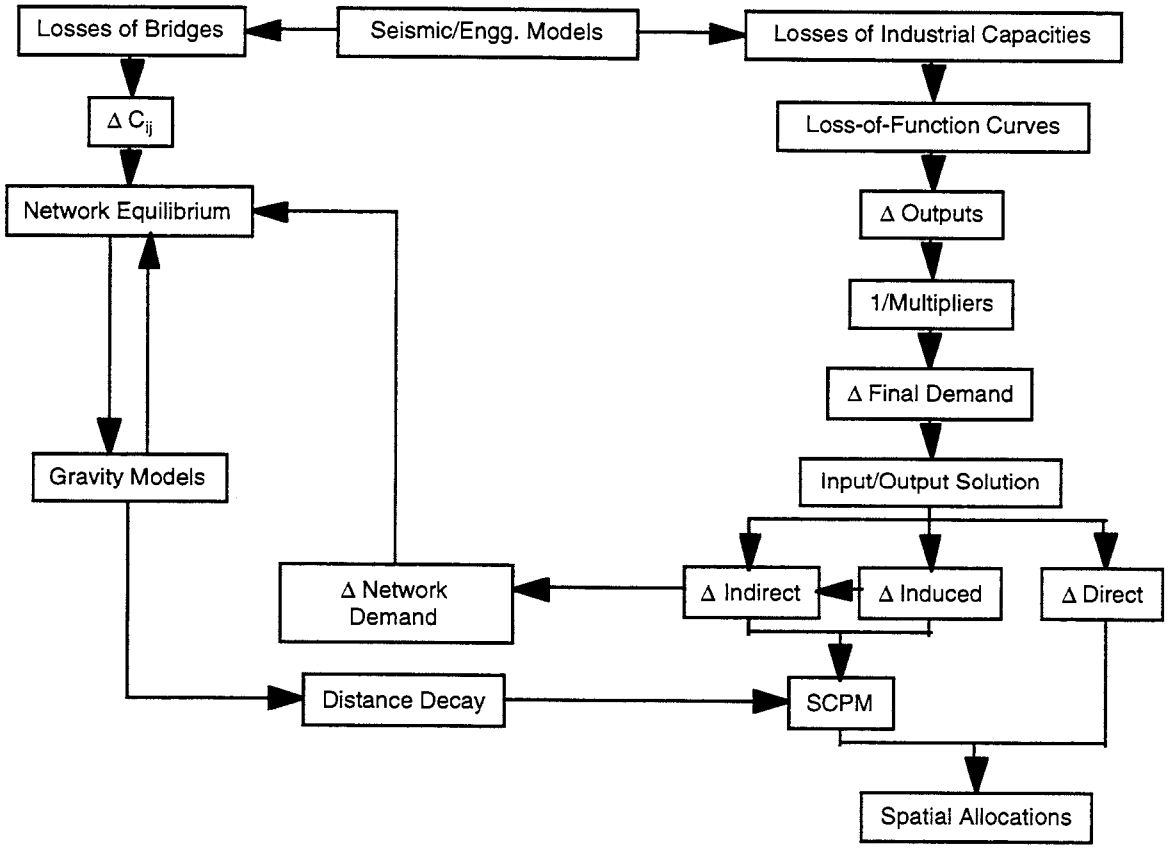

Figure 1: Summary of the Extended SCPModel

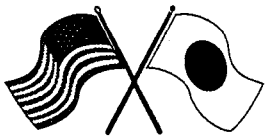

Appendices

Agenda

U.S. Side Participants

Japan Side Participants

NATIONAL CENTER FOR EARTHQUAKE ENGINEERING RESEARCH
Headquartered at the State University of New York at Buffalo

INSTITUTE OF INDUSTRIAL SCIENCE
INCEDE
UNIVERSITY OF TOKYO

NCEER-INCEDE Center-To-Center Workshop on
Earthquake Engineering Frontiers in Transportation Facilities

Agenda

Monday, March 10

8:30 – 9:00 Registration

9:00 – 10:00 **Opening Session**
Session Co-chairs: Ian M. Friedland and Kazuhiko Kawashima

Welcome and opening remarks – Dr. George C. Lee and Dr. Ken Sudo

NCEER's Mission and Goals for the Center to Center Project
George C. Lee and Andrea Dargush
Center-to-Center (INCEDE-NCEER) Cooperative Research and US-Japan Common Agenda on Earthquake Related Issues and the Role of INCEDE Towards Goals of IDNDR
Ken Sudo, *Tsuneo Katayama*, Kimiro Meguro, Anura S. Herath and Dushamante Dutta

10:00 – 10:20 Break

10:20 – 12:20 **Session 1: Ground Motion and Soils**
Session Co-chairs: Andrea Dargush and Tsuneo Katayama

Seismological Aspects of the Hyougo-ken Nambu Earthquake, the Kobe Earthquake, of 17 January 1995
Ken Sudo and Kimiro Meguro
Future Directions in a National Portrayal of Seismic Hazard for Highway and Bridge Design
Maurice S. Power
Long Period Ground Motion due to the 1995 Hyogen-ken Nambu, Japan Earthquake
Tatsuo Ohmachi, Shun'ichi Kataoka and Shojiro Kataoka
Site Response and Liquefaction Behavior
Ahmed-W. Elgamal, Korhan Adalier and Mourad Zeghal
Ground Displacements and Strain Caused by Soil Liquefaction
Masanori Hamada, Kazue Wakamatsu and Takehiro Shibuya
Reduction of Liquefaction Hazards by Deep Soil Mixing
Thomas D. O'Rourke and Siang H. Goh

12:20 – 13:30 Lunch

13:30 - 14:30 **Session 2: Underground Structures**

Session Co-chairs: Maurice Power and Tatsuo Ohmachi

GIS Assessment of Water Supply Damage from the Northridge Earthquake
Thomas D. O'Rourke and Selcuk Toprak

Effects of Liquefaction-induced Large Ground Displacements on Earthquake Resistance of Foundations of Buried Pipes
Masanori Hamada, Kazuto Kobayashi and Yoshifumi Akioka

Performance of Corrugated Metal Pipe (CMP) Culverts During Past Earthquakes
T. Leslie Youd and Chris J. Beckman

14:30 - 14:50 Break

14:50 - 16:50 **Session 3: Analysis & Structure Performance - Part I**

Session Co-chairs: Thomas O'Rourke and Masanori Hamada

Simulation of Collapse Process of Elevated Expressway Bridges Due to the Kobe Earthquake
Kimiro Meguro and Tsuneo Katayama

Evaluation of Bridge Damage from the 1994 Northridge, CA Earthquake
Nesrin I. Basöz and Anne S. Kiremidjian

Examination of Performance of a Menshin Elevated Highway Bridge During the Kobe Earthquake
Masato Abe, Yozo Fujino and Junji Yoshida

Liquefaction-induced Damage to Bridges
T. Leslie Youd

Intrepretation of Damage on the Hanshin Expressway (Kobe Line) Viaduct Based on Statistical Data and Dynamic Analysis
Yozo Fujino, Masato Abe and Satoko Abe

Seismic Response of Bridges to Differential Support Ground Motion
George Deodatis, Sanjay Arwade and Masanobu Shinozuka

16:50 - 17:00 **Group Photograph**

18:15 **Dinner Hosted by U.S. Side**

Dinner at Chang's Garden Restaurant; shuttle busses will leave from the University Inn front lobby at 6:15 pm

Tuesday, March 11

8:30 - 9:50 **Session 4: Analysis & Structure Performance - Part II**
Session Co-chairs: T. Leslie Youd and Yozo Fujino

Dynamic Response Behavior of Prestressed Concrete Viaduct Under Severe Earthquake
Wael Zatar, *Hiroshi Mutsuyoshi* and William Tanzo
Effect of Vertical Ground Motion on Bridge Deck Response
Chih-Peng Yu, Daniel S. Broekhuizen Jose M. Roesset, John E. Breen and *Michael E. Kreger*
Development and Application of a New Model for Fracture Behavior Analysis of Structures
Kimiro Meguro and *Hatem Tagel-Din*
To Isolate or not to Isolate: Insights from Field Tests
Stuart S. Chen, John B. Mander and Daniel A. Wendichansky

9:50 - 10:10 Break

10:10 - 11:50 **Session 5: Design and Retrofitting**
Session Co-chairs: Michael E. Kreger and Hiroshi Mutsuyoshi

The 1996 Seismic Design Specifications of Highway Bridges
Kazuhiko Kawashima and Shigeki Unjoh
Recommended Seismic Design Criteria for the Nation's Highway Bridges
Christopher Rojahn, Ronald L. Mayes and Richard V. Nutt
Pounding of Bridge Girders During Strong Ground Motion and its Countermeasure
Robert Jankowski, Yozo Fujino and Krzysztof Wilde
Standard and Innovative Retrofit Details and New Construction Details for Highway Bridges
James L. Foster, Jr.
A Model for Confinement Effect for Concrete Cylinders Confined by Carbon Fiber Sheets
Manabu Hosotani, *Kazuhiko Kawashima* and Jun-ichi Hoshikuma

11:50 - 13:10 Lunch

13:10 - 15:10 **Session 6: Earthquake Protective Systems**
Session Co-chairs: Christopher Rojahn and Masato Abe

Optimal Design of Bridge Bearings for Seismic Protection
Masato Abe and Yozo Fujino
Property Modification Factors and Response Modification Factors for Seismically Isolated Bridges
Michael C. Constantinou, Panos Tsopelas and Joseph Quarshie
The Restoring Force Characteristic of LRB Under the Influence of Variable Axial Loads and Rotational Deformations
Hirokazu Iemura, *Akira Igarashi*, Youzhen Chen and Hiroyuki Nakazima
Seismic Vibration Reduction of Highway Bridge by Real-time Structural Parameter Modification

(RSPM)
Mike Tong, Y.H. Wu, and George C. Lee
Retrofit of Existing Reinforced Concrete Bridges Using VE Dampers
Nishith Gupta, *Hiroshi Mutsuyoshi* and William Tanzo
Analytical Studies of Shape Memory Alloy Dampers for Structural Control of Base Isolated Structures
Krzysztof Wilde, Paolo Gardoni and Yozo Fujino

15:10 - 15:30 Break

15:30 - 16:10 **Session 7: Reconstruction Strategies, Social & Economic Impacts**
Session Co-chairs: James L. Foster and Akira Igarashi

Rapid Disaster Recovery: A Case Study for Bridge Replacement
Earl Seaberg
An Integrated Model of Bridge Performance, Highway Networks, and the Spatial Metropolitan Economy: Towards a General Model of How Losses due to Earthquake Impacts on Lifelines Affect the Economy
Peter Gordon, *James E. Moore II*, H. W. Richardson and Masanobu Shinozuka

16:10 - 17:00 **Session 8: Identification of Recommended Practices in Earthquake Damage Mitigation**
Session Co-chairs: Ian M. Friedland and Kimiro Meguro

Center-to-Center Reports and Products
Kimiro Meguro

Following this presentation, a discussion among participants on the identification and development of materials related to recommended practices for the prevention or mitigation of earthquake damage to highway systems.

17:00 - 17:20 **Resolutions and Closure**
Session Co-chairs: Ian M. Friedland and Kimiro Meguro

Proposed resolutions resulting from the workshop will be presented by Drs. George C. Lee and Ken Sudo.

18:15 **Reception and Dinner Hosted by Japan Side**
Reception (6:15 pm) and Dinner (7:00 pm) at the University Inn

Wednesday, March 12

8:30 - 11:30 NCEER Seismic Laboratory and Information Services Tour

NCEER - INCEDE Center-to-Center Workshop on Earthquake Engineering Frontiers in Transportation Facilities

U.S.-Side Participants

Dr. Nesrin Basöz
The John A. Blume Earthquake
Engineering Center
Stanford University
Department of Civil Engineering
Stanford, CA 94301
Tel: 415-725-3168
Fax: 415-725-9755
e-mail:

Dr. Stuart S. Chen
State University of New York at Buffalo
Department of Civil Engineering
242 Ketter Hall
Buffalo, NY 14260
Tel: 716-645-2114 Ext. 2428
Fax: 716-645-3733
e-mail: *ciechen@eng.buffalo.edu*

Dr. Michael Constantinou
State University of New York at Buffalo
Department of Civil Engineering
132 Ketter Hall
Buffalo, NY 14260
Tel: 716-645-2114 Ext. 2404
Fax: 716-645-3733
e-mail: *cieconst@ubvms.cc.buffalo.edu*

Ms. Andrea Dargush
Assistant Director for
Research and Education
National Center for Earthquake
Engineering Research
State University of New York at Buffalo
107 Red Jacket Quadrangle
Buffalo, NY 14261
Tel: 716-645-3391
Fax: 716-645-3399
e-mail: *dargush@acsu.buffalo.edu*

Dr. George Deodatis
Princeton University
Department of Civil Engineering
and Operations Research
E209 Engineering Quadrangle
Princeton, NJ 08544
Tel: 609-258-1624
Fax: 609-258-0998
e-mail: *deodatis@deo.princeton.edu*

Dr. Ahmad-W. Elgamal
Columbia University
Department of Civil Engineering
610 Mudd Building
New York, NY 10027
Tel: 212-854-1203
Fax: 212-854-6267
e-mail: *elgamal@civil.columbia.edu*

Mr. James L. Foster Jr.
Senior Engineer
California Department of Transportation
1801 30th Street
Sacramento, CA 95816
Tel: 916-227-8680
Fax: 916-227-8379
e-mail: *jfoster@trmx3.dot.ca.gov*

Mr. Ian M. Friedland
Assistant Director for
Bridges and Highways
National Center for Earthquake
Engineering Research
State University of New York at Buffalo
102 Red Jacket Quadrangle
Buffalo, NY 14261
Tel: 716-645-3391
Fax: 716-645-3399
e-mail: *imf@acsu.buffalo.edu*

Mr. Siang Huat Goh
Cornell University
School of Civil and Environmental Engineering
Hollister Hall
Ithaca, NY 14853
Tel: 607-255-4899
Fax: 607-255-9004
e-mail: *shg2@cornell.edu*

Dr. Michael Kreger
University of Texas at Austin
Ferguson Laboratory
10100 Burnet Road
Building 177
Austin, TX 78758
Tel: 512-471-4579
Fax: 512-471-1944
e-mail: *kreger@uts.cc.utexas.edu*

Dr. George C. Lee
Director
National Center for Earthquake
Engineering Research
State University of New York at Buffalo
109 Red Jacket Quadrangle
Buffalo, NY 14261
Tel: 716-645-3391
Fax: 716-645-3399
e-mail: *gclee@acsu.buffalo.edu*

Dr. John Mander
State University of New York at Buffalo
Department of Civil Engineering
230 Ketter Hall
Buffalo, NY 14260
Tel: 716-645-2114 Ext. 2418
Fax: 716-645-3733
e-mail: *jmander@ubvms.cc.buffalo.edu*

Dr. James E. Moore, II
University of Southern California
Urban and Regional Planning
Von KleinSmid Center 351
Los Angeles, CA 90089-0042
Tel: 213-743-2090
Fax: 213-743-2476
e-mail: *jmoore@rcf.usc.edu*

Dr. Thomas D. O'Rourke
Cornell University
School of Civil and Environmental Engineering
265 Hollister Hall
Ithaca, NY 14853
Tel: 607-255-6470
Fax: 607-255-9004
e-mail: *tdo1@cornell.edu*

Mr. Maurice S. Power
Vice President
Geomatrix Consultants, Inc.
100 Pine Street, Suite 1000
San Francisco, CA 94111
Tel: 415-434-9400
Fax: 415-434-1365
e-mail: *cmusacchia@geomatrix.com*

Mr. Joseph Quarshie
State University of New York at Buffalo
Department of Civil Engineering
204 Ketter Hall
Buffalo, NY 14260
Tel: 716-645-2114 Ext. 2436
Fax: 716-645-3733
e-mail: *quarshie@acsu.buffalo.edu*

Mr. Christopher Rojahn
Executive Director
Applied Technology Council
555 Twin Dolphin Drive, Suite 270
Redwood City, CA 94065
Tel: 415-595-1542
Fax: 415-593-2320
e-mail: *crojahn@atcouncil.org*

Dr. Vladimir Rzhevsky
State University of New York at Buffalo
Department of Civil Engineering
220 Ketter Hall
Buffalo, NY 14260
Tel: 716-645-2114 Ext. 2409
Fax: 716-645-3733
e-mail:

Mr. Earl Seaberg
Senior Engineer
California Department of Transportation
1801 30th Street
Sacramento, CA 95816
Tel: 916-227-8427

Fax: 916-227-8379
e-mail: *eseaberg@trmx3.dot.ca.gov*

Dr. Mai Tong
State University of New York at Buffalo
Department of Civil Engineering
141 Ketter Hall
Buffalo, NY 14260
Tel: 716-645-3019 Ext. 2444
Fax:
e-mail:

Mr. Selcuk Toprak
Cornell University
School of Civil and Environmental Engineering
Hollister Hall
Ithaca, NY 14853
Tel: 607-255-4292
Fax: 607-255-9004
e-mail: *st31@cornell.edu*

Dr. Panos Tsopelas
State University of New York at Buffalo
Department of Civil Engineering
142 Ketter Hall
Buffalo, NY 14260
Tel: 716-645-2114 Ext. 2435
Fax: 716-645-3733
e-mail: *tsopelas@abraham.eng.buffalo.edu*

Dr. Yihui Wu
Visiting Scholar
State University of New York at Buffalo
Ketter Hall
Buffalo, NY 14260
Tel: 716-645-2114
Fax: 716-645-3733
e-mail:

Dr. T. Leslie Youd
Brigham Young University
Department of Civil and Environmental Engineering
368 Clyde Building
P.O. Box 24009
Provo, UT 84602-4081
Tel: 801-378-6327
Fax: 801-378-4449
e-mail: *tyoud@byu.edu*

NCEER-INCEDE Center-to-Center Workshop on Earthquake Engineering Frontiers In Transportation Facilities

Japan-Side Participants

Dr. Masato Abe
Department of Civil Engineering
University of Tokyo
7-3-1 Hongo, Bunkyo-ku
Tokyo, 113, Japan
Tel: 81-3-5802-3312
Fax: 81-3-5689-7292
e-mail: *masato@kyouryou.t.u-tokyo.ac.jp*

Dr. Dushmanta Dutta
Research Associate
International Center for
Disaster-Mitigation Engineering
Institute of Industrial Science
University of Tokyo
7-22-1 Roppongi, Minato-ku
Tokyo, 106, Japan
Tel: 81-3-3402-6231
Fax: 81-3-3402-4165
e-mail: *dutta@incede.iis.u-tokyo.ac.jp*

Dr. Yozo Fujino
Department of Civil Engineering
University of Tokyo
7-3-1 Hongo, Bunkyo-ku
Tokyo, 113, Japan
Tel: 81-3-5802-3312
Fax: 81-3-5689-7292
e-mail: *fujino@kyouryou.t.u-tokyo.ac.jp*

Dr. Masanori Hamada
Department of Civil Engineering
Waseda University
3-4-1 Okubo, Shinjyuku-ku
Tokyo, 169, Japan
Tel: 81-3-3208-0349
Fax: 81-3-3208-0349
e-mail: *hamada@mn.waseda.ac.jp*

Dr. Akira Igarashi
Department of Civil Engineering
Kyoto University
Yoshida-Honmachi, Sakyo-ku
Kyoto, 606-01, Japan
Tel: 81-75-753-5087
Fax: 81-75-753-5926
e-mail: *iemura@catfish.kuciv.kyoto-u.ac.jp*

Mr. Robert Jankowski
Department of Civil Engineering
University of Tokyo
7-3-1 Hongo, Bunkyo-ku
Tokyo, 113, Japan
Tel: 81-3-5802-3312
Fax: 81-3-5689-7292
e-mail:

Dr. Tsuneo Katayama
Director General
National Research Institute for
Earth Science and Disaster Prevention
3-1, Tennodai
Tsukuba, 305, Japan
Tel: 81-298-51-1620
Fax: 81-298-51-3246
e-mail:

Dr. Kazuhiko Kawashima
Department of Civil Engineering
Tokyo Institute of Technology
2-12-1 O-okayama, Meguro-ku,
Tokyo, 152, Japan
Tel: 81-3-5734-2922
Fax: 81-3-3729-0728
e-mail: *kawasima@cv.titech.ac.jp*

Dr. Kimiro Meguro
International Center for
Disaster-Mitigation Engineering
Institute of Industrial Science
University of Tokyo
7-22-1 Roppongi, Minato-ku
Tokyo, 106, Japan
Tel: 81-3-3402-6231
Fax: 81-3-3402-4165
e-mail: *meguro@incede.iis.u-tokyo.ac.jp*

Dr. Hiroshi Mutsuyoshi
Department of Civil Engineering
Saitama University
255 Shimo-okubo
Urawa, 338, Japan
Tel: 81-48-858-3553
Fax: 81-48-855-9361
e-mail: *mutuyosi@p.mtr.civil.saitama-u.ac.jp*

Dr. Tatsuo Ohmachi
Interdisciplinary Graduate School of
Science and Engineering
Tokyo Institute of Technology
4259 Nagatsuda, Midori-ku
Yokohama, 226, Japan
Tel: 81-45-924-5605
Fax: 81-45-922-3840
e-mail: *ohmachi@enveng.titech.ac.jp*

Dr. Ken Sudo
Director
International Center for
Disaster-Mitigation Engineering
Institute of Industrial Science
University of Tokyo
7-22-1 Roppongi, Minato-ku
Tokyo, 106, Japan
Tel: 81-3-3402-6231
Fax: 81-3-3402-4165
e-mail: *sudo@incede.iis.u-tokyo.ac.jp*

Mr. Hatem Tagel-Din
International Center for
Disaster-Mitigation Engineering
Institute of Industrial Science
University of Tokyo
7-22-1 Roppongi, Minato-ku
Tokyo, 106, Japan
Tel: 81-3-3402-6231
Fax: 81-3-3402-4165
e-mail: *hsayed@rattle.iis.u-tokyo.ac.jp*

Dr. Krzysztof Wilde
Department of Civil Engineering
University of Tokyo
7-3-1 Hongo, Bunkyo-ku
Tokyo, 113, Japan
Tel: 81-3-5802-3312
Fax: 81-3-5689-7292
e-mail:

State University of New York at Buffalo
Red Jacket Quadrangle
Buffalo, New York 14261
Telephone: 716/645-3391
FAX: 716/645-3399

ISSN 1088-3800